Keele UNIVERSITY

Determining the role of epigenetics in telomerase regulation

Fatma Dogan

A thesis submitted in partial fulfilment of the requirements of

Keele University

for the degree of

Doctor of Philosophy (Ph.D)

October 2022

Abstract

Telomeres are guanine-rich 5′-TTAGGG-3′ repeats found at the ends of human chromosomes that protect chromosomes from degradation and also provide stabilization. Telomerase macromolecule is the primary enzyme responsible for telomere elongation. Telomerase has a critical role in cell proliferation, tumourigenesis, and therapy resistance by modifying many signalling pathways. The human telomerase reverse transcriptase enzyme (hTERT) is responsible for encoding the catalytic subunit of telomerase. It is demonstrated that TERT promoter mutations might increase telomerase activation, but regulation of the telomerase gene is incompletely understood with epigenetic, transcriptional, and posttranscriptional modifications all combined. Epigenetic alterations are just as significant as genetic mutations in a normal cell's transformation into cancer. Understanding the epigenetic molecular mechanism behind telomerase regulation and the responsible genes holds significant prospects for cancer treatment. Pluripotent stem cells provide a valuable tool to better understand this mechanism as telomerase activity is downregulated in stem cells during their differentiation. The link between telomerase activity and differentiation may provide an excellent tool for studying the epigenetic regulation of telomerase.

Physiological oxygen (physoxia) microenvironments affect several cellular aspects, including proliferation, metabolic activity, stemness, and differentiation. This environment also plays a critical role in TERT gene regulation and epigenetic changes such as histone modifications and DNA methylation. The role of oxygen tension on driving promoter modifications of the TERT gene in cancer and pluripotent stem cells (PSC) is poorly understood either *in vitro* or *in vivo*. Therefore, further research is required to determine the association between telomerase, epigenetics, and physiological oxygen microenvironment.

Here, various cancer cell lines and hESCs (embryonic stem cells) were studied to determine the role of low oxygen in the epigenetic regulation of telomerase and epigenetic associated genes, including TERT, DNMTs, HDACs, and differentiation markers for stem cells. This study design enabled an exploration of differences in molecular mechanisms of TERT regulation in different cell types. To understand physoxia effects, cells were cultured in an atmospheric oxygen incubator, 2% O_2 -Pre-gassed media (pre-conditioned to 2% O_2 in a HypoxyCool unit) in a 2% O_2 incubator and an oxygen controlled chamber to provide a fully defined 2% O_2 environment (tri-gas workstation). In this study, we investigated the effect of different oxygen tensions on proliferation, telomerase activity, TERT gene, promoter methylation and telomere length association with stem cell differentiation.

Reduced oxygen culture increased the proliferation rate, metabolic activity and stemness of ESCs. qRT-PCR data showed that EBs express three germ layer differentiation markers during extensive culture while retaining pluripotency and telomerase activity beyond the levels observed with monolayer differentiated cells. Monolayer and 3D differentiated cells displayed slower onset of differentiation in physoxia. Also, downregulated TERT expression was correlated to telomerase activity during differentiation with a higher telomerase enzyme activity in physoxia. A significant increase in promoter methylation was noted during the differentiation of ESCs and EBs correlated to decreased telomerase expression. Further, DNMT3B inhibition with nanaomycin A decreased methylation on the promoter and increased TERT expression, associated with increased enzyme activity in stem cells and cancer cell models. However, DNMT1 inhibitor (decitabine) treated cells had no consistent results in cancer cells. Additionally, CHIP data showed a considerable decrease in DNMT3B antibody binding to TERT promoter regions after nanaomycin A treatment compared to untreated cells.

Overall, our data for the first time demonstrated that DNMT3B binding to TERT promoter increases methylation in differentiated stem cells and cancer cells using CHIP qPCR. TERT promoter displayed an oxygen-sensitive methylation pattern associated with the DNMT3B enzyme activity in monolayer and 3D differentiated ESCs. Together these data suggest that DNMT3B inhibition positively regulates TERT gene expression and telomerase activity in stem cells and cancer cells.

Publications

Dogan, Fatma, Rakad M Kh Aljumaily, Mark Kitchen, Nicholas R. Forsyth. 2022. "Physoxia Influences Global and Gene-Specific Methylation in Pluripotent Stem Cells." BioRxiv preprint, March, 2022.03.21.484908. https://doi.org/10.1101/2022.03.21.484908.

Dogan, F.; Forsyth, N.R. Telomerase Regulation: A Role for Epigenetics. Cancers 2021, 13, 1213. https://doi.org/10.3390/cancers13061213.

Dogan, Fatma, and Nicholas R. Forsyth. 2021. "Epigenetic Features in Regulation of Telomeres and Telomerase in Stem Cells." Emerging Topics in Life Sciences 5 (4): 497–505. https://doi.org/10.1042/ETLS20200344.

Dogan, F.; Aljumaily, R.M.K.; Kitchen, M.; Forsyth, N.R. DNMT3B Is an Oxygen-Sensitive De Novo Methylase in Human Mesenchymal Stem Cells. Cells 2021, 10, 1032. https://doi.org/10.3390/cells10051032.

Conference Abstracts

▪ **F. Dogan**, N. Forsyth, `Mimicking Physiological Oxygen in Cell Cultures`, Innovative cell culture system; Keele University Seminar series, 23 Sep 2021, (Invited speaker).

▪ **F. Dogan**, N. Forsyth, `Environmental And Spatial Considerations For Transcriptional And Epigenetic Fidelity Of Pluripotent Stem Cells` Biomarkers UK 8-9 Nov 2021, Oxford Global Conferences Manchester, (Invited speaker).

▪ **F. Dogan**, N. Forsyth, `Telomerase activity regulation is promoter methylation-and oxygen-sensitive in differentiated pluripotent stem cell` EMBO Conference: Chromatin and Epigenetics, 17-20 May 2021, (Poster presentation and flash talk).

- **F. Dogan,** R. A. Jumaily, N. Forsyth, `Telomerase activity regulation and differentiation onset are oxygen-sensitive in differentiating pluripotent stem cells` TERMIS Conference (SYIS). 26-29 May 2020. Virtual, (Oral presentation).

- **F. Dogan**, N. Forsyth, `Down-regulation of telomerase activity in differentiating stem cells and the role of hypoxia on epigenetic regulation of TERT `Telomere Network UK Meeting University of Leicester, 10-11 Sep 2019, (Poster presentation).

- **F. Dogan**, N. Forsyth, `An attractive therapeutic target for cancer: Telomerase and Epigenetic approaches` ILAS/PGR conference, (3 Minute Thesis competition and poster), 16 Nov 2020.

- **F. Dogan**, N. Forsyth, `Telomerase activity regulation is promoter methylation-sensitive in 3D stem cell aggregates 6th Annual Keele Postgraduate Conference, 25 May 2021. (Poster presentation).

Acknowledgements

First, I would like to thank my supervisor, Professor. Nicholas R Forsyth for his guidance and advice throughout my project and for supporting every step of my PhD. Prof Forsyth supported me to develop my career as an independent researcher, and his research experience has helped keep my project on track. I am genuinely grateful for all the helpful and valuable suggestions to my publications and thesis from my mentor, who has unending patience when revising the manuscripts. Additionally, I would like to thank Dr Mark Kitchen, who has provided valuable support with the pyrosequencing assay.

I would certainly like to share my gratitude (in no particular order) to Jacob, Vibin, Shiko, Trisha and Tasmin. You are more than friends and have always been there for me through my best and worst times. I would also like to thank all the administration/PGR staff (Zara Richards, Keele) and Keele (Katy Cressy and John Misra) for all of the support over the past three years. I would also like to thank all the Guy Hilton research centre members, including receptionists, lab-technicians, PhD students, and post-doc students.

I would also like to share my genuine respect for my parents. A special thanks to my mother, Selime Dogan and father, Fikri Dogan, for your support over the years. Especially, my moms` love and support throughout my entire life mean more than anything. Also, I would like to thank my sister, Gulsum and brother Kadir for believing me more than I believed in myself and for encouragement throughout my study.

Contents

List of Figures

List of Tables

Abbreviations

3D	Three-dimensional
hESC	Human embryonic stem cell
hPSCs	Human pluripotent stem cells
hTR/ hTERC	The human telomerase RNA component
hTERT	Human telomerase reverse transcriptase
DNA	Deoxyribonucleic acid
HIF-1	Hypoxia-inducible factor 1
PHD	Prolyl hydroxylases
VHL	von Hippel–Lindau
Sp1	Specificity Protein 1
WT1	Wilms' tumour 1 suppressor
c-MYC	cellular MYC proto-oncogene
E2F-1	E2F transcription factor 1
Mad1	Mitotic arrest deficiency 1
AP-1	Activating protein-1
ER	Estrogen receptor
GABP	GA-binding protein
CTCF	CCCTC-binding factor
DNMT	DNA methyltransferase
HAT	Histone acetyltransferase
HDAC	Histone deacetylase
SIRT	Sirtuin 1
TSA	Trichostatin A
BSA	Bovine Serum Albumin
FBS	Fetal bovine serum
PSA	Penicillin-Streptomycin-Amphotericin B Solution

NEAA	Non-Essential Amino Acid
SMYD3	SET and MYND domain-containing protein 3
H3K4	Lysine 4 on histone 3
5meC	5-methylcytosine
miRNA	MicroRNA
mRNA	Messenger Ribonucleic Acid
3`UTR	3` untranslated region
cDNA	Complementary DNA
TRAP	Telomeric repeat amplification protocol
PCR	Polymerase chain reaction
qRT-PCR	Quantitative Real time PCR
EBs	Embryoid bodies
hMSCs	Human mesenchymal stem cells
iPSCs	Induced pluripotent stem cells
HCC	Hepatocellular carcinoma
TERRA	Telomere repeat-containing RNA
TRF1/2	Telomeric repeat-binding factors 1 and 2
POT1	Protection of telomeres 1
CTCF	CCCTC binding factor
ALT	Alternative lengthening of telomeres
SMYD3	SET and MYND domain-containing protein 3
SSEA	Stage-Specific Embryonic Antigen
ALP	Alkaline phosphatase
UTSS	Transcription start site
THOR	TERT hypermethylated oncological region

Keele University

CHAPTER 1: INTRODUCTION

Epigenetics defines the heritable change in gene function without changing the DNA sequence and focuses on understanding gene regulation with various associated modifications. Epigenetic changes might switch gene activity on or off with environmental influences, but they do not change the genome (Deans and Maggert, 2015). Chemical alterations of DNA have critical roles in mammalian development, differentiation, disease, and maintenance of cellular identity through the control of gene expression (Reik, 2007). Further, DNA methylation and histone modifications are dynamic and strongly associated with differentiation, stem cell renewal, and replicative senescence (Bork et al., 2010; Huang et al., 2014a).

The telomerase reverse transcriptase enzyme (abbreviated as TERT in humans) encodes the catalytic subunit of telomerase which together with the telomerase RNA component (TERC), comprises the fundamental unit of the enzyme complex. However, the expression of TERT is a rate-limiting determinant for telomerase enzyme activity in most cells (Counter et al., 1998). TERT is considered as a significant gene in carcinogenesis. It is a potential target for cancer treatment and is also a vital stem cell marker for immortality. However, the mechanisms of gene activation or silencing of TERT across somatic, cancer and stem cells remain open for discussion. Promoter mutations in TERT may induce telomerase activation in tumour cells. Additional factors, including epigenetic marks, transcriptional, and post transcriptional modifications are also essential in telomerase activation. Moreover, epigenetic mechanisms might be responsible for reversible silencing of the TERT gene in several biological processes such as differentiation and ageing (Lai et al., 2005; Eitsuka et al., 2018). During differentiation in mouse and human pluripotent stem cells (PSC), TERT and telomerase activity levels decrease with the emergence of a maturing population of cells (Armstrong et al., 2000, 2005; Tzukerman et al., 2000). Therefore, stem cells can be valuable tools to assess epigenetic regulation of TERT and related genes during differentiation and when considered alongside cancer cells has potential to aid a comprehensive understanding of the underlying epigenetic regulation of this gene.

Embryonic stem cells are derived from the inner cell mass at the blastocyst stage of embryonic development and express high levels of telomerase activity (Thomson et al., 1998). ESCs possess limitless proliferation, differentiation, and a self-renewal capacity distinct from other cells. They can differentiate into the three germ layers and form a range of tissue cell types that make up an adult organism (Sathananthan and Trounson, 2005). The association between stem cells and their niche is critical to maintaining proliferation, differentiation, cell fate regulation, and self-renewal. The stem cells niche is a dynamic and complex structure that

includes extracellular matrix, adhesion molecules, matrix glycoproteins, soluble signalling factors, physical parameters, and environmental signals like oxygen (Lane et al., 2014). Communication and contact between these factors are crucial in three-dimensional space. Cells react to every signal from within their specialized microenvironment through multiple pathways. Oxygen is an important signalling molecule and environmental factor for many cellular functions. Cells can sense and adapt to different oxygen tensions via hypoxia-inducible factors (HIFs) (Zhu and Bunn, 2001). The HIF transcription factor regulates several cellular events and is activated when cells or tissues are exposed to oxygen levels below their physiological or adaptive norm. Moreover, this transcription factor plays a significant part in cellular responses during a reduction in oxygen levels. It has various downstream effects such as apoptosis, tumour proliferation, inflammatory responses, activation pathways, and hypoxic recovery (Ziello et al., 2007). It is believed that hypoxia-responsive pathways are activated in order to survive pathological situations, including inflammatory and tumourigenic processes. Low (<2%) oxygen concentrations have a key role for the mammalian embryo, cardiovascular system, and placenta development by activating HIF, also affect cell behaviour, differentiation, proliferation, the formation of specific cell subtypes, and gene expression (Dunwoodie, 2009). Additionally, the impact of reduced oxygen on the differentiation of stem cells is controversial; for instance, some studies suggest that a low oxygen microenvironment increases differentiation potential in human stem cells, however, other studies emphasize that reduced oxygen tension (1-2% O_2) decreased differentiation of human mesenchymal stem cells (hMSCs) (Prado-Lopez et al., 2010; Volkmer et al., 2010; Kwon et al., 2017). The TERT core promoter region contains several binding sites for different transcription factors, including HIF1, c-Myc (cellular MYC proto-oncogene), Sp1 (Specificity Protein 1) and WT1 (Wilms' tumour 1 suppressor) transcription factors (Kyo et al., 2008). HIF1 is one of the significant transcription factors for the TERT promoter, which comprises two HIF-1 consensus sequences at -165 and +51 positions (Nishi et al., 2004). HIF-1α upregulation induces telomerase activity by considerably increased TERT transcription, and HIF1 binding motifs are responsible for its overexpression (Kyo et al., 2008). For these reasons, the effects of the physiological environment should be considered when assessing the epigenetic regulation of TERT and the expression of associated genes in differentiating pluripotent stem and tumour cell lines.

1.1 Telomeres and Telomerase Regulation

Telomerase is a ribonucleoprotein DNA-protein enzyme responsible for telomere elongation and was first discovered by Greider and Blackburn in 1985. Telomeres are guanine-rich tandem repeats at the ends of human chromosomes that protect chromosomes from degradation and stabilise chromosomes (Moyzis et al., 1988). Hayflick et al. first showed a finite lifespan and described cellular senescence in normal human fibroblasts (Hayflick, 1965). Cell replication results in telomere shortening correlated with the induction of cellular senescence (Harley et al., 1990). In 1978, telomeres were identified as tandem repeats end of the chromosomes (Blackburn and Gall, 1978). After that, the telomerase enzyme was discovered in the model organism Tetrahymena (Greider and Blackburn, 1985). Since their discovery, researchers have focused on the role of telomerase and telomeres in ageing, cancer, and disease. The TERT gene locus is located on the short arm of chromosome band 5 (5p15.33), and it is more than 2 Mb away from the telomere (Cong et al., 2002).

Generally, human telomere length ranges from 5 to 15 kb, and each cell division causes telomere repeat loss of 50–200 bp because of end replication problems (Klapper et al., 2001). During the 5`- 3` synthesis of DNA, the lagging strand is unlikely to be uncovered after removing the primer. As a result, each cell division causes a decrease in telomeric repeats because of the origin of replication (Lingner et al., 1995). The lagging strand, consisting of short DNA fragments and RNA primers, provides a 3' end for DNA polymerase-driven extension during DNA replication. The end-replication problem is encountered during the 5`-3` synthesis of DNA because DNA polymerases can only add nucleotides to 3`OH groups (***Fig 1.1***). The polymerase cannot replicate the last primer on the lagging strand after removing the RNA primer, resulting in a progressive shortening of telomeric repeats (Lingner et al., 1995). Telomerase is able to extend/maintain these telomere repeats. It is a ribonucleoprotein DNA polymerase enzyme consisting of two essential subunits. These subunits consist of highly conserved catalytic subunit TERT (1132 amino acids, 127 kDa) (Nakamura et al., 1997) and telomerase RNA component and also both components are required for telomerase activity (Autexier and Lue, 2006). There is a direct correlation between TERT mRNA level expression and telomerase activity (Ito et al., 1998) because the TERC component is constitutively expressed (Avilion et al., 1996).

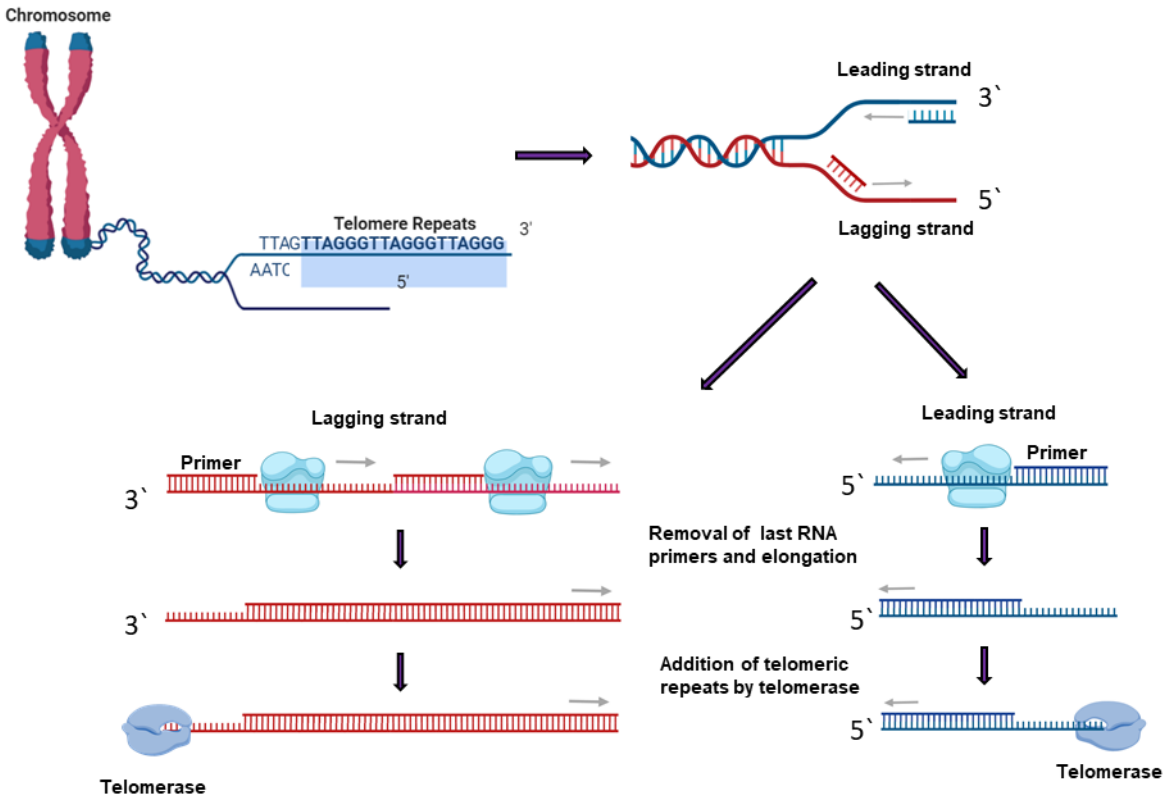

Figure 1.1. **Telomerase and the chromosome end replication problem**. Schematic representation of the replication of the lagging and leading strand DNA. Nucleotides are continuously added to the leading strand during DNA replication, and the lagging strand is replicated in the 3' – 5' direction. The lagging strand is produced in many small pieces called Okazaki fragments, each of which begins with its RNA primer. Telomere specific problem occurring on the leading and lagging strand is removing the last RNA primer. Telomerase enzyme with telomere binding proteins can extend the size of this 3' overhang.

Expression of the telomerase enzyme in normal cells is very low or undetectable, but it is overexpressed in cancer cells. Telomerase enzyme activity remains the primary mechanism for maintaining telomere repeats because 85-90% of cancer cells have telomerase activity (Kim et al., 1994). The rate-limiting catalytic subunit of TERT is essential for telomerase. It is known that embryonic stem cells, induced pluripotent stem cells, and germ-line cells have a strong ability to maintain their telomere length and display constitutive telomerase activity (Liu et al., 2007b).

On the other hand, some cancer cells are telomerase negative, so they adopt a different telomere maintenance mechanism (Bryan et al., 1995). In these cells, the telomere length is

extended by a telomerase-independent mechanism called the alternative lengthening of telomeres (ALT) (Henson et al., 2002). The presence of the ALT mechanism in mammalian cells is based on DNA homologous recombination and a small number of cells, approximately 10-15% of cancers, maintain their telomeres through this mechanism (Bailey et al., 2004). The presence of ALT was revealed by observing the continuity of telomere length in hundreds of reproductive populations without telomerase activity (Minasi et al., 2019). ALT positive cells are characterized by highly heterogeneous telomere lengths (Grobelny et al., 2000). After this finding, scientists announced another discovery related to ALT.

Non-coding RNAs are small RNA molecules, but they are not translated into functional proteins. Instead, they target epigenetic modifying enzymes or transcription factors to regulate gene expression. A unique non-coding RNA called telomeric repeat-containing RNA (TERRA) is transcribed by RNA polymerase II from mammalian subtelomeric region toward chromosome ends, following transcription, located to telomere repeats to maintain telomere length (Azzalin et al., 2007; Farnung et al., 2012). TERRA localizes at chromosome ends, and plays a significant role in regulating telomerase activity and heterochromatin formation at telomeres (Azzalin et al., 2007; Schoeftner and Blasco, 2008). TERRA contains the telomeric repeat RNA sequence UUAGGG, which can be variable in length between 200bp and several kilobases (Novakovic et al., 2016). Interestingly, TERRA appears more abundant in ALT cells than in telomerase-positive cells in general but not exclusively (Arora et al., 2014), and up-regulated levels of TERRA are represented in ALT cells (Lovejoy et al., 2012; Episkopou et al., 2014). Despite the alternative mechanism, telomerase enzyme activity remains the primary mechanism for maintaining telomere repeats (Cong et al., 2002). Different functions of TERRA have been shown, including recruitment of telomerase (Cusanelli et al., 2013; Lalonde and Chartrand, 2020), telomerase inhibition (Redon et al., 2010; Chu et al., 2017), heterochromatin formation at telomeres, and telomere elongation (Deng et al., 2009). TERRA stimulates telomerase recruitment and activity in model organism yeast with human-like telomeres (Moravec et al., 2016). TERRA-like oligonucleotides provide evidence of blocking telomerase activity in human and mouse cell extracts *in vitro* with a correlation between high expression of TERRA and short telomeres in various cell lines (Schoeftner and Blasco, 2008). Further, TERRA acts as a negative regulator of telomerase activity in mouse ESCs (Chu et al., 2017), although the purpose of TERRA as a general inhibitor of telomerase remains controversial. TERRA has the same complementarity sequence as telomerase RNA template, and *in vitro* studies showed that TERRA behaves as a competitive telomerase inhibitor (Redon et al., 2010).

It remains to be determined what the precise role of TERRA is in ALT and telomerase positive cells and whether they provide the same functionality.

1.2 Telomeres and Telomerase Activity in Stem Cells and Cancer Cells

Telomerase enzyme activity in normal cells can be detected at low levels (Hornsby, 2007). Its enzyme activity is detected at high levels in germ, stem cells, and many cancers. Telomerase activity and TERT gene expression are required for the maintenance of human embryonic stem cells (hESCs) pluripotency features (Armstrong et al., 2005). A prognostic role of telomerase activity and its association with the more aggressive phenotype of cancer has been proposed (Kulić et al., 2016). Telomerase is more commonly expressed than other tumour markers (Armstrong and Tomita, 2017). However, telomerase activity is not always related to telomere length in cancer cell lines. Instead, it may only sustain cell proliferation and stable chromosome ends (Januszkiewicz et al., 2003). Normal somatic cells do not display telomerase activity, so telomere repeats will get progressively shorter with age. In other words, human somatic cells lose their telomere repeats after multiple cell divisions due to the absence of telomerase activity. Usually, cells undergo a growth arrest called replicative senescence, or 'M1', when telomere shortening reaches a critical level. After telomere shortening reaches a critical level, it induces senescence. However, if protective tumour suppressive mechanisms such as p53, ATM, p16 are inactivated in cells, they can maintain cell proliferation despite chromosomal instability because of the erosion of telomeres. After many replications, the cells reach a crisis, or 'M2', represented by high apoptosis and genomic instability levels. Telomerase enzyme can become reactivated and may start carcinogenesis (Hackett and Greider, 2002) (***Fig 1.2***). Based on its high expression, a prognostic role for telomerase activity and its association with the more aggressive cancer phenotype has been proposed (Kulić et al., 2016; Armstrong and Tomita, 2017).

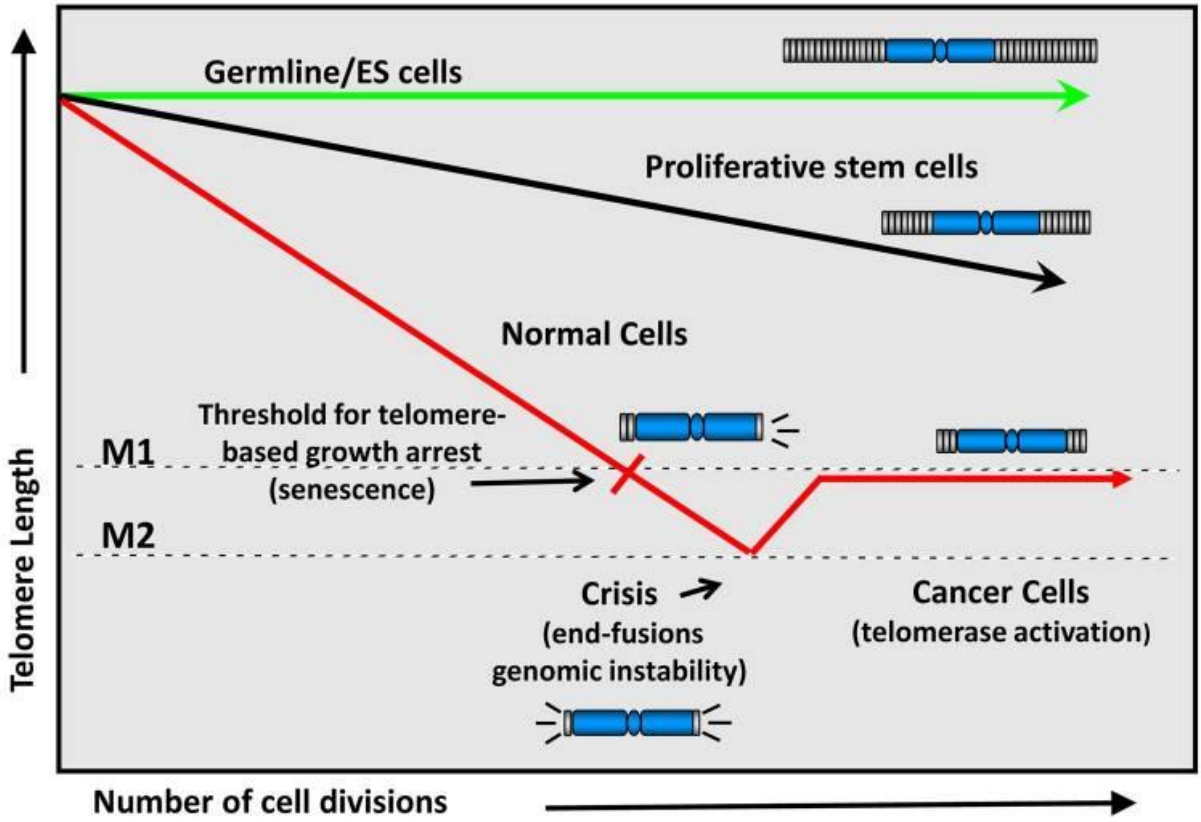

Figure 1.2. **Telomerase activation in cancer cells.** Telomere length is longer in stem cells than normal and cancer cell lines (Shay and Wright, 2011). Proliferative stem cells represent high telomerase activity, but they have less telomere length than germline or ES cells (Kim and Shay, 2018). Human somatic cells lose their telomere repeats after multiple cell divisions due to the absence of telomerase activity. Typically, cells undergo a growth arrest called replicative senescence when telomere shortening reaches a critical level. However, cells can escape from senescence following the dysregulation of cell cycle checkpoints, such as p53, ATM, p16. After exceeding the crucial step, the cells reach a crisis, or 'M2', represented by high levels of apoptosis and genomic instability. Some cells can bypass crisis by reactivating telomerase stabilizing telomere ends and may achieve immortality via telomerase activation and downregulation of tumour suppressor genes.

1.3 Stem Cells

The term "stem cell" was first proposed by Russian histologist Alexander Maksimov in the early 1900s (Konstantinov, 2000). All stem cells can proliferate, self-renew, differentiate into a range of tissue cell types, and repair damaged tissue (Becker et al., 1963) (Watt and Hogan, 2000). They can produce all kinds of tissue that form an adult organism during development.

The hESCs can be characterized by pluripotency markers, namely specific transcription factors and surface antigens (Zhao et al., 2012). Stem cells can be classified as either embryonic or non-embryonic. Embryonic stem cells are derived from the inner cell mass found in the embryo at the preimplantation blastocyst stage. Non-embryonic stem cells include adult stem cells, cord blood stem cells, fetal stem cells, and induced pluripotent stem cells (Bindu A, 2011). Potency is the capacity to differentiate into specific cell types and form any mature cells (***Fig 1.3***). Stem cells are grouped as totipotent, pluripotent, multipotent, and unipotent stem cells according to their differentiating features to different cell types (Kumar et al., 2010). Their unique immortal and regenerative abilities confer a potential to treat diseases with cell-based therapies.

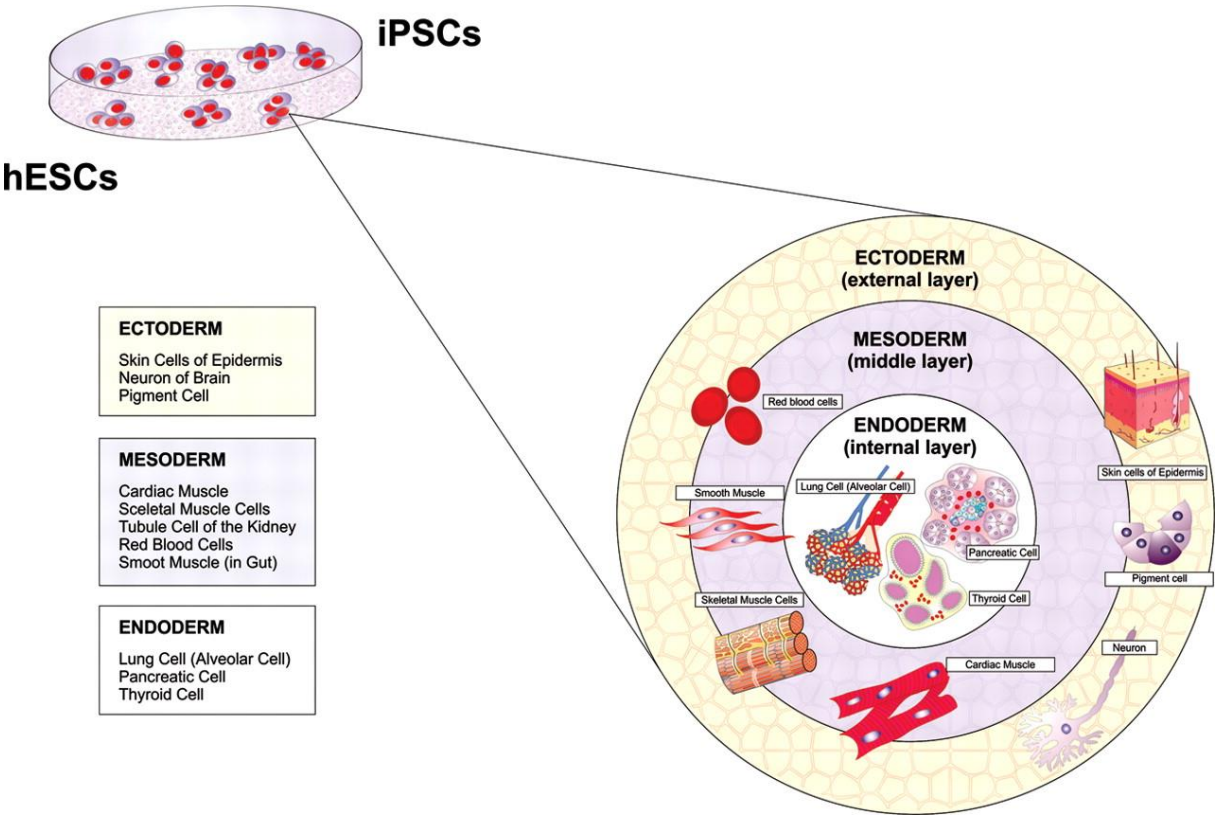

Figure 1.3. **Three germ layer differentiation potential of hPSCs.** Pluripotent hESCs and iPSCs have the potential to differentiate into all cell types of tissue cells (Volarevic et al., 2011). Several experimental approaches can be used to direct hPSCs differentiation to specific lineages. For example, embryoid bodies formed from PSCs can produce three germ layers and mimic *in vitro* embryogenesis.

1.4 Differentiation and Telomerase

Telomerase activity is high in ESCs, and TERT gene expression is involved in maintaining hESCs pluripotency features such as unlimited proliferation and self-renewal (Thomson et al., 1998; Romito and Cobellis, 2016). TERT overexpression and increased telomerase activity maintain colony-forming ability, proliferation, resistance to apoptosis, and show higher fractions of cells in S phase (synthesis phase) of the cell cycle of hESCs (Armstrong et al., 2005). However, upregulation of TERT can give rise to teratoma in hESCs, while downregulation of TERT can lead to loss of proliferation, decreased S phase, and increased G1 phase in hESC (Yang et al., 2008). Telomere shortening leads to senescence, and negatively affects stem cell features such as function, mobilization and proliferative capacity, especially in hematopoietic stem cells, skin stem cells, and neuronal stem cells, and these studies confirm that telomeres and telomerase are required for maintenance of stem cell features (Vaziri et al., 1994; Allsopp et al., 2001; Ferron et al., 2004; Flores et al., 2005). Embryonic stem cells, induced pluripotent stem cells, and germ-line cells can maintain their telomere length and telomerase activity (Hiyama and Hiyama, 2007). Telomerase enzyme activity and TERT expression are down-regulated during differentiation in pluripotent stem cells and cancer stem cells (Armstrong et al., 2005; Teichroeb et al., 2016). Knockdown of TERT in hESC resulted in spontaneous differentiation and loss of pluripotency. These cells were also unable to generate stable colonies hESCs (Yang et al., 2008), while the Sexton study's results did not represent any decrease in pluripotency and proliferation. Still, they also report differentiation and decreased self-renewal after 75 days in TERT knockout cells (Sexton et al., 2014).

Downregulation of telomerase activity is associated with cell differentiation and is negatively correlated with cell proliferation in human neural precursor cells (Ostenfeld et al., 2000). Induction of differentiation in leukaemia (HL-60 human promyelocytic leukaemia cells, K-562 human erythroid leukaemia cells), epithelial (293 immortal human kidney cells), and embryonal (murine embryonal stem cells) stem cells down-regulated telomerase activity (Sharma et al., 1995) and also telomere length was downregulated during B cell differentiation (Weng et al., 1997). Downregulation of telomerase may be a consequence of differentiation. Differentiation related specific intracellular signal cascades such as protein kinases and transcription factors might induce cell differentiation and telomerase activity. Meanwhile, antisense telomerase inhibited telomerase activity in glioma cells (U251-MG), resulting in either apoptosis or differentiation (Kondo et al., 1998). There is no particular evidence to

conclude telomerase directly controls the differentiation process, but telomerase activity impacts the proliferation and differentiation decision.

There are two common ways to differentiate hESCs spontaneously: the first one is monolayer culture, and the second one is through culture as three-dimensional (3D) aggregates known as embryoid bodies (EBs) (Simunovic and Brivanlou, 2017). Embryoid bodies occur as three-dimensional aggregates of hESCs in ultra-low attachment culture vessels during differentiation toward the three germ lineages (ectoderm, mesoderm and endoderm) (Itskovitz-Eldor et al., 2000a; Sathananthan and Trounson, 2005). Differentiation of EBs has similarities with embryogenesis, such as secretion of growth factors, repressors, cell interactions, and mimicry of structures of the developing embryo (Finley et al., 2003; Kemp et al., 2005; Rivera-Pérez and Magnuson, 2005; van den Brink et al., 2014). The 3D spatial organisation between cells can be replicated on a tissue culture through EBs. 3D formation of EBs has topographical differences when compared to a 2D layer of cells grown on a cell culture plate. EB formation is a powerful technique for studying the three germ lineages in early mammalian development. *In vitro* 3D culture opens a new avenue for more physiological human tissue models. There are limitations as well; for instance, embryoid bodies are unfortunately not perfectly organised (Berge et al., 2008), and the varying size of the EBs can alter differentiation and functional cell lineages. It is noteworthy that the oxygen concentration is 50% lower in the core of large EBs compared to smaller EBs (Van Winkle et al., 2012). For example, small EBs can apoptose while large EBs show necrosis in the core. Differentiated EBs can nevertheless produce several cell types associated with the three different embryonic germ layers with good cell viability (Van Winkle et al., 2012; Pettinato et al., 2014).

Telomerase enzyme activity may have an essential role in cell differentiation because it is correlated with cell proliferation, stemness, differentiation and self-renewal. Stem cells are valuable tools for understanding this mechanism. Because during differentiation, telomerase activity is downregulated in stem cells. The link between telomerase activity and differentiation may provide a model to study the regulation of telomerase activity.

1.5 Epigenetics and Genetics

Waddington (1942) defined epigenetics as the correlation between phenotype and genotype changes in mammalian embryonic development and tissue-specific gene function in the fruit-

fly Drosophila melanogaster (Sharma et al., 2010; Waddington, 2012). Traditional studies of genetics describe genes and their functions, while epigenetics provides an exciting new area of molecular genetics study by explaining the gene expression process (Mattick and Makunin, 2006). Nowadays, epigenetics is recognized as a reversible and heritable alteration in gene expression without changes in the primary DNA sequence (Deans and Maggert, 2015). Epigenetic mechanisms can change chromatin and DNA structure by methylation of cytosine bases in DNA, histone remodeling, and posttranslational modifications of histone proteins such as nucleosome remodelling and non-coding RNAs (including microRNAs) (Sharma et al., 2010). Non-coding RNAs are functional RNA molecules that control transcriptional, post-transcriptional gene expression levels and the synthesis of proteins but do not encode a functional protein (Mattick and Makunin, 2006). Epigenetic modifications play a pivotal part in the differentiation of stem cells and the diagnosis, prognosis, or cancer development. Genetic and epigenetic changes contribute to the initiation and progression of cancer and are associated with malignant transformation (Jones and Laird, 1999). Consequently, recent advances in epigenetics have contributed to our knowledge of cancer progression and the association of epigenetic alterations.

Gene mutations significantly affect the transcription of the TERT gene in cancer. Single nucleotide polymorphisms, especially cytosine to thymidine transitions at −124 bp and −146 bp upstream of the translation start site, are very common promoter mutations close to the transcription start site (Horn et al., 2013; Borah et al., 2015). However, additional factors, including epigenetic, transcriptional and posttranscriptional modifications may also have a role to play. Together genetic and epigenetic mechanisms are associated with TERT dysregulation in cancer, including TERT amplification (3%), TERT structural variants (3%), TERT promoter structural variants (5%), TERT promoter mutations (31%) and epigenetic modifications through TERT promoter methylation (53%) (Castelo-Branco et al., 2013; Barthel et al., 2017; Leão et al., 2019).

1.6 Gene Regulation by Epigenetic Mechanism

Epigenetics regulates gene modification that manifests in the effects of environment on phenotype (Feil and Fraga, 2012). DNA methylation plays a substantial role in the differentiation of stem cells via silencing pluripotency genes or establishing tissue-specific methylation patterns (Huang et al., 2014a). There are various epigenetic mechanisms including

DNA methylation, packaging of DNA by histone proteins, or non-coding RNAs which regulate gene expression (Bird, 2007). DNA methylation describes the addition of methyl groups to cytosine residues in DNA molecules to form 5-methylcytosine (5mC), which can block transcription factor binding or decrease binding of gene regulatory elements to promoter or enhancer regions, resulting in changes in gene expression. DNA methyltransferase (DNMT) enzymes regulate this significant process. Three major active DNA methyltransferases are DNMT1, DNMT3A, and DNMT3B which drive the methylation pattern of genomic DNA (Ting et al., 2006). DNMT3A and DNMT3B are essential to catalysing *de novo* methylation of DNA sequences during gametogenesis, embryogenesis, and somatic tissue development, while DNMT1 maintains global DNA methylation following DNA replication (Li, 2002) (***Fig 1.4***). In addition, DNMT1 tends to methylate the hemimethylated DNA faster, progressive and more accurately (Hermann et al., 2004).

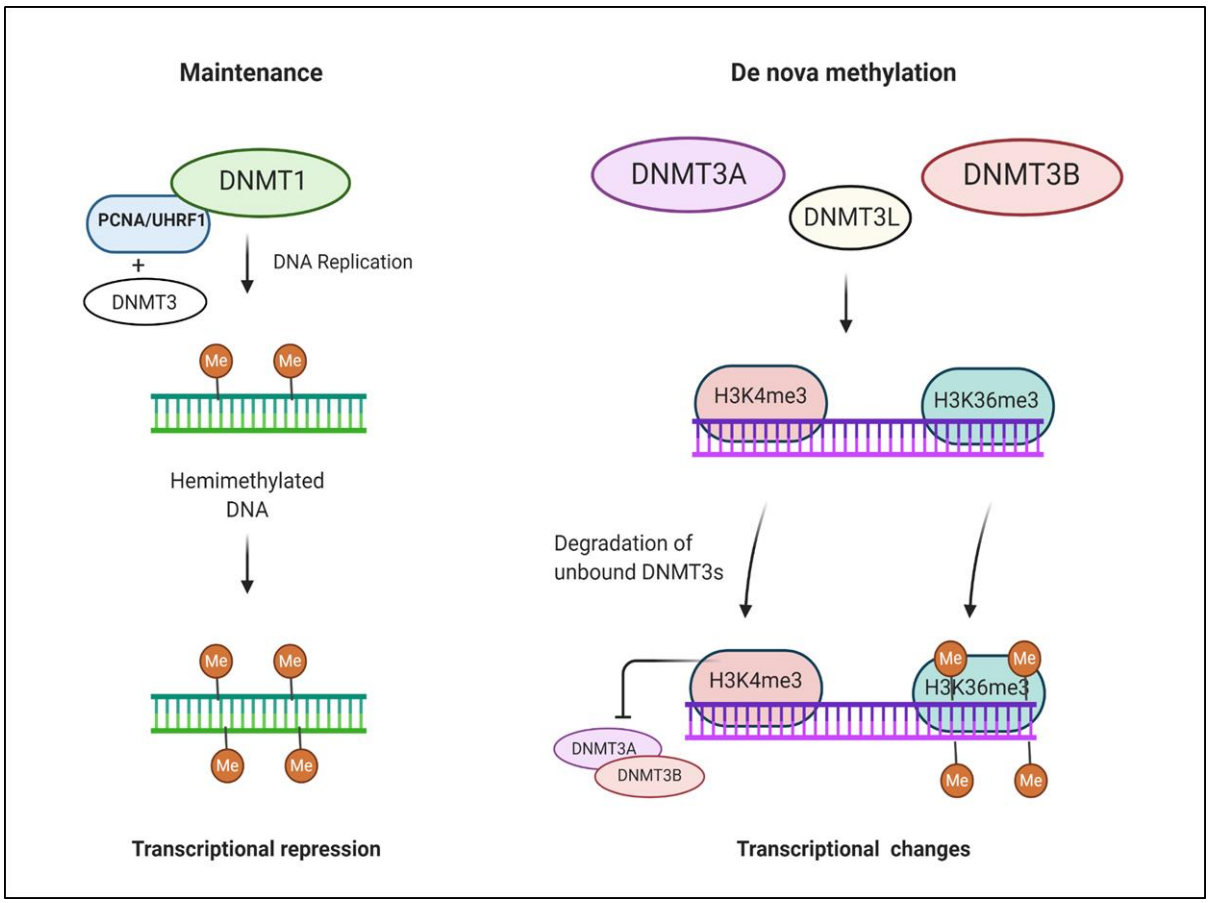

Figure 1.4. **Mechanism of DNA methyltransferases (DNMTs).** DNMT3A and DNMT3B *de nova* methyltransferases localize on methylated CpG-rich locus to maintain a uniform methylation pattern. DNMT3B targets the gene body to methylate that cytosine locus and

correlates with the presence of H3K36me3. DNMT3B acts as a maintenance enzyme to form new methylation patterns during differentiation.

DNA methylation regulates gene expression through various mechanisms. For instance, transcription factors are unable to attach to their binding site after methylation or recruitment of ‘repressor proteins which interplay with methylated cytosine to change chromatin structure and induce gene silencing (Moore et al., 2013). The expression level of DNMT3B is considerably low in somatic adult cells. In contrast, aberrant DNMT3B expression is observed in cancer cells and it is thought that DNMT3B expression may be required for tumour cell survival (Beaulieu et al., 2002; Ostler et al., 2007). Moreover, DNMT3A and DNMT3B expression are found at a high level in undifferentiated cells like embryonic stem cells, but DNMT3B is down-regulated during cell differentiation (Watanabe et al., 2002; Li et al., 2007; Liao et al., 2015). However, several studies have indicated that DNMTs are required to differentiate ESCs, and their absence can inhibit the differentiation process (Okano et al., 1999; Jackson et al., 2004) (***Fig 1.5***).

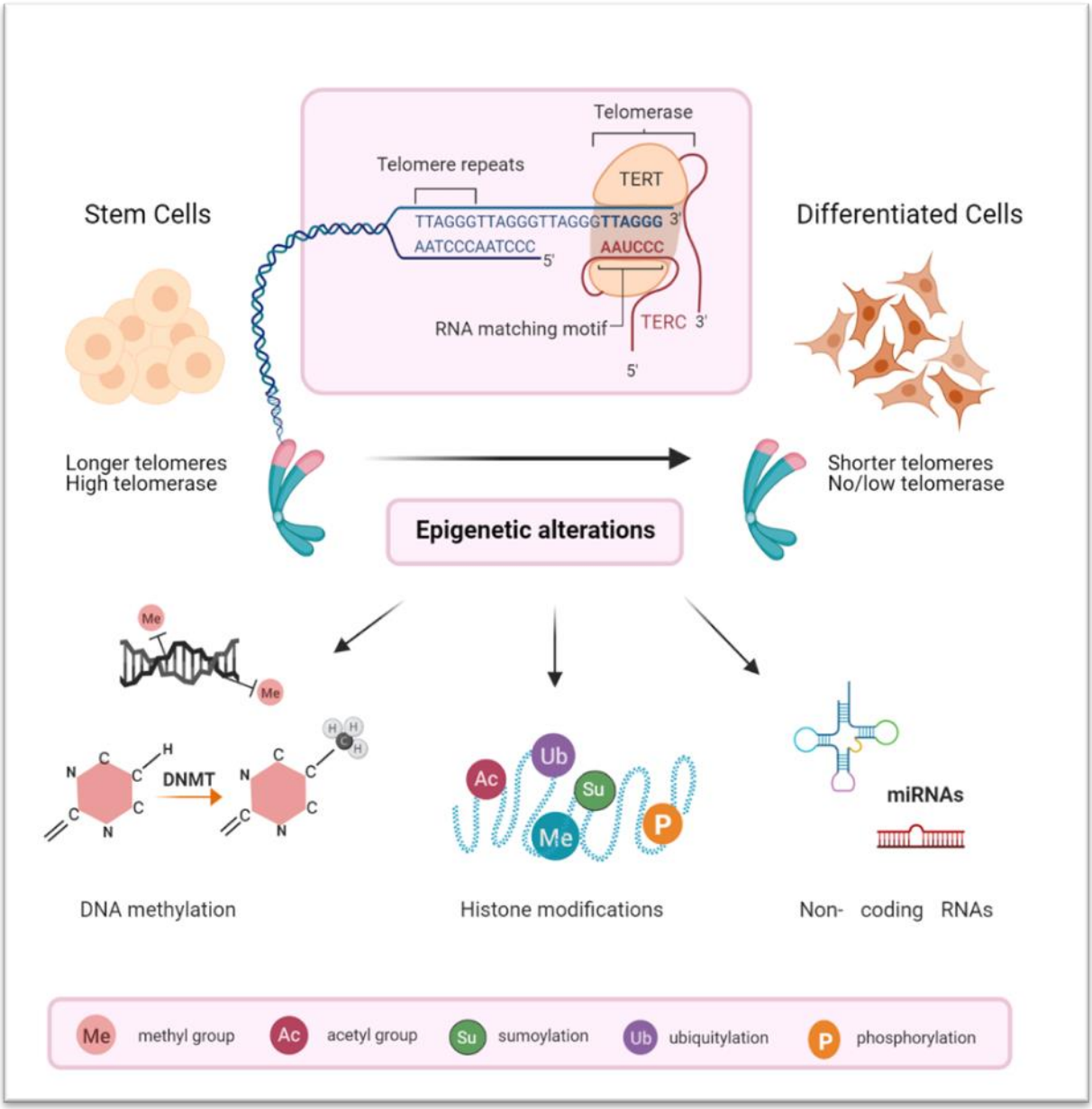

Figure 1.5. **Epigenetic alterations play a role in telomerase down-regulation during stem cell differentiation**. Epigenetic mechanism occurs as covalent modifications, including DNA methylation (e.g. cytosine methylation), non-coding RNAs and histone modifications (e.g. acetylation, methylation, phosphorylation, ubiquitination and sumoylation).

Another critical mechanism of epigenetics is histone modification. Methylation, phosphorylation, acetylation, ubiquitylation, and sumoylation are the most known covalent post-translational modification of histones (***Fig 1.6***). They are responsible for gene expression changes by modifying histone structure or recruiting remodelling enzymes. Histone acetyltransferases (HATs) and histone deacetylases (HDAC) enzyme families regulate

acetylation of the histones (Xhemalce et al., 2011). HDACs are crucial epigenetic regulators of gene expression, chromosome structure, control of cellular stability and they are associated with the loss of genomic integrity in cancer cells. HDACs catalyze the removal of the acetyl groups on histones added by the HATs (Seto and Yoshida, 2014). HATs acetylate specific lysine residues on histones (H2B, H3, and H4), and these enzymatic components increase DNA accessibility by interacting with different molecules (Bannister and Kouzarides, 2011). Histone methylation, a transfer of methyl groups to amino acids, occurs in the arginine, lysine and histidine residues on the histone proteins (Bedford and Clarke, 2009; Ng et al., 2009). Typically, three methylation forms are common on histone lysine residues: mono-, di- and trimethylation and are determined using selective antibodies that distinguish each of the methylated residues of histone. According to recent results, H3 Lys9 mono- and dimethylation are enriched in silent regions within euchromatin, while trimethylation is localized at pericentric heterochromatin (Rice et al., 2003). HDAC inhibitor trichostatin A treatment induces significant expression of TERT mRNA and telomerase activity via Sp1 sites on the promoter in somatic cells but not in cancer cells (Takakura et al., 2001).

Non-coding RNAs are functional RNA molecules that are not translated into protein and can target epigenetic modifying enzymes or transcription factors to regulate gene expression. TERRAs, the non-coding RNAs that protect telomeres, are essential epigenetic regulators (Khanduja et al., 2016). They are transcribed from telomeres. Further, there is a possible relationship between TERRAs and telomeric chromatin structure. The absence of TERRAs showed decreased heterochromatic marks (Montero et al., 2018). In summary, DNA methylation, histone methylation-acetylation and non-coding RNAs play a pivotal role in epigenetic regulation of TERT expression in various biological processes such as ageing and cancer (Lewis and Tollefsbol, 2016).

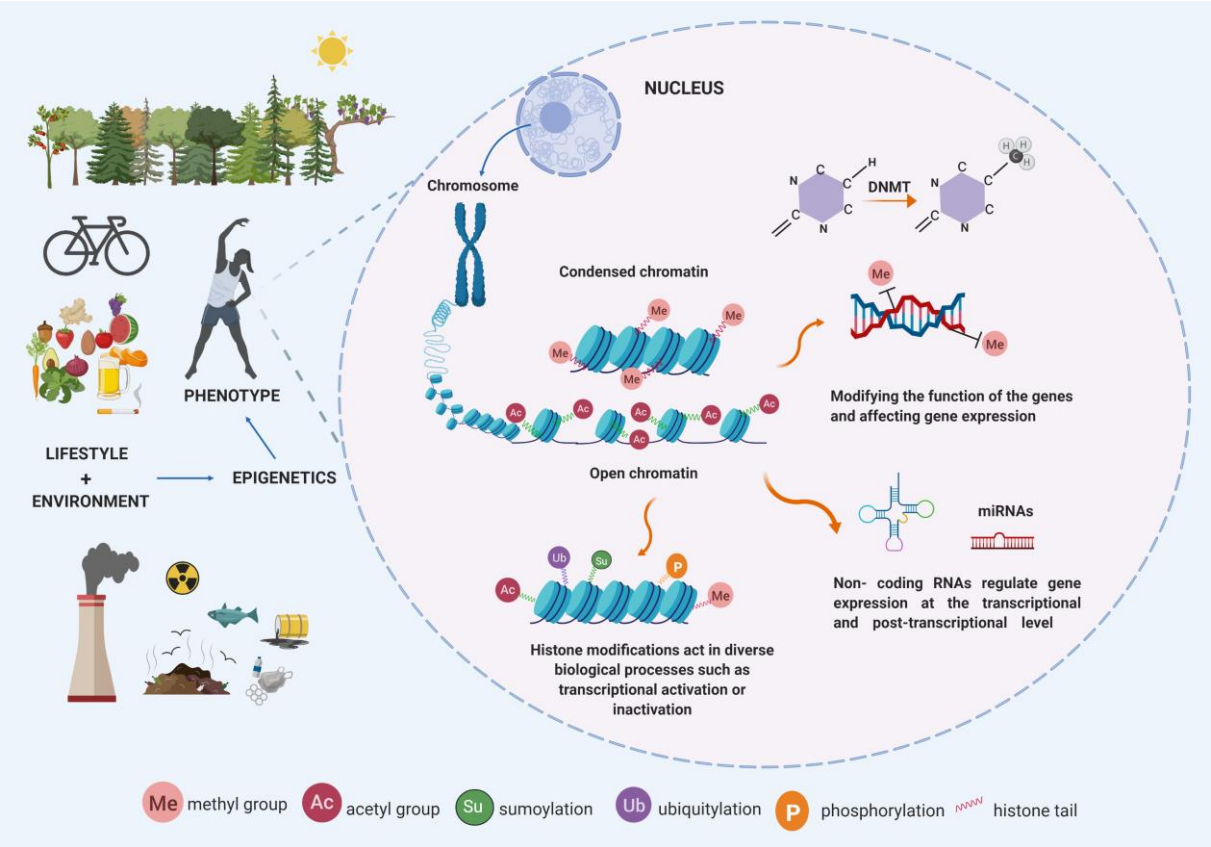

Figure 1.6. **The effect of environmental factors and lifestyles on epigenetic, gene activation and organism phenotype.** Epigenetic modifications have essential roles in chromatin structure and gene expression. DNA is coiled around eight histone proteins to form chromatin. Less condensed chromatin exhibits transcriptionally active, and more condensed chromatin exhibits a transcriptionally silent gene state. Epigenetic mechanism occurs as covalent modifications of either DNA or histone proteins. The most studied epigenetic marks are DNA methylation (including cytosine methylation and hydroxymethylation) and histone modification (including. acetylation, methylation, phosphorylation, ubiquitination and sumoylation). In addition, non-coding RNAs are significant in regulating human protein-coding genes and are also associated with DNA methylation and histone modification.

1.6.1 TERT promoter methylation in ESCs and cancer cells

DNA methylation regulates gene expression through various mechanisms. Generally, transcription factors cannot attach to their binding site after methylation due to the recruitment of repressor proteins that interplay with methylated cytosine to change chromatin structure and induce gene silencing (Moore et al., 2013). The TERT promoter region includes many GC

motifs (72 CpG sites, 500 bases upstream of the transcriptional start site into the first exon), and the methylation pattern of the promoter affects its gene expression (Devereux et al., 1999). The TERT gene is localized on the short arm of chromosome 5 (5p.15:33) and consists of 16 exons and 15 introns spanning approximately 40 kb gene body (Cong et al., 1999; Yuan et al., 2019).

Genistein is a natural isoflavone and induces apoptosis by inhibiting NF-κB pathway *in vitro* (Luo et al., 2014). It can upregulate tumour suppressor gene expression, including p53, p21, and p16 by inhibiting DNA demethylation and histone modification (Kikuno et al., 2008; Majid et al., 2008). Genistein changes the DNA methylation patterns of the promoter and hypomethylated CpG dinucleotides on the E2F-1 recognition site allowing increased E2F-1 binding. Also, genistein downregulates cMYC protein expression (Li et al., 2009). Genistein also represses the transcription of TERT, and expression of DNMT1, DNMT3A, and DNMT3B were reduced considerably after MCF-7 cells were treated with genistein (Li et al., 2009). DNMTs inhibition causes hypomethylation of the TERT promoter (Berletch et al., 2008), resulting in increased binding of the E2F-1 (E2F transcription factor 1) to the TERT promoter (Li et al., 2009). E2F-1 repressor of transcription of the human TERT gene or c-Myc as an activator of TERT binding to specific sites may depend on the methylation status and chromatin structures of the TERT promoter (Crowe et al., 2001). Furthermore, genistein can remodel the chromatin structures on the promoter by activating H3K9 trimethylation or deactivating H3K4 dimethylation (Li et al., 2009). As a result, TERT inhibition is connected to epigenetic modulating of DNMTs via methylation of the promoter region of the gene (Berletch et al., 2008; Li et al., 2009).

Methylation analysis methods rely on bisulfite conversion, a chemical deamination reaction followed by sequencing. Unmethylated cytosines are converted into uracils (and subsequently thymidines), while methylated cytosines remain intact during bisulfite conversion (Li and Tollefsbol, 2011). The TERT promoter is unmethylated generally in normal cells and hypermethylated in many cancer cells associated with its expression and telomerase activation (Yuan and Xu; Dessain et al., 2000). Upstream of the transcription site (UTSS) of the TERT promoter is partially or fully hypermethylated in malignant paediatric brain tumours which possess high TERT expression. In contrast, normal brain tissue or low-grade tumours are unmethylated or hypomethylated, indicating that TERT promoter is differently methylated in normal and tumour tissues. Additionally, it was demonstrated that UTSS hypermethylation was related to the progression of the tumour (Dessain et al., 2000; Castelo-Branco et al., 2013). The

TERT promoter was hypermethylated in different telomerase positive tumour samples, but telomerase negative normal tissues exhibited hypomethylation (Guilleret et al., 2002). These telomerase positive cell lines demonstrated the same pattern in the region −441 to −218 from the translational start site, including 27 CpG motifs. Further, telomerase activity and TERT mRNA levels are associated with the methylation pattern of the promoter region (Guilleret et al., 2002). However, in previous studies, the methylation status of up to 72 CpG sites extending from 500 bases upstream of the transcriptional start site of the TERT promoter was evaluated in different cancer cell lines. In contrast, no correlation between specific CpG sites or groups of CpG sites and TERT expression was noted (Devereux et al., 1999).

Renaud et al. have demonstrated the partial methylation of TERT promoter, between −160 to −80 bp in tumour cell lines and tumour tissues such as; breast, bladder and cervix cancer (Renaud et al., 2007). Interestingly, hypermethylation of TERT promoter may suppress CTCF (CCCTC-binding factor) transcriptional repressors binding to CCCTC binding regions on TERT promoter (Renaud et al., 2005). When the CpG island is not methylated, CTCF binds this region and inhibits transcriptional regulation of the TERT gene (Renaud et al., 2007). CTCF binds to unmethylated sites of the TERT promoter region in telomerase-negative cells but not in telomerase-positive cells because of methylation. CTCF binding to the TERT regulatory region is associated with the repression of TERT expression and down-regulation of telomerase in human breast cancer cells. Correlated to these results, Zinn and colleagues reported that -150 to +150 from UTSS of TERT promoter, which includes CTCF binding site, presents active chromatin remodelling and lack of methylation. Therefore these patterns provide an active transcription of the TERT gene, however, the -600 bp UTSS region is highly methylated in breast, lung, colon cancer cells and immortalized cell lines (***Table 1.1***) (Zinn et al., 2007).

According to Castelo-Branco et al., UTSS methylation is increased during the transformation of pediatric brain tumours from low to high grade and elevated methylation of UTSS was related to tumour progression (Castelo-Branco et al., 2013). Analysis of one TERT CpG site (cg11625005) indicated that normal brain tissues and low-grade tumours were not hypermethylated, however, malignant tumours were hypermethylated. This methylation site was differently methylated between malignant and non-malignant tissues. TERT promoter hypermethylation also appears related to lymph node metastasis, aggressive histological features, and poor prognosis in gastric cancer patients (Wu et al., 2016).

There is a TERT hypermethylated oncological region (THOR) upstream of the TERT promoter (***Fig 1.7***), which contains 52 CpG sites in the 433-bp genomic region (Lee et al.,

2019). Following this data, the TERT promoter activity was suppressed in unmethylated THOR samples, while hypermethylation of this region showed an increased promoter activity (Lee et al., 2019). Also, hypermethylation of TERT oncological regions was common in TERT positive tumour cell lines regardless of TERT promoter mutations, and 905 cancers had only THOR hypermethylation in a variety of tumour cell lines that lacked TERT promoter mutations (Lee et al., 2019). Takasawa et al. demonstrated that the distal promoter region of TERT, located between − 2056 and − 1566 nt, was more methylated in induced pluripotent stem cells (iPSCs) than in somatic cells. Also, there was a correlation between DNA methylation in the distal region and TERT expression (Takasawa et al., 2018) (***Table 1.1***).

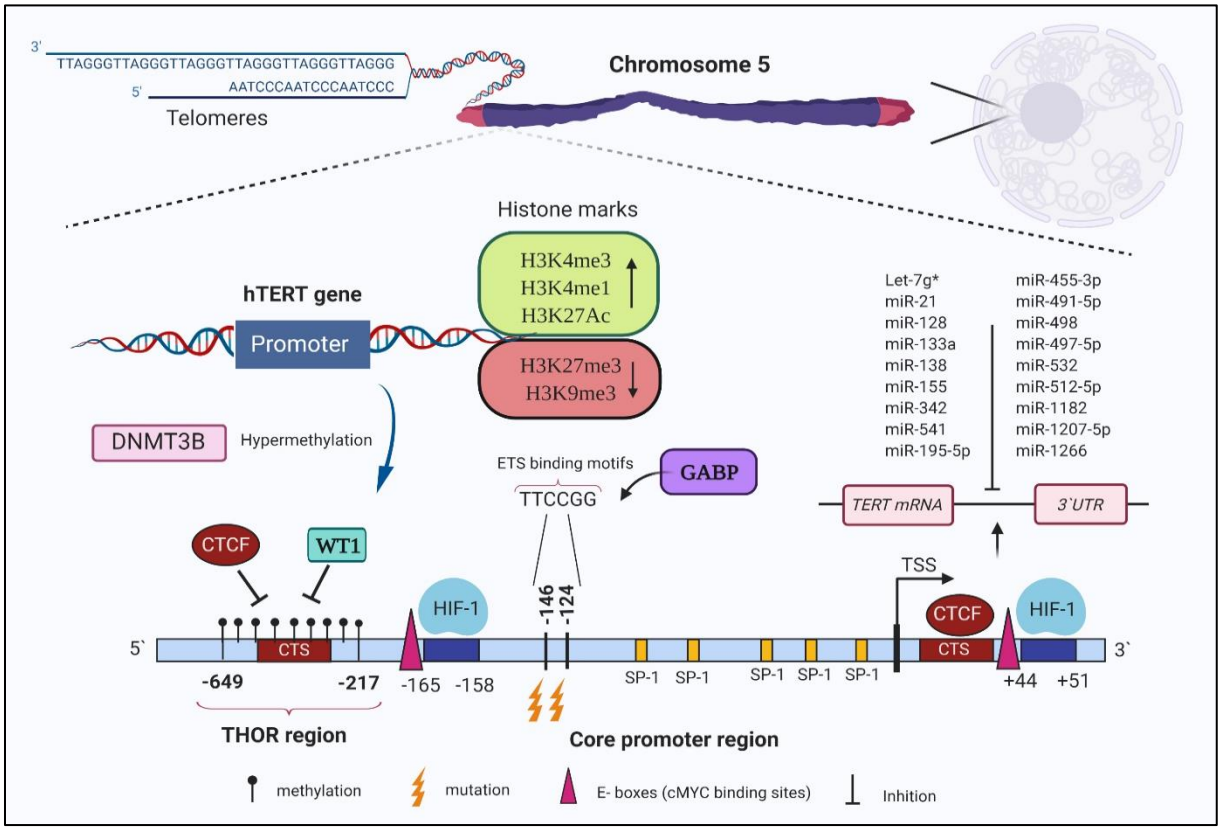

Figure 1.7. **The promoter region of TERT in cancer and promoter binding sites for various transcription factors and repressors**. The specific mutations and hypermethylated region upstream to TSS (THOR) are represented. Cancer-specific mutations control recruitment of GA-binding protein (GABP) transcription factor to the promoter and increase gene expression. Promoter methylation might regulate transcriptional activators (c-Myc) and repressors (WT1 and CTCF) recruitment to target sites, leading to gene overexpression. Black dots show methylated CpG sites. ETS: E-twenty-six; ATG: start codon, TSS: transcription start site.

Table 1-1. **Methylation pattern of the TERT promoter in different cancer cells** (Dogan and Forsyth, 2021)

Cell Types	Region Tested	Methylation Status
SUSM-1, CMV, SiHA, MDA-231/435, Calu 1/3/6, HTB 57/178/182, SW480, HTC 116 (Telomerase +)	From −500 UTSS to +50 first exon (72 CpG sites)	Partial or total methylation
A549, HTB183(Telomerase +) NHF, MRC-5/p27 (Telomerase −)	From −500 UTSS to +50 first exon (72 CpG sites)	Unmethylated
U2OS, telomerase-negative breast carcinoma, VA13 GM847	Promoter region	Partial or total methylation
CT1485 (Telomerase +) WI38, HA-1 pre-crisis cell strain, JFCF-6T/5K pre-crisis cell strain, IMR90, BJ fibroblast, adrenal carcinoma (Telomerase −)	Promoter region	Unmethylated
J82, T24, MCF-7, A431, HeLa, Co115, HT29, SW480, H520, SW2, PC-3,	27 CpG sites −441 to −218 relative to UTSS	Partial or total hypermethylation and correlation with TERT mRNA expression and telomerase activity
Tumour tissues from brain, breast, bladder, colon, kidney, lung, soft tissue		
Saos-2, U2-OS (Telomerase −)	27 CpG sites −441 to −218 relative to UTSS	Partial or total hypermethylation
Normal tissues; skin, brain, bladder, muscle, kidney, heart, placenta, testis, colon		Unmethylation and telomerase negative
HeLa, SW480, Tumour tissues (breast, bladder and cervix) (Telomerase +)	−100 to +100	75 to 100% methylation
	−165 to −100	0 to 55% methylation
BJ fibroblasts (Telomerase −)	−165 to +100 relative to UTSS	3 to 23% hypomethylation
Caco-2, HCT116, RKO, SW480, MCF7, MDA-MB-231, MDA-MB-435S, MDA-MB-453, H82, H157, H209, H146, H358, H417, H549, H747, H1299, U1752, DMS53, HL-60, KG-1a, Jurkat, Raji, LCL	−600 bp relative to UTSS	Partial or total methylation and TERT expression
	−150 to +150 relative to UTSS	Partial or unmethylation
Hepatocarcinoma cell lines HepG2, SNU-182, SNU-398, HCC Tissue (Telomerase +)	−165 to +49 relative to UTSS	10 HCC clones and HepG2 Hypo/unmethylated 12 HCC clones and SNU-182, SNU-398 hypermethylated and reduced TERT
Normal liver tissue (Telomerase −)	−165 to +49 relative to UTSS	Hypermethylated and reduced TERT
Malignant pediatric brain tumours	5 CpG sites located UTSS	Hypermethylation TERT expression
Neuroblastoma	UTSS	Highly methylated
Hepatocellular carcinoma	−452 to −667 and −974 to −1419 relative to UTSS	Hypermethylation and high TERT expression

Gastric cancer	25 CpG sites located −555 from UTSS	Hypermethylation and high TERT expression
Haematopoietic cell lines including Jurkat, THP1, K562, cervical cancer and embryonic kidney cells	−60 to +20 relative to ATG	Hypermethylation and TERT expression
Normal peripheral blood cell populations (granulocytes, T cells, B cells and monocytes)	−60 to +20 relative to ATG	Unmethylated
Acute myeloid leukaemia, myelodysplastic syndrome	−520 to −400 relative to ATG	Hypermethylation
Thyroid cancer	−541 to −578 relative to ATG	Hypermethylation
Prostate cancer	52 CpG –140 to –572 relative to the UTSS	Hypermethylation
Melanoma	26 CpG –482 to –667, relative to the ATG	Hypermethylation and positively correlated with the TERT expression
Melanoma	−945 to −669bp relative to UTSS	Hypermethylation and positively correlated with the TERT expression
Pancreatic cancer	Position –575 relative to the UTSS	Hypermethylation
Colon, blood, breast, prostate, brain, lungs, bladder, ovaries, bone, skin cancers	52 CpG sites −100 to −600 located UTSS	Hypermethylation and upregulated TERT expression
Bladder cancers	5 CpG sites in –140 to –572 region relative to UTSS	Hypermethylation and higher TERT expression
Primary metastatic medulloblastoma	5 CpG sites localized at −600 bp UTSS region	Hypermethylation
Thyroid Cancer Cell Lines	−662 to +174 relative to UTSS	Hypermethylation of upstream promoter and correlated with TERT expression

A recent study has shown that TERT stimulates DNMT3B expression and methylation in hepatocellular carcinoma (HCC), and increased TERT and DNMT3B expression are associated with shorter survival of HCC patients. TERT collaborates with the transcription factor Sp1, then stimulates abnormal DNMT3B expression and cancer-specific methylation in HCC (Yu et al., 2018b). A substantial decrease was observed after TERT inhibition with siRNA in both DNMT3B gene and protein levels. All-trans retinoic acid (ATRA) is used to differentiate human leukaemia cells. ATRA causes inhibition of telomerase activity and changes the expression of DNMTs that may regulate hypoacetylation and hypermethylation of the TERT

promoter during differentiation (Love et al., 2008). Significantly, the results showed an increased level of DNMT3A expression but downregulated DNMT1 and DNMT3B gene expressions after ATRA exposure. Another study with a natural isoflavone (genistein) demonstrated a similar decrease in telomerase activity, DNMT1 and DNMT3B expression in breast cancer cells (Li et al., 2009). It has been suggested that DNMTs inhibition results in hypomethylation of the E2F-1 recognition site at the TERT promoter, allowing increased binding of this repressor leading to reduced TERT transcription (Berletch et al., 2008). DNMT3B over-expression can induce the TERT promoter hypermethylation and activate TERT transcription. On the other hand, TERT induction might further up-regulate DNMT3B expression, which may generate a positive feedback loop between them in cancer cells (Yuan and Xu). hESCs differentiation is strongly associated with decreased DNMT3A and DNMT3B expression, similar to reduced TERT expression (Phipps et al., 2009). These results indicate that the epigenetic regulators DNMTs, especially DNMT3B and the TERT gene, could have a feedback loop during differentiation and also in cancer cells.

1.6.2 Transcriptional regulation of telomerase and telomeres by histone modifications

DNA is coiled around eight histone proteins to form a condensed chromatin structure. Modifications within the histone proteins affect the interactions between the nucleosome and DNA, therefore, histone tails can regulate chromatin structure and gene accessibility (Saha et al., 2006). Methylation of histone tails on lysine and arginine residues might induce repression or activation of genes related to methylation level and methylated residue (Strahl and Allis, 2000). For example, mono and dimethylation of H3K9 within the promoter region represents inactivated gene expression, while trimethylation of H3K9 indicates increased gene expression. On the other hand, histone acetylation of H3K9 is related to open chromatin and gene transcription (Lewis and Tollefsbol, 2016).

Epigenetic alteration of the TERT gene promoter is strongly associated with TERT upregulation in stem cells and cancer cells (Seynnaeve et al., 2017). DNA methylation, histone acetylation, and histone methylation also affect the regulation of TERT transcription (Dessain et al., 2000; Liu et al., 2016). For example, mono-, di- and trimethylation histon3-lysine9 (H3-K9) are associated with the repression of gene expressions or the formation of heterochromatin regions. It has been indicated that H3-K4 hypoacetylation and H3-K9 methylation diminish

TERT expression in telomerase-negative cell lines, on the other hand, H3 and H4 hyperacetylation and K4-H3 methylation are associated with TERT transcription in telomerase positive cells (Atkinson et al., 2005; Sui et al., 2013). Histone modification at the hTR and TERT promoters are strongly related to increased or activated gene expression in normal, ALT, or cancer cell lines (Atkinson et al., 2005). SET and MYND domain-containing protein 3 (SMYD3), a histone methyltransferase, can bind to the TERT promoter and activate TERT transcription through histone H3-K4 dimethylation (H3K4me2) or trimethylation (H3K4me3) in human fibroblasts and cancer cells (Liu et al., 2007). H3K4me3 is suggested as a positive marker for gene activation. Increased TERT mRNA level was observed after overexpression of SMYD3. In addition, suppressing SMYD3 led to suppressed H3K4me3 within the TERT core promoter and also decreased the ability of c-Myc and Sp1 to bind the promoter in cancer cell lines (Guccione et al., 2006; Liu et al., 2007).

Zinn and colleagues reported that the transcription start site of the TERT promoter (-150 to +150) presents active chromatin remodelling and a lack of methylation. Therefore, these patterns provide an active transcription of the TERT gene, also the -600 bp UTSS region is highly methylated in breast, lung, colon cancer cells and immortalized cell lines (Zinn et al., 2007). Otherwise, both H3K9ac and H3K4me2, which are considered active chromatin signs, and H3K9me3 and H3K27me3, which are common signs for methylated inactive DNA, were observed in the TERT promoter (Zinn et al., 2007). Recently, luciferase reporter assay results demonstrated that TERT promoter activity gradually decreased 5-10 fold after 14 days of differentiation of hESCs (Cheng et al., 2017). Additionally, histone markers H3K4me3 and H4Ac were mainly observed in hESCs-(wt) containing single-copy bacterial artificial chromosome reporter, including a 160-kb human genomic sequence comprising the whole TERT locus, but during differentiation, these positive marker`s levels considerably down-regulated (Cheng et al., 2017). It has been concluded that the H3K4me3 and H4Ac have a significant role in epigenetic regulation and are associated with the TERT promoter activities in ESCs and differentiated cells. Moreover, it has been reported that a considerable increase in levels of H3K9me3 and H3K27me3 is related to gene silencing (Cheng et al., 2017).

Chromatin modifications have significant roles in determining constitutive heterochromatin characteristics of telomeres and subtelomeric regions in mammals (Blasco, 2007). Telomeric regions are enriched in heterochromatin marks like mono-, di- and trimethylation histon3-lysine9 (H3K9) (Benetti et al., 2007). H3K9me3 (histone H3 Lys9 trimethylation), H4K20me3 (histone H4 Lys20 trimethylation and HP1 (heterochromatin protein 1) are common

mammalian telomere marks (Cacchione et al., 2019). However, heterochromatin methylation marks differ on human and mouse telomeres (***Table 1.2***). Interestingly, a decreased level of H3K9me3, H4K20me3 and decreased binding of HP1 at telomeric repeats, and consequently, less heterochromatin structure is observed in mice with short telomeres (Benetti et al., 2007a). Telomere repeats are generally enriched with dimethylated and trimethylated H3K9 in wild-type control mice (García-Cao et al., 2004). However, less dimethylated and trimethylated H3K9 but more monomethylated H3K9 are observed in embryonic stem cells and embryonic fibroblast cells from SUV39DN mice, which do not express Suv39h1 and Suv39h2 histone methyltransferase. Histone methylation may be a significant way to elongate telomere lengths because telomere length was longer in SUV39DN mice (null with the histone methyltransferases Suv39h1 and Suv39h2) than control mice (García-Cao et al., 2004). Cubiles and colleagues reported no enriched H3K9me3 marks but instead increased H4K20me1 and H2K27Ac are observed in the human telomeres at the heterochromatic region in laboratory cell lines K562, MCF-7, and HepG2), primary cell lines (HSMM, NHLF, and HMEC) and embryonic stem cells on telomeres. H3K9me3 is detected in subtelomeric regions (Cubiles et al., 2018). In general, the epigenetic nature of telomeres differs between human and mouse telomeres, and studies demonstrate some controversial results of heterochromatic marks concerning H3K9me3, H4K20me3, and H3K27me3 (***Table 1-2***). Overall, we noted that H3K9me3 has a significant place in silenced genes and embryonic stem cells. Additionally, H3K9me3, H3K27me3, H3K36me3, H4K20me1, H3K4me1, H3K4me2, H3K4me3, H3K27ac, H3K9ac and H3K72me2 are described as being common studied epigenetic features of human telomere repeats (Ernst et al., 2011; Cubiles et al., 2018).

Table 1-2. **Common histone modifications on human and mouse telomeres**

	Human telomere	Mouse telomere
H3K9me3 Chromatin compaction, silencing	**Enriched** (Arnoult et al., 2012) (Montero et al., 2018) (Negishi et al., 2015)	**Enriched** (García-Cao et al., 2004b) (Garcia-Cao et al, 2004). (Gonzalo et al., 2006) (Udugama et al., 2015)(Saksouk et al., 2014)
	Not enriched (Cubiles et al., 2018) (Rosenfeld et al., 2009)(Vaquero-Sedas and Vega-Palas, 2019)	
H3K27Ac Active chromatin	**Enriched** (Cubiles et al., 2018) (Negishi et al., 2015) (Rosenfeld et al., 2009)(Vaquero-Sedas and Vega-Palas, 2019)	**Enriched** (Akiyama et al. 2015)
H3K4me3 Active chromatin	**Enriched** (Rosenfeld et al., 2009)	**Enriched** (Akiyama et al. 2015) (Cao et al., 2009)

H4K20me3 Chromatin compaction, silencing	**Enriched** (Montero et al., 2018) (Kourmouli et al., 2004) (Nelson et al., 2016)	**Enriched** (Schotta et al., 2008)(Schoeftner and Blasco, 2010) (Gonzalo et al., 2006) (Benetti et al., 2007b)
		Not enriched (Saksouk et al., 2014)
H4K20me1 Chromatin compaction, silencing	**Enriched** (Cubiles et al., 2018) (Vaquero-Sedas and Vega-Palas, 2019)	**Enriched** (Benetti et al., 2007).
H3K27me3 Chromatin compaction, silencing	**Enriched** (Rosenfeld et al., 2009) (Montero et al., 2018), (Arnoult et al., 2012)	**Not enriched** (Saksouk et al., 2014)
HP-1 Chromatin compaction, silencing	**Enriched** (Montero et al., 2018)	**Enriched** (García-Cao et al., 2004b) (Garcia-Cao et al, 2004).

1.6.3 Transcription factors and regulation of TERT promoter

Transcriptional dysregulation of TERT is important for telomerase activation in tumour cells. Recent studies have emphasized the impact of transcription factor binding, DNA and histone modifications, especially around the core promoter (Khattar and Tergaonkar, 2017). The TERT promoter contains GC rich sequences and E-boxes as binding sites for transcription factors but lacks TATA or CAAT box transcriptional regulatory elements (Wick et al., 1999). Various transcription factors have been studied for TERT gene regulation, including transcriptional activators Sp1, c-Myc, Mad1 (mitotic arrest deficiency 1), Ap-1 (activating protein-1), ER (estrogen receptor), HIF1s and the repressors p53, WT1. Hypoxia-inducible factor family transcription factors (HIF-1α, HIF-2α and HIF-3α) are activated to regulate cellular response under hypoxic conditions (Semenza, 2011). HIF1 is one of the most significant transcription factors for TERT promoter, which comprises two HIF-1 consensus sequences between -165/-158 and +44/+51 region (Nishi et al., 2004) **(*Fig 7*)**. HIF-1α upregulation induces telomerase activity by considerably increased TERT transcription, and these two HIF1 binding motifs are the main reason for this overexpression (Kyo et al., 2008). HIF1a is oxygen-dependent and allows cellular adaption to low oxygen tension; on the other hand, the HIF-1β subunit is constitutively expressed in most cells (Bárdos and Ashcroft, 2004).

p53 with the assistance of the Sp1 transcription factor (possible other TFs), suppresses TERT gene transcription through binding at -1877 and -1240 upstream of the promoter regions. Moreover, p21 has a significant role in regulating p53 dependent TERT suppression, so p53 and p21 expression regulate the TERT gene repression (Kanaya et al., 2000; Lai et al., 2005).

Other important transcription factors are c-Myc and Mad1, which bind E-box consensus sites (5′-CACGTG-3′) at positions -165 and +44 promoter region of TERT to regulate gene activity (Takakura et al., 1999). Inhibition of HDAC accelerates TERT protein degradation, decreases telomerase activity, induces senescence, reduces gene transcription and promoter activation in rat vascular smooth muscle cells (Qing et al., 2016). On the other hand, HDAC inhibitor trichostatin A increases telomerase activity throughout transcriptional activation of TERT promoter in normal cells (Qing et al., 2016). In this regulation, the transcription factor Sp1 has a significant role because overexpression of Sp1 with enhanced responsiveness to HDAC inhibitor (Takakura et al., 2001). According to studies, histone deacetylation may have a repressive feature on the TERT gene in normal cells (Takakura et al., 2001; Cheng et al., 2017). Alternatively, Zhu et al. claimed that cell proliferation and apoptosis were induced after histone deacetylase inhibitors in ovarian cancer, but telomerase activity remained at the same level (Zhu et al., 2007). Another study demonstrated that telomerase activity and TERT gene expression were downregulated in brain cancer cells after exposure to HDAC inhibitors (Khaw et al., 2007). Therefore, HDAC inhibitors might have various influences on the telomerase and TERT gene activity in different cancer cells.

1.7 Epigenetics and Hypoxic Response

In the human body, tissue oxygen levels vary among organs and typically range from <2 - 9% *in vivo* (Jagannathan et al., 2016). Gene expression, transcription factors, and epigenetic regulation of gene or chromatin modification enzyme activities are likely to be altered *in vitro* compared to human bodies (Jagannathan et al., 2016) because *in vitro* experiments are traditionally conducted at normoxia conditions in standard cell culture incubators (21% O_2).

Epigenetic modifications significantly affect cellular responses to low oxygen environments and hypoxia-induced transcription factors. Epigenetics is essential to initiate hypoxic response pathways and to continue the post hypoxic phenotype (Watson et al., 2009) (***Fig 1.8***). HIF-1 transcription factors target several histone demethylase enzyme genes during cellular response to the low oxygen environment, such as HAT enzyme catalytic domain CBP/p300 (Kallio et al., 1998; Watson et al., 2010). Human umbilical vein endothelial cells were studied to understand changes in telomere length and telomerase activity in different levels of low oxygen tension, where growth advantage was observed in lower oxygen levels (Guan et al., 2012b). Telomerase activity increased in endothelial cells with long telomeres after culture in low

oxygen tension (Guan et al., 2012a, 2012b). Further, significantly longer telomeres and increased mRNA levels of TERT, HIF1A were observed in rat heart and lung tissue cells cultured in reduced oxygen tension (Wang et al., 2018). This result supported that reduced oxygen tension can induce telomere length elongation, and TERT mRNA levels were closely associated with HIF-1α and hypoxia responses. Beyond that, the TERT core promoter region contains several transcription factor binding sites, e.g., c-Myc, Sp1, WT1 and two HIF-1 binding sites (Kyo et al., 2008).

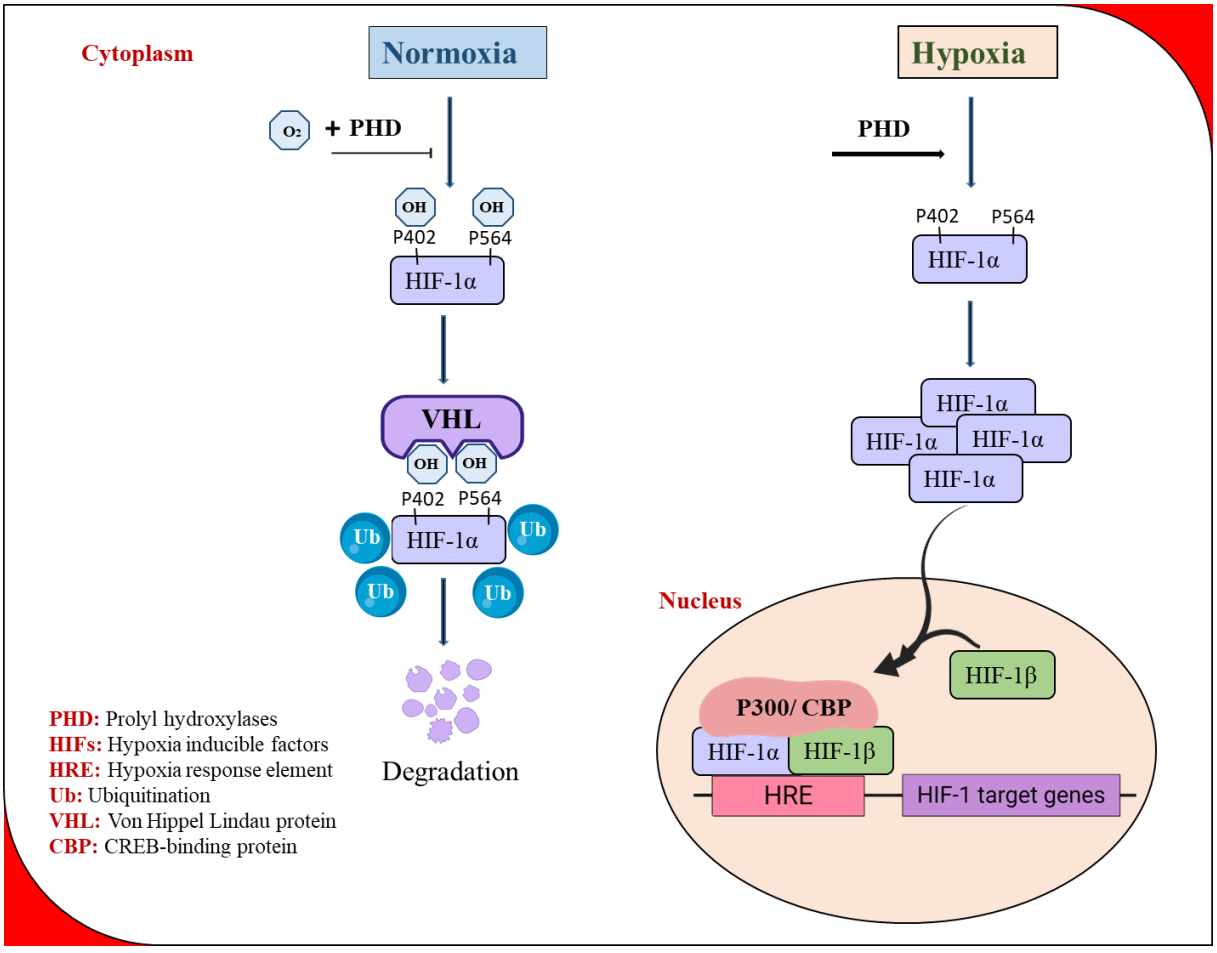

Figure 1.8. **Regulation of hypoxia-inducible factors response to oxygen concentrations**. Prolyl hydroxylases (PHD), activated by oxygen, lead to hydroxylation of HIF-1α at residues 402 and 564, followed by recognition by the tumour suppressor protein von Hippel–Lindau (VHL). In normal oxygen tension, pVHL tumour suppressor protein binds to and targets HIF for degradation by ubiquitination. On the other hand, in hypoxic conditions, pVHL does not bind to HIF, consequently, its levels increase within the cell, where it then binds to downstream

hypoxia response elements within the nucleus resulting in the activation of the genes expression that facilitate its survival within hypoxic conditions.

HIF-1α upregulation induces telomerase activity by considerably increased TERT transcription, and these two HIF1 binding motifs are the main reason for this overexpression (Kyo et al., 2008). Different studies show that hypoxia induces decreased global methylation in tumour and cancer cell lines (Shahrzad et al., 2007; Skowronski et al., 2010). Johnson et al. demonstrated chromatin alterations and epigenetic changes such as decreased H3K9me2, increased H3K9ac and H3K4me3 levels in the promoter region under hypoxia, and the same epigenetic changes were noticed at the promoters of the hypoxia-inducible genes (Johnson et al., 2008; Perez-Perri et al., 2011). Chronic tissue hypoxia conditions have been demonstrated as a natural process of the ageing prostate and organs (Aalami et al., 2003; Tanaka et al., 2006). Watson et al. have highlighted considerably increased DNA methylation (especially DNMT3B) and H3K9 acetylation in prostate cells by chronic hypoxia (Watson et al., 2009). Chronic hypoxic conditions induce significant modifications genome-wide, including epigenetic regulation of histone acetylation and DNA methylation. Expression of DNMT3B was increased in the hypoxic prostate cell line and might be responsible for maintaining global hypermethylation because no considerable alteration was observed in the DNMT1 and DNMT3A activity (Watson et al., 2009).

Scientific Aim and objectives

Telomerase is expressed in most cancer cells. TERT promoter mutations might increase telomerase activation, but epigenetic, transcriptional and posttranscriptional modifications are as crucial as mutations. Therefore, it is essential to understand these mechanisms, and there is a need to further research to comprehend the association between telomerase, epigenetic and physiological oxygen microenvironments.

Stem cells are a good model for understanding epigenetic responses to related environmental clues for cellular links. Their differentiation process provides a model to research the regulation of telomerase activity. It is noteworthy that ESCs and cancer cells both have high telomerase activity. Instead of focusing on one type of cell, we aim to look from a broad perspective at epigenetic regulation of telomerase. We seek to understand how alterations in the physiological environment can affect the expression of TERT in telomerase positive tumour cells, somatic cells and stem cell populations.

The overall aims of this project:

- Investigate the impacts of the different oxygen conditions on characteristics of embryonic stem cells and differentiated stem cells
- Investigate the effects of reduced oxygen on TERT promoter, gene expression, telomerase, and telomere length during differentiation
- Assess the association between DNMT1, DNMT3A, DNMT3B and TERT expression in stem cells and cancer cells models
- Evaluate the CpG methylation pattern of TERT promoter regions during the differentiation of hESCs and cancer cells
- Determine the impact of epigenetic drugs on the TERT gene, promoter methylation and telomerase enzyme, including Nanaomycin A (DNMT3Bi) and Decitabine (DNMTi).
- Determine specific binding of DNMT3B on TERT promoter and examine methylation changes

Keele University

CHAPTER 2: MATERIALS AND METHODS

2.1 Materials

Table 2-1. **List of materials, catalogue numbers and suppliers.**

Name	Catalogue number	Supplier
Agarose	BP1356-500	Fisher Scientific
Bovine serum albumin (BSA)	BP9703-100	Fisher Scientific
4′,6-Diamidino-2-phenylindole (DAPI)	D9542	Sigma-Aldrich
Paraformaldehyde	P/0840/53	Fisher Scientific
GeneRuler Low Range DNA Ladder	SM1193	Thermo Scientific
Direct Load Wide Range DNA Marker	D7058	Sigma-Aldrich
Dimethyl sulfoxide (DMSO)	D2650	Sigma-Aldrich
Dulbecco's Modified Eagle Medium (DMEM) – 4.5 g/L glucose	BE12-709F	Lonza
RPMI1640	12-918F	Lonza
EDTA (0.5 M), pH 8.0	AM9260G	Fisher Scientific
Ethylenediamine tetra-acetic acid (EDTA)	BP2482-1	Fisher Scientific
Trypan blue	T8154	Sigma-Aldrich
Trypsin	15090	Life Technologies
β-mercaptoethanol	10368072	Fisher Scientific
Essential 8™ Medium	A1517001	Life Technologies
Vitronectin (VTN-N) Recombinant Human Protein	A14700	Life Technologies
Knockout DMEM	10389172	Fisher Scientific
L-Glutamine	BE17-605E	Lonza
Non-essential amino acids NEAA	BE13-114E	Lonza

Penicillin, streptomycin, amphotericin B (PSA)	BE17-745E	Lonza
Poly(2-hydroxyethyl methacrylate), Poly(2-HEMA)	P3932-10G	Sigma-Aldrich
Methanol	M/3900/17	Fisher Scientific
Ethanol (absolute)	E0650/17	Fisher Scientific
Ethidium bromide	E1510	Sigma-Aldrich
Decitabine (DNA Methyltransferase Inhibitors)	A10292-10	Adooq Bioscience
Nanaomycin A	A13477-5	Adooq Bioscience
Bradford Reagent	B6916	Sigma-Aldrich
RIPA Lysis Buffer	20-188	Merck Millipore
Absolute Human Telomere Length Quantification qPCR Assay Kit	SC-8918	Caltag Medsystems Limited
FBS (foetal bovine serum)	DE14-801F	Lonza
Cell Proliferation Reagent WST-1	5015944001	Sigma-Aldrich
LIVE/DEAD Viability/Cytotoxicity Kit	L3224	ThermoFisher Scientific
Flow cytometry staining buffer	FC001	R&D system
Gel Loading Buffer (0.05% bromophenol blue, 40% sucrose, 0.1 M EDTA, 0.5% SDS)	G2526	Sigma-Aldrich
Go Taq G2 Flexi DNA polymerase	M7801	Promega
QuantiFast SYBR Green RT-PCR Kit	204154	Qiagen
RNeasy Mini Kit	74104	Qiagen
DNeasy Blood & Tissue Kit	69504	Qiagen
QIAshredder mini spin columns	79656	Qiagen
TRAPeze RT Telomerase Detection Kit	S7710	Merck Millipore

TITANIUM™ Taq DNA Polymerase	639208	Takara Bio
EpiQuik DNMT1 Activity/Inhibition Assay Ultra Kit	P-3006A-96	Epigentek
EpiQuik DNMT3B Activity/Inhibitor Screening Assay	P-3007A-96	Epigentek
EpiQuik Nuclear Extraction Kit	OP-0002-1	Epigentek
PyroMark Gold Q24 Reagents	970802	Qiagen
PyroMark Denaturation Solution	979007	Qiagen
PyroMark PCR Kit	978703	Qiagen
Annealing Buffer	979009	Qiagen
TE buffer	P7589	Invitrogen
Streptavidin sepharase	17-5113-01	GE Healthcare
Triton X-100	9002-93-1	Sigma-Aldrich
Cy™ AffiniPure Goat Anti-Rabbit IgG (H+L)	111-165-003	Jacksonimmuno
Goat anti-Mouse IgG1 Cross-Adsorbed Secondary Antibody	A-21125	Thermofisher
Rabbit anti-Goat IgG (H+L) Secondary Antibody	A- 11078	Thermofisher
Goat anti-Mouse IgG3 Cross-Adsorbed Secondary Antibody	A- 21155	Thermofisher
Goat anti-Mouse IgM Secondary Antibody	A- 21042	Thermofisher
Donkey anti-Mouse IgG Secondary Antibody	A- 21203	Thermofisher
Anti-TERT Antibody	ABE2075	Sigma Aldrich
Human Pluripotent Stem Cell Marker Antibody Panel	SC008	R&D Systems
Richard-Allan Scientific™ HistoGel™ Specimen processing gel	12006679	Fisher Scientific

Epredia™ SuperFrost Plus™ Adhesion slides	10149870	Fisher Scientific
Tris-EDTA buffer 100X	T9285	Sigma
Human Nestin Antibody	MAB1259	R&D system
Human alpha-Fetoprotein/AFP Antibody	MAB1369	R&D system
Human/Mouse Brachyury Antibody	AF2085	R&D system
PE/Cyanine5 anti-mouse/human CD11b Antibody	101209	BioLegend
PE/Cyanine5 Rat IgG2b, κ Isotype Ctrl Antibody	400609	BioLegend
Retinoic acid ATRA	R2625	Sigma-Aldrich
ChIP DNA Purification Kit	58002	Active Motif
ChIP-IT® Express Enzymatic Kit	53009	Active Motif
ChIP-IT® Control Kit – Human	53010	Active Motif
DNMT3B antibody	ab13604	Abcam
SYBR Green Master Mix	A46109	Thermofisher

2.2 General cell culture techniques

Two different hESC lines (SHEF1, SHEF2) were provided from the laboratory stock of Guy Hilton Research Centre, Keele University and used under approval from the UK Stem Cell Bank (UKSCB) (Aflatoonian et al., 2010). MG-63 (human osteosarcoma cell line), SH-SY5Y (neuroblastoma cell line), COV362 (human ovarian epithelial-endometroid carcinoma), A549 (human lung carcinoma), Jurkat cells (acute lymphocytic leukaemia), HL-60 (promyelocytic leukaemia cells) and IMR-90 (human fetal lung fibroblast) cell lines were obtained from the laboratory stock of Guy Hilton Research Centre, Keele University.

2.2.1 Cell culture conditions

Cells were cultured in the following three different conditions:

- Standard cell culture incubator 21% O_2 (21% AO)
- 2% O_2-Pre-gassed media and in a 2% O_2 incubator (2% PG)
- 2% O_2-Pre-gassed media and a fully defined 2% O_2 environment in a Workstation oxygen controlled chamber (2% WKS)

All cells were incubated at 37^o C in humidified air and 5% CO_2 incubator and handled in a standard class II biological safety laminar flow cabinet (21% AO), a nitrogen-regulated tri-gas controlled incubator set at 2% O_2, 5% CO_2 and handled in a standard class II biological safety laminar flow cabinet (2% PG), or a tri-gas incubator set at 2% O_2 in the presence of 5% CO_2 but handled in a sealed workstation (2% WKS) (SCI-TIVE, Baker Ruskinn Ltd, UK). Media in both reduced oxygen settings was pre-conditioned to 2% O_2 with a HypoxyCool unit. Mycoplasma testing was performed for each cell line by Guy Hilton technician team. Before experiments in physoxia, all cell types were culturing at least five passages in reduced oxygen conditions (2% PG and 2% WKS). Cells were checked regularly under an inverted microscope (Nikon TS100, Japan). In this study, long term effect was assessed because many studies focused on short term reduced oxygen effects (24h and three days), and there is not enough information about the effect of long term low oxygen tension on stem cells and cancer cells.

2.2.2 Hypoxic media

Cell culture media was deoxygenated to a 2% O_2 level at 4^{o}C in a HypoxyCool unit (Baker Ruskinn Ltd, UK) to provide the reduced oxygen conditions. Firstly, the media bottle caps were replaced with vented caps (ThermoFisher, UK), which maintain media sterility and allow gas change within the media in a sterile hood. Afterwards, the media bottles were placed in the HypoxyCool unit. The system was programmed with standard cycle parameters (O_2 level, temperature, shaker speed, and runtime) for three hours. Then, vented caps were changed with original media bottle caps in the class II biological safety cabinet and media were stored in the fridge (***Fig 2.1***).

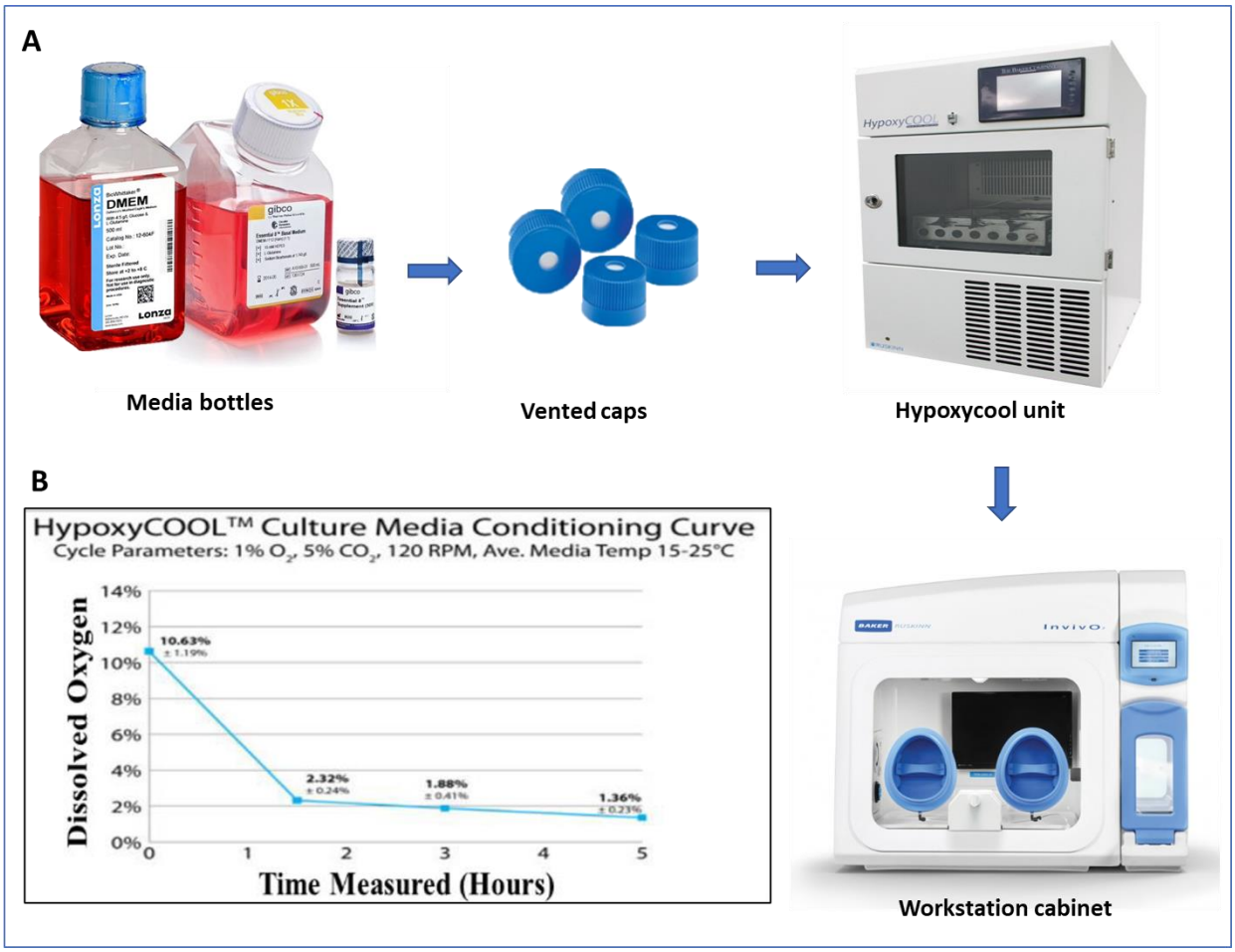

Figure 2.1. **Preparing deoxygenated media in Hypoxycool unit. A)** Caps from the media bottles were aseptically replaced with vented caps in class II biological safety cabinet and then placed into the Hypoxycool unit. It reduces the dissolved oxygen concentration and maintains media sterility, temperature and pH in the media to use in oxygen-regulated, closed-culture systems. **B)** Graph represents dissolved oxygen within the media over time. Source: The Baker Company.

2.2.3 Cell sub-culture and expansion

All cell culture procedures were performed using disposable sterile consumables in a Class II microbiological safety cabinet. Cells were cultured in standard tissue culture T25, T75 vented flasks or multi-well culture plate. Cells were sub-cultured regularly when they had reached 80-90% confluence. They were rinsed with calcium and magnesium-free PBS, and exposed to 1ml 1% trypsin/PBS or 0.5mM of ethylenediaminetetraacetic acid (EDTA) in PBS for passaging, then incubated for 3-5 minutes at 37°C until cells began to detach. After detachment, 2 ml of

media was added, and the cells were collected. Suspension cells Jurkat and HL-60 were collected in 15 ml tubes without trypsin treatment. Cells suspension are then centrifuged at 1300 rpm for 3 minutes to collect pellet the cells and supernatant removed. Finally, the fresh media was added to the pellet by gently pipetting at the correct dilution (1:4 to 1:10). All cells were checked routinely under an inverted microscope (Nikon TS100, Japan) to ensure they were healthy and checked for confluency. Mycoplasma testing was performed routinely for cell lines by the Guy Hilton technician team to ensure no contamination.

2.2.4 Cell counting

Cells were collected and diluted in culture media. 10 µl of the cell suspension was mixed with 10 µl volume of trypan blue and was loaded into a haemocytometer adhered with a coverslip. Cells were counted from 1 mm^2 corner squares under a microscope, and the mean number of 3 squares was multiplied by 10^4 and the dilution factor calculating cells/ml. Cell numbers were counted every two days. Population doubling (PD) time was calculated with a split ratio of cells at sub-culture (for example, 1:2 equals 1 PD). Also, cell counts were performed at sub-culture using trypsin/EDTA and haemocytometer to determine confluency.

2.2.5 Cryopreservation of cells

To cryopreserve the cells for future use, confluent cells were exposed to trypsin/EDTA. Following detachment, cells were harvested and re-suspended in 1ml freezing media, comprising 10% dimethyl sulphoxide (DMSO) in fresh media and immediately transferred into a cryovial. The cryovial was placed into a Mr Frosty container and then into a -80^{o}C freezer overnight before transfer into liquid nitrogen for long-term storage.

Cryovial taken out from liquid nitrogen was rapidly placed in a 37°C water bath and thawed for 1 minute to recover frozen cells. The thawed cells were diluted slowly using a pre-warmed growth medium and centrifuged at 1000 rpm for three minutes, the supernatant removed, and the pellet re-suspended in fresh media.

2.2.6 Cell sub-culture, expansion and characterization of hESCs

Xeno-free, E8 media (Life Technologies, USA) was used to grow hESC and media was prepared with 10ml Essential 8 Supplement (Life Technologies, USA). Essential 8 Supplement (10 ml, 50X) was thawed at 2-8^{o}C overnight and was mixed with 490 ml Essential 8 basal media to prepare 500 ml of complete Essential 8 basal medium (E8M), then stored in the fridge.

hESCs frozen vials were thawed rapidly in a water bath (37^{o}C) with gentle agitation following removal from liquid nitrogen. Thawed cells were added to 4ml of complete E8M, then centrifuged at 1300 rpm for 3 minutes, and the supernatant removed. The cell pellet is then re-suspended in 3ml of medium and seeded into one well of a six-well plate coated with vitronectin (rhVTN-N, Recombinant Human Protein) (Life Technologies, USA). The working vitronectin solution (5 µg/ml) was prepared for coating by adding 60µl rhVTN-N to 6ml of Dulbecco's phosphate buffer saline (PBS) without calcium and magnesium (Gibco). Then 1ml of vitronectin solution was added to each well of a 6-well tissue culture plate, followed by incubation at room temperature 1 hour before use. After incubation, the vitronectin solution was discarded, and 2ml of fresh E8M culture media was added. hESCs were cultured within the three different oxygen conditions; 21% AO, 2% PG and 2% WKS. hESCs regularly fed with fresh E8M every day. Confluent cells were sub-cultured enzymatically using 0.5mM EDTA.

Cells were sub-cultured regularly when they reached 80-90% confluence, the media was removed, and cells were washed with calcium and magnesium-free PBS. Cells were exposed to 1ml (1 well of a 6-well plate) 0.5mM of EDTA in PBS solution for 5 minutes. EDTA-based dissociation solution can minimize cell death and allow rapid cell attachment upon re-plating and resumption of the cell cycle. Culture vessels were incubated for 3-5 minutes at 37°C until cells began to detach. After detachment, 2 ml of media was added, and the cells were collected. Cells suspension are then centrifuged at 1300 rpm for 3 minutes to collect pellet the cells and supernatant removed. Finally, the fresh media was added to the pellet at the correct dilution (between a 1:4 and 1:8 split ratio).

2.3 Spontaneous differentiation

hESCs were grown in 6-well vitronectin-coated culture plates for 48 hours in E8M before switching into spontaneous differentiation medium (Knockout DMEM, 10% FBS, 1% NEAA,

1% PSA, 1% L-glutamine and 0.1 mM β mercaptoethanol). The medium was changed every three days.

Two different spontaneous differentiation methods were used for differentiation experiments; the monolayer 2D differentiation method, where cells were attached to a dish and 3D embryoid bodies (EBs) formation. The same media Knockout DMEM were used for both techniques. Monolayer differentiated cells were characterised at different time points; days 5, 10, 20 and 40. ESC cells are typically plated in a differentiation medium to form EBs with the conventional technique and cultured to form aggregates without attachment to the well plate.

Embryoid body formation protocol

After hESC reached 70-90% confluency, the cells were washed once and then incubated in EDTA/PBS for 3–5 minutes to dissociate colonies into cell clumps. Then cells were collected using warm media in a 15 mL conical tube and centrifuged at 1300 rpm for 3 minutes at room temperature.

To form self-aggregated EBs, suspended cells were transferred into six-well low attachment plates (poly-HEMA coated) via 1:1 passage (about 10^6 hESCs each well) to allow self-aggregation in 37°C incubator overnight. On the second day, EBs were formed in various sizes. After EBs formed, media was changed by tilting the plate at a 30°–45° angle to allow the EBs to gather at the bottom of the well. Gently most media was removed with a pipette, and the Knockout DMEM medium was changed every two days. In the end, cells were collected at different time points (5d, 10d, 20d).

2.4 Characterization of human embryonic stem cells

Undifferentiated hESC were seeded in 96 well-plates coated with vitronectin and maintained in E8 basal Medium over 96 hours before immunocytochemistry. Spontaneous differentiation of hESCs was assessed at three different time points; days 5, 10, 20 and 40. Cells are characterised using the Human Pluripotent Stem Cell Marker Antibody Panel (R&D systems, UK).

2.4.1 Immunocytochemistry fixing and staining protocol

Cells were washed twice with PBS, then fixed with 4% paraformaldehyde solution and incubated for 20 minutes at room temperature. After fixation, cells were rewashed three times with 1% BSA in PBS for 5 minutes. Then 0.3% Triton™ X-100 with 1% BSA in PBS was added for 45 minutes to permeabilise and block the cells for non-specific antibody binding. While blocking the cells, reconstituted primary antibodies were diluted in PBS containing 0.3% Triton™ X-100 with 1% BSA to a final concentration of 10 μg/ml.

The cells were incubated with primary diluted antibodies after blocking, including mouse anti-human ALP monoclonal, goat anti-human Nanog polyclonal, goat anti-human OCT-3/4 polyclonal, mouse anti-human SSEA-4 monoclonal or mouse anti-human SSEA-1 monoclonal antibody at 1μg/100μL and incubated at 2-8°C overnight. Then, cells were washed three times with 1% BSA in PBS for 5 minutes. After that, secondary antibodies (5μg/ml) in PBS containing 1% BSA were added to ALP (Goat anti-Mouse IgG1, Thermofisher, UK), Nanog and OCT-3/4 (Rabbit anti-Goat IgG, Thermofisher, UK), SSEA-4 (Goat anti-Mouse IgG3, Thermofisher, UK) and SSEA-1 (Goat anti-Mouse IgM, Thermofisher, UK). Samples were incubated with secondary antibodies for one hour at room temperature in the dark. Non-specific staining of the nuclei was visualised with 4, 6 Diamidino-2-phenylindole (DAPI) at 1 μg/ml in PBS for 5-10 minutes. Again cells were washed three times with 1% BSA in PBS for 5 minutes. Finally, cells were covered with PBS and immediately imaged using a Nikon fluorescence microscope (Nikon TZ1; Leica, Germany).

2.4.2 Histogel embedding and sectioning of EBs

EBs fixed with 10% neutral buffered formalin before embedding in histogel for 15-20 minutes at room temperature and washed with 5 ml PBS twice. Richard-Allan Scientific™ HistoGel™ Specimen processing gel (Fisher Scientific, UK) was melted in a microwave for 10-15 seconds until it became viscous. Then, 96 well plate lid was used to embed EBs in histogel and left to sit for 20 minutes. On the same day or later, histogel embedded EBs exposed to serial dilution of ethanol and isopropanol. First, samples were subjected to 70% ethanol for 60 minutes, then 80% ethanol for 60 minutes, 90% ethanol for 60 minutes, 100% ethanol for another 60 minutes. After ethanol, samples were subjected to freshly prepared 100%

isopropanol which does not interfere with wax. Once ethanol dehydration series and isopropanol treatments were done, samples were ready for paraffin embedding.

Firstly, the wax melter is switched on to melt the wax inside. Meanwhile, the floatation bath was filled up with deionised water to the brim, and the temperature was maintained between 40°C - 50°C. EBs embedded and dehydrated histogels were placed into the metal tray filled with wax inside the wax melter and then incubated for two hours. Once all set, EBs in the metal tray was placed under the wax dispenser and filled with wax gently, avoiding air bubbles. EBs were positioned to the centre of the tray, and immediately labelled white cassettes were pressed onto the tray. Assembled tray was quickly transferred to the cooling stage to solidify wax and EBs inside.

For sectioning, 8µm and 10 µm thin sections were prepared and placed into a floatation bath. Epredia™ SuperFrost Plus™ Adhesion slides (Fisher Scientific, UK) were used to attach the EBs sections and let them dry for 30 minutes. Slides with captured EBs sections were then placed into an oven for 4 hours at least to increase attachment between samples and slides. The slides were immersed again in a descending alcohol series to remove the paraffin wax and dehydrate the tissue as described below.

i. Place slides in 100% Xylene - 3 minutes
ii. Place slides in 100% Xylene - 3 minutes
iii. Place slides in 100% IMS - 3 minutes
iv. Place slides in 100% IMS - 30 seconds
v. Place slides in 90% IMS - 30 seconds
vi. Place slides in 80% IMS - 30 seconds
vii. Place slides in 70% IMS - 30 seconds
viii. Place slides in distilled water - 30 seconds (twice this step)

After the dehydration, slides were let to dry completely and stored at room temperature.

2.4.3 Heat-induced antigen retrieval and staining of EBs slides with differentiation markers

Most formalin-fixed samples require antigen retrieval steps because formaldehyde is a highly reactive compound. It contains a variety of chemical modifications, such as methylene bridges that can mask antigenic sites in immunohistochemistry. Antigen retrieval is a method used to reduce or break these chemical modifications to restore the antigenicity of the sample. There are two standard methods, including enzymatic and heat-induced antigen retrieval. The enzymatic method might damage the morphology of the sections, therefore, we prefer to use

the heat-mediated antigen retrieval method. Heat treatment reverses some cross-links and allows restoring antigenicity.

Antigen retrieval buffer was prepared using 5mL of Tris-EDTA buffer 100X (Sigma, UK), 495mL of ddH_2O, 250 µL Tween 20 (pH 9.0), and it can be stored at room temperature for three months or at 4°C for more extended storage. Antigen retrieval buffer was used for microwave treatment (750 W) for 5 minutes and then 10 minutes cooling down after each heat treatment. This step was repeated for three cycles and avoided drying out any samples. After the last heat treatment, samples were let cool down for 20 minutes. Slides were washed three times with 1% BSA in PBS for 5 minutes. Then 0.3% Triton™ X-100 with 1% BSA in PBS was used for 45 minutes to permeabilise and block the cells for non-specific antibody binding. While blocking the cells, reconstituted primary antibodies were diluted in PBS containing 0.3% Triton™ X-100 with 1% BSA to a final concentration of 1µg/150 µl. Pap pen was used to mark a circle around EBs samples to create a hydrophobic barrier and use less primary antibody in immunohistochemistry and incubated for 15 minutes to let it dry. 50 µl of antibody solution was added carefully to each sample's hydrophobic circle. Slides were placed into a tray that contained water to decrease the evaporation of the primary antibody, and the tray was sealed with foil. Samples were carefully placed into a fridge at 2-8°C for overnight incubation. Human nestin antibody (monoclonal mouse IgG1) (R&D Systems, UK), human alpha-fetoprotein/AFP antibody (monoclonal mouse IgG_{2B}) (R&D Systems, UK), human/mouse brachyury antibody (polyclonal goat IgG) were used for immunohistochemistry experiments.

Then cells were washed with 1% BSA in PBS three times for 5 minutes. After that, secondary antibodies (5µg/ml) in PBS containing 1% BSA were added to Nestin (anti-Mouse IgG1, Thermofisher, UK), AFP (anti-Mouse IgG, Thermofisher, UK) and Brachyury (anti-Goat IgG, Thermofisher, UK). Samples were incubated with secondary antibodies in the dark for one hour at room temperature. Non-specific staining of the nuclei was visualised with 4, 6 Diamidino-2-phenylindole (DAPI, Roche, UK) at 1 µg/ml in PBS for 5-10 minutes. Samples were washed with 1% BSA in PBS three times for 5 minutes. Finally, slides were covered with mounting media and coverslips, then immediately, samples were imaged using a Nikon fluorescence microscope (Nikon TZ1; Leica, Germany).

2.5 Cancer and normal cell lines

MG-63 (human osteosarcoma cell line), SH-SY5Y (neuroblastoma cell line), COV362 (human ovarian epithelial-endometroid carcinoma), A549 (human lung carcinoma), Jurkat cells (acute lymphocytic leukaemia), HL-60 (promyelocytic leukaemia cells) and IMR-90 (human fetal lung fibroblast) cell lines were obtained from the laboratory stock of Guy Hilton Research Centre, Keele University (***Table 2-2***). All cell lines were incubated at 37^{o}C at three different oxygen conditions. The cells were checked regularly to control confluency and passaged if it is required. Cancer cells and non-cancer control cells were maintained in DMEM (Lonza, USA) or RPMI (Lonza, USA), which contains 10% FBS, 1% NEAA, 1% PSA (Penicillin-Streptomycin-Amphotericin B) and 1% L-Glutamine. The medium was changed regularly to maintain optimum conditions and ensure no contamination. The cells were seeded in T25 and T75 flasks at a split ratio of 1:4 to 1:10 and growth in DMEM media, including 10% FBS, 1% PSA, 1% NEAA and 1% L-Glutamine. The cell viability and number of cells were determined using the trypan blue dye.

Table 2-2. **Cancer cell lines summary**

Cell lines	**Description**
MG-63 human osteosarcoma cell line (Adherent, P7)	Cells were obtained from a seventeen-week old male embryo with osteogenic sarcoma (Billiau et al., 1977).
SH-SY5Y neuroblastoma cell line (Adherent, P7)	Cells were initially isolated from a 4-year-old female with a metastatic bone tumour in 1970 (Biedler et al., 1978).
COV362 human ovarian epithelial-endometroid carcinoma (Adherent, P10)	Cells were obtained from the pleural effusion of a human ovarian epithelial-endometroid carcinoma (van den Berg-Bakker et al., 1993).
A549 human lung carcinoma (Adherent, P15)	Cells were derived from a 58-year-old Caucasian male in 1972 (Giard et al., 1973).

Jurkat cells Acute lymphocytic leukaemia (Non-Adherent)	Cells were obtained from the peripheral blood of a 14-year-old patient with relapsing Acute lymphocytic leukaemia (ALL) (Schneider et al., 1977).
IMR-90 human fetal lung fibroblast (Adherent, P12)	Non-cancer adherent IMR-90 cells (ATCC® CCL186™) were isolated from lung tissue of a 16-week-old female Caucasian foetus (Nichols et al., 1977).
HL-60 promyelocytic leukaemia cells (Non-Adherent)	Promyeoloblasts were isolated from the peripheral blood by leukapheresis from a 36-year-old Caucasian female with acute promyelocytic leukaemia (Collins, Gallo, & Gallagher, 1977)

2.6 LIVE/DEAD Cell Viability Assay

The LIVE/DEAD Viability Assay (Thermo Scientific, USA) has two colour fluorescence dyes based on measuring intracellular esterase activity and plasma membrane integrity. Calcein AM and ethidium homodimer (EthD-1) probes quickly distinguish live cells from dead cells by simultaneously staining with green-fluorescent calcein to show intracellular esterase activity and red-fluorescent EthD-1 to indicate loss of plasma membrane integrity. The polyanionic dye calcein produces a bright uniform green fluorescence in live cells. EthD-1 enters cells via damaged membranes and binds nucleic acids, producing intense red fluorescence. These optimal dyes are suitable for use with fluorescence microscopes with relatively low levels of background fluorescence and apply to most eukaryotic cells.

Cell preparation and staining protocol

Adherent cells were cultured on sterile glass coverslips in 48 well plates. EBs were grown in low attachment well plates after being washed two times with 500 µl PBS to remove serum which may contain serum esterase activity. Control dead cell samples were prepared using 70% methanol for 30 minutes of treatment. The LIVE/DEAD reagent stock solutions were removed from the freezer and warmed at room temperature. Cells were treated with 1 µl calcein AM and 1 µl EthD-1 in 500 µl PBS for each condition and then incubated at room temperature for 40

minutes. After treatment with reagents, cells were washed with PBS twice and imaged using a confocal microscope. EthD-1 was viewed with filters for Texas Red® dye, and Calcein was viewed simultaneously with FITC dye.

2.7 Flow cytometry

Flow cytometry (FC) is a common technique used to detect the physical and chemical characteristics of a population of cells as they flow past single or multiple lasers. Each cell is analyzed for visible light scatter and one or multiple fluorescence parameters through labelling cells with fluorescent antibodies. In the end, fluorescent light emission from the cells is detected and converted to electronic signals, processed, and visualised on a monitor for analysis. Flow cytometry measures the morphology and specific characteristics of a large number of individual cells. It can provide information about the properties of cells (morphology, cellular and physical properties, cell cycle stage).

Flow cytometry was used to identify the differentiation marker for HL-60 cells. Cells (approximately $5x10^5$) were obtained from a T25 flask at 90% confluence for each treatment and resuspended in flow cytometry buffer prepared with 0.5% BSA and 2 mM EDTA in PBS. After centrifuge, the supernatant was removed, and the cell pellet was washed twice in flow cytometry buffer. CD11b and relevant PE/Cyanine5 isotype control (rat IgG2b) were diluted in flow cytometry buffer. The diluted concentration of antibody (5 µl for 10^6 cells in 200 µl volume) and secondary antibody control were used for 200 µl cell suspension (5 µl for 10^6 cells). HL-60 cells were incubated on ice for 40 min in the dark, then centrifuged at 1200 rpm for 5 minutes. The supernatant was discarded, then the cell pellet was washed in flow cytometry buffer twice with centrifugation at 1200 rpm for 5 minutes on each occasion. The cell pellet was then re-suspended in a flow cytometry buffer. PerCP/Cyanine5.5 has a maximum absorption of 482 nm and a maximum emission of 690 nm, so we used the Cy5 channel in flow cytometry settings. For each run, 50.000 events were recorded via analysis on the Beckman Coulter Cytomics FC 500 flow cytometer. Data analysis was performed with Flowing Software CytExpert 2.4.

2.8 Drug Treatment of Cancer Cells

Before drug treatment experiments, the appropriate cell number was determined using Cell Proliferation Reagent WST1 (Water Soluble Tetrazolium Salts, Sigma-Aldrich). The WST-1 is an easy and sensitive reagent for performing a quantitative cell proliferation assay, cell viability assay, or cytotoxicity assay in mammalian cells. The stable tetrazolium salt WST-1 is cleaved to a soluble formazan dye by cellular mitochondrial dehydrogenase that is only active in metabolically intact cells (***Fig 2.2***). Therefore, the amount of the dye generated by dehydrogenase activity is directly proportional to the number of living cells. The formazan dye generated by viable cells can be quantified using the microplate reader at 450 nm absorbance.

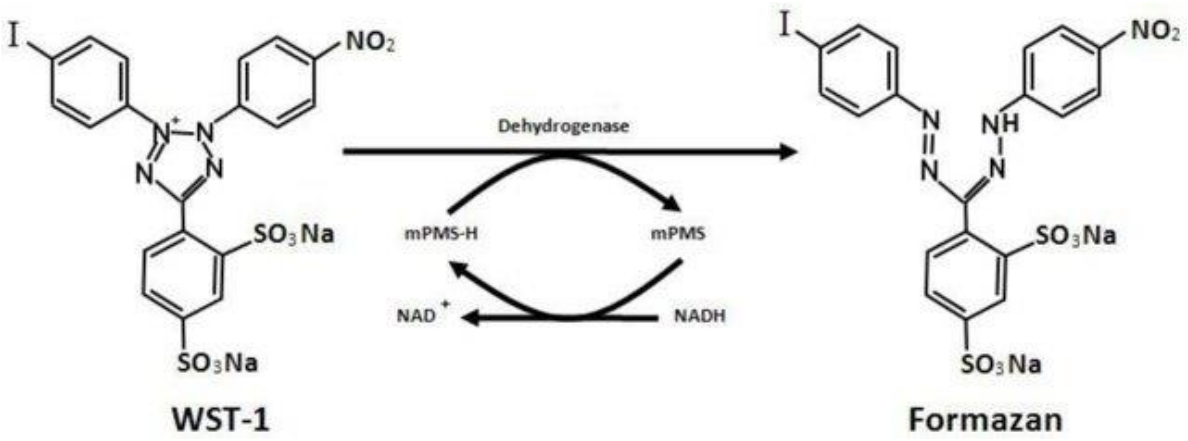

Figure 2.2. **Mechanism of the WST-1 reduction to highly water-soluble formazan dye by cellular dehydrogenase with intermediate electron acceptor (such as mPMS).** Abbreviation: mPMS: 1-methoxy-5-methyl-phenazinium methyl sulfate; NADH: Nicotinamide adenine dinucleotide.

The WST-1 is performed for spectrophotometric quantification of cell proliferation and viability in cell populations using the 96-well-plate format. Cells were seeded in 96 wells plates in a final volume of 100 µl/well culture medium for seven days under three oxygen conditions. After adding 10 µl/well WST-1 assay reagent to the cell culture media, the plate was shaken to mix contents. The plate was incubated for between 0.5 and 4 hrs in a 37°C incubator. The amount of formazan dye generated directly correlates to the number of viable cells with a spectrophotometer. The absorbance of the samples was analysed against the blank control using a microplate reader. There was a linear correlation between absorbance at 450 nm and

incubation time for up to 120 min. The cell line's growth characteristics and log phase were determined before starting drug treatment experiments. In the stationary phase of cell growth, cellular proliferation slows down because the cell population becomes confluent, and the cells are most susceptible to injury. Cell death predominates after the stationary phase, and the death phase starts (***Fig 2.3***).

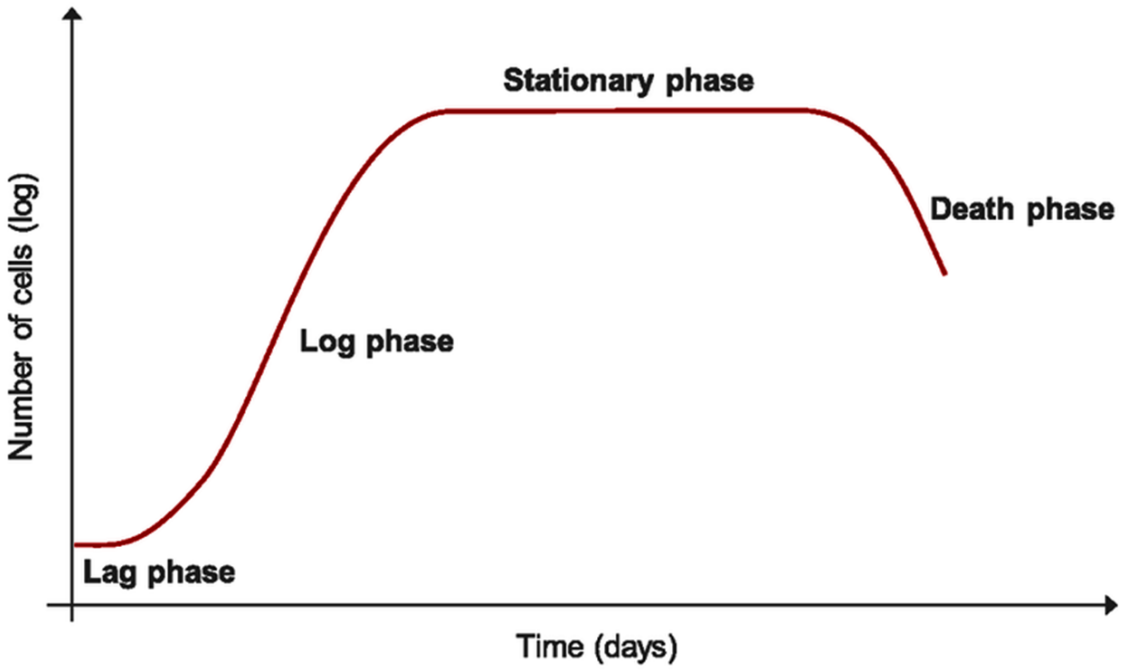

Figure 2.3. **A typical growth curve and phases in cell culture**. The growth curve indicates the number of live cells in a cell population over a time period. First, it starts with a lag phase where cells do not proliferate or divide. Then, cells begin to proliferate exponentially in the logarithmic phase. Once cells reach the confluency, proliferation slows down in the stationary phase. The final stage is called the death phase, where cell death predominates, and the number of live cells declines.

Following proliferation assays, cancer and somatic cells were treated with different Nanaomycin A and Decitabine doses under the normoxic and hypoxic conditions to determine maximum non-toxic drug doses. The DNMT3B selective inhibitor (nanaomycin A) and DNMT1 inhibitors (decitabine) were purchased from Adooq Bioscience (USA). Nanaomycin A is soluble in DMSO. Stock solutions of nanaomycin A were prepared in DMSO; therefore, we used the same amount of DMSO treated cells as a control for this experiment. Decitabine

can dissolve in water and DMSO. Stock solutions were prepared for decitabine in water, therefore, we used untreated cells as a control for this experiment. Prepared stock solutions were stored at -20ºC.

Maximum drug dose was determined with serial dilution of drugs ranging from 20 µM to 80 nM. The media was changed twice over seven days with a measured drug dose. Only culture media was used in the control wells. After seven days, WST1 reagent was used to measure the cytotoxicity and viability of cells for different drug doses.

2.9 Nuclear protein extraction

EpiQuik nuclear extraction kit (Insight Biotechnology, UK) was used to isolate nuclear proteins to perform DNMT enzyme assay. $3x10^6$ cells were collected for protein extraction and washed with PBS twice to remove media. The pellets were stored in -80 for later use in the extraction step.

NE1 solution was diluted with distilled water at a 1:10 dilution (1X) on the ice, then DTT solution (dithiothreitol) and PIC (1000X Protease inhibitor cocktail) were added to ice-cold diluted NE1 (1X) at a 1:1000 dilution. DTT reduces disulfide bonds and stabilizes proteins as a reducing agent. Cell pellets were re-suspended in 200 µl of diluted NE1 solution (1X) in a micro-centrifuge vial, and samples were incubated on ice for 10 minutes. Then, samples were vortexed for 10 seconds and centrifuged for one minute at 12,000 rpm. The cytoplasmic extract was carefully separated from the nuclear pellet.

DTT solution and PIC were added to NE2 lysis buffer at a 1:1000 dilution. 40 µl of NE2 containing DTT and PIC working solution was added to the nuclear pellet. The extract was incubated on ice for 15 minutes with a vortex every 3 minutes (about 5 seconds) to increase nuclear protein extraction. After incubation, samples were centrifuged for 10 minutes at the highest speed, around ~14,000 rpm at 4°C, and the supernatant was transferred into a new labelled micro-centrifuge vial. Bradford protein assay was used to measure protein. The protein extract was aliquoted and quick-frozen on dry ice and stored at -85°C to -75°C until further use.

2.10 Bradford Assay

Bradford assay is useful to learn the amount of protein in unknown samples, so total protein concentrations were measured using this assay from the cell lysates. Seven dilutions of BSA (Bovine serum albumin) standard were prepared with a range of 100 µg/ml to 1500 µg/ml protein. Unknown protein samples were diluted to obtain the same range concentration as standard. Blank was set for three well, and 6 µl each of standard solution or unknown protein sample were added as a triplicate to an appropriately labelled well. Bradford reagent 94 µl was added to each well and mixed. Finally, the plate was incubated at room temperature (RT) for at least 5 minutes or maximum 1 hour. Absorbance was measured at OD 595 nm. The protein concentration was determined by comparing the unknown samples to the standard curve prepared using the protein standards (BSA) (***Fig 2.4***).

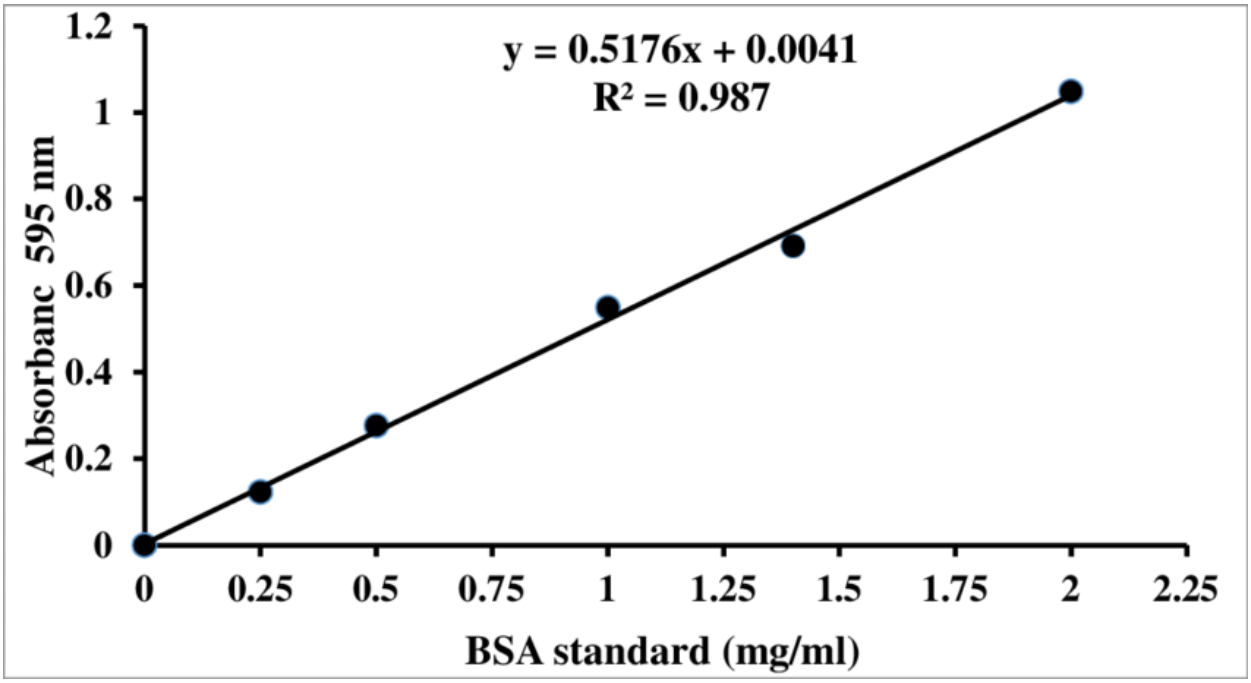

Figure 2.4. **The graph represents a standard curve for the Bradford Protein Assay**. BSA was prepared as a standard with different dilutions (X-axis), and absorbance was measured at = 595 nm. Each data point on Y-axis shows an average of three absorbance readings.

2.11 DNMT3B Activity Colorimetric Assay

EpiQuik™ DNA Methyltransferase 3B Activity/Inhibitors Assay Core Kit (Insight Biotechnology, UK) was used to analyse DNMT3B activity. De novo methyltransferase DNMT3B can methylate both unmethylated and hemimethylated DNA (Norvil et al., 2018). This assay is designed for screening DNMT3B activity or inhibition, and the strip wells are coated with the unique cytosine-rich DNA substrate. DNMT3B enzyme (not included) can methylate the DNA substrate by transferring a methyl group to cytosine. Afterwards, methylated DNA substrate can be detected with an anti-5mC antibody. The amount of methylated DNA is proportional to enzyme activity. This assay contains MT1 (10X Wash Buffer), MT2 (DNMT Assay Buffer), MT3 (Adomet, 8 mM), MT5 (Capture Antibody), MT6 (Detection Antibody), MT7 (Developing Solution), MT8 (Stop Solution), Enhancer Solution and 8-Well Substrate-Coated Strips.

First of all, the number of wells was determined for this assay and MT1 10X Wash Buffer was diluted in distilled water at a 1:10 ratio. Then, MT3 Adomet was diluted with MT2 Assay Buffer (at a 1:4 ratio) to 1.6 mM. Blank control wells were labelled, then 3 µl (10 µg) untreated control and 3 µl (10 µg) nanaomycin A treated samples were added to appropriate wells. After samples were prepared, 27 µl of MT2 and 3 µl of diluted MT3 were added to each well. The wells were mixed and covered with parafilm to avoid evaporation and incubated at 37°C for 90 minutes. After incubation, wells were aspirated and washed three times with 150 µl of 1X Wash Buffer. MT5 (Capture Antibody) was diluted (at a 1:1000 ratio) with 1X Wash Buffer. Diluted MT5 solution (50 µl) was added to each well, and the plate was incubated at room temperature for 60 minutes on an orbital shaker (50-100 rpm). After incubation with capture antibody, wells were aspirated and washed three times with 150 µl of 1X Wash Buffer. Detection antibody (MT6) was diluted (at a 1:1000 ratio) with 1X Wash Buffer. The diluted detection antibody (50 µl) was added to each strip well and incubated at room temperature for 30 minutes. After incubation with detection antibody, wells were aspirated and washed with 150 µl of 1X Wash Buffer four times. Enhancer Solution was also diluted (at a 1:5000 ratio) with 1X Wash Buffer. Diluted enhancer solution (50 µl) was added to each strip well and incubated at room temperature for 30 minutes. After incubation with enhancer solution, wells were aspirated and washed with 150 µl of 1X Wash Buffer four times. MT7 developing solution (100 µl) was added to each well and incubated at room temperature for 2-10 minutes in the dark. The colour change was monitored in the wells where a blue colour developed in the wells with DNMT3B enzyme activity. Finally, stop solution MT8 (50 µl) was added to each well to stop the reaction

when the colour in the no inhibitor control well turned light blue. After the stop solution, the colour changed to yellow and immediately absorbance was read on a microplate reader at 450 nm within 5-15 minutes. We calculated DNMT3B activity using the following formula:

$$\text{Dnmt activity (OD/h/}\mu\text{g)} = \frac{\text{(No inhibitor OD – blank OD)} \times 1000}{\text{Dnmt3B (ng) added in the reaction} \times \text{hour}^{*}}$$

2.12 DNMT1 Activity Colorimetric Assay

EpiQuik™ DNMT1 Activity/Inhibition Assay Ultra Kit (Colorimetric) (Insight Biotechnology, UK) was used to analyse DNMT1 activity after decitabine treatment. This assay is designed for screening DNMT1 activity or inhibition from nuclear extracts with an optimal range of 5-20 µg. A universal unique cytosine-rich DNA substrate is stably coated onto microplate wells in this assay. DNMT1 enzymes (not included) can methylate the DNA substrate by transferring a methyl group to cytosine from AdoMet. Afterwards, methylated DNA can be detected with an anti-5mC antibody (recombinant DNMT1). The amount of methylated DNA is proportional to enzyme activity. This assay contains MO1 (10X Wash Buffer), MO2 (DNMT1 Assay Buffer), MO3 (Adomet, 50X), MO4 (DNMT1 Enzyme Control, 50 µg/ml), MO5 (Capture Antibody, 1000 µg/ml), MO6 (Detection Antibody, 400 µg/ml), MO7 (Developer Solution), MO8 (Stop Solution), and 8-Well Assay Strips.

Firstly, the number of wells was determined for this assay and MO1 10X Wash Buffer was diluted in distilled water at a 1:10 ratio. MO3 Working Buffer was prepared by adding 2 µl of MO3 (Adomet) into 8 µl of MO2 (DNMT1 Assay Buffer). Blank control and positive control wells were labelled, then 3 µl (10 µg) untreated control, 3 µl (10 µg) decitabine treated samples, and 2 µl of MO4 positive control (DNMT1 Enzyme Control) were added to appropriate wells. After samples were prepared, 30 µl of this diluted MO3 was added to each well. The wells were mixed and covered with adhesive covering film to avoid evaporation and incubated at 37°C for 90 minutes. After incubation, the reaction solution was aspirated, and wells were washed with 150 µl of 1X MO1 Wash Buffer three times. MO5 (Capture Antibody) was diluted in 1X MO1 Wash Buffer at a ratio of 1:1000. Diluted MO5 solution (50 µl) was added to each well and covered with Parafilm M. The plate was incubated at room temperature for 60 minutes. After

incubation with capture antibody, wells were aspirated and washed three times with 150 µl of 1X Wash Buffer. MO6 (Detection Antibody) was diluted with 1X Wash Buffer at a ratio of 1:2000. 50 µl of diluted MO6 was added to each well, then carefully covered with Parafilm M and incubated at room temperature for 30 min. After incubation with detection antibody, wells were aspirated and washed with 150 µl of 1X Wash Buffer four times. Enhancer solution was diluted with 1X Wash Buffer at a ratio of 1:5000. Diluted enhancer solution (50 µl) was added to each well and covered with Parafilm M to incubate for a further 30 minutes. After incubation with enhancer solution, wells were aspirated and washed five times with 150 µl of 1X Wash Buffer. 100 µl of MO8 Developer Solution was added to each well and incubated at room temperature for 1 to 10 min at dark. The colour change was monitored in the sample and control wells. The blue colour was developed in the wells with DNMT1 enzyme activity. Finally, stop solution MU9 (50 µl) was added to each well to stop the reaction when the colour in the positive control wells turned medium blue. After the stop solution, the colour changed to yellow and immediately absorbance was read on a microplate reader at 450 nm within 2-15 minutes. We calculated DNMT1 activity using the following formula:

$$\textit{DNMT Activity (OD/h/mg)} = \frac{\textit{(Sample OD – Blank OD)}}{\textit{(Protein amount (µg)* x hour**)}} \textbf{ x } \textit{1000}$$

2.13 Telomerase Activity

The TRAPeze® RT Telomerase Detection Kit was used through the use of Amplifluor® primers to detect telomerase activity.

2.13.1 Principles of the Technique

The telomerase detection kit contains Amplifluor® primers, one buffer and two enzyme systems based on polymerase chain reaction (PCR). Amplifluor® primers have energy transfer moieties designed to emit a fluorescence signal only when incorporated into PCR products. The

net increase of fluorescence in the reaction vessel directly shows the amount of amplified DNA produced in the PCR reaction. This protocol includes two reaction steps. Firstly, the telomerase enzyme in the sample adds some telomeric repeats onto the 3' end of a substrate oligonucleotide (TS). Then in the second step, the Taq polymerase enzyme amplifies these extended products using PCR with the TS and fluorescein-labelled Amplifluor® RP (reverse) primers. These reactions produce a fluorescent ladder with six base increments starting at 61 nucleotides: 61, 67, 73, 79, etc. Generated fluorescence emission is correlated directly proportional to the number of TRAP (Telomeric repeat amplification protocol) products and telomerase activity (***Fig 2.5***).

Telomerase positive control cells, minus telomerase control template TSR8, TSK and heat-treated telomerase negative control templates (-85°C for 20 minutes to inactivate the enzyme) were used as a control in the assay. TSR8 quantitation control provides a method for quantitating telomerase activity relative to TSR8 product amplification by generating a standard curve. TSK control template is an artificial PCR control to assess PCR inhibitor status and as a positive control for PCR amplification.

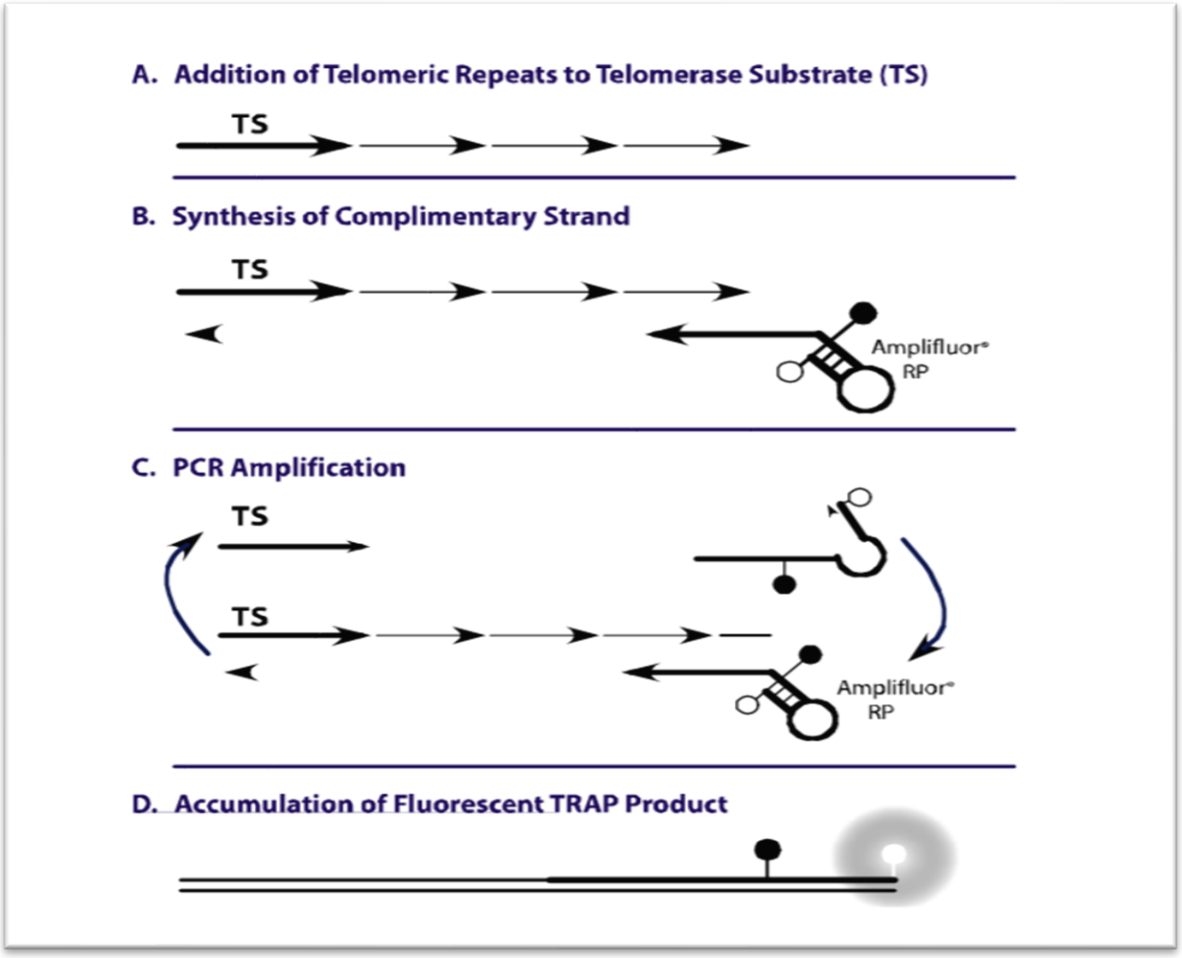

***Figure 2.5*. The principle of telomerase detection kit.** Short arrows on the line show telomere repeats (GGTTAG). The small filled circles symbolize the quencher molecule while the open circles represent the fluorophore (energy donor) (TRAPEZE® RT Telomerase Detection Kit/ S7710)

2.13.2 Extract Preparation

Pellets of cells were washed once with PBS, re-pelleted, and all PBS carefully removed. After removal of PBS, the cell pellet can be stored at -85°C to -75°C or kept on dry ice. Telomerase in frozen cells or tissues is stable for approximately one year at -85°C to -75°C. The cells or tissue should be resuspended in CHAPS Lysis Buffer (3-((3-cholamidopropyl) dimethylammonio)-1-propanesulfonate) when samples were thawed for extraction. CHAPS lysing buffer contains 10 mM Tris-HCl, pH 7.5, 1 mM MgCl2, 1 mM EGTA, 0.1 mM benzamidine, 5 mM β-mercaptoethanol, 0.5% 3-[3-cholamidopropyl-dimethyl-amino]-1-propane-sulfonate, and 10% glycerol.

Cell pellets were resuspended in 200 µL of CHAPS Lysis Buffer/10^5-10^6 cells. Also, 200 µL of CHAPS Lysis Buffer was used to prepare the positive control cell extract (provided in TRAP kit). The suspension was incubated on ice for 30 minutes. Samples were spun in a microcentrifuge at 12,000 x g for 20 minutes at 4°C. 160 µL of the supernatant was transferred into a fresh tube, and a Bradford assay was used to determine the protein concentration (10-750 ng/µL). The remaining extract was aliquoted, quick-frozen on dry ice, and stored at -85°C to -75°C. The extract is stable for at least 12 months when stored at -85°C to -75°C.

2.13.3 Preparation of Controls, PCR Reactions and TRAP Amplification

Different reaction controls were used in this protocol: Control Template TSR8, Telomerase Positive Extract Control, Minus Telomerase control, No Template Control (NTC), and Heat Treated sample control.

Four dilutions of Control Template TSR8 were provided within the kit as 20 amoles/µL (attomolar/µL). Next, 1:10 serial dilutions of the stock concentration were prepared with CHAPS Lysis Buffer to obtain TSR8 concentrations of 2 amoles/µL, 0.2 amoles/µL and 0.02 amoles/µL. TSR8 standard curves provide a method for quantitating telomerase activity relative to TSR8 product amplification (***Table 2-3***).

Table 2-3. **Dilution of Control Template TSR8**

TSR8 Concentration	Volume of TSR8 Stock	Volume of Diluent CHAPS Lysis Buffer
1. 20 amoles/µL	No dilution	-
2. 2 amoles/µL	2 µL of #1	18 µL
3. 0.2 amoles/µL	2 µL of #2	18 µL
4. 0.02 amoles/ µl	2 µL of #3	18 µL

Telomerase-positive cell extract was prepared using 200 µL of CHAPS Lysis Buffer and the control cell pellet (10^6 cells) provided in the kit. The aliquoted lysate was stored at -75°C to -85°C. Before the experiment, stock aliquots were diluted at 1:10 with CHAPS Lysis buffer and 2 µL (300 ng) positive control was used for each set of TRAPeze® RT Telomerase Assays.

Assays were performed with 2 µL CHAPS Lysis Buffer substituted for the cell/tissue extract as a minus telomerase control. At the same time, TRAPeze® RT assay was run with 2 µL of Nuclease-Free Water substituted for the cell/tissue extract as a No Template Control (NTC). Due to the design of this assay, a certain level of primer dimer formation inevitably occurs with the Amplifluor primers in the absence of telomerase activity. This NTC occurs below the lowest level of detection of the assay and will not affect data analysis when sample activity is detected above this lowest limit. TSK Normalization Standard Curve was generated as an optional feature of this analysis to assess PCR performance and inhibitors in the cell or tissue extract samples (***Table 2-4***).

Table 2-4. **Assay design for TRAPeze® RT Telomerase Detection**

	1	2	3	4	5	6	7	8	9	10	11	12
A	TSR8 40 amoles			Sample 1			Sample 1—Heat Treated			Sample 1		
B	TSR8 4 amoles			Sample 2			Sample 2—Heat Treated			Sample 2		
C	TSR8 0.4 amoles			Sample 3			Sample 3—Heat Treated			Sample 3		
D	TSR8 0.04 amoles			Sample 4			Sample 4—Heat Treated			Sample 4		
E	Positive Extract (1000 cells)			Sample 5			Sample 5—Heat Treated			Sample 5		
F	Minus Telomerase Control			Sample 6			Sample 6—Heat Treated			Sample 6		
G	NTC			Sample 7			Sample 7—Heat Treated			Sample 7		
H				Sample 8			Sample 8—Heat Treated			Sample 8		
	5X TRAPEZE® RT Reaction Mix			5X TRAPEZE® RT Reaction Mix			5X TRAPEZE® RT Reaction Mix			5X TRAPEZE® Control Reaction Mix		

A1 – D3: 4 TSR8 quantitation controls
E1 – E3: **1000 cell equivalents** of telomerase positive extract control
F1 – F3: Minus telomerase control
G1 – G3: No Template Control (NTC)
A4 – H9: 8 experimental samples and heat-treated controls
A10 – H12: 8 experimental samples with TSK template and Control Reaction Mix (Optional)

"Master Mix" was prepared by mixing the below-mentioned reagents except for the extract. Thaw all reagents, mix well and store on ice. A mix containing Taq polymerase was aliquoted 23.0 µL for each well of PCR Plate used for your real-time instrument. Experimental samples, heat-inactivated extracts or controls (300 ng) were added to the designated well. Heat-inactivated controls 10 µL of each sample extract were incubated at 85°C for 20 minutes (***Table 2-5***).

Table 2-5. **Master mix preparation for samples**

Required Controls and Samples	
5X TRAPEZE® RT Reaction Mix*	5.0 µL
Taq Polymerase (5 units/µL)	0.4 µL
Nuclease Free Water	17.6 µL
TSR8 dilutions, Positive extract control, Telomerase Negative, NTC, Experimental Samples +/- heat treatment)	2.0 µL
TOTAL VOLUME	**25 µL**

Optional Amplification	
RT Control Reaction Mix	5.0 µL
Taq Polymerase (5	0.4 µL
Nuclease Free Water	15.6 µL
Samples	2.0 µL
TSK Template	2.0 µL
TOTAL VOLUME	**25 µL**

2.13.4 PCR Amplification

PCR plate was placed in the thermocycler block. The real-time experiment was set up to include the following PCR parameters (***Table 2-6***). The melting curve has been added after PCR amplification step (***Fig 2.6***).

***Table 2-6*. PCR amplification parameters and example data for generation of the TSR8 standard curves.** (*) Temperature and stage where the Real-time fluorescent data should be collected.

PCR Amplification Parameters		
30°C	30 min	1 cycle
95°C	2.0 min	1 cycle
45 cycles		
94°C	15 sec	
59°C	60 sec	
*45°C	10 sec	

TSR8 Dilutions	Copies TSR8	Log	Experimental Avg. Ct
40 amoles	24,088,000	7.38	20.4
4 amoles	2,408,800	6.38	23.3
0.4 amoles	240,880	5.38	26.8
0.04 amoles	24,080	4.38	30.3

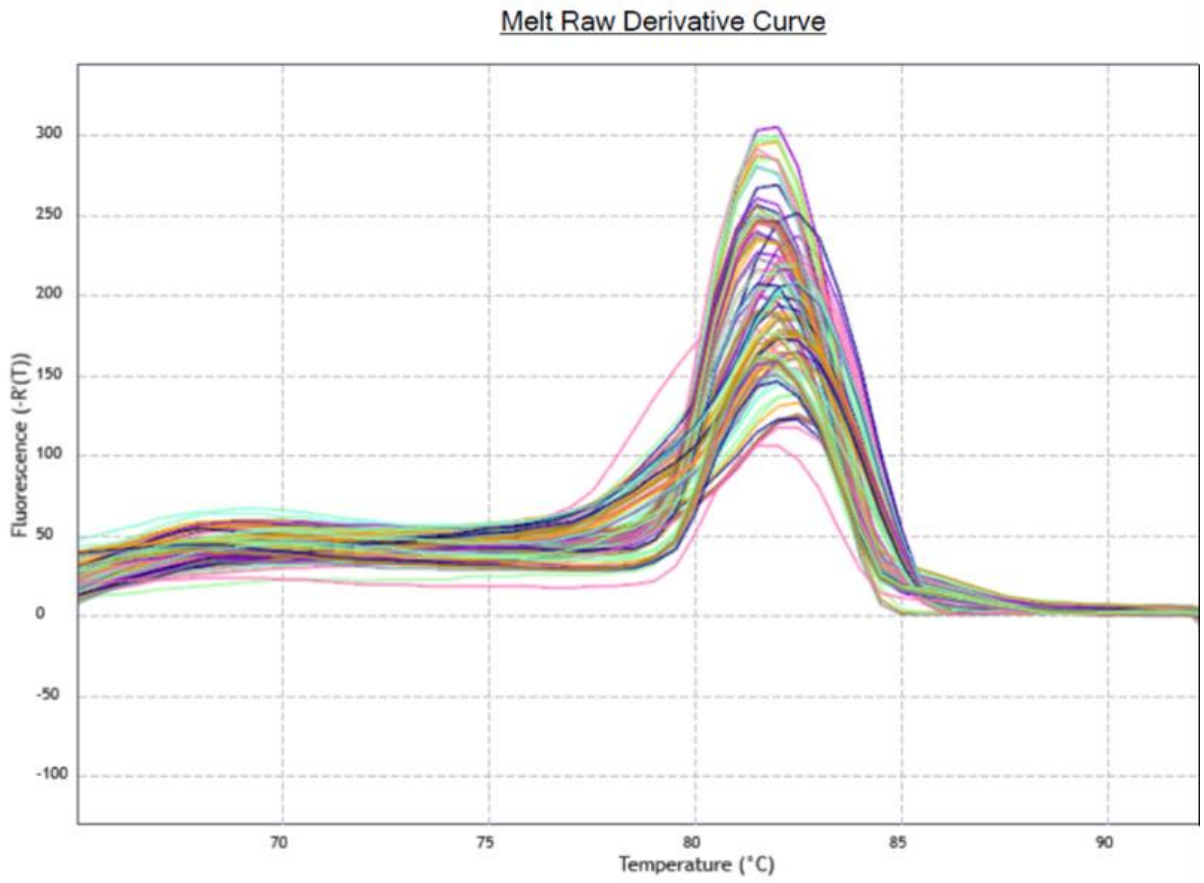

***Figure 2.6.* The melting curve for the qRT-PCR step of the TRAP assay to confirm specific PCR products in amplification.**

2.13.5 Data Analysis

The standard curve of the TSR8 template was used to quantitate telomerase activity via fluorometric detection. The $\log_{10}$ of the amoles per well for each reaction was calculated utilizing TSR8 standards.

2.14 Telomere Length Quantification with qPCR Assay

Absolute Human Telomere Length Quantification qPCR assay measures directly the average telomere length of the human cell population. Kit contains two main primer sets: telomere primer set amplifies telomere repeats, and single-copy reference (SCR) primer set recognizes a 100 bp-long region on human chromosome 17 and amplifies this sequence. The reference genomic DNA sample serves as a standard for data normalization with known telomere length and calculating the telomere length of target samples.

2.14.1 Cell pellet preparation

The cell suspensions were centrifuged at 3000 x g for 3 minutes with 1ml culture medium, the supernatant removed, and the pellet was washed twice with PBS by centrifugation. Then the supernatant was removed, and pellets were stored at -20^{o}C.

2.14.2 DNA Extraction

DNeasy Blood and Tissue kit (Qiagen) were used for DNA extraction. Cells were centrifuged for 3 min at 1300 rpm and resuspended in 200 µl PBS with 20 µl proteinase. 200 µl Buffer AL was added to samples and then mixed thoroughly by vortexing and incubated at 56°C for 10 min for lysing. After incubation, 200 µl ethanol (96–100%) was added and mixed thoroughly by vortexing. The mixture was pipetted and then transferred into a DNeasy Mini spin column placed in a 2 ml collection tube and centrifuged at ≥8000 rpm for 1 min. The flow-through and collection tube was discarded. Total DNA was attached to the DNeasy column membrane, and then the spin column was placed in a new 2 ml collection tube. 500 µl Buffer AW1 was added to wash and centrifuged for 1 min at ≥8000 rpm. The flow-through and

collection tube was again discarded. The spin column was placed in a new 2 ml collection tube. For the second wash, 500 µl Buffer AW2 was added and centrifuged for 3 min at 14,000 rpm. The spin column was transferred into a new 1.5 ml microcentrifuge tube. DNA was eluted by adding 200 µl Buffer AE to the centre of the spin column membrane and incubated for 1 min at room temperature (15–25°C). The spin column was centrifuged for 1 min at ≥8000 rpm in the final step.

2.14.3 Human Telomere Length Quantification PCR Protocol

Before use, Telomere primer set, Single-copy reference (SCR) primer set vials were warmed up at room temperature, and then the vials were centrifuged at 1,500x g for 1 minute. 200 µl nuclease-free H_2O was added to the telomere primer set to make a telomere primer stock solution and aliquoted as needed. Stock primers were stored at -20°C in the freezer. Next, a nuclease-free H_2O was added 200 µl to the SCR primer set to make an SCR primer stock solution and aliquoted again. Stock SCR primer was stored at -20°C in the freezer.

Two qPCR reactions were prepared for the reference genomic DNA sample, one with telomere primer stock solution and one with SCR primer stock solution. 20 µl qPCR reactions which include 1 µl Reference genomic DNA sample, 2 µl Primer stock solution (Telomere or SCR), 10 µ l2x qPCR master mix and 7 µl nuclease-free H_2O were prepared for one well.

Two separate qPCR reactions were prepared for each genomic DNA sample, one with telomere primer stock solution and one with SCR primer stock solution. 0.5 – 5 ng Genomic DNA template, 2 µl Primer stock solution (Telomere or SCR), 10 µl 2x qPCR master mix and Nuclease-free H2O (variable), total 20 µl qPCR reactions were prepared for one well.

Finally, the qPCR plate was sealed, and the qPCR program was set up as shown below, then data were analysed (***Table 2-7***). The melting curve was performed for each PCR, and gel electrophoresis showed the separation of the qPCR telomere product (***Fig 2.7***).

Table 2-7. **PCR setup with optimal annealing temperature**

Step	Temperature	Time	Number of cycles
Initial denaturation	95°C	10 min	1
Denaturation	95°C	20 sec	32
Annealing	52°C	20 sec	
Extension	72°C	45 sec	
Data acquisition	Plate read		
Optional	*Melting curve analysis*		1
Hold	20°C	Indefinite	1

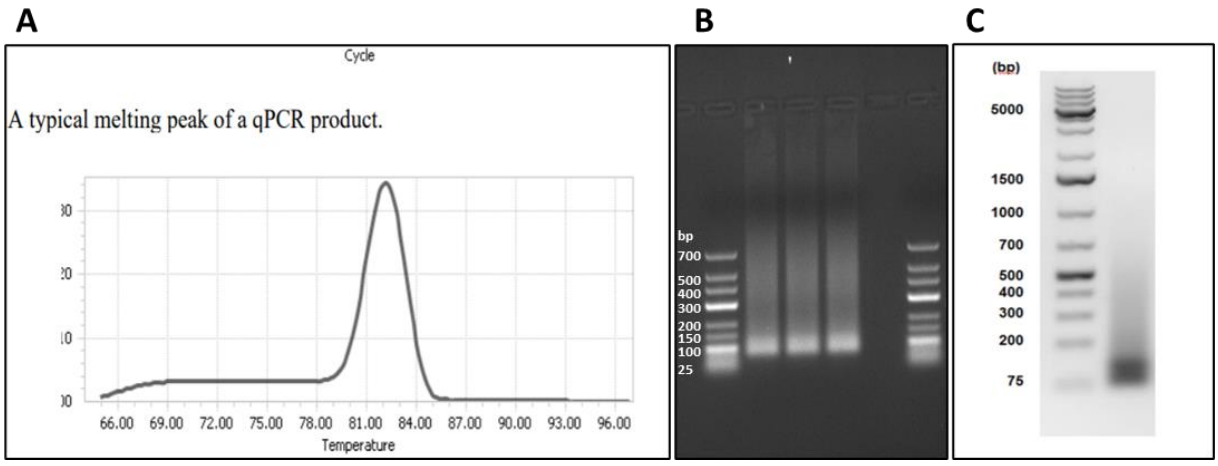

Figure 2.7. **Validation of PCR amplification with melting curve and gel electrophoresis**. The image represents the melt curve for a qRT-PCR step of telomere assay to confirm specific PCR products in amplification **(A)**. Separation of qPCR telomere product by agarose gel electrophoresis from our experiments **(B)**. A smeared band is observed as expected. Separation of qPCR telomere product was shown by agarose gel electrophoresis from manufacturer datasheet **(C)**.

2.14.4 Data Analysis

Data from qRT-PCR were analysed by the following calculations for this experiment:

ΔCq (TEL) indicates the quantification cycle number difference of telomere between the target and the reference genomic DNA samples. ΔCq (TEL) = Cq (TEL, target sample) - Cq (TEL, reference sample). Noteworthy that the value of ΔCq (TEL) can be positive, 0, or negative.

For single copy reference (SCR), ΔCq (SCR) is the quantification cycle number difference of reference between the target and the reference genomic DNA samples. ΔCq (SCR) = Cq (SCR, target sample) - Cq (SCR, reference sample). Noteworthy that the value of ΔCq (SCR) can be positive, 0, or negative.

$\Delta\Delta Cq = \Delta Cq\ (TEL) - \Delta Cq\ (SCR)$

Relative telomere length of the target sample to the reference sample (fold) = $2^{-\Delta\Delta Cq}$

The total telomere length of the target sample = Reference sample telomere length x $2^{-\Delta\Delta Cq}$

There are 92 chromosome ends in one diploid cell. Therefore, the results can be divided into 92 to calculate the average telomere length per chromosome end.

2.14.5 Statistical analysis

The experimental data and graphical displaying of data were performed using statistical software GraphPad Prism 8. A comparison among the groups was assessed using a two-way analysis of variance (ANOVA). The threshold for which statistically significant was accepted as $p<0.05$. Data are presented as mean ± SD, and each result represents a replicate of 3 independent experiments (n=3).

2.15 Gene expression analysis

2.15.1 RNA extraction

Cells were lysed with 350µl lysis buffer RLT, supplemented with 10µl/ml β mercaptoethanol. Qiashredder spin column (Qiagen) was used for 2 minutes of centrifugation at 12000 rpm (2×10^6 cells) to disrupt cells and increase RNA yield. After homogenisation, the lysate can be stored at -80°C for subsequent RNA extraction. RNA was extracted following the

manufacturer's protocol using the RNeasy® Mini Kit (Qiagen). Frozen lysates were defrosted on ice, and one volume of 70% ethanol was added. The final solution passed through an RNeasy mini spin column placed in a 2ml collection tube to allow total RNA to bind to the column membrane and centrifuged at 12000 rpm for 15 seconds before the flow-through was discarded. Next, the column membrane was washed twice with 700µl of RW1 washing buffer and then with 500µl of RPE washing buffer by centrifugation at 12000 rpm for 15 seconds and 2 minutes, respectively. The last step was repeated by centrifuging the column again at 12000 rpm for 1 minute to remove any residual fluid.

Then the spin column was transferred into a new 2ml microcentrifuge tube, and the membrane was soaked with 30µl RNeasy-free water for two minutes before being centrifuged at 12000 rpm for 1 minute. This step was repeated to increase the RNA concentration by transferring the RNA from the microcentrifuge tube back onto the RNase spin column and centrifuged again. The total RNA concentration was quantified using a NanoDropTM 2000/2000c Spectrophotometer (Thermo Scientific, USA) and stored at -20°C until required.

2.15.2 Reverse transcriptase-polymerase chain reaction (RT-PCR)

Quantitative real-time polymerase chain reaction (qRT-PCR) is a sensitive molecular technique combining reverse transcription of RNA into DNA (complementary cDNA) and amplification of specific DNA targets using PCR. RT-PCR is used to detect and compare mRNA expression levels from small samples. This technique is called real-time PCR because it monitors the amplification reaction using fluorescence. The fluorescent signal represents the relative abundance of the PCR product determined by comparing the cycle number. SYBR Green generates a fluorescent signal when bound to double-stranded DNA during amplification. A melting curve (dissociation curve) analysis is used to check real-time PCR reactions for primer-dimers and ensure reaction specificity during assay optimisation. Double-stranded DNA dissociates into a single-stranded DNA as the temperature of the reaction is raised, and these changes generate a melting curve with incorporated dye molecules. The specific PCR product of the reaction has a higher melting temperature while primer-dimers, non-specific or mismatched sequences generally have lower melting temperatures. Melting curves analysis is used to check real-time PCR reactions for primer-dimers and ensure reaction specificity during assay optimisation.

2.15.3 Primer design

PCR primers were designed to be complementary to template DNA sequences using several databases such as GenBank (http://www.ncbi.nlm.nih.gov/), NCBI Primer-BLAST, IDT (Integrated DNA technologies), OligoCalc and Ensembl. Next, primers were ordered from Sigma, including TERT, Nestin, AFP, Brachyury (TBXT), KDR, DNMT3A, DNMT3B and HDACs gene expression. Primers were designed as approximately 18 - 25 nucleotides in length, possess 40 - 60% GC content, and lack significant secondary structures. PCR amplicon length was chosen between 100 to 500 bp. Regions of complementarity at the 3' end of primers were minimised to reduce the potential for the formation of primer dimers. Also, both primer melting temperature (TM) differences were closely matched and carefully checked to be no more than 5°C. Primer sequences, TM temperature and product sizes are listed in (***Table 2-8)*.**

Table 2-8. **Primer sequences used in qRT-PCR**

Primers	**Sequence**		**Product size**	**TM (°C)**
TERT	F	CTTGCGGAAGACAGTGGTGAAC	178	53
	R	GAGACTGGCTCTGATGGAGGT		
DNMT1	F	GTGGGGGACTGTGTCTCTGT	204	56
	R	TGAAAGCTGCATGTCCTCACATTC		
DNMT3A	F	CAGCTTCCACGTTGCCTTCTG	69	56
	R	CATCTGCAAGCTGTCTCCCTTT		
DNMT3B	F	GACTCGAAGACGCACAGCTG	98	56
	R	CTCGGTCTTTGCCGTTGTTATAG		
HDAC1	F	ACTGCTAAAGTATCACCAGAGGG	233	54
	R	TGGCCTCATAGGACTCGTCA		
HDAC2	F	CATAGAATCCGCATGACCCATAAC	389	52
	R	TCAAGGATGGCAAGCACAATATCA		
GAPDH	F	GAGTCAACGGATTTGGTCGTATTG	220	59
	R	CGCTCCTGGAAGATGGTGATGG		
KDR	F	GTGGTCTCTCTGGTTGTGTATG	235	55
	R	CCTCCACACTTCTCCATTCTTC		
AFP	F	CGAGGGAGCGGCTGACATTATTAT	339	58
	R	TGGCCTTGGCAGCATTTCTCC		
	F	ATGAGCCTCGAATCCACATAGT		

TBXT	R	TCCTCGTTCTGATAAGCAGTCA	109	55
NESTIN	F	GCAGCGTTGGAACAGAGGTTGG	389	59
	R	TGGCACAGGTGTCTCAAGGGTAG		

RT-PCR reaction was performed on samples using the QuantiFast SYBR Green RT-PCR Kit (Qiagen). Firstly, 2x QuantiFast SYBR Green RT-PCR Master Mix containing QuantiFast RT Mix, template RNA, primers, and RNase-free water were thawed and placed on ice. The master mix was prepared according to ***Table 2-9,*** and every experiment included a negative control (without template RNA).

Table 2-9. **Master mix components and their volumes**

Component of Master mix	**Volume/sample**
2x QuantiFast SYBR Green RT-PCR Master Mix	6.25µl
Forward primer (1µM)	1µl
Reverse primer (1µM)	1µl
RNase free water	2.125µl
Template RNA (25ng)	2µl
QuantiFast RT Mix	0.125µl
TOTAL	**12.5µl**

The master mix was mixed thoroughly and dispensed in appropriate volumes into PCR tubes. Then template RNA was added 50ng/reaction to the PCR tubes. Reverse transcription reactions were performed at 50°C for 30 min just 1 cycle. The PCR amplification segment was started with an initial heating step at 95°C for 15 min to activate HotStarTaq DNA Polymerase. Then cycling step was performed 1 min 94°C denaturation, 1 min 50-60°C annealing and 1 min 72°C extension. The cycle number was around 25-40, and the final extension was run at 10 min 72°C.

2.15.4 Agarose gel electrophoresis

Following RT-PCR amplification, specific PCR products size were validated by agarose gel electrophoresis**.** To prepare the gel**,** 4 g of agarose powder was dissolved in 200ml 1x TAE buffer (Tris-acetate-EDTA), and 2% agarose gel containing 5 µl ethidium bromide was prepared and kept at room temperature for 45 minutes to cool down. Ethidium bromide is a fluorescent dye that can bind to double-stranded DNA and emit light in the visible spectrum to visualise DNA in gels. After the gel cooled, it was placed in an electrophoresis tank containing 1 x TAE buffer (Sigma), which completely covered the gel. Before loading, each sample was mixed with 1 µl gel loading buffer and carefully loaded into the gel wells. Then, the wide range DNA marker (Sigma) was loaded into the first wells to allow the determination of fragment size. All gel was run at 100 V for one hour. Gel images were captured with Syngene Genesnap software (***Fig 2.8***).

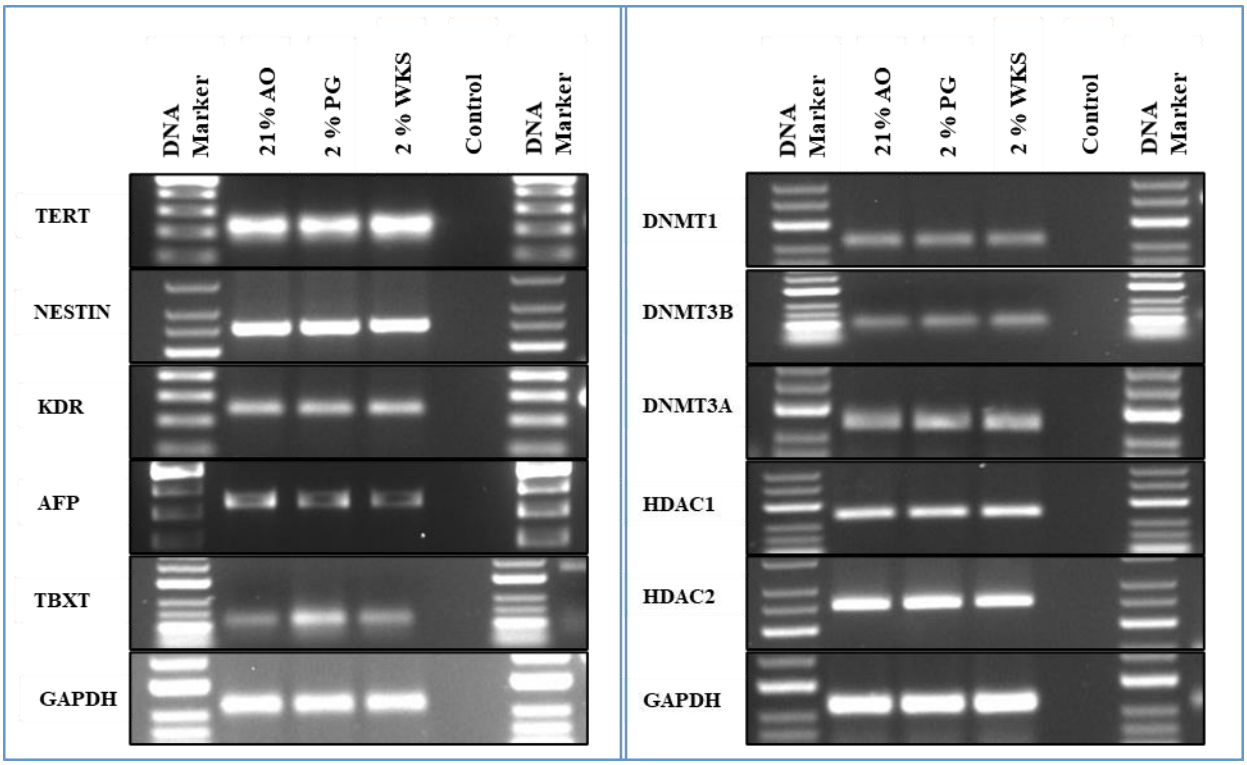

Figure 2.8. **PCR products in agarose gel**. 2% agarose gel validated specific PCR products from TERT, Nestin, KDR, AFP, TBXT, DNMTs, HDACs, and housekeeping gene GAPDH across three different oxygen tensions. The first and last wells indicate the DNA ladder. Gel images were captured with Syngene Genesnap software.

2.16 Pyrosequencing

Pyrosequencing is a DNA sequencing technique that can detect methylation levels of CpG sites within genes of interest. It is based on sequencing by synthesis. When DNA polymerase elongates the chain, the inorganic pyrophosphate (PPi) is released as a result of nucleotide incorporation by a polymerase. Each released pyrophosphate triggers a series of reactions that generates a detectable light. The energy for this reaction is supplied via the conversion of pyrophosphate to adenosine triphosphate (ATP). The light is produced as the result of luciferin oxidation by luciferase. The amount of light is proportional to the number of bases incorporated. Eventually, the pyrosequencing machine captures this light signal and plots it on a program. The quantitative results are generated as percentage values from the ratio of methylated to unmethylated cytosine residues within the CpG region (***Fig 2.9***).

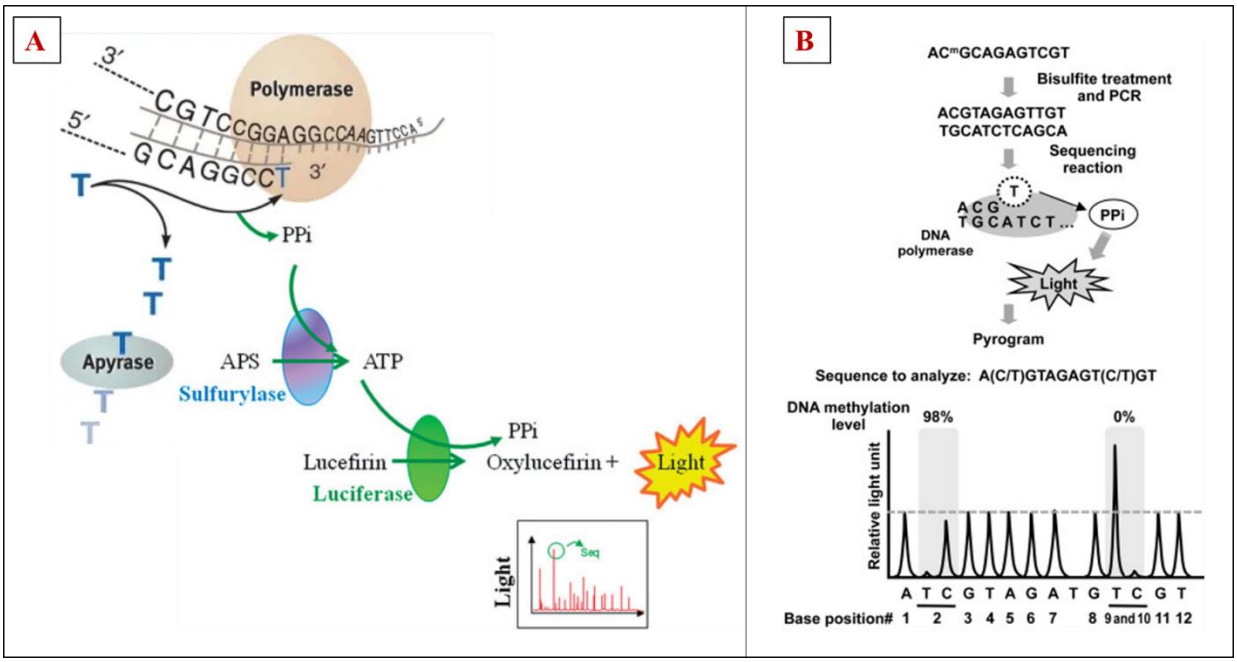

Figure 2.9. **The principle of pyrosequencing. (A)** This figure represents the chemical reactions during the sequencing. First, the sequencing primer is allowed to anneal with the DNA template in provided enzyme mixture of four enzymes (DNA polymerase, ATP sulfurylase, luciferase, and apyrase) and substrates (adenosine 5′-phosphosulfate (APS) and luciferin). Then, individual dNTPs are added to the reaction sequentially in a fixed order, programmed before the run. The incorporation of a nucleotide into the template is catalysed by DNA polymerase, and pyrophosphate (PPi) is released and converted to ATP by the sulfurylase enzyme in the presence of adenosine 5´-phosphosulfate substrate (APS). The luciferase enzyme

utilizes ATP to oxidize luciferin into oxyluciferin that produces light. This light is recorded by a charge-coupled device (CCD) camera in the form of a peak. The apyrase enzyme degrades any unutilized nucleotides, so it is important to reduce the background noise. **(B)** Bisulfite converted DNA was used for PCR amplification with one of the biotinylated primers. Streptavidin-coated sepharose beads capture the PCR amplicon containing a biotinylated end. The purified biotinylated strand is used as a template for pyrosequencing. A pyrosequencing primer (the third primer) is added to the mixture containing the purified biotinylated PCR strand, and pyrosequencing is carried out. Methylation in the PCR product is investigated by measuring pyrophosphate released at individual sites. The pyrophosphate is then converted into a light signal, and a program captures this light signal.

Bisulfite conversion is a common technique used for pyrosequencing. First, denatured genomic DNA is treated with sodium bisulfite, which leads to the deamination of unmethylated cytosines into uracils while methylated cytosines remain unchanged. Bisulfite based method is a common approach used to study DNA methylation and help in preparing genomic DNA for gene-specific DNA methylation analysis. Once DNA is converted, the methylation profile of the DNA can be determined by PCR amplification followed by DNA sequencing. In this thesis, we used sodium bisulphite to modify genomic DNA and pyrosequencing methods to measure methylation percentage at a specific gene (***Fig 2.10***).

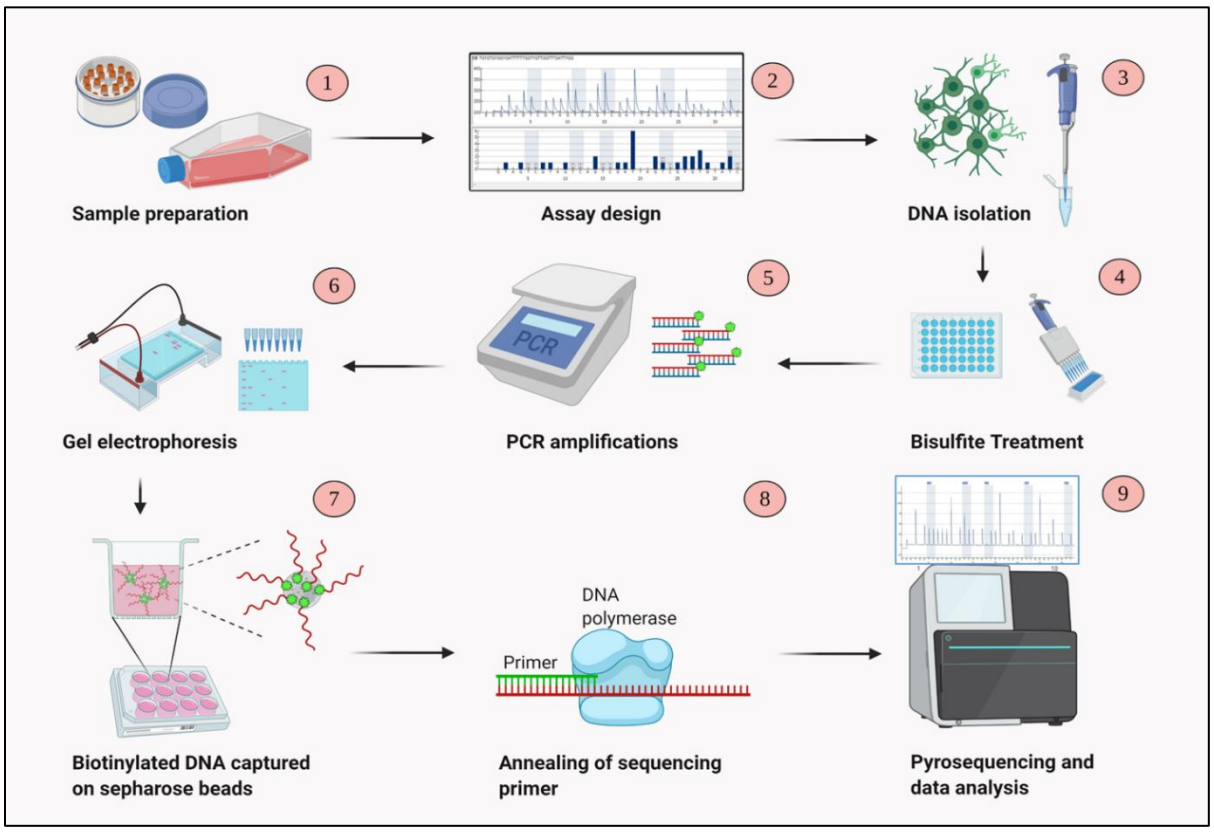

Figure 2.10. **An overview of the steps involved in DNA methylation analysis using pyrosequencing.** First, samples are prepared, and an assay is designed for each primer set. After DNA isolation from samples, bisulfite conversion of genomic DNA is performed for DNA methylation analysis. PCR amplifications are performed for target regions and checked with gel electrophoresis. Biotin labelled PCR amplicons are captured on sepharose beads. Then, PCR amplicons are used as a template for pyrosequencing. The sequencing data were analysed using the PyroMark software.

2.16.1 Bisulfite treatment of DNA

DNA denaturation and bisulfite conversion were performed using EZ DNA Methylation-Gold™ Kit (Zymo Research) in one step. Genomic DNA was isolated from cells as described in ***Section 2.14.2*** and 500ng DNA extractions were diluted in 20µl of DNases/RNase free. CT Conversion Reagent was prepared by adding 900 µl water, 300 µl M-Dilution Buffer, and 50 µl M-Dissolving Buffer per tube and it was shaken for 15 minutes to dissolve. DNA samples were transferred in a PCR tube, and 130 µl of the CT Conversion Reagent was added to each

sample. The samples were mixed by pipetting up and down. Then the thermal cycler ran at 98°C for 10 minutes and 64°C for 2.5 hours. After that, samples were stored at 4°C for up to 20 hours. After the conversion step, DNA product was mixed with 600µl M-Binding Buffer and transferred to a Zymo-Spin Column, then centrifuged at 13000 g for 30 seconds. The eluate was discarded, and 100 µl M-Wash Buffer was added to the column centrifuged at 13000 g for 30 seconds. Next, 200µl M-Desulphonation Buffer was added to the column followed by incubation at room temperature for 15-20 minutes. Following on from centrifugation at 13000 g for 30 seconds and 200 µl of M-Wash Buffer to the column was added, then centrifuged at 13000 g for 30 seconds. The flow-through was discarded, and this washing step was repeated one more time. New 1.5 ml microcentrifuge tubes were labelled, and the spin columns were transferred to microcentrifuge tubes. In the last step, 21µl M-Elution Buffer was added directly to the column matrix and centrifuged for 30 seconds at full speed to elute the DNA. The final product was quantified by spectrophotometry (single-stranded DNA measurements ssDNA) and stored at -20°C in sterile tubes for future use.

2.16.2 PCR Reaction for Converted DNA

Bisulphite converted DNA (2µl) was used as a template in PCR reactions. Primers were designed from the Pyrosequencing PyroMark software and supplied by Biomers (Germany). One primer was biotinylated at the 5'end for use as a template in the Pyrosequencing reaction. Primer sequences, locations and expected PCR product size are listed in ***Table 2-10*.**

Table 2-10. **TERT gene PCR primers for pyrosequencing.** Forward, reverse and sequencing primers are shown in this table. Also, CpG site locations, product size, and annealing temperature are listed.

CpG Locations	Annealing Temp (°C)	Forward primer	Reverse primer	Sequencing primer	Product size
Promoter region I (-	60°C	5'-gga agt aga aga tta tgt tgg agt aat t-3'	5'-aac aca cta act aca ccc ata at-3'	5'-aga tta tgt tgg agt aat taa tat t-3'	157 bp

1456, -1495 from TSS)					
Promoter region II (-674, -717 from TSS)	60°C	5'-aag ggt ggg aaa tgg agt ta-3'	5'-ccc caa att acc ctc cac cct ata c-3'	5'-ggg aaa tgg agt tag g-3'	157 bp
Promoter region III (-315, -348 from TSS)	59°C	5`tat gat gtg gag gtt ttg gga ata g -3`	5`acc taa aaa caa ccc taa atc t -3`	5`agg ttt tgg gaa tag g -3`	84 bp
Promoter region IV (-122, -171 from TSS)	59°C	5'-gga agg tga agg ggt agg a-3'	5'-tcc caa aac ctc cac atc ata -3	5'-ttt gtg tta gag aat tta ttg gga g-3	287 bp
Promoter region V (-67 -106 from TSS)	59°C	5'-gga agg tga agg ggt agg a-3'	5'-cct ccc tcc aat tac ccc aca ac-3'	5'-cca aac cca act ccc aat aaa t-3'	261 bp

PyroMark PCR Kit (Qiagen) was used to amplify samples in 25µl volumes containing 12.5µl 2x PyroMark PCR Master Mix, 2.5µl 10x CoralLoad® Concentrate, 5µl 5x Q-solution, 1µl $MgCI_2$ 25mM, 1µl RNase free water, 1µl of each forward and reverse primers. Initial DNA polymerase activation was performed with one cycle of 95°C for 15 minutes. Then the denaturation step was 94°C for 1 minute after touch-down cycling was used for the first 14 cycles, where the temperature was reduced by 0.5°C in each successive cycle. Next, 35 cycles of 95°C for 45 seconds, annealing at 55–63°C for 45 seconds and elongation at 72°C for 30 seconds followed by a final elongation step with one cycle at 72°C for 5 minutes (***Fig 2.11***). Successful PCR amplification was confirmed with gel electrophoresis through a 2% agarose gel as described in ***Section 2.15.4.***

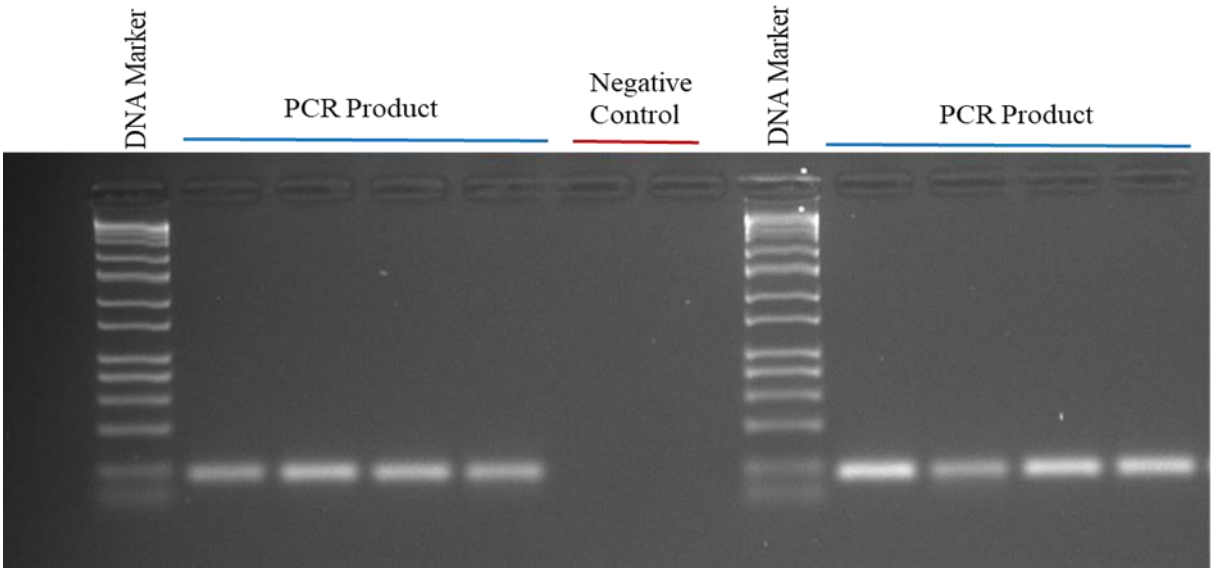

Figure 2.11. **Example of PCR products of promoter region II (-674, -717 from TSS) on a 2% agarose gel**. Bisulfite converted DNA was used for PCR amplification. Specific amplification was determined by the presence of correct size and single band products. Negative control indicates no template DNA.

2.16.3 Pyrosequencing

PCR products were used for the next step of pyrosequencing to determine the percentage of methylation within genes of interest. Biotin-labelled PCR amplicons were captured by mixing PCR products with streptavidin-sepharose beads (GE Healthcare). 40µl of Binding buffer (Qiagen), 29 µl of molecular grade water and 1µl of streptavidin-sepharose beads were added to each sample and incubated on a rotary shaker for 15 minutes to allow streptavidin beads to bind biotin-labelled strand. During the mixing step, 25 µl Annealing buffer (Qiagen) and 0.125 µl of the specific sequencing primer mix were added to each Q24 pyrosequencing plate. PCR samples were removed from the shaker, and beads with biotin labelled PCR amplicons were captured by the filter probes by lowering the Vacuum Prep Tool into the PCR tubes. Vacuum Prep Tool (with the captured sepharose beads) was placed into 70% ethanol solution to wash filters for 10 seconds and then put into denaturation solution (NaOH) for another 10 seconds to denature PCR product. After denaturation, a washing buffer was used for 18 seconds to purify the final biotinylated strands, and the vacuum pump was switched off. The Vacuum Prep Tool was carefully placed into the wells and shook for a few seconds while the beads were released

into the Q24 pyrosequencing plate filled with annealing mix. The plate was heated at 80 °C for 5 minutes on heat blocks and then incubated at room temperature to cool down for 3 minutes, where the sequencing primer anneals to the target ssDNA. Instrument parameters were selected according to the manufacturer's instructions. A determined amount of Pyromark Gold Q24 reagents (Qiagen), including the four nucleotides, the substrate and enzyme mix, were loaded into a pyrosequencing dispensation cartridge. Then the cartridge was carefully inserted into the pyrosequencing instrument, and the run was started. The sequencing data were analysed using the PyroMark software (***Fig 2.12***).

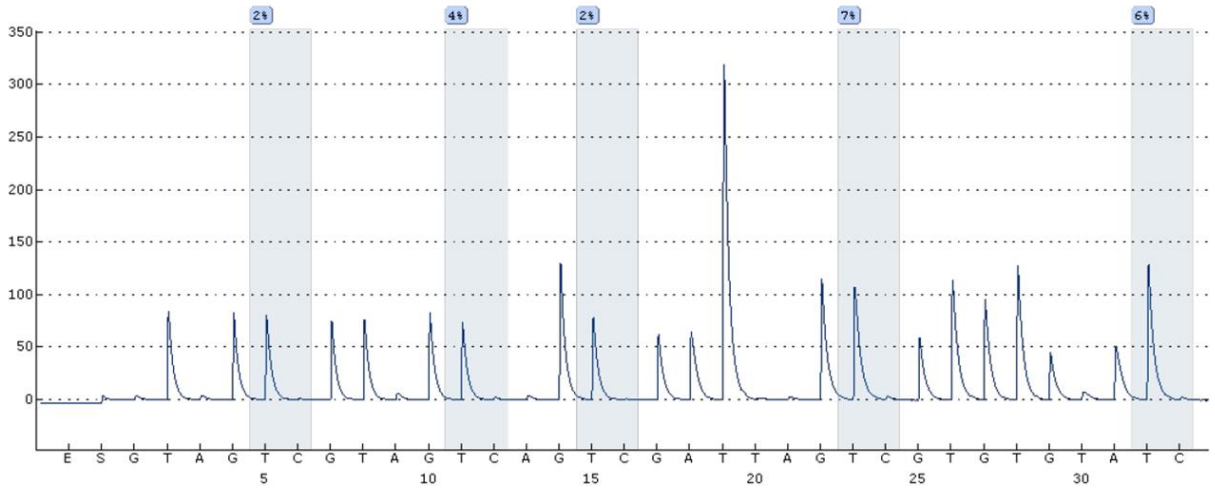

Sequence to analyze:
TGYGTGYGGYGATTTTTTGGTYGTTGGTTTGATTYGG

Position	1	2	3	4	5
Quality	Passed	Passed	Passed	Passed	Passed
Meth (%)	2	4	2	7	6

Figure 2.12. **Example of pyrosequencing result for TERT promoter region III (-315, -348 from TSS) in SHEF1 cells.** Blue highlighted columns represent 5 CpG sites and the percentage of methylation. The table summarises the data and the quality of the experimental sample.

2.16.4 Statistical analysis

The experimental data and graphical displaying of data were performed using statistical software GraphPad Prism 8. A comparison among the groups was assessed using a two-way analysis of variance (ANOVA). The threshold for which statistically significant was accepted

as $p<0.05$. Data are presented as mean ± SD, and each result represents a replicate of 3 independent experiments (n=3).

2.17 Chromatin Immunoprecipitation (ChIP)

ChIP is a useful technique for exploring protein-DNA binding interactions and their association with certain genomic regions. For example, histone proteins and transcription factors' targets in the genome can be determined, and various proteins can be mapped across the genome with ChIP experiments. Also, it can be used for exploring the existence of specific proteins at different locations in the genome (Das et al., 2004). ChIP-IT® Express Chromatin Immunoprecipitation Kit (Active Motif, USA) was used to investigate the binding of DNMT3B antibody to TERT promoter regions. First, cells are fixed using formaldehyde, and protein/DNA complexes have been stabilized via cross-linking. DNA is sheared into uniform smaller fragments with an enzymatic solution. DNA fragments interacted with specific DNMT3B protein are then captured with DNMT3B antibody and protein-G coated magnetic beads. Afterwards, proteins are removed, and DNA is purified for downstream analysis via qRT-PCR (***Fig 2.13***).

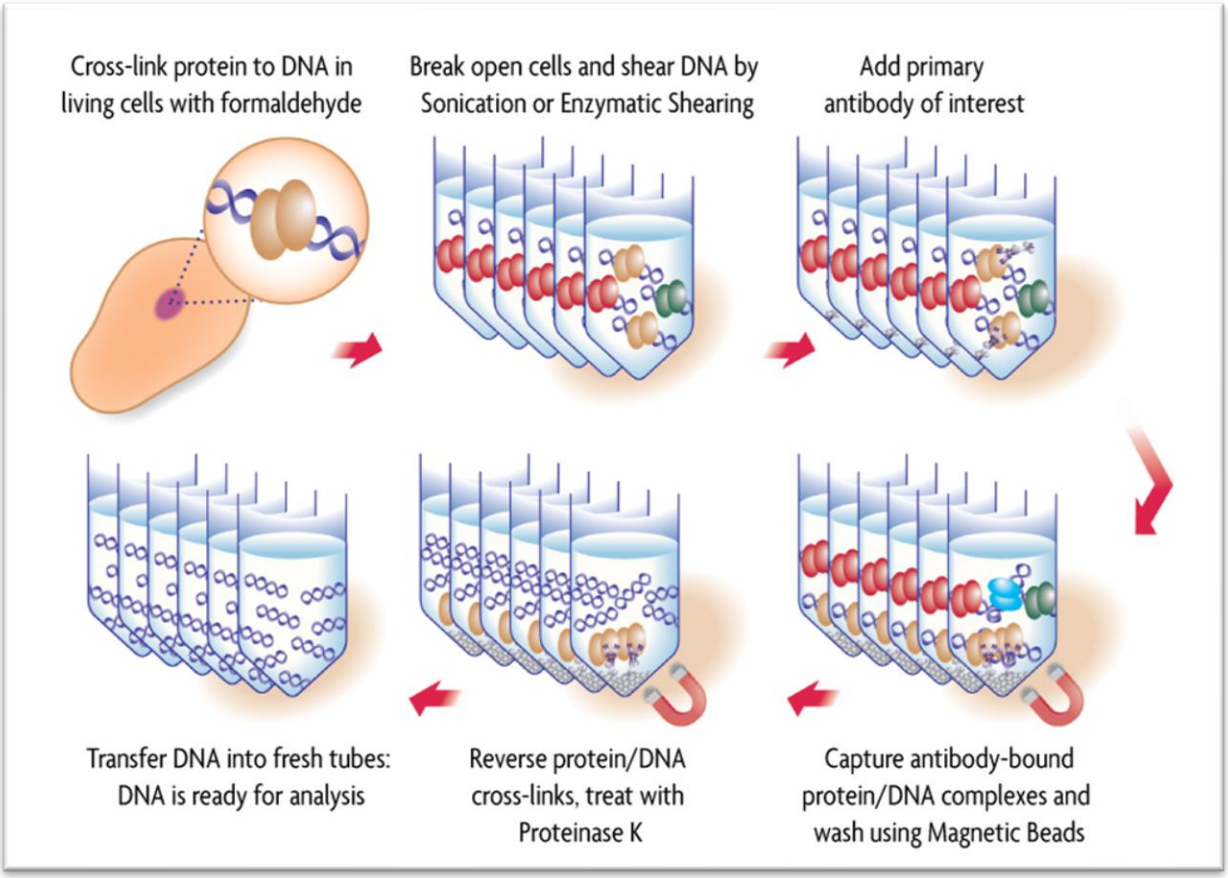

Figure 2.13. **The steps of chromatin immunoprecipitation using the ChIP-IT Express Kit.** DNA/protein interactions were preserved via cross-linking with formaldehyde. DNA is enzymatically sheared, then precipitated with DNMT3B antibody and Protein G Magnetic Beads. Following reversal of DNA/protein interactions, specific promoter regions of the TERT gene bound by DNMT3B protein were screened using qRT-PCR. (ChiP_mag_flowchart_web (Active Motif))

2.17.1 Cell fixation and Enzymatic Shearing

ChIP kit includes: RNase A (10 pg/pl), 5 M NaCl, 100 mM PMSF (phenylmethylsulfonyl fluoride, a serine protease inhibitor), Proteinase K (0.5 pg/pl), Proteinase K Stop Solution, Protease Inhibitor Cocktail (PIC), IX Lysis Buffer, 10X Glycine, 10X PBS, Elution Buffer AM2, Reverse Cross-linking Buffer, Chip Buffer 1, ChIP Buffer 2, Digestion Buffer, Enzymatic Shearing Cocktail, 0.5 M EDTA, Protein G Magnetic Beads and bar magnet.

Recommended number of cells (1.5×10^7) was used in this protocol. Methyl alcohol (10%) was added to formalin (37% formaldehyde) in the fixation step to prevent polymerization. Time for fixation, lysis of cells and enzymatic shearing conditions were optimized before the main experiments. Fixation solution was poured off, and cells were washed with 1X PBS. 1ml of 10X glycine was combined with 1ml 10X PBS and 8ml dH_2O. 10ml glycine stop solution was used at room temperature for 5 minutes on a shaker to stop the fixation reaction. After pouring off glycine stop solution, cells were rewashed with 10 ml ice-cold 1X PBS for 5 minutes and then PBS was removed. A cell scraping solution was prepared with 5 ml 1X PBS and 30 µl 100mM PMSF to collect cells. Then cells were scraped with a cell scraper in the ice-cold cell scraping solution. Collected cells were transferred to the 15 ml tube for 10 minutes of centrifugation at 2,500 rpm at 4°C. Cell pellet can be frozen at -80°C by adding1 µl 100 mM PMSF and 1 µl PIC.

The cell pellet was resuspended in 1ml cold lysis buffer supplemented with 5 µl PMSF+1 µl PIC and vortexed to mix properly, and then the mixture was incubated on ice for 30 minutes. The most critical part of shearing is properly preparing cell lysate so that enzymes can reach chromatin and work efficiently. Therefore, we used a dounce homogenizer to increase the lysis of cell membrane on ice and cells were broken down mechanically with 10 strokes to release nuclei. Also, we monitored 10 µl of cell lysis under a microscope to verify disturbed cell membranes. Once we started to see asymmetric debris with small dark dots (nuclei), samples were centrifuged for 10 minutes at 5,000 rpm at 4°C to pellet the nuclei, and the supernatant was carefully discarded. Nuclei pellet was resuspended in 350 µl digestion buffer with 1.75 µl PIC and 1.75 µl PMSF and incubated for 5 minutes at 37°C. During the waiting period, the enzymatic shearing cocktail was prepared by diluting 1:100 with 50% glycerol in dH_2O, and an optimized 10 µl enzymatic shearing cocktail solution was added to the nuclei and mixed. The mixture was incubated for 5 minutes at 37°C, and the reaction was stopped by adding 7 µl cold 0.5 M EDTA and incubated for 10 minutes on ice. The sheared chromatin samples were centrifuged for 10 minutes at 15,000 rpm at 4°C. The supernatant was carefully transferred into a fresh microcentrifuge tube, and it can be stored at -80°C. Before freezing, 50 µl of the ChIP sample was used in agarose gel to check shearing efficiency and DNA concentration (***Fig 2.14-2.15.B***).

2.17.2 ChIP DNA Purification

ChIP DNA Purification Kit (Active Motif, USA) was used to clean up 50 µl DNA sample and learn the concentration to set up the following step ChIP reactions. The purification kit included DNA Purification Binding Buffer, Wash Buffer, Elution Buffer, 3M Sodium Acetate, DNA purification columns and collection tubes.

First, 250 µl purification binding buffer was added to 50 µl of the ChIP sample and 5 µl of 3M sodium acetate, then mixed in the eppendorf tube. The sample colour was checked every time to ensure it was bright yellow as in ***Fig 2.14*** (**left**), 3M sodium acetate can be added to a lower pH level. After adjusting pH level, samples were transferred into DNA purification columns and placed into collection tubes to spin them at 14,000 rpm for 1 minute. The DNA purification columns were kept and washed with 750 µl wash buffer, and then samples were centrifuged at 14,000 rpm for 1 minute. This step was repeated once more for 2 minutes to remove the wash buffer properly from the column. Finally, 50 µl of elution buffer was added to the centre of the column matrix and waited for 1 minute. Then, samples were centrifuged at 14,000 rpm for 1 minute. The amount of DNA in the sample was detected using NanoDropTM 2000/2000c Spectrophotometer (Thermo Scientific, USA) and stored at -20°C until required.

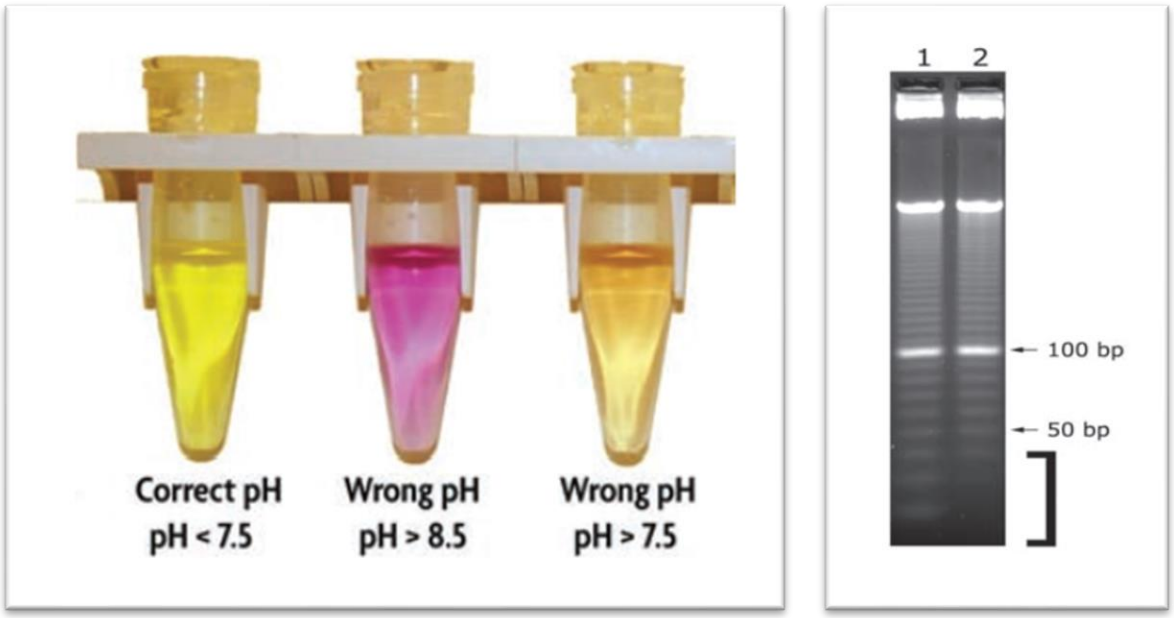

Figure 2.14. **DNA purification with ChIP DNA Purification Kit.** The sample colour indicates the pH level because the binding buffer includes pH indicator dye. pH is essential for the binding of DNA to the silica matrix of the purification column. The yellow colour indicates

the correct pH<7.5 in this figure (**left**). DNA will not bind to the purification column when pH is higher than 7.5. DNA fragments on a 5% agarose gel. The first sample is not purified, and the second sample is after purification (**right**).

2.17.3 Immunoprecipitation and washing magnetic-beads

The ChIP-IT® Control Kit (Active Motif, USA) was used to assess the non-specific binding of the DNMT3B antibody. This kit includes a positive control antibody (RNA pol II mouse monoclonal antibody), a bridging antibody for mouse IgG to enhance the binding affinity of mouse monoclonal antibodies and a negative control antibody (mouse IgG).

The chromatin samples were thawed on ice, and 10 µl was transferred into a microcentrifuge tube to use as an input DNA control in the following steps. Next, 25 µg of DNA was used for ChIP reactions. ChIP reactions were prepared using 25 µl Protein-G coated magnetic beads, 10 µl ChIP buffer 1, 20-60 µl sheared chromatin (25 µg), 1 µl PIC and dH_2O to complete the final volume 100 µl and 2 µg DNMT3B (mouse IgG) antibody. ChIP reactions were also performed with positive control 2 µg RNA pol II plus 2 µg bridging antibody and negative control IgG antibody with the same ingredients: 25 µl Protein-G coated magnetic beads, 10 µl ChIP buffer 1, 20-60 µl sheared chromatin (25 µg), 1 µl PIC and dH_2O to complete the final volume 100 µl. ChIP Controls are important for quality control of experiments. Once ChIP reactions were read, tubes were closed and incubated overnight at 4°C. Following overnight incubation, tubes were spun briefly to collect liquid and placed on the magnetic stand to pellet the magnetic beads from the liquid. Protein-G coated beads make ChIP protocol faster/more straightforward, and they possess a high binding affinity to IgG and decrease non-specific bindings. The liquid was carefully discarded, and beads were washed with 800 µl ChIP buffer 1, then 800 µl ChIP buffer 2. The remaining buffer was removed without disturbing the magnetic beads. 50 µl of elution buffer AM2 was used to elute DNA fragments from beads and incubated for 15 minutes at room temperature. 50 µl of Reverse Cross-linking Buffer was added to the tube, simultaneously reversing the cross-links while DNA was eluted from the beads. The supernatant was transferred to the new microcentrifuge tube. The input DNA sample was processed by adding 88 µl ChIP buffer 2 and 2 µl 5 M NaCl to complete the final volume 100 µl. ChIP and input DNA samples were incubated for 15 minutes at 95°C. Tubes were cooled to room temperature. 2 µl proteinase K solution was added to each tube and incubated for 60 minutes at 37°C. Lastly,

a 2 µl proteinase K stop solution was added once the tubes were cooled down to room temperature. The DNA product was used immediately or stored at -20°C.

2.17.4 qRT-PCR for detection of ChIP product

ChIP DNA and the control Input DNA samples were used in qRT-PCR. DNA samples were purified before PCR for each sample as recommended in the commercial kit. We used positive and negative control qPCR primers to eliminate variations in ChIP experiment steps. We used designed primers for TERT promoter regions for ChIP samples shown in ***Table 2-11***.

RT-PCR reaction was performed on samples using the SYBR Green Master Mix (Thermofisher, UK). Firstly, SYBR™ Green Master Mix (contains DNA polymerase), DNA, primers, and RNase-free water were thawed and placed on ice. The master mix was prepared using 15 µL SYBR™ Green Master Mix, 3 µL DNA samples, 1 µL (1µM) forward and reverse primers for a final volume of 20 µL. Reactions were cycled 36 times with the following steps per cycle: 95°C hot start for 10 minutes, 95°C denaturing for 20 seconds, 59°C (primer specific) annealing for 30 seconds, 72°C extension for 30 seconds and addition of melting curve. We also run serial dilutions of input DNA for each primer set to produce a standard curve with known DNA quantities, e.g. 0.005 ng, 0.05 ng, 0.5 ng, 5 ng, 50 ng. PCR amplicons were also checked in agarose gel to confirm the correct product size (***Fig 2.15.A***).

Table 2-11. **Designed PCR primers for TERT promoter in different regions in the ChIP experiment**. Promoter regions, annealing temperature, forward and reverse primer sequences, and product sizes are listed. PCR amplicons should ideally be around 50-200 bp in length for a successful real-time PCR step.

CpG Locations	Annealing Temp (°C)	Forward primer	Reverse primer	Product size
Promoter region II	59°C	5'-GGCGGGATGTG ACCAGATGTTG-3'	5'- GAAAGGGTGGG AAATGGAGCC -3'	134 bp
Promoter region III	55°C	5'-CTTCACGTCCGG CATTCGTG-3'	5'-CCTGATCCGGA GACCCAGG -3'	81 bp

Promoter region IV	58°C	5`-GGCCGATTCGA CCTCTCTCC -3`	5`-CGTCTGTGCCC GCGAATCCA -3`	164 bp
Promoter region V	58°C	5'-CCGGGCTCCCA GTGGATTCG -3'	5'-TGGAAGGTGAA GGGGCAGGAC -3	103 bp

GAPDH control primers were used for control samples. The reactions were also cycled for 36 repetitions. GAPDH positive control primers generate a 166 bp product enriched in the RNA pol II and input DNA samples. A negative IgG sample represents non-specific background. Reactions were cycled 36 times with the following steps per cycle: 95°C hot start for 10 minutes, 94°C denaturing for 20 seconds, 59°C (for GAPDH primers) annealing for 30 seconds, 72°C extension for 30 seconds and addition of melting curve.

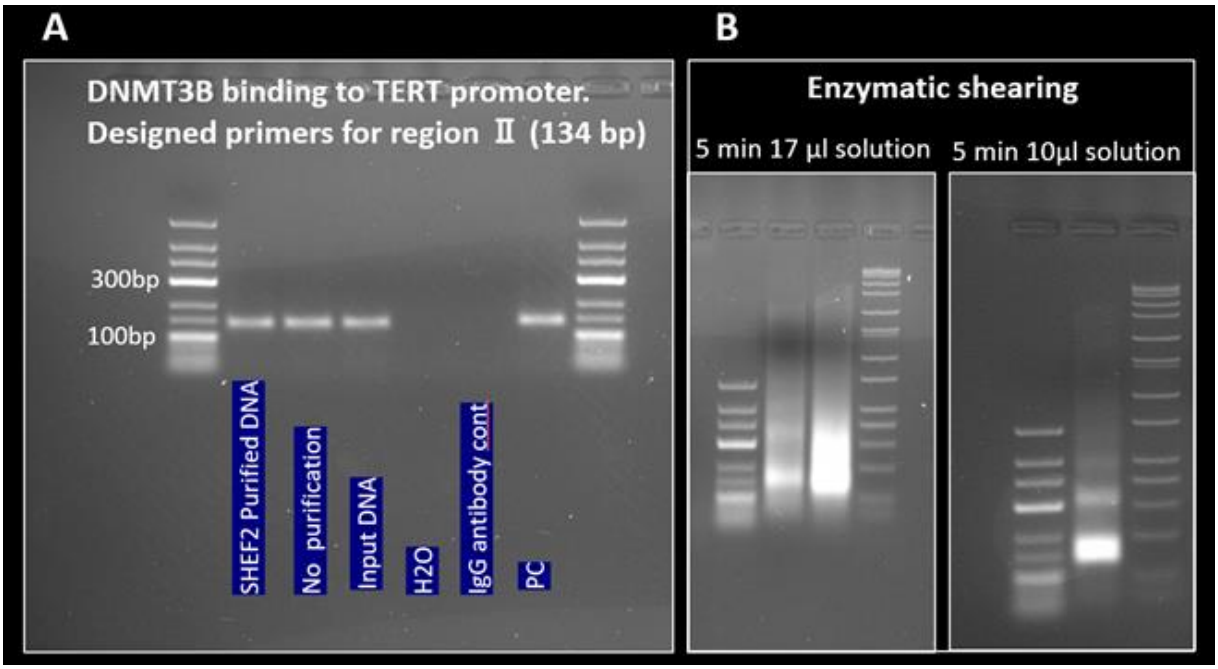

Figure 2.15. **Example of ChIP qPCR products from promoter region II on a 2% agarose gel.** ChIP DNA sample and input DNA were used for PCR amplification **(A).** Specific amplification was determined by the presence of correct size and single band products. Negative control H_2O indicates no template DNA. The enzymatic shearing step was optimised with different volumes of shearing solutions **(B).**

We also run serial dilutions of input DNA for each PCR to produce a standard curve with known DNA quantities, e.g. 0.005 ng, 0.05 ng, 0.5 ng, 5 ng, 50 ng (***Fig 2.16)***. DNA quantity was solved with the following formula in the ChIP and IgG samples: X = DNA quantity, Y = Ct, M = slope of the standard curve line and B = the Ct value where X =1.

(1) Y = M (log X) + B or log(X) = (y – B) - M

(2) Fold Enrichment = ChIP DNA quantity / IgG DNA quantity

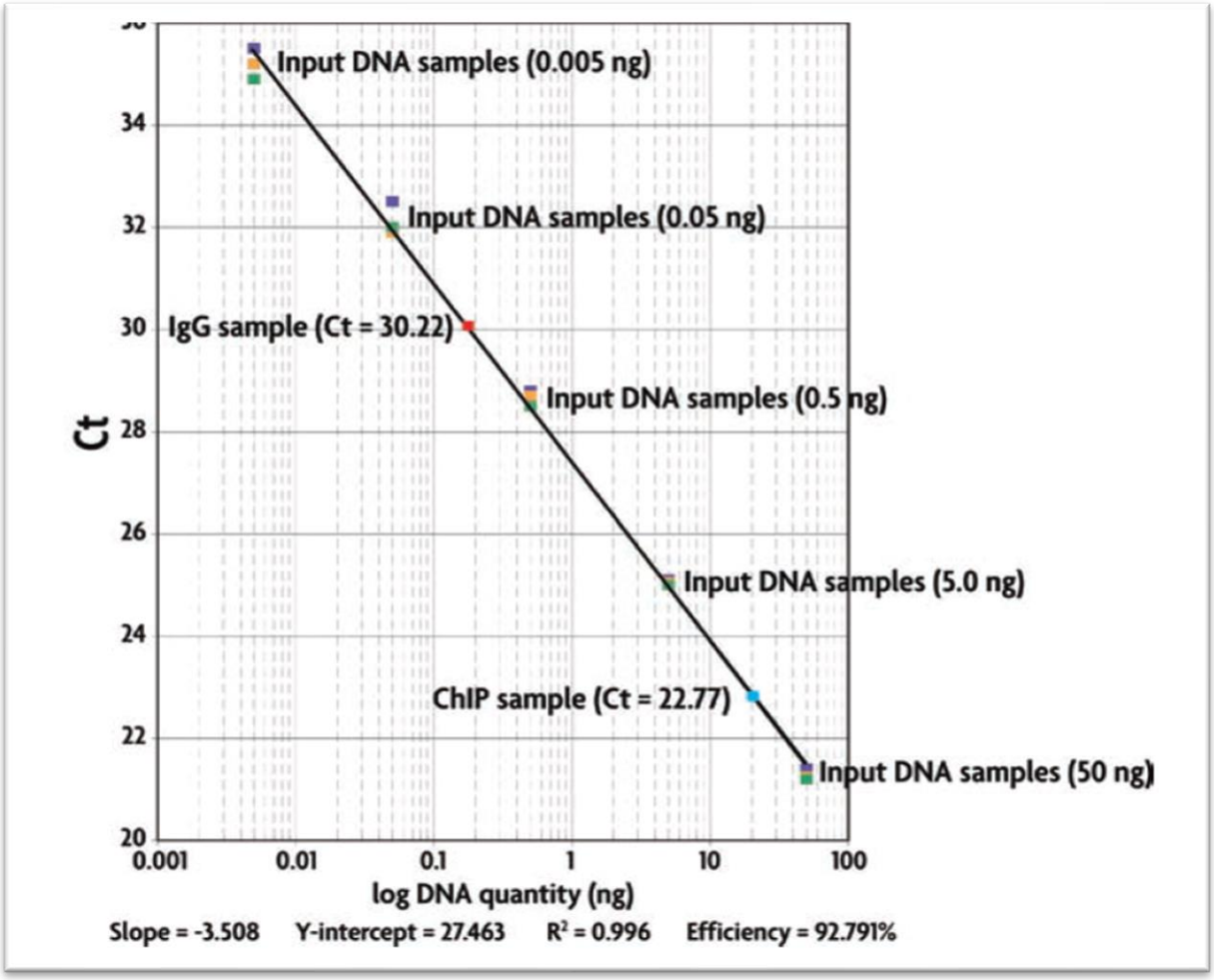

Figure 2.16. **An example of a standard curve with known DNA quantities.** A standard curve was produced from serial dilutions of input DNA samples with known concentrations and IgG sample. Y-axis represents the Ct values, and X-axis shows log DNA quantity (ng).

2.17.5 Statistical analysis

The experimental data and graphical displaying of data were performed using statistical software GraphPad Prism 8. A comparison among the groups was assessed using a two-way analysis of variance (ANOVA). The threshold for which statistically significant was accepted as $p<0.05$. Data are presented as mean ± SD, and each result represents a replicate of 3 independent experiments (n=3).

Keele University

CHAPTER 3: Telomerase activity regulation is promoter methylation and oxygen-sensitive in differentiated embryonic stem cell

3.1 INTRODUCTION

Telomerase enzyme is a telomere terminal transferase made of protein and RNA components, and it is responsible for telomere maintenance and elongation (Klapper et al., 2001; Takubo et al., 2002). Telomerase reverse transcriptase enzyme (TERT) encodes the catalytic protein subunit, and it is a rate-limiting factor for enzyme activity. The mechanisms of activation of TERT across cancer cells or, conversely, silencing during differentiation of stem and somatic cells remains poorly understood. Promoter mutations, epigenetics including DNA methylation, histone modification, non-coding RNAs and transcriptional or posttranscriptional modifications of TERT may all play roles in the regulation of telomerase activity.

Embryonic stem cells (ESCs) have unique properties, including self-renewal, differentiation into cell-type specific progenies, and high telomerase activity with long telomeres. Recent studies have suggested that decreased telomerase enzyme activity and TERT expression after differentiation were associated with epigenetic modifications (Lai et al., 2005; Eitsuka et al., 2018). It is correlated with the observation that somatic cells express very low or no detectable levels of telomerase (Hornsby, 2007). Albanell and colleagues reported a decreased telomerase activity during differentiation of maturation-sensitive human embryonal carcinoma and human promyelocytic leukaemia cell lines with retinoic acid treatment (Albanell et al., 1996). During stem differentiation and embryonic developmental programming, expression of genes related to self-renewal decreases, while lineage-specific genes are upregulated where epigenetic modifications can play a crucial role in cell fate (Wu and Sun, 2006). Due to their potential, ESCs have been used to investigate epigenetic changes during stem cell differentiation and early development as an *in vitro* model system. There is a complex interaction between the genetic and epigenetic basis of pluripotency (Loh, and Ng 2008). So far, evidence has demonstrated a unique epigenetic signature of undifferentiated ESCs compared to differentiated and somatic cells (Bibikova et al., 2006; Fouse et al., 2008; Altun et al., 2010). For example, DNMT3A, DNMT3B and TERT expression are down-regulated during differentiation (Phipps et al., 2009). Conversely, DNMT3A and DNMT3B are highly expressed in undifferentiated ESCs (Li et al., 2007; Liao et al., 2015). Further, ESCs express high DNMT3A and DNMT3B levels when compared to somatic cells (Okano et al., 1998).

The addition of methyl groups to cytosine residues (methylation) forms 5-methylcytosine (5mC) or oxidation (hydroxymethylation) of methyl groups that can regulate the transcription of genes. The three major DNA methyltransferases; DNMT1, DNMT3A, and DNMT3B control the process of methylation in mammals (Ting et al., 2006; Moore et al., 2013). On the other hand, the ten-eleven translocation family of dioxygenases (TETs) catalyse the successive oxidation of 5mC to 5-hydroxymethylcytosine (5hmC), which can be detected in the majority of tissues (Rasmussen and Helin, 2016; An et al., 2017). DNMT1 is mainly responsible for maintaining heritable methylation patterns during DNA replication and distinguishing hemimethylated DNA (Hermann et al., 2004). De novo methylation is catalyzed by DNMT3A and DNMT3B working in coordination with DNMT1 to establish DNA methylation patterns during gametogenesis, embryogenesis and somatic tissue development (Li, 2002). ESCs have a distinct DNA methylation signature compared to somatic cells (Huang et al., 2014a). Another recently identified enzyme is DNMT3L (DNA methyltransferase 3-like) which is highly expressed in ESCs and cooperates with DNMT3A and DNMT3B to stimulate their catalytic activity (Hata et al., 2002). DNA methylation changes, including gains and losses, are associated with lineage specification and cell fate during stem cell differentiation in hematopoietic progenitor cells and mature cells (Hodges et al., 2011; Suelves et al., 2016).

Oxygen tension in the tissue depends on the distance away from the vascular system, and it ranges from 1–14 % *in vivo* for most tissues (Jagannathan et al., 2016; Ast and Mootha, 2019). Accumulating pieces of evidence show that cells cultured in atmospheric oxygen conditions have higher oxidative stress due to the production of reactive oxygen species (ROS) than in physiological oxygen environments resulting in cellular or DNA damage, genomic instability, and senescence (Jagannathan et al., 2016). ESCs are generally cultured under air oxygen conditions (21% O_2), but they are derived from embryos that occupy a 2–5% physiological normoxia environment (Forristal et al., 2010). Low oxygen conditions affect stem cell characteristics such as proliferation, genomic stability, differentiation, pluripotency capacity, cells` physiology and epigenetic profile such as DNA methylation (Forsyth et al., 2006; Kwon et al., 2017; Widowati et al., 2017; Dogan et al., 2021). ESCs cultured in the physoxia condition (3%-5% O_2) prevent spontaneous differentiation compared to 21% AO (Ezashi T et al., 2005). Recently, it has been shown that removing methyl groups with oxidation of 5mC to 5hmC depends on oxygenases named TET enzymes that require oxygen as a cofactor (Kietzmann et al., 2017). Oxygen availability during embryonic development can differently regulate epigenetic landscape, cellular specification pathways, and cell functions (Burr et al., 2018). Physiological oxygen levels drive a significant decrease in global DNA methylation levels

across a range of cancer cell lines (Shahrzad et al., 2007). Oxygen and ROS have profound effects on epigenetic modification. Therefore, applying the physiological oxygen environment due to the crucial role of oxygen in determining epigenetic profiles is becoming more critical for a mammalian stem cell culture.

Understanding the epigenetic mechanisms involved in ESCs differentiation will help further understand telomerase silencing and the development of functional cells *in vitro*. All together, epigenetic regulators, oxygen tension, DNMTs and histone methyltransferases could play an essential role in the regulation of TERT during differentiation. In this study, we have tested the effect of different oxygen conditions on stem cell differentiation and telomerase activity. Further, we have investigated the association between TERT gene expression and methylation of the gene promoter.

3.2 RESULTS

3.2.1 Cell proliferation in three oxygen conditions

WST1 assay was performed to explore the effect of oxygen on cell proliferation and viability over seven days. SHEF1 and SHEF2 cells were seeded using the 96-well-plate format (100 µl/well) with a given cell number (cells/ml) and cultured for seven days. Cells became confluent in reduced oxygen conditions more rapidly. This method was reflected in the wells with high initial cell numbers showing a decrease in cell viability after a seven-day cell culture period. These results enabled the determination of the optimum cell number of SHEF1 and SHEF2 ($31x10^3$ cells/ml) for seven days of experimentation ***(Fig 3.1.A, B)***.

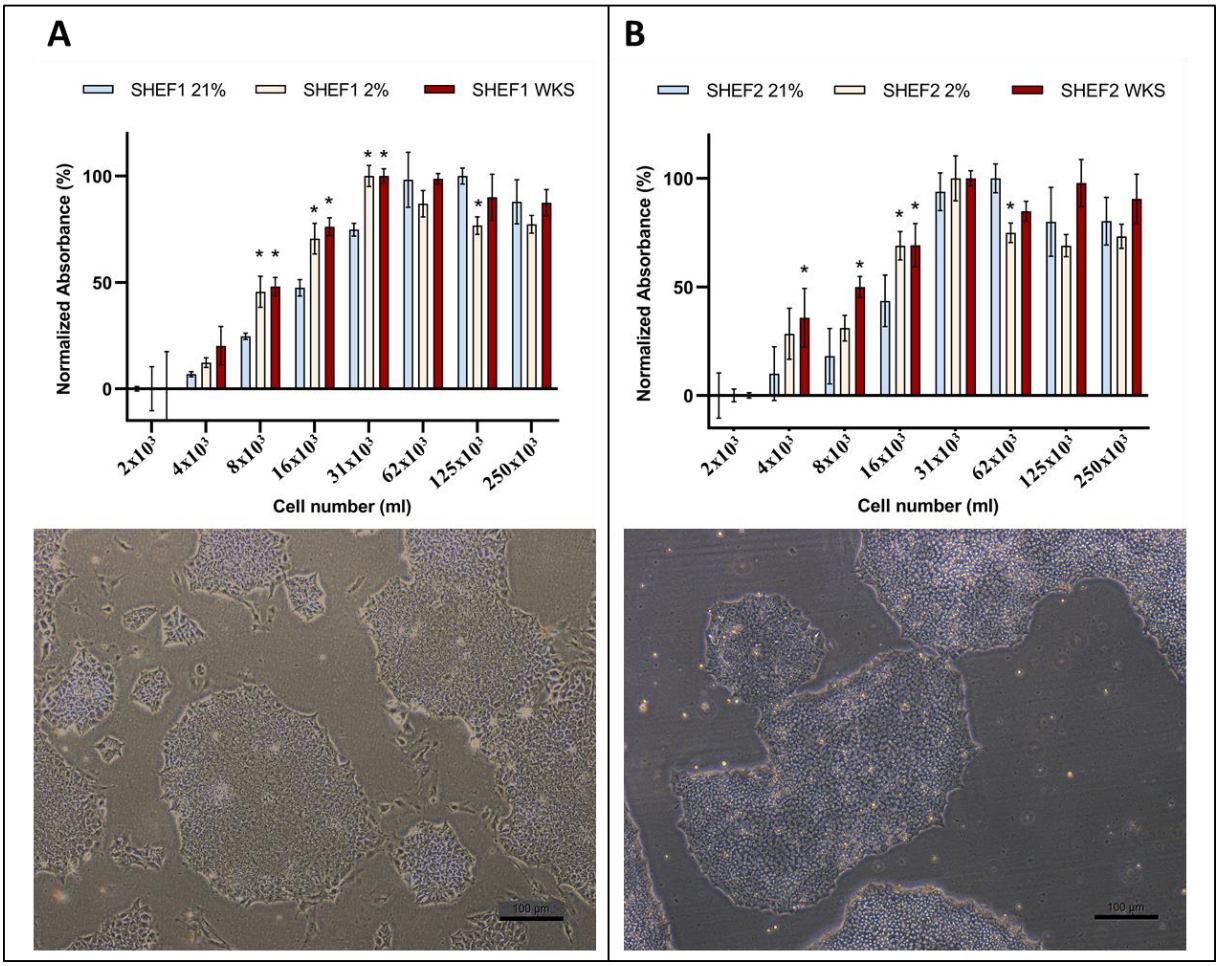

Figure 3.1. **Cell proliferation assay and colony formation of ESCs.** The optimum cell number for further experiments was assessed using WST1 assay in air oxygen and physoxia

conditions. A) SHEF1, B) SHEF2 in air oxygen (21% O_2) and physoxia (2% O_2 and WKS) and images represent cell morphology of SHEF1 **(A)** and SHEF2 **(B)** cells. * indicates $p<0.05$ versus air oxygen.

3.2.2 Analysis of Monolayer Spontaneous Differentiation of hESCs

hESCs were characterized by their expression of pluripotency markers, including transcription factors; Oct-3/4, Nanog, surface markers; SSEA-1, SSEA-4, and alkaline phosphatase enzyme activity (ALP). Differentiated hESCs also were stained with pluripotency marker antibodies to evaluate spontaneous monolayer differentiation during 5, 10, 20 and 40 days. Cells were seeded in 96 well-plates in three different conditions and analysed at selected time points via immunofluorescence staining.

During differentiation of SHEF1, the expression of pluripotent markers decreased in a time-dependent manner. ALP, SSEA-4 and OCT-3/4 expression decreased after five days in 21% AO (air oxygen), while Nanog expression reduced gradually over 20 days. SHEF1 cells in 21% AO and 2% PG showed a rapid increase in negative marker SSEA-1 after day 5 (***Fig 3.2.A).*** Differentiated SHEF1 cells in 2% PG displayed a considerable decrease in ALP and SSEA-4 markers after day 5, while OCT-3/4 expression was reduced after 10 days of differentiation. Nanog expression showed a decrease after day 20, while SSEA-1 illustrated a significant increase after day 5 in the 2% PG condition (***Fig 3.2.B)***. ALP and SSEA-4 markers in 2% WKS decreased after 5 days of differentiation, while expression of OCT-3/4 and Nanog significantly decreased after day 10 and day 20, respectively. SSEA-1 expression gradually increased during 20 days of differentiation in 2% WKS (***Fig 3.2.C)***. In conclusion, SSEA-1 negative pluripotency marker expression increased while positive markers ALP, SSEA-4, OCT-3/4, and Nanog expression decreased in all conditions during 20 days of spontaneous monolayer differentiation.

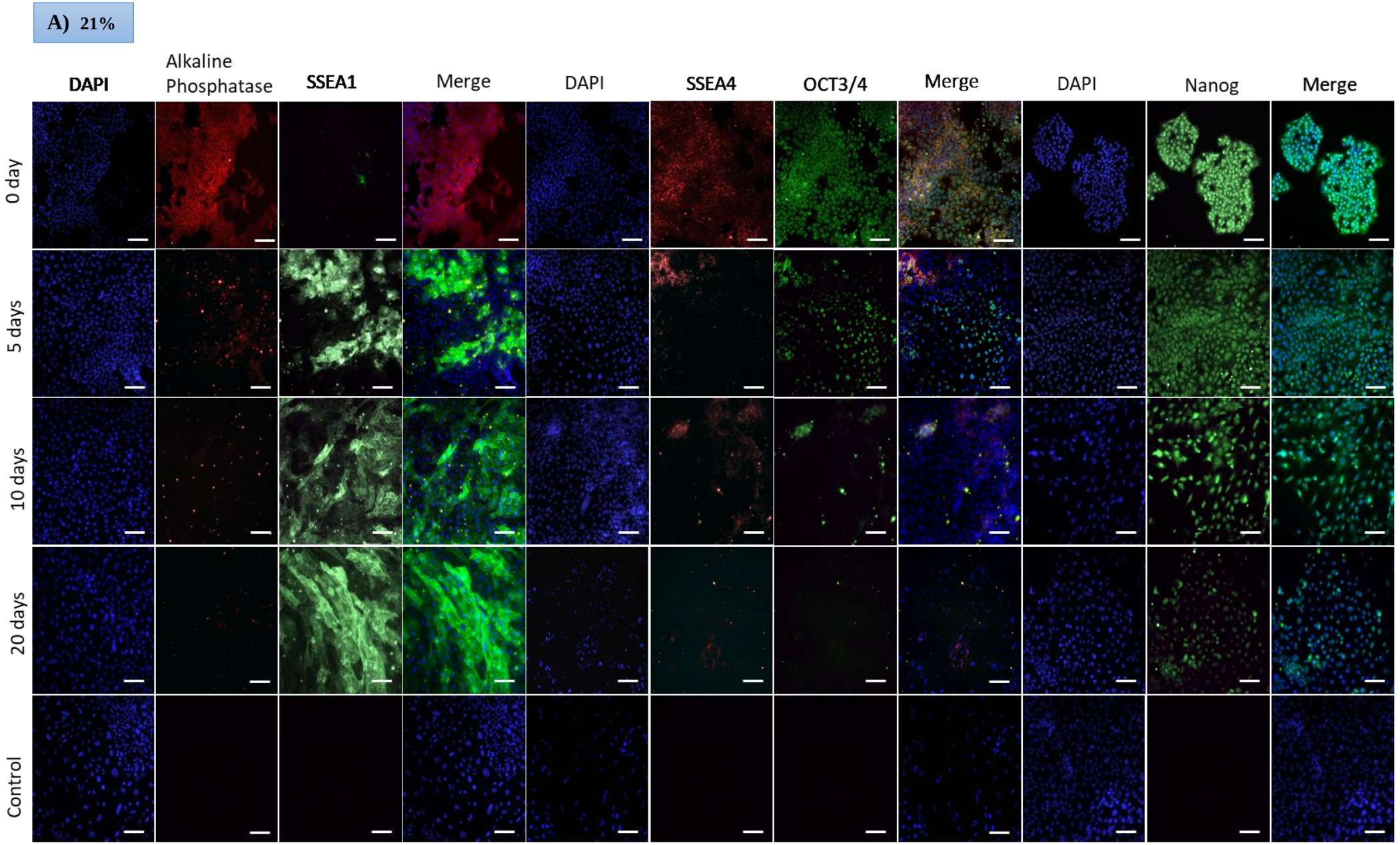
A) 21%
DAPI
Alkaline Phosphatase
SSEA1
Merge
DAPI
SSEA4
OCT3/4
Merge
DAPI
Nanog
Merge
0 day
5 days
10 days
20 days
Control

B) 2%

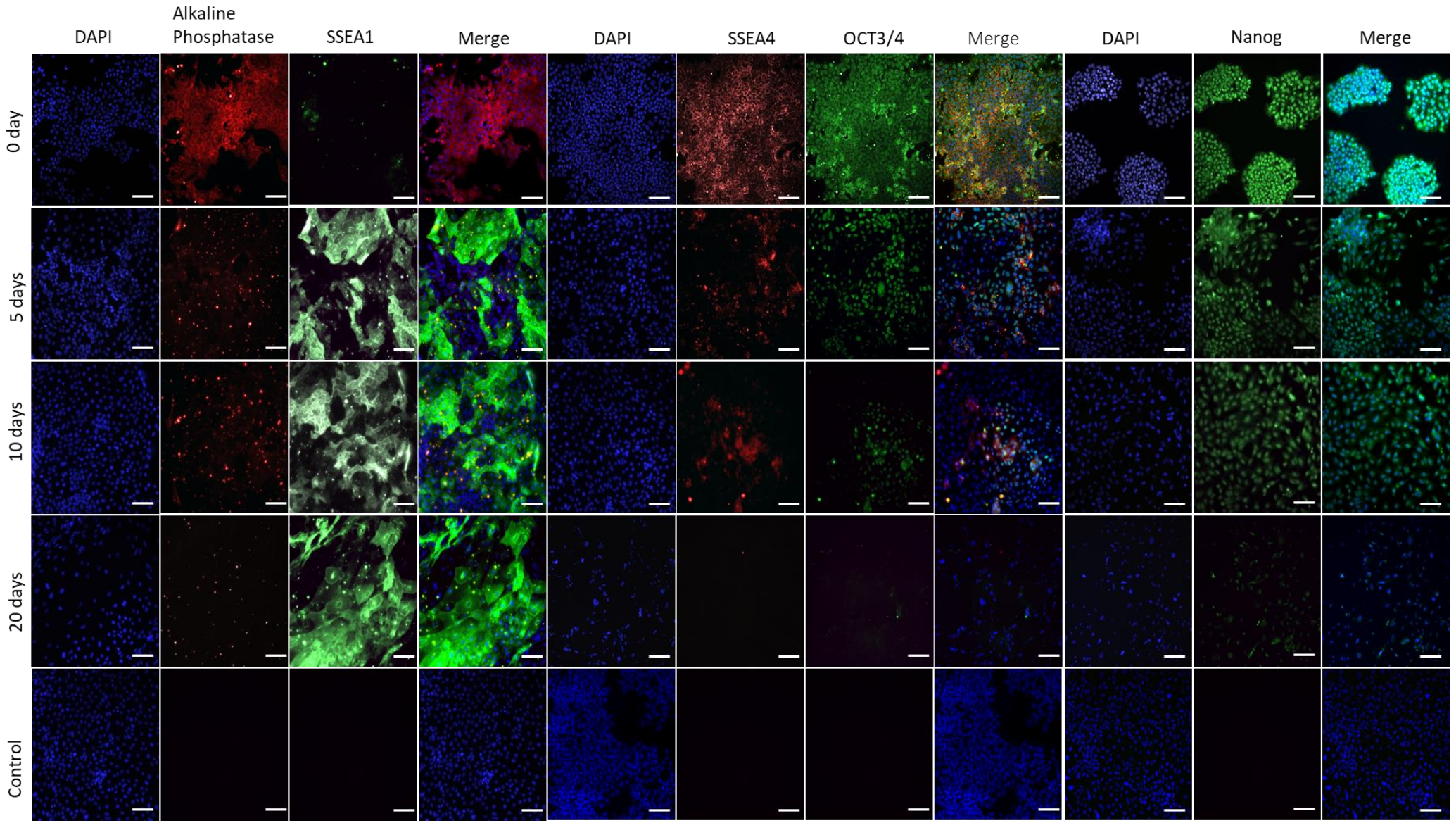
DAPI
Alkaline Phosphatase
SSEA1
Merge
DAPI
SSEA4
OCT3/4
Merge
DAPI
Nanog
Merge
0 day
5 days
10 days
20 days
Control

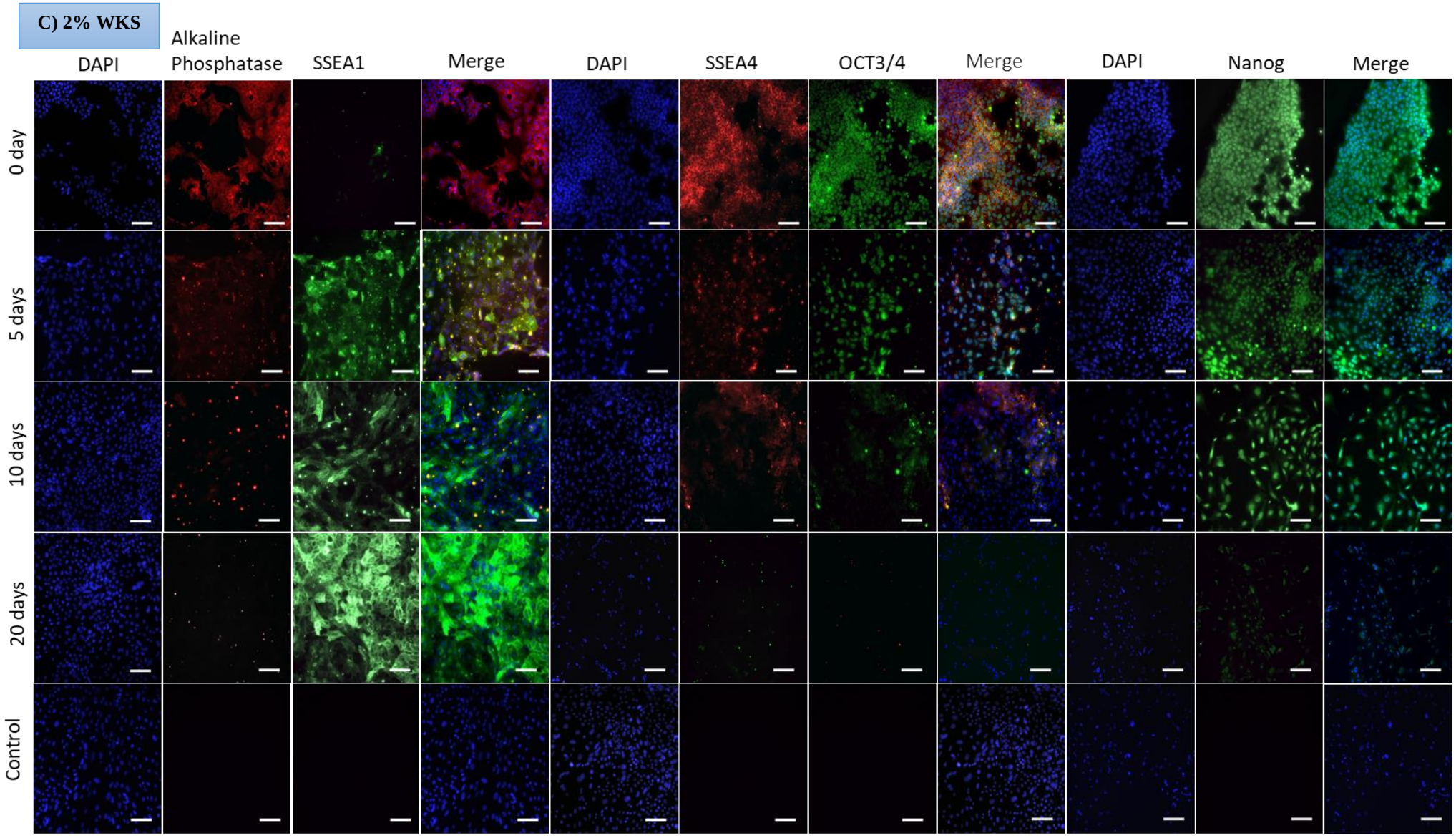

Figure 3.2. **Immunofluorescence staining of undifferentiated and differentiated SHEF1.** Cells were differentiated in **(A)** 21% AO, **(B)** 2% PG and (C) 2% WKS conditions at four-time points (0, 5, 10, 20 days). The scale bar represents 100 μm, 20X objective and red, green colour indicates antigen, blue DAPI. Images are representative of three independent samples, and secondary antibody controls also were given.

SHEF2 cells were also characterized by their expression of pluripotency markers, including Oct-3/4, Nanog, SSEA-1, SSEA-4 and ALP via immunofluorescence staining. Differentiated SHEF2 were stained with the same pluripotency marker antibodies to evaluate spontaneous monolayer differentiation during 5, 10 and 20 days. After differentiation of SHEF2, the expression of pluripotent markers gradually decreased in a time-dependent manner. ALP, SSEA-4 and OCT-3/4 expression decreased after 5 days in all conditions, while Nanog expression reduced after 10 days of differentiation. A reduced ALP, SSEA-4, OCT-3/4, and Nanog expression were noted in three culture environments after 10 and 20 days of differentiation. SHEF2 cells started to express the negative marker SSEA-1 after day 5, while cells cultured in 21% AO and 2% PG showed higher expression of SSEA-1 compared to 2% WKS samples after 10 and 20 days ***(Fig 3.3.A-C)***. In summary, SSEA-1 negative pluripotency marker expression increased while positive markers ALP, SSEA-4, OCT-3/4, and Nanog expression decreased in all conditions during 20 days of spontaneous monolayer differentiation ***(Fig 3.3)***.

In conclusion, undifferentiated cells expressed high levels of positive pluripotency markers (OCT-3/4, SSEA-4, Nanog, and ALP) but not negative pluripotency marker SSEA-1 in undifferentiated hESCs under 21% AO, 2% PG and 2% WKS conditions. Results demonstrate that hESCs pluripotency marker expressions are retained in all oxygen conditions.

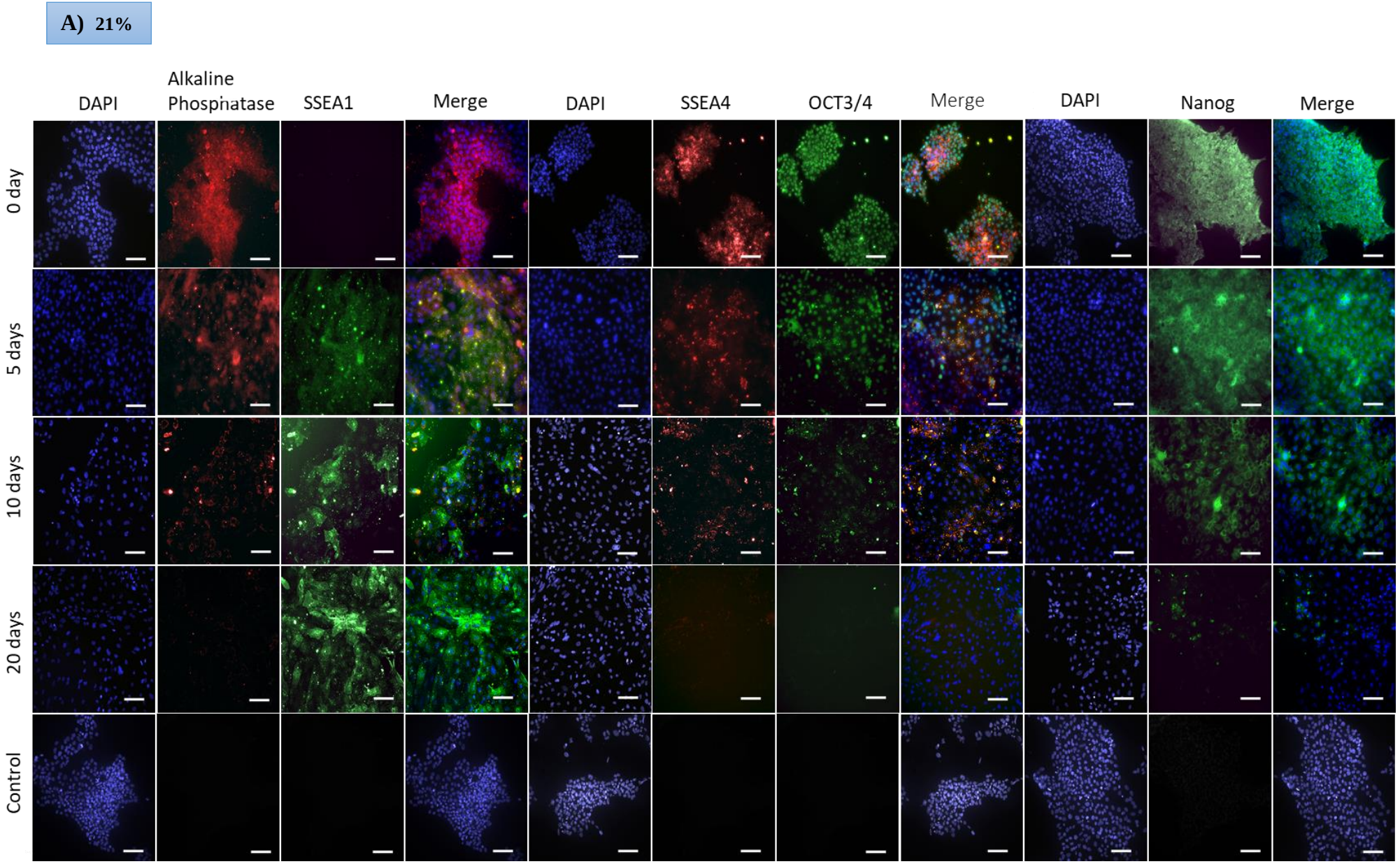
A) 21%
DAPI
Alkaline Phosphatase
SSEA1
Merge
DAPI
SSEA4
OCT3/4
Merge
DAPI
Nanog
Merge
0 day
5 days
10 days
20 days
Control

B) 2%

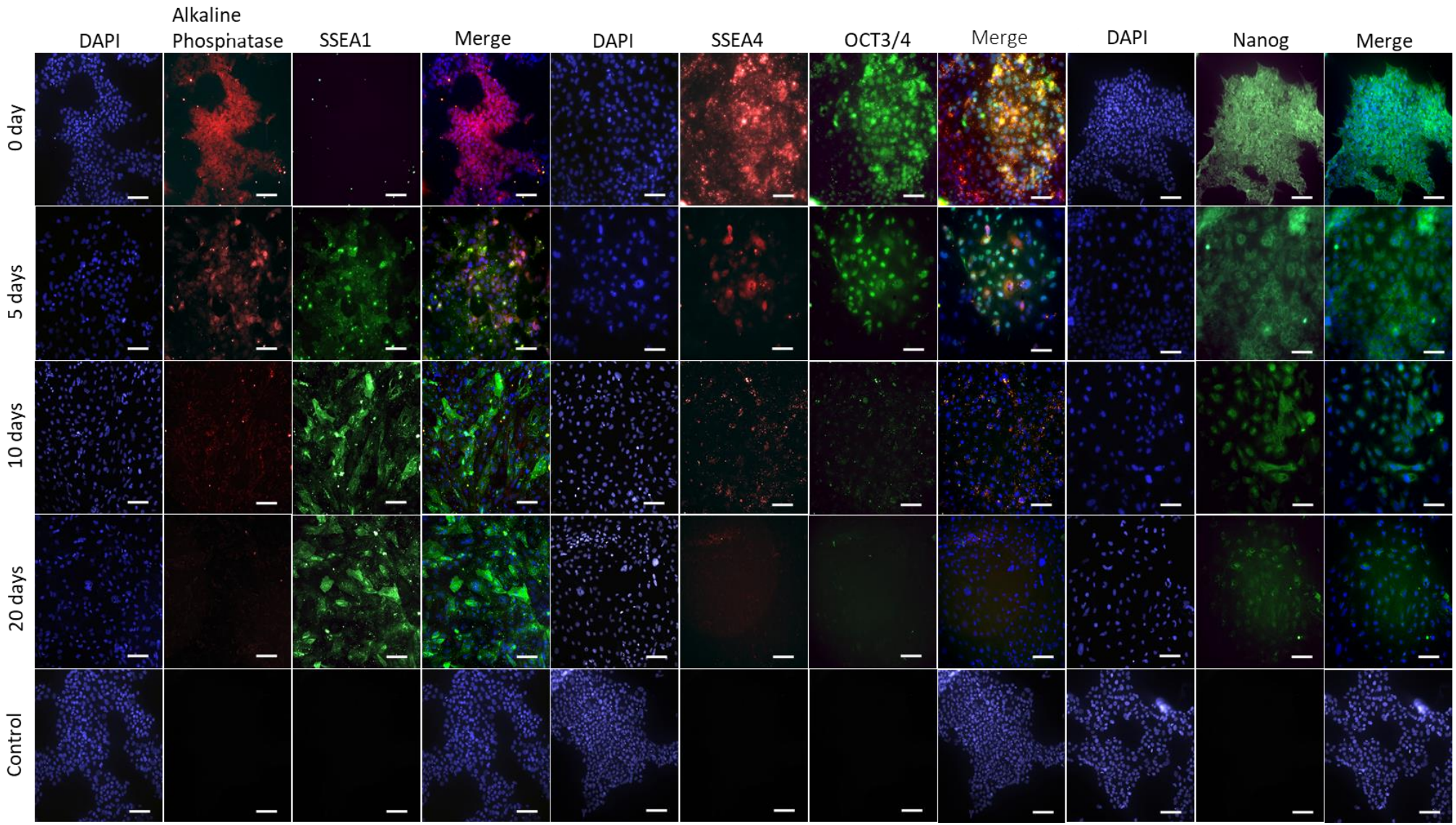
DAPI
Alkaline Phosphatase
SSEA1
Merge
DAPI
SSEA4
OCT3/4
Merge
DAPI
Nanog
Merge
0 day
5 days
10 days
20 days
Control

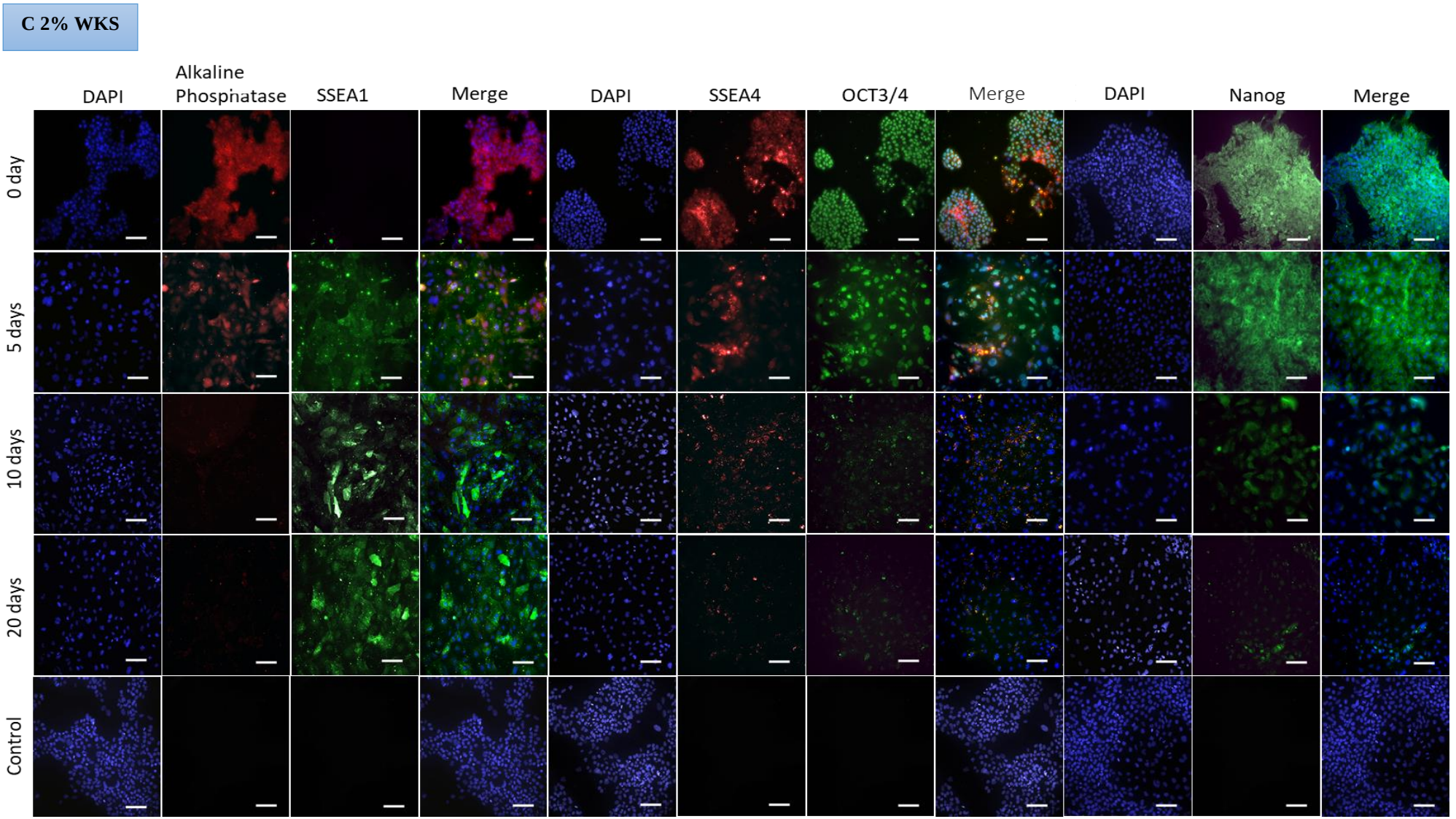

Figure 3.3. **Immunofluorescence staining of undifferentiated and differentiated SHEF2 cells.** Cells were differentiated in **(A)** 21% AO, **(B)** 2%PG and (C) 2% WKS conditions at four-time points (0, 5, 10, 20 days). The scale bar represents 100 µm, 20X objective and red, green colour indicates antigen, blue DAPI. Images are representative of three independent samples, and secondary antibody controls also were given.

3.2.3 Live dead cell imaging

LIVE/DEAD Cell Imaging Kit was used to identify live and dead cells to assess the health of the cells via fluorescence microscopy. The images show that cell viability was maintained during 40 days of differentiation, and there was no need to count dead cells. Green cells were live cells that had converted calcein-AM green via esterase activity, while red cells had compromised membranes allowing EthD-1 to enter cells and bind with nucleic acids ***(Fig 3.4)***.

Live dead cell analysis showed no significant changes in viability of differentiated SHEF1 at day 10 (94.8 ± 31.4%), 20 (96.1 ± 29%) and 40 (94.4 ± 25.7%) in AO. The percentage of differentiated live cells was 94.7 ± 40.4% on day 10, 95.3 ± 21.9% on day 20 and 94.3 ± 15.7% on day 40 in 2% PG condition. Differentiated SHEF1 cultured in 2% WKS showed 94.3 ± 5.6% cell viability on day 10, 94.7 ± 21.2% on day 20 and 95.4 ± 5.4% on day 40. Physoxia conditions displayed no difference in cell viability compared to AO. Differentiated SHEF2 also displayed no significant changes in viability at day 10 (96.7 ± 15.4%), 20 (96.0 ± 15.6%) and 40 (95.3 ± 28.3%) in 21% AO conditions. Differentiated live cells were calculated as 96.3 ± 32% on day 10, 95.3 ± 21.9% on day 20 and 96.3 ± 17.9% on day 40 in 2% PG condition. Differentiated SHEF1 cultured in 2% WKS showed 97 ± 18% cell viability on day 10, 96.3 ± 21.2% on day 20 and 97 ± 36.9% on day 40. Again, physoxia conditions represented no difference in cell viability compared to the AO microenvironment ***(Fig 3.5)***.

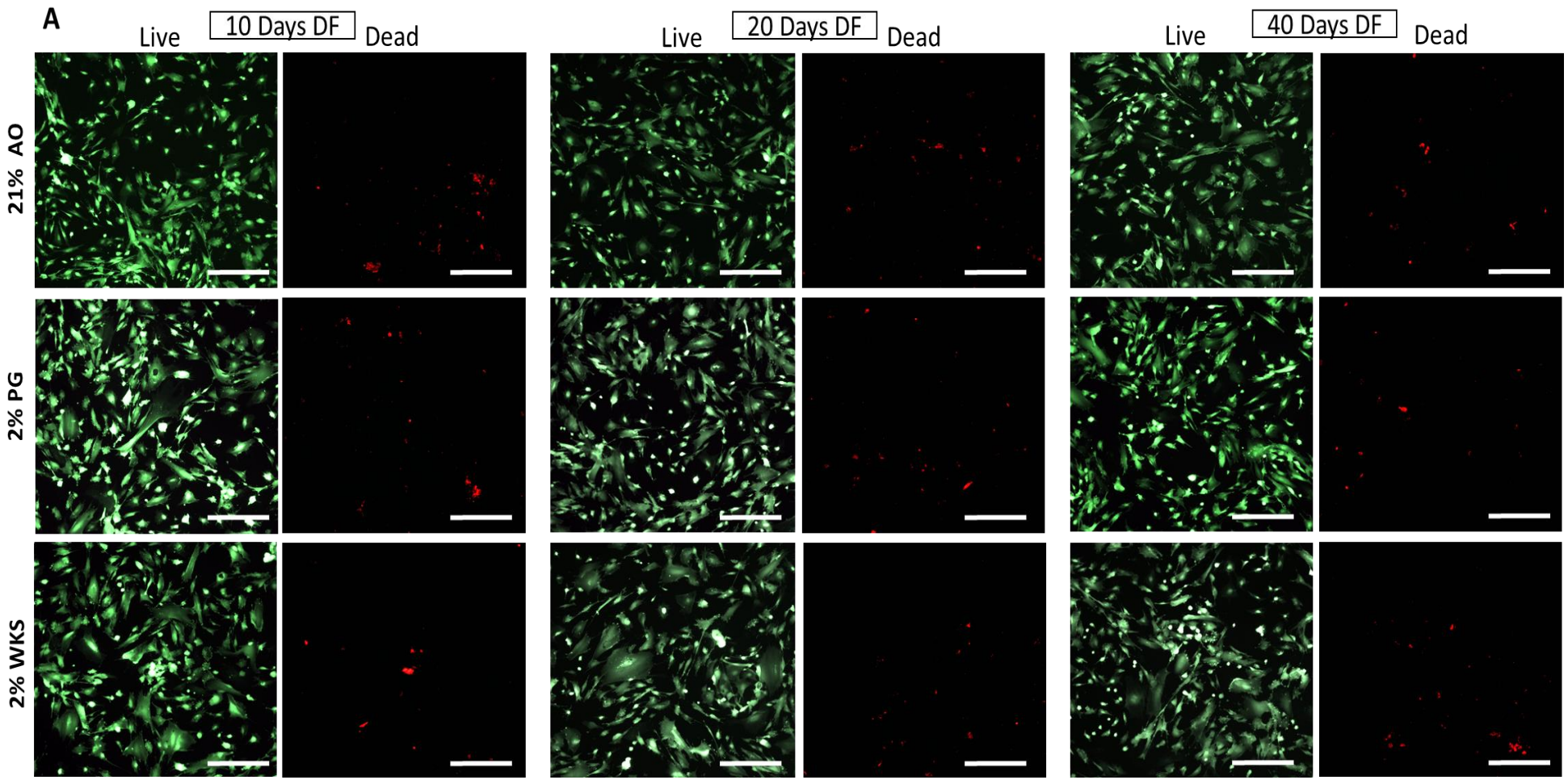
A
Live
10 Days DF
Dead
Live
20 Days DF
Dead
Live
40 Days DF
Dead
21% AO
2% PG
2% WKS

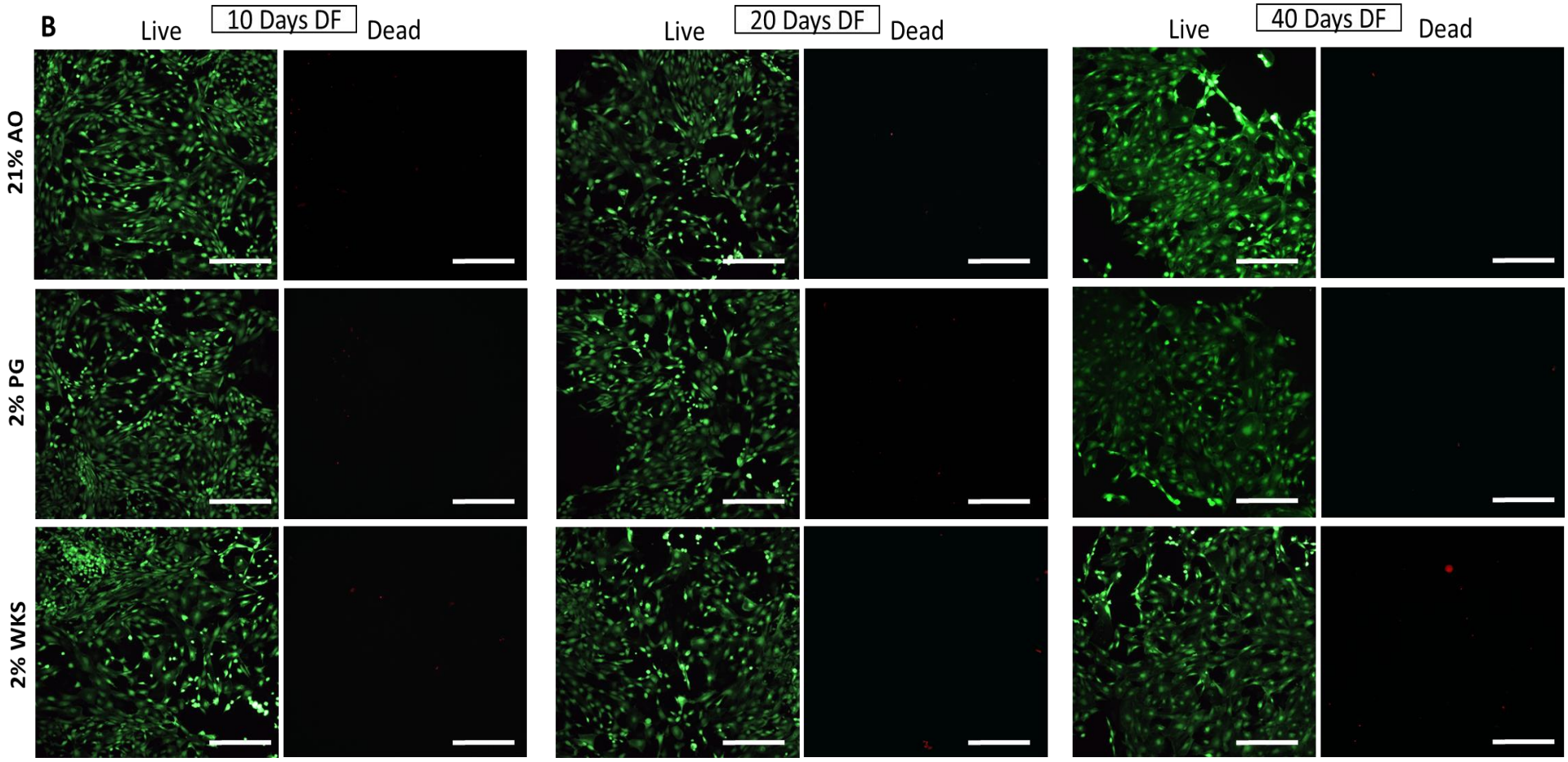

***Figure 3.4*. Live dead cell imaging and viability of differentiated ESCs.** SHEF1 **(A)** and SHEF2 **(B)** cells were differentiated in 21% AO, 2% PG and 2% WKS conditions. Images represent three independent samples for each condition, and the scale bar represents 100 μm.

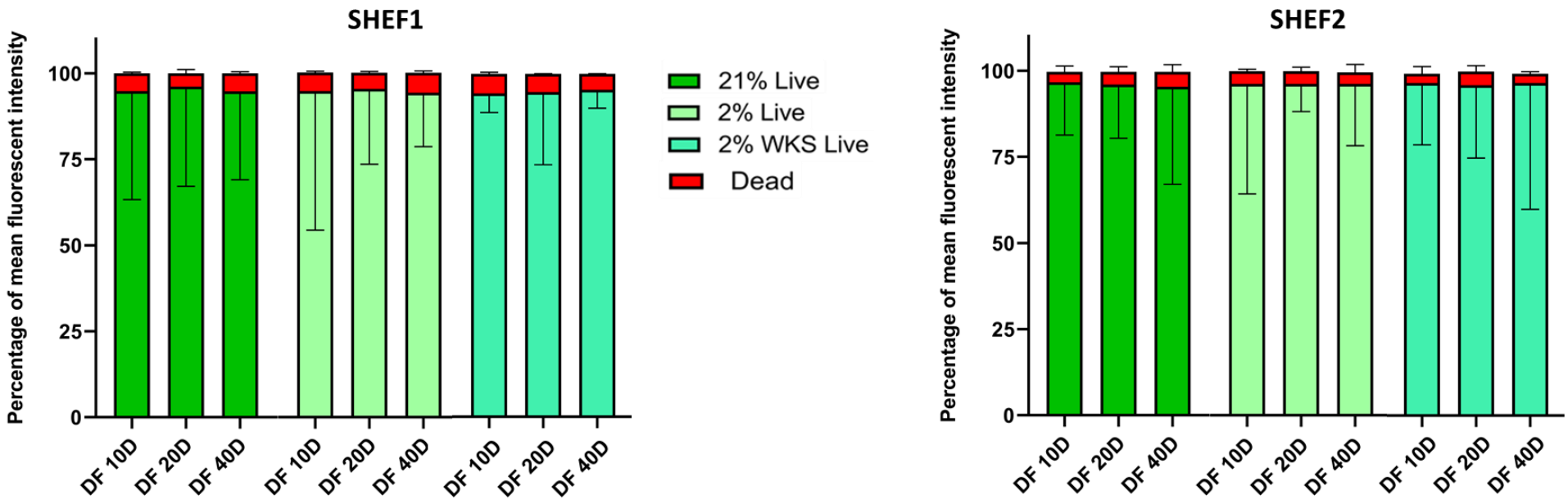

***Figure 3.5*. The mean fluorescent intensity of live and dead cells in SHEF1 and SHEF2 cells in 21% AO, 2% PG and 2% WKS conditions.** The fluorescent intensity of live cells is indicated with green shades, and the fluorescent intensity of dead cells is represented with red colour. Error bars were represented for live cells on the bottom and dead cells on the above column. The results are illustrated with three independent samples (n=3) for each condition.

3.2.4 Population doubling time in differentiated cells

The proliferation capacity of differentiated cells was evaluated every two days across a 40 day culture period in air oxygen and physoxic conditions. All conditions evidenced a short lag-phase in SHEF1 cells. We observed 40, 36 and 32.7 hours of doubling time after day 10 in 21% AO, 2% PG and 2% WKS conditions, respectively. The population doubling time of SHEF1 cells after 40 days of differentiation was calculated as 72, 68.6 and 62.6 hours in air oxygen, 2% PG and 2% WKS, respectively. However, cells were grown under air oxygen, and physoxia followed a consistent growth rate (an exponential growth curve) from day 0-to 36 and then began to slow (stationary phase) progressively until day 40. The exponential growth kinetics showed a significant increase in population doubling time in physoxia than air oxygen condition ***(Fig 3.6.A)***. Differentiated ESCs represented different cell morphology during differentiation ***(Fig 3.7).*** SHEF2 cells showed a similar trend with a short lag phase and consistent growth rate (an exponential growth curve) from day 0-to 36 and then began to slow (stationary phase) until day 40. Doubling times of SHEF2 cells cultured in 21% AO, 2% PG and 2% WKS were calculated as 34.3, 30 and 28.8 hours, respectively, during 10 day differentiation. The population doubling time of SHEF2 cells during 40 days of differentiation was calculated as 65.4, 62.6 and 57.5 hours in air oxygen, 2% PG and 2% WKS, respectively. Overall, both cell data indicate that cells cultured in 2% WKS proliferate faster than air oxygen. After day 15, differentiated cells displayed significantly increased population doubling time in physoxia versus AO ***(Fig 3.6)***.

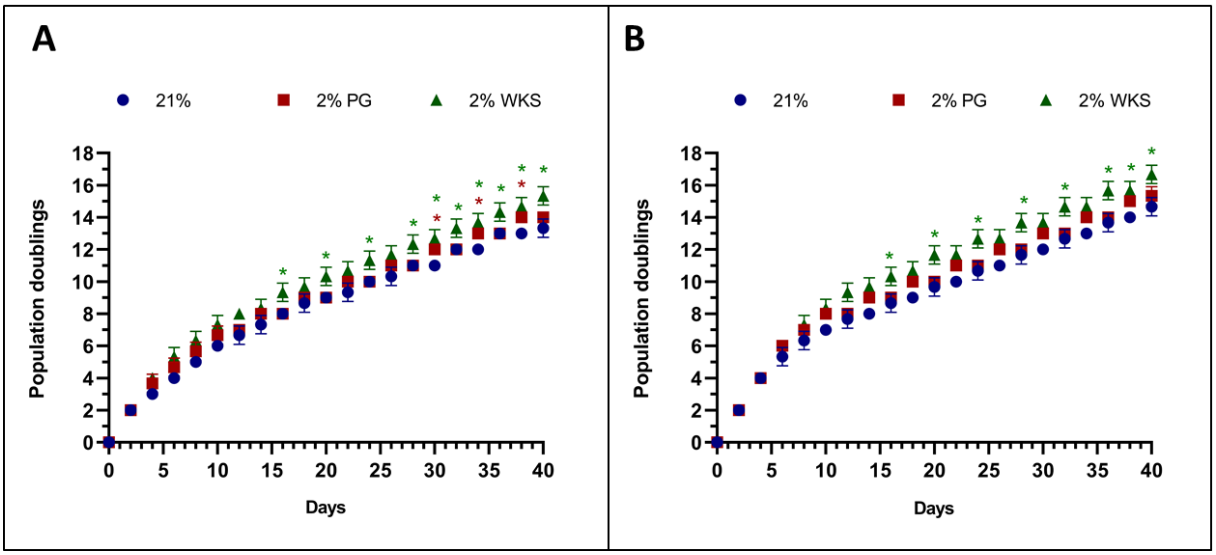

Figure 3.6. **Differentiated SHEF1 and SHEF2 cells population doubling time.** SHEF1 **(A)** and SHEF2 **(B)** cells differentiated in three oxygen conditions. The X-axis represents days in cell culture, and Y-axis shows the population doublings during 40 days of differentiation. The results are illustrated with three independent samples (n=3) for each condition. Data are represented as mean ± standard deviation (SD), *p<0.05.

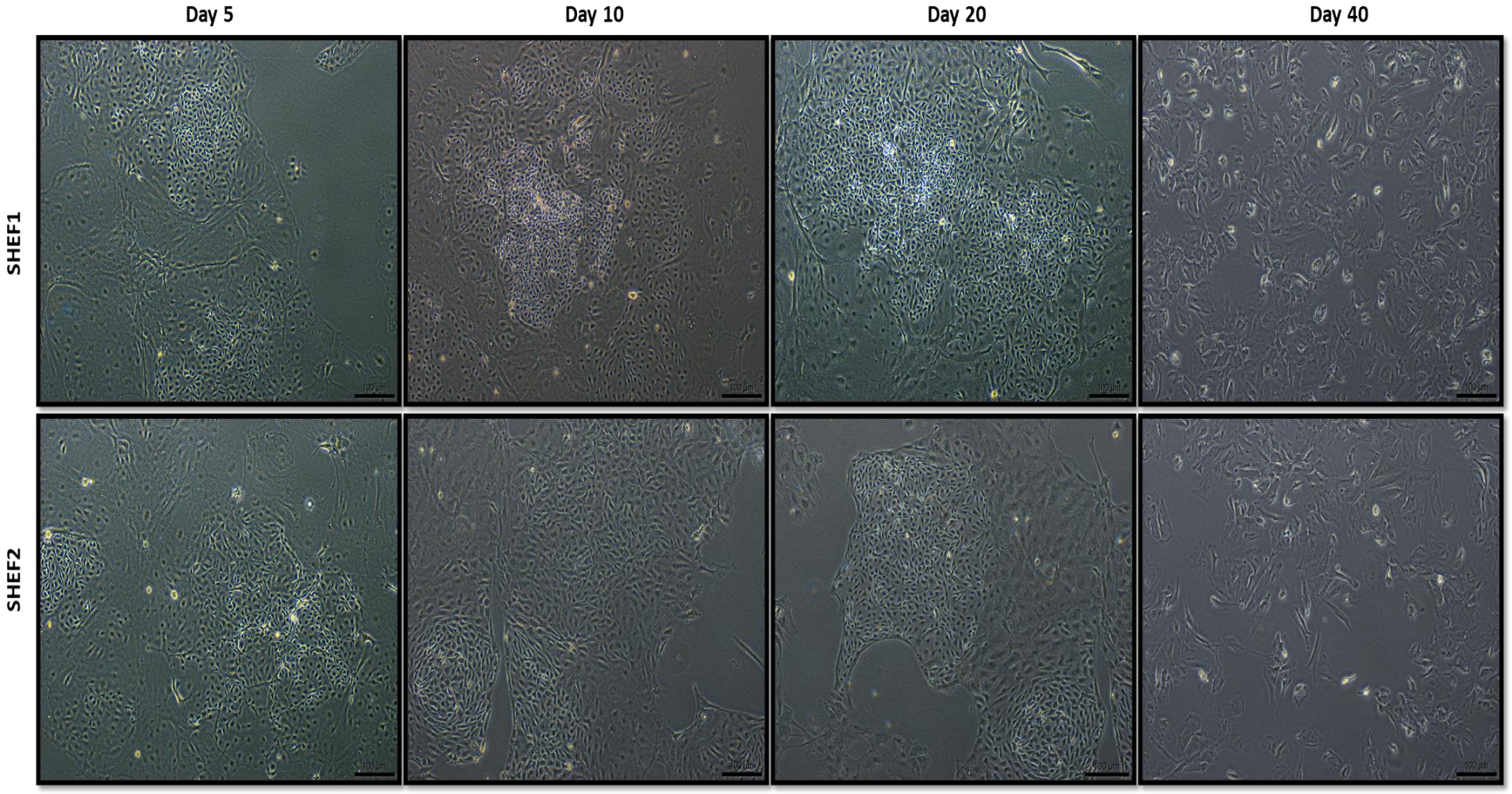

Figure 3.7. **Morphology of differentiated SHEF1 and SHEF2 cells.** Representative images showing cell morphology over time. Pictures are taken at 10X magnification, and the scale bar indicates 100 µm.

3.2.5 Three Germ Layer Differentiation Gene Expression

RT-qPCR was performed to examine relative gene expressions for three germ layer differentiation genes NES (Nestin, ectodermal marker), TBXT (T-Box Transcription Factor T, mesodermal marker), KDR (Kinase Insert Domain Receptor, mesodermal marker) and AFP (Alpha-fetoprotein, endodermal marker) in differentiated cells. No significant difference in NES expression was observed in undifferentiated SHEF1 cells cultured in 21% AO, 2% PG and 2% WKS. Monolayer differentiated SHEF1 cells cultured in 21% AO showed a significantly higher (1.88 ± 0.71, $p<0.001$) Nestin gene expression after 5 days. However, the level of relative Nestin expression was lower in differentiated cells cultured in 2% PG and 2% WKS (-0.34 ± 0.82 and -1.86 ± 0.34, respectively) on day 5. After 10 days differentiation, statistically significant downregulation was observed in 21% AO, 2% PG, and 2% WKS conditions (-1.67 ± 0.76, -1.91 ± 1.18 and -2.55 ± 0.72, $p<0.001$, respectively). Similar significant reductions were noted in 20 days differentiated cells grown under 21% AO, 2% PG and 2% WKS microenvironment (-1.08 ± 1.28, -1.45 ± 0.55 and -1.25 ± 0.76, $p<0.001$, respectively). The level of Nestin gene expression started to increase in differentiated cells following treatment with 2% WKS (0.004 ± 0.28) on day 40, and cells cultured in 2% WKS had significantly higher relative gene expression versus 21% AO (-1.33 ± 0.38) and 2% PG (-0.43 ± 0.73) in day 40. In addition, there was a significant decrease in gene expression in all conditions during differentiation compared to undifferentiated SHEF1 (***Fig 3.8.A)***. Expression of NES was significantly higher in 21% AO versus 2% WKS (-1.86 ± 0.30, $p<0.01$) microenvironment in undifferentiated SHEF2. There was a significant decrease in NES gene expression in differentiated SHEF2 at day 5 in 2% PG (-1.70 ± 1.12, $p<0.05$) and day 10, 20 in 2% WKS (-1.92 ± 0.35, $p<0.01$ and -5.85 ± 0.21, $p<0.05$) versus 21% AO. Interestingly, there was a significant decrease in NES expression on days 20 and 40 ($p<0.001$) in all conditions compared to undifferentiated SHEF2 (***Fig 3.8.B)***.

Similar variations in KDR gene expression was observed in monolayer differentiated cells cultured in three conditions with a significant increase during 10 ($p<0.01$), 20 ($p<0.001$) and 40 days ($p<0.001$) differentiation in all conditions compared to undifferentiated cells. There was a significant decrease in KDR gene expression at day 5 in 2% PG (0.80 ± 0.59, $p<0.05$) and 2% WKS (-0.93 ± 0.87, $p<0.01$) cultured SHEF1 cells versus 21% AO (1.14 ± 0.59). KDR expression increased gradually during 5, 10, 20 and 40 days monolayer differentiation (1.14 ±

0.59, 0.67 ± 0.51, 1.78 ± 0.41 and 1.43 ± 0.83, respectively) in cells following 21% AO treatment. The mean value of gene expression of cells cultured in 2% PG were 0.80 ± 0.59, 1.14 ± 0.47, 0.98 ± 0.82 and 0.77 ± 0.69 during monolayer differentiation at day 5, 10, 20 and 40, respectively. Differentiated cells grown under 2% WKS condition showed a significant increase at days 10, 20 and 40 (0.69 ± 0.59, 1.31 ± 0.59 and 1.66 ± 0.45, respectively) (***Fig 3.8.A)***. Undifferentiated SHEF2 cells cultured in 2% PG (-1.45 ± 0.18, $p<0.05$) and 2% WKS (-1.16 ± 0.68) showed a lower expression of KDR versus 21% AO. A significant decrease in gene expression was noted at day 5 in 2% PG (0.93 ± 1.11, $p<0.05$) versus AO. Also, we noted significantly less expression of KDR in 2% WKS at day 10 (1.76 ± 1.07, $p<0.05$) and 20 (1.93 ± 0.85, $p<0.01$) compared to 21% AO cultured cells. There was a significant increase in KDR expression after day 5, 10, 20 and 40 ($p<0.001$) in all conditions compared to undifferentiated SHEF2 cells (***Fig 3.8.B)***.

In general, the TBXT gene expression results showed that a higher mesodermal marker expression was noted during spontaneous differentiation in SHEF1 monolayer differentiated cells. Undifferentiated SHEF1 cells cultured in 2% PG (-1.46 ± 0.72, $p<0.05$) and 2% WKS (--0.59 ± 0.88) displayed a reduction compared to 21% AO condition. There was no significant difference in the three oxygen environments in differentiated SHEF1 cells. Mesodermal marker TBXT expression was significantly higher on days 5, 10, 20 and 40 ($p<0.001$) in differentiated SHEF1 versus undifferentiated cells in all conditions (***Fig 3.8.A)***. Undifferentiated SHEF2 cells cultured in 2% PG (-1.25 ± 1.13, $p<0.05$) and 2% WKS (-2.18 ± 1.34, $p<0.01$) displayed a significant reduction compared to 21% AO condition. TBXT expression was significantly higher on days 5, 10, 20 and 40 ($p<0.001$) differentiated SHEF2 versus undifferentiated cells in all conditions. 20 day differentiated SHEF2 cells in 2% PG (1.85 ± 0.95, $p<0.01$) and 2% WKS (1.87 ± 0.45, $p<0.01$) showed a significant reduction compared to 21% AO (3.32 ± 0.84). Also, 40 day differentiated SHEF2 cells in 2% PG (3.72 ± 0.53, $p<0.01$) showed a significant reduction compared to 21% AO (5.22 ± 0.46) (***Fig 3.8.B)***.

There was a variation in endodermal marker AFP gene expression in monolayer differentiated SHEF1 cells cultured in three conditions. There was no increase in the mean value of gene expression during 5, 10, 20 or 40 days of differentiation. SHEF1 cells cultured in 2% PG and 2% WKS physoxia conditions for 5 days (-2.95 ± 0.42 and -5.66 ± 0.37, $p<0.001$)) displayed a significant reduction in comparison to 21% AO (0.57 ± 0.56). Differentiated cells cultured for 10 days in 2% WKS (-5.08 ± 0.74, $p<0.01$) and 20 days in 2% PG (-3.40 ± 1.29, $p<0.01$) showed also a significant reduction in comparison to 21% AO (- 3.56 ± 0.57 and -1.05

± 0.94, respectively). However, the expression of AFP was significantly higher in cells cultured in 2% PG and 2% WKS (1.71 ± 1.19, $p>0.01$ and 0.06 ± 0.77, $p>0.001$, respectively) when compared to AO (-3.53 ± 0.55) at day 40 (***Fig 3.8.A)***. The expression of AFP was significantly lower in undifferentiated SHEF2 cells cultured in 2% PG and 2% WKS (-1.56 ± 0.73, $p>0.05$ and -2.31 ± 0.42, $p>0.001$, respectively) when compared to 21% AO. There was a significant decrease in AFP expression at day 5 differentiated SHEF2 cells in 2% PG (-2.92 ± 0.68, $p<0.01$) versus AO (0.15 ± 1.14). A significant decrease in AFP gene expression was noted at day 10 in WKS (-1.98 ± 0.59, $p<0.05$) versus 21% AO (-1.14 ± 0.19). There was a decrease in the mean value of AFP gene expression in differentiated SHEF2 cells at day 40 (***Fig 3.8.B)***.

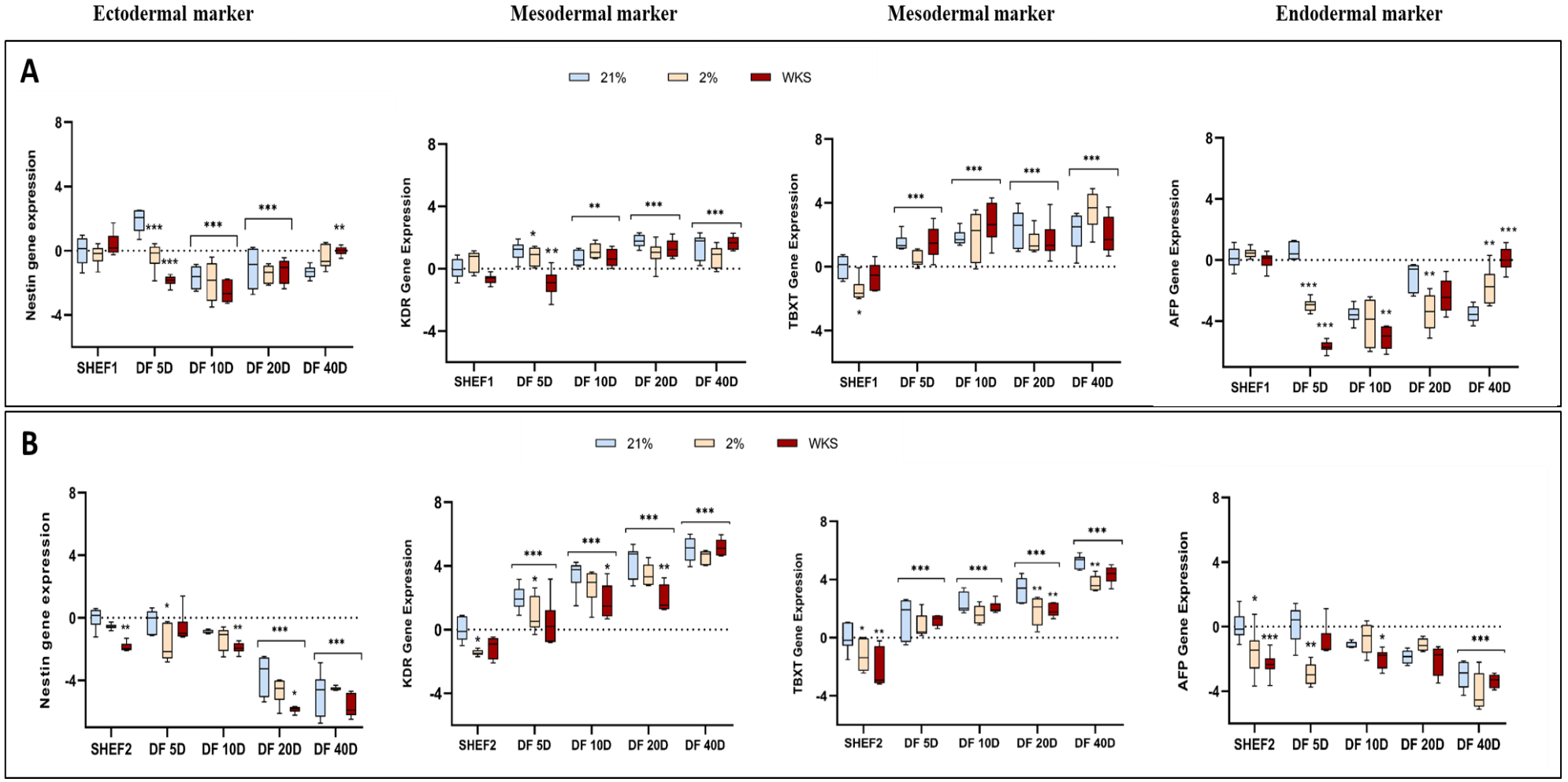

Figure 3.8. **Box and whisker plots of relative Nestin, KDR, TBXT and AFP gene expression.** SHEF1 **(A)**, SHEF2 **(B)** undifferentiated and differentiated cells were obtained in air oxygen (21% AO) and physiological oxygen conditions (2% PG and 2% WKS). The RT-qPCR expression ($2^{-\Delta\Delta CT}$) of the genes normalized to the expression of GAPDH. The box represents the interquartile range, the whisker illustrates the outer quartiles, and the line in the middle shows the median expression. Data are represented as n=3x3, *p<0.05, **p<0.01, ***p<0.001 vs air oxygen (21% AO). Bars with stars indicate a significant difference between differentiated and undifferentiated cells. The other stars compare physoxia conditions to 21% AO.

When the data from both stem cells were combined, a significant decrease in NES expression was noted at day 10 ($p<0.01$), 20 ($p<0.001$) and 40 ($p<0.001$) in all conditions when compared to undifferentiated SHEF cells. Also, there was a significant decrease in 2% PG, 2% WKS at day 5 (-1.02 ± 1.18, $p<0.001$, -1.25 ± 0.96, $p<0.01$) and in 2% WKS at day 10 (-2.24 ± 0.63, $p<0.05$) when compared to 21% AO (0.83 ± 1.29 and -1.28 ± 0.66) respectively.

Combined data from two undifferentiated ESCs showed a significant decrease in 2% WKS (-0.89 ± 0.56, $p<0.05$) compared to 21% AO. Also, there was a significant decrease in KDR gene expression of differentiated SHEF cells at day 5 in 2% PG and 2% WKS (0.87 ± 0.85, $p<0.05$ and -0.24 ± 1.34, $p<0.001$) and at day 20 in 2% WKS (1.62 ± 0.77, $p<0.01$) versus 21% AO (1.57 ± 0.79 and 3.03 ± 1.49), respectively. Overall, there was a significant increase in gene expression in all conditions during differentiation at day 10 ($p<0.01$), 20 ($p<0.001$) and 40 $p<0.001$) compared to undifferentiated SHEF cells.

Pooled data from two ESCs demonstrated that undifferentiated SHEF cells cultured in 2% PG (-1.35 ± 0.91, $p<0.01$) and 2% WKS (-1.38 ± 1.36, $p<0.01$) had significantly less TBXT expression versus AO, and 20 day differentiated EBs in 2% PG, 2% WKS (1.70 ± 0.82, 1.76 ± 0.87, $p<0.05$) compared to 21% AO (2.87 ± 1.09). Further, TBXT expression was higher in all conditions after 5, 10 and 20 days differentiation ($p<0.001$) versus 21% AO.

Pooled data from two stem cells demonstrated that AFP was decreased at day 5, ($p<0.01$) day 10 ($p<0.001$), 20 ($p<0.01$) and 40 ($p<0.001$) in all conditions compared to undifferentiated SHEF cells. Undifferentiated SHEF cells are grown under 2% WKS (-1.17 ± 1.28, $p<0.05$) had a significantly lower mean value versus 21% AO. There was a significant decrease in 2% PG, 2% WKS at day 5 (-2.94 ± 0.54, $p<0.001$, -3.29 ± 2.58, $p<0.01$) and in 2% WKS at day 10 (-3.53 ± 1.74, $p<0.001$) compared to 21% AO (0.36 ± 0.88 and -2.35 ± 1.33) respectively (***Fig 3.9)***.

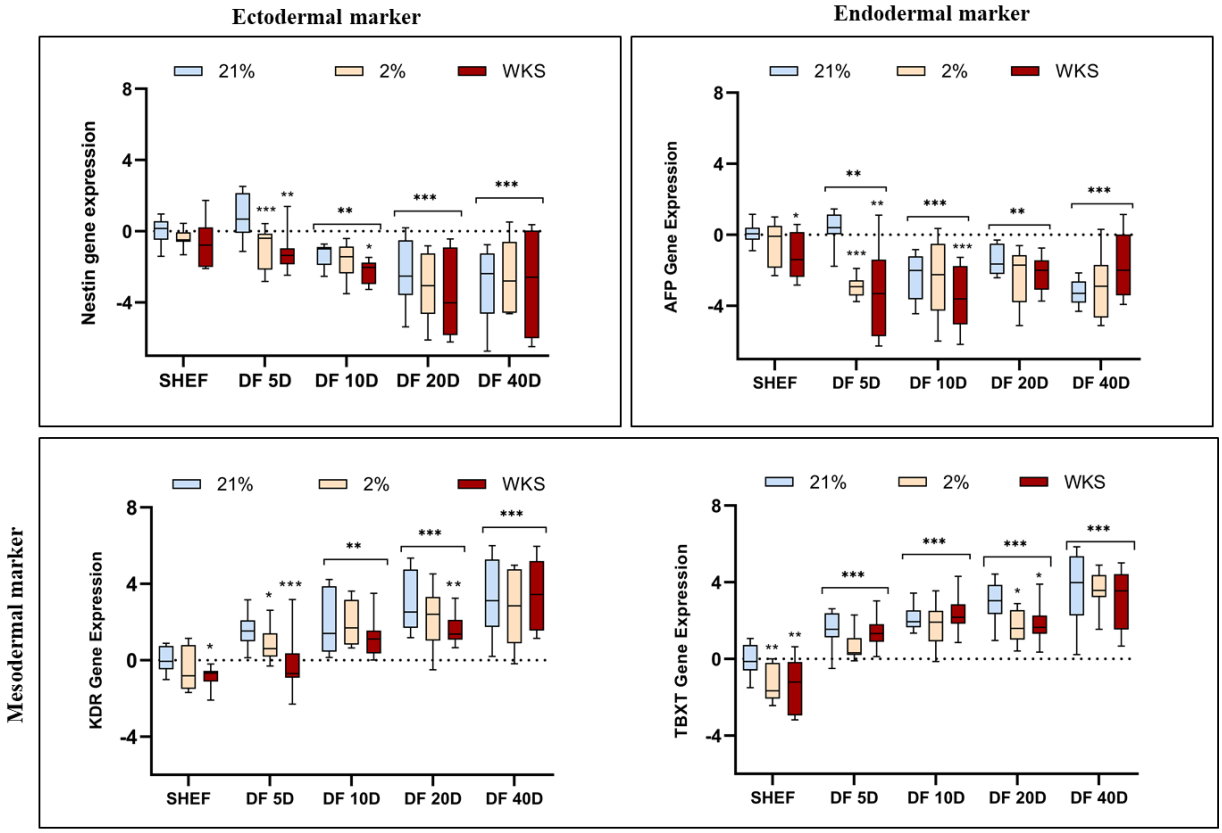

Figure 3.9. **Box and whisker plots of relative Nestin, KDR, TBXT and AFP gene expression.** SHEF1 and SHEF2 data were pooled together. Undifferentiated and differentiated cells were obtained in air oxygen (21% AO) and physiological oxygen conditions (2% PG and 2% WKS). The RT-qPCR expression ($2^{-\Delta\Delta CT}$) of the genes normalized to the expression of GAPDH. The box represents the interquartile range, the whisker illustrates the outer quartiles, and the line in the middle shows the median expression. Data are represented as n=3x3, *p<0.05, **p<0.01, ***p<0.001 vs air oxygen (21% AO). Bars with stars indicate a significant difference between differentiated and undifferentiated cells. The other stars compare physoxia conditions to 21% AO.

3.2.6 Telomerase Activity

To evaluate the telomerase activity in different oxygen conditions and during differentiation, TRAP assay was performed using the TRAPeze® Kit RT Telomerase Detection Kit (Millipore, USA). Cell number and protein concentration were established for each sample, and appropriate controls were used for each assay.

There were significant differences in the level of telomerase activity between air oxygen and reduced oxygen conditions 2%PG and 2%WKS in undifferentiated SHEF1 cells (5.35 ± 0.19, 5.62 ± 0.31, $p<0.05$ and 5.73 ± 0.38, $p<0.01$, respectively). A significant decrease was observed during 5 days, 10 days, 20 days, and 40 days differentiation of cells in air oxygen environment 4.67 ± 0.06, ($p<0.01$) and 3.70 ± 0.14, ($p<0.001$), 3.33 ± 0.13, ($p<0.001$) and 2.53± 0.03, ($p<0.001$), respectively compared to undifferentiated SHEF1 in 21% AO condition. Similar significant reductions were observed in SHEF1 cells grown under 2% PG reduced oxygen conditions at day 5, day 10, day 20, and 40 days (5.18 ± 0.07, $p<0.05$, 4.48 ± 0.13, $p<0.001$, 3.12 ± 0.04, $p<0.001$ and 2.30 ± 0.08, $p<0.001$, respectively) in comparison undifferentiated cells. Consistently, 5, 10, 20 and 40 days differentiated cells (5.18 ± 0.31, $p<0.05$, 4.10 ± 0.07, $p<0.001$, 3.96 ± 0.08, $p<0.001$ and 2.63 ± 0.03, $p<0.001$, respectively) showed significant difference in comparison undifferentiated SHEF1 cells cultured in workstation condition (2% WKS). Telomerase activity significantly decreased between all SHEF1 groups after 40 days of differentiation. A significant difference was observed on days 5 differentiated cells grown in 2% PG ($p<0.01$) and 2% WKS ($p<0.01$) compared to 21% AO condition. 10 days differentiated cells showed significant differences in 2% PG ($p<0.001$) and 2% WKS ($p<0.05$) when compared to cells cultured in 21% AO. Day 20 cells demonstrated a significant difference in 2% WKS ($p<0.001$) versus 21% AO, while day 40 differentiation had no significant differences between conditions. The average relative telomerase activity of differentiated and undifferentiated cells combined was 1.99 ± 0.35, 2.15 ± 0.44 and 2.07 ± 0.32 in 21% AO, 2% PG and 2% WKS heat-treated (HT) samples, respectively (***Fig 3.10)***. In addition, we showed a significant correlation between telomerase activity and the differentiation process in 21% AO (R^2=0.85), 2% PG (R^2=0.91) and 2% WKS (R^2=0.87) conditions using linear regression analysis.

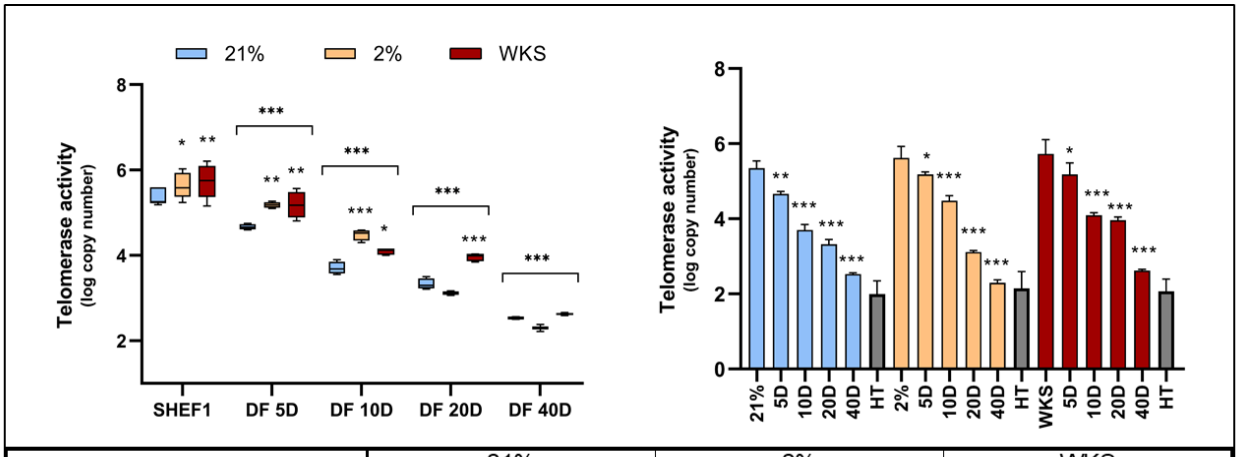

	21%	2%	WKS
R square	0.8548	0.9154	0.8715
P value	<0.0001	<0.0001	<0.0001
Deviation from zero?	Significant	Significant	Significant
Equation	Y = -0.07048*X + 4.991	Y = -0.08954*X + 5.484	Y = -0.07581*X + 5.472

Figure 3.10. **Decreased telomerase activity in differentiated SHEF1 cells with higher enzyme activity in physoxia.** SHEF1 cells were obtained in air oxygen (21% AO) and physiological oxygen conditions (2% PG and 2% WKS) at different time points. Data are represented as mean ± standard deviation (SD), n=3, *p<0.05, **p<0.01, ***p<0.001. HT (heat-treated control samples). Bars with stars indicate a significant difference between differentiated and undifferentiated cells. The other stars compare physoxia conditions to 21% AO.

There was no significant difference in undifferentiated SHEF2 cells cultured in 21% AO, 2% PG and 2% WKS (5.78 ± 0.16, 5.79 ± 0.14, 5.99 ± 0.14, respectively). After day 5, cells cultured in 2% PG and 2% WKS reduced oxygen conditions showed significantly higher enzyme activity (5.42 ± 0.36, p<0.001 and 5.65 ± 0.22, p<0.001) compared to AO condition (4.28 ± 0.05). Similar significant differences were observed in 2% PG and 2% WKS reduced oxygen conditions at day 10 (4.91 ± 0.59, p<0.001 and 5.23 ± 0.31, p<0.001) and day 20 (4.15 ± 0.31, p<0.01 and 4.44 ± 0.44, p<0.001) compared to AO (3.65 ± 0.22 and 3.33 ± 0.26, respectively). 2% PG condition (3.53 ± 0.52, p<0.001) showed a significant increase in comparison to AO (2.84 ± 0.29) cultured cells after 40 days of differentiation. Moreover, three conditions together showed significantly decreased (p<0.001) telomerase activity following 40 days of differentiation compared to undifferentiated cells. Overall, there is a significant difference in telomerase activity between air oxygen and reduced oxygen conditions, 2% PG and 2% WKS, in differentiated SHEF2 cells. The average relative telomerase activity of

differentiated and undifferentiated cells together was 2.81 ± 0.08, 2.99 ± 0.25 and 2.96 ± 0.12 in 21% AO, 2% PG and 2% WKS HT samples, respectively ***(Fig 3.11)***. Also, a similar significant correlation between telomerase activity and the differentiation process was observed in air oxygen (R^2=0.67), 2% PG (R^2=0.76) and 2% WKS (R^2=0.94) conditions using linear regression analysis.

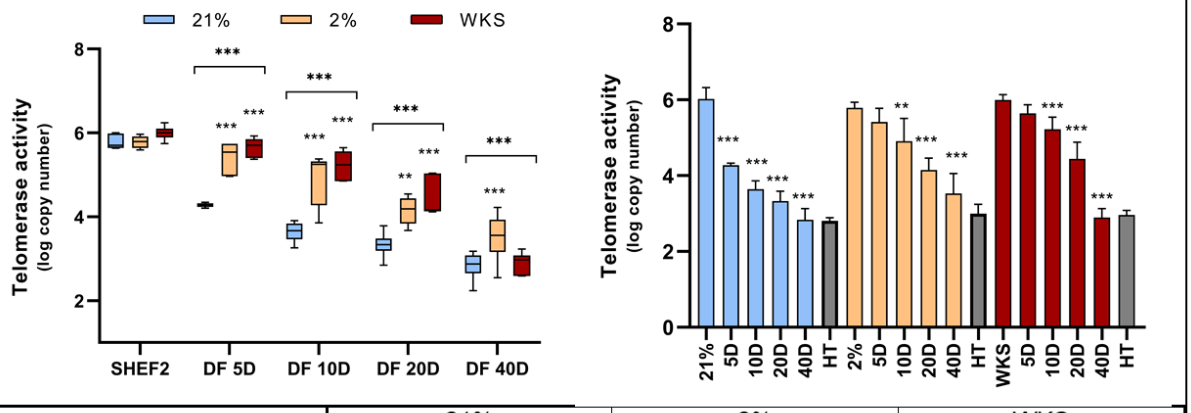

	21%	2%	WKS
R square	0.6728	0.7648	0.9418
P value	<0.0001	<0.0001	<0.0001
Deviation from zero?	Significant	Significant	Significant
Equation	Y = -0.06011*X + 4.876	Y = -0.05656*X + 5.608	Y = -0.07798*X + 6.010

Figure 3.11. **Decreased telomerase activity in differentiated SHEF2 cells with higher enzyme activity in physoxia.** SHEF2 cells were obtained in air oxygen (21% AO) and physiological oxygen conditions (2%PG and 2%WKS) at different time points. Data are represented as mean ± standard deviation (SD), n=3, *p<0.05, **p<0.01, ***p<0.001. HT (heat-treated control samples). Bars with stars indicate a significant difference between differentiated and undifferentiated cells. The other stars compare physoxia conditions to 21% AO.

Numerical data from two pluripotent stem cells were pooled for analysis purposes. There was no significant difference in undifferentiated stem cells cultured in 21% AO, 2% PG and 2% WKS (5.76 ± 0.42, 5.72 ± 0.23, 5.89 ± 0.29, respectively). After day 5, cells cultured in 2% PG and 2% WKS reduced oxygen conditions showed significantly higher enzyme activity (5.34 ± 0.31, p<0.001 and 5.50 ± 0.33, p<0.001) compared to AO condition (4.40 ± 0.19). Similar significant differences were observed in 2% PG and 2% WKS reduced oxygen conditions at day 10 (4.78 ± 0.53, p<0.001 and 4.88 ± 0.60, p<0.001) and day 20 (3.83 ± 0.56, p<0.01 and 4.29 ± 0.43, p<0.001) compared to AO (3.66 ± 0.19 and 3.33 ± 0.22, respectively). 2% PG (3.22

± 0.71, p<0.001) showed a significant increase in comparison to AO (2.76 ± 0.29) cultured cells after 40 days of differentiation. The average relative telomerase activity of differentiated and undifferentiated cells together was 2.34 ± 0.49, 2.54 ± 0.56 and 2.48 ± 0.52 in 21% AO, 2% PG and 2% WKS HT samples, respectively (***Fig 3.12)***. Also, a similar significant correlation between telomerase activity and the differentiation process was observed in air oxygen (R^2=0.70), 2% PG (R^2=0.74) and 2% WKS (R^2=0.88) conditions using linear regression analysis.

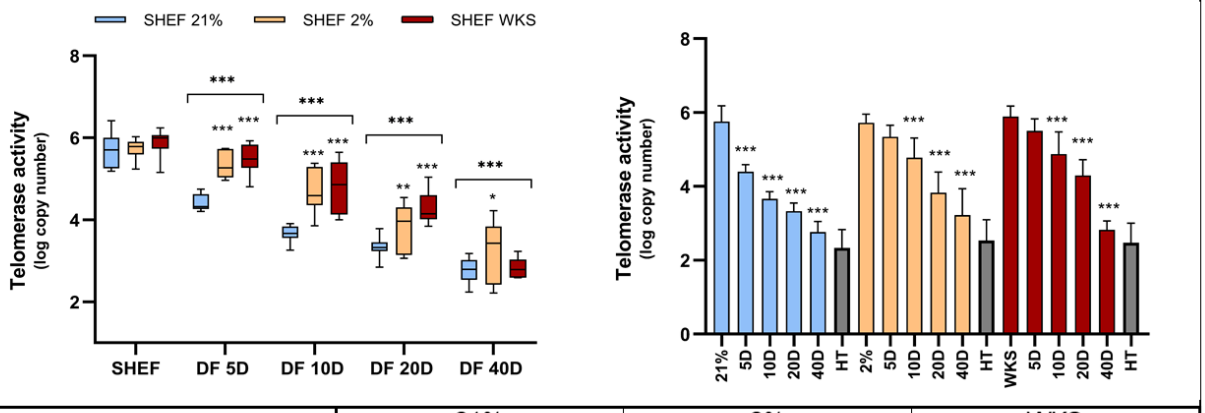

	21%	2%	WKS
R square	0.6962	0.7386	0.8782
P value	<0.0001	<0.0001	<0.0001
Deviation from zero?	Significant	Significant	Significant
Equation	Y = -0.06553*X + 4.982	Y = -0.06436*X + 5.547	Y = -0.07586*X + 5.818

***Figure 3.12*. Decreased telomerase activity in differentiated SHEF cells with higher enzyme activity in physoxia.** SHEF1 and SHEF2 data were pooled together. Cells were obtained in air oxygen (21% AO) and physiological oxygen conditions (2% PG and 2% WKS) at different time points. Data are represented as mean ± standard deviation (SD), n=3, *p<0.05, **p<0.01, ***p<0.001. HT (heat-treated control samples). Bars with stars indicate a significant difference between differentiated and undifferentiated cells. The other stars compare physoxia conditions to 21% AO.

3.2.7 TERT Protein Expression decreased during differentiation

We next sought to confirm that the loss of telomerase activity was associated with a decrease in TERT protein expression. SHEF1 and SHEF2 cells were stained with TERT

antibody at 0, 5, 10, 20 and 40 days of differentiation. SHEF1 stem cells showed high TERT protein expression in three conditions (***Fig 3.14.A)***, but after 5 days of differentiation, we observed reduced protein expression, which decreased further on day 10 (***Fig 3.13.B -C)***. Cells differentiated for 20 and 40 days showed low or undetectable levels of TERT protein (***Fig 3.13.D-E)***.

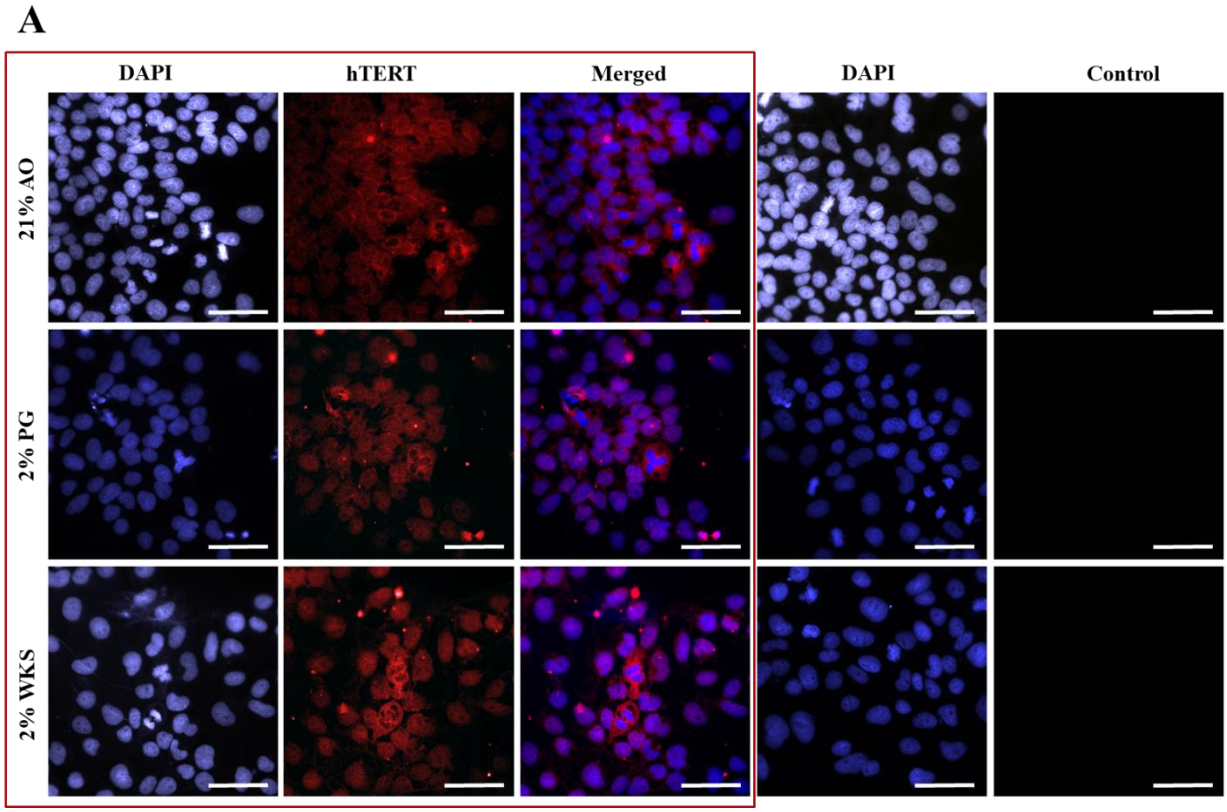

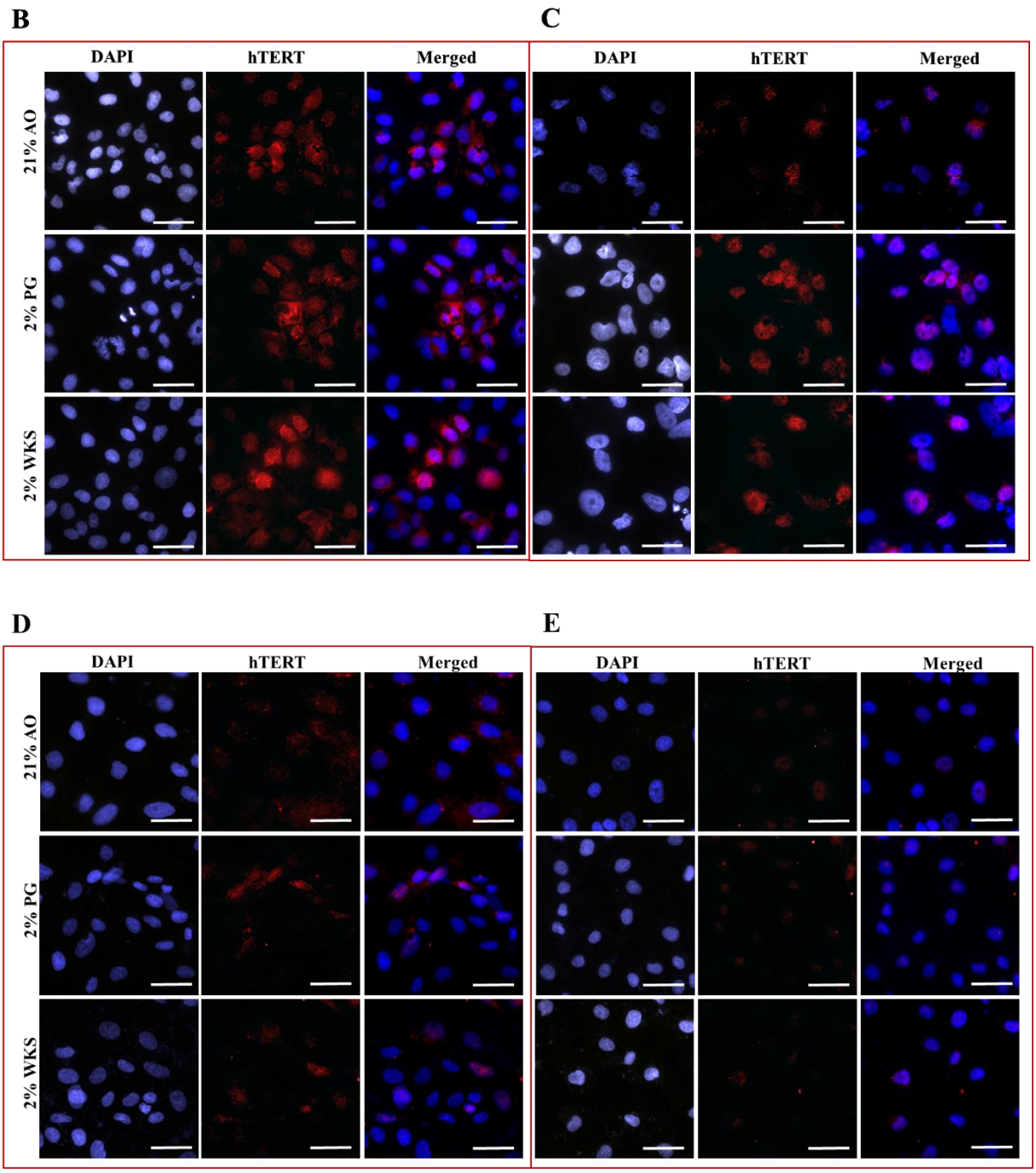

Figure 3.13. **Immunofluorescence staining for TERT protein of SHEF1. (A)** Undifferentiated, **(B)** 5 days differentiated, **(C)** 10 days differentiated, **(D)** 20 days differentiated and **(E)** 40 days differentiated cells were cultured in AO and physoxia (2% PG and 2% WKS) conditions. The scale bar represents **50** μm. Red colour indicates antigen, blue DAPI and secondary controls also are given.

TERT protein expression was determined in undifferentiated cells (day 0) and from spontaneous differentiated (5, 10, 20 and 40 days) SHEF2 cells to confirm TERT expression

and telomerase enzyme results. Similar to SHEF1 cells, undifferentiated SHEF2 cells expressed high TERT protein in all conditions (***Fig 3.14.A)***. SHEF2 stem cells showed high TERT protein expression in three conditions, but after 5 days of differentiation, we observed reduced protein expression. There was a decreased protein expression on day 10 (***Fig 3.14.B-C)***. Cell cultured and differentiated for 20 and 40 days showed a low or undetectable level of TERT protein (***Fig 3.14.D-E)***.

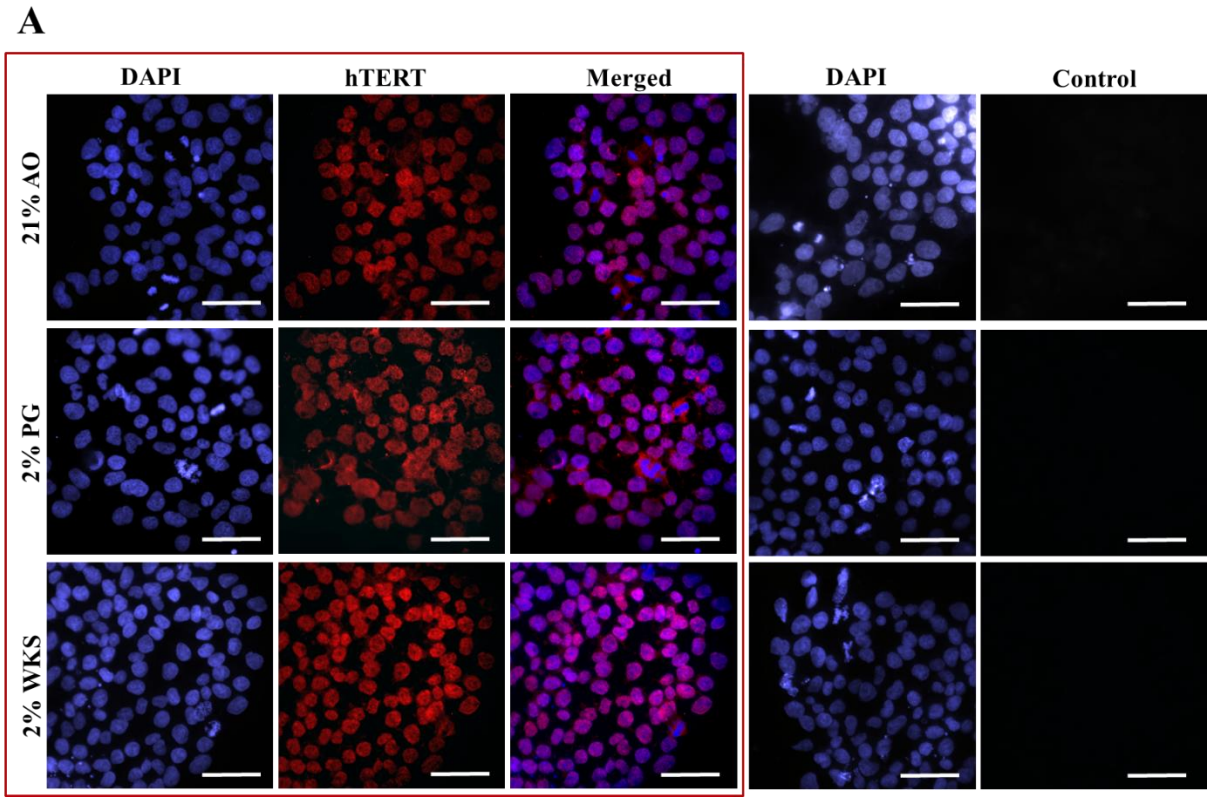

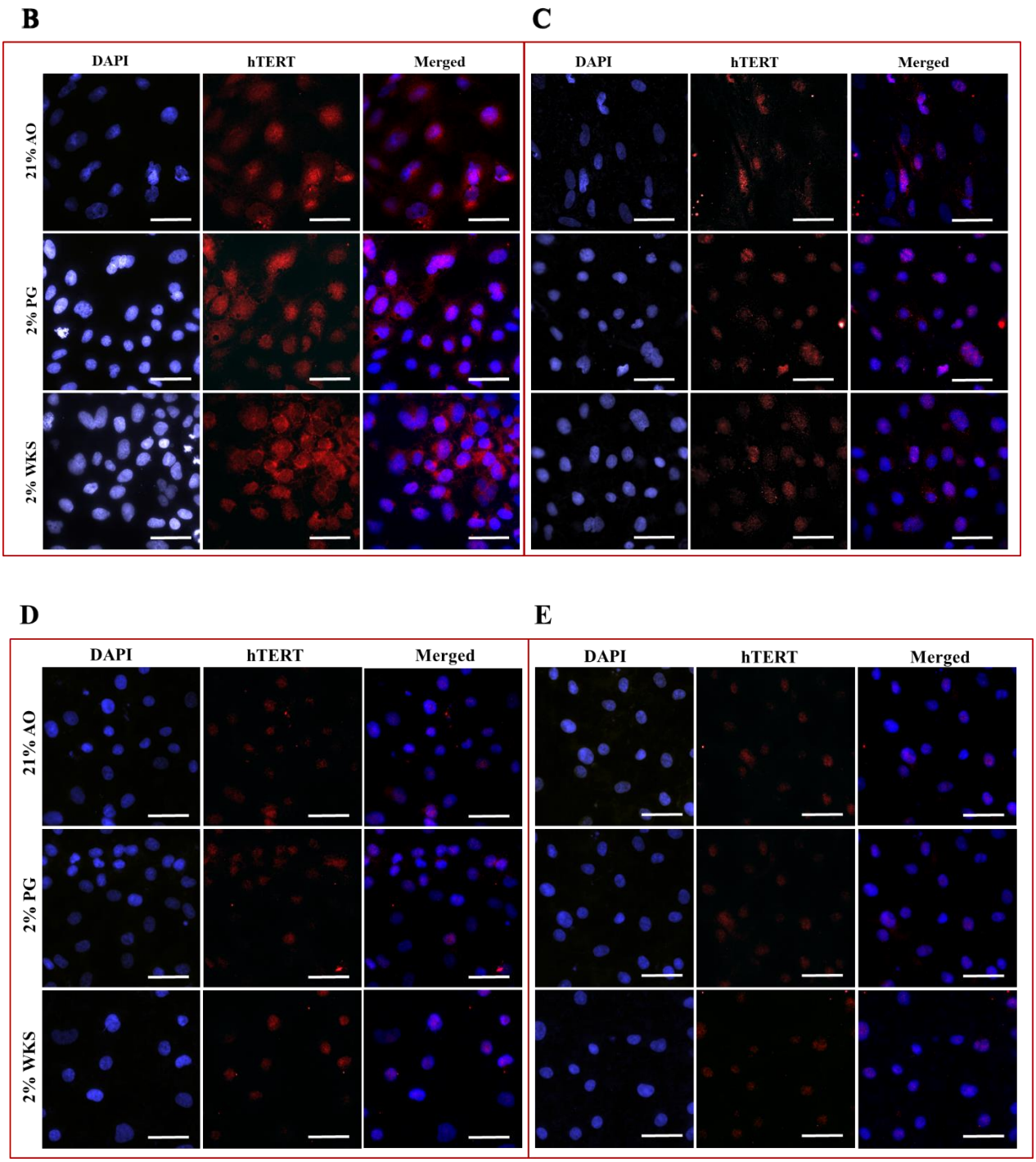

Figure 3.14. **Immunofluorescence staining for TERT protein of SHEF2. (A)** Undifferentiated, **(B)** 5 days differentiated, **(C)** 10 days differentiated, **(D)** 20 days differentiated and **(E)** 40 days differentiated cells were cultured in AO and physoxia (2% PG and 2% WKS) conditions. The scale bar represents **50** μm. Red colour indicates antigen, blue DAPI and secondary controls also are given.

3.2.8 TERT Gene Expression

To identify the effects of differentiation and physoxia, TERT gene expression was analysed with qRT-PCR in undifferentiated and differentiated cells. Relative gene expression in monolayer differentiated SHEF1 cells in comparison to undifferentiated cells was decreased at day 5 (-1.01 ± 0.31, p<0.001), day 10 (-2.28 ± 0.28, p<0.001), day 20 (-3.62 ± 0.39, p<0.001) and day 40 (-7.30 ± 0.68, p<0.001) in 21% AO. After 5-day differentiation, a significant reduction was observed in cells incubated in AO. Also, a significant increase in TERT gene expression at day 5 (-0.38 ± 0.05, p<0.05), day 10 (-1.41 ± 0.22, P<0.001) and day 20 (-2.96 ± 0.24, P<0.05) in 2% PG condition compared to 21% AO. A significant increase observed in undifferentiated SHEF1 cells incubated in 2% WKS (0.70 ± 0.87, p<0.01) versus 21% AO condition. TERT expression was significantly higher at 5 days (-0.22 ± 0.60, p<0.01), 10 days (-1.16 ± 0.39, p<0.001), 20 days (-1.53 ± 0.67, p<0.001), and 40 days (-5.41 ± 0.60, p<0.001) in differentiated SHEF1 in 2% WKS compared to AO environment. 2% WKS condition showed a significant increase at day 0 (p<0.01), day 5 (p<0.01), day 10 (p<0.001), day 20 (p<0.001) and day 40 (p<0.001) compared to AO environment (***Fig 3.15)***. A significant correlation between TERT gene expression and the differentiation process was observed in AO (R^2=0.97), 2% PG (R^2=0.98) and 2% WKS (R^2=0.89) conditions using linear regression analysis.

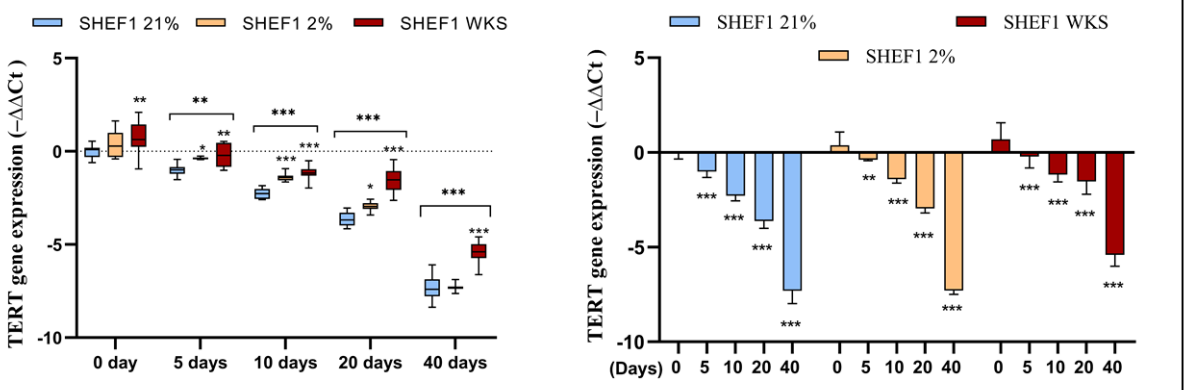

	SHEF1 21%	SHEF1 2%	SHEF1 WKS
R square	0.9713	0.9794	0.8901
P value	<0.0001	<0.0001	<0.0001
Deviation from zero?	Significant	Significant	Significant
Equation	Y = -0.1794*X - 0.1483	Y = -0.1920*X + 0.5465	Y = -0.1454*X + 0.6555

Figure 3.15. **Higher TERT gene expression in physoxia in SHEF1 cells.** SHEF1 undifferentiated and differentiated cells were obtained in air oxygen (21% AO) and physiological oxygen conditions (2% PG and 2% WKS). The RT-qPCR expression of the

TERT normalized to the expression of GAPDH. Data are represented as mean ± standard deviation (SD), n=3, *p<0.05, **p<0.01, ***p<0.001, ****p<0.0001 vs air oxygen (21% AO). Bars with stars indicate a significant difference between differentiated and undifferentiated cells. The other stars compare physoxia conditions to 21% AO.

TERT gene expression was higher in 2% PG (0.89 ± 0.48, p<0.001) and 2% WKS (1.35 ± 0.79, p<0.001) conditions in undifferentiated SHEF2 cells versus 21% AO. The mean value of TERT gene expression was downregulated in SHEF2 cells differentiated in 21% AO at day 5 (-0.79 ± 0.79), day 10 (-2.18 ± 1.22, p<0.001), day 20 (-2.91 ± 0.51, p<0.001) and day 40 (-4.35 ± 0.93, p<0.001) in comparison to undifferentiated cells. Cells differentiated in 2% PG showed a decrease after 5 days (0.20 ± 0.49) of differentiation and significant downregulation at day 10 (-0.45 ± 0.50, p<0.001), day 20 (-2.18 ± 0.64, p<0.001) and day 40 (-4.23 ± 0.93, p<0.001) in comparison to undifferentiated SHEF2 cells (0.89 ± 0.48). TERT gene expression was higher after 5 days differentiation in 2% PG (0.20 ± 0.49, p<0.01) and 2% WKS (1.26 ± 0.70, p<0.001) condition in comparison to 21% AO cultured cells (-0.79 ± 0.79). There was a significant reduction after day 10 (-0.71 ± 0.47, p<0.001), day 20 (-1.96 ± 0.64, p<0.001) and day 40 (-4.05 ± 0.75, p<0.001) in 2% WKS. SHEF2 cells cultured in 2% WKS condition showed a significant difference at day 0 (p<0.001), day 5 (p<0.001), day 10 (p<0.001), day 20 (p<0.001), day 40 (p<0.05). SHEF2 cells cultured in 2% PG showed a significant difference at day 0 (p<0.001), day 5 (p<0.01), day 10 (p<0.001), day 20 (p<0.001) when compared to AO environment (***Fig 3.16)***. A significant correlation between TERT gene expression and the differentiation process was observed in AO (R^2=0.76), 2% PG (R^2=0.90) and 2% WKS (R^2=0.86) conditions using linear regression analysis.

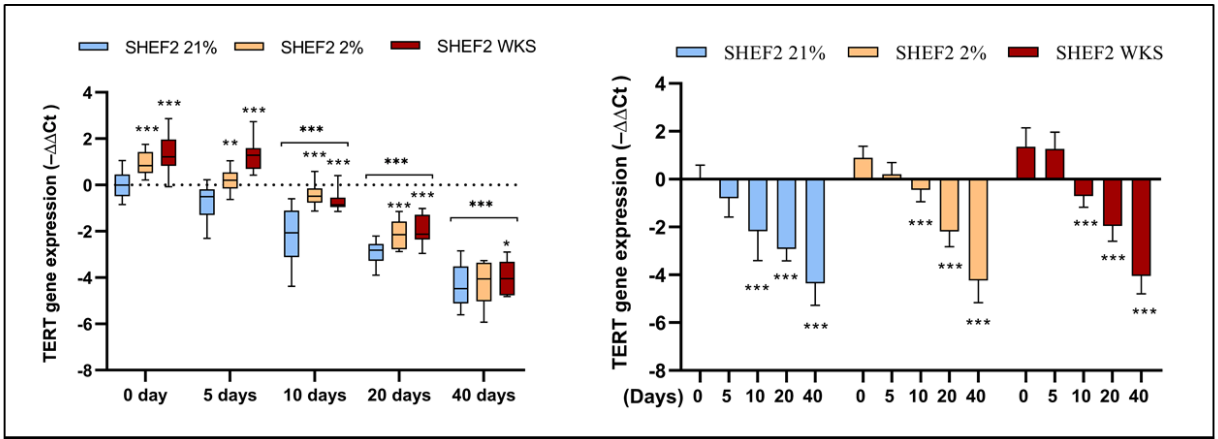

	SHEF2 21%	SHEF2 2%	SHEF2 2% WKS
R square	0.7559	0.9027	0.8634
P value	<0.0001	<0.0001	<0.0001
Deviation from zero?	Significant	Significant	Significant
Equation	Y = -0.1095*X - 0.3367	Y = -0.1310*X + 0.8251	Y = -0.1411*X + 1.308

Figure 3.16. **Higher TERT gene expression in physoxia in SHEF2 cells.** SHEF2 undifferentiated and differentiated cells were obtained in air oxygen (21% AO) and physiological oxygen conditions (2% PG and 2% WKS). The RT-qPCR expression of the TERT normalized to the expression of GAPDH. Data are represented as mean ± standard deviation (SD), n=3, *p<0.05, **p<0.01, ***p<0.001 vs 21% AO. Bars with stars indicate a significant difference between differentiated and undifferentiated cells. The other stars compare physoxia conditions to 21% AO.

Numerical data from two pluripotent stem cells were pooled for gene expression analysis purposes. There was a significant difference in undifferentiated stem cells cultured in 2% PG (0.73 ± 0.68, p<0.05) and 2% WKS (0.76 ± 0.72, p<0.05) in comparison to AO. TERT expression was downregulated in stem cells differentiated in AO at day 5 (-0.90 ± 0.59, p<0.05), day 10 (-2.23 ± 0.86, p<0.001), day 20 (-3.26 ± 0.57, p<0.001) and day 40 (-5.83 ± 1.71, p<0.001) in comparison to undifferentiated cells. Differentiation in physoxia 2% PG showed a significant downregulation at day 5 (-0.09 ± 0.45, p<0.05), day 10 (-0.92 ± 0.62 p<0.001), day 20 (-2.57 ± 0.61, p<0.001) and day 40 (-5.76 ± 1.71, p<0.001) in comparison to undifferentiated SHEF cells (0.73 ± 0.68). TERT gene expression was decreased after 5 days (0.52 ± 0.99) of differentiation in 2% WKS condition in comparison to undifferentiated SHEF cells. There was a significant reduction after day 10 (-0.93 ± 0.48, p<0.001), day 20 (-1.74 ± 0.67, p<0.001) and day 40 (-4.73 ± 0.96, p<0.001) differentiation. 2% WKS showed a significant difference at day 0 (p<0.05), day 5 (p<0.01), day 20 (p<0.001) in comparison to AO (***Fig 3.17)***. A significant correlation between TERT gene expression and the differentiation process was observed in AO

(R^2=0.81), 2% PG (R^2=0.86) and 2% WKS (R^2=0.85) conditions using linear regression analysis.

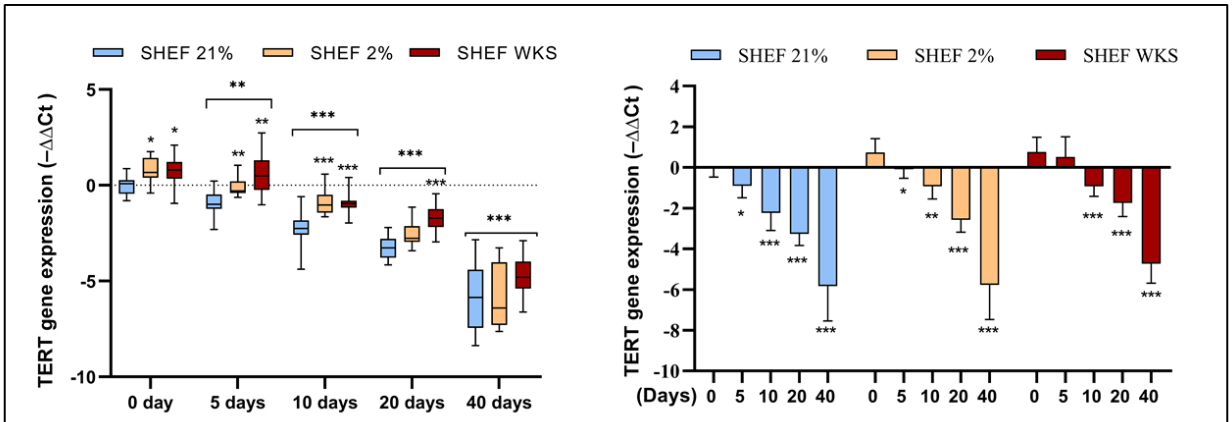

	SHEF 21%	SHEF 2%	SHEF WKS
R square	0.8102	0.8655	0.8548
P value	<0.0001	<0.0001	<0.0001
Deviation from zero?	Significant	Significant	Significant
Equation	Y = -0.1417*X - 0.3205	Y = -0.1625*X + 0.7146	Y = -0.1388*X + 0.8569

Figure 3.17. **Higher TERT gene expression in physoxia in SHEF cells.** SHEF1 and SHEF2 undifferentiated and differentiated cells data were gathered together in air oxygen (21% AO) and physiological oxygen conditions (2% PG and 2% WKS). The RT-qPCR expression of the TERT normalized to the expression of GAPDH. Data are represented as mean ± standard deviation (SD), n=3, *p<0.05, **p<0.01, ***p<0.001 vs 21% AO. Bars with stars indicate a significant difference between differentiated and undifferentiated cells. The other stars compare physoxia conditions to 21% AO.

3.2.9 Telomere Length

Telomere Length Quantification qPCR Assay (Sciencell Research Lab, USA) was performed to measure telomere length for samples collected from different oxygen conditions and differentiation time points**.** Generally, there was no significant difference in the mean telomere length value of undifferentiated SHEF1 cells under 21% AO (12.49 ± 1.08), 2% PG (11.86 ± 1.08) and 2% WKS (12.88 ± 1.56). At day 5, the mean value of telomere length was significantly higher in 2% WKS (11.12 ± 0.74) versus AO 21% (10.83 ± 0.51) and 2% PG (9.85 ± 0.98). All conditions together showed significant telomere shortening after day 5 (p<0.001), day 10 (p<0.001), day 20 (p<0.001) and day 40 (p<0.001). There was no significant

difference between 21% AO (9.41 ± 1.03) compared to 2% PG (9.63 ± 1.19) and 2% WKS (10.02 ± 0.96) on day 10. There was no significant change between AO (8.18 ± 1.25), 2% PG (7.84 ± 1.16) and 2% WKS (8.61 ± 0.62) on day 20. In addition, only 2% WKS (8.30 ± 0.72, $p<0.05$) conditions had a significant difference compare to 21% AO (7.19 ± 1.03), 2% PG (7.05 ± 1.43) at 40 days (***Fig 3.18)***. Telomerase activity was higher in physoxia and accompanied by higher doubling times in reduced oxygen conditions, so average telomere shortening was calculated as approximate ~260 bp per chromosome end in three conditions.

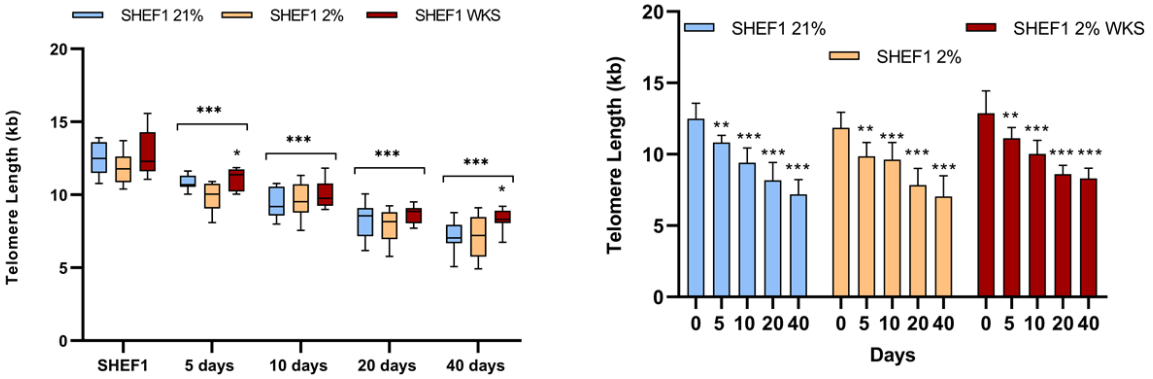

	SHEF 21%	SHEF 2%	SHEF WKS
R square	0.6916	0.6101	0.5889
P value	<0.0001	<0.0001	<0.0001
Deviation from zero?	Significant	Significant	Significant
Equation	Y = -0.1224*X + 11.55	Y = -0.1098*X + 10.98	Y = -0.1089*X + 11.89

Figure 3.18. **Decreased telomere length (kb) in differentiated SHEF1 cell populations.** The box represents the interquartile range, the whisker in the outer quartiles, and the line in the middle shows the median expression. Data are represented as n=3x3, *p<0.05, **p<0.01, ***p<0.001 vs 21% AO. Bars with stars indicate a significant difference between differentiated and undifferentiated cells. The other stars compare physoxia conditions to 21% AO.

Telomere Length Quantification qPCR Assay (Sciencell Research Lab, USA) was performed to measure telomere length for SHEF2 samples collected from different oxygen conditions and differentiation time points. Generally, there was a significant difference in the mean value of telomere length of undifferentiated SHEF2 cells 2% WKS (12.47 ± 0.79) versus 21% AO (11.20 ± 0.85) and 2% PG (11.59 ± 1.01) conditions. At day 5, the mean value of telomere length was higher in 2% WKS (11.07 ± 0.97) versus AO 21% (10.11 ± 0.66) and 2% PG (10.81 ± 0.51). All conditions together showed significant telomere shortening after day 5 ($p<0.05$), day 10 ($p<0.001$), day 20 ($p<0.001$), and day 40 ($p<0.001$). There was no significant

difference between 21% AO (9.98 ± 0.78) compared to 2% PG (9.79 ± 0.69) and 2% WKS (10.39 ± 0.85) at day 10. Also, there was no significant change between AO (8.66 ± 0.76), 2% PG (8.78 ± 1.05) and 2% WKS (9.65 ± 0.75) on day 20. In addition, 2% WKS 8.61 ± 0.93 conditions had no significant difference compare to 21% AO (7.64 ± 0.84), 2% PG (7.94 ± 0.83) at 40 days (***Fig 3.19)***. Telomerase activity was higher in physoxia and accompanied a shorter doubling time in reduced oxygen conditions. Also, average telomere shortening was approximate ~207 bp per chromosome end in three conditions.

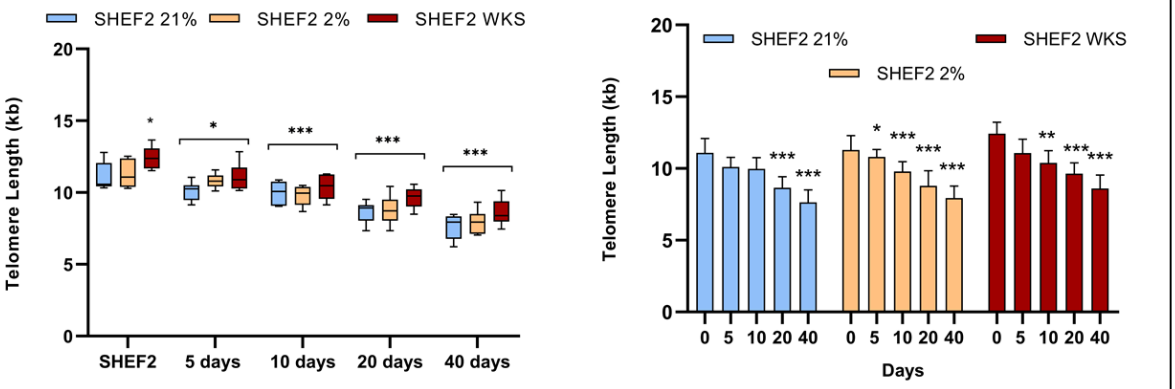

	SHEF2 21%	SHEF2 2%	SHEF2 WKS
R square	0.6821	0.6608	0.6408
P value	<0.0001	<0.0001	<0.0001
Deviation from zero?	Significant	Significant	Significant
Equation	Y = -0.08304*X + 10.74	Y = -0.08382*X + 10.98	Y = -0.08555*X + 11.71

Figure 3.19. **Decreased telomere length (kb) in differentiated SHEF2 cell populations.** The box represents the interquartile range, the whisker in the outer quartiles, and the line in the middle shows the median expression. Data are represented as n=3x3, *p<0.05, **p<0.01, ***p<0.001 vs air oxygen (21% AO). Bars with stars indicate a significant difference between differentiated and undifferentiated cells. The other stars compare physoxia conditions to 21% AO.

Numerical data from two pluripotent stem cells were pooled for telomere length analysis. There was a significant difference in the mean value of telomere length of undifferentiated stem cells 2% WKS (12.71 ± 1.28, p<0.05) versus 21% AO (11.94 ± 1.16) and 2% PG (11.75 ± 1.04). At day 5, the mean value of telomere length was significantly higher in 2% WKS (11.01 ± 0.81) versus AO 21% (10.5 ± 0.66) and 2% PG (10.23 ± 0.93). All conditions together showed significant telomere shortening after day 5 (p<0.001), day 10 (p<0.001), day 20 (p<0.001), and

day 40 (p<0.001). There was no significant difference between 21% AO (9.64 ± 0.95) compared to 2% PG (9.69 ± 0.99) and 2% WKS (10.17 ± 0.90) at day 10. Also, there was no significant change between AO (8.37 ± 1.07), 2% PG (8.22 ± 1.18) and 2% WKS (9.02 ± 0.83) on day 20. However, 2% WKS (8.43 ± 0.79) conditions had a significant difference compare to 21% AO (7.34 ± 0.98), 2% PG (7.35 ± 1.31) at 40 days (***Fig 3.20)***. Telomerase activity was higher in physoxia but doubling time was observed higher in reduced oxygen conditions, so average telomere shortening was calculated as ~240 bp in three conditions. All conditions together showed significant telomere shortening after day 5 (p<0.001), day 10 (p<0.001), and day 20 (p<0.001).

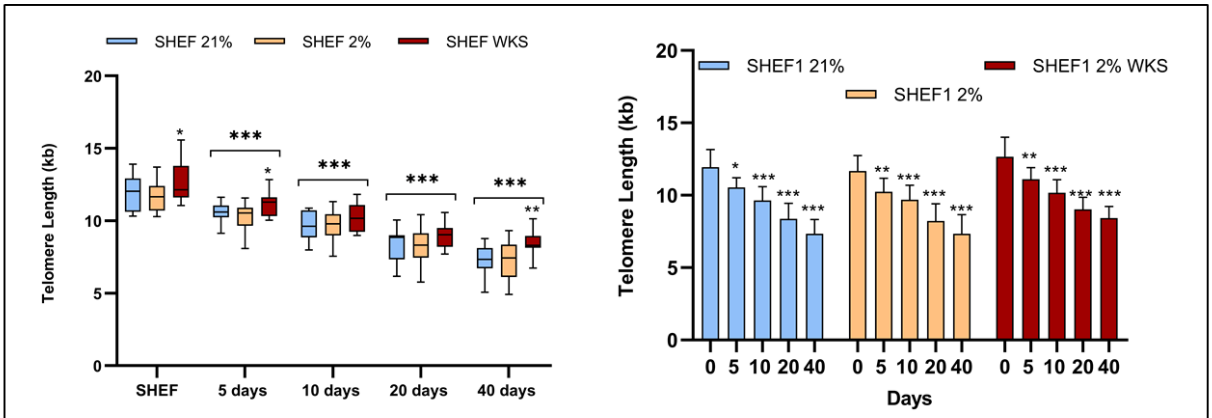

	SHEF 21%	SHEF 2%	SHEF WKS
R square	0.6659	0.6073	0.5902
P value	<0.0001	<0.0001	<0.0001
Deviation from zero?	Significant	Significant	Significant
Equation	Y = -0.1062*X + 11.19	Y = -0.1011*X + 10.99	Y = -0.09777*X + 11.77

Figure 3.20. **Decreased telomere length (kb) during differentiation and higher telomere length in physoxia in SHEF cell populations.** The box represents the interquartile range, the whisker in the outer quartiles, and the line in the middle shows the median expression. Data are represented as n=3x3, *p<0.05, **p<0.01, ***p<0.001 vs air oxygen (21% AO). Bars with stars indicate a significant difference between differentiated and undifferentiated cells. The other stars compare physoxia conditions to 21% AO.

3.2.10 TERT Gene-specific promoter methylation in hESC

The analysis thus far in ESCs indicated significant differences in telomerase activity and TERT gene expression in differentiated progeny from both reduced and air oxygen conditions. We next sought to determine if these changes in expression were reflected in the methylation

level of regions within the TERT promoter; region I (-1456, -1495 bp from TSS), II (-674, -717 bp from TSS), III (-315 -348 bp from TSS), IV (-122, -171 bp from TSS) and V (-67, -106 bp from TSS) by using pyrosequencing.

Region I showed higher CpG island methylation levels than all other regions and displayed no difference between conditions or during the differentiation process (average 85.53%)(***Fig 3.21***). However, there was a significantly elevated methylation in region II after 10 days (51.92%, and 51.54%, p>0.01), 20 days (62.01% and 56.43%, p>0.001) and 40 days (55.92% and 50.79%, p>0.001) of differentiation compared with undifferentiated cells (42.54% and 30.63%) in 21% AO and 2% WKS, respectively. Further, methylation levels in undifferentiated, 20 days, and 40 days differentiated SHEF1 cells cultured in 21% AO environment (p>0.001, p>0.01 and p>0.05, respectively) were significantly higher compared to the 2% WKS condition. A significant increase in methylation level was observed in region III after 10 (7.73% and 7.27%, p>0.001), 20 (10.67% and 11.53%, p>0.001), and 40 days (11.8% and 9.47%, p>0.001) of differentiation compared with undifferentiated cells (4% and 3.33%) in 21% AO and 2% WKS, respectively. In addition, the methylation level in 40 days differentiated SHEF1 cells cultured in 21% AO was significantly higher in comparison to 2% WKS condition (p>0.05). Significant elevation of methylation was also noted after 40 days differentiation (16.42%, and 16.22%, p>0.001) compared to undifferentiated cells (10.45% and 6%) in 21% AO and 2% WKS, respectively, in region IV. Undifferentiated and 20 days differentiated SHEF1 cells showed a significant decrease in region V methylation level following treatment with 2%WKS (3.93%, p>0.05 and 5,06%, p>0.001) compared with the 21% AO (5.69% and 8.78%). While significantly higher methylation levels were observed after 20 and 40 days of differentiation in both 21% AO (8.78% and 8.93%, p>0.001) and at 40 days in 2% WKS (7.91%, p>0.001) conditions. Pooled data from region II, III, IV and V indicated a significant increase in methylation level at day 10 (18.64% and 17.52%, p>0.001), 20 (22.84% and 20.36%, p>0.001), and 40 (23.18% and 21.17%, p>0.001) in AO and WKS compared to undifferentiated cells (15.72% and 10.88%), respectively ***(Fig 3.21.A)***. There was a significant difference between undifferentiated (p>0.001), day 20 (p>0.001) and day 40 differentiated cells (p>0.05).

Pooled regional analysis for differentiated and undifferentiated cells indicated that region V (5.51%, 7.29%, p>0.001), IV (9.79%, 12.08%, p>0.001), and II (47.83%, 53.72%, p>0.05) demonstrated a significant decrease in 2%WKS compared to AO excepting region III (7.9%, 8.55%). Similarly, combined data from these four regions (II, III, IV and V) showed

significantly less methylation in reduced oxygen compared to air oxygen (17.67%, 21.11%, p>0.05) ***(Fig 3.21. B)***.

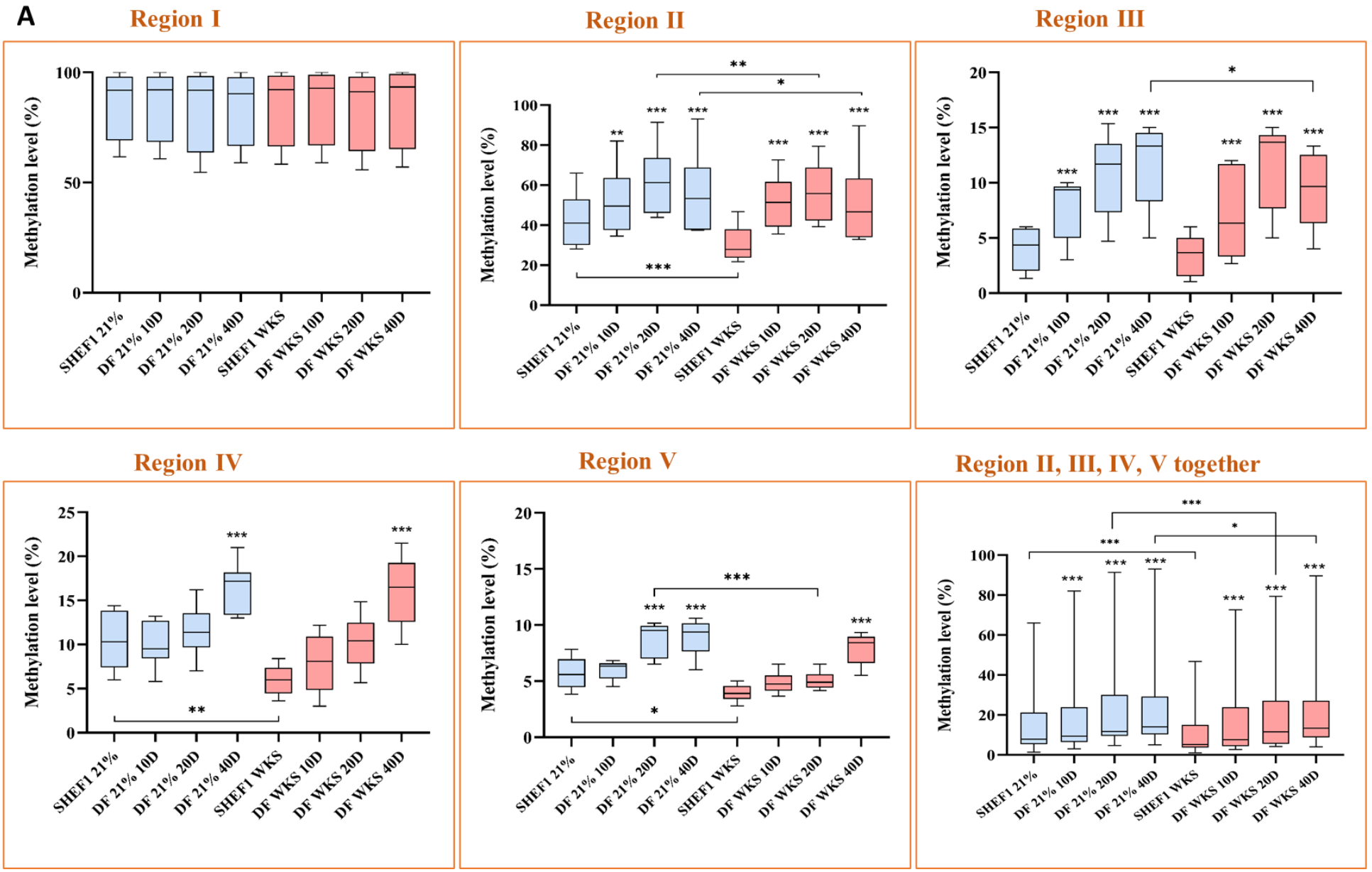
A
Region I
Region II
Region III
Region IV
Region V
Region II, III, IV, V together
Methylation level (%)
SHEF1 21%
DF 21% 10D
DF 21% 20D
DF 21% 40D
SHEF1 WKS
DF WKS 10D
DF WKS 20D
DF WKS 40D

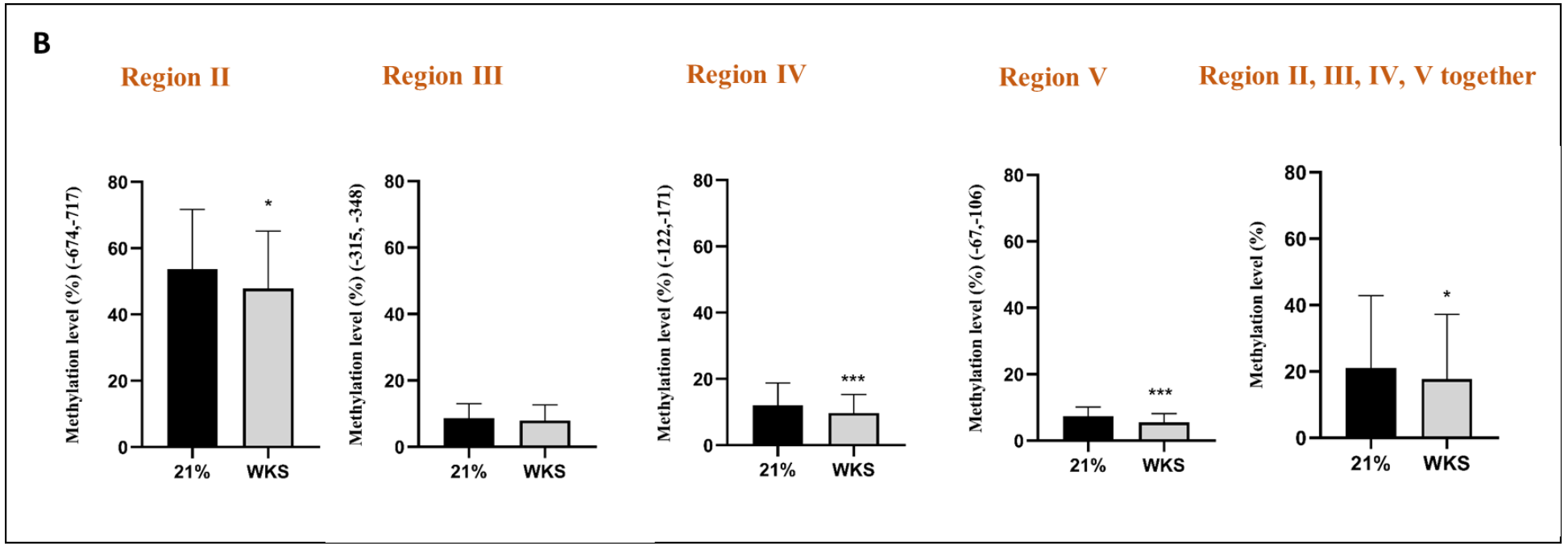

Figure 3.21. **The methylation levels of TERT promoter in 2% WKS compared to air oxygen in SHEF1 cells.** Different promoter regions relative to TSS were evaluated using pyrosequencing. **(A)** The median value of methylation was represented in the box and violin graph. Y-axis indicates DNA methylation level (%) at CpG sites, and X-axis represents the name of samples. Data presented as median (min-max). The stars indicate a significant difference between differentiated and undifferentiated cells. **(B)** The data from differentiated and undifferentiated cells together was indicated in this graph to compare two oxygen conditions. Y-axis indicates DNA methylation level (%) at CpG sites, and X-axis represents the conditions as mean ± SD. n=3, *p<0.05, **p<0.01, ***p<0.001.

Methylation results of SHEF2 showed that region I was highly methylated in comparison to all other regions (average 92.8%) with no difference between conditions or differentiation duration. Significantly higher methylation in region II was noted after 10 days (55.07%, $p>0.01$ and 53.18%, $p>0.001$), 20 days (58.28% and 56.67%, $p>0.001$), and 40 days (59.17% and 56.83%, $p>0.001$) of differentiation compared with in undifferentiated cells (47.39% and 38.97%) in 21% AO and 2% WKS, respectively. Undifferentiated cells cultured in AO showed significantly higher methylation ($p>0.01$) than cells cultured in 2% WKS. Methylation levels were significantly increased in region III after 10 days (16.33% and 13.20%, $p>0.001$), 20 days (19.83% and 14.15%, $p>0.001$), and 40 days (19.40% and 17.42%, $p>0.001$) of differentiation compared to undifferentiated cells (10.48% and 8.27%) in 21% AO and 2% WKS, respectively. Furthermore, undifferentiated ($p>0.05$) and 10 days ($p>0.01$), 20 days ($p>0.001$) differentiated SHEF2 cultured in AO showed a significantly higher methylation percentage compared to 2% WKS environment. We observed higher methylation levels in region IV in 21% AO at day 20 (10.78%, $p>0.01$) and 2% WKS conditions at day 10 (8.40%, $p>0.01$), 20 (9.62%, $p>0.001$), and 40 (10.63%, $p>0.001$) versus undifferentiated cells (9.25% and 6.54%, respectively). Cells cultured in 2% WKS showed significantly reduced methylation levels than those cultured in 21% AO ($p>0.001$) in region IV. There was a significant elevation of methylation in region V after 10 days (6.23% $p>0.001$), 20 days (6.74% $p>0.001$) and 40 days (6.73% $p>0.001$) differentiated cells versus undifferentiated cells cultured in 2% WKS condition (3.92%). Conversley, significant decreases were noted in region V methylation levels following treatment with 2%WKS (3.92%, $p>0.001$) compared with the 21% AO (5.70%) in undifferentited SHEF2. While, significantly higher methylation levels were observed at day 40 differentiation in 21% AO (7.07%, $p>0.01$). Pooled data from regions II, III, IV and V showed a significant increase in methylation levels at day 10 (21.08% and 19.59%, $p>0.001$), 20 (22.94% and 21.13%, $p>0.001$) and 40 (23.03% and 22.14%, $p>0.001$) in AO and WKS compared to undifferentiated cells (17.80% and 14.04%), respectively (***Fig 3.22.A)***. We also analysed differentiated and undifferentiated cells methylation data together for each region to compare differences between 21% AO and 2% WKS conditions. Region II (55.58%, 49.98%, $p>0.01$), III (16.62%, 13.30%, $p>0.01$), IV (10.05%, 8.92%, $p>0.05$), V (6.33% 5.79%, $p>0.05$) and data pooled from the four regions (20.88%, 18%, $p>0.05$) displayed significantly reduced methylation levels in reduced oxygen condition compared to AO ***(Fig 3.22.B)***.

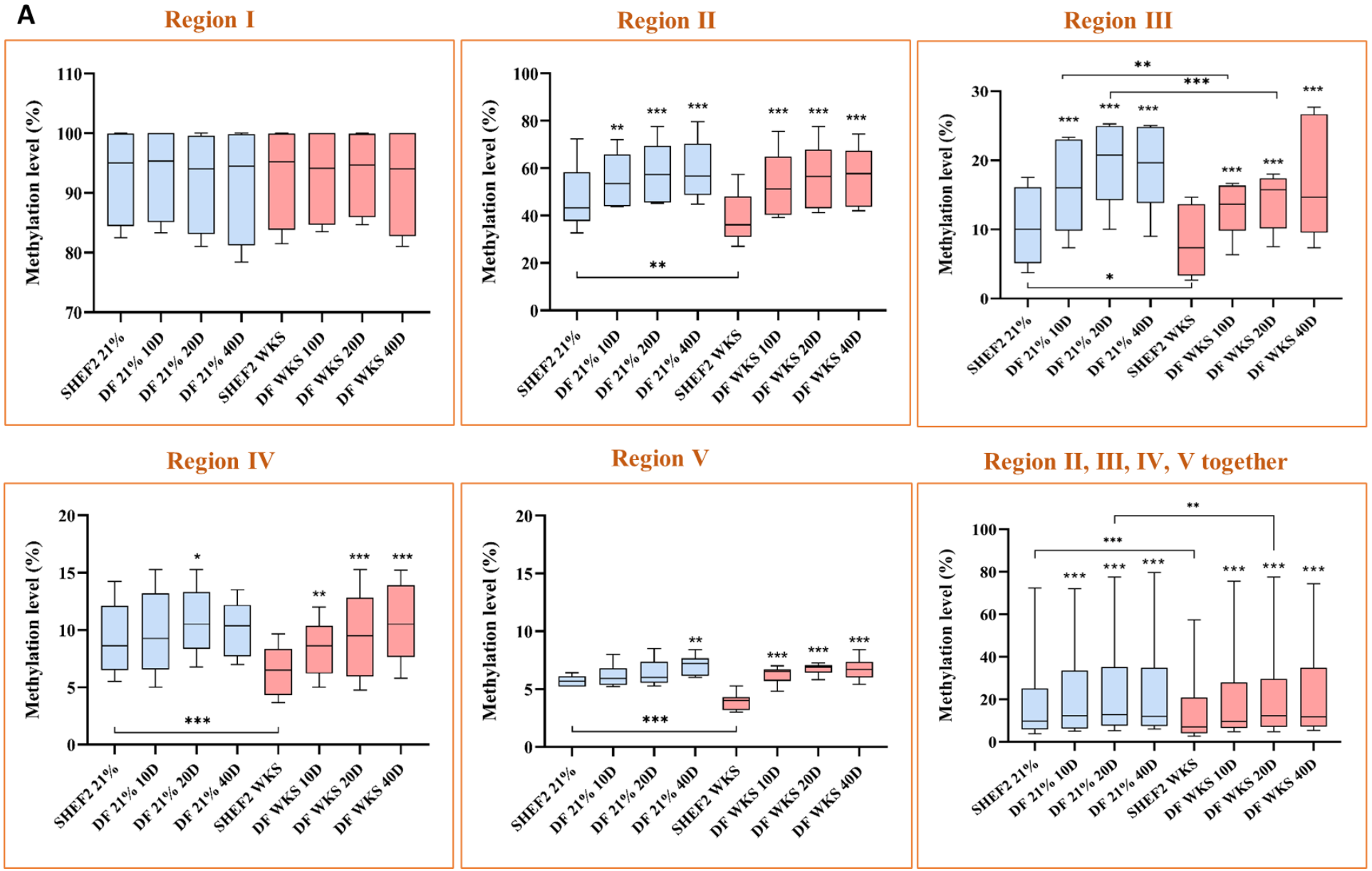
A
Region I
Region II
Region III
Region IV
Region V
Region II, III, IV, V together
Methylation level (%)
SHEF2 21%
DF 21% 10D
DF 21% 20D
DF 21% 40D
SHEF2 WKS
DF WKS 10D
DF WKS 20D
DF WKS 40D

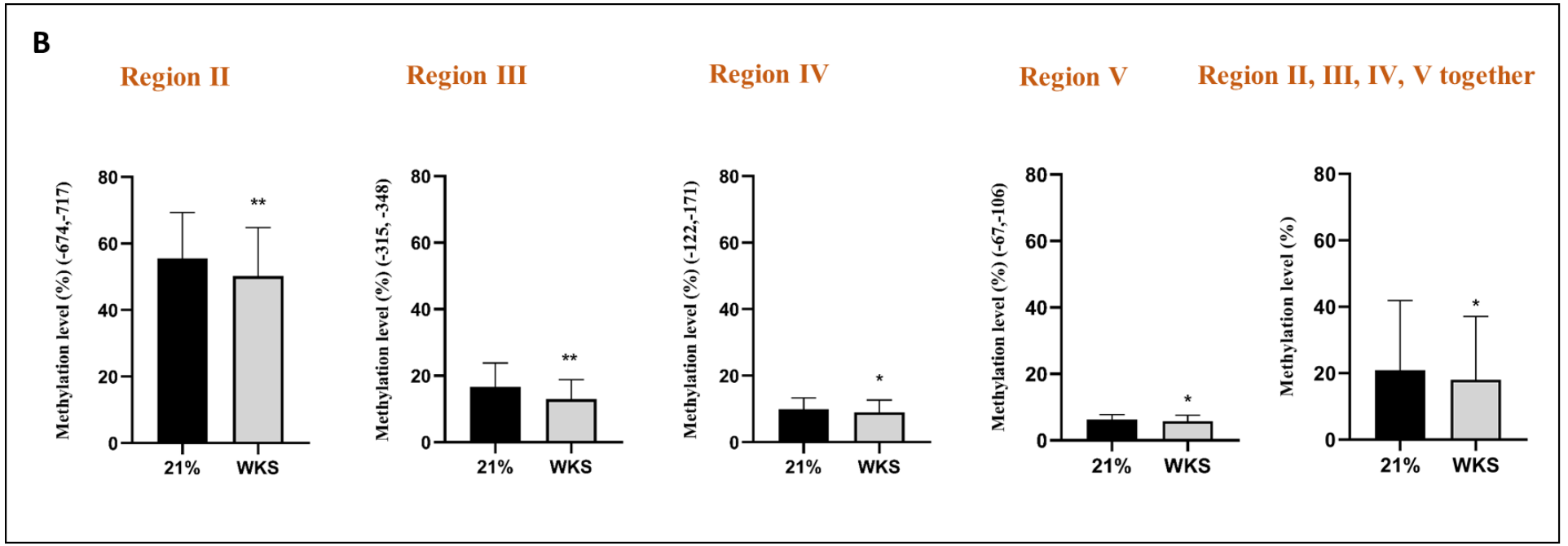

Figure 3.22. **The methylation levels of TERT in physoxia relative to air oxygen in SHEF2 cells.** Different promoter regions relative to TSS were evaluated using pyrosequencing. **(A)** The median value of methylation was represented in the box and violin graph. Y-axis indicates DNA methylation level (%) at CpG sites, and X-axis represents the name of cells. Data presented as median (min-max). The stars indicate a significant difference between differentiated and undifferentiated cells. **(B)** The data from differentiated and undifferentiated cells together was indicated in this graph to compare two oxygen conditions. The Y-axis indicates DNA methylation level (%) at CpG sites, and the X-axis represents the conditions as mean ± SD. n=3, *p<0.05, **p<0.01, ***p<0.001.

Pooled data from SHEF1 and SHEF2 indicated higher methylation levels in region I than in all other regions and no difference between conditions or differentiation stages (average 89.16%) (***Fig 3.23. A***). Significantly higher methylation was noted for region II after 10 days (51.40% and 52.28%, p>0.001), 20 days (60.34% and 56.53%, p>0.001), and 40 days (57.38% and 53.26%, p>0.001) of differentiation compared with undifferentiated cells (44.54% and 34.67%) in 21% AO and 2% WKS, respectively. Methylation levels in undifferentiated cells cultured in 21% AO environment (p>0.001) were significantly higher than 2% WKS. Increased methylation levels were observed in region III after 10 (12.03% and 10.23%, p>0.01), 20 (15.64% and 13.03%, p>0.001), and 40 days (15.60% and 13.47%, p>0.001) of differentiation compared with undifferentiated cells (7.58% and 5.80%) in 21% AO and 2% WKS, respectively. In addition, the methylation level in undifferentiated cells cultured in 21% AO environment (p>0.05) was significantly higher than the 2% WKS condition. There was a significant elevation of methylation in region IV after 40 days of differentiation (13.59%, and 13.11%, p>0.001) when compared to undifferentiated cells (9.92% and 6.20%) in 21% AO and 2% WKS, respectively, and 20 days differentiated cells in 2% WKS (10.03%). Undifferentiated cells displayed a significant decrease in methylation levels in 2% WKS (p>0.001) compared with 21% AO.

Pooled data from undifferentiated and 20 days differentiated cells showed a significant decrease in region V methylation levels in 2%WKS (3.93% and 5,81%, p>0.001) compared to 21% AO (5.69% and 7.84%). Elevated methylation levels were observed after 20 (7.84% and 5.82%, p>0.001) and 40 days (8.00% and 7.38%, p>0.001) differentiation in comparison to undifferentiated cells in 21% AO and 2% WKS, respectively. Region II, III, IV and V combined data showed a significant increase in methylation levels at day 10 (19.36% and 18.52%, p>0.001), 20 (23.09% and 20.78%, p>0.001) and 40 (23.16% and 21.44%, p>0.001) in AO and WKS conditions compared to undifferentiated cells (16.75% and 12.41%), respectively. Also, methylation results of undifferentiated cells (p>0.001), 20 days (p>0.001) and 40 days differentiated cells (p>0.01) showed there was a significant decrease in methylation level following treatment with 2% WKS when compared to 21% AO (***Fig 3.23. A***). We also analysed differentiated and undifferentiated cells methylation pooled data for each region to compare the difference between conditions. Region II (48.82% and 54.56%, p>0.001), region III (10.54% and 12.87%, p>0.01), region IV (9.40% and 11.15%, p>0.001), region V (5.63% and 6.85%, p>0.001) and data pooled from the four regions (21%, 17.83%, p>0.01) demonstrated a significant decrease in 2% WKS compared to 21% AO (***Fig 3.23. B).***

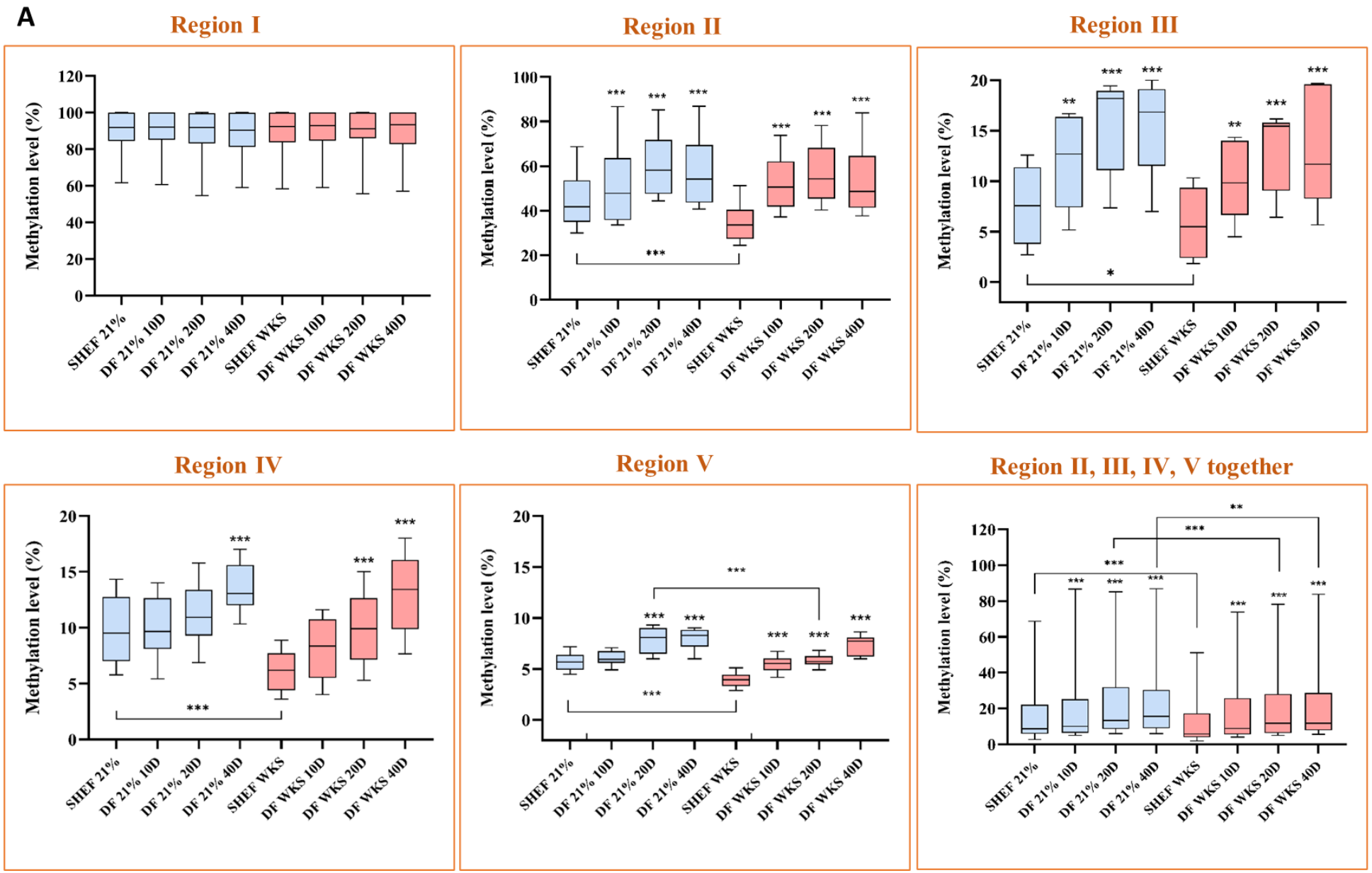
A
Region I
Region II
Region III
Region IV
Region V
Region II, III, IV, V together
Methylation level (%)
SHEF 21%
DF 21% 10D
DF 21% 20D
DF 21% 40D
SHEF WKS
DF WKS 10D
DF WKS 20D
DF WKS 40D

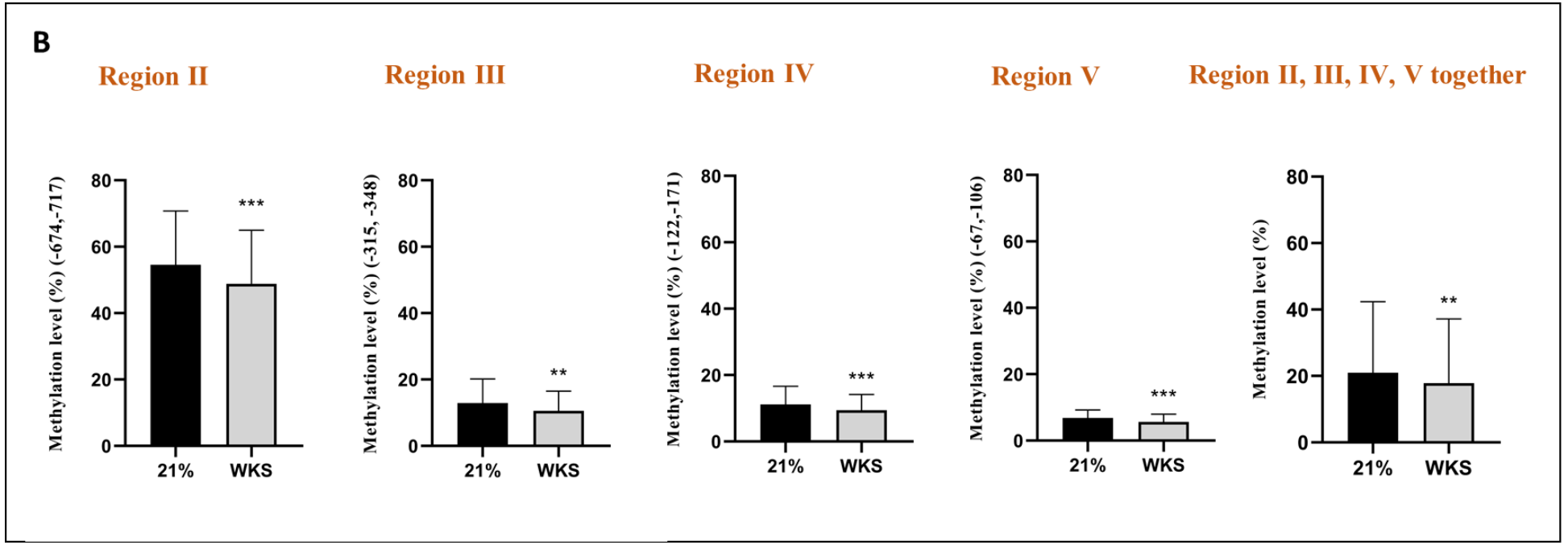

Figure 3.23. **The methylation levels of TERT in physoxia relative to air oxygen from pooled data (SHEF1 and SHEF2).** Different promoter regions relative to TSS were evaluated using pyrosequencing. **(A)** The median value of methylation was represented in the box and violin graph. Y-axis indicates DNA methylation level (%) at CpG sites, and X-axis represents the name of cells. Data presented as median (min-max). The stars indicate a significant difference between differentiated and undifferentiated cells. **(B)** The data from differentiated and undifferentiated cells together was indicated in this graph to compare two oxygen conditions. Y-axis indicates DNA methylation level (%) at CpG sites and represents the conditions as mean ± SD. n=3, *p<0.05, **p<0.01, ***p<0.001.

3.2.11 DNMTs Gene Expression in ESCs and their differentiation progeny in response to physiological oxygen condition

RT-qPCR was performed to examine the changes in the expression of DNMTs relative to TERT promoter methylation in response to the physiological oxygen environment. The results from differentiated SHEF1 showed a significant decrease in DNMT1 expression in 2% WKS (-0.49 ± 0.55 and -1.92 ± 1.30, $p<0.01$) in comparison to 21% AO (0.66 ± 0.93 and -0.56 ± 0.85) at day 5 and 10, respectively. The expression of DNMT1 was decreased significantly at 10 days and 40 days in differentiated cells ($p<0.01$ and $p<0.001$) versus undifferentiated cells. We also analysed differentiated and undifferentiated cells data together to compare the difference between conditions and observed a significant decrease in 2% WKS (-1.13 ± 0.75, $p<0.05$) in comparison to 21% AO (-0.37 ± 0.81) (***Fig 3.24.A)***. SHEF2 cells displayed a significant reduction in 2% WKS (-1.58 ± 0.99, $p<0.01$) conditions versus AO (-0.46 ± 0.46) at day 10. However, there was no change in DNMT1 expression in undifferentiated SHEF2 and 5, 20, and 40 days differentiated cells. But, expression of DNMT1 was decreased significantly in 10, 20 and 40 days differentiated cells ($p<0.001$) versus undifferentiated cells. We also analysed differentiated and undifferentiated SHEF2 cells data together, and there was no significant difference between conditions ***(Fig 3.24.B)***.

Similar significant reduction was observed in DNMT3B expression in differentiated SHEF1 cells grown under 2% WKS conditions at day 5 (-4.92 ± 1.31, $p<0.001$) and 10 (-5.34 ± 0.55, $p<0.001$) versus 21% AO (-0.95 ± 0.42 and -2.48 ± 0.86, respectively). Further, DNMT3B expression was decreased significantly during 5, 10, 20 and 40 days of differentiation ($p<0.001$) versus undifferentiated cells. Differentiated and undifferentiated SHEF1 data together showed a significant decrease in 2% WKS (-5.19 ± 2.74, $p<0.01$) conditions versus AO (-3.47 ± 3.20) ***(Fig 3.24.C)***. The results from undifferentiated SHEF2 showed a significant decrease in DNMT3B expression in 2% WKS (-1.21 ± 0.25, $p<0.05$) in comparison to 21% AO. A significant reduction in DNMT3B expression was noticed at day 20 (-9.87 ± 1.50, $p<0.01$) and 40 (-10.23 ± 0.75, $p<0.01$) from differentiation in 2% WKS in comparison to 21% AO (-8.12 ± 0.78 and -8.05 ± 0.87, respectively). Further, DNMT3B expression was decreased significantly during 5, 10, 20 and 40 days of differentiation ($p<0.001$) versus undifferentiated SHEF2. Differentiated and undifferentiated SHEF2 data together displayed a significant decrease in 2% WKS (-6.08 ± 3.70, $p<0.05$) conditions versus AO (-4.63 ± 3.22) ***(Fig 3.24.D)***.

A significant reduction in DNMT3A expression was noted for SHEF1 cells differentiated in 2% WKS at day 5 (-0.49 ± 0.89, $p<0.05$), day 10 (-1.40 ± 0.67, $p<0.05$) and day 20 (-2.10 ± 0.74, $p<0.001$) versus 21% AO (0.36 ± 0.57, -0.55 ± 0.55 and -0.22 ± 0.61, respectively).

Further, DNMT3A expression was decreased significantly after 10 ($p<0.05$), 20 ($p<0.01$) and 40 days of differentiation ($p<0.001$) versus undifferentiated SHEF1. Differentiated and undifferentiated SHEF1 data together showed a significant decrease in 2% WKS (-1.46 ± 1.01, $p<0.05$) conditions versus AO (-0.52 ± 0.99) ***(Fig 3.24.E)***. Undifferentiated SHEF2 samples displayed a significantly higher DNMT3A expression in 21% AO when compared to 2% WKS (-1.11 ± 0.66, $p<0.05$). There was no difference between conditions after differentiation. However, we noted reduced DNMT3A expression after 10, 20 and 40 days of differentiation ($p<0.001$) versus undifferentiated SHEF2**.** Differentiated and undifferentiated SHEF2 data together displayed no significant difference between 2% WKS (-2.05 ± 0.91) and AO (-1.96 ± 1.55) ***(Fig 3.24. F)***.

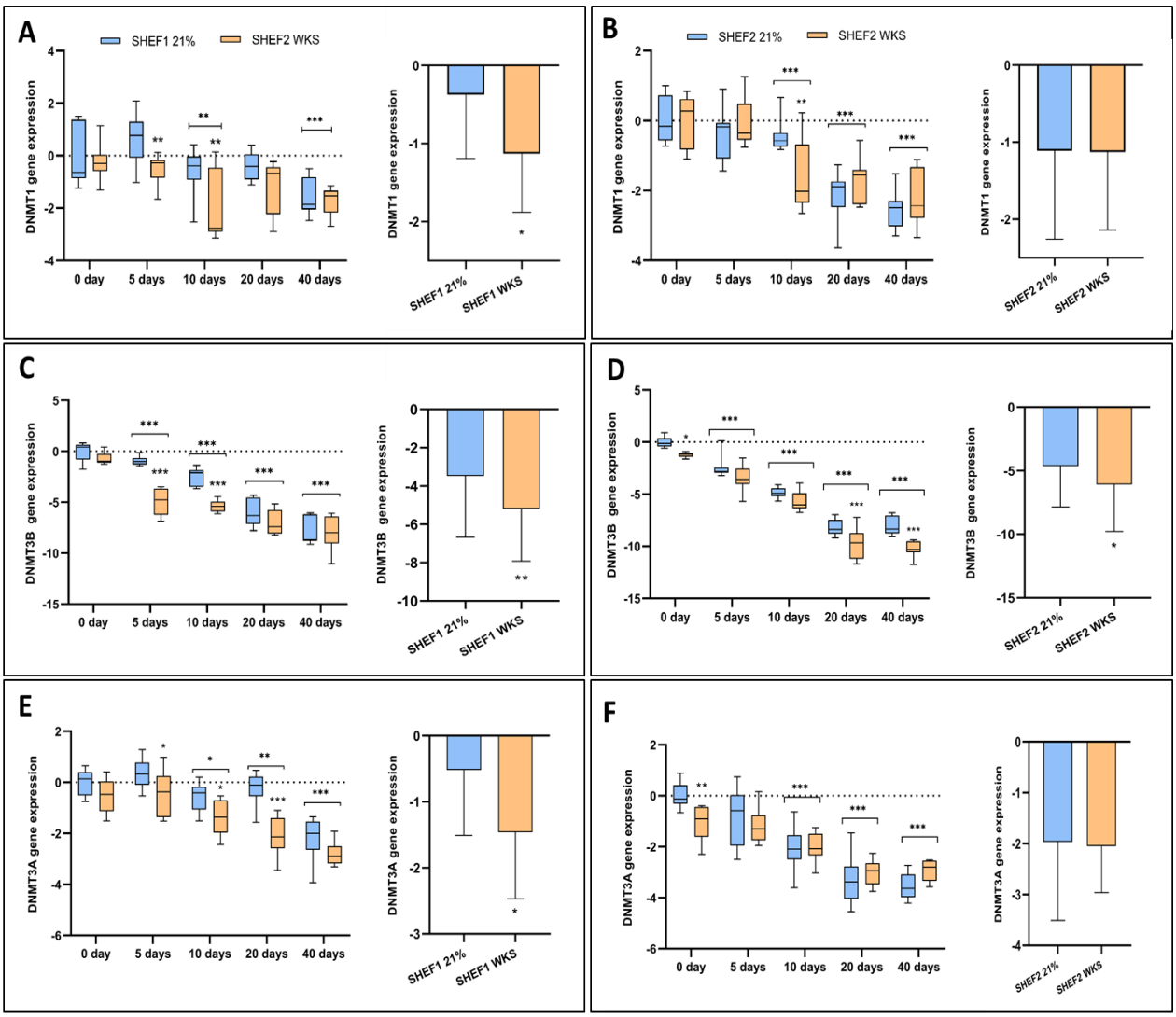

Figure 3.24. **DNMTs gene expression in SHEF cells.** DNMT1 **(A, B)**, DNMT3B **(C, D)** and DNMT3A **(E, F)** data were obtained from SHEF1 and SHEF2 undifferentiated and differentiated cells in 21% AO and 2% WKS. The RT-qPCR expression of the DNMTs normalized to the expression of GAPDH. Data are represented as mean ± standard deviation (SD), n=3, *p<0.05, **p<0.01, ***p<0.001 vs 21% AO. Bars with stars indicate a significant difference between differentiated and undifferentiated cells. The other stars compare 2%WKS to 21% AO.

3.2.12 Nanaomycin A treatment of undifferentiated and differentiated SHEF2 cells

To determine the impact of nanaomycin A (DNMT3B selective inhibitor) on epigenetic regulation of TERT, seven days of drug treatment was performed in different concentrations (5- 0.02 µM) using WST-1 cytotoxicity assay. The maximum drug dose without killing undifferentiated SHEF2 cells was determined as 40 nM, and cells cultured in WKS hypoxia condition were more sensitive to nanaomycin A doses ***(Fig 3.25. A)***. The maximum non-toxic drug dose was determined at 310 nM for differentiated cells ***(Fig 3.25. B)***. Interestingly, differentiated cells displayed higher tolerance to nanaomycin A treatment. Further, we used DMSO control, and there was no significant effect of DMSO on cell growth**.**

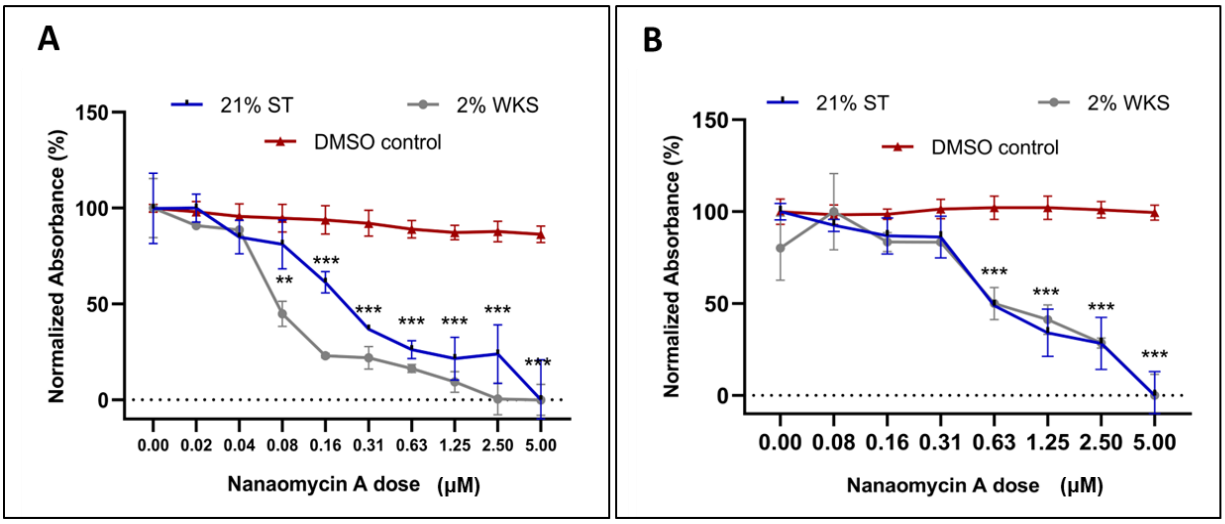

Figure 3.25. **Non-toxic nanaomycin A dose in undifferentiated and differentiated SHEF2 cells.** Undifferentiated **(A)** and differentiated SHEF2 cells **(B)** were treated with increasing doses of nanaomycin A ranging from 20 nM to 5 µM for seven days. Cell viability was plotted against nanaomycin A concentrations in µM. Data are represented as the mean of three wells and SD. The data were analyzed by GraphPad calculated maximum drug concentrations. Results are expressed relative to those obtained in the untreated DMSO control cells.

3.2.13 DNMT3B gene expression and enzyme activity after nanaomycin A treatment of undifferentiated and differentiated SHEF2 cells

The results from undifferentiated SHEF2 showed a significant decrease in DNMT3B expression after nanaomycin A treatment in 21% AO (-3.28 ± 0.66, $p<0.001$) and 2% WKS (-3.47 ± 1.17, $p<0.001$) in comparison to untreated cells in AO and WKS. A significant reduction in DNMT3B expression was noticed at day 5 in 21% AO (-4.92 ± 0.83, $p<0.001$) and 2%WKS (-5.15 ± 1.26, $p<0.01$) in comparison to untreated cells in AO (-2.45 ± 1.00) and WKS (-3.41 ± 1.19). A significant reduction in DNMT3B expression was noticed at day 20 (-9.87 ± 1.50, $p<0.01$) and 40 (-10.23 ± 0.75, $p<0.001$) untreated samples in 2%WKS in comparison to 21% AO (-8.12 ± 0.78 and -8.05 ± 0.87, respectively). In contrast to the above, nanaomycin A treated cells displayed an increase at day 20 in 21% AO (-6.41 ± 0.84, $p<0.01$) and 2%WKS (-7.28 ± 1.15, $p<0.01$) in comparison to untreated cells. Also, we noted an increase in 40 days differentiated SHEF2 (-8.33 ± 1.65, $p<0.01$) after nanaomycin A treatment versus untreated samples in 2% WKS ***(Fig 3.26. A)***. Further, DNMT3B expression was decreased significantly during 5, 10, 20 and 40 days of differentiation ($p<0.001$) versus undifferentiated SHEF2. Differentiated and undifferentiated SHEF2 data together displayed a significant decrease in 2% WKS (-6.08 ± 3.70, $p<0.05$) conditions versus AO (-4.63 ± 3.22) ***(Fig 3.26. B).***

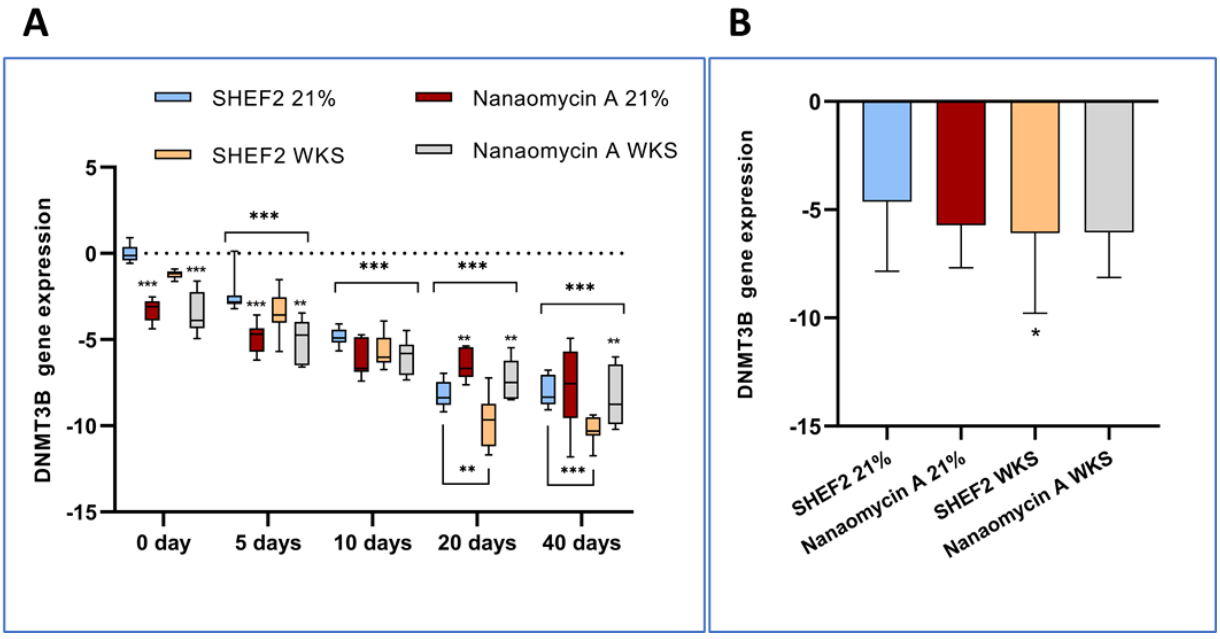

Figure 3.26. **DNMT3B expression in untreated and nanaomycin A (DNMT3B selective inhibitor) treated SHEF2 samples in 2% WKS. (A)** The RT-qPCR expression of the

DNMT3B normalized to the expression of GAPDH. Bars with stars indicate a significant difference between differentiated and undifferentiated cells. The other stars compare untreated cells to nanaomycin A treatment. **(B)** Differentiated and undifferentiated SHEF2 data were pooled together. Data are represented as mean ± standard deviation (SD), n=3, *p<0.05, **p<0.01, ***p<0.001 vs 21% AO.

We used EpiQuik™ DNMT3B Activity Assay Kit to screen DNMT3B inhibitor nanaomycin A and tried to understand the drug's effect on cells by measuring the enzyme activity. Undifferentiated SHEF2 displayed the highest DNMT3B activity, and we normalized absorbance values to the undifferentiated SHEF2 cells. An unpaired t-test was used to compare treated and untreated cells, and a one-way ANOVA test was used for comparing differentiated versus undifferentiated cells. Nanaomycin A treated undifferentiated SHEF2 cells showed a significant decrease in DNMT3B activity (0.65 ± 0.16, p<0.05) versus untreated samples (1.00 ± 0.08). Further, nanaomycin A treated differentiated cells demonstrated decreased enzyme activity at day 5 (0.55 ± 0.05, p<0.05), day 20 (0.35 ± 0.03, p<0.01) and 40 (0.19 ± 0.04, p<0.01) in comparison to untreated samples (0.87 ± 0.02, 0.54 ± 0.05 and 0.48 ± 0.09). There was a significant reduction in the enzyme activity at day 10 (p<0.001),20 (p<0.001), and 40 (p<0.001) of differentiation when compared to undifferentiated SHEF2 ***(Fig 3.27).***

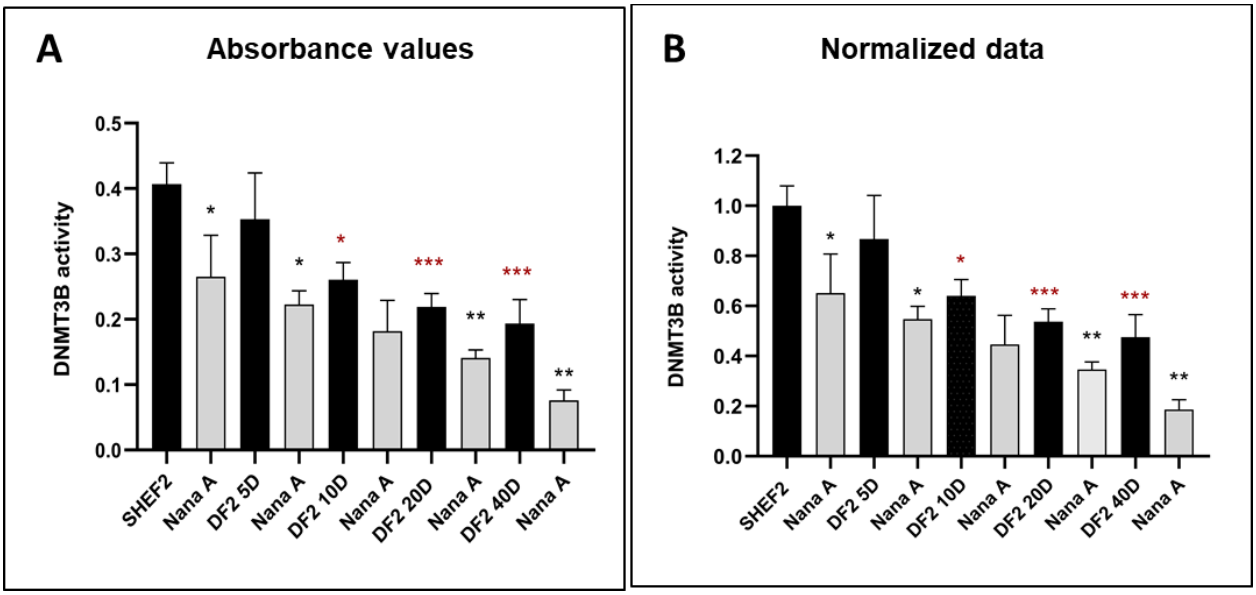

Figure 3.27. **DNMT3B enzyme activity in untreated and nanaomycin A (DNMT3B**

selective inhibitor) treated SHEF2 samples in 2% WKS. (A) measured absorbance for each sample, **(B)** normalized to undifferentiated SHEF2 absorbance values.

3.2.14 Nanaomycin A treatment increase TERT expression and Telomerase activity

We used SHEF2 cells treated with nanaomycin A in 2% WKS to investigate the impact of the DNMT3B inhibition on TERT gene expression and telomerase activity. No significant change was observed in TERT gene expression in undifferentiated SHEF2 cells treated with nanaomycin A (1.35 ± 0.79, $p<0.001$) versus untreated cells following culture in 2% WKS. The mean value of TERT gene expression was downregulated in SHEF2 cells differentiated for 10, 20 and 40 days ($p<0.001$) in comparison to undifferentiated cells. Differentiated cell treated with nanaomycin A for 20 days (-0.59 ± 0.92, $p<0.01$) and 40 days (-2.08 ± 1.51, $p<0.001$) which showed a significantly higher TERT expression in comparison to untreated cells (1.96 ± 0.64 and -4.05 ± 0.75) in 2% WKS ***(Fig 3.28. A)***.

There was no significant difference in telomerase activity in undifferentiated SHEF2 cultured in 2% WKS and treated with nanaomycin A (5.90 ± 0.19) compared to untreated cells (5.99 ± 0.14). Also,we noted no significant change following nanaomycin A treatment at day 5, 10 and 20 (5.36 ± 0.10, 4.93 ± 0.23 and 4.54 ± 0.16) from differentiation compared to untreated cells in 2% WKS (5.65 ± 0.22, 5.23 ± 0.31 and 4.44 ± 0.44, respectively). However, 40 days of differentiated SHEF2 cells after nanaomycin A treatment showed a significantly higher telomerase activity (4.22 ± 0.19, $p<0.001$) in comparison to untreated cells (2.84 ± 0.29) in 2% WKS ***(Fig 3.28. B)***.

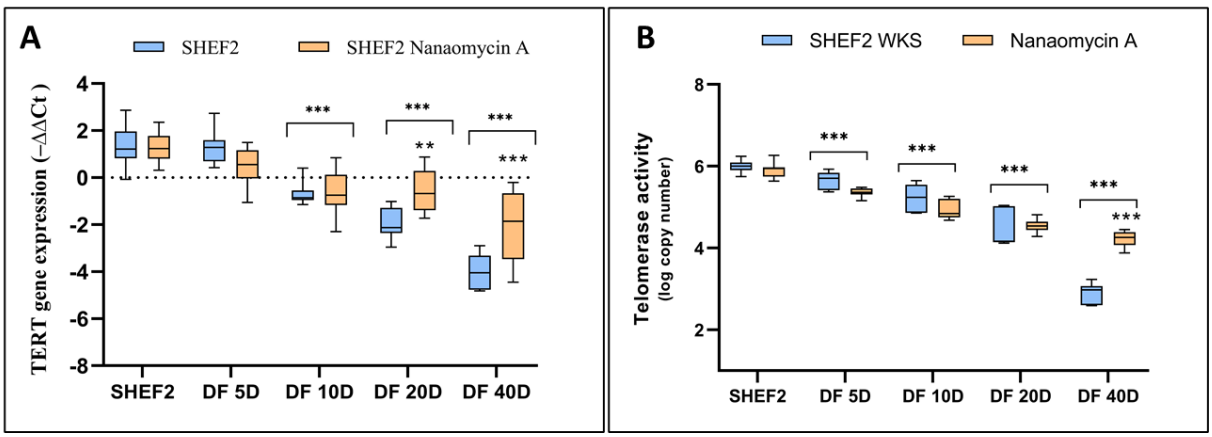

Figure 3.28. **TERT expression and telomerase enzyme activity in untreated and nanaomycin A (DNMT3B selective inhibitor) treated SHEF2 samples in 2% WKS. (A)** The RT-qPCR expression of the TERT normalized to the expression of GAPDH. **(B)** Telomerase activity detection with TRAP Assay. Data are represented as mean ± standard deviation (SD), n=3, *p<0.05, **p<0.01, ***p<0.001 vs 21% AO. Bars with stars indicate a significant difference between differentiated and undifferentiated cells. The other stars compare 2%WKS to 21% AO.

3.2.15 TERT gene-specific promoter methylation after nanaomycin A treatment

Methylation results of SHEF2 showed that region I was highly methylated compared to all other regions with no difference during differentiation. Although, TERT promoter methylation level significantly decreased after nanaomycin A treatment in undifferentiated cells (93% to 69%, p>0.001), 10 days (92.94% to 73.58%, p>0.001), 20 days (93.50% to 65.25%, p>0.001), and 40 days (93.25% to 82.83%, p>0.05) differentiated cells in 2% WKS. Furthermore, differentiated and undifferentiated cells' methylation data together were analysed for each region to compare differences between treated and untreated samples. Overall, undifferentiated and differentiated cells pooled data showed that there was a significant reduction in methylation level of region I following nanaomycin A treatment (69.03%, p>0.001) compared to untreated cells (92.96%) (***Fig 3.29. A)***. Significantly reduced methylation level in region II was noted after nanaomycin A treatment in undifferentiated cells (38.97% to 11.39%, p>0.001), 10 days (53.18% to 15.33%, p>0.001), 20 days (56.67% to 16.44%, p>0.001), and 40 days (56.83% to 24.17%, p>0.001) of differentiation in 2% WKS, respectively. Data pooled from region II displayed significantly reduced methylation levels in nanaomycin A treated (15.80%, p>0.001) compared to untreated cells (49.98%) (***Fig 3.29. B)***. Methylation levels were significantly decreased in region III after nanaomycin A treatment in undifferentiated cells (8.27% and 3.93%. p<0.05), 10 days (13.20% and 5.67%, p>0.01), 20 days (14.15% and 10%, p>0.05), and 40 days (17.42% and 7.93%, p>0.001) differentiated cells, respectively. Data pooled from region III displayed significantly reduced methylation levels in nanaomycin A treated (6.88%, p>0.001) compared to untreated cells (13.30%) (***Fig 3.29. C)***. Conversely, there were no significant changes in methylation levels following nanaomycin A treatment versus untreated cells in region IV in undifferentiated cells (6.54%, 7.83%), at days 10 (8.40%, 9%), 20 (9.62%, 9.71%), and 40 (10.63%, 11.46%) of differentiation in % WKS conditions. Pooled data from

treated and untreated samples (9.5% and 8.8%) also showed no significant changes in methylation level in region IV (***Fig 3.29. D)***. There was no significant change in methylation following nanaomycin A treatment versus untreated cells in region V in undifferentiated cells (3.92%, 3.75%) on days 10 (6.23%, 6.12%), 20 (6.74%, 6.21%), and 40 (6.73%, 6.46%) of differentiation in % WKS conditions (***Fig 3.29. E)***. Pooled data from treated and untreated samples (5.63% and 5.91%) also showed no significant changes in methylation level in region V. Pooled data from all regions (I, II, III, IV and V) showed a significant decrease in methylation levels following nanaomycin A treatment versus untreated cells in region V in undifferentiated cells (15.49% vs 24.93%, $p>0.001$), at days 10 (18.05% vs 29.71%, $p>0.001$), 20 (18.09% vs 31.11%, $p>0.001$) and 40 (22.29% vs 31.81%, $p>0.001$) of differentiation in WKS (***Fig 3.29. F)***. Differentiated and undifferentiated cells' methylation data together for all regions showed a significant decrease following nanaomycin A treatment (18.48%, $p<0.01$) when compared to untreated cells (29.39%).

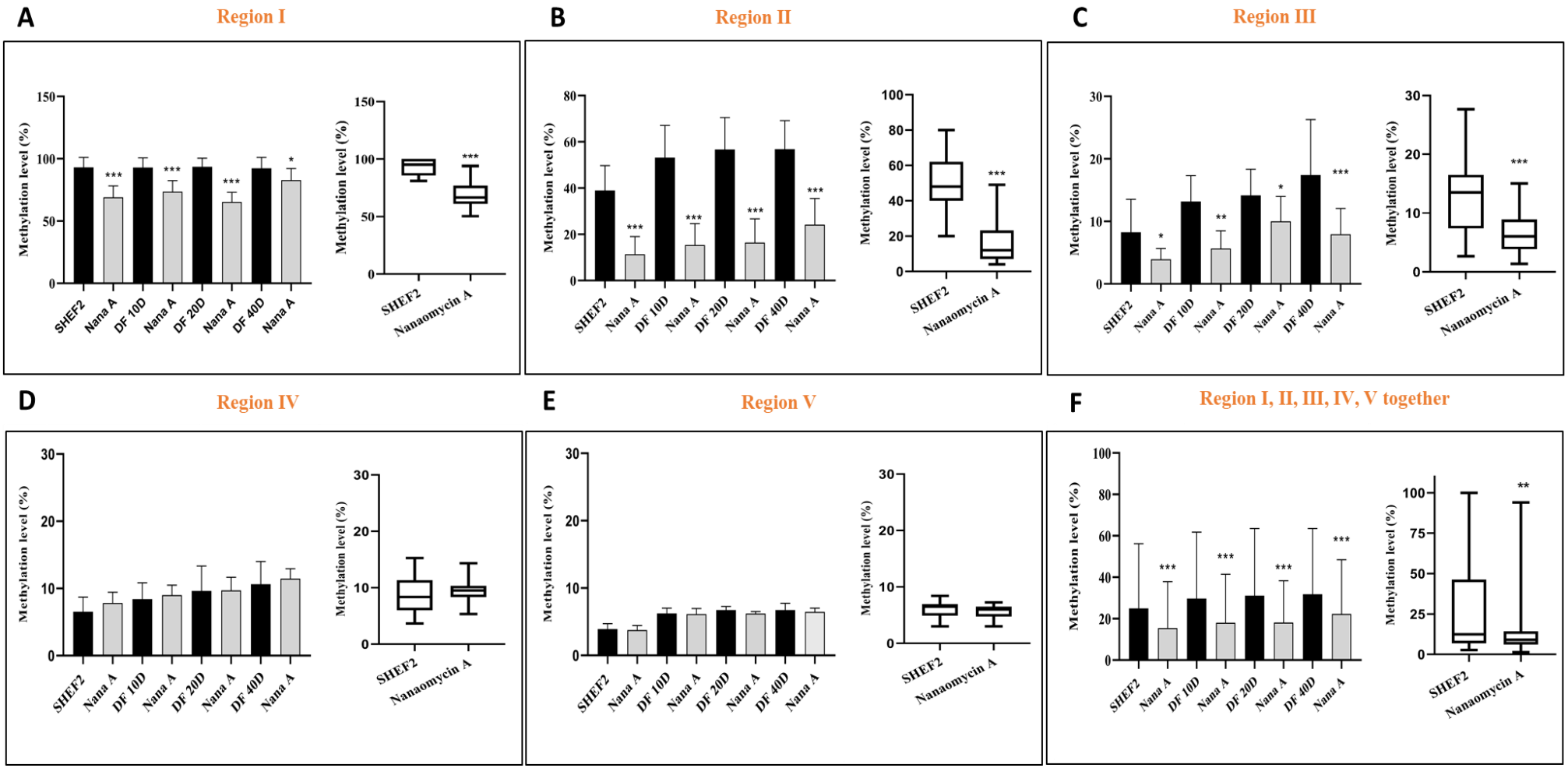

Figure 3.29. **The methylation levels of TERT promoter following nanaomycin A treatment versus untreated SHEF2 cells in 2% WKS.** Regions I **(A)**, II **(B),** III **(C)**, IV **(D)**, V **(E)** and pooled data from all regions **(F)** relative to TSS were analysed using pyrosequencing. Y-axis indicates DNA methylation level (%) at CpG sites, and X-axis represents the name of cells. Data presented as median (min-max) and as mean ± SD, n=3, *p<0.05, **p<0.01, ***p<0.001.

3.2.16 Binding of DNMT3B Antibody on TERT promoter region using CHIP (Chromatin immunoprecipitation) qPCR tool

ChIP-qPCR is a powerful tool that allows the specific matching of proteins or histone modifications to regions of the genome. We performed CHIP to examine DNMT3B-induced TERT promoter methylation in differentiated SHEF2 cells in 21% AO and 2% WKS. After DNMT3B antibody treatment, the immunoprecipitated DNA was detected by qPCR following the protocol described in method chapter (***chapter 2.17, Page 75***). CHIP assay results suggest that DNMT3B binding increases in the TERT promoter during differentiation. We performed qPCR for different regions of TERT promoter. DNMT3B binding to region II was significantly increased in differentiated SHEF2 cells at day 10 (3.11 ± 0.51, $p<0.01$), day 20 (3.45 ± 0.33, $p<0.001$) and day 40 (3.89 ± 0.17, $p<0.001$) when compared to undifferentiated SHEF2 cells (2.49 ± 0.61). There was no significant change between conditions, but we noted slightly less binding of DNMT3B to region II in 2% WKS versus AO ***(Fig 3.30. A)***. Results from region III demonstrated similar statistically significant elevated DNMT3B binding on the promoter after 20 days (4.59 ± 0.45, $p<0.001$) and 40 days (4.90 ± 0.39, $p<0.001$) of differentiation versus undifferentiated cells (3.65 ± 0.40) ***(Fig 3.30. B)***. In contrast to region II, we noted a significantly higher DNMT3B binding to the region III on the promoter in WKS (3.91 ± 0.09 and 5.16 ± 0.18, $p<0.05$) versus AO (3.38 ± 0.41 and 4.63 ± 0.38) in undifferentiated and 40 days differentiated SHEF2, respectively. Results from region IV showed a similar statistically significant elevated DNMT3B binding on the promoter after 20 days (3.03 ± 0.19, $p<0.001$) and 40 days (3.07 ± 0.18, $p<0.001$) of differentiation versus undifferentiated cells (2.51 ± 0.30). Also, there was no significant change between conditions, but we noted slightly less binding of DNMT3B to region IV in 2% WKS when compared to AO ***(Fig 3.30. C)***. CHIP results from region V displayed a similar pattern to the other regions. We noted significantly increased binding of DNMT3B on TERT promoter at day 10 (2.46 ± 0.28, $p<0.01$), 20 (2.68 ± 0.18, $p<0.001$), and 40 (2.78 ± 0.14, $p<0.001$) in 2% WKS when compared to 21% AO (2.10 ± 0.43). Furthermore, two-way ANOVA was carried out, and no significant change between conditions was observed in region V ***(Fig 3.30. D)***. Lastly, pooled data from all regions showed that there was a significant increase in DNMT3B binding to the TERT on proximal promoter region during 10 days (3.07 ± 0.67, $p<0.05$), 20 days (3.44 ± 0.79, $p<0.001$) and 40 (3.66 ± 0.86, $p<0.001$) days differentiation compared to 21% AO (2.69 ± 0.73). Also, no significant change between conditions was observed ***(Fig 3.30. E)***.

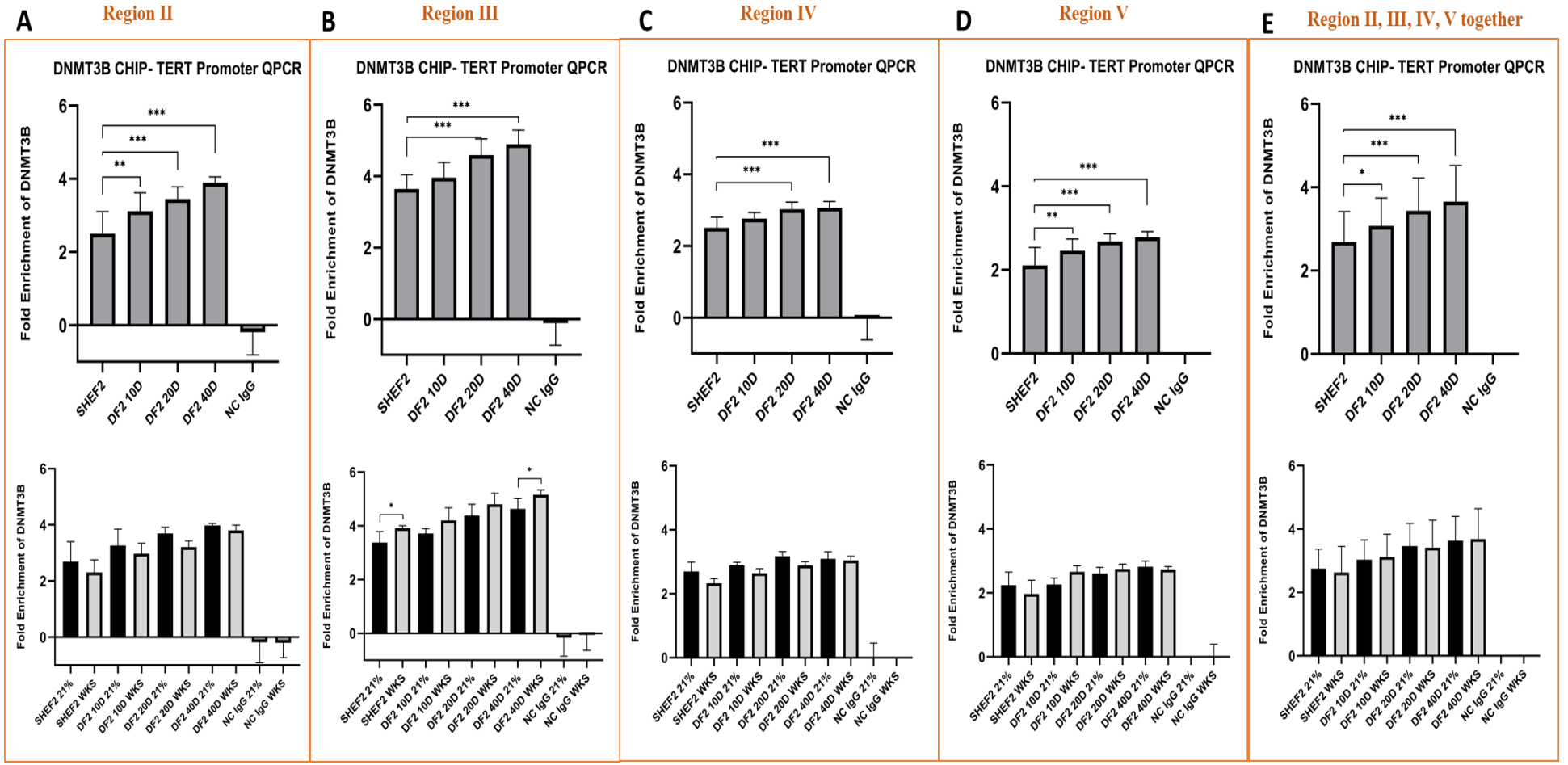

Figure 3.30. **Binding of DNMT3B enzyme on TERT promoter regions using CHIP (Chromatin immunoprecipitation) qPCR tool.** Primers were designed for region II **(A)**, III **(B)**, IV **(C)**, V **(D),** and we also analysed the data pooled together from all regions **(E)**. Data are represented as mean ± standard deviation (SD), n=3, *p<0.05, **p<0.01, ***p<0.001 vs 21% AO.

3.2.17 HDACs Gene Expression in undifferentiated and differentiated ESCs in response to physiological oxygen condition

RT-qPCR was performed to examine the changes in the expression of HDAC1 and HDAC2 expression in response to physiological oxygen environment. The two way ANOVA showed a significant decrease in HDAC1 expression in 2% WKS at day 5 (-1.09 ± 0.43, $p<0.001$), day 20 (-1.26 ± 0.67, $p<0.05$) and day 40 (-1.16 ± 0.62, $p<0.01$) in comparison to 21% AO (0.42 ± 0.40, -0.69 ± 0.70 and -0.43 ± 0.47, respectively) in differentiated SHEF1. Further, there was a significant decrease in gene expression after 20 ($p<0.01$) and 40 days ($p<0.05$) from differentiation. Differentiated and undifferentiated SHEF1 data together displayed a significant decrease in HDAC1 expression in 2% WKS (-1.01 ± 0.35, $p<0.05$) conditions versus AO (-0.21 ± 0.43) ***(Fig 3.31. A)***. Similar reductions were noted with undifferentiated SHEF2 in 2%WKS (-0.76 ± 0.67, $p < 0.01$) when compared to 21% AO. We also noted statistically significant reduction at day 10 in 2% WKS (-1.93 ± 0.91, $p<0.001$) versus 21% AO (-0.53 ± 0.73). Further, there was a significant decrease in gene expression after 20 ($p<0.001$) and 40 days ($p<0.001$) from differentiation. Differentiated and undifferentiated SHEF2 data together displayed a significant decrease in HDAC1 expression in 2% WKS (-1.99 ± 1.08, $p<0.05$) conditions versus AO (-1.19 ± 1.31) ***(Fig 3.31. B)***.

In contrast to the above, HDAC2 displayed no statistically significant changes in SHEF1 samples. Only there was a significant decrease in gene expression after 20 ($p<0.01$) and 40 days ($p<0.001$) from differentiation. However, differentiated and undifferentiated SHEF1 combined data displayed no significant change in HDAC2 expression in 2% WKS conditions versus AO ***(Fig 3.31. C)***. Interestingly, SHEF2 cells showed an increase in HDAC2 gene expression in 2% WKS at day 40 (-1.30 ± 1.48, $p<0.05$) when compared to 21% AO (-2.69 ± 1.51). Further, there was a significant decrease in gene expression after 20 and 40 days ($p<0.001$) from differentiation. Differentiated and undifferentiated SHEF2 data together displayed a significant increase in HDAC2 expression in 2% WKS (-0.68 ± 0.97, $p<0.01$) conditions versus AO (-1.61 ± 1.14) ***(Fig 3.31. D)***

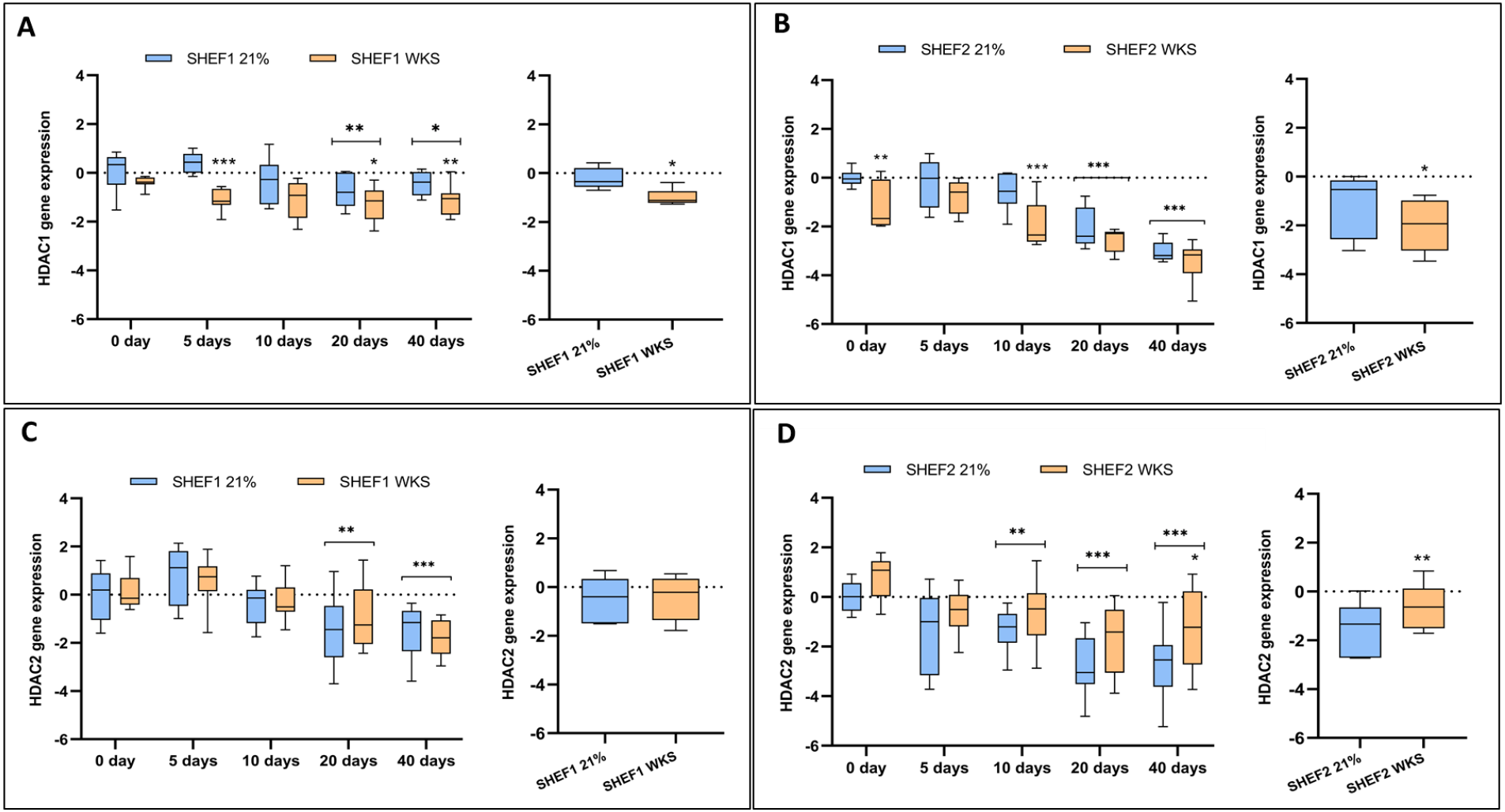

Figure 3.31. **Decreased HDACs gene expression in differentiated SHEF cells.** HDAC1 (A, B), and HDAC2 (C, D) expression data were obtained from SHEF1 and SHEF2 undifferentiated and differentiated cells in 21% AO and 2% WKS. The RT-qPCR expression of the DNMTs normalized to the expression of GAPDH. Data are represented as mean ± standard deviation (SD), n=3, *p<0.05, **p<0.01, ***p<0.001 vs 21% AO. Bars with stars indicate a significant difference between differentiated and undifferentiated cells. The other stars compare 2%WKS to 21% AO.

3.3 DISCUSSION AND CONCLUSION

Stem cells have the potential to generate human tissues, treatment of genetic disorders and widespread research studies due to their unlimited proliferation and capacity for differentiation into a broad range of cell types (Stojkovic M et al., 2004; Volarevic et al., 2011). ESCs and iPSCs exhibit high proliferation, colony formation, high expression of Oct-4 and Nanog, alkaline phosphatase activity, and telomerase activity which maintain stable telomeres (Huang et al., 2014b). Differentiated stem cells display decreased telomerase activity and TERT gene expression (Sharma et al., 1995; Albanell et al., 1996; Armstrong et al., 2005; Cheng et al., 2017). Telomerase is correlated to the proliferation capacity of stem cells and is silenced as cells differentiate, indicating that telomerase has a significant role in embryonic development (Greenberg RA et al., 1998; Forsyth et al., 2002). Furthermore, telomerase can repress cell differentiation (Kim et al., 1994). Many studies have explored the importance of epigenetic mechanisms such as DNA methylation and histone modifications on cellular processes, including differentiation and embryonic developmental programming (Li, 2002; Huang et al., 2014a). In addition, physiological oxygen condition is an essential microenvironment component of stem cell biology and stem cell fate (Ma et al., 2009). Early development occurs in the absence of vascularization, and blastocyst develops within the fluid-filled uterine cavity and has no direct access to blood supplied oxygen source. Researchers suggested that embryos adapt to reduced oxygen concentrations, and ESCs are best maintained in the range of 2–5% physiological normoxia (Fischer B and BD, 1993; Ezashi T et al., 2005). Low oxygen conditions are associated with higher proliferation, colony initiating cells, stemness, survival, reduced chromosomal abnormalities, change of metabolic activity, and maintenance of the undifferentiated state with elevated levels of nuclear TERT (Ivanovic et al., 2000; Forsyth et al., 2006; Dunwoodie, 2009; Prado-Lopez et al., 2010; Radan et al., 2014; Kwon et al., 2017). Importantly, HIF1α is identified as an upstream trans activator of the TERT promoter which possesses HIF1 binding motifs (Kyo et al., 2008). Altogether, stem cells and their differentiation process provide a good model for understanding the regulation of telomerase activity and epigenetic responses to related environmental clues like oxygen. In this chapter, we investigated the effect of different oxygen environments on characteristics of stem cells, telomere length, telomerase enzyme and gene expression, moreover, we tested the hypothesis DNA methylation pattern on the TERT promoter can change during differentiation and are impacted by physiological oxygen.

We observed that reduced oxygen culture (2% PG and 2% WKS) increased the proliferation rate of ESCs in comparison to AO. Our finding is correlated with previous studies, which have demonstrated that the proliferation rate and metabolic activity of stem cells were increased and morphology improved under low oxygen conditions (Forsyth et al., 2006; Forristal et al., 2010; Rajala et al., 2011). These findings confirm that ESCs grow better under low oxygen culture, indicating an improved balance between proliferation and metabolic activity compared to widely used 21% AO, representing a hyperoxic non-physiological condition. When stem cells are cultured in non-physiological conditions, they undergo a set of changes, including metabolism, oxidative stress, reduced proliferation, stemness, self-renewal, differentiation potential, and morphology (Ezashi T et al., 2005; Mas-Bargues et al., 2019). We also noted a shorter doubling time in reduced oxygen culture compared to 21% AO in differentiated cells. Monitoring oxygen levels is therefore critical, especially when differentiation of the culture is required for stem cell therapy, regenerative medicine and tissue engineering.

To characterise the undifferentiated state of ESCs, expression of surface markers SSEA-1, SSEA-4, specific transcription factors Oct-3/4, Nanog, and ALP enzyme activity were explored. Undifferentiated SHEF1 and SHEF2 cells expressed positive markers SSEA-4, Oct-3/4, Nanog, and ALP enzyme activity (Fox N et al., 1981; Adewumi et al., 2007; Zhao et al., 2012), and displayed decreases in expression of pluripotency markers (OCT-4, SSEA-4, Nanog and ALP) and increased SSEA-1 expression during spontaneous differentiation in all conditions (Solter and Knowles, 1978). We noted a rapid increase of SSEA-1 (Solter and Knowles, 1978; Noisa et al., 2012) after 5 days of differentiation with no expression of SSEA-1 in undifferentiated ESCs. OCT-4 plays a critical role in early embryonal stem cell potency and self-renewal. At the same time, Nanog has a crucial role in the second embryonic cell fate after the formation of the early blastocyst and works with Oct-4 to support stem cell potency and self-renewal (Cavaleri and Schöler, 2003). Nanog expression is downregulated early during ESC differentiation and defines stem cell identity (Chambers I et al., 2003). Our results showed that ALP and SSEA-4 expression notably decreased after 5 days while Nanog expression reduced gradually over 20 days of differentiation across all three oxygen conditions with no significant differences between physoxia and air oxygen conditions. Interestingly, OCT-3/4 expression slowly reduced in physiological oxygen conditions compared to 21% AO, indicating low oxygen conditions support continued stem cell potency and self-renewal through OCT-4 expression. Air oxygen is suggested to promote spontaneous cell differentiation (Kurosawa et

al., 2006). A study suggests that low oxygen culture promotes directed differentiation towards functional endothelial cells from hESCs (Prado-Lopez et al., 2009).

ESCs are isolated from pre-implantation blastocysts and can differentiate into all embryonic lineages (Itskovitz-Eldor et al., 2000a). The spontaneous differentiation status of the ESCs was analyzed by following the expression pattern of four different lineage-specific molecular markers using RT-PCR, including NES (ectoderm), TBXT (mesoderm), KDR (mesoderm) and AFP (endoderm). NES was initially identified as a marker of neural stem cells. NES expression also indicates ectoderm germ layer differentiation of EBs (Khoo et al., 2005). Immunofluorescent staining results showed NES expression within the neuroectoderm region in FGF2-supplemented EBs. Suppression of NES expression leads to increased expression of pluripotency markers that demonstrated a functional factor at the time of stem cell differentiation (Kim et al., 2010). Our observations of monolayer stem cell differentiation showed that there is no ectodermal marker NES expression in both ESCs. EBs express upregulated germ layer-specific genes associated with each of the three germ layers, including AFP (for endoderm), Sox-1 (for ectoderm) and Brachyury (for mesoderm) after 20 days of culture (Pettinato et al., 2014). Brachyury-positive cells localize in the middle layer of the embryoid colony (Poh et al., 2014). Furthermore, ESCs can generate multiple mesodermal derivatives when directed towards mesodermal differentiation. Mesodermal phenotypes were previously identified with the KDR (VEGFR2) surface marker, which is a well-defined early mesodermal differentiation marker (Yamashita et al., 2000; Evseenko et al., 2010). Correlated to these results, we observed increased expression of mesodermal markers, TBXT and KDR expression in hESC during differentiation with a significantly less expression in physiological oxygen culture than AO. AFP is a major plasma protein produced primarily by the liver in a developing fetus and diagnostic biomarkers for hepatocellular carcinoma or liver disease (Marzinke and Dufour, 2020). AFP concentrations may increase after liver injury or when hepatocytes regenerate or proliferate (Sell, 2008). Also, AFP protein may localize in the fetal central nervous tissues at an early development period to contribute to cell differentiation of the neuronal system (Pasqualini, Kincl, and Sumida 1991). EBs formed from mouse embryonic stem cells express endoderm marker genes, including AFP, during the processes of early development and strongly after that (Abe et al., 1996). We noted that monolayer spontaneous differentiated stem cells have no increased expression level of AFP during 40 days of differentiation. In summary, ESCs monolayer differentiation is accompanied by downregulation of pluripotency related genes and increased expression of mesodermal markers.

ESCs provide a useful *in vitro* model of early human developmental processes and investigate the role of epigenetic mechanisms behind telomerase regulation and TERT silencing during differentiation. As described previously, telomerase enzyme activity correlates with cell differentiation and proliferation. Induction of differentiation in leukaemia cells, epithelial and embryonal stem cells show decreased telomerase activity and TERT expression (Sharma et al., 1995; Armstrong et al., 2005). Furthermore, downregulation of TERT in hESCs resulted in reduced proliferation, increased the numbers of cells in the G1 phase, induced differentiation and an inability to generate stable ESCs sublines (Yang et al., 2008; Sexton et al., 2014). In line with these results, our TRAP assay and immunofluorescent staining of TERT protein data confirmed a gradual downregulated telomerase activity during 40 days of differentiation in both ESCs. On the other hand, we assessed the effect of oxygen on differentiation and telomerase activity. Telomerase activity was significantly higher in both ESCs cultured in physiological oxygen niches when compared to AO. Similar to these results, we observed a significant decrease in TERT expression during differentiation and a significantly higher gene expression was noted in reduced oxygen cultured cells.

Amit and colleagues showed that human ES cell lines after long cell culture continue to proliferate actively, express high levels of telomerase and retain normal karyotypes where telomere lengths are maintained between 8 and 12 kb in the high passage (Amit M et al., 2000). Reduced oxygen culture increases the replicative life span of the cells (Jagannathan et al., 2016). The average telomere length was noted as 11.94 kb in 21% AO, 11.67 in 2% PG and 12.66 kb in 2% WKS in each chromosome end, and there was a significant increase in average telomere length in 2% WKS. These results are in line with our telomerase activity and TERT expression results. Furthermore, there was a significant decrease in telomere length in both ESCs after differentiation.

Hyperoxia (atmospheric oxygen) reduces telomerase RNA component levels and limits telomerase activity and telomerase-mediated telomere lengthening in TERT-transduced bone marrow endothelial cells (Napier et al., 2010). Even overexpression of TERT does not prevent telomere loss in endothelial cells cultured in atmospheric oxygen, which indicates the effect of oxidative stress on telomere erosion (Napier et al., 2010). Oxidative stress is due to the generation of reactive oxygen species (ROS) in cells cultured at atmospheric oxygen higher than cells cultured in physiological levels (Atkuri et al., 2007). ROS has an impact on the cellular response, epigenetic regulation of many gene expressions and activates redox-sensitive factors related to inflammatory and apoptotic signalling (Okazaki and Maltepe, 2006; Ivanovic,

2009; Jagannathan et al., 2016). Taken together, we need to consider the benefits of using lower oxygen tension for primary cells and tissues. Conflicting with these results, researchers observed increased telomere lengths of T helper, T cytotoxic, natural killer and B cells from blood samples following hyperbaric oxygen therapy on thirty-five healthy adults (aged 64 and older), and they suggested a significant decrease in the number of senescent T helpers after hyperbaric oxygen therapy (Hachmo Y et al., 2020).

DNA methylation and hydroxymethylation have essential roles in PSCs functions, differentiation process, cell fate, and maintenance of characteristics in low oxygen environments (Watson et al., 2010; Xu et al., 2011; Huang et al., 2014a; Mariani et al., 2014). Epigenetic modifications such as DNA methylation, histone modification, and non-coding RNAs are significant regulators of the telomerase gene (Lewis and Tollefsbol, 2016; Dogan and Forsyth, 2021). OCT-4 and Nanog essential transcription factors in undifferentiated ESCs become methylated during differentiation (Mitsui K et al., 2003; Gopalakrishnan et al., 2008; Altun et al., 2010; Pelosi et al., 2011). The presence of 5mC at gene control elements such as promoters and enhancers is often associated with repression transcription (Di Croce L et al., 2002; Miller and Grant, 2013). The importance of DNA methylation in stem cell differentiation and cellular programming has been shown in many studies. In this chapter, we also focused on the impact of physoxia on DNA methylation of TERT promoter regions in human PSCs. We found that proximal TERT promoter methylation is oxygen-sensitive, and there is a significant decrease in methylation percentage in physiological conditions. In addition, there was a substantial increase in methylation level during the differentiation of both ESCs. Notably, pluripotent cell samples and somatic cells methylation results demonstrated that a distinct methylation pattern distinguishes pluripotent stem cells from somatic cells (Huang et al., 2014a). Distal promoter regions (-2056 and -1566 nt) of TERT were found to be highly methylated in line with our results, while -1415 to -638 nt region represented distinct methylation signature in pluripotent stem cells versus somatic cells correlated to gene expression levels (Takasawa et al., 2018). We observed that the distal promoter (region I, -1456, -1495 from TSS) has a high methylation level in all conditions with no significant difference during differentiation compared to other regions which reside in the proximal promoter. All together, methylation alteration of the TERT promoter is strongly linked to its regulation in stem cells (Seynnaeve et al., 2017). Our data showed that there is a strong link between telomerase activity and TERT proximal promoter methylation.

DNMT1 is responsible for the methylation maintenance during replication. It has a strong affinity for the hemimethylated DNA while DNMT3A and DNMT3B work together with DNMT1 and are involved in de novo methylation, particularly during early development (Gopalakrishnan et al., 2008). DNMT3A and DNMT3B are highly expressed during embryonic development (Turek-Plewa and Jagodziński, 2005) and in undifferentiated ESCs (Okano et al., 1998; Liao et al., 2015) but down-regulated after post-differentiation (Phipps et al., 2009). Deleting DNMT1 and DNMT3B enzymes results in embryonic lethality or postnatal (DNMT3A deletion) lethality confirming their essential roles in the development of mice models (E et al., 1992; Thomson et al., 1998; Okano et al., 1999). Further research showed that deletion of DNMT1 resulted in a global loss of DNA methylation followed by rapid cell death in human ESC (Liao et al., 2015). The changes in the expression of DNMTs in response to reduced oxygen could be related to changes in the TERT promoter methylation. DNMTs gene expression experiments were performed at undifferentiated and differentiated cells exposed to different oxygen conditions at different time points (5, 10, 20 and 40 days). Our results showed a significant reduction in the expression of de novo methyltransferase DNMT1, DNMT3B and DNMT3A during differentiation in both ESCs. Our results showed a sharp decrease in expression of DNMT3B during pluripotent stem cell differentiation in line with previous studies (Gifford et al., 2013). Importantly, DNMT3B showed a significant decrease in physiological oxygen (2% WKS) in both ESCs. Our lab's previous experiment results demonstrated a decline in global 5mC in PSCs exposed to physiological oxygen conditions (2% PG and 2% WKS) following a significant transcriptional and translational downregulation of DNMT3B (Dogan et al., 2022). Additionally, DNMT3B displayed reduced transcription accompanied by decreased protein expression in MSCs following physoxia treatment (2% WKS) (Dogan et al., 2021). In summary, downregulated global methylation correlates to DNMT3B expression in response to reduced oxygen conditions. There was a link between a higher methylation level of TERT proximal promoter and DNMT3B in 21% AO. Therefore, we hypothesized that the oxygen-sensitive methylation pattern of TERT promoter might be associated with the DNMT3B enzyme activity.

Next, we used nanaomycin A selective inhibitor to target DNMT3B and performed a cytotoxicity assay to determine non-toxic drug doses for differentiated and undifferentiated ESCs. We also performed qRT-PCR to investigate the effect of nanaomycin A on DNMT3B gene expression. Molecular docking studies of a binding model of nanaomycin A with DNMT3B suggest that the catalytic site of DNMT3B forms a hydrogen bond network with Glu697, Arg731, Arg733 and Arg832 for stabilization of the protein-ligand complex (Dirk et

al., 2010; Kuck et al., 2010). Kuck and colleagues showed that nanaomycin A (5 μmol/L) induced no changes in transcript levels of DNMT3B or DNMT1 in A549 cells, but nanaomycin A revealed selective inhibition of DNMT3B using biochemical *in vitro* methylation assays. (Kuck et al., 2010). Nanaomycin A induced genomic demethylation and showed antiproliferative effects in human cancer cells by reactivating transcription of the RASSF1A tumour suppressor gene (Kuck et al., 2010). There was a significant decrease in DNMT3B gene expression after nanaomycin A treatment in undifferentiated and 5, 10 days differentiated SHEF2 cells, while we observed an increase in gene expression after 20 days of differentiation. We also evaluated the DNMT3B enzyme activity with a colourimetric assay. Nanaomycin A treated cells displayed a decrease in enzyme activity as expected. Then, we investigated the effect of DNMT3B inhibition on TERT gene expression and telomerase activity. Interestingly, we observed an increase in TERT gene expression after 20 days of differentiation and telomerase activity after 40 days of differentiation compared to untreated cells. Pyrosequencing data showed that DNMT3B inhibitor treatment reduced TERT promoter methylation, associated with increased gene and enzyme activity. Most importantly, for the first time, we showed that DNMT3B binding to TERT promoter increases methylation in differentiated stem cells using CHIP qPCR. On the other hand, elevated TERT and DNMT3B expression were associated with shorter survival of hepatocellular carcinoma patients (Yu et al., 2018b). Yu and colleagues suggested that TERT promotes *DNMT3B* transcription because *TERT* inhibition resulted in a decrease in both DNMT3B gene and protein expressions.

Recent studies have reported that DNMT1and DNMT3B promoters possess a hypoxia response element (HRE) which is a DNA recognition site for HIFs (Skowronski et al., 2010; Watson et al., 2014). Watson et al. showed that oxygen tension could drive DNMT1 and DNMT3B expression via the transcription factor HIF-1α in myocardial tissue (Watson et al., 2014). Their study evidenced that mutated HIF-1α-binding site resulted in reduced DNMT1 and DNMT3B promoter activity while stabilized nuclear HIF-1α protein expression contributed to an increased expression of DNMT1 and DNMT3B. Furthermore, hESCs cultured in long term culture in reduced oxygen tension showed a decreased expression of HIF-1α (Forristal et al., 2010). In line with this, we noted significant downregulation of HIF-1α expression in physoxia conditions in undifferentiated and differentiated PSCs (Dogan et al., 2022). In addition, there was a decrease in HIF-1α expression in 2% physoxia environment in human mesenchymal stem cells (Dogan et al., 2021). We believe that a possible mechanism for the observed reduction in DNMT3B expression in the physoxia condition might be due to decreased HIF-1α expression.

In conclusion, understanding the mechanism behind reversible silencing of the TERT gene during differentiation, embryonic development, ageing or activation in cancer cells promise massive potential for future clinical applications, cancer treatment, diagnosis, prognosis and cellular ageing research. Epigenetic mechanisms can be responsible for the regulation of TERT and other related gene regulations. Therefore, investigating the epigenetic memory of cell origin is essential to stem cell biology and cancer research (Lai et al., 2005; Jones and Baylin, 2007; Eitsuka et al., 2018). This chapter has highlighted the link between DNA methylation of TERT promoter and gene expression correlated to telomerase enzyme. Also, we demonstrated the effect of the oxygen environment in this model with the downstream effects, including proliferation, metabolic activity, differentiation and pluripotency features. Notably, stem cell models will contribute to developing useful epigenetic engineering tools for brand new clinical applications.

3.3.1 Summary

In this Chapter, we have provided some key observations; the effect of different oxygen environments on stem cell characteristics, including telomere length, telomerase enzyme and TERT expression, and DNA methylation patterning on the TERT promoter. ***Figure 3.32*** provides an outline of experiments performed in chapter 3.

In summary, the reduced oxygen culture increased the proliferation rate of ESCs. Monolayer differentiated cells showed no ectodermal or endodermal markers expression, but increased mesodermal markers expression was observed during differentiation with slower onset of differentiation in physoxia. A significant decrease in telomerase activity, TERT expression and telomere length was observed during differentiation. Telomerase activity, TERT expression and telomere length were significantly higher in physiological oxygen.

We also demonstrated DNA methylation pattern on TERT promoter regions in human ESCs. Proximal TERT promoter methylation was oxygen-sensitive. There was a substantial increase in methylation level during differentiation. For the first time, a strong link between telomerase activity and TERT proximal promoter methylation was associated with DNMT3B enzyme activity. DNMT3B inhibitor treatment reduced TERT promoter methylation associated with increased TERT gene and telomerase activity. CHIP-qPCR data revealed that DNMT3B binding to TERT promoter was correlated with increased methylation during differentiation and associated with decreased TERT gene and telomerase activity. This study showed the importance of understanding ESCs behaviours and epigenetics in different oxygen environments.

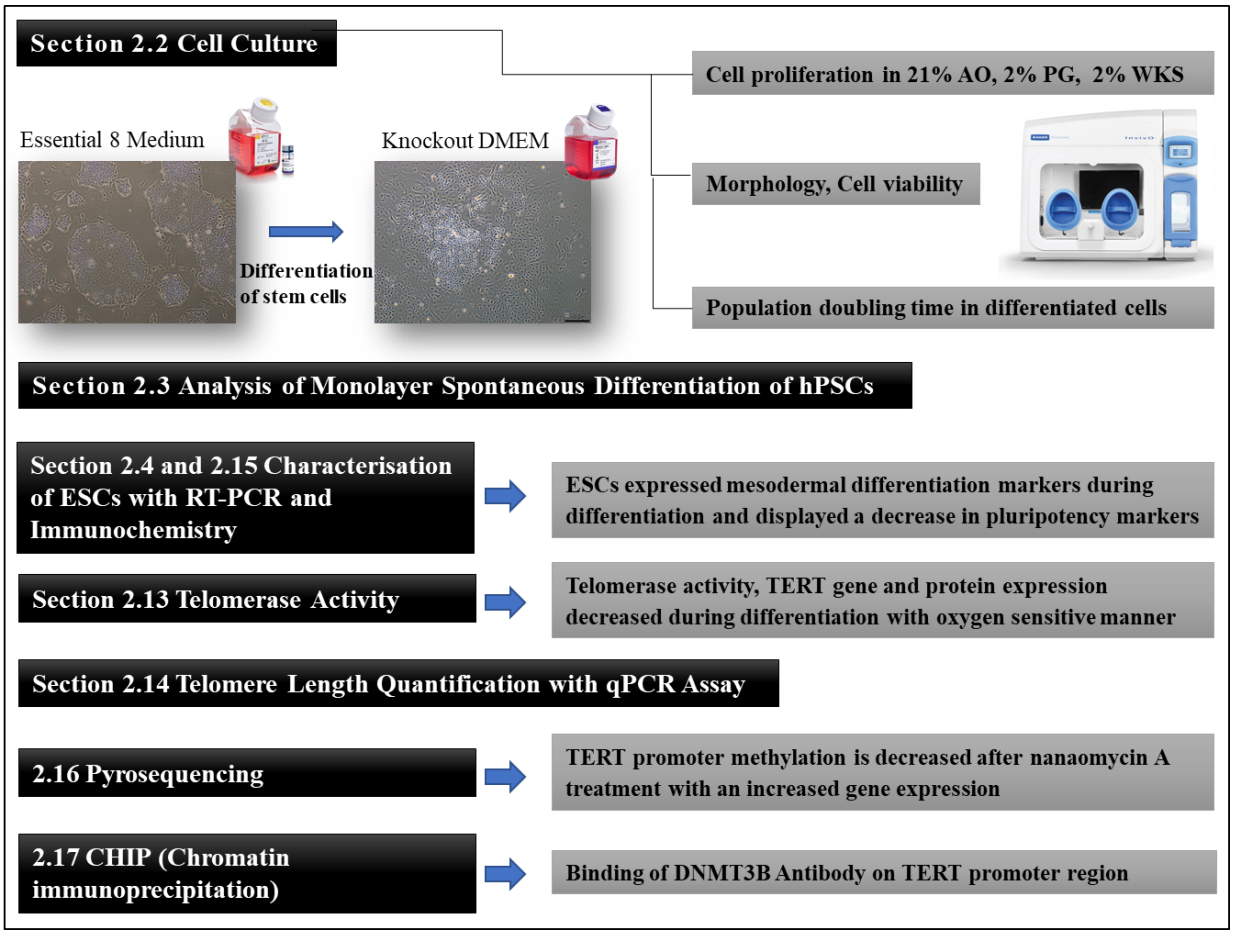

***Figure 3.32*. Summary of the methodology in chapter 3.**

Keele University

CHAPTER 4: Three germ layer differentiation of the embryoid body: Low oxygen modulates the epigenetic state of 3D aggregates of pluripotent cells and their differentiated progeny

4.1 INTRODUCTION

ESCs are pluripotent cells isolated from the inner cell mass (ICM) of the pre-implantation blastocyst. Post fertilisation, human embryos reach 100-200 cells after 4–5 days in the blastocyst stage (Fischbach and Fischbach, 2004; Khan and Ackerman, 2021) (***Fig 4.1***). On day 5, the blastocyst looks like a fluid-filled sphere with an inner cell mass (ICM) surrounded by a trophectoderm epithelium (TE). The ICM is a disc of cells that ultimately can develop into the fetus. The extra-embryonic TE surrounds the ICM and forms essential tissues during pregnancy, such as the placenta (Yamanaka et al., 2006; Stephenson et al., 2010). ESCs derived from the pre-implantation blastocyst display the unique properties of pluripotency, self-renewal, and the potential to differentiate into, in principle, every cell type in the body (>220 individual types) (Shevde, 2012; Rathjen and Rathjen, 2013; Klimanskaya et al., 2020).

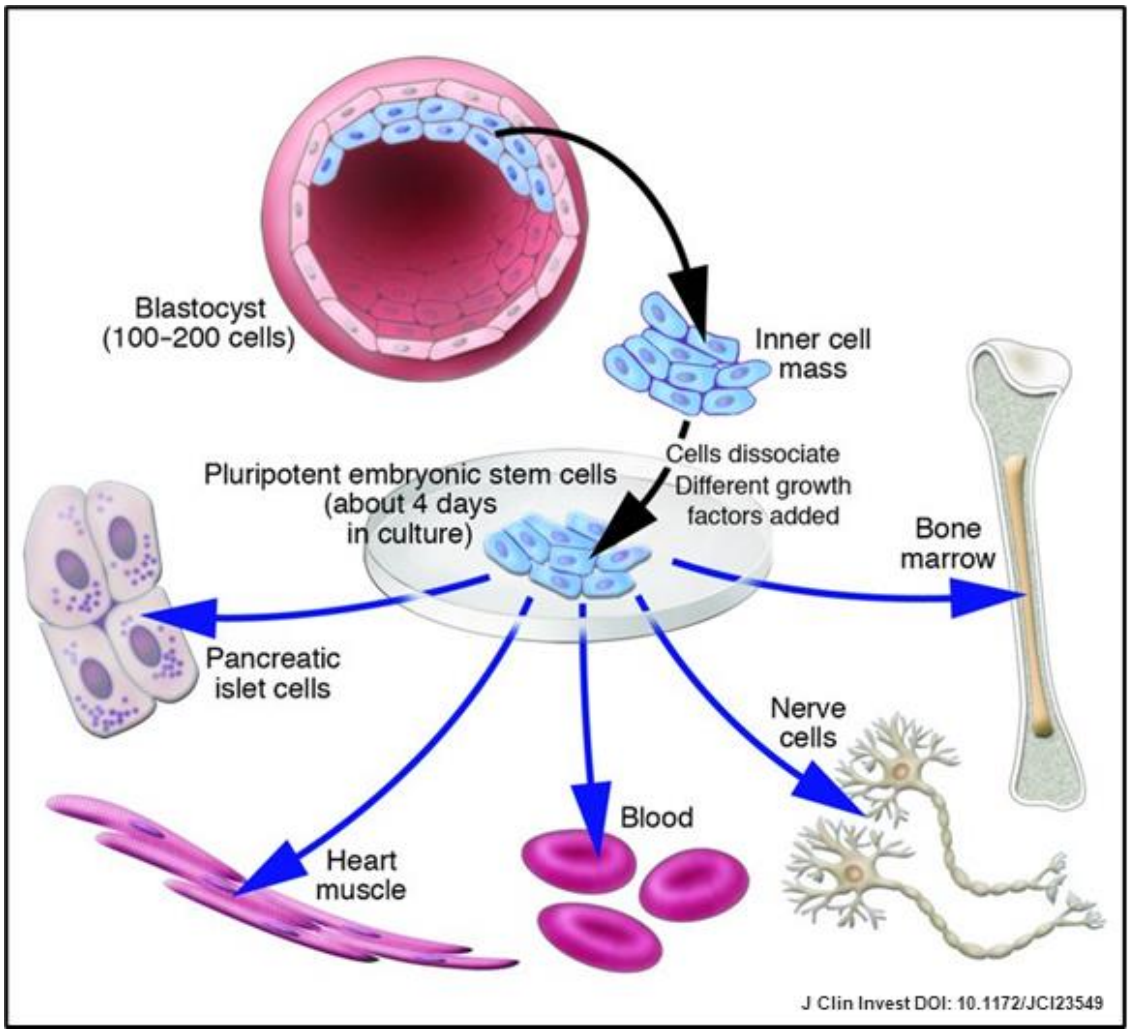

Figure 4.1. **Embryonic stem cells are originated from the inner cell mass (ICM) of the pre-implantation blastocyst.** Isolated cells in this pluripotent state are cultured for a long period in the presence of growth factors. These pluripotent stem cells can differentiate into all types of cells in the human body, such as cardiomyocytes, nerve cells, or bone marrow.

Embryoid bodies (EBs) are three-dimensional aggregates derived from spontaneously differentiated ESCs cultured in suspension culture that generate all three germ layers (ectoderm, endoderm, and mesoderm) in a manner similar to the early embryo (Desbaillets et al., 2000; Jackson et al., 2010). EBs are structurally similar to the pre-gastrulation embryo and show gastrulation-like events, including gene expression (Sadasivam et al., 2007). EBs do not mimic primitive streak formation (the start of gastrulation) and cell movements associated with gastrulation. Still, they share similarities with gastrulation, such as the ability to generate all three germ layers (Coucouvanis and Ft Martin, 1995). EBs often develop a central cavity similar to the early steps of pre-implantation development, and cavity formation in EBs or embryos

occurs by apoptosis. Basically, the central cavity is surrounded by the viable cells in contact with the basement membrane, and the cells in the interior part undergo apoptosis (Murray and Edgar, 2000).

EBs can be formed spontaneously from cell suspension culture and the hanging drop culture method with a defined cell number in nonadhesive microwells (Torisawa et al., 2007) and stirred vessel bioreactors (Schroeder et al., 2005). Alternative techniques for EB formation use microfabrication technologies, stirred mixed suspension culture systems, or spinning 96-well, round-bottomed, low-attachment plates (Ng et al., 2005). Suspension culture is the easiest and most straightforward method for EB formation, where a range of sizes and shapes of EBs are produced and can help obtain large quantities of differentiated cells (Walker et al., 2021). In addition, EBs grow better in serum-containing media and reach a maximum size of approximately 30,000 cells/EB by day 12 of differentiation (Dang et al., 2002). EBs tend to aggregate together and increase cell number or complexity as three embryonic germ layers are formed (Mansergh et al., 2009). EB growth optimisation experiments show that the ideal cell number for hanging drop culture is 500–1000 cells per 10 μl, and they can reach the largest EBs sizes with 15% and 20% serum concentration (Mansergh et al., 2009). Previous studies have reported that hESCs cultured in biomimetic 3D amniogenic culture system, 3D soft-gel, or microfluidic devices can form embryonic sac-like structures that mimic the early postimplantation embryo and amnion development to provide a 3D extracellular environment (Shao et al., 2017; Zheng et al., 2020).

Telomerase activity and TERT gene expression are higher in pluripotent stem cells to maintain hESCs pluripotency and self-renewal features (Thomson et al., 1998; Romito and Cobellis, 2016). However, TERT and telomerase activity levels decrease in pluripotent stem cells during the differentiation process (Armstrong et al., 2000, 2005; Tzukerman et al., 2000). TERT transcription is the primary and rate-limiting step of forming active telomerase (Aisner et al., 2002). Studies have indicated that TERT expression is highly regulated and correlated with telomerase activity, whereas TERC RNA and telomerase-associated proteins are expressed ubiquitously in adult cells (Jia et al., 2011). Transcriptional regulation of TERT is a complex process and involves the binding of transcription factors at the promoter and epigenetic factors, including DNA methylation and histone modifications of the TERT locus (Zhu et al., 2010; Saha et al., 2017). Telomerase activity decreased significantly after day four, and there was a correlation between TERT expression and telomerase activity in mouse EBs cultured in a differentiation medium (Armstrong et al., 2000). Cheng et al. have shown that TERT promoter

activity was significantly repressed by 55%, and TERT mRNA level decreased in EBs cultured for two weeks compared to undifferentiated ESCs using chromatinized BACs. Repressed TERT promoter was correlated to downregulated TERT expression during ESC differentiation (Cheng et al., 2017, 2019). Downregulated TERT expression was accompanied by increased H3K9me3 and H3K27me3 repressive marks at the TERT promoter (Cheng et al., 2017). EBs consist of a range of asynchronously differentiated and undifferentiated cells in their structure, therefore, Cheng and colleagues cultured adherent cells from EBs and removed the suspension cells to allow differentiation of fibroblast-like cells in an osteogenic medium for three weeks. The results of differentiated fibroblast-like culture showed that TERT promoter activities decreased to 18% (Cheng et al., 2019). Further studies have shown that ESC hanging drop-derived EBs displayed TERT and telomerase activity on day 14 (Madonna et al., 2008).

There are bioethical barriers to culturing *in vivo* human embryos beyond 14 days post-fertilisation. The 14-day rule originated because body form, axes, and primitive streak appear as hallmarks of gastrulation onset after 15 days of development of a human embryo from gamete mixing. Using an embryo for research is prohibited after the appearance of the primitive streak by the Human Fertilisation and Embryology Authority (HFEA) (HFE Act, 1990). Therefore, mimicking embryonic development provides a powerful experimental system to advance knowledge of human embryology and reproduction, furthermore, these systems based on stem cells provide ethical alternatives (Zheng et al., 2019). EBs embryo-like features could assist in the rational design of differentiation protocols of hPSCs for disease modelling and cell therapy and provide a valuable tool to study the relatively inaccessible stages of mammalian development. Modelling embryogenesis in a dish can be used in high-throughput drug and toxicity screens to understand pregnancy failure and birth defects better.

4.2 RESULTS

4.2.1 Embryoid body formation

SHEF1 embryoid bodies were grown under three different conditions (21% AO, 2% PG and 2% WKS). The size of EBs ranged from 10 µm to 150 µm in diameter (***Fig 4.2***). The mean size of EBs was 60 to 110 µm in 21 %, while 2% PG was 60-80 µm. On the other hand, EBs were distributed around 50-70 µm in diameter in 2% oxygen controlled workstation condition. The diameters of EBs cultured in 21% AO, 2% PG and 2% WKS were measured as 80.03 µm, 63.58 µm and 64.91 µm, respectively (***Fig 4.2)***.

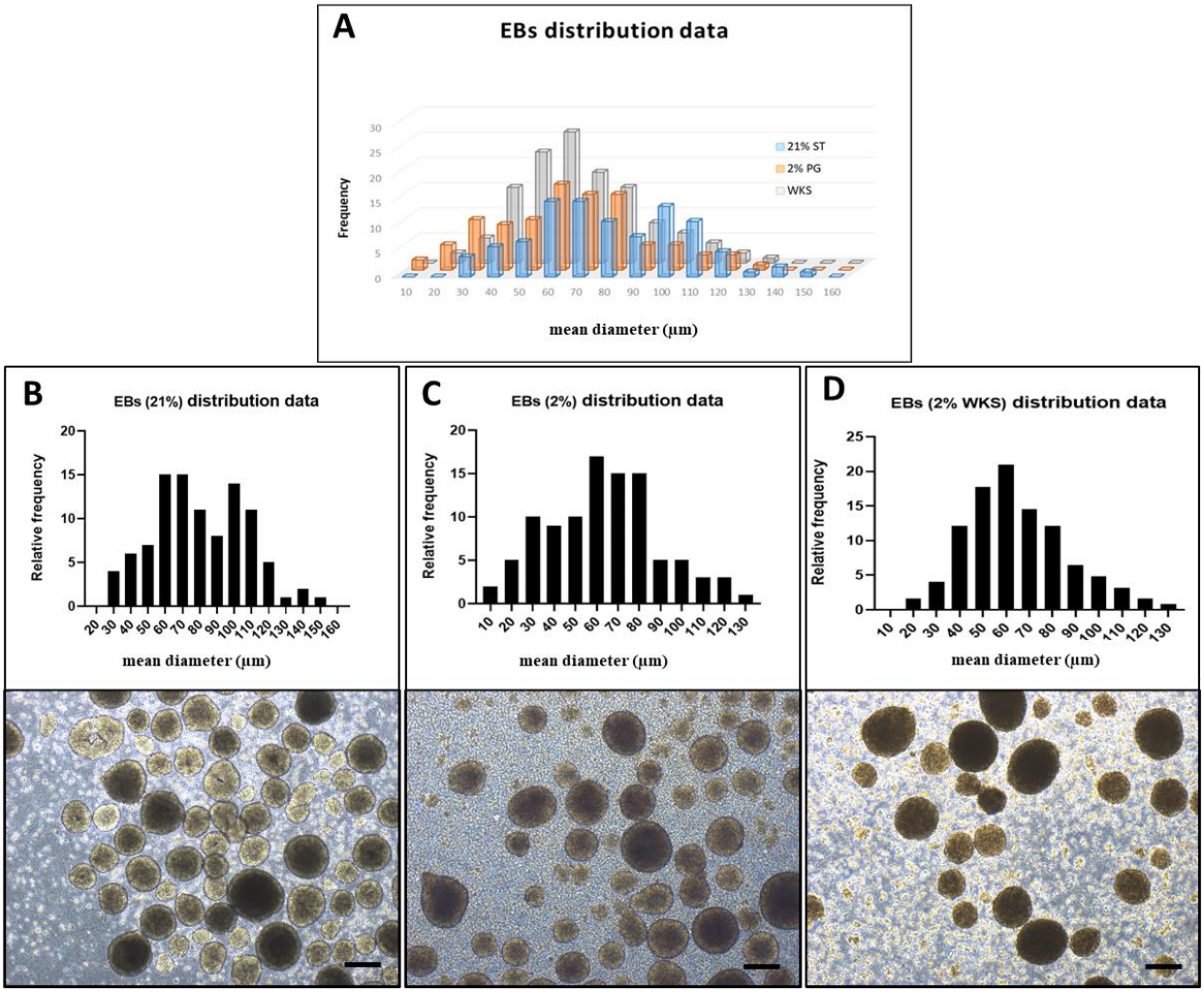

***Figure 4.2*. Five-days-old EBs of varying sizes were derived from hESCs in suspension**. The size distribution of EBs from SHEF1 cells was represented in differing oxygen conditions

(**A**). Histogram of frequency distribution data and morphology of EBs were shown in 21% AO (**B)**, 2% PG (**C),** and 2% WKS (**D)** conditions. The scale bar represents 100 µm, and n=100 EBs were counted for each condition using Image J software.

Embryoid bodies obtained from SHEF2 cells were grown under three different conditions (21% AO, 2% PG and 2% WKS). The diameter of EBs ranged from 30 µM to 170 µM. The mean size of EBs was ~ 60 µM in air oxygen and 2% physoxia environments. EBs cultured in air oxygen ranged from 60-80 µM in diameter, while the size of EBs also ranged from 60 to 80 µM in 2% PG condition. Meanwhile, EBs developed within oxygen controlled workstations ranged from 50 to70 µM in diameter. The mean value of EBs was measured as 80.11 µM, 79.09 µM and 65.80 µM for 21%, 2% PG, and WKS, respectively (***Fig 4.3)***.

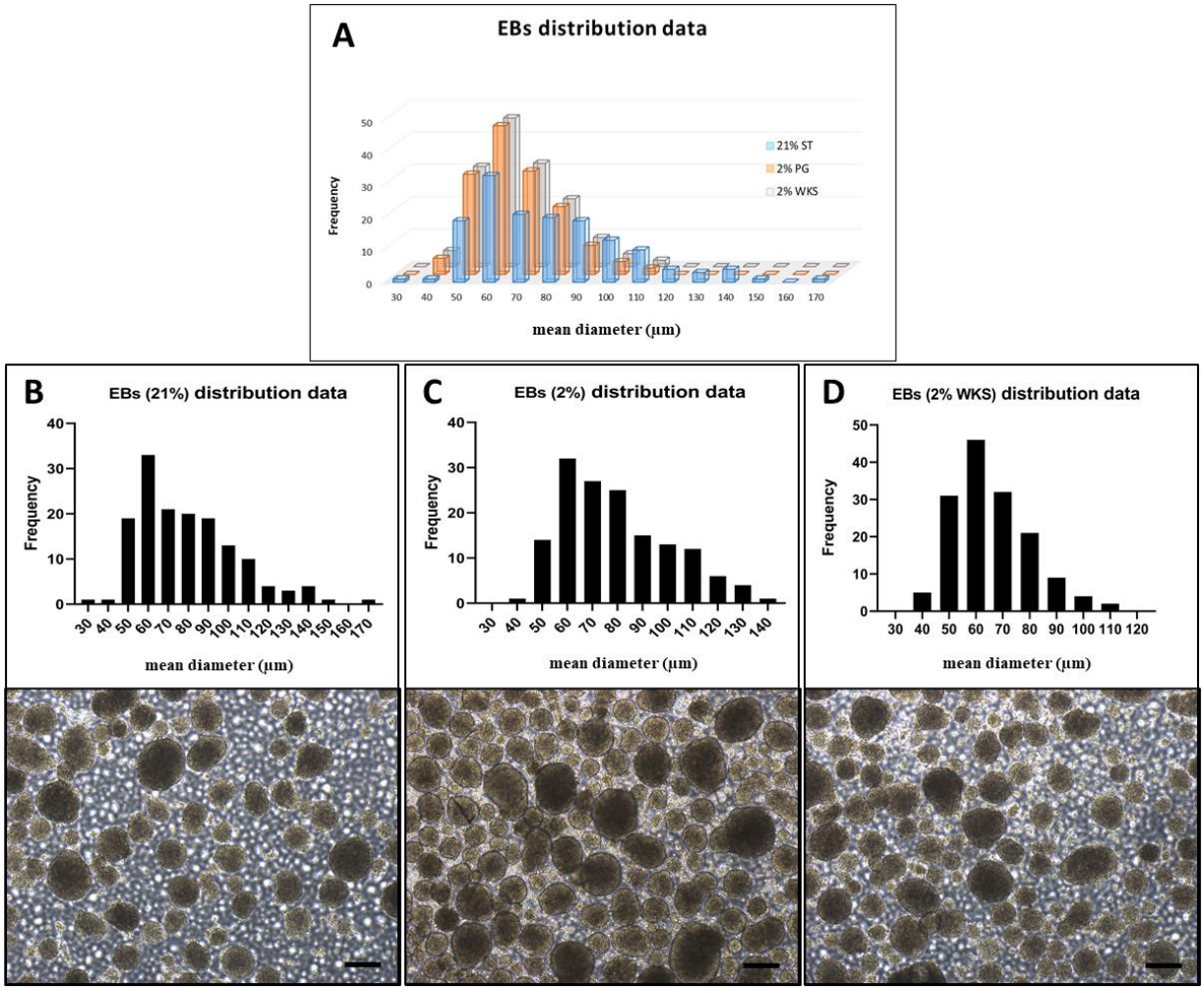

***Figure 4.3*. Five-days-old EBs of varying sizes were derived from hESCs in suspension**. The size distribution of EBs from SHEF2 cells was represented in differing oxygen conditions

(**A**). Histogram of frequency distribution data and morphology of EBs were shown in 21% AO (**B)**, 2% PG (**C),** and 2% WKS (**D)** conditions. The scale bar represents 100 μm, and n=150 EBs were counted using Image J software for each condition.

Live dead cell analysis determined higher viability of SHEF1 EB cells on day 5 (94.68 ± 5.77%) when compared to both days 10 (89.4 ± 2.56%) and 20 (85.28 ± 1.65%) in air oxygen. The percentage of live cells within EBs was 90.57 ± 6.06% on day 5, 86.36 ± 2.33% on day 10 and 81.85 ± 4.99% on day 20 in 2% PG condition. EBs cultured in 2% WKS showed 85.81 ± 4.68% cell viability on day 5, 83.59 ± 6.41% on day 10 and 76.07 ± 1.83% on day 20 (***Fig 4.4, 5)***. There were more apoptotic cells in 2% PG ($p<0.05$) and 2% WKS ($p<0.01$) conditions versus AO in SHEF1 EBs, and we noted increased apoptosis with differentiation (***Fig 4.5***).

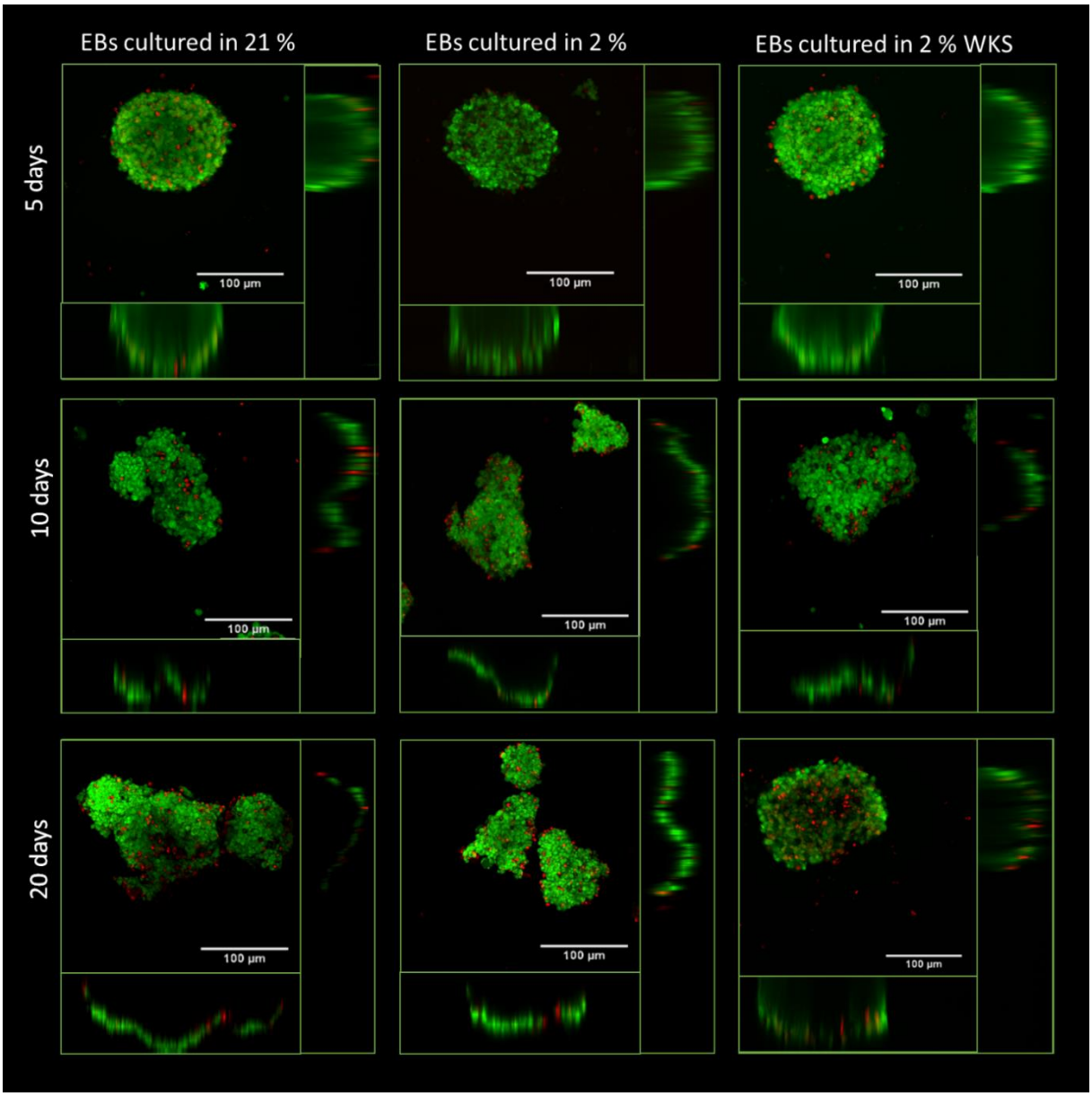

Figure 4.4. **Confocal images from live-dead cell analysis of EBs**. The pictures illustrate live cells (green) and dead cells (red) in EBs formed from SHEF1 cells at days 5, 10 and 20 in 21% AO, 2% PG and 2% WKS conditions. The scale bar represents 100 µm, representative of three independent samples for each condition.

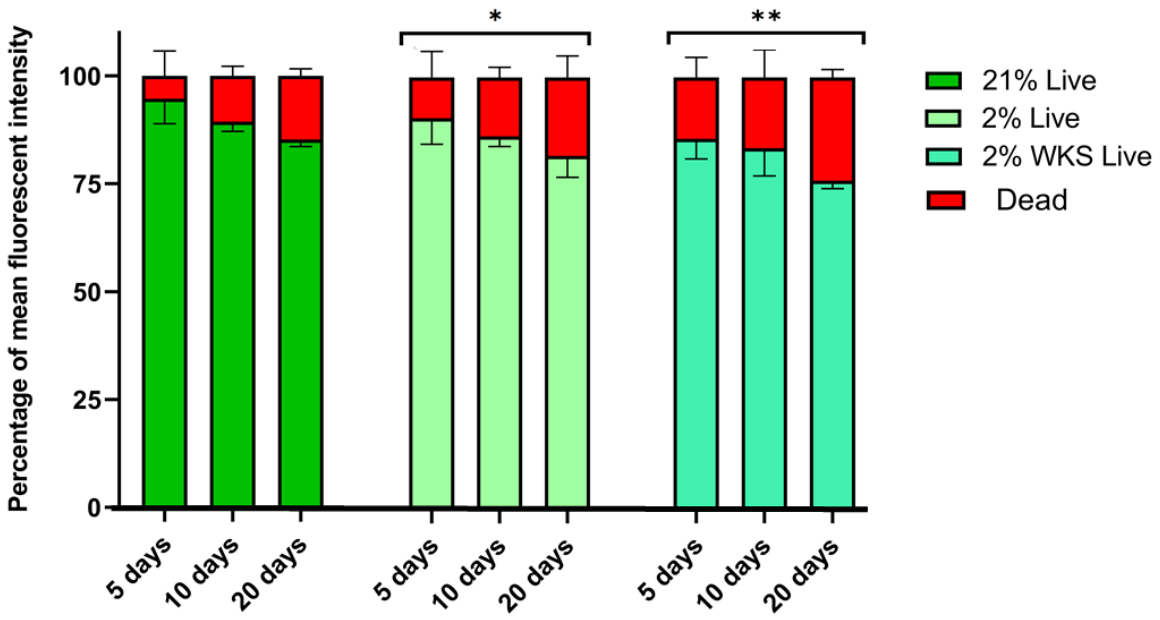

Figure 4.5. **Increased apoptosis during differentiation of SHEF1 EBs**. The percentage of mean fluorescent intensity of live and dead cells were represented in EBs formed from SHEF1 cells in 21% AO, 2% PG and 2% WKS conditions. The fluorescent intensity of live cells is indicated by green and dead cells by red. The results are represented with three independent samples (n=3) for each condition.

Live dead cell analysis identified higher viability of EBs formed from SHEF2 cells on day 5 (95.02 ± 1.21%) when compared to days 10 (89.63 ± 3.73%) and 20 (87.51 ± 3.34%) in air oxygen. Meanwhile, there was no significant change in cell viability in low oxygen conditions compared to AO microenvironment. The percentage of live cells in EBs was calculated as 95.09 ± 3.81% on day 5, 92.83 ± 4.91% on day 10 and 91.25 ± 3.99% on day 20 in 2% PG condition. Also, the cell viability of EBs cultured in 2% WKS were 97.22 ± 0.80% at day 5, 93.59 ± 3.11% at day 10 and 92.31 ± 4.41% at day 20 (***Fig 4.6, 4.7)***. We also noted increased apoptosis with differentiation in SHEF2 EBs (***Fig 4.7***).

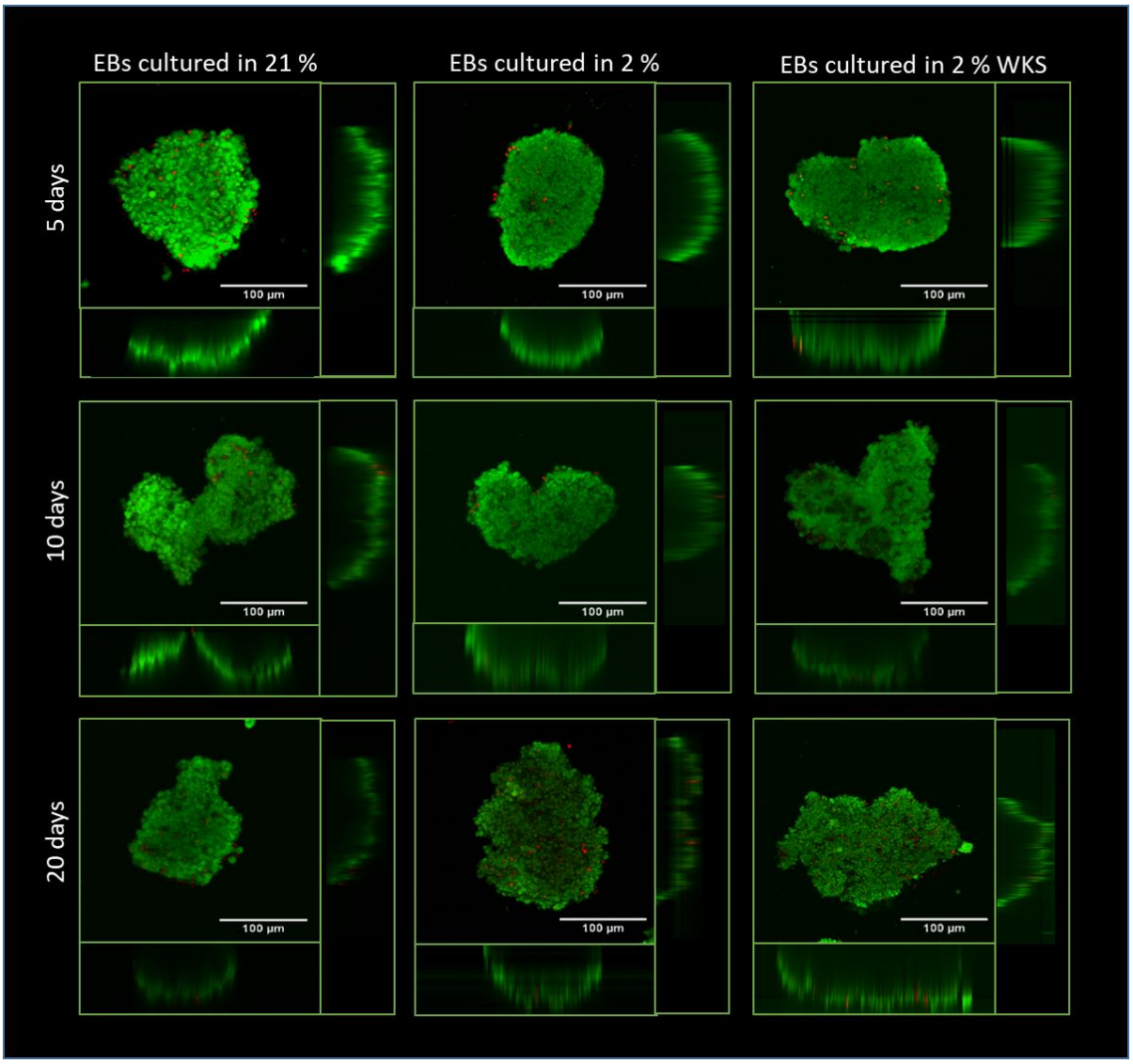

Figure 4.6. **Confocal images from live-dead cell analysis of EBs**. The pictures illustrate live cells (green) and dead cells (red) in EBs formed from SHEF2 cells at days 5, 10 and 20 in 21% AO, 2% PG and 2% WKS conditions. The scale bar represents 100 µm, representative of three independent samples for each condition.

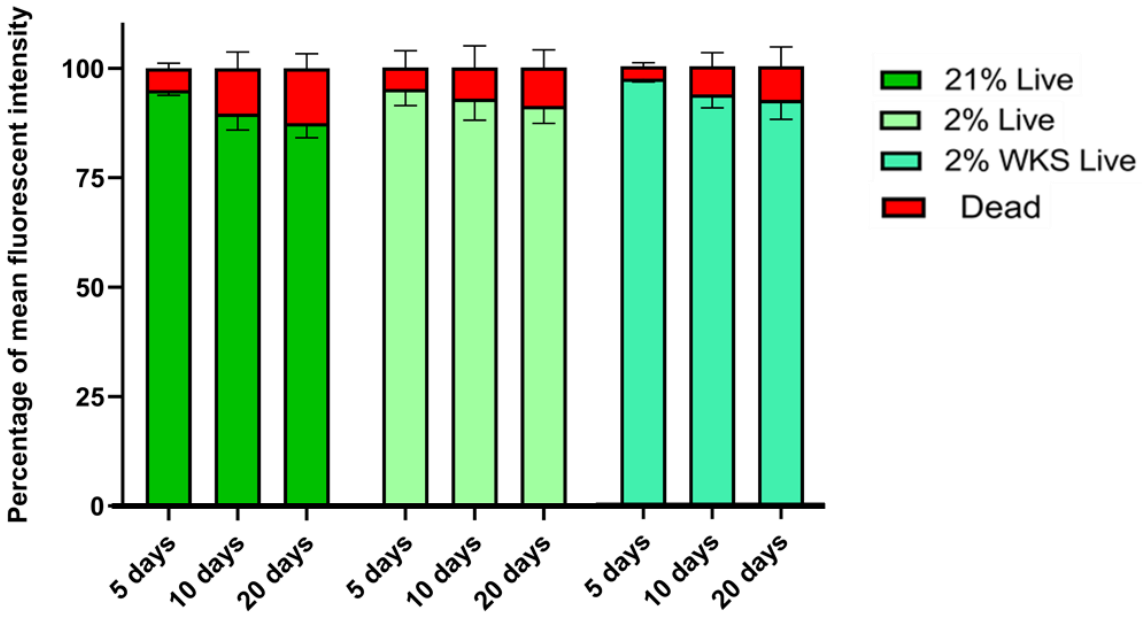

Figure 4.7. **Increased apoptosis during differentiation of SHEF2 EBs.** The percentage of mean fluorescent intensity of live and dead cells were represented in EBs formed from SHEF2 cells in 21% AO, 2% PG and 2% WKS conditions. The fluorescent intensity of live cells is indicated by green and dead cells by red. The results are represented with three independent samples (n=3) for each condition.

4.2.2 Three germ layer Differentiation Gene Expression Results

RT-qPCR was performed to examine relative gene expressions during spontaneous three germ layer differentiation, including NES (Nestin), TBXT (T-Box Transcription Factor T), KDR (Kinase Insert Domain Receptor), and AFP (Alpha-fetoprotein) in differentiated EBs.

Spontaneous differentiation with EBs formation displayed a different pattern of Nestin gene expression versus monolayer differentiated cells. EBs expressed elevated ectodermal marker when compared to monolayer differentiated cells. NES expression was increased at day 5 (2.77 ± 1.51), 10 (3.62 ± 0.38), and 20 (3.37 ± 0.52) in differentiated versus undifferentiated SHEF1 EBs in 21% AO. Significantly higher ectodermal differentiation was noted in 21% AO (3.62 ± 0.38, $p<0.05$) versus 2% WKS (1.99 ± 0.84) at day 10. Relative NES expression was 2.39 ± 0.93 fold at day 5, 3.07 ± 0.94 fold at day 10 and 3.99 ± 0.72 fold at day 20 differentiation in 2% PG EBs versus undifferentiated cells. NES expression displayed increases at days 5 (1.16

± 0.58), 10 (1.99 ± 0.84), and 20 (3.11 ± 0.83) in 2% WKS EBs. Overall, there was a significant increase in NES expression in all conditions during EB differentiation compared to undifferentiated SHEF1 cells (***Fig 4.8.A)***.

NES expression was significantly higher in 21% AO versus 2% WKS (-1.86 ± 0.30, $p<0.001$) undifferentiated SHEF2 cells and also with EBs at day 5 in 21% AO (4.06 ± 0.94) versus 2% PG (2.72 ± 1.65, $p<0.05$) and 2% WKS (0.09 ± 1.01, $p<0.001$). There was a significant increase in NES expression at days 10 (4.98 ± 0.65, 5.25 ± 0.28 and 4.96 ± 1.04, $p<0.001$) and 20 EBs (5.23 ± 0.72, 5.30 ± 0.86 and 4.24 ± 0.48, $p<0.001$) in 21% AO, 2% PG and 2% WKS, respectively versus undifferentiated cells (***Fig 4.8.B)***. When the data from both stem cells were combined, EBs displayed a significant increase in NES expression at days 5, 10, and 20 ($p<0.001$) in all conditions combined versus undifferentiated cells. Particularly, there was a significant decrease in 2% WKS at day 5 (0.63 ± 0.96, $p<0.001$) and day 20 (3.67 ± 0.88, $p<0.05$) compared to 21% AO at day 5 and 20 (3.41 ± 1.38 and 4.30 ± 1.14), respectively (***Fig 4.9.A)***.

KDR expression was significantly lower in SHEF1 EBs cultured in 2% WKS at day 5 (-1.54 ± 0.68, $p<0.05$) and 2% PG at day 10 (-0.01 ± 0.56, $p<0.05$) versus 21% AO at days 5 and 10 (0.31 ± 1.17 and 1.32 ± 0.78), respectively. EBs in 21% AO condition had higher expression at days 5, 10, and 20 (0.31 ± 1.16, 1.32 ± 0.78 and 2.17 ± 0.37, respectively) versus 21% AO undifferentiated SHEF1. A significant increase in gene expression was noted at day 20 in 21% AO, 2% PG and 2% WKS (2.16 ± 0.37, 1.91 ± 0.79 and 1.21 ± 0.69, $p<0.001$) compared to undifferentiated SHEF1 cultured in 21% AO (0.00 ± 0.64), 2% PG (0.51 ± 0.67) and 2% WKS (-0.66 ± 0.32), respectively (***Fig 4.8.A)***. All together EBs demonstrated that cells cultured in air oxygen showed consistently higher mesodermal gene expression patterns than physoxia condition. SHEF2 EBs in 21% AO at days 5, 10 and 20 (4.03 ± 1.0, 5.49 ± 0.46 and 4.79 ± 1.91, $p<0.001$) displayed a significant increase in KDR gene expression compared to undifferentiated cells. Also, there was a significant decrease in KDR expression at day 5 (2.24 ± 1.35, $p<0.05$) and day 10 EBs (3.61 ± 1.01, $p<0.05$) in 2% WKS conditions versus AO at day 5 (4.03 ± 1.00) and day 10 EBs (5.49 ± 0.46) (***Fig 4.8.B)***. Combined data demonstrated a significant decrease in 2% WKS in undifferentiated cells (-0.89 ± 0.56, $p<0.05$) compared to 21% AO. Further, significant decreases in KDR expression in differentiated EBs in 2% WKS at day 5 (0.35 ± 2.22, $p<0.05$), 10 (1.61 ± 2.30, $p<0.01$), and 20 (2.38 ± 1.35, $p<0.05$) was noted versus 21% AO at days 5, 10, and 20 (2.17 ± 2.20, 3.41 ± 2.26, and 3.48 ± 1.89,

respectively). Also, EBs cultured for 10 days in 2% PG microenvironment (2.18 ± 2.32, $p<0.001$) displayed a significant reduction versus 21% AO at day 10 EBs (***Fig 4.9.C)***.

Undifferentiated SHEF1 cells cultured in 2% PG (-1.46 ± 0.72, $p<0.05$) and 2% WKS (-0.59 ± 0.88) displayed reduced TBXT expression compared to 21% AO. TBXT, mesodermal marker, expression was significantly higher in days 5 ($p<0.01$), 10 ($p<0.001$), and 20 ($p<0.001$) EBs versus undifferentiated SHEF1 cells. There was a sigificant reduction in 2% WKS (-0.39 ± 0.61, $p<0.05$) versus 21% AO (1.03 ± 0.96) at day 5. No significant difference were noted in 21% AO (2.27 ± 0.79 and 1.90 ± 0.91), 2% PG (1.89 ± 0.85 and 2.89 ± 1.21), and 2% WKS (2.65 ± 0.81 and 2.03 ± 0.61) EBs at days 10 and 20, respectively (***Fig 4.8.A)***. Undifferentiated SHEF2 in 2% PG (-1.25 ± 1.13, $p<0.05$) and 2% WKS (-2.18 ± 1.34, $p<0.01$) displayed a significant reduction compared to 21% AO condition. Also, 5 day cultured EBs in 2% WKS (0.51 ± 0.71, $p<0.001$) showed a significant reduction compared to 21% AO at day 5 (2.21 ± 0.39). No significant difference was noted in 21% AO (1.96 ± 0.27 and 2.27 ± 0.73), 2% PG (1.36 ± 0.09 and 2.27 ± 1.44) and 2% WKS (2.30 ± 0.62 and 2.91 ± 0.73) cultured EBs at days 10 and 20, respectively (***Fig 4.8.B)***. Pooled data demonstrated that undifferentiated hESC in 2% PG (-1.35 ± 0.91, $p<0.001$) and 2% WKS (-1.38 ± 1.36, $p<0.001$) had significantly less TBXT expression versus AO. Significantly less expression of TBXT was noted in 5 days differentiated EBs in 2% WKS (0.06 ± 0.78, $p<0.001$) when compared to 21% AO at day 5 (1.62 ± 0.94). Altogether, TBXT was highly expressed after 5, 10, and 20 days of differentiation ($p<0.001$) versus undifferentiated cells (***Fig 4.9.D)***.

Endodermal marker AFP expression was elevated after 5, 10, and 20 days ($p>0.001$) of differentiation versus undifferentiated SHEF1. EBs in 2% PG and 2% WKS conditions for 5 days (2.15 ± 0.69 and 1.86 ± 0.27, $p<0.001$) displayed a significant reduction in comparison to 5 days EBs in 21% AO (4.21 ± 1.18). EBs in 2% PG and 2% WKS for 10 days (2.84 ± 0.96, $p<0.01$ and 2.09 ± 0.41, $p<0.001$) also displayed a significant reduction in comparison to 21% AO (3.99 ± 0.56), respectively. However, there was no significant difference between 21% AO, 2% PG and 2% WKS (2.88 in ± 0.51, 3.21 ± 0.46 and 3.15 ± 0.51) SHEF1 at day 20 (***Fig 4.8.A)***. The expression of AFP was significantly lower in undifferentiated SHEF2 in 2% PG and 2% WKS (-1.56 ± 0.73, $p>0.05$ and -2.31 ± 0.42, $p>0.001$, respectively) compared to 21% AO. In addition, there was a significant decrease in AFP expression in day 10 EBs in 2% PG and 2% WKS (2.78 ± 0.82 and 2.45 ± 0.59, $p<0.05$) versus day 10 EBs in AO (4.29 ± 0.79). EBs cultured for 5 and 20 days displayed no significant difference between 21% AO (1.66 ± 1.43 and 4.89 ± 1.39), 2% PG (0.81 ± 1.83 and 4.86 ± 0.58), and 2% WKS (1.27 ± 0.93 and

3.44 ±1.47) (***Fig 4.8.B)***. Overall, AFP expression was higher after 5, 10, and 20 days of differentiation ($p<0.001$) versus 21% AO. Pooled data demonstrated that EBs displayed a significant increase in AFP expression at days 5, 10, and 20 when all conditions were combined. Undifferentiated SHEF cultured in 2% WKS (-1.17 ± 1.28, $p<0.05$) had a significantly lower mean value versus 21% AO. Also, EBs in 21% AO (2.94 ± 1.83 and 4.14 ± 0.62) showed higher expression levels than 2% PG (1.48 ± 1.49 and 2.81 ± 0.85, $p<0.01$) and 2% WKS (1.56 ± 0.72, $p<0.05$ and 2.27 ± 0.52, $p<0.001$) at days 5 and 10, respectively. Lastly, there was no significant change of relative gene expression of AFP between conditions at day 20 (***Fig 4.9.B)***.

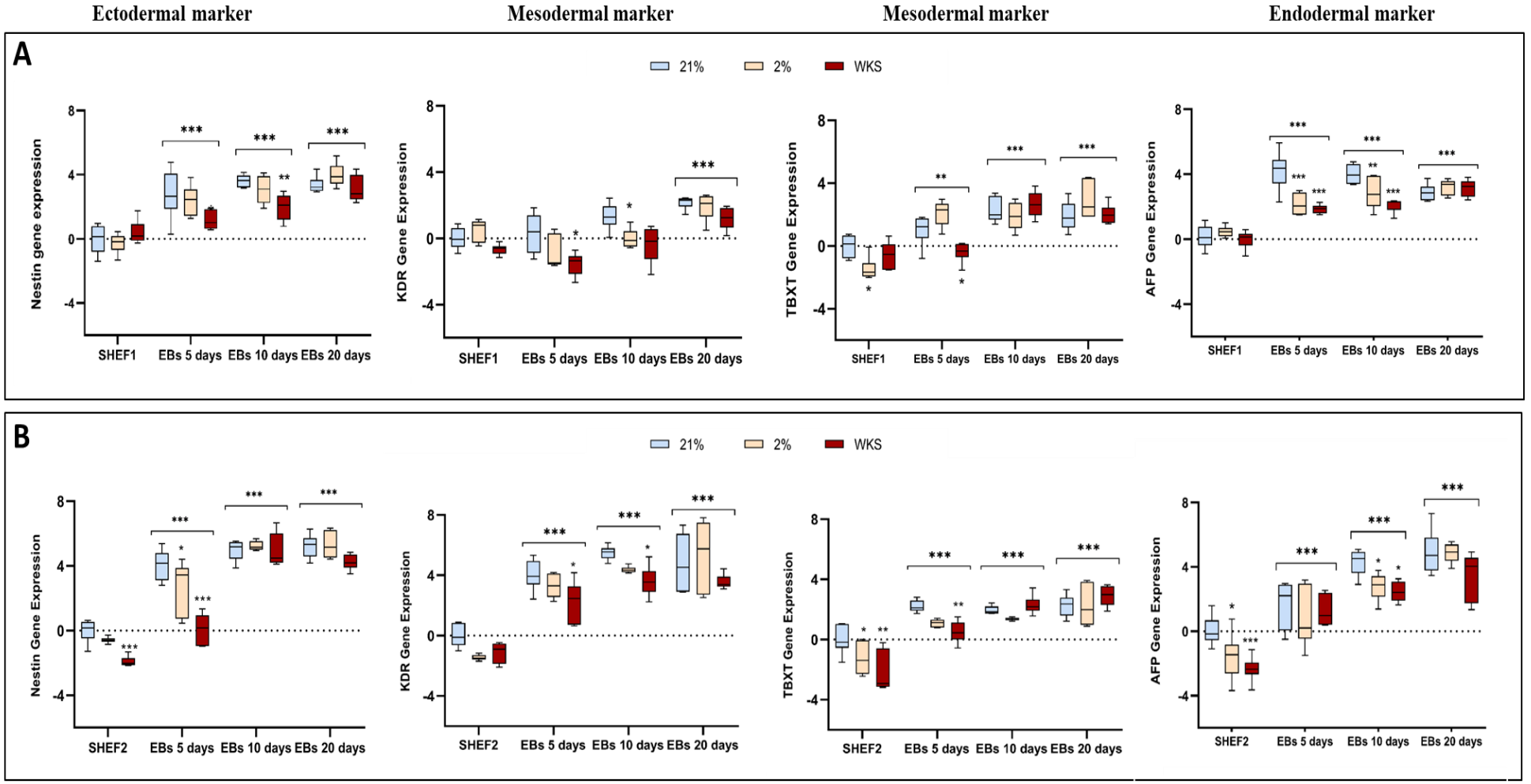

Figure 4.8. **Increased expression of Nestin, KDR, TBXT and AFP differentiation markers**. SHEF1 (**A**), SHEF2 (**B**) undifferentiated cells and differentiated EBs were obtained in air oxygen (21% AO) and physiological oxygen conditions (2% PG and 2% WKS). The RT-qPCR expression ($2^{-\Delta\Delta CT}$) of the genes normalised to the expression of GAPDH. The box represents the interquartile range, the whisker illustrates the outer quartiles, and the line in the middle shows the median expression. Data are represented as n=3x3, *p<0.05, **p<0.01, ***p<0.001 vs 21% AO. Bars with stars indicate a significant difference between differentiated and undifferentiated cells. The other stars compare physoxia conditions to 21% AO.

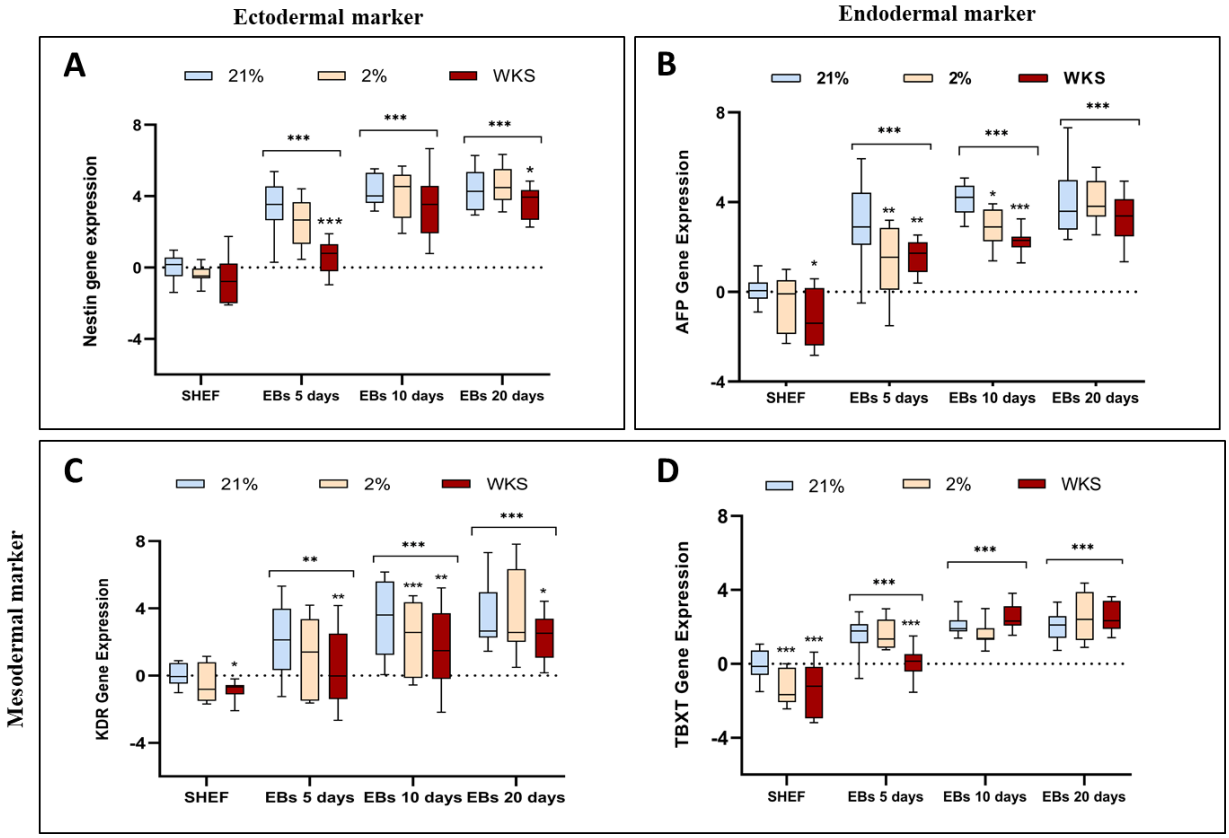

***Figure 4.9*. Increased expression of Nestin, AFP, KDR and TBXT differentiation markers.** SHEF1 and SHEF2 EBs data were pooled together. Undifferentiated and differentiated cells were obtained in air oxygen (21% AO) and physiological oxygen conditions (2% PG and 2% WKS). The RT-qPCR expression ($2^{-\Delta\Delta CT}$) of the Nestin **(A)**, AFP **(B)**, KDR **(C)** and TBXT **(D)** genes normalised to the expression of GAPDH. The box represents the interquartile range, the whisker illustrates the outer quartiles, and the line in the middle shows the median expression. Data are represented as n=3x3, *p<0.05, **p<0.01, ***p<0.001 vs air oxygen (21% AO). Bars with stars indicate a significant difference between differentiated and undifferentiated cells. The other stars compare physoxia conditions to 21% AO.

4.2.3 Three Germ Layer Differentiation Markers Expression

EBs were characterized by their expression of pluripotency markers SSEA-1 and alkaline phosphatase. Also, EBs were stained with three germ layer differentiation markers Nestin, AFP and Brachyury to evaluate spontaneous monolayer differentiation during 5, 10 and 20 days. During differentiation of EBs, pluripotent marker alkaline phosphatase expression decreased at

day 20 in 21% AO and 2% PG but not in 2% WKS. EBs started to express SSEA-1 marker on day 5, and it was higher on days 10, 20 in both SHEF1 and SHEF2 EBs (***Fig 4.10.A, B, C***).

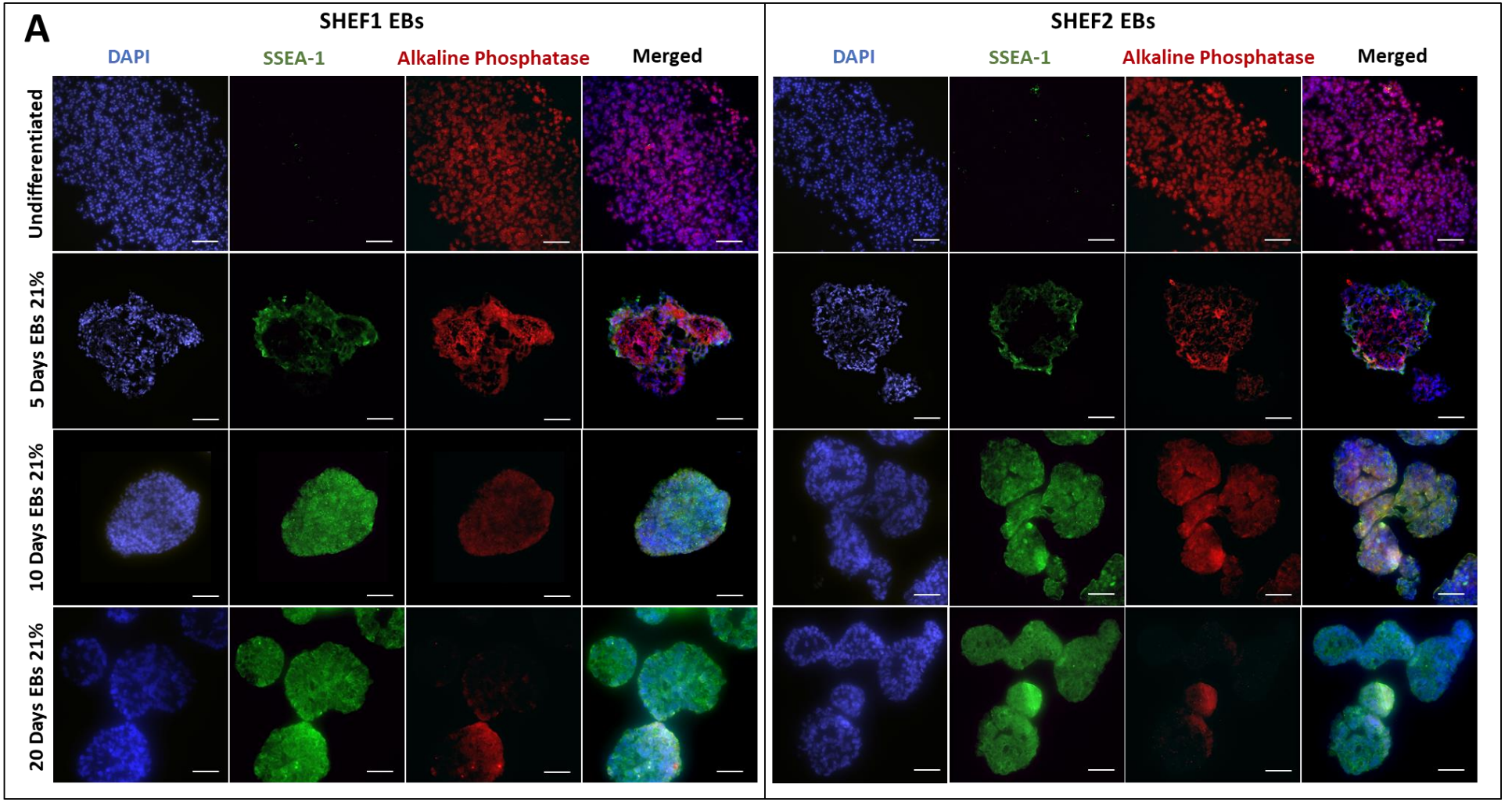
A
SHEF1 EBs
SHEF2 EBs
DAPI
SSEA-1
Alkaline Phosphatase
Merged
DAPI
SSEA-1
Alkaline Phosphatase
Merged
Undifferentiated
5 Days EBs 21%
10 Days EBs 21%
20 Days EBs 21%

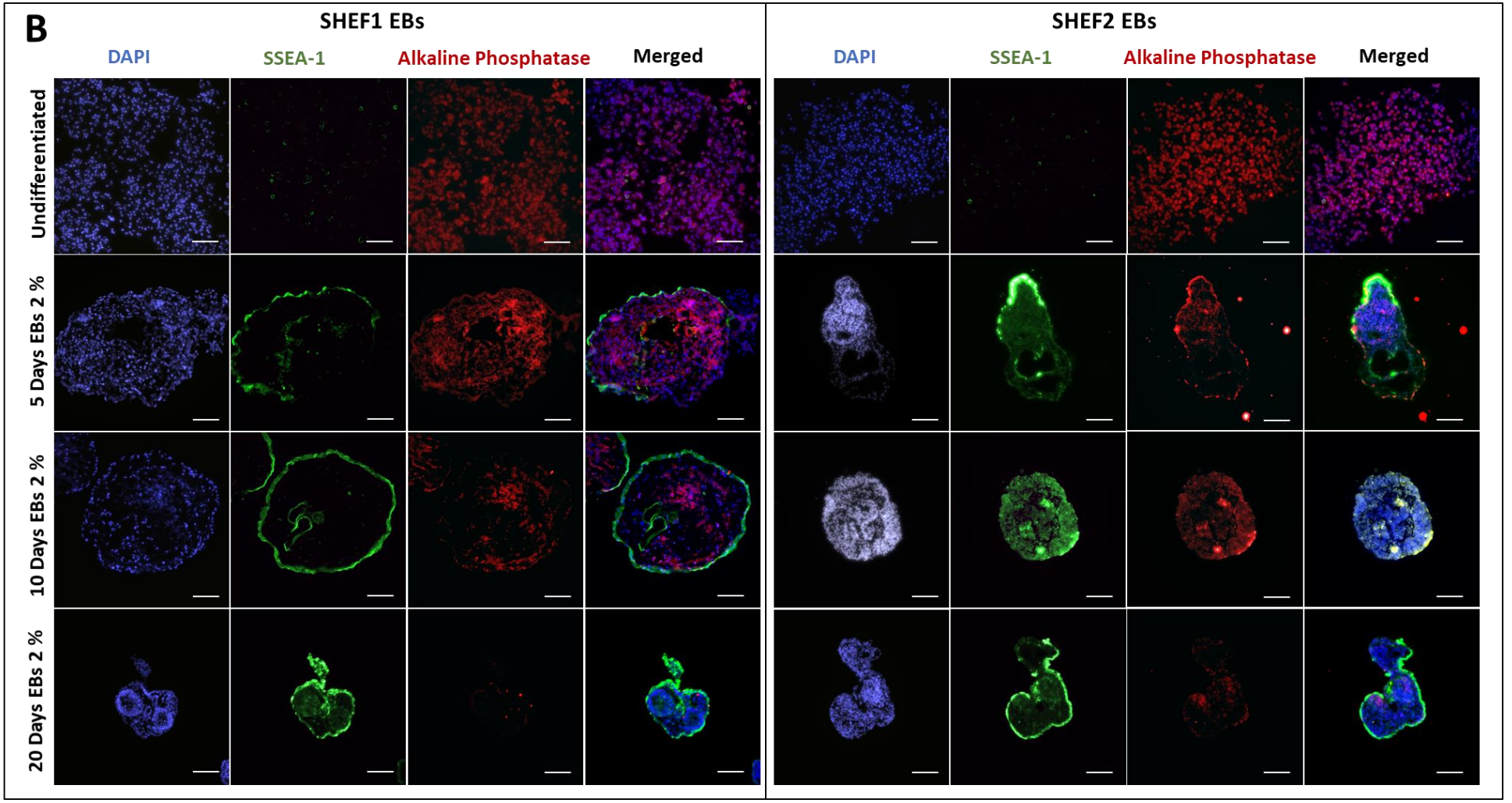
B
SHEF1 EBs
SHEF2 EBs
DAPI
SSEA-1
Alkaline Phosphatase
Merged
DAPI
SSEA-1
Alkaline Phosphatase
Merged
Undifferentiated
5 Days EBs 2 %
10 Days EBs 2 %
20 Days EBs 2 %

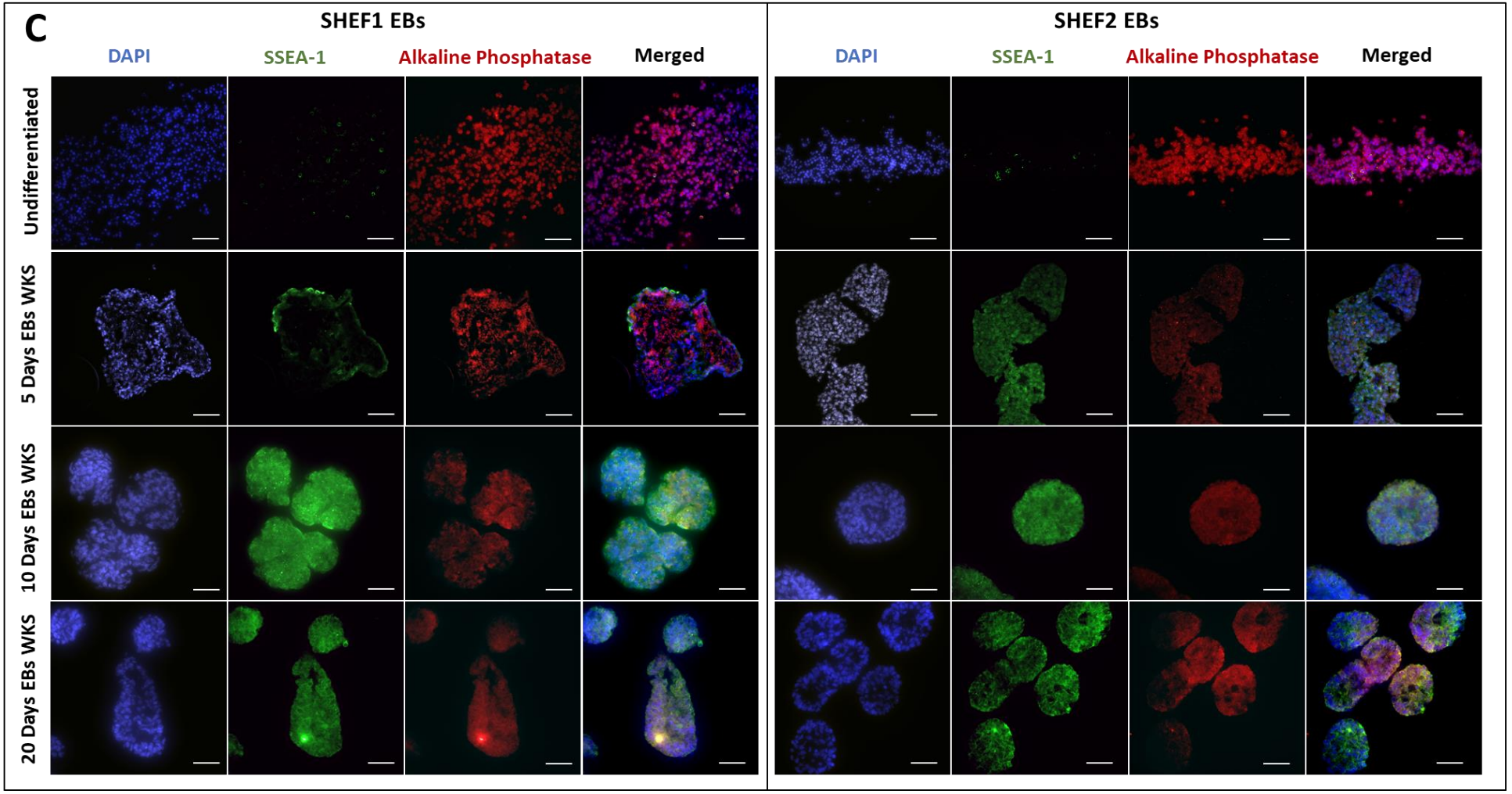

Figure 4.10. **Immunostaining of pluripotency markers in undifferentiated SHEF and EBs.** Cells were cultured in **(A)** 21% AO, **(B)** 2% PG and **(C)** 2% WKS for 20 days. The scale bar represents 100 µm. The red and green colours indicate specific antigens, blue represents DAPI. Images are representative of three independent samples.

AFP expression was characterized in SHEF1 and SHEF2 EBs in 21% AO, 2% PG and 2% WKS *(**Fig 4.11.A, B, C**).* AFP expression was increased during the formation of EBs in both cell lines in all conditions. Different sizes of EBs were observed from immunohistochemistry experiments which may be due to some variations in incubation parameters during cell culture.

Nestin expression was increased after five days of EBs formation, and there was a higher expression at day 20 EBs cultured in 21% AO (***Fig 4.12.A**)*. SHEF2 EBs showed high Nestin expression at days 5, 10 and 20 in 21% AO. Also, EBs cultured in 2% PG and 2% WKS showed a rapid increase in Nestin marker at days 5, 10 and 20 (***Fig 4.12.B, C***).

SHEF1 and SHEF2 EBs in 21% AO displayed considerably high Brachyury expression on days 5 and 10, but there was a decrease on day 20 (***Fig 4.13.A*)**. EBs cultured in 2% PG showed moderate expression of early differentiation marker Brachyury at days 5, 10 and 20 (***Fig 4.13.B***). SHEF1 EBs cultured in 2% WKS showed high Brachyury expression at days 5, 10 and 20, but SHEF2 EBs displayed a decrease after days 10 and 20 (***Fig 4.13.C**)*.

Overall, SSEA-1 negative pluripotency marker expression increased while positive marker alkaline phosphatase expression decreased during 20 days of EBs formation. EBs showed expression of three germ layer differentiation markers.

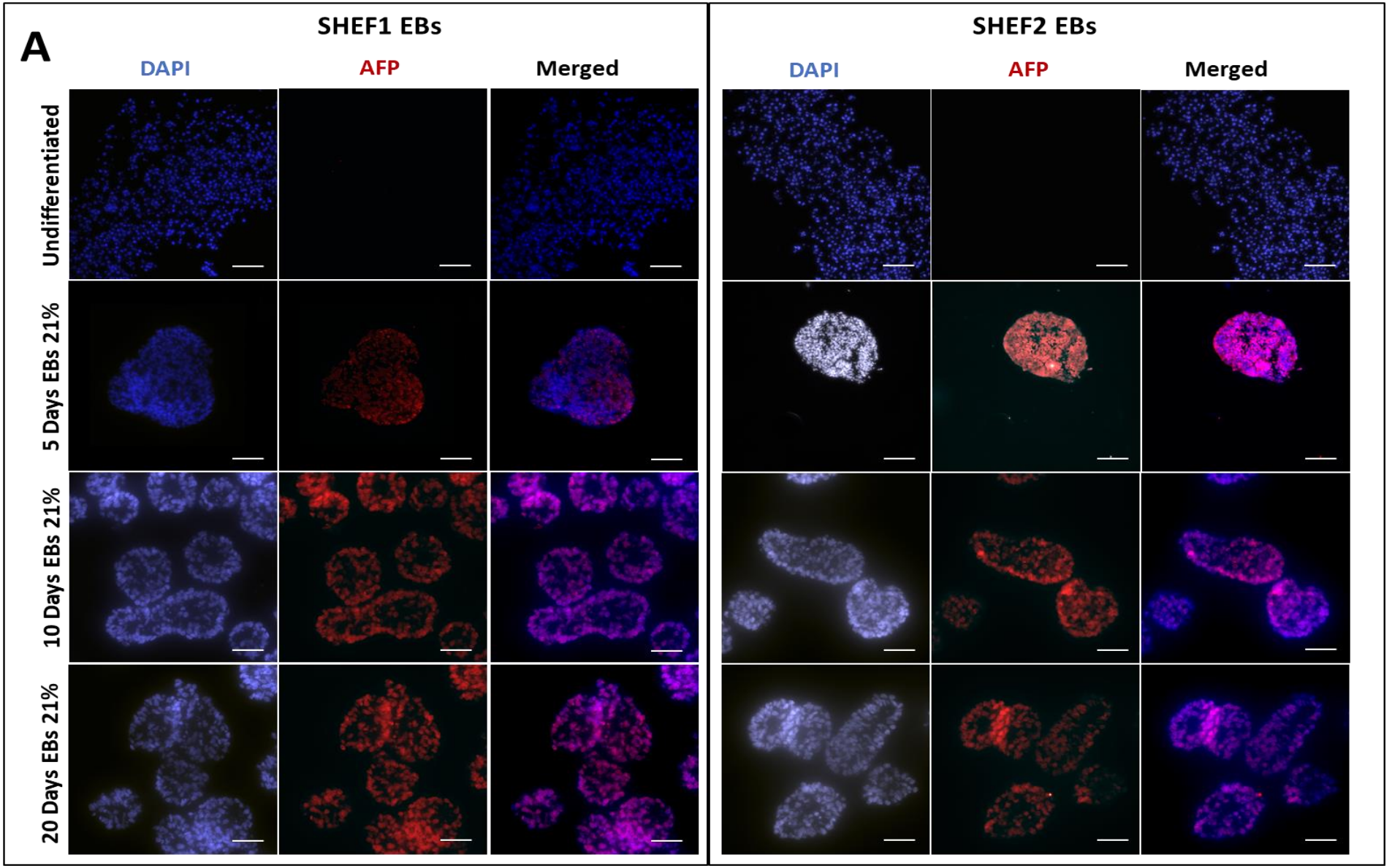
A
SHEF1 EBs
SHEF2 EBs
DAPI
AFP
Merged
DAPI
AFP
Merged
Undifferentiated
5 Days EBs 21%
10 Days EBs 21%
20 Days EBs 21%

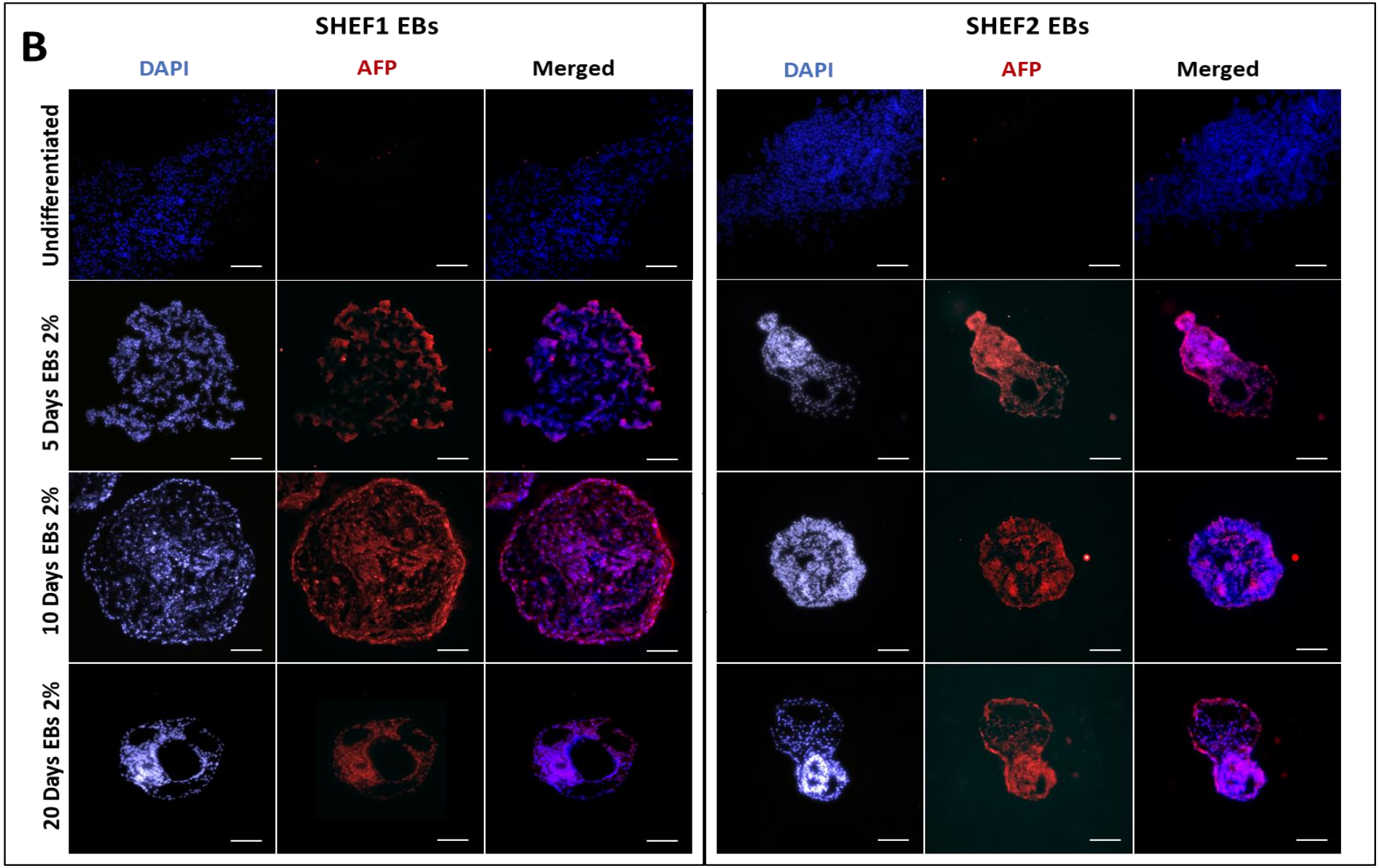
B
SHEF1 EBs
SHEF2 EBs
DAPI
AFP
Merged
DAPI
AFP
Merged
Undifferentiated
5 Days EBs 2%
10 Days EBs 2%
20 Days EBs 2%

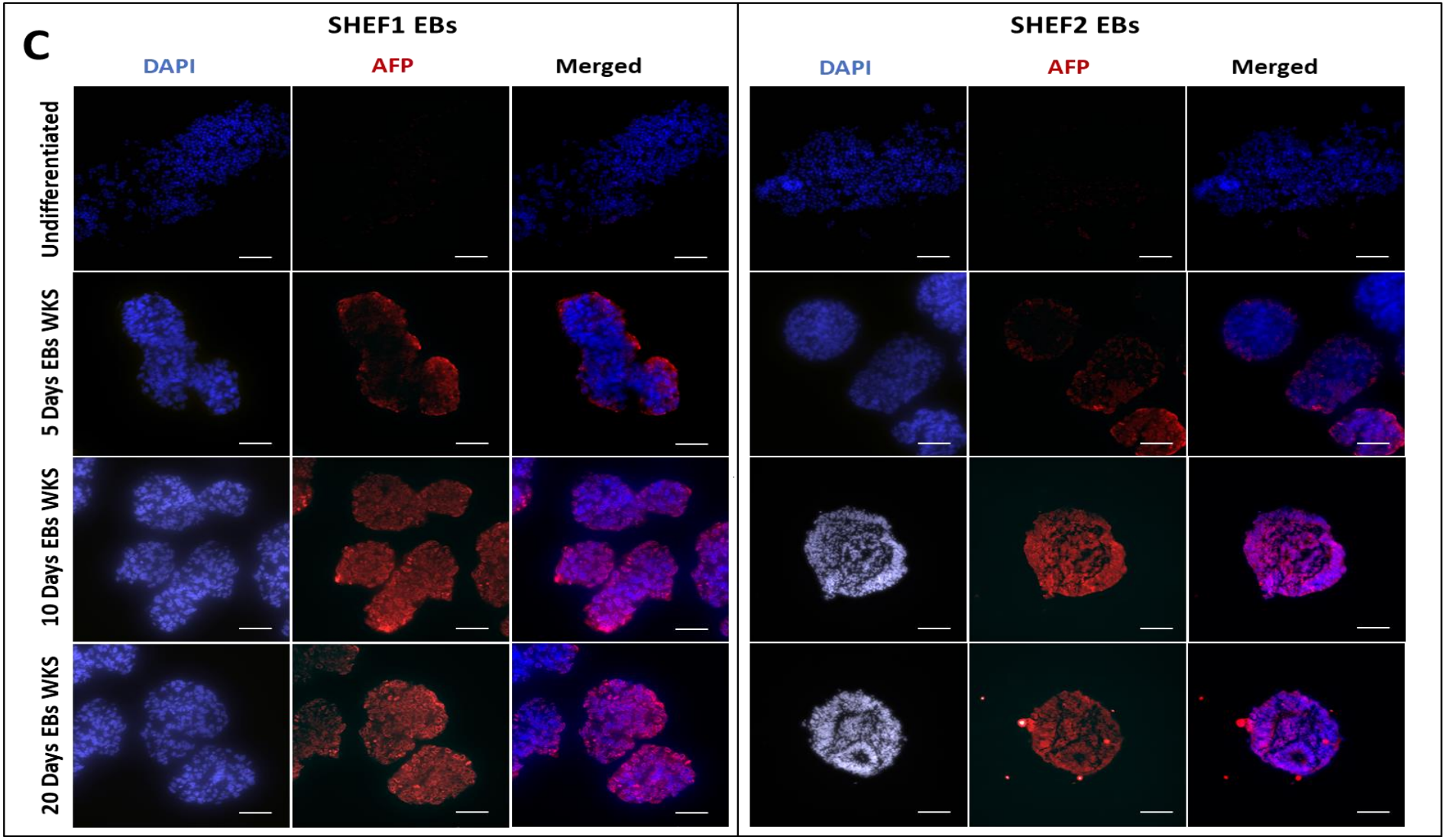

Figure 4.11. **Immunostaining of differentiation markers in undifferentiated SHEF and EBs.** Cells were cultured in **(A)** 21% AO, **(B)** 2% PG and **(C)** 2% WKS for 20 days. The scale bar represents 100 μm. The red and green colours indicate specific antigens, and blue represents DAPI. Images are representative of three independent samples.

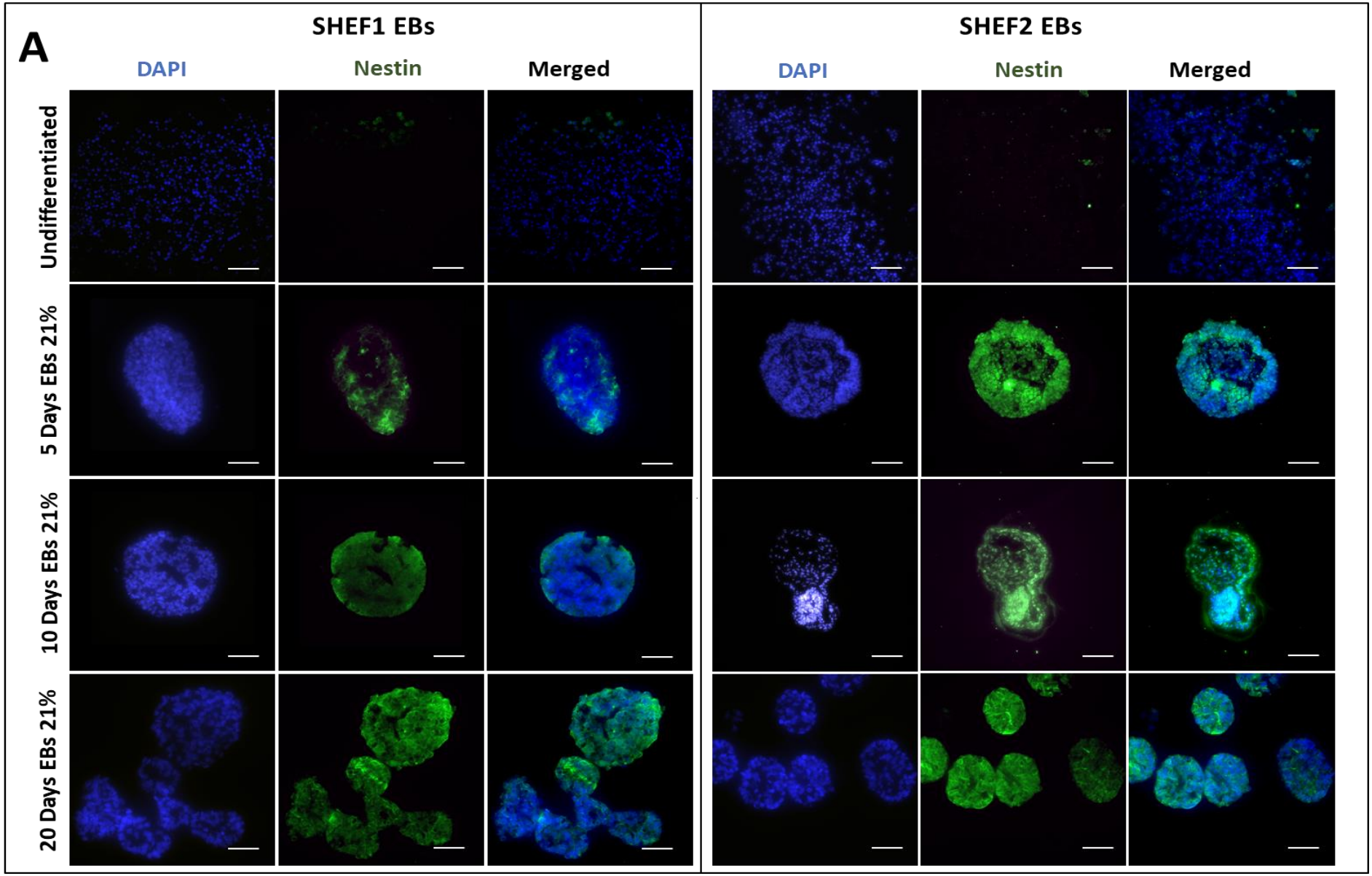
A
SHEF1 EBs
SHEF2 EBs
DAPI
Nestin
Merged
DAPI
Nestin
Merged
Undifferentiated
5 Days EBs 21%
10 Days EBs 21%
20 Days EBs 21%

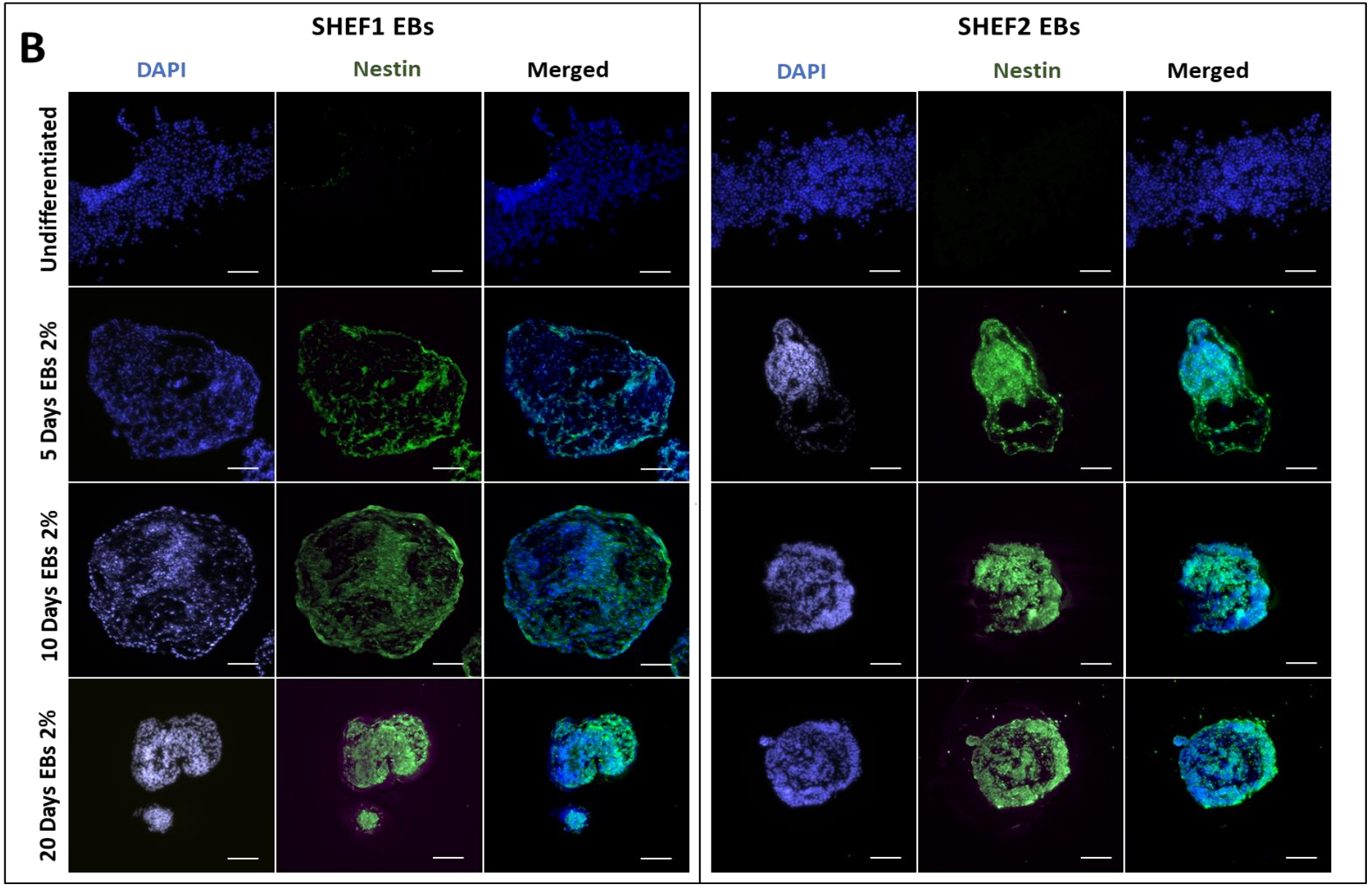
B
SHEF1 EBs
SHEF2 EBs
DAPI
Nestin
Merged
DAPI
Nestin
Merged
Undifferentiated
5 Days EBs 2%
10 Days EBs 2%
20 Days EBs 2%

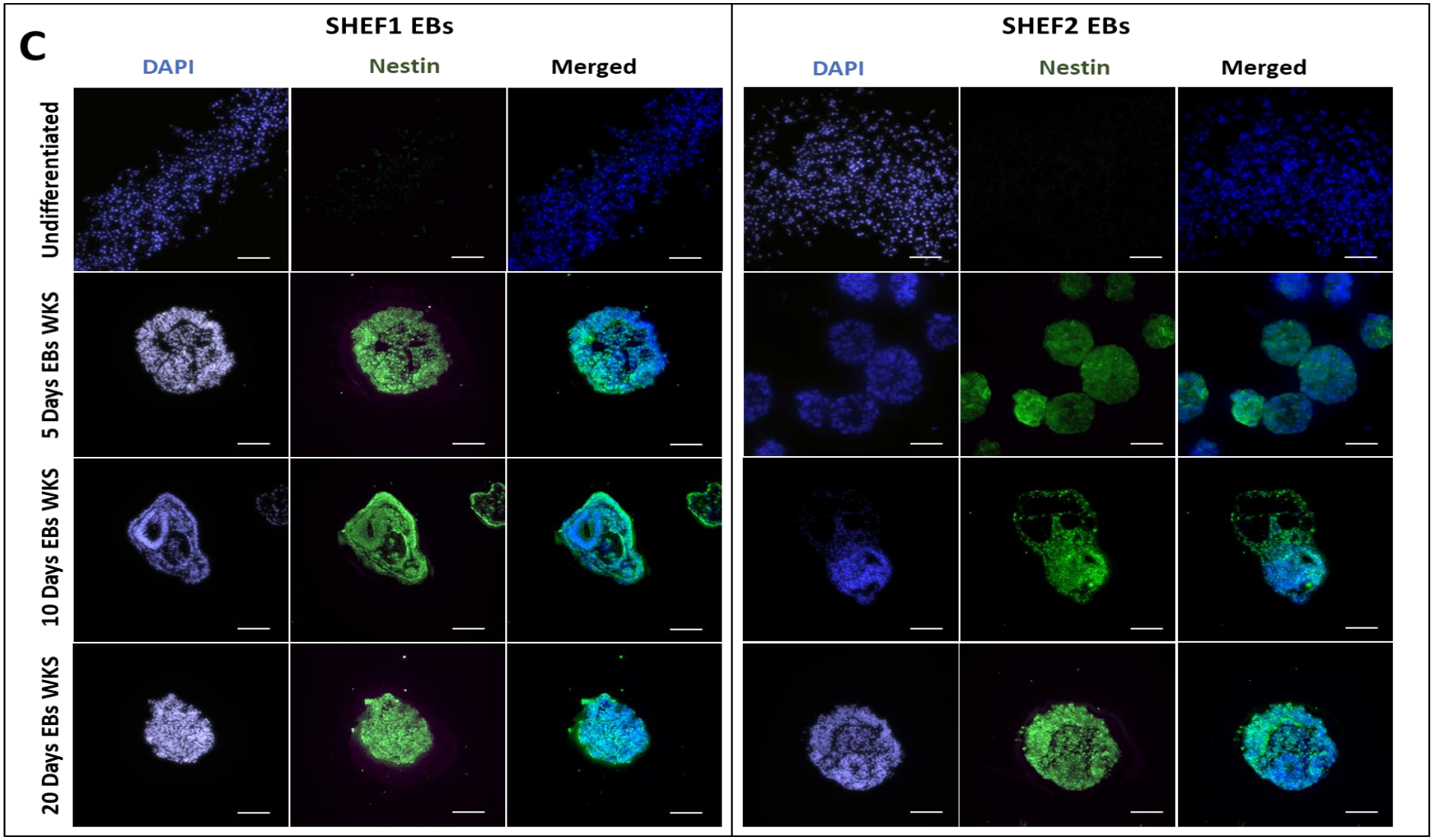

Figure 4.12. **Immunostaining of differentiation markers in undifferentiated SHEF and EBs.** Cells were cultured in **(A)** 21% AO, **(B)** 2% PG and **(C)** 2% WKS for 20 days. The scale bar represents 100 μm. The red and green colours indicate specific antigens, and blue represents DAPI. Images are representative of three independent samples.

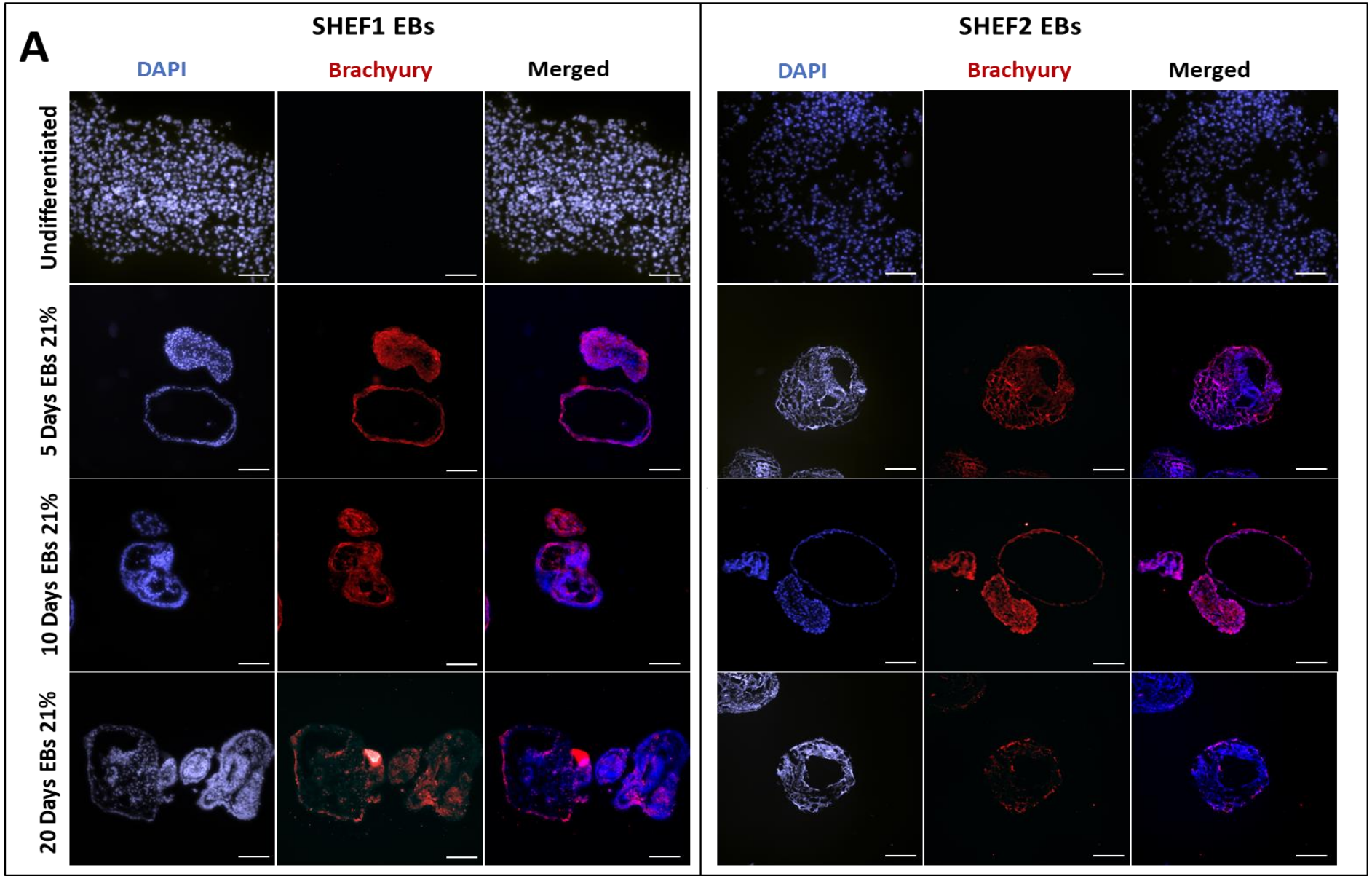
A
SHEF1 EBs
SHEF2 EBs
DAPI
Brachyury
Merged
DAPI
Brachyury
Merged
Undifferentiated
5 Days EBs 21%
10 Days EBs 21%
20 Days EBs 21%

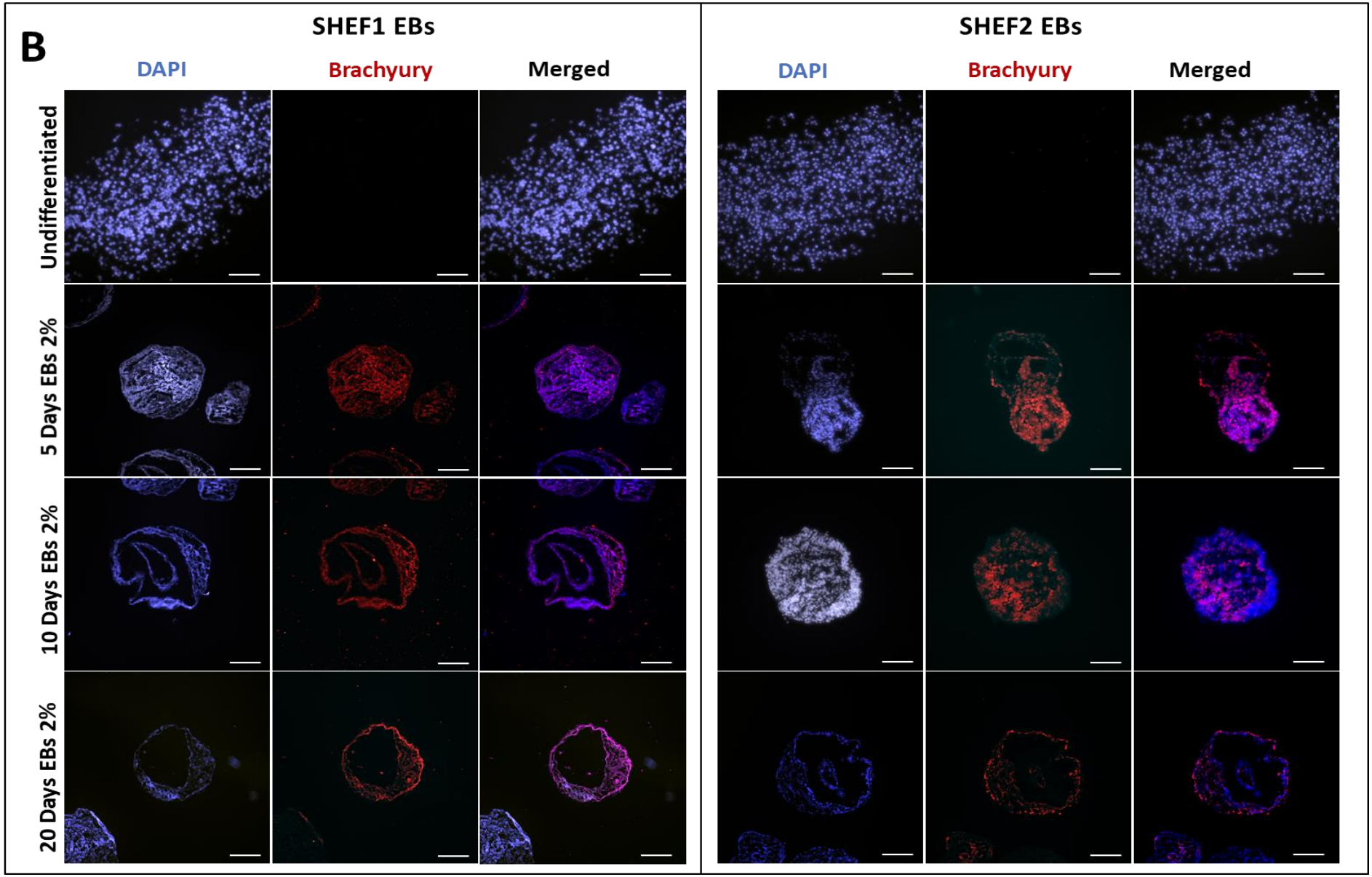
B
SHEF1 EBs
SHEF2 EBs
DAPI
Brachyury
Merged
DAPI
Brachyury
Merged
Undifferentiated
5 Days EBs 2%
10 Days EBs 2%
20 Days EBs 2%

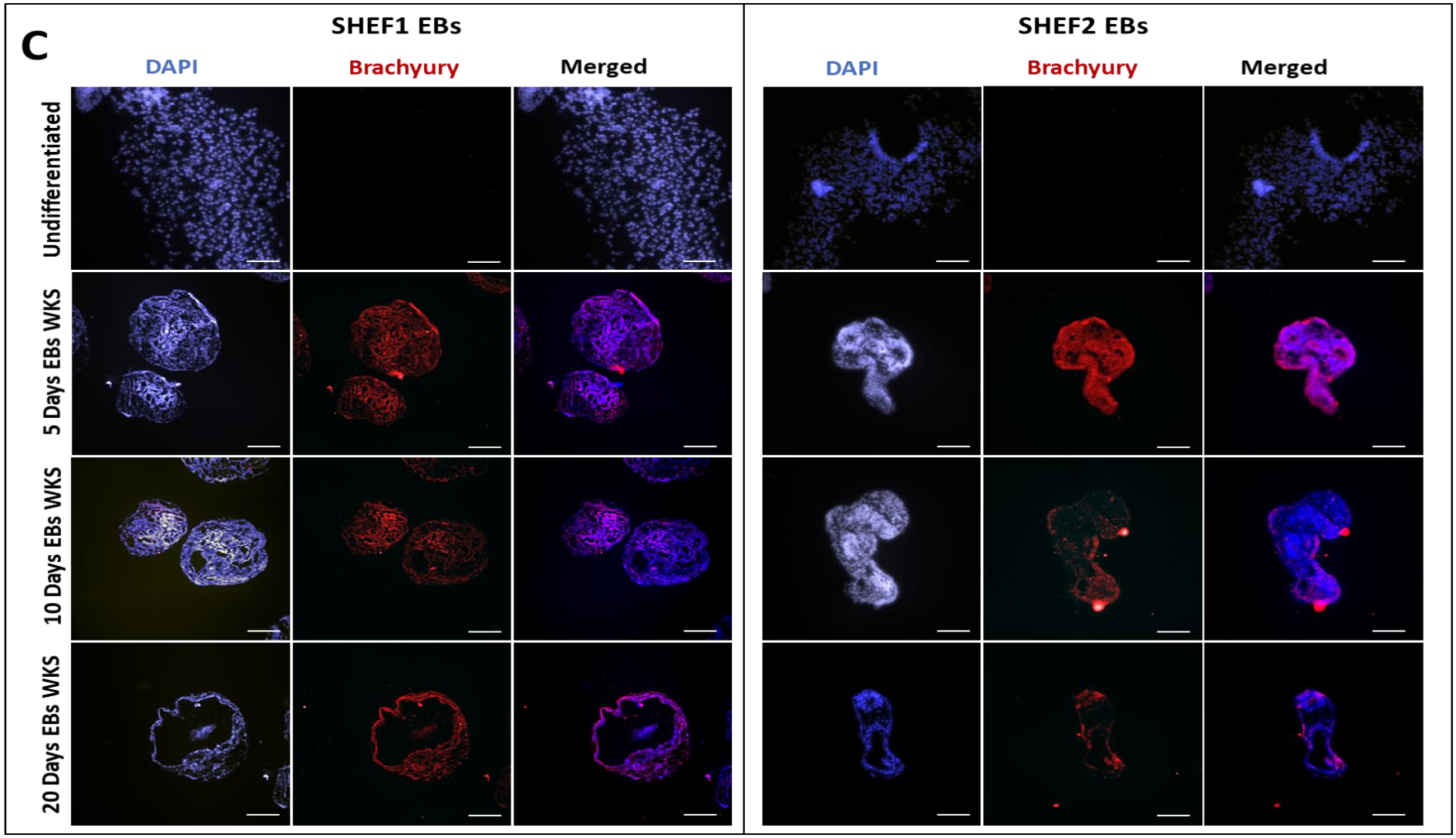

Figure 4.13. **Immunostaining of differentiation markers in undifferentiated SHEF and EBs.** Cells were cultured in **(A)** 21% AO, **(B)** 2% PG and **(C)** 2% WKS for 20 days. The scale bar represents 100 μm. The red and green colours indicate specific antigens, and blue represents DAPI. Images are representative of three independent samples.

4.2.4 Telomerase Activity

To evaluate the telomerase activity in different oxygen conditions and differentiation time points, TRAP assay was performed using the TRAPeze® Kit RT Telomerase Detection Kit (Millipore, USA).

Telomerase activity was evaluated in 3D aggregates of SHEF1 in different oxygen conditions and time points. There was a significant increase in telomerase activity in SHEF1 undifferentiated cells cultured in 2% PG and 2% WKS (5.62 ± 0.31 and 5.73 ± 0.38, $p<0.05$) versus 21% AO (5.35 ± 0.19). However, no significant change were observed between EBs cultured in 21% AO, 2% PG, or 2% WKS at days 5 (5.43 ± 0.12, 5.11 ± 0.56 and 5.29 ± 0.19) or 10 (5.11 ± 0.44, 5.09 ± 0.88 and 5.26 ± 0.18), respectively. In addition, EBs showed a significantly higher telomerase activity when compared to monolayer differentiated cells at day 10 ($p<0.05$). EBs cultured for 20 days showed an increased expression of telomerase in 2% PG (4.04 ± 0.51, $P<0.05$) and 2% WKS (4.35 ± 0.22, $p<0.01$) compared to 21% AO (3.37 ± 0.38) (***Fig 4.14.A)***. There was a significant decrease at day 20 compared to undifferentiated cells in all conditions (***Fig 4.14.B)***. A moderate correlation between telomerase activity and the differentiation process was observed in 21% AO ($R^2=0.76$) and 2% WKS ($R^2=0.78$) conditions using linear regression analysis (***Fig 4.14)***.

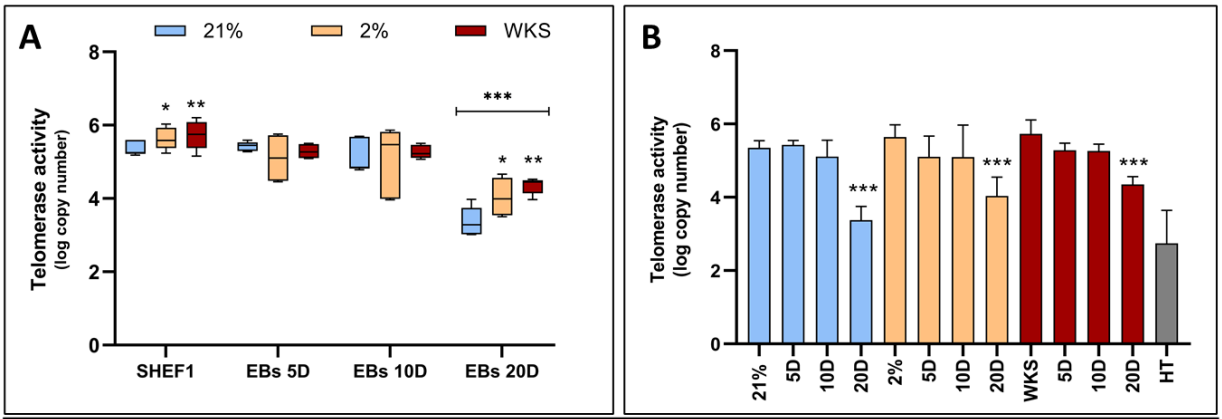

	21%	2%	WKS
R square	0.7556	0.4955	0.7763
P value	<0.0001	0.0001	<0.0001
Deviation from zero?	Significant	Significant	Significant
Equation	Y = -0.1044*X + 5.731	Y = -0.07579*X + 5.628	Y = -0.06605*X + 5.734

***Figure 4.14*. Telomerase activity detection with Real-time PCR.** SHEF1 EBs cells were cultured in air oxygen (21% AO) and physiological oxygen conditions (2% PG and 2% WKS) at different time points. Data are represented as mean ± standard deviation (SD), n=3, *p<0.05,

**p<0.01, ***p<0.001. HT (heat-treated control samples). Bars with stars indicate a significant difference between differentiated and undifferentiated cells. The other stars compare physoxia conditions to 21% AO.

Telomerase activity was also evaluated in 3D aggregates of SHEF2 during 20 days of culture. There was no significant difference in undifferentiated SHEF2 cells cultured in 21% AO, 2% PG, or 2% WKS (5.78 ± 0.16, 5.79 ± 0.14, 5.99 ± 0.14, respectively). No significant changes were observed between EBs cultured in 21% AO, 2% PG and 2% WKS (5.05 ± 0.16, 5.23 ± 0.31 and 5.28 ± 0.24, respectively) at day 5. EBs cultured for 10 days showed decreased expression of telomerase in 2% PG (4.26 ± 0.49, p<0.05) in comparison to air oxygen cultured EBs (4.99 ± 0.19). On the other hand, there was a significant increase in enzyme activity in 2% WKS (3.67 ± 0.09 p<0.05) compared to 21% AO (3.11 ± 0.32) after 20 days of differentiation (***Fig 4.15.A)***. Similar to previous results, all three conditions together showed significantly decreased (p<0.001) telomerase activity following the differentiation process compared to undifferentiated cells (***Fig 4.15.B)***. A strong correlation between telomerase activity and the differentiation process was observed in 21% AO (R^2=0.91), 2% PG (R^2=0.91), and 2% WKS (R^2=0.94) conditions using linear regression analysis (***Fig 4.15)***.

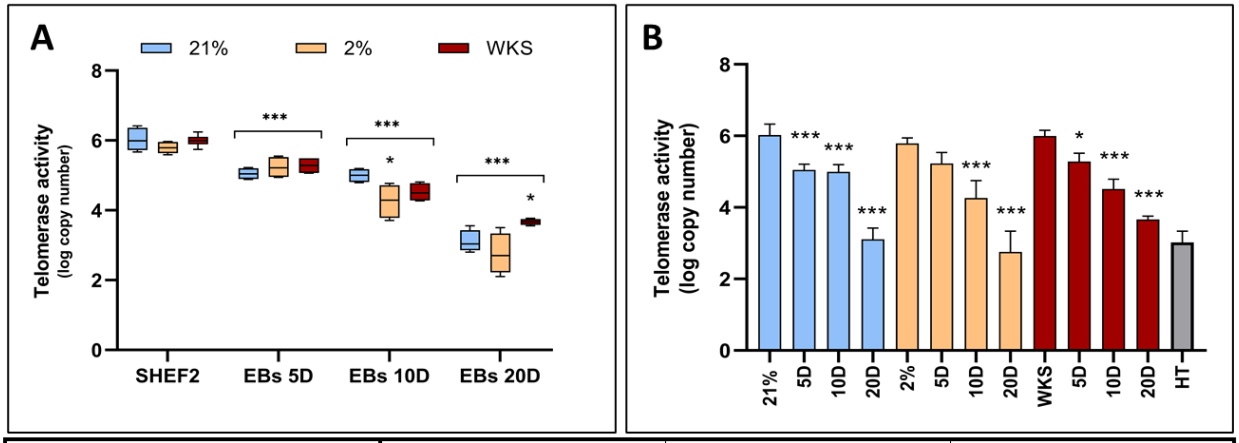

	21%	2%	WKS
R square	0.9124	0.9143	0.9443
P value	<0.0001	<0.0001	<0.0001
Deviation from zero?	Significant	Significant	Significant
Equation	Y = -0.1393*X + 6.016	Y = -0.1542*X + 5.853	Y = -0.1178*X + 5.908

***Figure 4.15*. Telomerase activity detection with Real-time PCR.** SHEF2 EBs cells were cultured in air oxygen (21% AO) and physiological oxygen conditions (2% PG and 2% WKS) at different time points. Data are represented as mean ± standard deviation (SD), n=3, *p<0.05,

**p<0.01, ***p<0.001. HT (heat-treated control samples). Bars with stars indicate a significant difference between differentiated and undifferentiated cells. The other stars compare physoxia conditions to 21% AO.

Telomerase activity was analysed from SHEF1 and SHEF2 pooled data in different oxygen conditions and time points. There was no significant increase in telomerase activity in undifferentiated cells in 21% AO, 2% PG, or 2% WKS (5.68 ± 0.43, 5.71 ± 0.25 and 5.86 ± 0.31). Also, no significant change were observed between EBs cultured in 21% AO, 2% PG, or 2% WKS at days 5 (5.28 ± 0.24, 5.16 ± 0.46 and 5.28 ± 0.19) or 0 (5.07 ± 0.35, 4.76 ± 0.83 and 4.97 ± 0.44), respectively. However, EBs cultured for 20 days showed an increased expression of telomerase in 2% PG (3.52 ± 0.83) and 2% WKS (4.07 ± 0.39 p<0.001) compared to 21% AO (3.27 ± 0.36) (***Fig 4.16.A)***. There was a significant decrease at day 20 compared to undifferentiated cells in all conditions (***Fig 4.16.B)***. A moderate correlation between telomerase activity and the differentiation process was observed in 21% AO (R^2=0.82), 2% PG (R^2=0.64) and 2% WKS (R^2=0.79) conditions using linear regression analysis (***Fig 4.16)***.

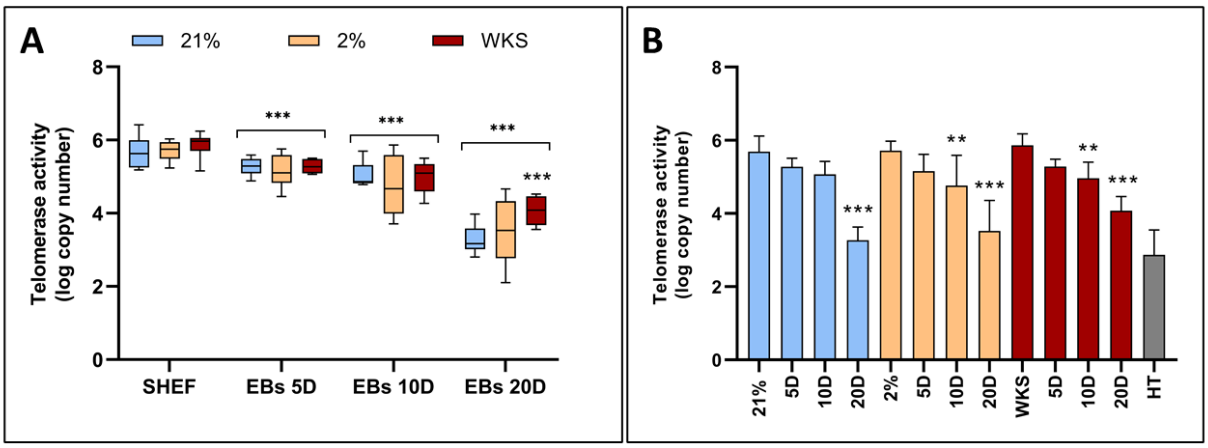

	21%	2%	WKS
Goodness of Fit			
R square	0.8224	0.6416	0.7935
P value	<0.0001	<0.0001	<0.0001
Deviation from zero?	Significant	Significant	Significant
Equation	Y = -0.1196*X + 5.863	Y = -0.1081*X + 5.732	Y = -0.08750*X + 5.815

Figure 4.16. **Telomerase activity detection with Real-time PCR.** SHEF1 and SHEF2 EBs data were pooled together. Cells were cultured in air oxygen (21% AO) and physiological oxygen conditions (2% PG and 2% WKS) at different time points. Data are represented as mean ± standard deviation (SD), n=3, *p<0.05, **p<0.01, ***p<0.001. HT (heat-treated control

samples). Bars with stars indicate a significant difference between differentiated and undifferentiated cells. The other stars compare physoxia conditions to 21% AO.

4.2.5 TERT Gene Expression

TERT gene expression was analysed using RT-qPCR in differentiated EBs to investigate the effects of differentiation and reduced oxygen.

Undifferentiated SHEF1 in 2% WKS showed a significant increase (0.70 ± 0.87, $p<0.05$) in TERT expression compared to 21% AO. EBs cultured for 5 days in 2% PG (-0.53 ± 0.57, $p<0.05$) and 2% WKS (0.33 ± 0.54, $p<0.01$) displayed significanly increased relative gene expression versus EBs cultured in 21% AO (-1.08 ± 0.62). A significant increase was observed in EBs incubated in 2% WKS at day 10 (0.17 ± 0.31, $p<0.05$) compared to 21% AO condition (-0.95 ± 0.60). However, EBs cultured for 20 days showed no significant difference between 21% AO (-1.31 ± 0.65), 2% PG (-1.09 ± 0.57), or 2% WKS (-1.38 ± 0.21). The relative TERT gene expression decreased at day 5 ($p<0.05$), day 10 ($p<0.05$), day 20 ($p<0.001$) differentiated EBs in all conditions together versus undifferentiated cells (***Fig 4.17.A)***. A weak correlation between TERT gene expression and the differentiation process was observed in 21% AO (R^2=0.32), 2% PG (R^2=0.42) and 2% WKS (R^2=0.65) conditions using linear regression analysis (***Fig 4.17)***.

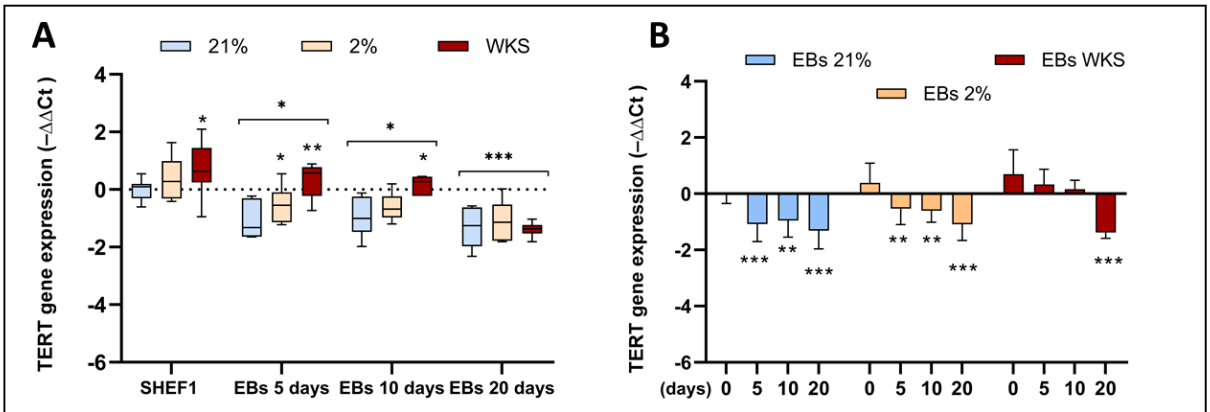

	EBs 21%	EBs 2%	EBs WKS
R square	0.3184	0.4196	0.6466
P value	0.0003	<0.0001	<0.0001
Deviation from zero?	Significant	Significant	Significant
Equation	Y = -0.05598*X - 0.3363	Y = -0.06702*X + 0.1331	Y = -0.1029*X + 0.8497

Figure 4.17: **TERT gene expression results.** SHEF1 undifferentiated and differentiated cells EBs were obtained in 21% AO and physiological oxygen conditions (2% PG and 2% WKS). The RT-qPCR expression of the TERT normalised to the expression of GAPDH. Data are represented as mean ± standard deviation (SD), n=3, *$p<0.05$, **$p<0.01$, ***$p<0.001$ vs 21%

AO. Bars with stars indicate a significant difference between differentiated and undifferentiated cells. The other stars compare physoxia conditions to 21% AO.

TERT gene expression was higher in 2% PG (0.89 ± 0.48, p<0.001) and 2% WKS (1.35 ± 0.79, p<0.001) conditions in undifferentiated SHEF2 versus 21% AO. After 5 days of EBs formation, there was no significant change in TERT expression in 2% PG (-1.23 ± 0.46) and 2% WKS (-0.98 ± 0.84) versus EBs cultured in 21% AO (-0.68 ± 0.91). No significant change was observed in EBs incubated in 2% PG (-3.15 ± 0.43) and 2% WKS for 10 days (-2.40 ± 0.46) compared to 21% AO condition (-2.49 ± 0.26). However, EBs cultured for 20 days showed a significant difference in 2% PG (-3.01 ± 0.50) and 2% WKS (-2.75 ± 0.45) versus 21% AO (-3.87 ± 0.75) (***Fig 4.18.A)***. The relative TERT gene expression significantly decreased at days 5 (p<0.001), 10 (p<0.001), and 20 (p<0.001) differentiated EBs in all conditions together versus undifferentiated cells (***Fig 4.18.B)***. A moderate correlation between TERT gene expression and the differentiation process was observed in 21% AO (R^2=0.83), 2% PG (R^2=0.74) and 2% WKS (R^2=0.72) conditions using linear regression analysis (***Fig 4.18)***.

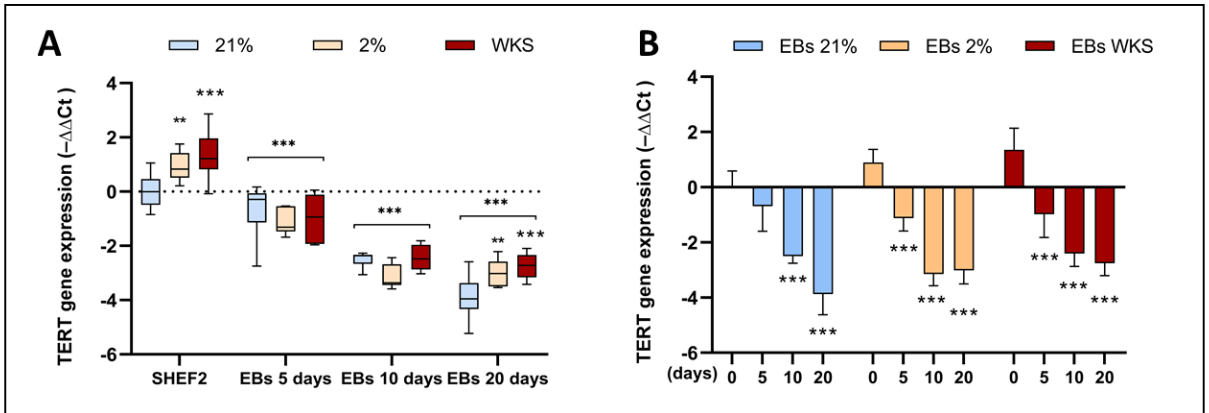

	21%	2%	WKS
R square	0.8309	0.7368	0.7220
P value	<0.0001	<0.0001	<0.0001
Deviation from zero?	Significant	Significant	Significant
Equation	Y = -0.2015*X + 0.0008889	Y = -0.2102*X + 0.3730	Y = -0.2143*X + 0.8153

Figure 4.18. **TERT gene expression results.** SHEF2 undifferentiated and differentiated cells EBs were obtained in 21% AO and physiological oxygen conditions (2% PG and 2% WKS). The RT-qPCR expression of the TERT normalised to the expression of GAPDH. Data are represented as mean ± standard deviation (SD), n=3 *p<0.05, **p<0.01, ***p<0.001 vs 21%

AO. Bars with stars indicate a significant difference between differentiated and undifferentiated cells. The other stars compare physoxia conditions to 21% AO.

Numerical data from SHEF cells were pooled for expression analysis purposes. There was a significant difference in undifferentiated stem cells cultured in 2% PG (0.73 ± 0.68, $p<0.01$) and 2% WKS (0.76 ± 0.72, $p<0.01$) in comparison to AO. There was no significant change in gene expression in EBs at day 5 following 21% AO (-0.88 ± 0.78), 2% PG (-0.83 ± 0.59), and 2% WKS (-0.32 ± 0.96) culture. EBs cultured for 10 days in 2% WKS (-1.12 ± 1.38, $p<0.05$) displayed significantly higher gene expression versus EBs cultured in 21% AO (-1.72 ± 0.91). However, EBs cultured for 20 days showed no significant difference between 21% AO (-2.60 ± 1.48), 2% PG (-2.05 ± 1.12), or 2% WKS (-2.07 ± 0.78) (***Fig 4.19.A)***. The relative TERT gene expression significantly decreased at day 5 ($p<0.05$), 10 ($p<0.001$), and 20 ($p<0.001$) differentiated EBs in all conditions together versus undifferentiated cells (***Fig 4.19.B)***. A weak correlation between TERT gene expression and the differentiation process was observed in 21% AO (R^2=0.48), 2% PG (R^2=0.44) and 2% WKS (R^2=0.51) conditions using linear regression analysis (***Fig 4.19)***.

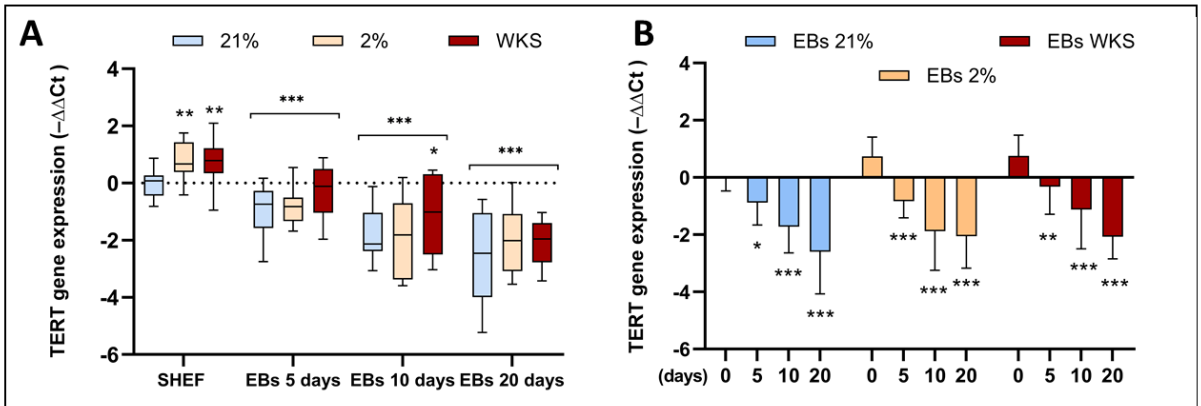

	EBs 21%	EBs 2%	EBs WKS
R square	0.4865	0.4381	0.5135
P value	<0.0001	<0.0001	<0.0001
Deviation from zero?	Significant	Significant	Significant
Equation	Y = -0.1277*X - 0.1828	Y = -0.1314*X + 0.1443	Y = -0.1374*X + 0.5147

***Figure 4.19*. TERT gene expression results.** SHEF1 and SHEF2 EBs data were gathered together in 21% AO and physiological oxygen conditions (2% PG and 2% WKS). The RT-qPCR expression of the TERT normalised to the expression of GAPDH. Data are represented as mean ± standard deviation (SD), n=3 *$p<0.05$, **$p<0.01$, ***$p<0.001$ vs 21% AO. Bars with

stars indicate a significant difference between differentiated and undifferentiated cells. The other stars compare physoxia conditions to 21% AO.

4.2.6 Telomere Length

Telomere Length Quantification qPCR Assay (Sciencell Research Lab, USA) was performed to measure telomere length for EBs differentiated in different oxygen conditions and time points**.** There was no significant difference in the mean telomere length value of undifferentiated SHEF1 in 21% AO (12.49 ± 1.08 kb), 2% PG (11.86 ± 1.08 kb) and 2% WKS (12.88 ± 1.56 kb). The mean value of telomere length in 5 days differentiated EBs was measured as 2% WKS (11.54 ± 0.71 kb), AO 21% (12.33 ± 1.74 kb), and 2% PG (11.98 ± 0.51 kb). There was a significantly longer telomere length in EBs differentiated in 2% WKS (11.81 ± 1.42 kb) versus 21% AO (9.96 ± 1.99 kb) at day 10. Moreover, we noted significantly longer telomere lengths in EBs differentiated in 2% PG (10.85 ± 0.64 kb) and 2% WKS (10.91 ± 1.20 kb) compare to 21% AO (9.16 ± 1.54 kb) at day 20 (***Fig 4.20.A)***. All conditions together showed significant telomere shortening after day 10 ($p<0.01$) and day 20 ($p<0.001$) (***Fig 4.20.A)***. The relative telomere length is significantly decreased at day 10 ($p<0.001$), 20 ($p<0.001$) in AO and at day 20 ($p<0.01$) in 2% WKS EBs versus undifferentiated cells (***Fig 4.20.B)***. There was a weak correlation between telomere length and the differentiation process in 21% AO ($R^2=0.47$), 2% PG ($R^2=0.10$) and 2% WKS ($R^2=0.25$) conditions using linear regression analysis (***Fig 4.20)***.

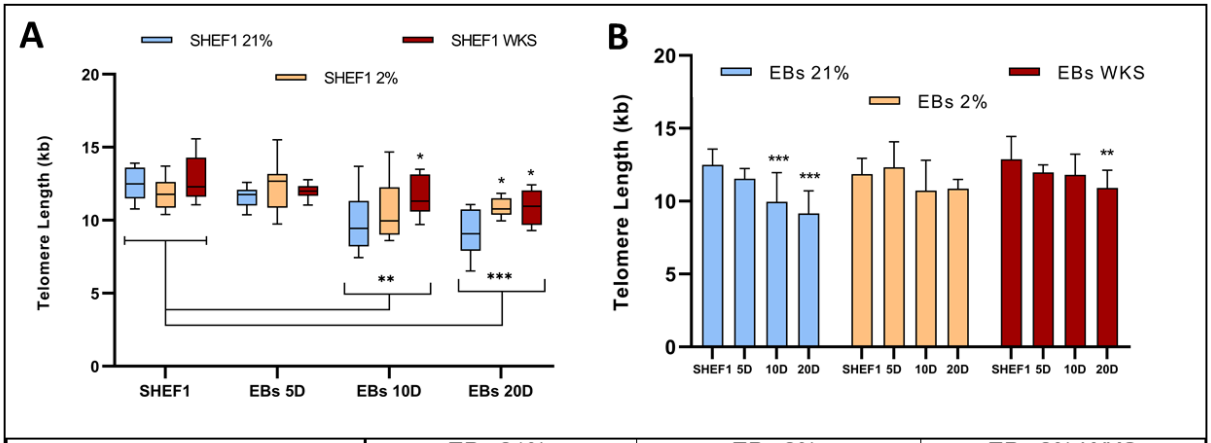

	EBs 21%	EBs 2%	EBs 2% WKS
R square	0.4698	0.09948	0.2497
P value	<0.0001	0.0505	0.0012
Deviation from zero?	Significant	Not Significant	Significant
Equation	Y = -0.1720*X + 12.31	Y = -0.06469*X + 12.00	Y = -0.09371*X + 12.73

Figure 4.20. **The relative mean of Telomere length (kb) on each chromosome end in differentiated EBs and undifferentiated SHEF1 populations.** The box represents the interquartile range. The whisker illustrates the outer quartiles, and the line in the middle shows the median expression. Data are represented as n=3x3, *p<0.05, **p<0.01, ***p<0.001 vs air oxygen (21% AO). Bars with stars indicate a significant difference between differentiated and undifferentiated cells. The other stars compare physoxia conditions to 21% AO.

Telomere Length Quantification qPCR Assay was performed to measure telomere length for SHEF2 EB samples differentiated in different oxygen conditions and time points**.** There was a significant difference in the mean telomere length value of undifferentiated SHEF2 in 21% AO (11.20 ± 0.85 kb) and 2% PG (11.59 ± 1.01 kb) versus 2% WKS (12.47 ± 0.79 kb, p<0.01). No significant difference between 21% AO (11.36 ± 0.72), 2% PG (11.04 ± 1.24), and 2% WKS (11.27 ± 1.14 kb) conditions was noted in differentiated EBs telomere length at day 5. There was also no significant difference in telomere length in EBs differentiated in 2% PG (10.83 ± 0.69 kb), 2% WKS (10.82 ± 0.79 kb), and 21% AO (10.24 ± 1.03 kb) at day 10. However, we noted significantly longer telomere lengths in EBs differentiated in 2% WKS (10.11 ± 0.97 kb) compared to 21% AO (9.01 ± 0.48 kb) at day 20 (***Fig 4.21)***. All conditions together showed significant telomere shortening after day 10 (p<0.01) and day 20 (p<0.001) (***Fig 4.21.A)***. The relative telomere length is significantly decreased at day 20 (p<0.001) in AO, 2% PG, 2% WKS and at day 5 (p<0.01), day 10 (p<0.01) in 2% WKS EBs versus undifferentiated cells (***Fig 4.21.B)***. There was a weak correlation between telomere length and the differentiation process

in 21% AO (R^2=0.56), 2% PG (R^2=0.39) and 2% WKS (R^2=0.44) conditions using linear regression analysis (***Fig 4.21)***.

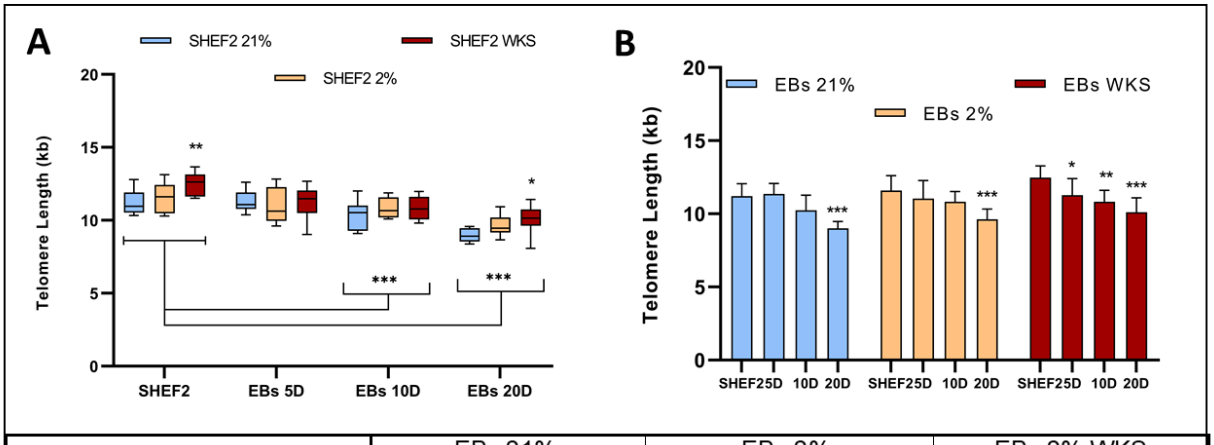

	EBs 21%	EBs 2%	EBs 2% WKS
R square	0.5564	0.3884	0.4389
P value	<0.0001	<0.0001	<0.0001
Deviation from zero?	Significant	Significant	Significant
Equation	Y = -0.1213*X + 11.51	Y = -0.09581*X + 11.61	Y = -0.1103*X + 12.13

Figure 4.21. **The relative mean of Telomere length (kb) on each chromosome end in differentiated EBs and undifferentiated SHEF2 populations.** The box represents the interquartile range. The whisker illustrates the outer quartiles, and the line in the middle shows the median expression. Data are represented as n=3x3, *p<0.05, **p<0.01, ***p<0.001 vs air oxygen (21% AO). Bars with stars indicate a significant difference between differentiated and undifferentiated cells. The other stars compare physoxia conditions to 21% AO.

Numerical data of telomere lengths from two pluripotent stem cell lines were pooled for telomere length analysis purposes. We noted significantly longer telomere lengths of undifferentiated stem cells in 2% WKS (12.71 ± 1.28 kb, p<0.05) versus 21% AO (11.94 ± 1.16 kb) and 2% PG (11.75 ± 1.04 kb). No significant difference between 21% AO (11.45 ± 0.70), 2% PG (11.69 ± 1.61 kb), and 2% WKS (11.63 ± 0.93 kb) was noted in differentiated EB telomere lengths at day 5. There was a significantly longer telomere in EBs differentiated in 2% WKS (11.32 ± 1.22 kb) versus 21% AO (10.10 ± 1.55 kb) at day 10. We also noted significantly longer telomere lengths in EBs differentiated in 2% WKS (10.51 ± 1.14 kb) compared to 21% AO (9.08 ± 1.11 kb) at day 20 (***Fig 4.22)***. All conditions together showed significant telomere shortening after day 10 (p<0.001) and day 20 (p<0.001) (***Fig 4.22)***. The relative telomere length is significantly decreased at day 5 in 2% WKS (p<0.05), at day 10

(p<0.01) in AO, 2% WKS and at day 20 (p<0.001) in AO, 2% PG, 2% WKS EBs versus undifferentiated cells (***Fig 4.22.B)***. There was a weak correlation between telomere length and the differentiation process in 21% AO (R^2=0.47), 2% PG (R^2=0.19) and 2% WKS (R^2=0.31) conditions using linear regression analysis (***Fig 4.22)***.

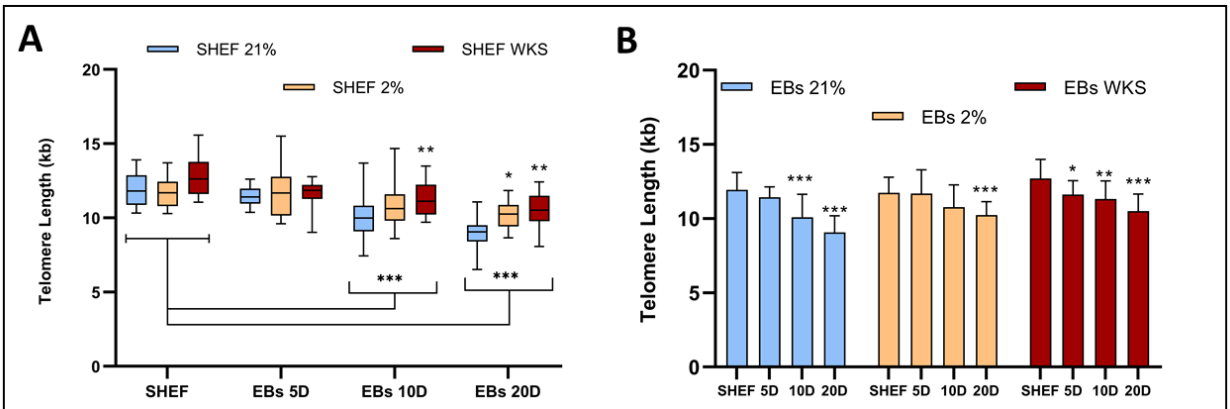

	EBs 21%	EBs 2%	EBs 2% WKS
R square	0.4774	0.1869	0.3125
P value	<0.0001	0.0001	<0.0001
Deviation from zero?	Significant	Significant	Significant
Equation	Y = -0.1490*X + 11.95	Y = -0.08142*X + 11.82	Y = -0.1038*X + 12.46

Figure 4.22. **The relative mean of Telomere length (kb) on each chromosome end in differentiated EBs and undifferentiated SHEF populations.** The box represents the interquartile range. The whisker illustrates the outer quartiles, and the line in the middle shows the median expression. Data are represented as n=3x3, *p<0.05, **p<0.01, ***p<0.001 vs air oxygen (21% AO). Bars with stars indicate a significant difference between differentiated and undifferentiated cells. The other stars compare physoxia conditions to 21% AO.

4.2.7 TERT Gene-specific promoter methylation in hESC-derived EBs

We investigate the methylation pattern of TERT promoter in EBs cultured for 5, 10 and 20 days in two extreme conditions. We wanted to compare conserved physiological oxygen with air oxygen tension because 2% WKS data showed more consistent results. To investigate the methylation level of TERT promoter, region I (-1456, -1495 bp from TSS), II (-674, -717 bp from TSS), III (-315 -348 bp from TSS), IV (-122, -171 bp from TSS) and V (-67, -106 bp from TSS) were determined by using pyrosequencing (***chapter 2, Table 2-10, page 71***).

Region I showed a higher methylation level (~89.33%) than the other regions and displayed no significant difference between conditions or differentiation processes. Significant increases were observed for region II in 21% (70.89%, 75.42% and 73.42% p>0.001) and WKS (52.67%, 58.94% and 60.96% p>0.001) conditions at day 5 , day 10 and day 20, respectively compared to undifferentiated cells (42.54% and 30.63%). Air oxygen cultured EBs showed significantly higher methylation levels at each time point (p>0.001) in comparison to reduced oxygen cultured cells. Region III results showed that EBs had a significant increase in methylation in 21% AO (8.13%, 9.5% and 10.6% p>0.001) and 2% WKS (5.33% p>0.05, 6.1% p>0.01 and 5.2% p>0.05) compared to undifferentiated SHEF1 (4% and 3.33%) at 5 days, 10 days and 20 days, respectively. Moreover, there were significant differences between conditions at day 5 (p>0.01), day 10 (p>0.001) and day 20 (p>0.001). Undifferentiated SHEF1 cells displayed significantly higher methylation in region IV in 21% AO (10.45%, p>0.01) versus 2% WKS (6%). Region IV demonstrated that the methylation level of EBs was significantly elevated at day 20 in 21% AO (10.75%) when compared to reduced oxygen conditions (6.95%, p>0.01). No significant increase at days 5 or 10 differentiation were noted for 21% AO and 2% WKS conditions. Undifferentiated SHEF1 cells displayed a significantly higher methylation in region V in 21% AO (5.69%, p>0.05) versus 2% WKS (3.93%). Methylation of SHEF1 EBs for region V showed higher methylation at days 10 (5.87%, p>0.05) and 20 (6.61%, p>0.01) in air oxygen compared to reduced oxygen condition (4.79%, and 5.05%, respectively). The data combined from region II, III, IV and V showed that a significant increase in methylation levels at day 10 (21.86% and 17.04%, p>0.001), 20 (23.95% and 18.87%, p>0.001) and 40 (24.77% and 19.11%, p>0.001) in AO and WKS conditions compared to undifferentiated cells (15.72% and 10.88%), respectively. There was a significant difference between undifferentiated (p>0.001), day 5 (p>0.001), day 10 (p>0.001) and day 20 (p>0.001) EBs ***(Fig 23.A)***. We also analysed pooled data from differentiated EBs for each region to compare the difference between conditions. Region II (50.26% and 65.21%, p>0.001), region III (5.08% and 8.20%, p>0.01), region IV (6.79% and 9.10%, p>0.001), region V (4.49% and 5.54%, p>0.01) and data pooled from the four regions (16.04% and 20.91%, p>0.05) demonstrated a significant decrease in 2% WKS compared to 21% AO ***(Fig 4.23.B)***.

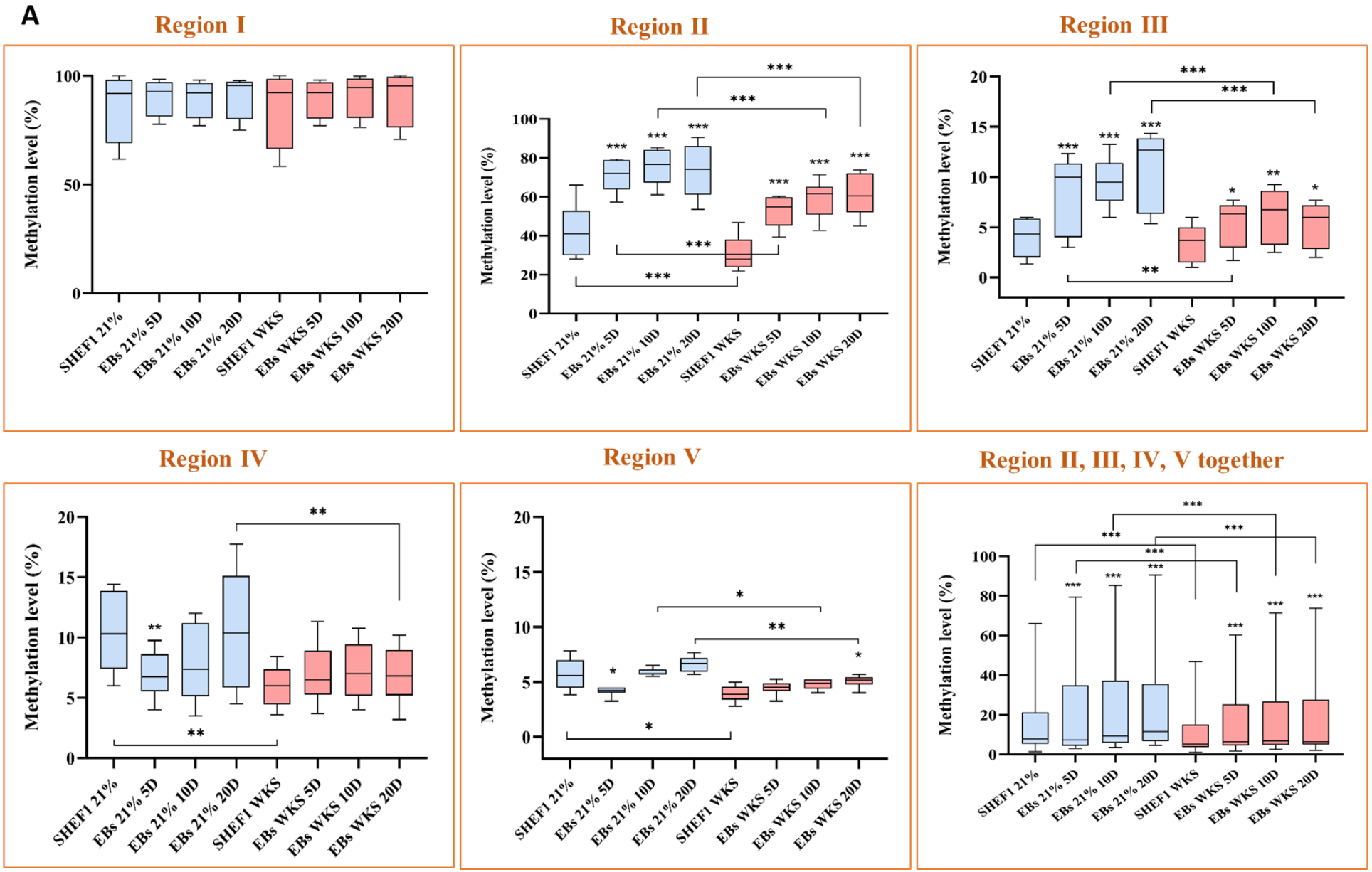
A
Region I
Region II
Region III
Region IV
Region V
Region II, III, IV, V together
Methylation level (%)
SHEF1 21%
EBs 21% 5D
EBs 21% 10D
EBs 21% 20D
SHEF1 WKS
EBs WKS 5D
EBs WKS 10D
EBs WKS 20D

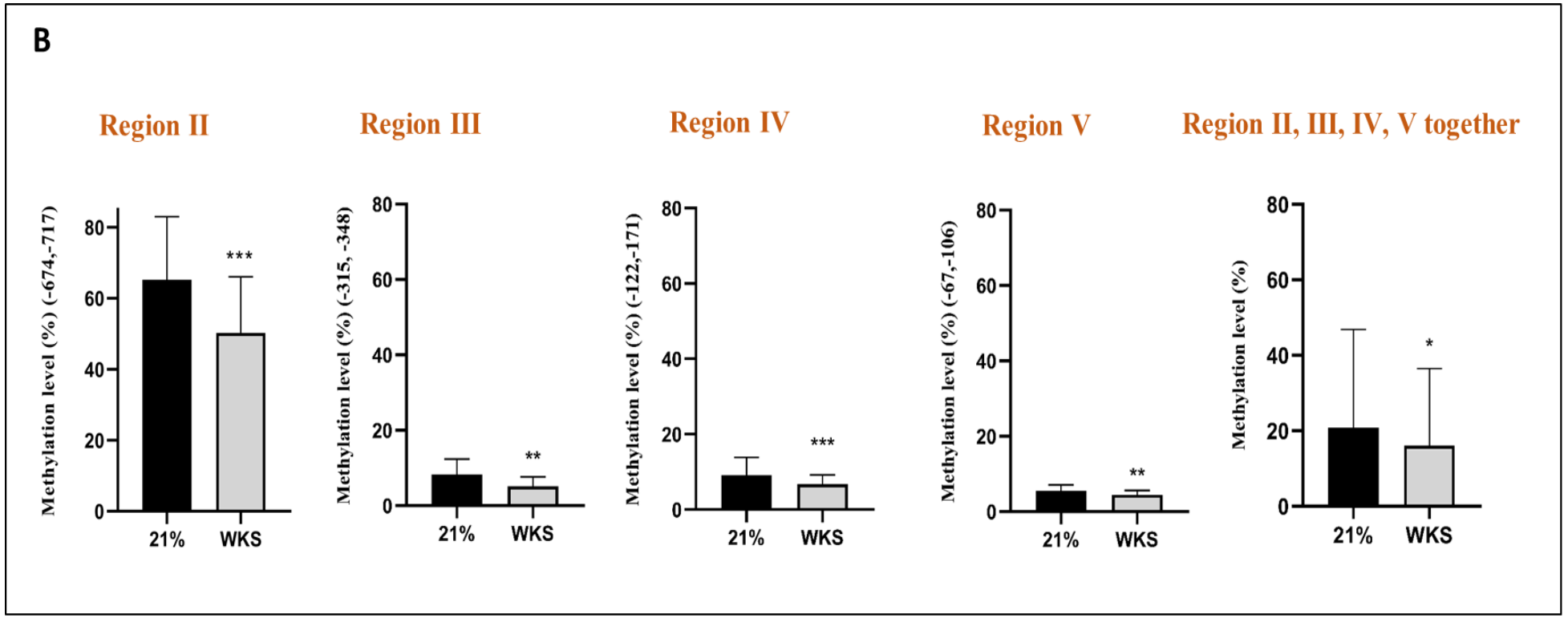

Figure 4.23. **Reduced methylation levels of TERT promoter in pooled data from SHEF1 EBs in physoxia**. Different promoter regions relative to TSS were evaluated using pyrosequencing. **(A)** The median value of methylation was represented in the box and violin graph. Y-axis indicates DNA methylation level (%) at CpG sites, and X-axis represents the name of cells. Data presented as median (min-max). The stars indicate a significant difference between differentiated and undifferentiated cells. **(B)** The data from 5, 10 and 20 days differentiated EBs together were indicated in this graph to compare two oxygen conditions. Y-axis indicates DNA methylation level (%) at CpG sites, and X-axis represents the CpG sites as mean ± SD, n=3, *p<0.05, **p<0.01, ***p<0.001 relative to air oxygen.

Region I in SHEF2 cells showed higher methylation level (~91.95%) than the other regions with no significant difference between conditions or differentiation process (***Figure 4.24)***. Significant increases were observed for region II in 21% (56.94%, p>0.001, 54.95% p>0.01 and 57.39%, p>0.001) and WKS (47.21%, p>0.01, 49.96%, p>0.001 and 51.11% p>0.001) conditions at days 5, 10, and 20, respectively compared to undifferentiated cells (47.39% and 38.97%). EBs cultured in 21% AO showed significantly higher methylation levels at days 5 (p>0.01), 20 (p>0.001) and undifferentiated cells (p>0.05) in comparison to reduced oxygen cultured cells. Region III from EBs had a significantly higher methylation in 21% AO (14.40% p>0.05) at day 20 and 2% WKS at days 10 and 20 (12.55% p>0.01 and 14.90% p>0.001) compared to undifferentiated SHEF2 (10.48% and 8.27%), respectively. Moreover, there were significant differences between conditions in undifferentiated SHEF2 (p>0.05). Region IV demonstrated that methylation levels of EBs were significantly higher at days 10 (15.78%, p>0.01) and 20 (28.04%, p>0.001) compared to undifferentiated cells (9.25%) in 21% AO. EBs cultured in reduced oxygen 2% WKS had higher metyhlation level after day 10 (17.19%, p>0.001) and 20 (21.56%, p>0.001) differentiation versus undifferentiated SHEF2 (6.54%). There was no significant increase at differentiation day 5 in either condition. Day 20 differentiated EBs displayed significantly higher mehylation in region IV in 21% AO (28.04%, p>0.01) versus 2% WKS (21.56%). Undifferentiated SHEF2 cells displayed a significantly higher methylation in region V in 21% AO (5.70%, p>0.001) versus 2% WKS (3.92%). Methylation results of SHEF2 EBs for region V showed that there were increases in metyhlation level at 10 days (7.33%, p>0.01) and 20 days (8.00%, p>0.001) cultured EBs in in 21% AO. In addition, there were increases in methylation levels at day 5 (7.11%, p>0.001), 10 (8.00%, p>0.001) and 20 (9.11%, p>0.001) cultured EBs in in 21% AO ***(Fig 4.24.A)***.

The data combined from region II, III, IV and V showed a significant increase in methylation levels at day 5 (22.16% and 18.25%, p>0.001), 10 (23.96% and 22.24%, p>0.001), 20 (28.55% and 24.84%, p>0.001) and 40 (24.77% and 19.11%, p>0.001) in AO and WKS conditions compared to undifferentiated cells (17.80% and 14.04%), respectively. There was a significant difference between undifferentiated (p>0.001), day 5 (p>0.001) and day 20 (p>0.001) EBs. We also analysed pooled data from differentiated SHEF2 EBs for each region to compare the difference between conditions. Region II (49.98% and 55.58%, p>0.01), region III (13.30% and 16.62%), region IV (8.92% and 10.05%), region V (5.80% and 6.33%) and data pooled from the four regions (18.00% and 20.88%) demonstrated decreases in 2% WKS compared to 21% AO ***(Fig 4.24.B)***.

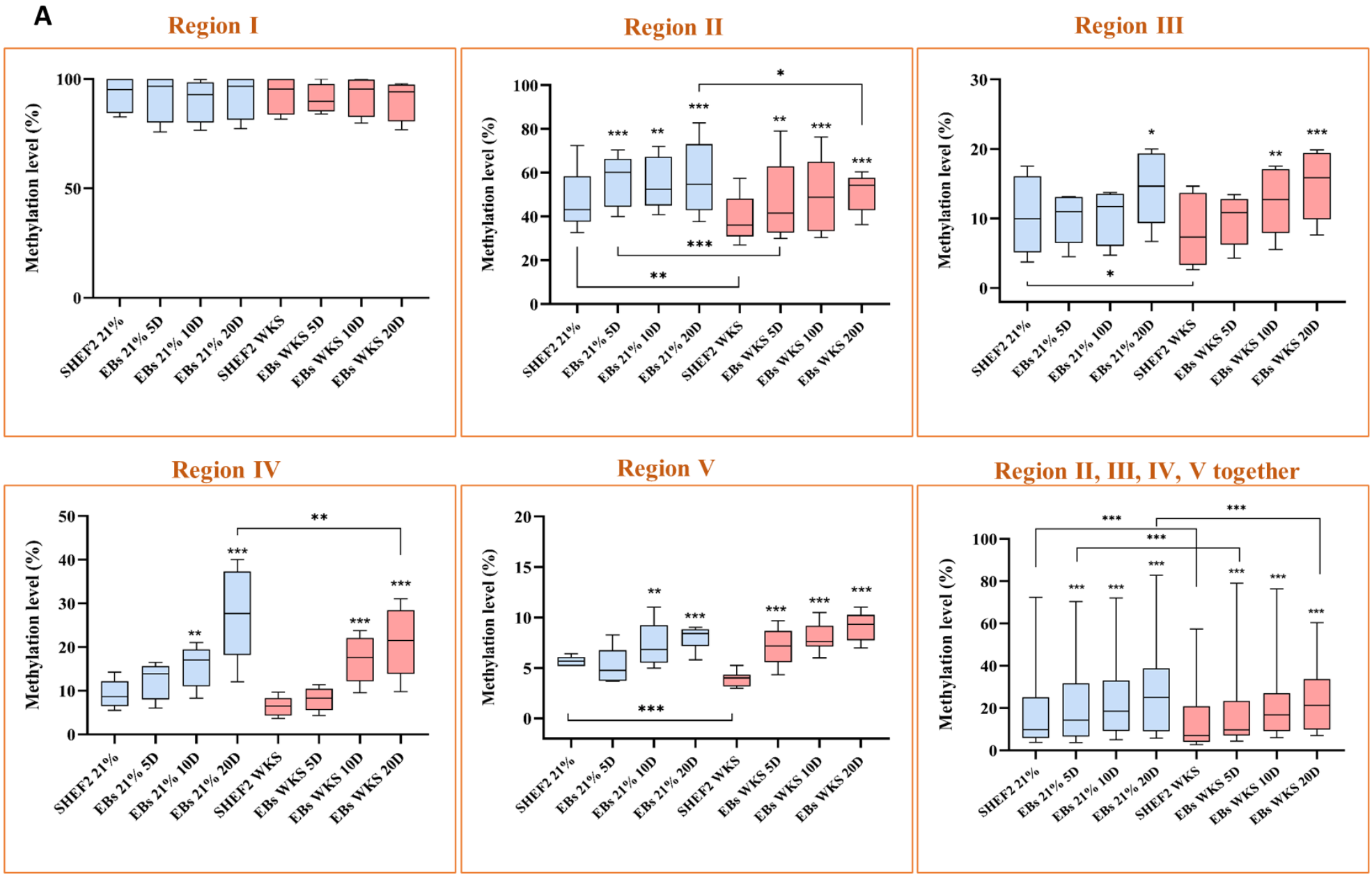
A
Region I
Region II
Region III
Region IV
Region V
Region II, III, IV, V together
Methylation level (%)
SHEF2 21%
EBs 21% 5D
EBs 21% 10D
EBs 21% 20D
SHEF2 WKS
EBs WKS 5D
EBs WKS 10D
EBs WKS 20D

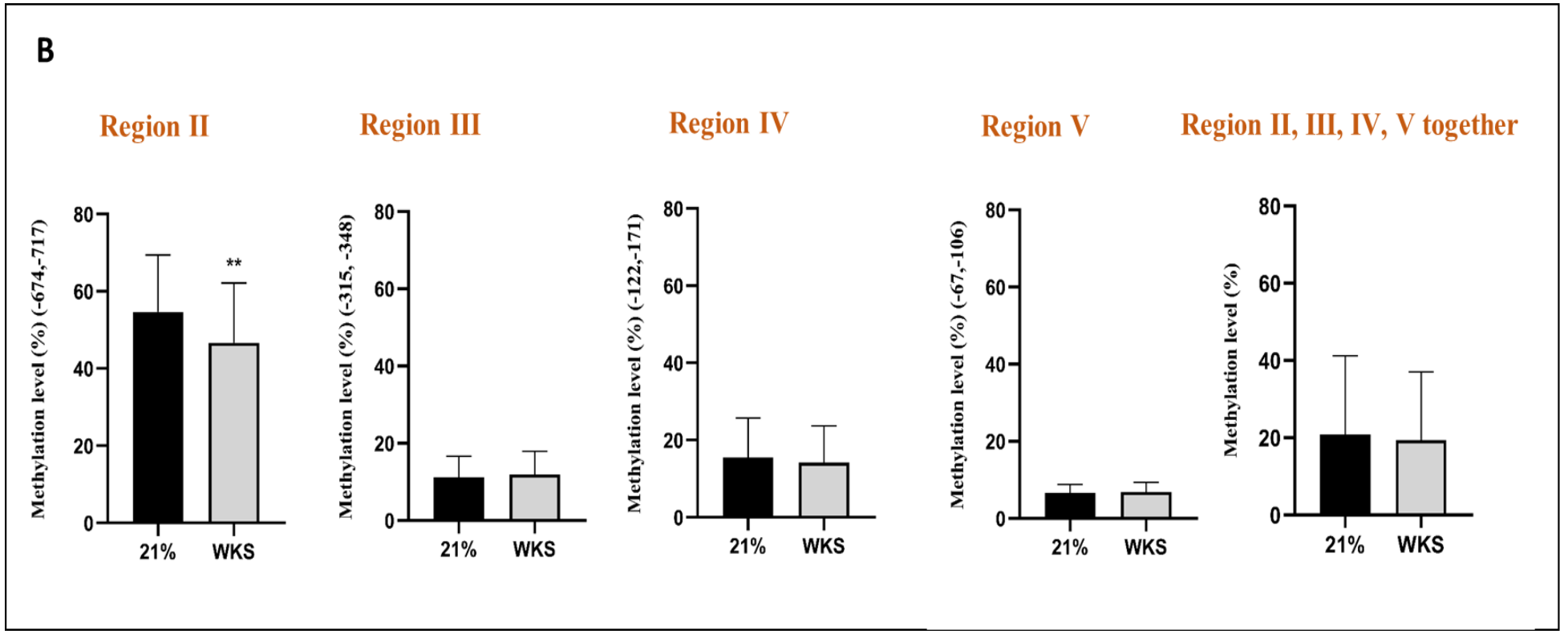

Figure 4.24. **Reduced methylation levels of TERT promoter in pooled data from SHEF2 EBs in physoxia**. Different promoter regions relative to TSS were evaluated using pyrosequencing. **(A)** The median value of methylation was represented in the box and violin graph. Y-axis indicates DNA methylation level (%) at CpG sites, and X-axis represents the name of cells. Data presented as median (min-max). The stars indicate a significant difference between differentiated and undifferentiated cells. **(B)** The data from 5, 10 and 20 days differentiated EBs together were indicated in this graph to compare two oxygen conditions. Y-axis indicates DNA methylation level (%) at CpG sites, and X-axis represents the CpG sites as mean ± SD, n=3, *p<0.05, **p<0.01, ***p<0.001 relative to air oxygen.

Combined data from SHEF1 and SHEF2 EBs showed higher methylation levels in region I than the other regions and no significant difference between conditions or differentiation process (average 90.64%). Significantly elevated methylation was noted in region II after 5 (63.92% and 49.94%, p>0.001), 10 (64.46% and 53.62%, p>0.001), and 20 days (64.67% and 56.74%, p>0.001) differentiation compared with undifferentiated cells (44.54% and 34.67%) in 21% AO and 2% WKS, respectively. Methylation levels in undifferentiated stem cells and days 5, 10, and 20 EBs in 21% AO environment (p>0.001) were significantly higher than those in 2% WKS. A significant increase in methylation was observed in region III after 20 days (13.07%, p>0.001) in 21% AO and after 10, 20 days (10.06% and 12.25%, p>0.001) of differentiation in 2% WKS compared with undifferentiated cells (7.58% and 5.80%), respectively. There was a significant elevation of methylation in region IV at 20 days of differentiation EBs (18.16%, and 13.44%, p>0.001) compared to undifferentiated cells (9.92% and 6.20%) in 21% AO and 2% WKS, respectively and 10 days differentiated cells in 2% WKS (12.27%). Methylation of undifferentiated cells showed a significant decrease in methylation levels following treatment with 2% WKS (p>0.05) compared with the 21% AO. In addition, the methylation levels in 20 days EBs cultured in 21% AO (p>0.01) were significantly higher than 2% WKS. Undifferentiated SHEF cells showed a significant decrease in the region V methylation level in 2%WKS (3.93%, p>0.001) compared with 21% AO (5.69%). Significantly higher methylation levels were observed in 20 days EBs (7.48% p>0.001) in 21% AO and 5, 10, and 20 days EBs (5.59%, 6.39% and 7.08%, p>0.001) in comparison to undifferentiated SHEF cells in 21% AO and 2% WKS, respectively. Region II, III, IV and V combined data showed a significant increase in methylation level at days 5 (21.44% and 17.44%, p>0.001), 10 (22.81% and 20.34%, p>0.001), and 20 (25.74% and 22.07%, p>0.001) in AO and WKS compared to undifferentiated cells (16.75% and 12.41%), respectively. Undifferentiated cells (p>0.001), 5 (p>0.001), 10 (p>0.01), and 20 days EBs (p>0.001) showed a significant decrease in methylation levels following treatment with 2% WKS compared with the 21% AO (***Fig 4.25.A***).

We also analysed pooled data from differentiated SHEF1 and SHEF2 EBs for each region to compare the difference between conditions. Region II (48.46% and 59.84%, p>0.001), region III (9.56% and 10.11%), region IV (10.13% and 12.14%, p>0.01), region V (5.61% and 6.06%, p>0.05) and data pooled from the four regions (17.76% and 20.87%, p>0.01) demonstrated an overall decrease in 2% WKS compared to 21% AO (***Fig 4.25.B***).

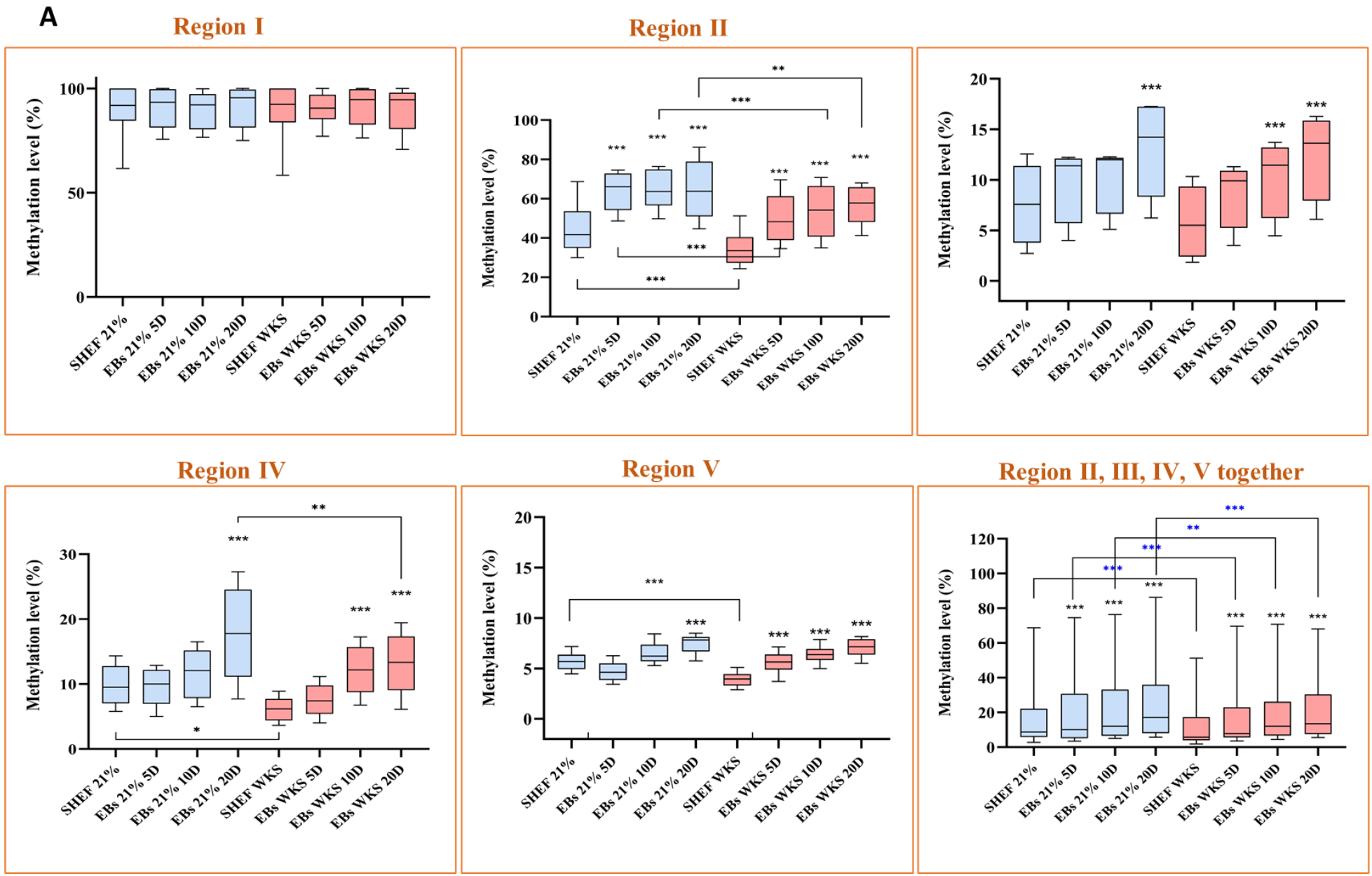
A
Region I
Region II
Region II, III, IV, V together
Region IV
Region V
Methylation level (%)
SHEF 21%
EBs 21% 5D
EBs 21% 10D
EBs 21% 20D
SHEF WKS
EBs WKS 5D
EBs WKS 10D
EBs WKS 20D

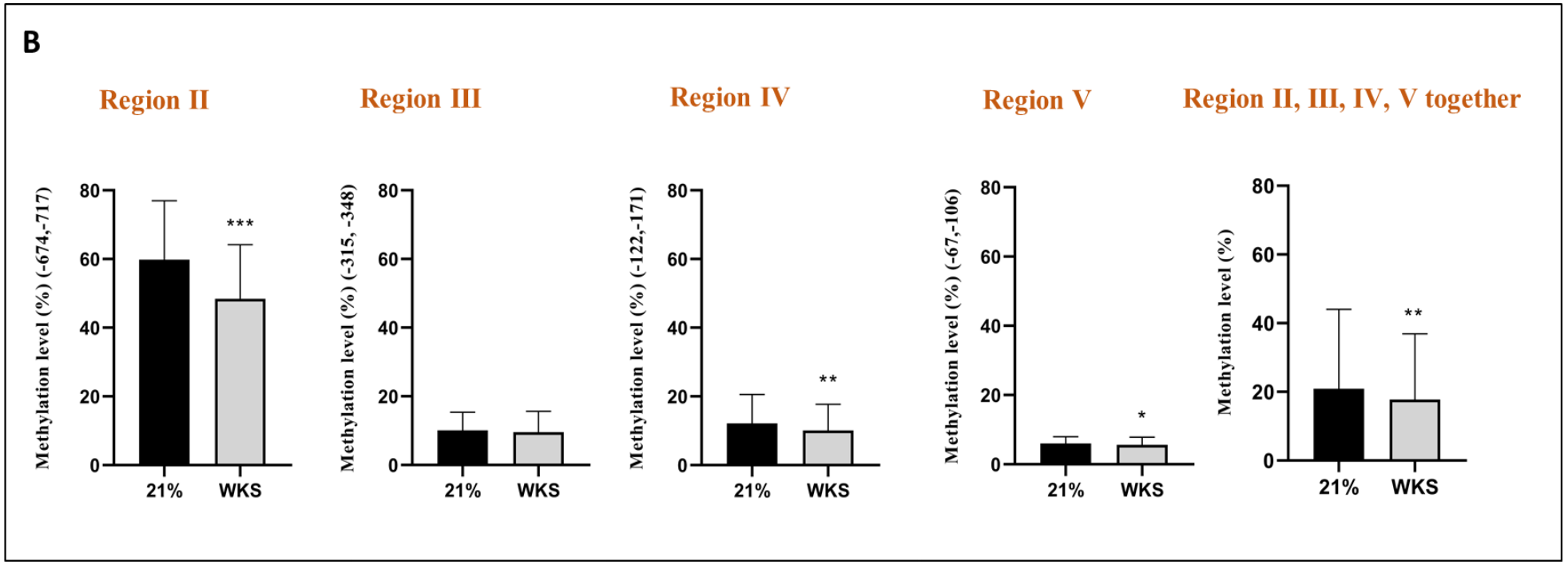

Figure 4.25. **Reduced methylation levels of TERT promoter in pooled data from SHEF EBs in physoxia**. Different promoter regions relative to TSS were evaluated using pyrosequencing. **(A)** The median value of methylation was represented in the box and violin graph. Y-axis indicates DNA methylation level (%) at CpG sites, and X-axis represents the name of cells. Data presented as median (min-max). The stars indicate a significant difference between differentiated and undifferentiated cells. **(B)** The data from 5, 10 and 20 days differentiated EBs together were indicated in this graph to compare two oxygen conditions. Y-axis indicates DNA methylation level (%) at CpG sites, and X-axis represents the CpG sites as mean ± SD, n=3, *p<0.05, **p<0.01, ***p<0.001 relative to air oxygen.

4.2.8 DNMTs gene expression in 3D aggregates of pluripotent cells and their differentiation progeny in response to physiological oxygen condition

RT-qPCR was performed to examine changes in the expression of DNMTs relative to TERT promoter methylation in response to the physiological oxygen environment in SHEF1 EBs. DNMT1 expression displayed no significant changes in undifferentiated SHEF1 cells cultured in 2% WKS (-0.12 ± 1.12) versus AO. EBs differentiated from SHEF1 showed no significant change in DNMT1 expression in 2% WKS (-1.58 ± 0.67, -2.33 ± 0.92, and -3.62 ± 0.90) in comparison to 21% AO (-2.16 ± 1.76, -1.99 ± 1.17 and -2.46 ± 0.96) at days 5, 10, and 20, respectively. We also explored differentiated EBs data to compare conditions and observed a significant decrease in 2% WKS (-2.20 ± 0.24) in comparison to 21% AO (-2.51 ± 1.03) (***Fig 4.26.A)***.

Undifferentiated SHEF2 displayed no significant change in 2% WKS (0.01 ± 0.79) versus 21% AO. There was no change in DNMT1 expression in SHEF2 EBs at days 5 and 10 in 2% WKS (-1.83 ± 1.56 and -2.37 ± 0.89) in comparison to 21% AO (-1.83 ± 2.29 and -3.10 ± 1.50), respectively. DNMT1 was decreased significantly in 2% WKS at day 20 differentiated EBs (6.65 ± 0.97, $p<0.01$) versus 21% AO (-3.92 ± 2.09). We also explored differentiated SHEF2 EBs data, and there was no significant difference between conditions ***(Fig 4.26.B)***.

DNMT3A expression in undifferentiated SHEF1 showed no significant change in 2% WKS (-0.43 ± 0.67) versus 21% AO. No significant reduction in DNMT3A expression was noted for SHEF1 EBs differentiated in 2% WKS at day 5 (-2.47 ± 0.67), day 10 (-2.27 ± 1.15) and day 20 (-3.46 ± 1.27) versus 21% AO (-2.35 ± 0.99, -2.16 ± 1.97 and -3.01 ± 1.29, respectively). Further, differentiated SHEF1 EBs data together showed no significant decrease in 2% WKS (-2.74 ± 0.63) versus AO (-2.51 ± 0.45) ***(Fig 4.26.C)***.

Undifferentiated SHEF2 samples displayed significantly less DNMT3A expression in 2% WKS (-1.13 ± 0.56, $p<0.05$) when compared to 21% AO. There was no difference between conditions after differentiation of EBs. No significant reduction in DNMT3A expression was noted for SHEF2 EBs differentiated in 2% WKS at day 5 (-0.18 ± 0.99), day 10 (-1.20 ± 1.12) and day 20 (-2.16 ± 0.50) versus 21% AO (-1.28 ± 0.83, -1.17 ± 1.67 and -1.75 ± 1.54, respectively). Differentiated SHEF2 EBs data displayed no significant difference between 2% WKS (-1.18 ± 0.99) and AO (-1.40 ± 0.31) conditions ***(Fig 4.26.D)***.

No significant reduction in DNMT3B expression was observed in differentiated SHEF1 EBs in 2% WKS at days 5 (-2.18 ± 0.92), 10 (-2.82 ± 0.64), and 20 (-4.16 ± 1.92) versus 21% AO (-1.74 ± 1.78, -1.87 ± 1.87 and -4.20 ± 0.91, respectively). Further, DNMT3B expression in undifferentiated SHEF1 showed no significant difference in 2% WKS (-0.83 ± 0.49) versus 21% AO. Differentiated SHEF1 EBs data together showed no significant decrease in DNMT3B expression in 2% WKS (-3.05 ± 1.01) versus AO (-2.60 ± 1.39) ***(Fig 4.26.E)***.

Undifferentiated SHEF2 showed a significant decrease in DNMT3B expression in 2% WKS (-1.42 ± 0.63, $p<0.05$) in comparison to 21% AO. A significant reduction in DNMT3B expression was noted at day 5 (-0.91 ± 1.02, $p<0.05$) and 10 (-2.04 ± 0.72, $p<0.01$) in 2% WKS in comparison to 21% AO (0.56 ± 2.14 and 0.31 ± 0.89, respectively). Further, SHEF2 EBs showed no significant decrease in DNMT3B expression at day 20 in 2% WKS (-3.66 ± 1.21) in comparison to 21% AO (-2.37 ± 1.16). Differentiated SHEF2 EBs data taken together indicated a significant decrease in 2% WKS (-2.21 ± 1.39) condition versus AO (-0.71 ± 1.51) ***(Fig 4.26.F)***.

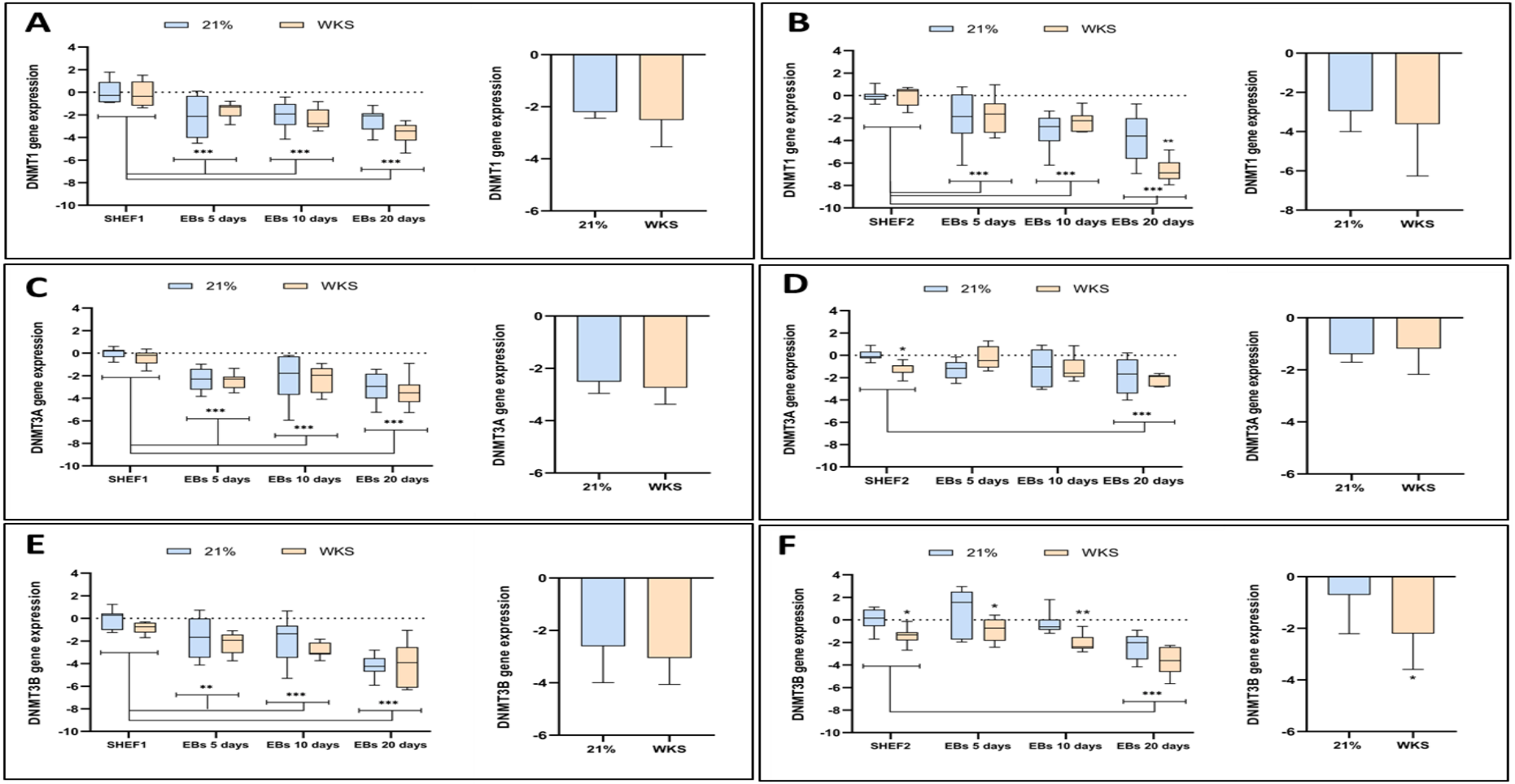

Figure 4.26. **Reduced DNMTs expression in differentiated hESCs.** DNMT1 **(A, B)**, DNMT3B **(C, D)** and DNMT3A **(E, F)** data were obtained from SHEF1 and SHEF2 undifferentiated and differentiated EBs in 21% AO and 2% WKS. The RT-qPCR expression of the DNMTs normalised to the expression of GAPDH. Data are represented as mean ± standard deviation (SD), n=3, *p<0.05, **p<0.01, ***p<0.001 vs 21% AO. Bars with stars indicate a significant difference between differentiated and undifferentiated cells. The other stars compare 2%WKS to 21% AO.

4.3 DISCUSSION

Embryonic stem cells derived from the inner cell mass (ICM) of pre-implantation embryos have a remarkable potential to differentiate into many different cell types (Wobus, 2001). ESCs can form floating three-dimensional embryo-like aggregates and initiate spontaneous differentiation toward the three germ lineages in suspension culture. EBs can differentiate into various types of cells, such as neuronal cells, cardiomyocytes (Boheler et al., 2002), skeletal muscle cells (Salani et al., 2012), and adipocytes (Xiong et al., 2013). EBs can differentiate spontaneously into beating cardiomyocytes that localise between the epithelial layer and mesenchymal basal layer (Hescheler et al., 1997; Boheler et al., 2002). There are unique challenges to effectively directing the differentiation of the three-dimensional structure of EBs compared to the more homogeneously controlled differentiation of ESCs in monolayer cultures. The local extracellular microenvironment comprising physical and chemical signals is crucial for 3D organisation and structure of EBs, while current strategies have primarily focused on differentiation of EBs from the exterior, such as spatially controlling EB size, culturing EBs on extracellular matrices or adding soluble factors to the media to direct their differentiation (Bratt-Leal et al., 2009).

Following dissociation in cell culture, hESCs cells frequently display poor survival, but some researchers suggest that ROCKi (p160 rho-associated coiled-coil kinase inhibitor) enhances the survival of dissociated hESCs in culture and preserves their pluripotency (Watanabe et al., 2007). However, Pettinato and colleagues showed no differences in viability, pluripotency, size, and spherical geometry of EBs regardless of ROCK-i supplementation. They maintained EBs for up to 30 days with high viability evident during prolonged culture (Pettinato et al., 2014). In our experiments, we noted similar EBs formation results with ROCKi and no- ROCKi, therefore, we used media without ROCK-i to decrease experimental variations. Additionally, we observed bigger EBs sizes in air oxygen versus physoxia conditions. Cameron and colleagues demonstrated that cell proliferation or expansion was slowed and apoptosis increased by 5% reduced oxygen exposure during 10 and 16 days of EB development compared to AO (Cameron et al., 2008). Inconsistent with the above, our live/dead cell assay results revealed that SHEF1 cells cultured in 2% WKS had significantly higher dead cells within the EBs versus 21% AO. Still, there was no significant difference in SHEF2 cells. Also, we noted increased number of dead cells after EBs formation after 10 and 20 days of differentiation in three oxygen conditions compared to 5 days EBs which was

consistent with development. Apoptotic cells might be reflective of central cavity formation during the development of EBs.

Some studies have suggested that physiological oxygen (5%) enhanced the formation of mouse ESC and iPSC-derived EBs. The number of EBs was significantly lower in air oxygen tension compared to 5% oxygen after 5 days in suspension culture (Garreta et al., 2014). Researchers induced endodermal differentiation by exposing EBs to high concentrations of activin A in adherent culture and performed immunostaining for endodermal markers. ESCs derived EBs cells showed a higher amount of Foxa2 and Sox17 endodermal markers in both oxygen conditions, while iPSC-derived EBs cells demonstrated lower expression of these markers in air oxygen tension compared to 5% oxygen condition on day 6 (Garreta et al., 2014). Their qPCR data showed that ESCs derived EBs expressed higher levels of Foxa2 in air oxygen tension versus 5% oxygen, while no significant change was noted for the Sox17 between conditions. iPSC-EBs differentiated adherent cultures revealed lower Foxa2 and Sox17 gene expression in air oxygen tension than 5% oxygen condition consistent with protein expression data on day 6 (Garreta et al., 2014).

EBs spheroid structures exhibit heterogeneous patterns of differentiated cells. EBs can express three germ layer markers; ectodermal (Sox1, Nestin, Pax6, GFAP, Olig2, neurofilament 68Kd, and tubulin-b3), mesoderm (Brachyury-T, Desmin, Flk-1, Msp1/2, Isl-1, αlfa-actin, zeta-globin, and Runx2) and endoderm (Foxa2, Sox17, GATA 4/6, α-fetoprotein, and albumin) (Itskovitz-Eldor et al., 2000b; Qin et al., 2008; Pekkanen-Mattila et al., 2010). Our study demonstrated an increased expression of ectodermal marker Nestin, endodermal markers KDR and TBXT, mesodermal marker AFP after EBs formation at days 5, 10 and 20. Moreover, EBs cultured in physoxia showed lower expression of these differentiation markers when compared to 21% AO. We demonstrated elevated three germ layer differentiation markers (Nestin, AFP and TBXT) expression with immunohistochemistry. Different EBs sizes were observed from immunohistochemistry experiments which may be due to some variations in incubation parameters during cell culture. Many pieces of evidence support the importance of oxygen on the regulation of stem cell potency, differentiation, and low oxygen tension increases the growth and establishment of new mouse and human ESC lines from blastocysts (Ludwig et al. 2006; Wang, Thirumangalathu, and Loeken 2006). In the same manner, physoxia has improved enhanced efficiency of the generation of induced pluripotent stem cells from mouse and human somatic cells (Yoshida et al., 2009; Shimada et al., 2012).

TERT protein is synthesised in the cytoplasm and functions in the nuclei but shuttles between the nucleus and the cytoplasm (Wong et al., 2002). Also, TERT protein has an extra-nuclear function that regulates an insulin-insensitive pathway involved in glucose uptake or basal glucose transport in human and mouse skeletal muscle cells (Shaheen et al., 2014). iPSCs were successfully formed from mice TERT-KO fibroblasts by introducing the four reprogramming factors, but it was less efficient compared to wild type fibroblasts (Kinoshita et al., 2014). After injecting TERT-KO reprogrammed cells into mice, cells form teratomas after 3-4 weeks. Also, they are capable of forming EBs spheroid structures and all three germ layers. EBs derived from WT and TERT-KO iPSCs express less pluripotent cell markers (Nanog and Oct3/4), while they highly express three germ layer markers, including GATA6 and Sox17 (endoderm markers), Flk1 (a mesoderm marker), and Nestin (an ectoderm marker) (Kinoshita et al., 2014).

The myogenesis of ESC-derived EBs, which express both TERT and myocardin A, was performed using the three-dimensional hanging-drop culture system where myogenic cells developed clearly in the EBs. In addition, TRAP assays showed that the nuclear proteins of murine ESC-derived EBs contained significant telomerase activity in beating EBs at day 14 (Madonna et al., 2008). Spontaneous differentiated ESCs derived EBs showed telomerase activity and TERT gene expression even after 20 days of culture. Consistent with the above, we noted slightly decreased telomerase activity and TERT gene expression in EBs compared to undifferentiated cells. However, we noted that EBs mostly maintained telomerase activity, TERT gene expression, and telomere length more consistently than monolayer differentiated ESCs. Further, there was a higher telomerase activity and gene expression in physoxia associated with longer telomeres in reduced oxygen tension. Several studies have reported the effect of reduced oxygen conditions on telomerase and TERT. For instance, increased cell survival and maintenance of the undifferentiated hESCs were noted in 2% O_2 culture with elevated nuclear TERT level, but no significant difference in telomerase activity was observed (Radan et al., 2014). In general, we noted higher telomerase activity, TERT gene expression, and telomere length in spontaneous differentiated EBs. EBs cultures are capable of only about 40 population doublings *in vitro* due to senescence and telomeric shortening in monolayer culture (Shamblott, 2001). In conflict with our observations, researchers reported that EBs were telomerase-negative. After many population doublings and absence of telomerase lead cells to senescence and eventually telomere attribution. Shamblott et al., 2001, determined that embryoid-derived cultures were telomerase-negative and suggested that epigenetic processes

such as DNA methylation were likely involved in the transition of ESC into EB. DNA methylation regulates gene expression through various mechanisms. For instance, transcription factors are unable to attach to their binding sites after methylation or through recruitment of repressor proteins that interplay with methylated cytosine to change chromatin structure and induce gene silencing (Moore et al., 2013). Genome-wide DNA methylation status (247 CpG islands that potentially have tissue-dependent and differentially methylated regions) was lower in fetal tissue and EBs compared to ESCs. Therefore, this suggested that global methylation decreased as ESC-derived EBs developed (Kremenskoy et al., 2003). We specifically investigated TERT promoter methylation and the effect of oxygen on methylation patterns. We noted increased TERT proximal promoter methylation during EB formation compared to undifferentiated ESCs. We also observed that the distal promoter (region I, -1456, -1495 from TSS) had a high methylation level in all conditions with no significant difference during differentiation compared to other proximal promoter regions. We found that methylation of the proximal TERT promoter region (including region II, III, IV and V) is oxygen-sensitive. There is a significant decrease in methylation percentage in physiological conditions versus 21% AO.

Understanding the epigenetic profile of naive cells is essential to stem cell biology and cancer research. DNA methylation profiles will be important for developing precise epigenetic engineering tools, and understanding the development of functional cells with epigenetic memory has massive potential for clinical applications (Jones and Baylin, 2007). DNA methylation on gene promoters during differentiation and lineage commitment ensures cellular identity associated with activation/repression of lineage-specific genes and loss of pluripotency in ESCs (Ziller et al., 2013). Significantly, the catalytically active DNMT3B level reduces sharply during PSCs differentiation as cells mature and DNMT3B is generally not expressed in somatic tissues (Gifford et al., 2013; Gordon et al., 2013). DNMT3B expression was downregulated in EBs versus undifferentiated ESCs and more starkly decreased in reduced oxygen compared to 21% AO. We hypothesise that there is a link between higher methylation levels on TERT proximal promoter and higher expression of DNMT3B in 21% AO. Therefore, we further hypothesised that the oxygen-sensitive methylation pattern of TERT promoter might be associated with the DNMT3B enzyme activity, as observed in monolayer differentiated ESCs.

In summary, EBs express three germ layer differentiation markers during extensive culture while retaining pluripotency and telomerase activity beyond the levels observed with monolayer differentiated cells. Further, there was a strong link between DNMT3B expression

and TERT promoter methylation in monolayer differentiated and ESC EBs. EBs provide an opportunity to mechanistically study early differentiation events of 3D aggregates of pluripotent cells enabling *in vitro* genetic manipulation studies during periods reflective of early development. ESCs are commonly differentiated *in vitro* by spontaneous self-assembly in suspension culture into 3D cell aggregates called embryoid bodies (EBs), which mimic many of the hallmarks of early embryonic development. Yet, the 3D organisation and structure of EBs also present unique challenges to effectively direct the differentiation of the cells. The control of the pluripotency of ESCs, iPSCs and their guided differentiation toward specific cell types are major hurdles for their successful use in future clinical applications.

4.3.1 Summary

In this chapter, we have explored some key observations on the effect of different oxygen environments on EBs characteristics, including telomere length, telomerase activity and TERT expression and DNA methylation patterning on the TERT promoter. ***Figure 4.27*** provides an outline of experiments performed in chapter 4.

In summary, we noted larger EBs in air oxygen versus physoxia and increased apoptosis with differentiation in SHEF2 EBs, consistent with development. Apoptotic cells can be forming a central cavity during the development of EBs. An increased expression of ectodermal marker Nestin, endodermal markers KDR and TBXT, and mesodermal marker AFP was observed after EBs formation with slower onset of differentiation in physoxia. EBs maintained telomerase activity, TERT gene expression, and telomere lengths to a greater extent than seen with monolayer differentiated ESCs. Similar to monolayer differentiated cells, there was a higher telomerase activity and gene expression in physoxia associated with longer telomeres. We noted increased TERT proximal promoter methylation during EB formation compared to undifferentiated ESCs, and it was oxygen sensitive. Similar to monolayer differentiated cells, the distal promoter (region I, -1456, -1495 from TSS) showed a high methylation level in all conditions with no significant difference during differentiation.

This chapter suggested that monolayer differentiated cells and EBs have differences and some similarities in their characteristics and epigenetics in different oxygen environments.

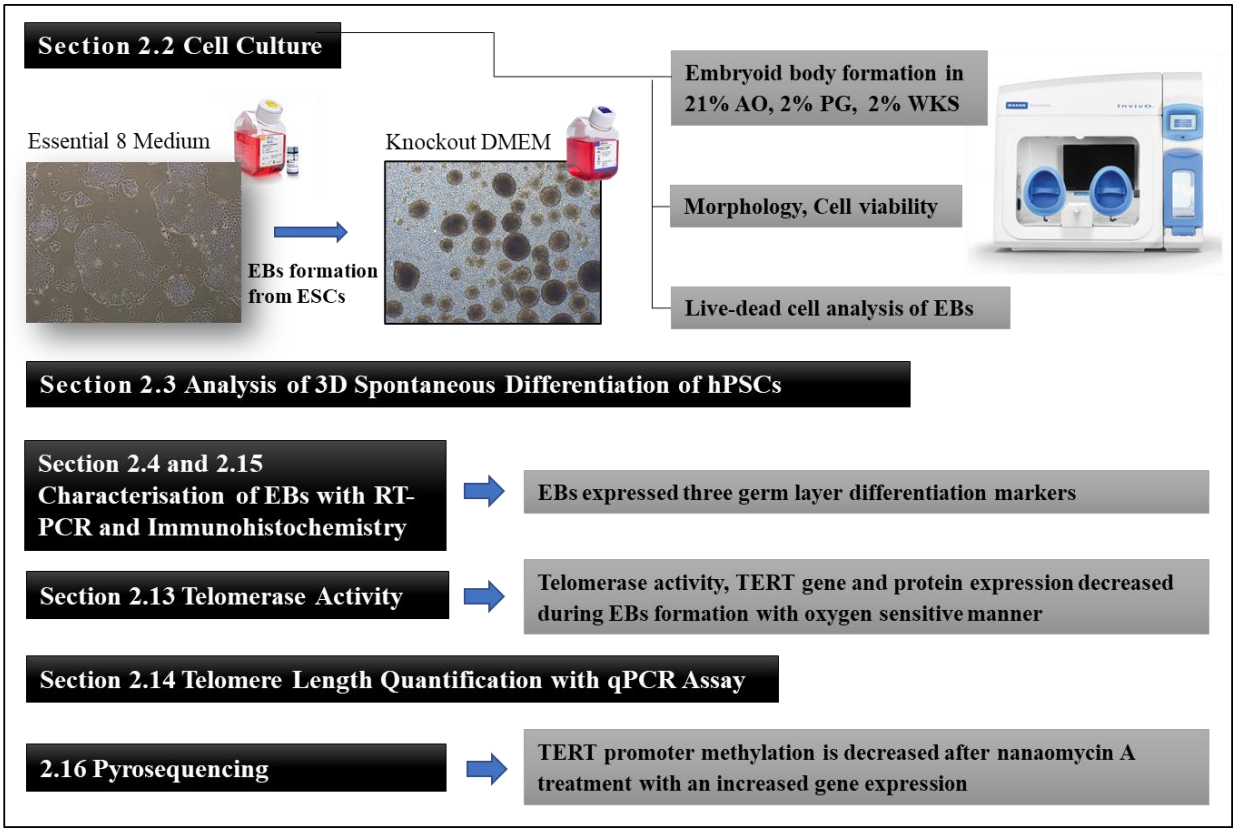

Figure 4.27. **Summary of the methodology in chapter 4.**

Keele University

CHAPTER 5: DNMT3B inhibition positively regulates TERT and telomerase activity and is accompanied by reduction of TERT promoter methylation in cancer cell lines

5.1 INTRODUCTION

Telomerase reactivation and telomere maintenance are crucial requirements for the immortality of cancer cells, while telomerase activity is repressed in mature somatic cells. Consistently, TERT expression and telomerase activity are detectable in the vast majority of primary human cancers (85%–90%) (Kim et al., 1994; Shay, 2016). Rapidly growing and proliferating cancer cells possess shorter telomeres, a barrier to immortalisation and cancer progression. Therefore, cancer cells reactivate telomerase enzyme activity to overcome telomere shortening and maintain critical levels of telomeres to enable continued proliferation (Hackett and Greider, 2002; Januszkiewicz et al., 2003). These features make telomerase and telomeres attractive targets for cancer therapy (Wright and Shay, 2000). There are many telomerase inhibitors, but none are yet clinically approved, and it remains a challenging target for drug or vaccine development (Vonderheide, 2008; George et al., 2020). New strategies for potential anticancer drugs, including the development of telomerase inhibitors, targeting TERT promoter, telomerase and TERT targeting immunotherapies, or drugs that target telomeric DNA, are ongoing (Gomez et al., 2016; Mizukoshi and Kaneko, 2019). The mechanisms of *TERT* reactivation in cancer cells and the silencing of *TERT* in somatic cells remain open to debate. TERT reactivation in cancer is most commonly associated with genetic alterations in TERT gene/promoter and epigenetic modifications through TERT promoter methylation (Castelo-Branco et al., 2013; Barthel et al., 2017; Leão et al., 2019).

Epigenetics describes the correlation between genotype and phenotype changes and explains the process of reversible and heritable gene regulation (Mattick and Makunin, 2006; Deans and Maggert, 2015). Chemical modification of DNA or RNA can regulate gene transcription without changing genetic code. DNA methylation, histone modification, and non-coding RNAs are the prominent epigenetic marks that regulate telomeres and telomerase activity (Dogan and Forsyth, 2021). Also, these epigenetic modifications may have a role in reversible activation or silencing of TERT in biological processes, including development and differentiation and increased TERT expression in cancers (Dogan and Forsyth, 2021). There are many reports explaining the regulation of TERT through epigenetic mechanisms (Cong et al., 2002; Lewis and Tollefsbol, 2016), where hypermethylation of the TERT gene correlates with telomerase activity (Guilleret et al., 2002). The human TERT promoter possesses a large CpG island (485 CpGs, −1800 to +2300 relative to ATG) within the promoter region, exons 1

and 2 (UCSC Genome Browser). TERT promoter contains 52 CpG sites in the 433-bp genomic region, a hypermethylated oncological region (THOR). It is differentially methylated between somatic cells and most cancers (Castelo-Branco et al., 2016) (***chapter 1, Fig 1.7, Page 20***). Hypermethylation of CpG islands within a gene promoter is often associated with gene silencing (Moore et al., 2013). However, the hypermethylated THOR region is associated with increased promoter activity and TERT expression in cancer (Lee et al., 2019). ChIP was applied to demonstrate that hypermethylation of the TERT promoter reduced binding of CTCF (transcriptional repressor) to the CCCTC binding region and prevented CTCF dependent inhibition of TERT expression (Renaud et al., 2007). TERT promoter hypermethylation at specific CpG islands (THOR) has diagnostic and prognostic value in prostate, pancreatic and brain tumours (Castelo-Branco et al., 2013, 2016; Faleiro et al., 2017) and is a potentially accessible biomarker for malignancy and patient outcome in paediatric gliomas (Castelo-Branco et al., 2013). Upstream of the TERT promoter transcription site is hypermethylated in malignant paediatric brain tumours, which is related to the progression of a tumour, while normal brain tissues or low-grade tumours are hypomethylated (Dessain et al., 2000; Castelo-Branco et al., 2013). Guilleret and colleagues emphasised the correlation between TERT methylation and gene expression in telomerase positive cancer cells (Guilleret and Benhattar, 2004). The driving mechanism of hypermethylation of TERT promoter is unclear in oncogenesis. DNA methyltransferase enzymes may induce methylation and promote cancer progression. DNMT1 has a preference for hemimethylated DNA during the replication process (Jones and Liang, 2009) and is transcribed mostly during the S-phase of the cell cycle (Robertson et al., 2000). DNMT3B is responsible for de novo DNA methylation, and aberrant upregulation of DNMT3B is common during early oncogenesis. Therefore, it might induce promoter hypermethylation resulting in transcriptional activation of TERT gene, which promotes cancer progression. DNMT3B is highly expressed in several cancer cells, including colorectal carcinoma, hematopoietic cell lines, bladder and breast cancer and is linked to increased tumour cell survival (Beaulieu et al., 2002; Ostler et al., 2007). TERT upregulation may further promote DNMT3B expression and generate a positive feedback loop in cancer cells (Yu et al., 2018b; Yuan et al., 2019).

A significant factor in epigenetic regulation is oxygen. TERT promoter region between −165 and +51 contains two HIF1 consensus sequences in the proximal promoter region that mediate upregulation of the gene (Nishi et al., 2004). HIF1A is activated in response to low oxygen levels and induces telomerase activity via TERT transcription in cervical and

choriocarcinoma cells (Yatabe et al., 2004; Kyo et al., 2008), indicating that low oxygen tension might be a selective advantage for tumour cell survival. Studies have shown that low oxygen tension induces reduced global DNA methylation in cancer cell lines (Shahrzad et al., 2007; Skowronski et al., 2010). Reduced oxygen also increases telomere length and TERT expression in rat heart and lung tissue associated with HIF-1α (Wang et al., 2018). HIF overexpression is linked to higher vascular density, cell survival, metastasis, tumour grade, and resistance to conventional therapies (Poon et al., 2009). Low oxygen (1% O_2) upregulates the expression level of DNMT1 and DNMT3A, but not DNMT3B in Hep3B cells (Liu et al., 2011). Conflicting, increased levels of DNMT3B were noted in prostate cells in a low oxygen condition (1% O_2) while no alteration was observed in DNMT1 and DNMT3A activity (Watson et al., 2009).

The human promyelocytic leukaemia-derived cell line, HL-60, retains the potential for differentiation through all-trans retinoic acid (ATRA) treatment resulting in a progressive increase in the proportion of mature neutrophil cells (Breitman et al., 1980; Martin et al., 1990; Manda-Handzlik et al., 2018). CD11b is a standard cell surface marker used to identify myeloid differentiation of the HL-60 induced by ATRA (Hicksteinsgli, Back, and Collins 1989). ATRA can cross the cell membrane and be transferred to the nucleus by intracellular lipid-binding proteins (CRABPII or FBP5), and they can bind vitamin D related nuclear receptors, ligand-dependent retinoic acid receptors (RAR) and thyroid hormone receptors (Al Tanoury et al., 2013). HL-60 expresses high levels of telomerase activity, however, telomerase and TERT protein are reportedly suppressed during the differentiation of HL-60 cells (Xu et al., 1999; Liu et al., 2004). Following ATRA treatment, HL-60 cells differentiate into CD11b+ mature granulocytes and monocytes (Kim et al. 1999). TERT is downregulated with 2 μM ATRA treatment in HL-60 at day 12, and DNMTs expression changes during this process (Love et al., 2008). DNMT3B was repressed at day 6, DNMT1 expression progressively decreased, and DNMT3A increased from day 6 to day 12 of treatment (Love et al., 2008). Epigenetic changes, including the hypoacetylation and hypermethylation of TERT promoter, are associated with ATRA-induced inhibition of telomerase activity. The downregulation of TERT expression in the HL-60 differentiation model may be helpful for investigating TERT promoter methylation during myeloid cell differentiation.

Recent advances in epigenetics have contributed to our knowledge of cancer progression and the association of epigenetic alterations in this process. In this chapter, we investigated the

effect of different oxygen tensions on proliferation, telomerase activity, TERT gene and telomere length. Also, we optimised DNMT inhibitors (nanaomycin A, decitabine) concentration and determined TERT expression and telomerase activity in inhibitor-treated cells. We have investigated DNMT3B binding to TERT promoter after nanaomycin A treatment. Overall, we investigated DNMT3B inhibition effect on the TERT promoter hypermethylation, TERT expression and telomerase activity in different cancer cells. Further, telomerase activity, gene expression and promoter methylation were analysed in differentiated and undifferentiated HL-60 model. In conclusion, DNMT3B methylation on TERT promoter was independent of differentiation. A significant decrease in DNMT3B binding to TERT promoter was noted after nanaomycin A treatment compared to untreated cells. DNMT3B inhibition can decrease TERT promoter methylation, further, it can increase TERT expression and telomerase activity.

5.2 RESULTS

5.2.1 The effect of reduced oxygen on the proliferation of cancer cells

Proliferation and viability of cancer cell lines were first explored. Different densities of cells (serial dilution of 250.000 cells/ml) were cultured in 96-wells plate formats in a final volume of 100 µl/well in three conditions (21% AO, 2% PG and 2% WKS) to determine optimal cell numbers for seven-day experimentation. IMR-90 (fibroblasts isolated from the fetal lung tissue) and SH-SY5Y cells showed a higher proliferation rate in physoxia conditions during the logarithmic phase, where cells actively proliferate with an exponential increase. However, higher proliferation rate was noted for A549, COV362, MG-63, and Jurkat cells cultured in 21% AO during the logarithmic phase. Cells are the most viable in the logarithmic phase. We determined cell numbers in this phase for the following drug experiments as $31x10^3$ cells/ml for A549 (***Fig 5.1.A***) and $15x10^3$ cells/ml for IMR-90 (***Fig 5.1.B***), COV362 (***Fig 5.1.C***), MG-63 (***Fig 5.1.D***), SH-SY5Y (***Fig 5.1.E***), Jurkat cells (***Fig 5.1.F***) before they reached the stationary phase.

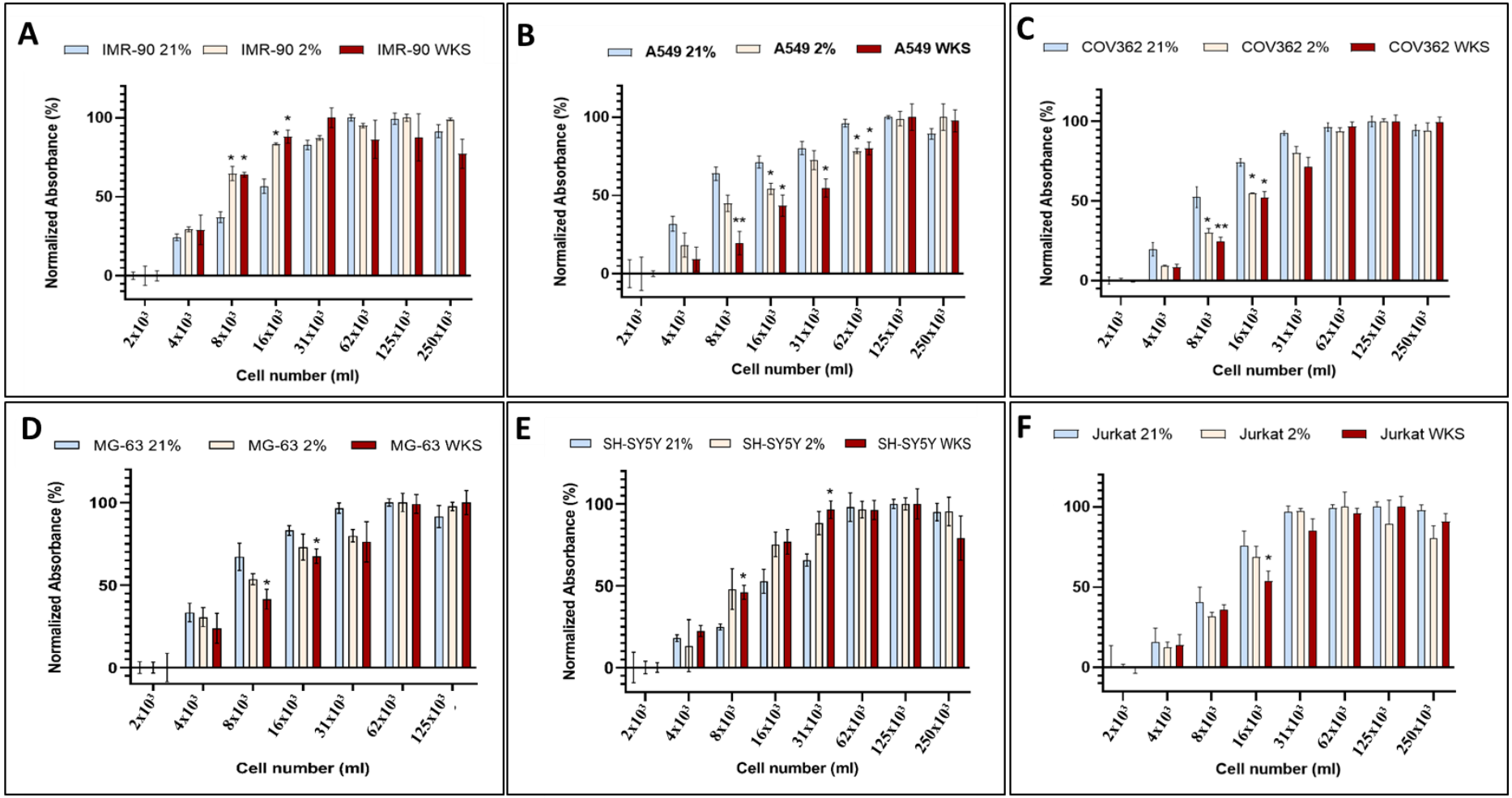

Figure 5.1. **Effect of reduced oxygen on the proliferation rate of cancer cells.** Serial dilution of cells was seeded to 96 well plates. Cell proliferative ability was measured using WST-1 assay after seven days. Data are shown as mean ± standard deviation (SD) of 3 independent experiments. Two-way ANOVA was conducted to determine the significant differences *$p < 0.05$, **$p < 0.01$, ***$p < 0.001$ versus 21% AO.

5.2.2 Telomerase activity, gene expression and telomere length in cancer cells

TRAP assay was performed using the TRAPeze® Kit RT Telomerase Detection Kit (Millipore, USA) to evaluate the telomerase activity in different oxygen conditions for cancer cells. IMR-90 showed the lowest telomerase activity compared to cancer cells. There was a higher telomerase activity in 2% WKS (2.12 ± 0.61, $p<0.01$) in comparison to 21% AO (1.43 ± 0.01) and heat-treated samples (1.26 ± 0.08). However, A549 cells showed significantly less telomerase activity in 2% WKS (4.77 ± 0.17, $p<0.01$) compared to 21% AO (5.20 ± 0.20). No significant difference was noted between 21% AO, 2% PG, and 2% WKS in COV362 (4.62 ± 0.01, 4.43 ± 0.01, and 4.65 ± 0.55, respectively) and MG-63 cells (4.34 ± 0.16, 4.35 ± 0.04, and 4.51 ± 0.33, respectively). There was higher telomerase activity in 2% WKS (4.68 ± 0.30, $p<0.05$) compared to 21% AO (4.68 ± 0.30) in SH-SY5Y cells. We noted higher telomerase activity in 2% PG condition (5.95 ± 0.02) versus 21% AO (5.44 ± 0.01) in Jurkat cells (***Fig 5.2.A*)**. Cancer cell lines generally showed a higher telomerase activity than control IMR-90 cells (***Fig 5.2*)**.

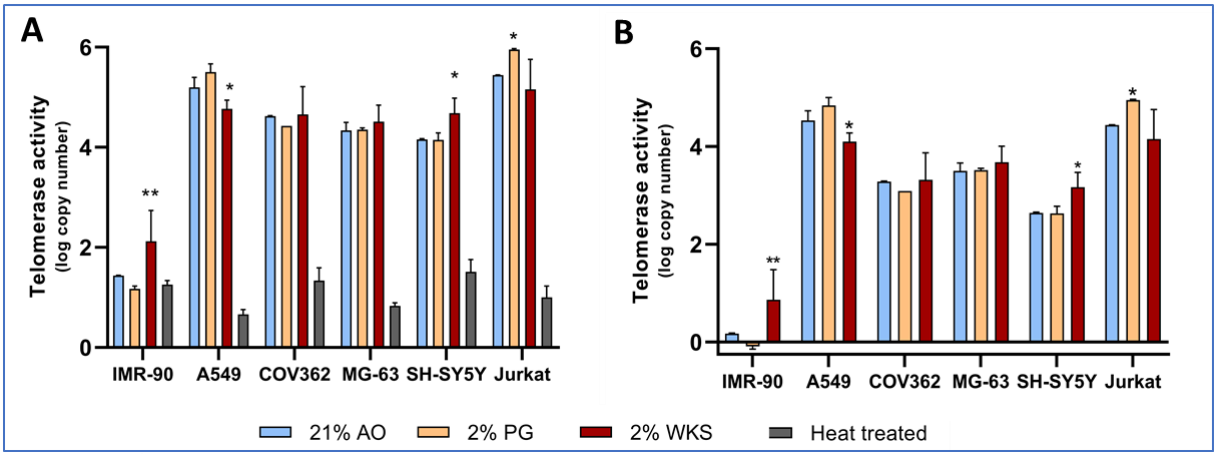

Figure 5.2. **High telomerase activity in cancer cells with TRAP assay.** Cancer and somatic cells were cultured in air oxygen (21% AO) and physiological oxygen conditions (2% PG and 2% WKS). (**A**) Real-time PCR data is represented with HT (heat-treated) control samples. (**B**) Data is normalised to HT samples. Data are represented as mean ± standard deviation (SD), n=3, *$p<0.05$, **$p<0.01$, ***$p<0.001$. The stars compare physoxia conditions to 21% AO.

TERT gene expression was analysed using RT-qPCR to determine any correlation between telomerase activity and the effect of different oxygen exposures to cancer cells. IMR-90 cells showed increased expression of TERT expression correlated to telomerase activity in 2% WKS (1.41 ± 0.91, $p<0.05$) versus 21% AO. Similar to telomerase activity, cancer cell lines showed higher TERT expression when compared to IMR-90. No significant difference was noted for A549 (3.67 ± 1.06, 3.71 ± 0.28 and 2.60 ± 1.03), COV362 (2.96 ± 0.90, 2.71 ± 0.45 and 2.82 ± 0.49), MG-63 (3.39 ± 0.45, 2.97 ± 0.14 and 3.31 ± 0.49), and Jurkat cells (6.12 ± 0.86, 6.09 ± 0.79 and 6.16 ± 0.83) between 21% AO, 2% PG, 2% WKS conditions, respectively. There was a higher expression of TERT gene in 21% AO (5.10 ± 0.42, $p<0.05$) versus 2% PG (4.11 ± 0.33) in SY-SY5Y cells. Lastly, Jurkat cells displayed the highest telomerase activity and TERT expression compared to other cells (***Fig 5.3***).

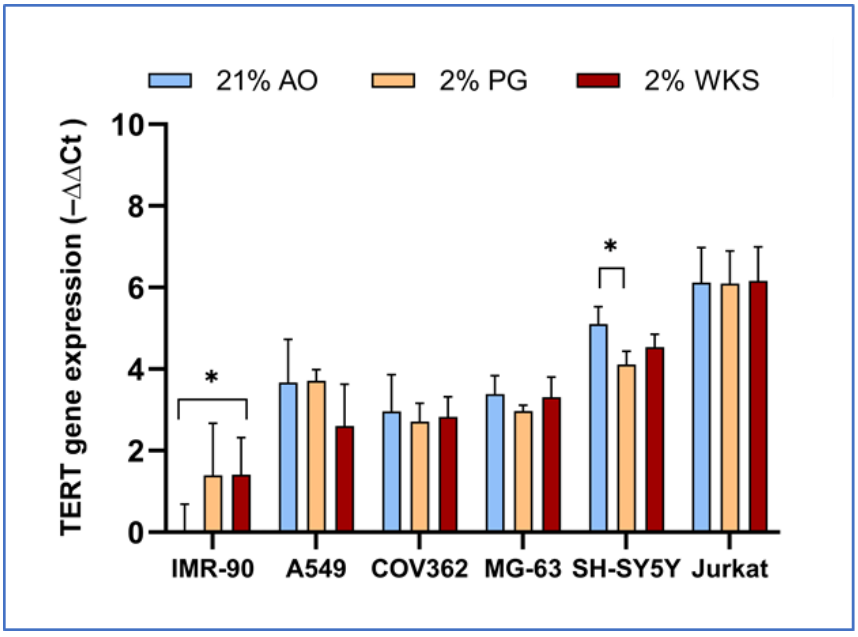

Figure 5.3. **No consistent pattern of TERT gene expression in physoxia in cancer cells.** Cancer and somatic cells were cultured in 21% AO and physiological oxygen conditions (2% PG and 2% WKS). The RT-qPCR expression of the TERT normalised to the expression of GAPDH. Data are represented as mean ± standard deviation (SD). n=3, *$p<0.05$, **$p<0.01$, ***$p<0.001$ vs 21% AO.

Telomere Length Quantification qPCR Assay (Sciencell Research Lab, USA) was performed to measure mean telomere lengths in cancer cells. IMR-90 in 2% WKS (5.69 ± 0.29,

p<0.05) showed longer telomeres than 21% AO (5.09 ± 0.48). There was no significant difference in the mean value of telomere lengths in A549 (4.93 ± 0.52, 4.60 ± 0.81 and 4.73 ± 0.75), COV362 (5.01 ± 0.55, 5.57 ± 1.20 and 5.42 ± 0.59), MG-63 (5.14 ± 0.78, 4.32 ± 0.51 and 4.81 ± 0.98), SH-SY5Y (4.97 ± 0.39, 4.91 ± 0.55 and 5.14 ± 0.67) or Jurkat cells (5.37 ± 0.88, 5.53 ± 0.56 and 5.41 ± 0.86) between 21% AO, 2% PG, 2% WKS conditions, respectively (***Fig 5.4***).

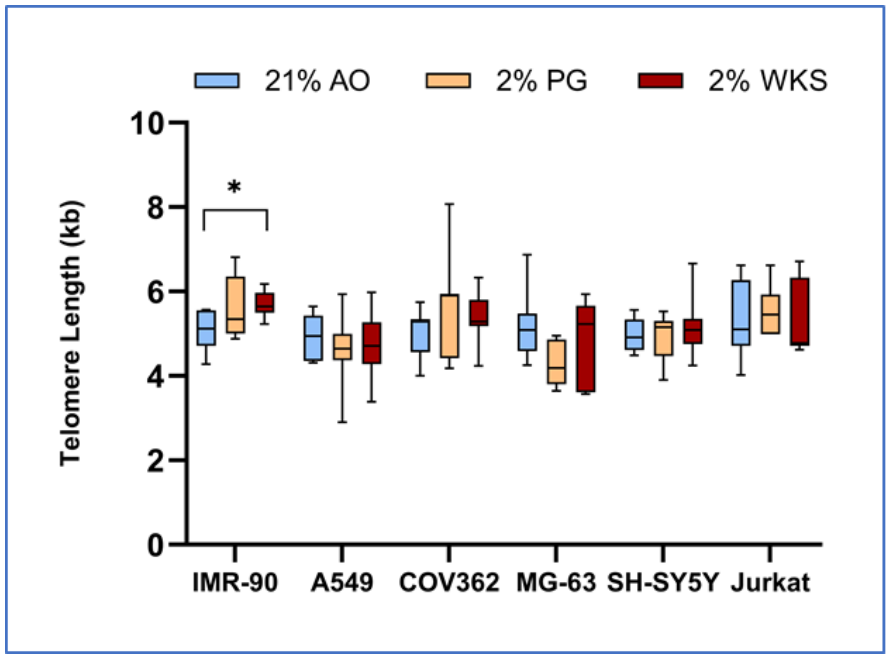

Figure 5.4. **No consistent pattern of telomere length in physoxia in cancer cells.** The box represents the interquartile range, the whisker illustrates the outer quartiles, and the line in the middle shows the median expression. Data are represented as n=3x3, *p<0.05, **p<0.01, ***p<0.001 vs air oxygen (21% AO).

5.2.3 Non-toxic dose establishment of nanaomycin A (DNMT3B inhibitor) and decitabine (DNMT1 inhibitor) in cancer and somatic cell lines

Serial dilutions (10 µM- 0.08 µM) nanaomycin A were used to determine the maximum non-toxic drug dose over seven days. The maximum non-toxic nanaomycin A dose was determined as 0.31 µM for IMR-90 in three oxygen conditions (***Fig 5.5.A***), and it was 0.63 µM for A549 in 21% AO, 2% PG but 0.31 µM for A549 in 2% WKS (***Fig 5.5.B***). COV362 cells represented the non-toxic nanaomycin A dose as 1.25 µM in all three oxygen tensions (***Fig***

5.5.C). MG-63 showed 0.63 µM as a non-toxic nanaomycin A dose in 21% AO, 2% PG and 2% WKS (***Fig 5.5.D***). The maximum non-toxic nanaomycin A dose was determined as 0.31 µM in 21% AO, 2% PG and 0.16 in 2% WKS in SH-SY5Y cells (***Fig 5.5.E***). The maximum non-toxic drug dose was determined as 0.31 µM in 21% AO, 2% WKS and 0.16 in 2% PG in Jurkat cells (***Fig 5.5.F***). Overall, the maximum non-toxic drug dose was determined as 0.31 µM for IMR-90, SH-SY5Y, and Jurkat cells, 0.63 µM for A549 and MG-63, and 1.25 µM for COV362. DMSO, used as a carrier, control displayed no significant effect on cell growth (***Fig 5.5***).

Serial dilutions of decitabine (20 µM-0.08 µM) were used for cytotoxicity assays to determine maximum non-toxic drug doses. The maximum non-toxic decitabine dose was 0.16 µM for IMR-90 in 21% AO, 2% WKS conditions and 0.31 µM in 2% PG (***Fig 5.6.A***). A549 cells showed 0.63 µM in 21% AO but 0.31 µM in 2% PG and 2% WKS as a non-toxic decitabine dose (***Fig 5.6.B***). COV362 cells represented the non-toxic decitabine dose as 0.63 µM in 2% PG and 0.31 µM in 21% AO, 2% WKS tensions (***Fig 5.6.C***). MG-63 showed 0.63 µM as a non-toxic decitabine dose in 2% PG and 0.31 µM in 21% AO, 2% WKS (***Fig 5.6.D***). The maximum non-toxic decitabine dose was 0.63 µM in 21% AO and 0.31 in 2% PG, 2% WKS in SH-SY5Y cells (***Fig 5.6.E***). The maximum non-toxic drug dose was determined as 0.31 µM in 2% PG and 0.16 in 21% AO, 2% WKS in Jurkat cells (***Fig 5.6.F***). Overall, the maximum non-toxic drug dose was determined as 0.16 µM for IMR-90, Jurkat, and 0.31 µM for A549, COV362, MG-63 and SH-SY5Y cancer cells. As decitabine was water-soluble, therefore, untreated cells were included as a control group (***Fig 5.6***).

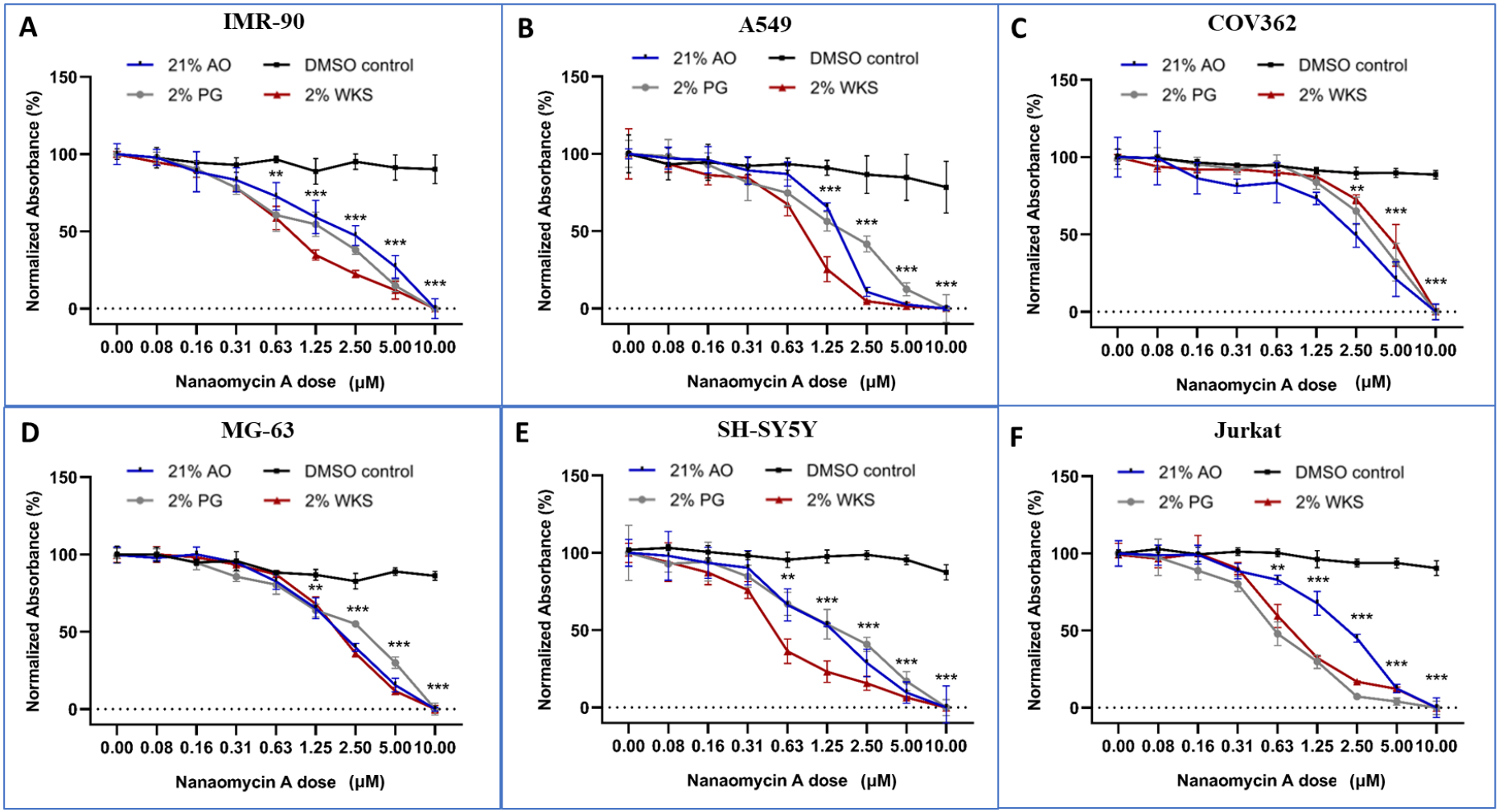

Figure 5.5. **Determining non-toxic nanaomycin A dose with cytotoxicity assay in cancer and normal cell lines.** Serial dilution of 10 μM nanaomycin A was performed using 1/2 of the previous dilution as the input to the next dilution in each step. Data are represented as n=3, *p<0.05, **p<0.01, ***p<0.001 vs DMSO control.

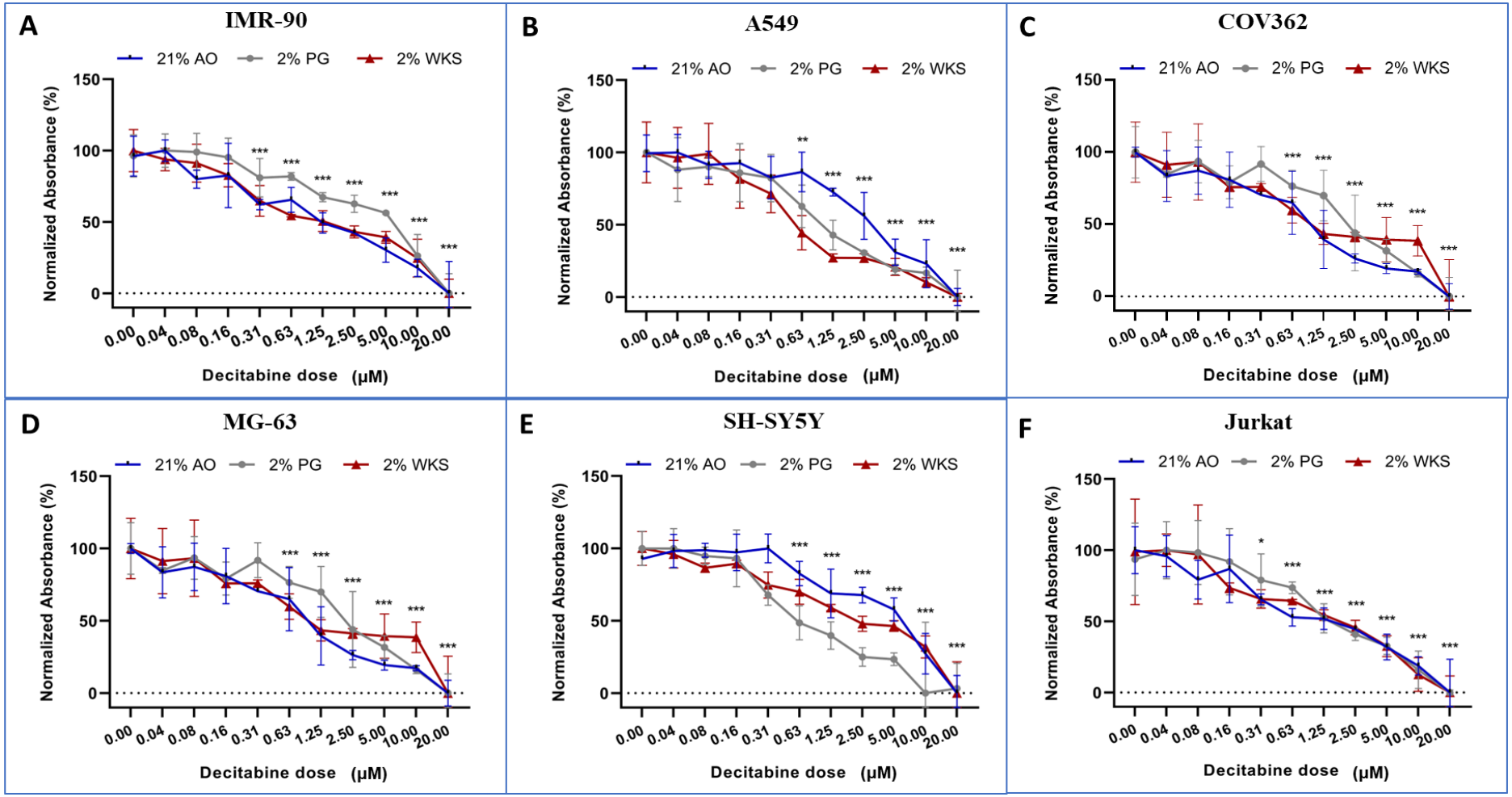

Figure 5.6. **Determining non-toxic decitabine dose with cytotoxicity assay in cancer and normal cell lines.** Serial dilution of 20 μM decitabine was performed using 1/2 of the previous dilution as the input to the next dilution in each step. Data are represented as n=3, *p<0.05, **p<0.01, ***p<0.001 vs untreated control.

5.2.4 Nanaomycin A inhibited DNMT3B Activity in cancer cells

We next sought to determine DNMT3B enzymatic activity following on from nanaomycin A treatment in cells cultured in 2% WKS. We noted a significant inhibition after nanaomycin A treatment in IMR-90 (0.35 ± 0.20, p<0.001), A549 (0.46 ± 0.15, p<0.01), COV362 (0.27 ± 0.05, p<0.001), MG-63 (0.41 ± 0.13, p<0.001), SH-SY5Y (0.43 ± 0.15, p<0.001) and Jurkat cells (0.42 ± 0.17, p<0.001) versus normalized controls (***Fig 5.7***).

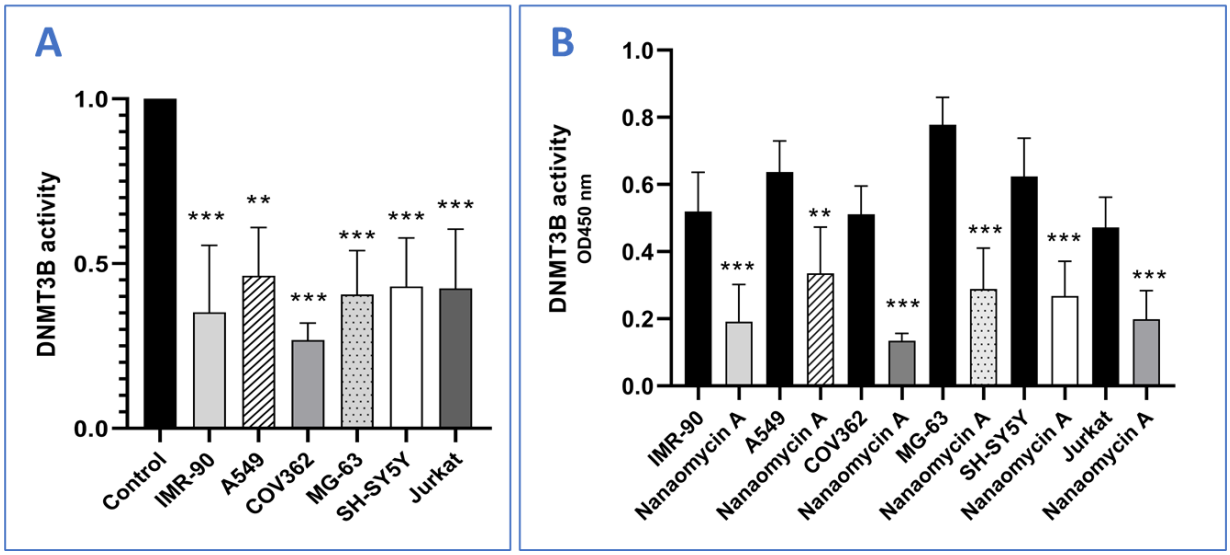

Figure 5.7. **Nanaomycin A induced inhibition of DNMT3B activity in cancer cells cultured in 2% WKS**. DNMT3B enzyme activity was measured in untreated (black column) and nanaomycin A (DNMT3B selective inhibitor) treated cancer samples. **(A)** The absorbance values of drug-treated cancer cells were normalised to untreated cells, **(B)** The measured absorbance for untreated and nanaomycin A treated samples were represented. A dose of 0.31 µM nanaomycin A were used for IMR-90, SH-SY5Y, and Jurkat cells, 0.63 µM for A549 and MG-63, and 1.25 µM for COV362.

5.2.5 Decitabine inhibited DNMT1 Activity in cancer cells

DNMT1 Activity/Inhibition was next established following exposure to decitabine treatment. Significant inhibition after decitabine treatment was noted in IMR-90 (0.27 ± 0.07, p<0.001), A549 (0.34 ± 0.13, p<0.001), COV362 (0.19 ± 0.07, p<0.001), MG-63 (0.33 ± 0.04,

p<0.001), SH-SY5Y (0.25 ± 0.10, p<0.001), and Jurkat cells (0.23 ± 0.12, p<0.001) versus normalized controls (***Fig 5.8***).

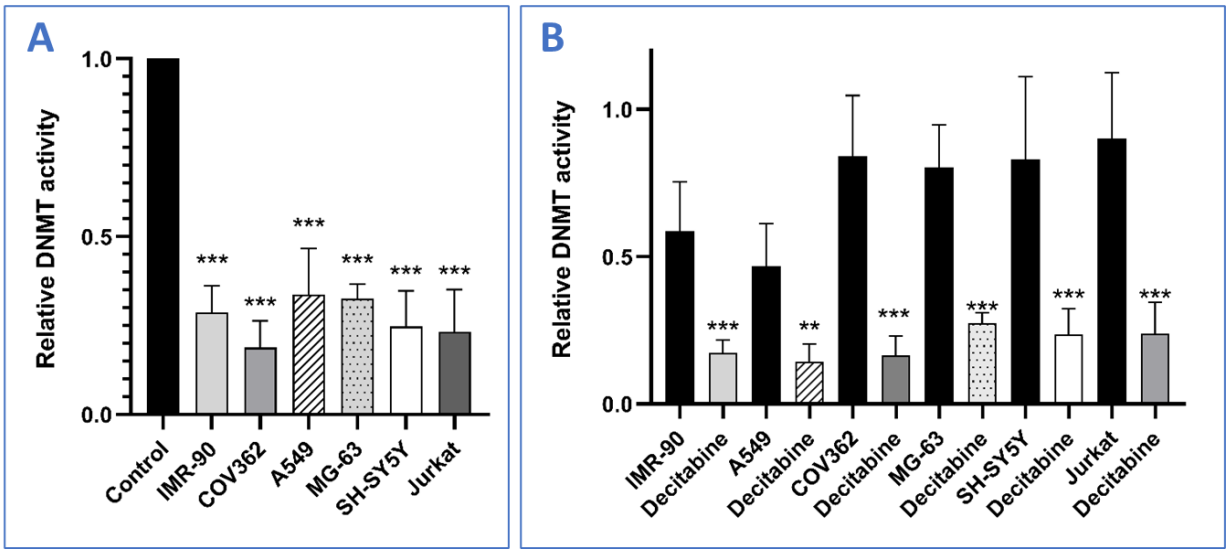

Figure 5.8. **Decitabine induced inhibition of DNMT1 activity in cancer cells cultured in 2% WKS**. DNMT1 enzyme activity was measured in untreated (black column) and decitabine (DNMT1 inhibitor) treated cancer samples. **(A)** The absorbance values of drug-treated cancer cells were normalised to untreated cells, **(B)** The measured absorbance for untreated and decitabine treated samples were represented. A dose of 0.16 μM nanaomycin A were used for IMR-90, Jurkat, and 0.31 μM for A549, COV362, MG-63 and SH-SY5Y cancer cells.

5.2.6 Nanaomycin A and decitabine decreased DNMT gene expression

We performed qRT-PCR to investigate the effect of DNMT inhibitors on DNMT3B and DNMT1 gene expressions. Nanaomycin A exposed IMR-90 cells displayed significantly reduced DNMT3B expression (-1.37 ± 0.55, p<0.01). Further, we noted decreased COV362 (-1.08 ± 0.66), SH-SY5Y (-0.96 ± 1.57), and Jurkat (-1.09 ± 1.14). However, nanaomycin A treatment had no significant effect on DNMT3B expression in A549 (0.21 ± 0.94) and MG-63 (0.19 ± 0.66) (***Fig 9.A***).

Decitabine treated IMR-90 and A549 cells showed significantly decreased DNMT1 expression (-1.80 ± 0.43 and -3.81 ± 1.22, p<0.001). MG-63 (-0.41 ± 0.87), SH-SY5Y (-0.86

± 1.17) and Jurkat cells (-1.08 ± 0.91) displayed reduced DNMT1 expression compared to untreated cells except for COV362 cells (0.36 ± 0.43). Overall, we noted that cancer cells exposed to decitabine showed decreased DNMT1 expression (***Fig 5.9.B***).

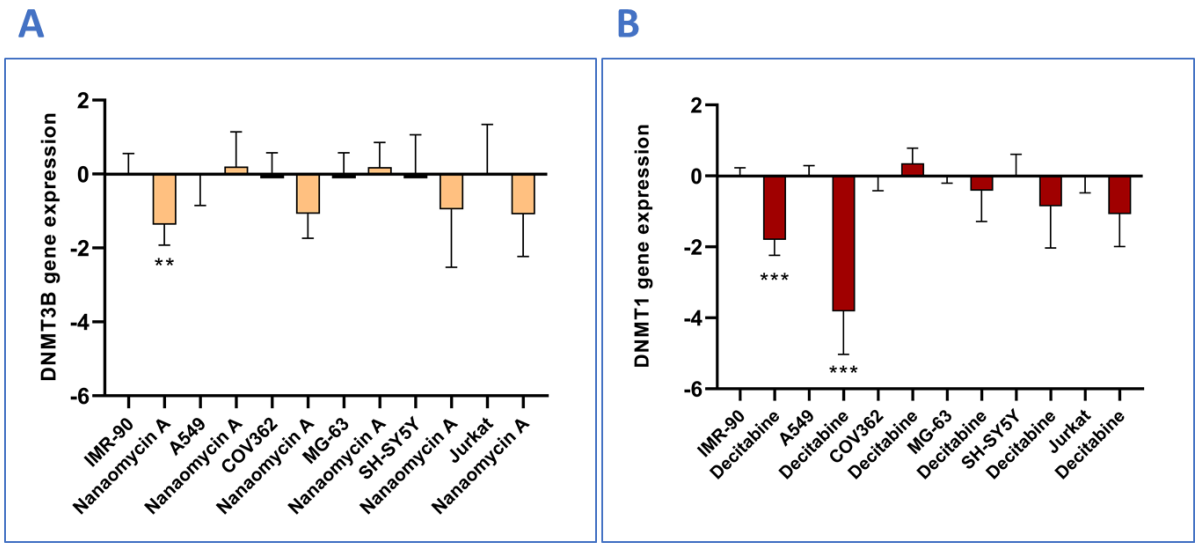

Figure 5.9. **DNMT3B and DNMT1 gene expression after nanaomycin A and decitabine treatment.** Cancer cells were cultured in 2% WKS. DNMT3B and DNMT1 expression normalised to the expression of GAPDH. Data are represented as mean ± standard deviation (SD). n=3, *p<0.05, **p<0.01, ***p<0.001 vs untreated control sample. The stars compare untreated cells to drug treatment.

5.2.7 Nanaomycin A significantly reduced methylation levels in cancer cells

After inhibition of DNMTs, we investigated TERT promoter methylation. We used the pyrosequencing method to determine the methylation level of five different regions (I, II, III, IV and V) of TERT promoter. We observed that IMR-90 somatic cells and ESCs were consistent and highly methylated in region I, while cancer cells displayed irregular methylation patterns on TERT promoter region I. In general, cancer cells represented irregular methylation patterns across all regions.

IMR-90 cells showed a significant decrease in methylation level in region I following nanaomycin A (76.58%, p<0.01) treatment versus untreated cells (83.17%). However,

decitabine (84%) had no significant effect on region I promoter methylation. A549 treated with nanaomycin A demonstrated reduced methylation in region I (48.17%, $p<0.001$) when compared to untreated cells (86.92%). Decitabine exposed A549 cells had no significant change in methylation in region I (79.67%). A significant decrease was also noted in the methylation level of region I after nanaomycin A exposure (53.92%, $p<0.01$) versus untreated SH-SY5Y cells (58.57%), and no difference in decitabine treated cells was noted (57.08%). Significantly lower methylation levels were observed after nanaomycin A (68.92%, $p<0.001$) or decitabine (69.92%, $p<0.001$) treatment versus untreated MG-63 (82.08%). Jurkat showed significantly reduced methylation on region I after either nanaomycin A (60.62%, $p<0.001$) and decitabine (59.83%, $p<0.001$) treatment versus untreated cells (73.33%). COV362 displayed no difference after nanaomycin A (73.08%) and decitabine (74.83%) treatment versus untreated cells (75.42%)**.** Overall, IMR-90, A549, MG-63, SH-SY5Y and Jurkat cells showed a decreased methylation after nanaomycin A treatment but not COV362 in region I. Only MG-63 and Jurkat represented reduced methylation after decitabine treatment in region I (***Fig 5.10.A, Table 5-1)***.

IMR-90 cells showed no difference in methylation levels of region II following nanaomycin A (41.44%) and decitabine (41%) treatment versus untreated cells (42.06%). A549 showed a significant decrease in methylation level in region II following nanaomycin A (52.94%, $p<0.001$) treatment versus untreated cells (68.56%), while decitabine treated cells (87.67%, $p<0.001$) had higher methylation levels in region II. Further, COV362 displayed a significant reduction in region II after nanaomycin A treatment (81.44%, $p<0.001$) but decitabine exposed cells (90.25%) had no significant difference versus untreated cells (90.22%). Similarly, significantly lower methylation levels were observed in SH-SY5Y exposed to nanaomycin A (29.67%, $p<0.001$) treatment versus untreated cells (40.56%) but not decitabine treated cells (40.39). MG-63 treated with nanaomycin A (76.38%, $p<0.001$) and decitabine (77.44%, $p<0.001$) demonstrated reduced methylation percentage in the region II when compared to untreated cells (91.28%). No significant change was noted in the methylation level of region II after nanaomycin A exposure (68.10%) and decitabine (78.33%) versus untreated Jurkat (73.32%). Overall, A549, COV362, MG-63 and SH-SY5Y showed a decreased methylation pattern after nanaomycin A treatment but not IMR-90 and Jurkat cells in region II. Only A549 and MG-63 represented reduced methylation after decitabine treatment in region II (***Fig 5.10.B, Table 5-1).***

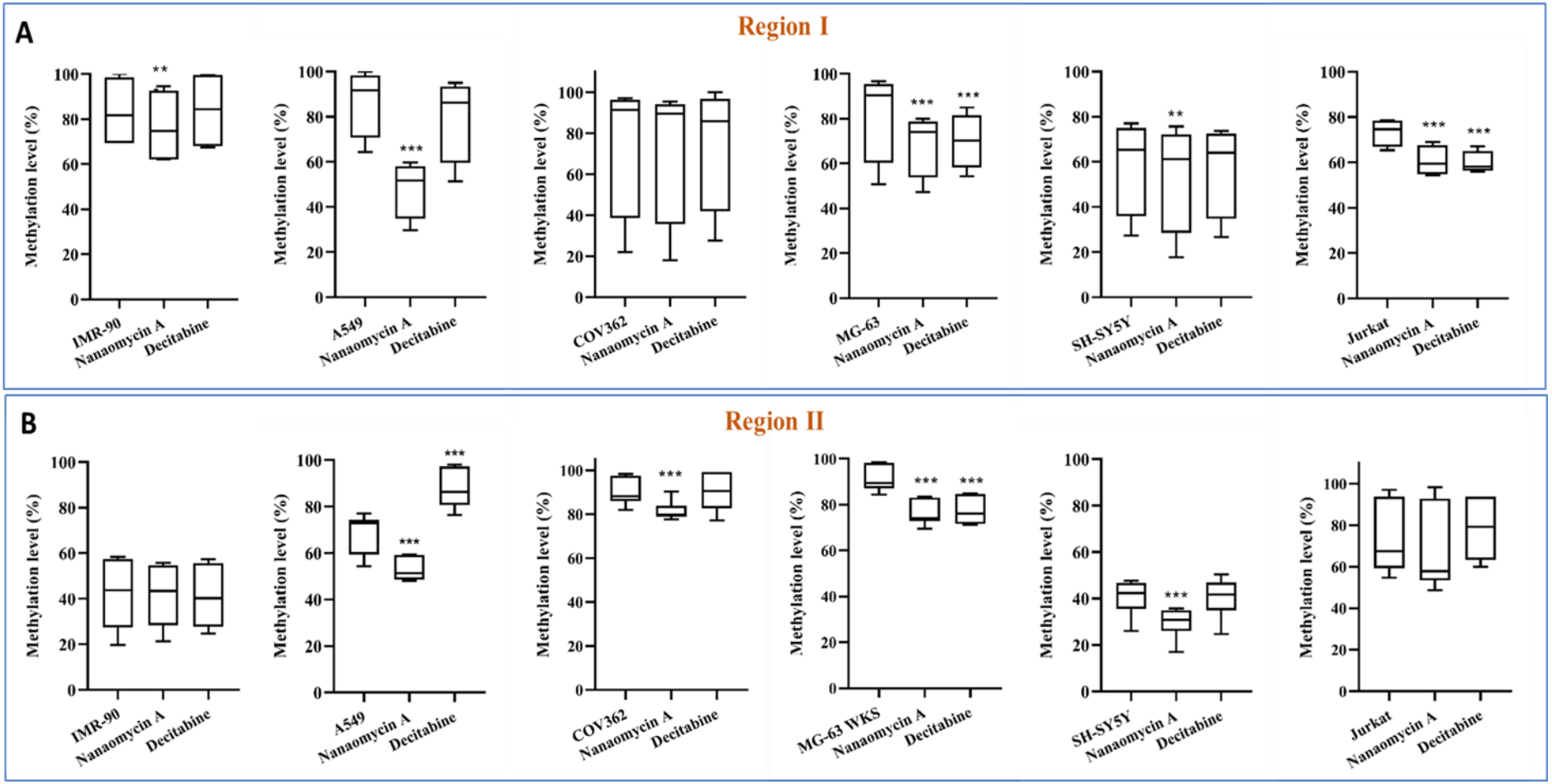

Figure 5.10. **Decreased methylation levels on TERT promoter after nanaomycin A treatment in cancer cells cultured in 2% WKS.** Different promoter regions **(A**, region I and **B,** region II) relative to TSS were evaluated using pyrosequencing. The median value of methylation was represented in the box and violin graph. Y-axis indicates DNA methylation level (%) at CpG sites, and X-axis represents the name of cells. Data presented as median (min-max) ± SD. n=3, *p<0.05, **p<0.01, ***p<0.001. The stars compare untreated cells to drug treatment.

Region III on TERT promoter was hypomethylated in IMR-90, and there was no significant change in methylation level following nanaomycin A treatment (6.80%). Still, higher methylation was noted after decitabine treatment (9.67%, $p<0.05$) versus control IMR-90 cells (7.33%). A549 showed a significant decrease in methylation level of region III following nanaomycin A (45.07%, $p<0.001$) and decitabine (67.47%, $p<0.01$) treatment versus untreated cells (81.27%). COV362 displayed a significant reduction after nanaomycin A (73.87%, $p<0.001$) and decitabine exposure (82.30%, $p<0.01$) when compared to untreated cells (86.20). Similarly, MG-63 treated with nanaomycin A (36.60%, $p<0.001$) and decitabine (46.10%, $p<0.01$) demonstrated reduced methylation in region III when compared to untreated cells (56.08%). SH-SY5Y exposed to nanaomycin A (18.20%, $p<0.001$) displayed a lower methylation level than in untreated cells (22.47%), while decitabine treated cells were unchanged (21.80%). A significant decrease was also noted in the methylation level of region III after nanaomycin A exposure (75.75%, $p<0.001$) in Jurkat when compared to untreated cells (87.90%), while decitabine (85.80%) induced no significant change versus control. Overall, A549, COV362, MG-63, SH-SY5Y and Jurkat showed a decreased methylation pattern after nanaomycin A treatment but not IMR-90 in region III. IMR-90 represented increased methylation, but A549, COV362 and MG-63 indicated a decreased methylation pattern after decitabine treatment in region III (***Fig 5.11.A, Table 5-1)***.

IMR-90 showed a significant decrease in methylation levels in the region IV following nanaomycin A (6.13%, $p<0.001$) versus untreated cells (10.79%), while there was an increase in methylation after decitabine (15.21%, $p<0.01$) treatment. Also, COV362 displayed a significant decrease in methylation levels after nanaomycin A (15.50%, $p<0.001$), but decitabine treated cells showed an increase (27.69%, $p<0.01$) versus untreated cells (23.67%) on the promoter region IV. However, nanaomycin A treated A549 (6.54%) had no significant change in region IV promoter methylation versus control cells (7%), while decitabine exposed A549 displayed higher methylation (9%, $p<0.01$). MG-63 had significantly lower methylation levels after nanaomycin A (23%, $p<0.001$) treatment versus untreated cells (42.66%) and no difference in decitabine exposed cells (41.63). Further, a significant decrease was noted in methylation level after nanaomycin A exposure (15%, $p<0.001$) versus untreated SH-SY5Y (27.71%) and no difference was observed again in decitabine exposed cells (29.63%). On the other hand, Jurkat displayed a significant decrease in methylation levels after nanaomycin A (71.71%, $p<0.001$) and decitabine (76.80%, $p<0.05$) treatment versus untreated cells (82.38%, respectively) on the promoter region IV. Overall, IMR-90, COV362, MG-63, SH-SY5Y and

Jurkat showed a decreased methylation pattern after nanaomycin A treatment but not A549 in region IV. IMR-90, A549 and COV362 represented increased methylation, but Jurkat showed a decreased methylation pattern after decitabine treatment in region IV (***Fig 5.11.B, Table 5-1).***

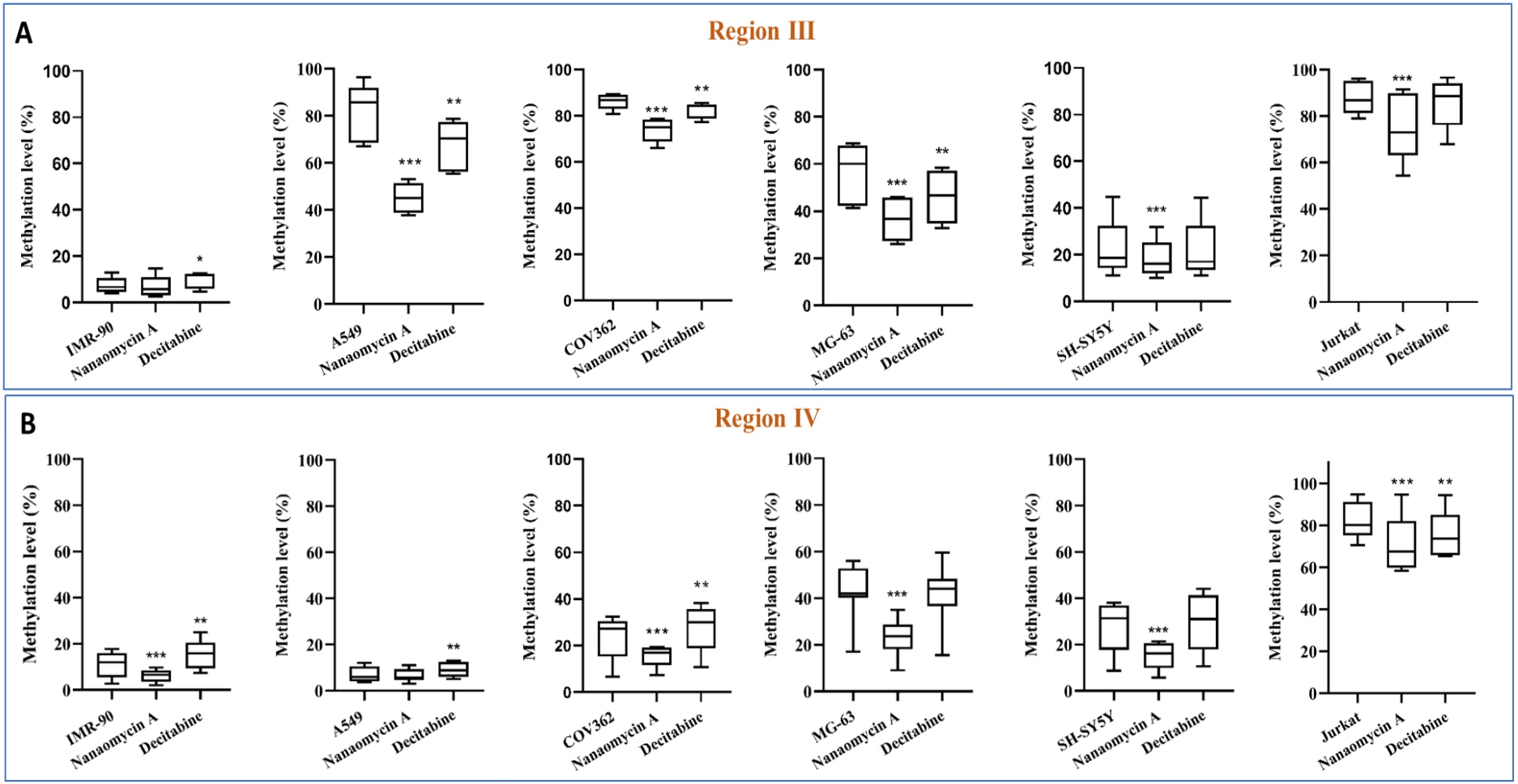

Figure 5.11. **Decreased methylation levels on TERT promoter after nanaomycin A treatment in cancer cells cultured in 2% WKS.** Different promoter regions **(A**, region III and **B,** region IV) relative to TSS were evaluated using pyrosequencing. The median value of methylation was represented in the box and violin graph. Y-axis indicates DNA methylation level (%) at CpG sites, and X-axis represents the name of cells. Data presented as median (min-max) ± SD. n=3, *p<0.05, **p<0.01, ***p<0.001. The stars compare untreated cells to drug treatment.

Region V was less methylated after nanaomycin A treatment (8.72%, $p<0.05$) in IMR-90 versus control cells (12.79), while a higher methylation level was noted following decitabine treatment (16.89%, $p<0.01$). A549 showed no difference in methylation level at region V following nanaomycin A (5.17%) treatment, but there was a significant increase in methylation level after decitabine treatment (7.33%, $p<0.01$) when compared to control (4.61%). Further, COV362 displayed a significant reduction after nanaomycin A treatment (7.67%, $p<0.05$) but decitabine exposed cells (13.61%, $p<0.05$) had a higher methylation percentage at region V versus untreated cells (10.28). Similarly, SH-SY5Y had significantly lower methylation levels following nanaomycin A (18.8%, $p<0.001$) and higher methylation levels after decitabine treatment (47.06%, $p<0.001$) than untreated cells (32.72%). MG-63 treated with nanaomycin A (14.33%, $p<0.001$) demonstrated reduced methylation percentage at region V when compared to untreated cells (24.5%), and no significant change was noted in methylation level after decitabine exposure (27.5%). A significant decrease was reported in the methylation level of region V after nanaomycin A exposure (42.83%) versus untreated Jurkat cells (69.72%), but no difference was observed in decitabine exposed cells. Overall, IMR-90, COV362, MG-63, SH-SY5Y and Jurkat showed a decreased methylation pattern after nanaomycin A treatment but not A549 in region V. IMR-90, A549, COV362 and SH-SY5Y represented increased methylation after decitabine treatment in region V (***Fig 5.12.A, Table 5-1)***.

Lastly, pooled data from these five TERT promoter regions indicated that IMR-90 had no significant change on promoter methylation levels after nanaomycin A (23.80%) and decitabine (29.43%) treatment versus untreated cells (26.72%). A549 displayed a significant reduction after nanaomycin A (28.24%, $p<0.01$) and no significant change in methylation levels following decitabine treatment (44.75%) versus control (43.07%). Similar to above, we observed a significant decrease in methylation levels of TERT promoter following nanaomycin A (41.06%, $p<0.05$) treatment versus untreated COV362 (52.38%) and no difference in decitabine treated samples (53.66%). Further, MG-63, SH-SY5Y and Jurkat cells displayed a significant reduction after nanaomycin A (40.93%, 24.68% and 65.20% $p<0.001$) treatment when compared to untreated cells (56.16%, 34.78% and 78.25%), but no significant difference was noted in decitabine treated cells (50.78%, 37.90% and 73.92%), respectively. Pooled data showed that A549, COV362, MG-63, SH-SY5Y and Jurkat showed a decreased methylation pattern after nanaomycin A treatment but no significant change after decitabine treatment. IMR-90 displayed no significant change after both drug treatments (***Fig 5.12.B***).

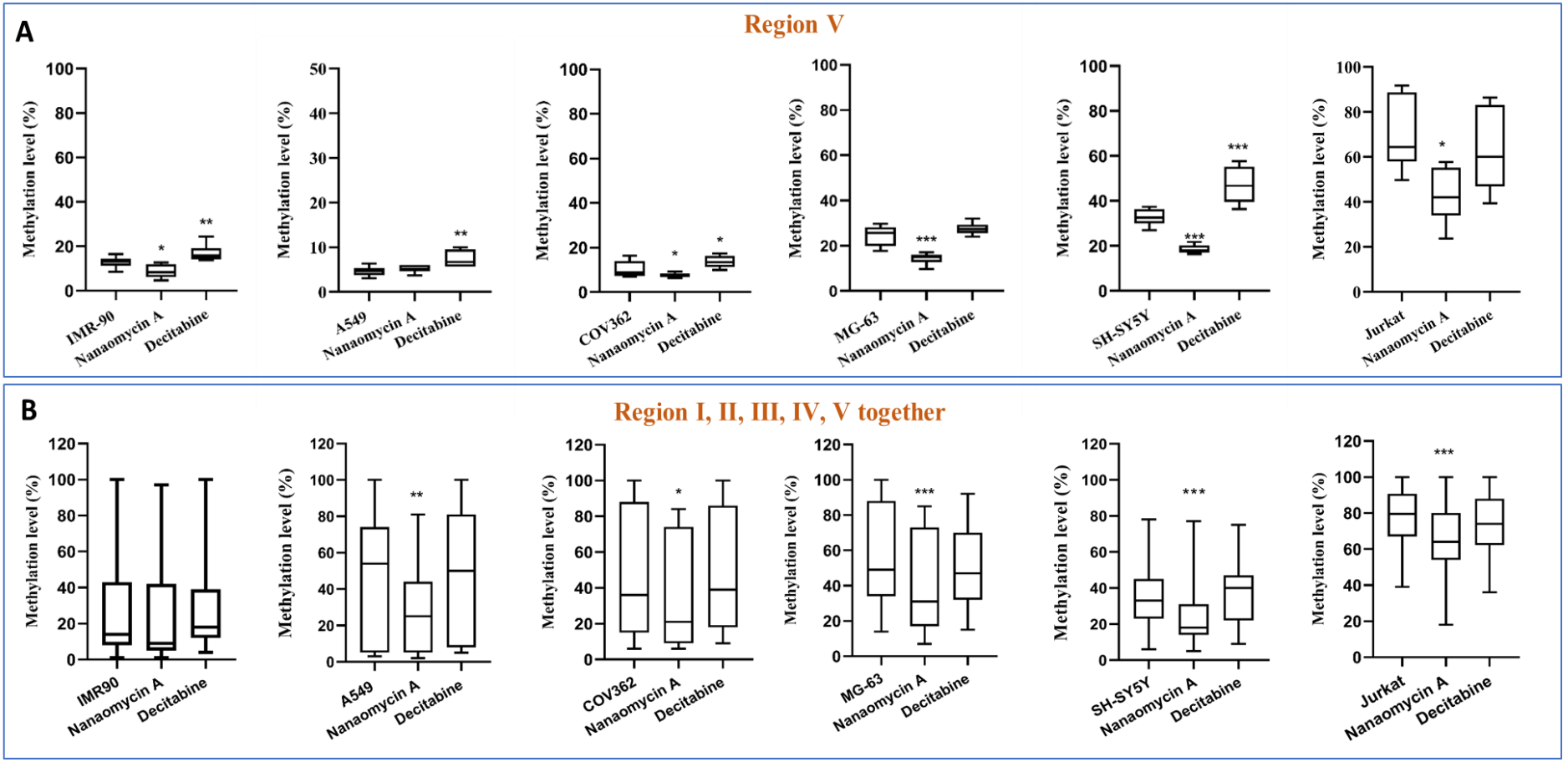

Figure 5.12. **Decreased methylation levels on TERT promoter after nanaomycin A treatment in cancer cells cultured in 2% WKS.** Different promoter regions **(A)** (region V) and **(B) (**all regions together) relative to TSS were evaluated using pyrosequencing. The median value of methylation was represented in the box and violin graph. Y-axis indicates DNA methylation level (%) at CpG sites, and X-axis represents the name of cells. Data presented as median (min-max) ± SD. n=3, *p<0.05, **p<0.01, ***p<0.001. The stars compare untreated cells to drug treatment.

Table 5-1. **The methylation levels of TERT promoter in cancer cells cultured in 2% WKS.** The columns representing different promoter regions (region I and II, III, IV and V relative to TSS were evaluated using pyrosequencing. The percentage of methylation (%) at CpG sites was represented in individual boxes. Data were presented as mean ± SD. n=3, *p<0.05, **p<0.01,***p<0.001. The stars compare untreated cells to drug treatment.

Cell Type	Region I	Region II	Region III	Region IV	Region V
IMR-90	83.17	42.06	7.33	10.79	12.79
Nanaomycin A	** 76.58	41.44	6.80	*** 6.13	* 8.722
Decitabine	84	41	* 9.67	** 15.21	** 16.89
A549	86.92	68.56	81.27	7.00	4.611
Nanaomycin A	*** 48.17	*** 52.94	*** 45.07	6.54	5.167
Decitabine	79.67	*** 87.67	** 67.47	** 9	** 7.33
COV362	75.42	90.22	86.20	23.67	10.28
Nanaomycin A	73.08	*** 81.44	*** 73.87	*** 15.5	* 7.667
Decitabine	74.83	90.25	** 82.3	** 27.69	* 13.61
MG-63	82.08	91.28	56.08	42.66	24.5
Nanaomycin A	*** 68.92	*** 76.38	*** 36.60	*** 23.00	*** 14.33
Decitabine	*** 69.92	*** 77.44	** 46.1	41.63	27.5
SH-SY5Y	58.75	40.56	22.47	27.71	32.72
Nanaomycin A	*** 53.92	*** 29.67	*** 18.20	***15.00	*** 18.5
Decitabine	57.08	40.39	21.80	29.63	*** 47.1
Jurkat	73.33	73.32	87.90	82.38	69.72
Nanaomycin A	*** 60.62	68.10	*** 75.75	*** 71.71	* 42.83
Decitabine	*** 59.83	78.33	85.8	** 76.8	62.83

5.2.8 Nanaomycin A treated cancer cells display higher telomerase activity and TERT expression

We next evaluated telomerase activity in drug-treated cancer and somatic cells cultured in 2% WKS conditions. IMR-90 showed the lowest telomerase activity compared to cancer cells. Nanaomycin A treated IMR-90 (2.82 ± 0.02, p<0.01) demonstrated a higher telomerase activity when compared to untreated cells in 2% WKS (2.12 ± 0.61). No significant change was noted for decitabine treated IMR-90 cells (2.10 ± 0.07). A549 showed no significant difference after nanaomycin A (4.78 ± 0.06) and decitabine treatment (4.50 ± 0.7) versus untreated cells (4.77 ± 0.17). COV362 displayed a higher telomerase activity after nanaomycin A treatment (5.38 ± 0.04, p<0.01) compared to untreated cells (4.65 ± 0.55), but decitabine treated cells (4.74 ± 0.11) showed no significant difference in 2% WKS. Only MG-63 treated with nanaomycin A (4.91 ± 0.06, p<0.05) and decitabine (4.94 ± 0.04, p<0.05) displayed higher telomerase activity compared to untreated cells (4.51 ± 0.33). In contrast above, decitabine treated SH-SY5Y showed decreased telomerase activity (4.30 ± 0.22, p<0.05) while nanaomycin A treated cells still had a significantly high telomerase activity (4.98 ± 0.22, p<0.15) in comparison to

untreated cells (4.68 ± 0.30). Also, we noted lower telomerase activity in decitabine treated Jurkat cells (4.51 ± 0.11) in 2% WKS when compared to control cells (5.15 ± 0.60) while there was no change in nanaomycin A treated cells (5.39 ± 0.15) (***Fig 5.13.A*)**. We also used heat-treated samples as an internal control for IMR-90 (1.26 ± 0.17), A549 (1.10 ± 0.49), COV362 (1.32 ± 0.18), MG-63 (1.02 ± 0.21), SH-SY5Y (1.42 ± 0.24), and Jurkat (0.92 ± 0.17) in this assay (***Fig 5.13.A)***.

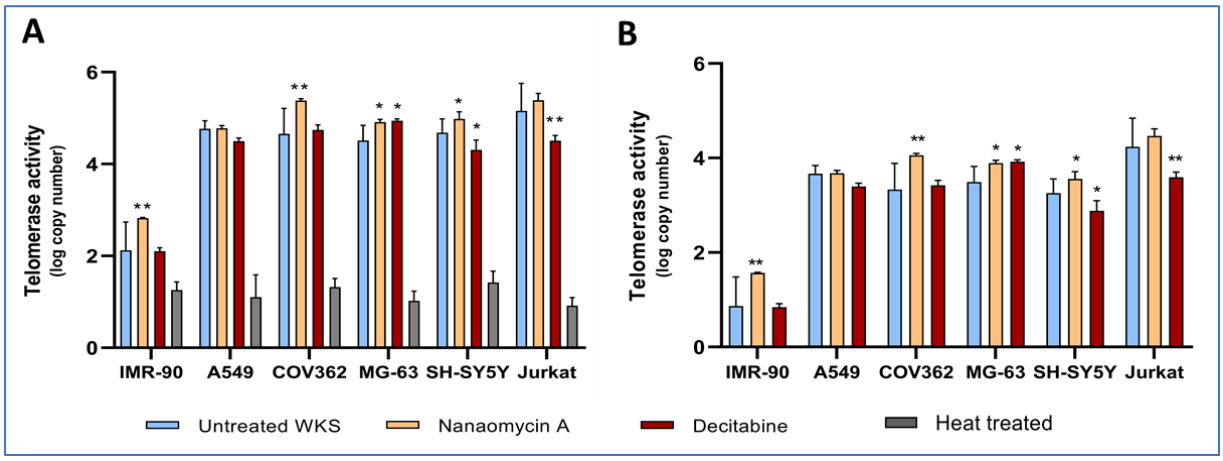

Figure 5.13. **Increased telomerase activity in nanaomycin A treated cancer cells.** Cancer and somatic cells were treated with nanaomycin A and decitabine in physiological oxygen condition (2% WKS) for seven days. (**A**) Real-time PCR data is represented with HT (heat-treated) control samples. (**B**) Data is normalised to HT samples. Data are represented as mean ± standard deviation (SD), n=3, *p<0.05, **p<0.01, ***p<0.001. The stars compare untreated cells to drug treatment.

Similar to telomerase activity, we noted increased TERT gene expression in nanaomycin A treated cancer cells except A549. Nanaomycin A exposed IMR-90, COV362, MG-63, SH-SY5Y and Jurkat cells (1.09 ± 0.58, 1.14 ± 0.60, 0.84 ± 0.43, 1.12 ± 0.51 and 1.14 ± 0.77, p<0.01) cells displayed significantly increased TERT expression. Further, we noted slightly decreased TERT expression after decitabine treatment in IMR-90 (-0.20 ± 0.70), COV362 (-0.66 ± 0.54) and Jurkat cells (-0.79 ± 1.54) while slightly increased TERT expression in MG-63 (0.69 ± 0.36, p<0.05) and SH-SY5Y (0.44 ± 0.77) versus control cells (***Fig 5.14)***.

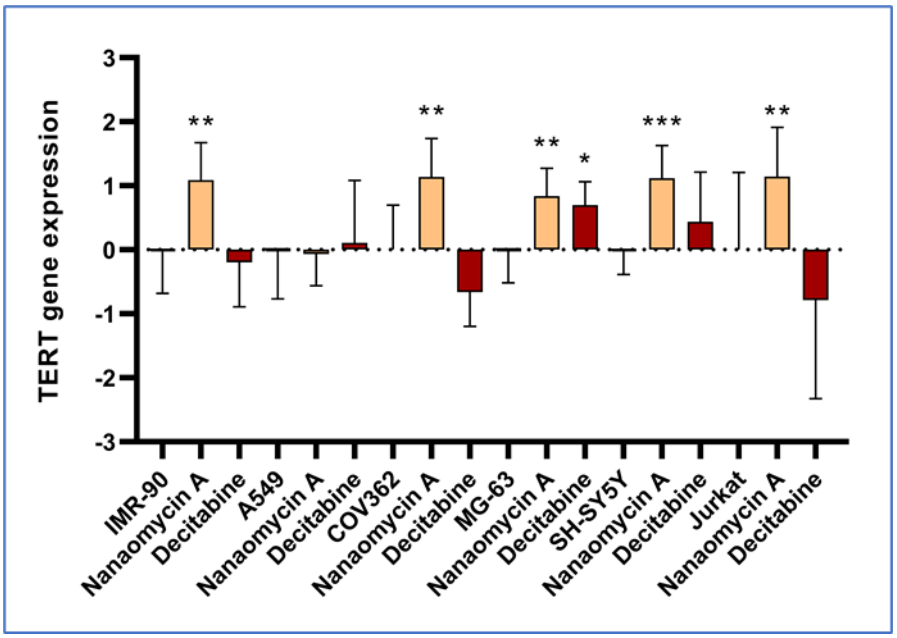

Figure 5.14. **Decreased TERT gene expression after nanaomycin A and decitabine treatment.** Cancer cells were cultured in 2% WKS. TERT expression normalised to the expression of GAPDH. The orange column indicates nanaomycin A treated samples, and the red column shows decitabine treated samples. Data are represented as mean ± standard deviation (SD). n=3, *p<0.05, **p<0.01, ***p<0.001 vs untreated control sample. The stars compare untreated cells to drug treatment.

5.2.9 Binding of DNMT3B Antibody on TERT promoter region using CHIP (Chromatin immunoprecipitation) qPCR in COV362 Cancer cell

We next performed CHIP to examine DNMT3B-induced TERT promoter methylation in differentiated COV362 cells in 2% WKS. Following the protocol described in the method chapter (***chapter 2.17, Page 75***), the immunoprecipitated DNA after DNMT3B antibody treatment was detected by qPCR. CHIP results suggested that nanaomycin A decreased DNMT3B binding at TERT promoter in COV362 cells. We performed qPCR for different regions of TERT promoter (regions II, III, IV and V). Region I was omitted due to high methylation levels in cancer cells such as COV362 and ESCs. From previous data (***chapter 3, Fig 3.23, page 133 and chapter 4, Fig 4.25, page 206***), region I distal TERT promoter region has no significant contribution to TERT gene regulation. Therefore, we designed primers for proximal promoter regions for ChIP experiments.

DNMT3B binding to region II was significantly decreased in nanaomycin A treated (2.14 ± 0.62, $p<0.001$) COV362 versus control untreated cells (3.83 ± 0.35). We noted a similar reduction in DNMT3B binding at region III (3.00 percentage of 0.49, $p<0.05$) after nanaomycin A exposure for seven days versus untreated cells (3.69 ± 0.34). We also noted a significant reduction after nanaomycin A treatment at region IV (1.03 ± 0.23, $p<0.001$) compared to control (1.76 ± 0.29). Nanaomycin treated cells (1.03 ± 0.23, $p<0.01$) showed decreased DNMT3B binding on the promoter compared to control samples (2.07 ± 0.42) at region V. In addition, more DNMT3B binding to TERT promoter was noted in regions II and III than in regions IV and V (***Fig 5.15***). The fold enrichment of DNMT3B on TERT promoter was consistent with previously calculated methylation percentage in these regions (***Table 5-1***). There was a higher DNMT3B binding and methylation at the regions II and III. In contrast, less DNMT3B binding was noted at regions IV and V consistent with less methylation.

Pooled data from all regions showed that there was a significant reduction (1.85 ± 0.84, $p<0.001$) in DNMT3B binding to the TERT proximal promoter region after nanaomycin A treatment compared to control (2.92 ± 1.01). GAPDH (5.28 ± 0.26) was included as an internal control for ChIP experiments.

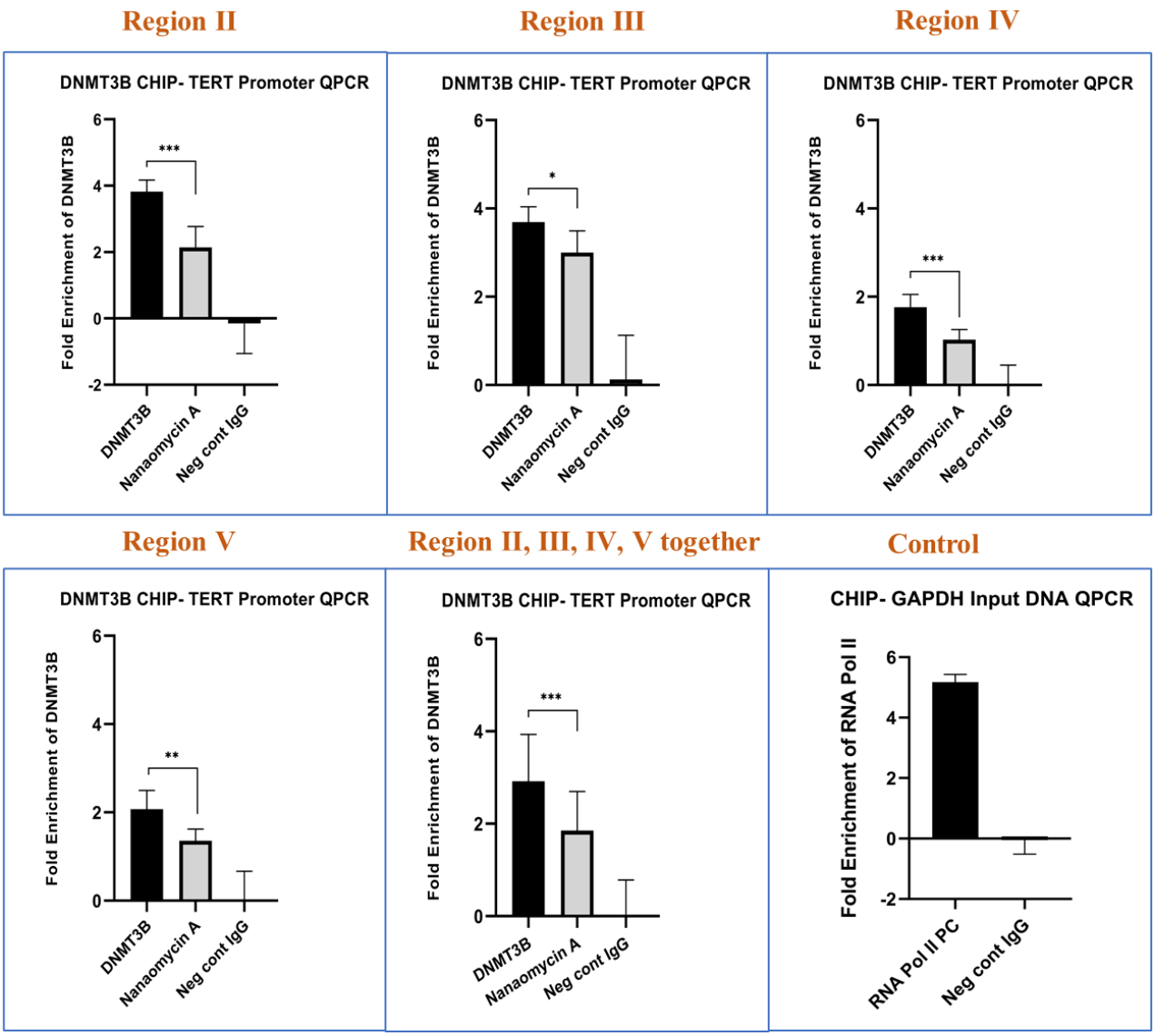

Figure 5.15. **Decreased DNMT3B binding on TERT promoter regions after nanaomycin A treatment.** DNMT3B binding was assessed using the CHIP (Chromatin immunoprecipitation) qPCR tool. Primers were designed for regions II, III, IV, V, and we also analysed the data pooled from all regions. Positive control RNA pol II and negative isotype control were indicated. Data are represented as mean ± standard deviation (SD). n=3, *p<0.05, **p<0.01, ***p<0.001 vs untreated cells in 2% WKS.

ATRA treated HL-60 cells can differentiate into monocytes

HL-60 can differentiate into monocytes, and TERT promoter activity decreases rapidly following the loss of telomerase activity during differentiation (Dongmei and Yuan, 2003). All-trans-retinoic acid (ATRA) initiates granulocyte-like cell differentiation in HL60. We used HL-

60 differentiation as a model to explore promoter methylation changes associated with downregulated telomerase during cancer cell differentiation and to determine if previously identified changes in the hESC model were consistent or not. Firstly, we confirmed the differentiation of HL60 utilising expression of CD11b as a marker (***Fig 5.16.A)***. We compared differentiation in both 21% AO and 2% WKS to compare the effect of the oxygen microenvironment. Different concentrations of ATRA were considered to determine the optimal concentration for differentiation experiments. CD11b expression was was noted as 85.93% and 86.30% in 21% AO, also, 78.62% and 77.72% in 2% WKS after 1 µM and 2 µM ATRA treatments compared to isotype control (26.98 ± 6.70 and 10.81 ± 0.05), respectively. We noted the highest percentage of CD11b positive events with a 5 µM concentration of ATRA in 21% AO and 2% WKS (89.67 ± 8.89 and 89.00 ± 3.77) compared to isotype control. Finally, we determined that positive events were 82.22% and 80.28% with 8µM ATRA supplementation in 21% AO and 2% WKS, respectively. We determined 5uM ATRA as optimal for HL-60 differentiation (***Fig 5.16.B)***.

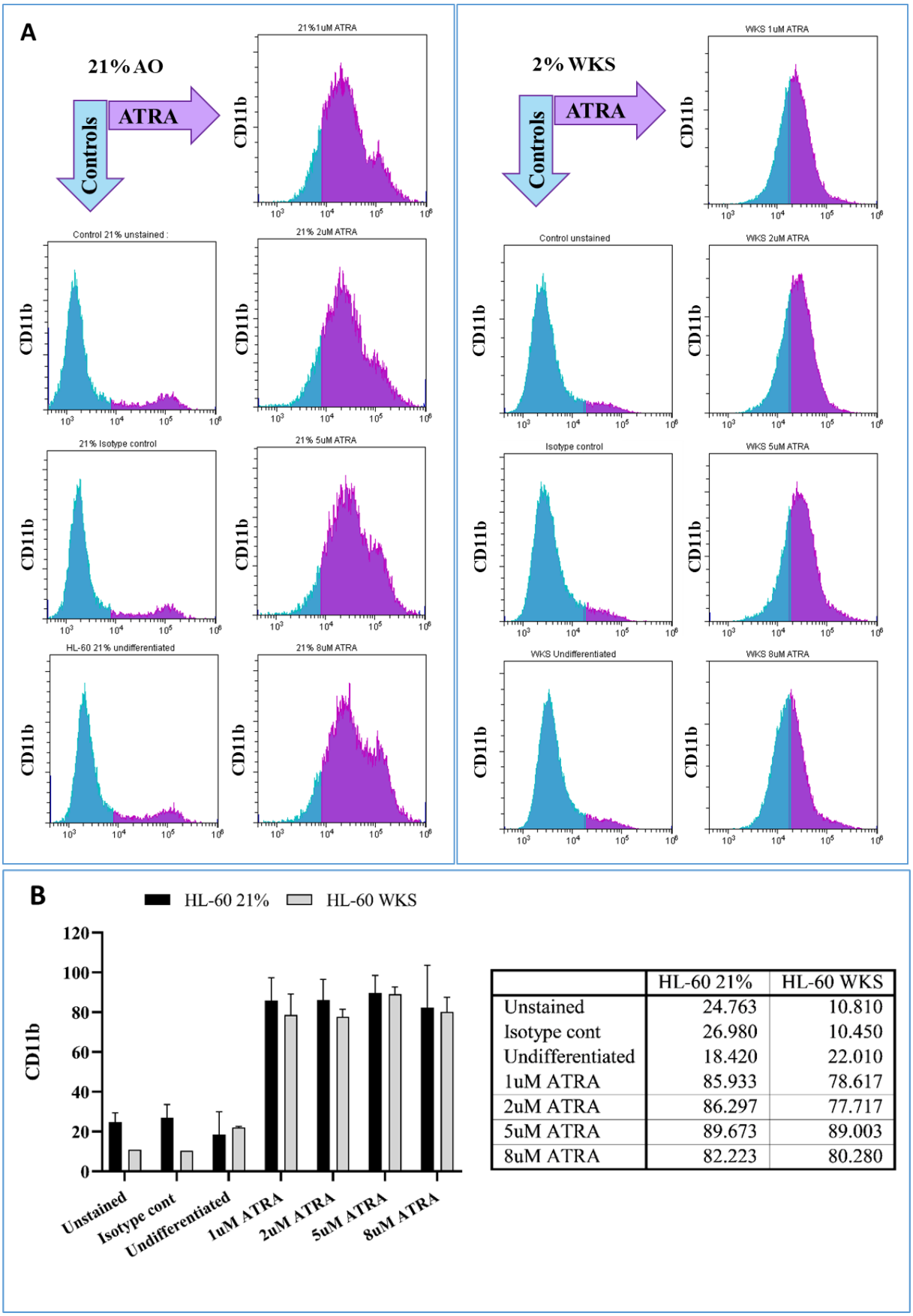

	HL-60 21%	HL-60 WKS
Unstained	24.763	10.810
Isotype cont	26.980	10.450
Undifferentiated	18.420	22.010
1uM ATRA	85.933	78.617
2uM ATRA	86.297	77.717
5uM ATRA	89.673	89.003
8uM ATRA	82.223	80.280

Figure 5.16. **Increased CD11b cell surface marker in HL-60 cells after ATRA treatment.**

CD11b was quantified by flow cytometry in ATRA differentiated HL-60 cells cultured under

21% AO and 2% WKS. **A)** Overlay histograms of HL-60 cells from Flowing Software. **B)** The percentage of positive events was quantified relative to the relevant isotype control (IgG2b) and data represented in a bar graph. ATRA treated samples were positive for CD11b marker after each experiment at both oxygen tensions (21% AO and 2%WKS). The X-axis indicates % of positive events. Data are presented as mean ± standard deviation (SD), n=3.

Induction of morphological differentiation with ATRA in HL-60 cells

Typically, HL-60 possess large round nuclei, but cells develop myelocyte and granulocytic nuclear segmentation following ATRA-induced differentiation. HL-60 cells acquired segmented, polymorphological nuclei after five days of differentiation (***Fig 5.17***). We counted those granulated and segmented nuclei after differentiation and compared them to round large nuclei numbers, which represent undifferentiated HL-60 cells. A total of 250 nuclei were quantified in a minimum of three fields to do statistical analyses. Segmented and polymorphological nuclei were counted as differentiated (155 and 160 nuclei) after ATRA treatment compared to regular round nuclei (95 and 90 nuclei) in 21% AO and 2% WKS, respectively (***Fig 5.18***). There was a significantly high number of segmented nuclei in 21% AO and 2% WKS ($p<0.05$) after ATRA treatment, but no significant difference was observed between conditions.

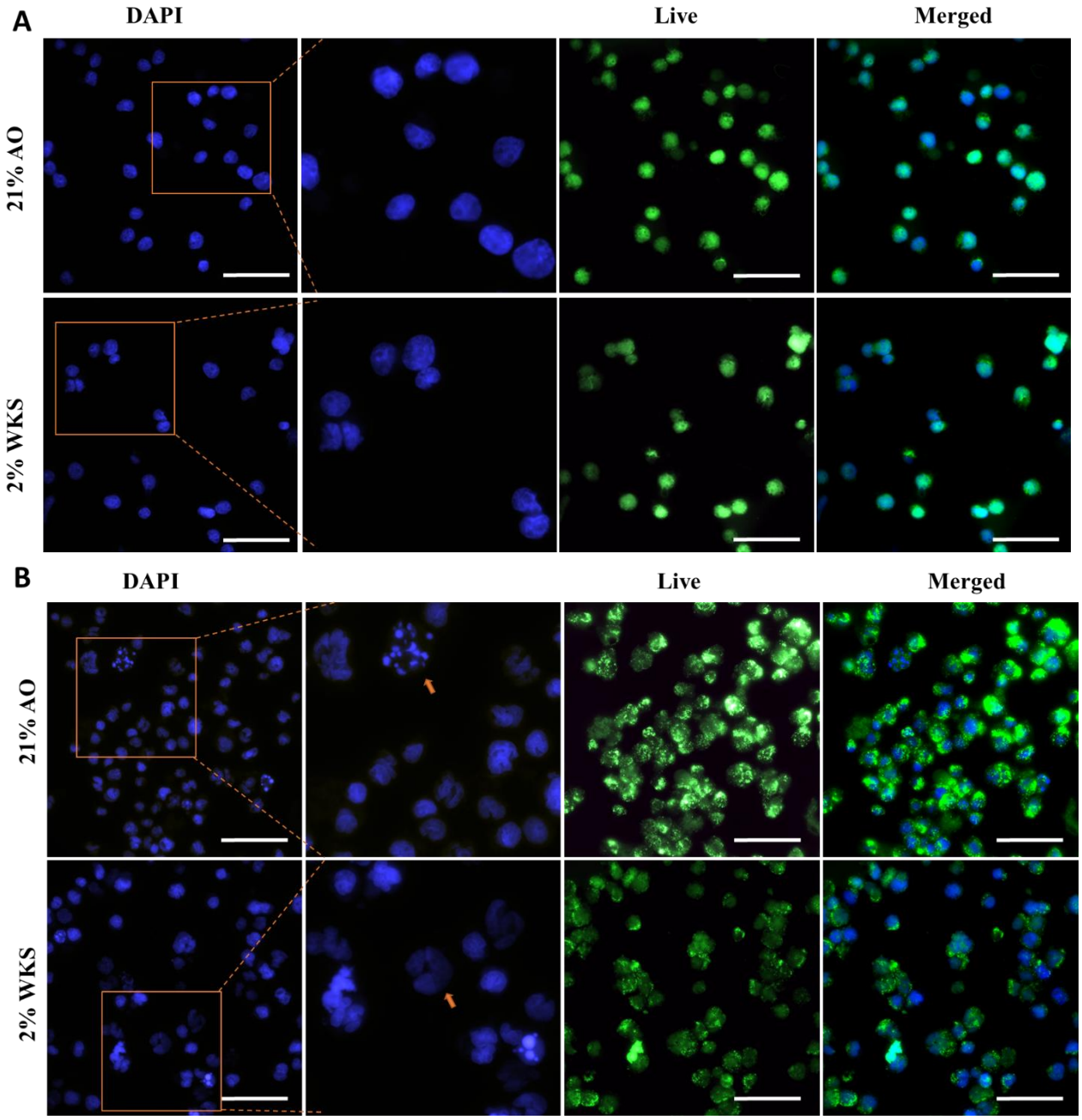

Figure 5.17. **ATRA treatment induces myeloid differentiation and illustrates distinct nuclei morphology in HL-60 cells.** Nuclei staining with DAPI in undifferentiated HL-60 cell **(A).** Induction of morphological differentiation with ATRA in HL-60 cells after five days of differentiation **(B).** The green colour represents live cells, and orange arrows show an example of segmented nuclei. The scale bar represents 50 μm, 20X and 40X objectives were used. The green colour indicates live cells, and blue represents DAPI. Images are representative of three independent samples.

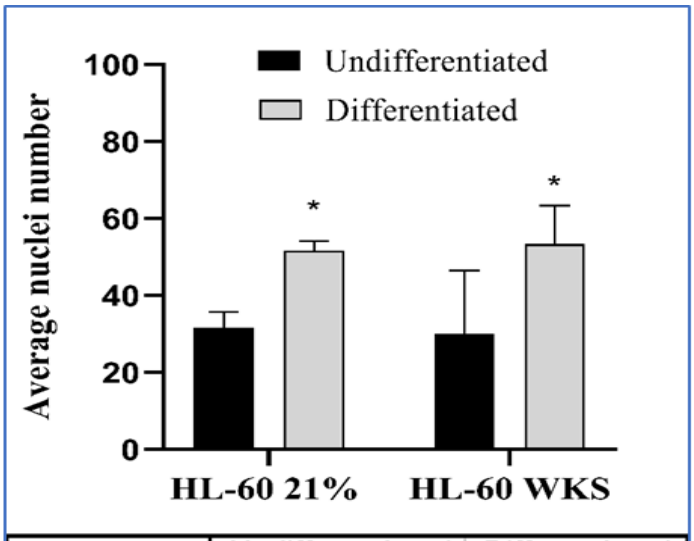

	Undifferentiated	Differentiated
HL-60 21%	95	155
HL-60 WKS	90	160

Figure 5.18. **Many segmented or polymorphological nuclei were observed after ATRA treatment with no significant difference between conditions.** Segmented and polymorphological nuclei were quantified after differentiation of HL-60 cells using ATRA. The total nuclei count was 250 in minimum of three independent field views to do statistical analyses for each oxygen tension.

5.2.10 Differentiated HL-60 display downregulated telomerase activity and TERT expression

The level of telomerase activity in HL-60 cultured in 2% WKS (5.21 ± 0.53, $p<0.001$) was significantly higher than 21% AO (4.47 ± 0.23). Following ATRA treatment, no difference was noted between oxygen conditions. There was a decrease in telomerase activity after seven days of ATRA treatment in 21% AO and 2% WKS conditions (4.49 ± 0.21 and 4.77 ± 0.19). A similar decrease in telomerase activity was noted in 21% AO and 2% WKS after 10 (3.89 ± 0.21 and 4.07 ± 0.12, $p<0.001$) and 20 days (4.13 ± 0.14 and 3.94 ± 0.23, $p<0.01$) of ATRA treatment. Nanaomycin A exposed HL-60 cells showed higher telomerase activity in 21% AO and 2% WKS (5.01 ± 0.35 and 5.46 ± 0.07, $p<0.01$, respectively). However, ATRA/nanaomycin A treated cells showed significantly lower telomerase activity at days 5, 10, and 20 ($p<0.01$) in 21% AO (4.17 ± 0.16, 4.18 ± 0.42, and 4.22 ± 0.20) and 2% WKS (4.23 ± 0.15, 4.10 ± 0.14, and 4.13 ± 0.20), respectively (***Fig 5.19.A)***.

TERT gene expression was analysed with qRT-PCR in HL-60 to investigate the effects of ATRA, nanaomycin A, and physoxia. Relative TERT expression was higher in undifferentiated HL-60 cultured in 2% WKS (2.01 ± 0.82, $p<0.01$) in comparison to 21% AO. ATRA treated HL-60 cultured in 2% WKS (0.56 ± 0.98, $p<0.001$ and -0.33 ± 0.91, $p<0.01$) displayed significantly higher telomerase expression compared to 21% AO (-1.72 ± 1.52 and -2.02 ± 1.32) at days 10 and 20, respectively. Further, ATRA treated HL-60 demonstrated downregulated TERT expression correlated to telomerase activity at day 5 ($p<0.01$), 10, and 20 ($p<0.001$). On the other hand, Nanaomycin treatment increased TERT expression ($p<0.001$) in both 21% AO and 2% WKS conditions (2.31 ± 1.14 and 3.25 ± 0.97). Lastly, there was no significant change in TERT expression in HL-60 cells treated with ATRA/nanaomycin A (***Fig 5.19.B)***.

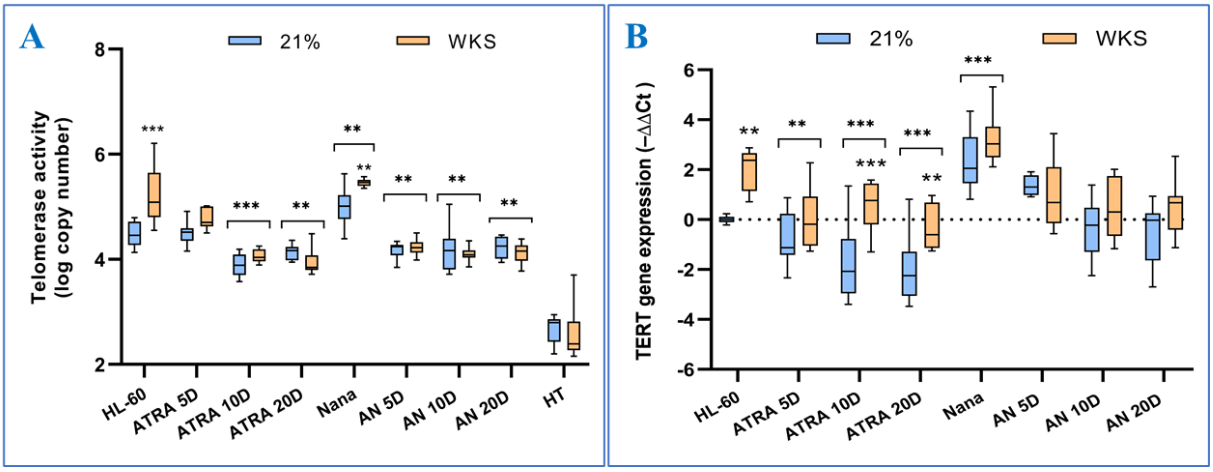

Figure 5.19. **Decreased telomerase activity and TERT expression after differentiation with ATRA.** HL-60 cells were treated with ATRA for differentiation and nanaomycin A in physiological oxygen condition (2% WKS). Real-time PCR data are represented as mean ± standard deviation (SD), n=3, *p<0.05, **p<0.01, ***p<0.001. HT (heat-treated control samples). Bars with stars indicate a significant difference between differentiated and undifferentiated cells. The other stars compare untreated cells to drug treatment.

5.2.11 Differentiated HL-60 display decreased DNMT3B expression with Nanaomycin A treatment

RT-qPCR was performed to examine the changes in the expression of DNMT3B after ATRA/nanaomycin A treatment in HL-60. Undifferentiated cells cultured in physoxia had higher DNMT3B expression (1.73 ± 0.86, $p<0.01$) than air oxygen tension (0.01 ± 0.85).

DNMT3B expression was downregulated in both conditions after differentiation at days 10 (-1.80 ± 1.11 and -0.45 ± 1.74, p<0.001) and 20 (-2.74 ± 0.61 and -2.72 ± 1.29, p<0.01) with no significant difference between conditions. Moreover, nanaomycin A treated cells displayed significantly decreased DNMT3B expression (-1.27 ± 0.81 and -0.64 ± 0.80, p<0.001). Noteworthy, an ATRA/nanaomycin A combination decreased DNMT3B expression significantly (-2.01 ± 1.21 and -1.07 ± 1.65, p<0.001) versus only ATRA treated HL-60 cells at day 5 (0.29 ± 0.96 and 0.95 ± 0.87). There was also reduced gene expression in ATRA/nanaomycin A treated cells at days 10 (-1.64 ± 0.90 and -1.19 ± 1.46, p<0.001) and 20 (-4.04 ± 0.85 and -3.82 ± 0.78, p<0.001) in both 21% and 2% WKS, respectively. HL-60 showed the lowest DNMT3B expression after 20 days of culture with ATRA/nanaomycin A (***Fig 5.20)***.

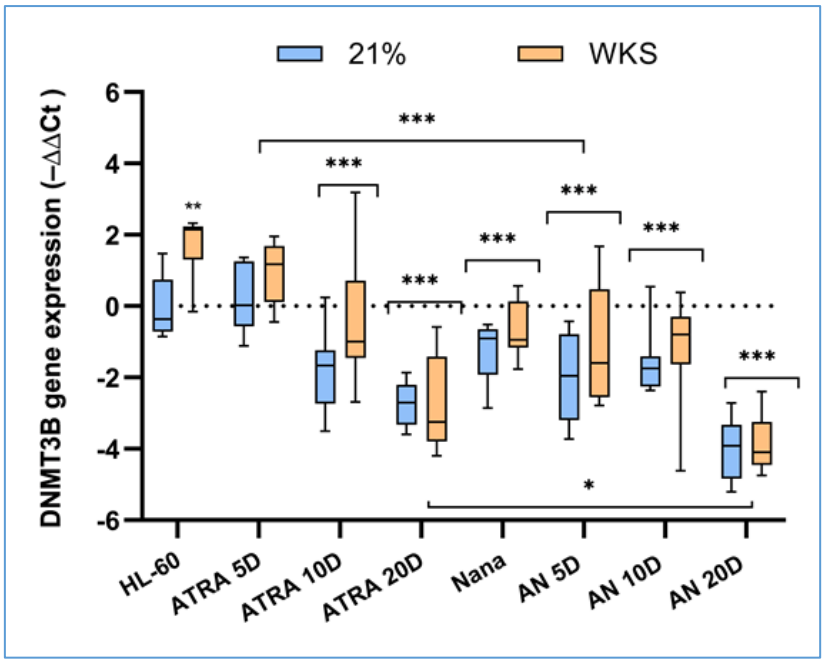

Figure 5.20. **DNMT3B gene expression after ATRA and nanaomycin A treatment.** HL-60 cells were cultured in 21% AO and 2% WKS. DNMT3B expression normalised to the expression of GAPDH. Data are represented as mean ± standard deviation (SD). n=3, *p<0.05, **p<0.01, ***p<0.001 vs untreated control sample. Bars with stars indicate a significant difference between differentiated and undifferentiated cells. The other stars compare untreated cells to drug treatment.

5.2.12 TERT promoter methylation in HL-60

The analysis thus far in HL-60 cells indicated significant differences in telomerase activity and TERT gene expression in differentiated progeny from both reduced and air oxygen conditions. We next sought to determine if these changes in expression were reflected in the methylation level of regions within the TERT promoter; region I (-1456, -1495 bp from TSS), II (-674, -717 bp from TSS), III (-315 -348 bp from TSS), IV (-122, -171 bp from TSS) and V (-67, -106 bp from TSS) by using pyrosequencing. In general, methylation results did not correlate with TERT expression and telomerase activity in HL-60 cells.

Region I distal promoter showed higher CpG island methylation levels than all other regions and displayed no difference during the differentiation process in 21% AO condition; only a decreased methylation was noted after ATRA/nanaomycin A treatment (85.42 ± 10.17, $p<0.01$) versus undifferentiated HL-60 in 2% WKS (92.08 ± 4.79) at day 10. We also noted a significant change in methylation level of ATRA/nanaomycin A treated cells cultured in 21% AO and 2% WKS between days 5 (85.83 ± 6.92 and 92.33 ± 5.60, $p<0.05$) and 10 (93.67 ± 6.98 and 85.42 ± 10.17, $p<0.001$), respectively (***Fig 5.21.A***).

Region II showed decreased methylation after ATRA treatment in 21% AO at day 5 (76.17 ± 11.42), 10 (55.21 ± 13.54, $p<0.001$) and 20 (51.50 ± 11.65, $p<0.001$) versus undifferentiated cells (89.61 ± 7.49). Moreover, there was a significant reduction in the methylation level of region II after nanaomycin A treatment (49.88 ± 8.33, $p<0.001$) in 21% AO. ATRA/nanaomycin A treated cells had lower methylation at day 5 (53.50 ± 8.89, $p<0.001$), day 10 (58.79 ± 10.89, $p<0.001$,) and day 20 (63.22 ± 15.09, $p<0.01$) versus undifferentiated cells (89.61 ± 7.49). Further, we noted a significant decrease in methylation of region II after ATRA/nanaomycin A treatment at day 10 (52.28 ± 13.66, $p<0.05$) versus undifferentiated cells (69.94 ± 8.55) in 2% WKS. There was a significant difference between 21% AO and 2% WKS oxygen tension in ATRA treated HL-60 cells at day 5 (76.17 ± 11.42 and 57.44 ± 10.29, $p<0.001$), day 10 (55.21 ± 13.54 and 74.67 ± 9.13, $p<0.001$) and day 20 (51.50 ± 11.65 and 75.56 ± 9.62, $p<0.001$), respectively (***Fig 5.21.B***).

Region III results were inconsistent, and it was challenging to interpret with TERT expression and telomerase activity data. There was a significant decrease after ATRA treatment at day 10 (33.75 ± 10.85, $p<0.01$) and day 20 (19.07 ± 6.67, $p<0.001$) in 21% AO condition compared to undifferentiated cells (42.20 ± 16.45). We observed a reduction after nanaomycin A (31.60 ± 10.15, $p<0.001$) and ATRA/nanaomycin A treatment at day 5 (29.50 ± 9.21,

p<0.001), day 10 (38.65 ± 13.46), and day 20 (18.73 ± 7.22, p<0.001). However, ATRA treated cells in 2% WKS showed increased methylation at day 5 (42.95 ± 12.35, p<0.05) and 10 (42.93 ± 10.99, p<0.05) but decreased at day 20 (20.07 ± 8.55, p<0.001) and in ATRA/nanaomycin A treated cells at day 10 (18.20 ± 7.53, p<0.05) versus undifferentiated HL-60 (35.13 ± 9.99). There was a significant difference between conditions in ATRA treated cells at day 10 (33.75 ± 10.85 and 42.93 ± 10.99, p<0.01) and ATRA/nanaomycin A treated cells at day 5 (29.50 ± 9.21 and 39.53 ± 12.99, p<0.001), 10 (38.65 ± 13.46 and 18.20 ± 7.53, p<0.001), and 20 (18.73 ± 7.22 and 27.93 ± 9.14, p<0.01) (***Fig 5.21.C***).

Region IV had a significant decrease after nanaomycin A (16.58 ± 7.17 and 16.46 ± 9.54, p<0.01) and ATRA/nanaomycin A treatment at day 5 (14.92 ± 8.83 and 14.63 ± 7.78, p<0.001) versus undifferentiated cells in 21% AO and 2% WKS (19.21 ± 15.44 and 19.38 ± 14.11, respectively). However, ATRA/nanaomycin A treated cells at day 10 displayed higher methylation levels in 21% AO and 2% WKS (22.88 ± 5.13 and 23.04 ± 5.98, respectively). No significant change was recorded between conditions after treatments (***Fig 5.21.D***).

Conversely, increased methylation was noted at region V after ATRA treatment at day 5 (27.72 ± 14.11, p<0.01), day 10 (27.67 ± 8.19, p<0.001), and day 20 (30.28 ± 10.49, p<0.001) versus undifferentiated cells (17.94 ± 15.21). Nanaomycin A treated cells showed higher methylation (23.50 ± 14.28, p<0.01). In addition, there was higher methylation after ATRA/nanaomycin A treatment at day 10 (24.50 ± 9.76, p<0.001) and day 20 (29.06 ± 9.12, p<0.001) in 21% AO. In physoxia, we noted higher methylation after 10 (25.39 ± 10.07, p<0.05) and 20 days (28.22 ± 9.88, p<0.001) of ATRA treatment, while we observed lower methylation after ATRA/nanaomycin A treatment at day 5 (20.56 ± 11.32, p<0.05) versus 2% WKS control cells (22.78 ± 15.75). Undifferentiated cells, 5 days of ATRA, and 20 days of ATRA/nanaomycin A treatment showed a significant difference between 21% AO and 2% WKS (p<0.001) condition in region V (***Fig 5.21.E)***.

Pooled data from regions I, II, III, IV, and V demonstrated a significant reduction in methylation after ATRA treatment at day 10 (32.91 ± 17.26, p<0.001), day 20 (30.27 ± 16.00, p<0.001) and nanaomycin A treatment (29.24 ± 16.07, p<0.001) when compared to undifferentiated cells cultured in 21% AO (40.40 ± 32.50). In addition, we noted a similar decrease in ATRA/nanaomycin A treated cells at day 5 (28.45 ± 17.71, p<0.001), day 10 (35.04 ± 17.41, p<0.001) and day 20 (32.49 ± 20.24, p<0.001) in 21% AO. In physoxia, we noted a similar decrease in ATRA/nanaomycin A treated cells at day 5 (30.17 ± 18.54, p<0.001), day 10 (29.44 ± 15.97, p<0.001), and day 20 (33.23 ± 19.90, p<0.001) versus undifferentiated cells

(35.48 ± 23.78). However, pooled data showed a higher methylation level after ATRA treatment on day 10 (39.24 ± 23.54, $p<0.001$) versus undifferentiated cells culture in 2% WKS. Further, undifferentiated cells, 5 days and 10 days of ATRA, and 10 days of ATRA/nanaomycin A treatment showed a significant difference between 21% AO and 2% WKS ($p<0.001$) in pooled data from all regions (***Fig 5.21.F***).

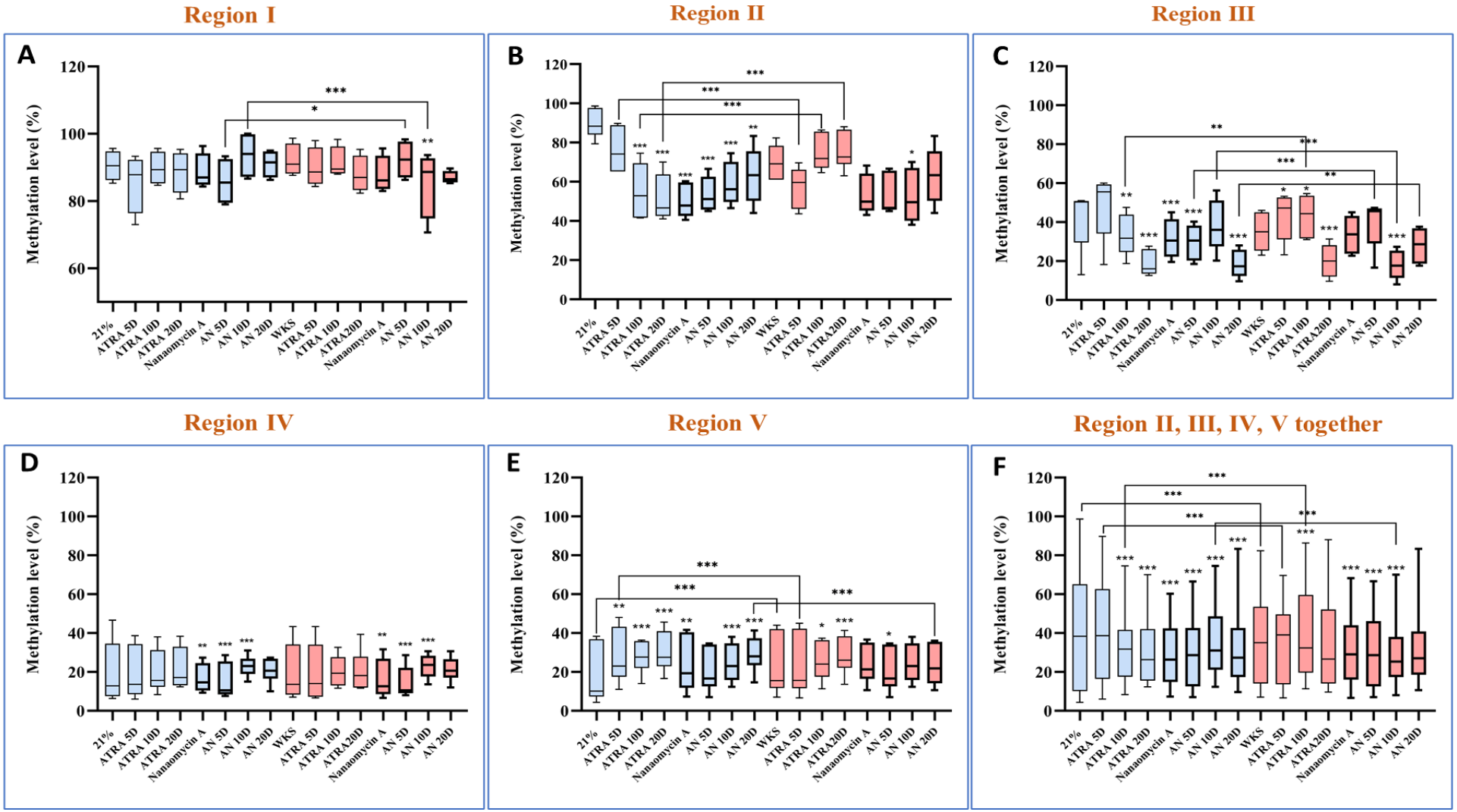

Figure 5.21. **The methylation levels of TERT promoter in HL-60 cells cultured in 21% AO and 2% WKS**. Different promoter regions (region I **(A)**, II **(B),** III **(C)**, IV **(D)**, V **(E)** and all regions together **(F)**) relative to TSS were evaluated using pyrosequencing. Data presented as median (min-max). The median value of methylation was represented in the box and violin graph. Y-axis indicates DNA methylation level (%), and X-axis represents the treatment name. n=3, *p<0.05, **p<0.01, ***p<0.001. The stars compare untreated versus treated cells

5.3 DISCUSSION

Cancer cells can activate telomerase to avoid senescence and apoptosis by stabilising their telomeres, reducing genomic instability levels. Genetic and epigenetics together contribute to the regulation of TERT expression in human cancers (Dratwa et al. 2020; Leão et al. 2019). Further, epigenetic modifications have essential roles in important cellular functions, including embryonic development, differentiation of stem cells, and the development of cancer. Accumulation of genetic and epigenetic changes can result in dysregulation of cancer-related genes, but underlying epigenetic regulation of many oncogenes remains ambiguous (Sharma et al., 2010). DNA methylation is one of the most studied epigenetic processes. It is involved in X-chromosome inactivation, genomic imprinting, regulation of gene transcription, silencing of retroviral and transposable DNA elements, maintenance of genome stability and chromatin organisation (Li and Zhang, 2014). Global hypomethylation, hypermethylation of CpG islands in gene promoters, and increased mutation rate at methylated CpG dinucleotides are the major reasons for disturbed DNA methylation profiles in cancer, and they cause alterations of crucial genes and downstream signalling pathways (Sadikovic et al., 2008). At this point, the mechanism behind TERT promoter methylation and the effect on gene expression is controversial. Therefore, we aimed to explore the methylation changes on TERT promoter after treatment with DNMT inhibitors in different cancer models. In this chapter, we also used the HL-60 differentiation model to investigate the role of DNMT3B enzyme on the TERT promoter.

First, the proliferation of cancer cell lines was explored in different oxygen conditions. We observed a significant decrease in the proliferation rate of A549, COV362, MG-63 and Jurkat cells cultured in both reduced oxygen conditions. At the same time, there was an increase in the proliferation rate of IMR-90 and SH-SY5Y in reduced oxygen tension (***Fig. 1***). Previous studies have observed that HCT116, HeLa cervical carcinoma and HTB-30 breast carcinoma cells lose their proliferation ability within hypoxic conditions as a result of the modulation of metabolic mechanisms, cell cycle regulation, as well as the development of epigenetic modifications (Box and Demetrick, 2004; Hubbi et al., 2013). In contrast, some studies have shown that low oxygen tension promotes proliferation in HCT116 and RKO colon cancers (Dang et al., 2006). Also, activation of HIF-2α promotes proliferation in renal clear cell carcinoma through enhanced c-Myc transcriptional activity (Gordan et al., 2007). Overall, we noted that the proliferation of cancer cells was oxygen-sensitive and depended on the cancer type, in agreement with Shahrzad et al. Further, they suggested that metabolic mechanisms and

cell cycle regulation were also oxygen-sensitive (Shahrzad et al. 2007). There is a correlation between proliferation and abnormal DNA methylation at global and gene-specific levels in several cancer models (Gossage and Eisen 2010; Shahrzad et al. 2007).

Following proliferation experiments, we performed telomerase activity, TERT expression, and telomere length analysis in cancer cells. IMR-90, SH-SY5Y and Jurkat displayed higher telomerase activity in reduced oxygen conditions, IMR-90 showed higher TERT expression and telomere length in 2% WKS. Consistent with our findings, reduced oxygen increases TERT gene expression and telomerase activity to protect cells against genetic stress induced by low oxygen tension in solid tumours (Seimiya et al., 1999; Yatabe et al., 2004). They suggested a correlation between telomerase activation and resistance to apoptotic cell death under reduced oxygen tension. Reduced oxygen tension promotes the TERT promoter activity and enhances endogenous TERT expression in choriocarcinoma cell lines (Nishi et al., 2004).

Next, we optimised nanaomycin A drug dose for cancer cells and IMR-90. The maximum non-toxic drug dose was determined as 0.31 µM for IMR-90 fibroblast, SH-SY5Y and Jurkat cells, 0.63 µM for A549, MG-63 and 1.25 µM for COV362 cancer cells. Interestingly, some cancer cells displayed higher tolerance to nanaomycin A treatment. Molecular dynamics studies of DNMT3B showed that nanaomycin A selectively inhibits DNMT3B interactions with Arg731, Arg733, Arg832, and the catalytic Cys651, in addition, reactivates silenced tumour suppressor genes in human cancer cells (Caulfield and Medina-Franco, 2011). IC50 (the half-maximal inhibitory concentration) values are measured for HCT116 as 0.4 µmol/L, A549 as 4.1 µmol/L, and HL-60 as 0.8 µmol/L after 72 hours of incubation where nanaomycin A treatment induces genomic demethylation (Kuck et al., 2010). Noteworthy, epigenetics abnormalities like altered global methylation patterns of cancer cells are important regulators of gene expression independent of genetic mutations (Jones and Baylin, 2007). Moreover, we also determined the maximum non-toxic drug dose of FDA-approved DNMT inhibitor 5-aza-2′-deoxycytidine (decitabine). DNA methylation induces silencing of tumour suppressors in cancers, so a reversal of promoter DNA hypermethylation with demethylating agent decitabine is effective in treating haematological neoplasms (Issa et al., 2005; Yu et al., 2018a). Interestingly, DNMT1 gene expression is positively correlated with decitabine sensitivity, while DNMT3B gene expression displays more resistance to decitabine in pancreatic (Simó-Riudalbas et al., 2011) and ovarian cancers (Stewart et al., 2015). Previous publications confirm that DNMT3B is a challenging oncogene in solid human cancers, and a high gene dosage of DNMT3B is correlated with elevated resistance to the inhibitory effect of DNA demethylating

agents like decitabine (Simó-Riudalbas et al., 2011). We performed DNMT and DNMT3B activity/inhibition colourimetric assay to examine the effect of DNMTs inhibitors. Similar to the above literature, DNMT1 inhibitor decitabine induced a significant decrease in DNMT1 enzyme activity in all cancer cells and nanaomycin A treated cells showed a considerable decrease in DNMT3B enzyme. Following enzyme assay, we conducted gene expression to investigate changes at the mRNA level. Most cancer cells showed a decreased gene expression of DNMT3B after nanaomycin A treatment and gene expression of DNMT1 after decitabine treatment. Overall, decreased DNMT1 and DNMT3B enzyme activity accompanied reduced gene expression. Conflicting our results, chronic treatment with decitabine cause up-regulation of DNMT1 gene expression in lung cancer cells, which may explain why genomic DNA is remethylated in decitabine-treated patients (Yan et al., 2015). Cell proliferation and viability are drastically reduced in mouse T-ALL cells treated with 25, 50, and 100nM nanaomycin A accompanied by a decrease in DNMT3B gene expression (Poole et al., 2017). On the other hand, nanaomycin A treated HCT116, A549, and HL-60 cell lines showed no changes in transcript levels of DNMT3B or DNMT1 (Kuck et al., 2010), and they suggested that nanaomycin A does not directly degrade DNMT3B or DNMT1 in drug-treated cells. HDAC inhibitor vorinostat reduced the binding activities of DNMT1 and DNMT3B on TERT promoter in A549 cancer cells (Li et al., 2011).

We examined telomerase activity and TERT expression in nanaomycin A-treated cancer cells. There was an increase in telomerase and TERT expression after nanaomycin A treatment in cancer cells, while decitabine treated cells had no consistent results. The Stögbauer study demonstrated decreased proliferation and cell viability after incubation with decitabine from 1 to 10 μM doses in malignant meningioma cells. Reduced proliferation and viability were independent of TERT expression, telomerase activity, or TERT promoter methylation but associated with promoter methylation of distinct tumour suppressor genes and oncogenes (Stögbauer et al., 2020). However, some studies showed upregulated TERT transcription after decitabine treatment by reducing CpG methylation in HeLa cell lines (Kato et al., 2021). The data from Cancer Genome Atlas demonstrated that shorter survival in HCC patients has correlated to upregulation of TERT and DNMT3B expression; further, TERT positively regulates DNMT3B expression in HCC cells (Yu et al., 2018b). However, there is no direct study about the effect of nanaomycin A on telomerase or TERT.

Some studies have demonstrated a correlation between TERT promoter methylation and gene repression or activation in normal, immortalised, and several cancer cell lines; however, other studies reported no association between gene expression and methylation pattern of the promoter (Devereux et al., 1999; Dessain et al., 2000; Guilleret et al., 2002). The data from the ESCs (***chapter 3, Fig 3.29-30, Page 143-145***) and nanaomycin A treated cancer cells suggested an effect of DNMT3B on TERT promoter methylation. Therefore, we investigated the methylation signature of cancer cells after nanaomycin A and decitabine treatment in reduced oxygen tension. Nanaomycin A treated cells showed decreased methylation in all TERT proximal promoter regions except distal promoter region I, while decitabine treated cells displayed no significant changes across all regions. There was a correlation between increased TERT expression and promoter methylation in nanaomycin A treated cells. Love et al. supported our data and suggested that methylation status of upstream of the translation start site (14 CpG sites, -300 to -368 bp from TSS) in the TERT promoter becomes hypermethylated, resulting in loss of expression of TERT (Love et al., 2008). Renaud et al. showed partial demethylation of the TERT core promoter (−160 to −80 bp from TSS) in telomerase-positive breast, bladder, and cervical cancer (Renaud et al., 2007). However, methylation results are conflicted with hypermethylated region THOR and elevated telomerase activity in many cancers (Guilleret et al., 2002; Castelo-Branco et al., 2013). Controversial questions about the relationship between TERT promoter region methylation and gene expression remain. Most studies have focused on the core promoter of TERT, and maybe this is one of the reasons why there are different results (Guccione et al., 2006; Arita et al., 2013; Castelo-Branco et al., 2013).

Further, we have explored DNMT3B inhibition and increased TERT expression via CHIP. Interestingly, there is a significant decrease in DNMT3B antibody binding to TERT promoter regions after nanaomycin A treatment compared to untreated cells. These results show that DNMT3B inhibition can decrease TERT promoter methylation, and simultaneously increase TERT expression and telomerase activity. It is noteworthy that the fold enrichment of DNMT3B on TERT promoter was consistent with previously calculated methylation percentage in the regions II, III, IV and V in COV362 (***Table 5-1***). There was a higher DNMT3B binding on regions II and III, where a higher methylation percentage was measured in COV362.

Many studies have shown that ATRA treatment significantly induces downregulation of TERT gene and protein compared to untreated HL-60 (Dongmei and Yuan, 2003; Liu et al., 2004). Love et al. suggested that ATRA treatment reduced cellular proliferation and induced apoptosis in the HL-60. Also, 2 μM ATRA induced inhibition of telomerase activity and

downregulation of TERT through hypoacetylation and hypermethylation of the TERT promoter during 12 days of treatment (Love et al., 2008). We observed reduced telomerase activity after ATRA and a combination of nanaomycin A/ATRA treatment during 20 days of differentiation. However, only nanaomycin A treated undifferentiated HL-60 cells displayed higher telomerase and TERT expression versus controls. We noted a decrease in TERT expression after ATRA treatment during 20 days of differentiation, and TERT expression was higher in reduced oxygen tension 2% WKS versus 21% AO. Lastly, we investigated methylation patterns and the link between TERT expression and methylation, but there was no correlation between methylation and TERT expression in ATRA and nanaomycin A/ATRA treated cells. Only nanaomycin A treated cells showed reduced methylation at promoter regions. Therefore, it might explain increased TERT expression and telomerase activity in these samples.

In conclusion, data from cancer cells suggest that DNMT3B methylation on TERT promoter is independent of stem cell differentiation, and telomerase regulation is associated with DNMT3B enzyme activity. The de novo methylase DNMT3B plays a significant role in TERT promoter methylation linked to the oxygen culture and is correlated directly with TERT transcription and telomerase activity in cancer cells. DNA methylation, histone modification, and non-coding RNAs are responsible for regulating telomeres and telomerase activity in several biological processes, including increased TERT expression in cancers, development and differentiation. Therefore, we believe answers behind epigenetic modifications can improve cancer treatment, diagnosis, and prognosis.

5.3.1 Summary

The stem cell differentiation process provides a model to research on the regulation of telomerase activity. ESCs and cancer cells both have high telomerase activity. Instead of focusing on one type of cell, we aimed to look from a broad perspective at epigenetic regulation of telomerase. We aimed to understand better TERT regulation in telomerase positive tumour cells and stem cell models in different physiological environments.

In summary, the proliferation of cancer cells was oxygen-sensitive and depended on the cancer type. IMR-90, SH-SY5Y, and Jurkat displayed higher telomerase activity in reduced oxygen conditions. Decitabine and nanaomycin A treated cells showed decreased DNMT1 and DNMT3B enzyme activity, respectively, accompanied by reduced DNMT1 and DNMT3B gene expressions. Further, there was an increase in telomerase and TERT expression after nanaomycin A treatment in cancer cells, while decitabine treated cells displayed variable responses. Nanaomycin A treated cells displayed decreased methylation in all TERT proximal promoter regions except distal promoter region I, while decitabine treated cells displayed no significant changes across all regions. There was a correlation between increased TERT expression and decreased promoter methylation in nanaomycin A treated cells. CHIP data showed a considerable decrease in DNMT3B antibody binding to TERT promoter regions after nanaomycin A treatment compared to untreated cells. DNMT3B inhibition can decrease TERT promoter methylation, and simultaneously increase TERT expression and telomerase activity (***Table 5-2***). Additionally, the fold enrichment of DNMT3B on TERT promoter was consistent with previously calculated methylation percentage in the regions II, III, IV and V in COV362. There was a higher DNMT3B binding on regions II and III, where a higher methylation percentage was measured in COV362. Overall, data from cancer cells and nanaomycin A treatment suggested that the impact of DNMT3B methylation on TERT promoter was independent of stem cell differentiation, and telomerase regulation is associated with DNMT3B enzyme activity. The de novo methylase DNMT3B plays a significant role in TERT promoter methylation and telomerase regulation linked to the oxygen culture in cancer cells. Also, methylation results demonstrated a distinct methylation pattern that distinguishes pluripotent stem cells from somatic cells (***Table 5-3***).

Table 5-2. **Change in TERT expression, telomerase activity and methylation in drug-treated samples versus untreated cells in 2% WKS.**

	TERT Gene		Telomerase Activity		Methylation (All regions)	
Treatment	**Nanaomycin A**	**Decitabine**	**Nanaomycin A**	**Decitabine**	**Nanaomycin A**	**Decitabine**
IMR-90	↑	---	↑	---	---	---
A549	---	---	---	---	↓	---
COV362	↑	---	↑	---	↓	---
MG-63	↑	↑	↑	↑	↓	---
SH-SY5Y	↑	---	↑	↓	↓	---
Jurkat	↑	----	---	↓	↓	---

Table 5-3. **Distinct methylation pattern in cancer cells and differentiated stem cells.**

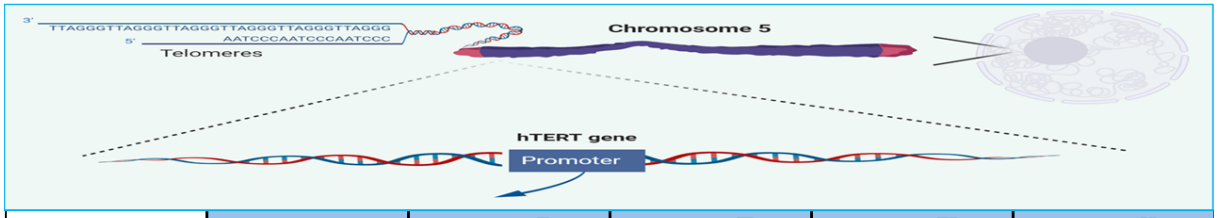

Cell Type	Region Ⅰ	Region Ⅱ	Region Ⅲ	Region Ⅳ	Region Ⅴ
IMR-90	83.17	42.06	7.33	10.79	12.79
A549	86.92	68.56	81.27	7.00	4.61
COV362	75.42	90.22	86.20	23.67	10.28
MG-63	82.08	91.28	56.08	42.66	24.5
SH-SY5Y	58.75	40.56	22.47	27.71	32.72
Jurkat	73.33	73.32	87.90	82.38	69.72
SHEF 21%	89.73	44.54	7.58	9.92	5.70
SHEF 10 Days DF	89.83	51.40	12.03	9.89	6.06
SHEF 20 Days DF	88.42	60.34	15.64	11.25	7.84
SHEF 40 Days DF	88.38	57.38	15.60	13.59	8.00
SHEF WKS	89.33	34.67	5.80	6.20	3.93
SHEF 10 Days DF	89.55	52.28	10.23	8.15	5.49
SHEF 20 Days DF	89.00	56.53	13.03	10.03	5.81
SHEF 40 Days DF	89.08	53.26	13.47	13.11	7.38

Increased methylation

THOR Region

Keele University

CHAPTER 6: Discussion, Conclusion and Future Work

6.1 Discussion

For decades, genetic mutations have been thought to be critical for cancer treatment, but after extensive research, epigenetics aberrations are now casting new light on cancer progression and therapy (Sharma et al., 2010; Nebbioso et al., 2018). Epigenetic alterations are potentially reversible, and their expected state can be restored in the cell (Falahi et al., 2014). Therefore, epigenetic therapy has vast implications for clinical prevention and treatment of many diseases because of the reversibility of epigenetic aberrations, unlike genetic mutations (Yoo and Jones, 2006). The abnormalities on global DNA and gene-specific methylation are observed in cancers, and this has highlighted the role of epigenetics on gene expression independent of genetic mutations in cancer biology (Wajed et al., 2001; Baylin and Bestor, 2002). Especially, it has been shown that altered methylation of CpG islands within tumour suppressor genes promotes carcinogenesis in many studies (Baylin and Bestor, 2002; Nishida et al., 2008). Some studies have suggested that reduced oxygen induces epigenetic and genetic instability, contributing to cancer development (Perez-Perri et al., 2011; Camuzi et al., 2019; Tang et al., 2021). Low oxygen tension modulates multiple signalling pathways within the cell, including proliferation, self-renewal, differentiation, metabolism, DNA damage, senescence, survival and apoptosis-related pathways (Rios et al., 2016; Zhi et al., 2018). On the other hand, air oxygen (21% O_2) induces genomic instability, increases cellular complexity, and creates barriers to clonogenicity (Forsyth et al., 2006; Agrawal et al., 2016). Air oxygen drives coordinate the repression of hundreds of genes supporting developmental potential in hESCs and hMSCs (Agrawal et al., 2016). Moreover, high oxygen tension (21% AO) in tissue culture is associated with increased ROS production, resulting in cellular, DNA damage, genomic instability and senescence (Jagannathan et al., 2016). Typically, ESCs are derived from embryos that occupy between 2–5% physiological normoxia environment (Forristal et al., 2010), while the oxygen level in tumour tissues ranges between 1%–2% O_2 and below depending on the size and stage of the tumour (Muz et al., 2015). Moreover, the impact of the oxygen environment on global DNA and gene-specific methylation of cancer cells or stem cells is little studied so far. Physiological oxygen levels drive a significant decrease in global DNA methylation levels (5mC) across cancer cell lines and stem cells (Shahrzad et al., 2007; Dogan et al., 2021).

In this project, we aimed to understand the impact of the local oxygen microenvironment on TERT methylation profiles in cancer and stem cells. Cells were cultured in physiological oxygen conditions (2% PG and 2% WKS) to mimic the native oxygen microenvironment and

21% AO to mimic standard tissue culture conditions. The effect of different oxygen microenvironments on various cell functions was investigated, including proliferation, metabolic activity, differentiation, TERT expression, telomerase activity and telomere length. Firstly, characterisation experiments for undifferentiated and differentiated cells were performed to ensure the status of cells in the three oxygen microenvironments. Immunofluorescence staining for pluripotency markers and qRT- PCR for germ layer differentiation markers were performed to dynamically monitor the status of germ lineage organization of spontaneously monolayer differentiated stem cells and EBs. There was a gradual decrease in pluripotency markers OCT-4, NANOG, SSEA-4 and ALP after differentiation of stem cells in all conditions, while negative marker SSEA-1 showed an increase similar to previous studies (Solter and Knowles, 1978; Noisa et al., 2012; Zhao et al., 2012). Immunostaining results showed no significant differences between physoxia and air oxygen conditions in pluripotency markers. However, ALP and SSEA-4 expression notably decreased after five days, while Nanog expression reduced gradually over 20 days of differentiation across all three oxygen conditions. OCT-3/4 expression was slowly reduced in physiological oxygen conditions compared to 21% AO. Possibly, low oxygen conditions support stem cell potency and self-renewal through OCT-4 expression. Some studies support that reduced oxygen culture promotes stem cell differentiation (Kurosawa et al., 2006; Prado-Lopez et al., 2009), while many studies that showed the low oxygen tension did not significantly change the expression of pluripotency markers of stem cells (Forsyth et al., 2006; Forristal et al., 2010; Basciano et al., 2011; Närvä et al., 2013). Many researchers have demonstrated that the reduced oxygen microenvironment promotes proliferation, inhibits senescence, and reduces chromosomal abnormalities of several stem cells, including hESCs and MSCs (Forsyth et al., 2006; Bentivegna et al., 2013; Choi et al., 2015). We also noted an enhanced proliferation, metabolic activity, stemness and slower differentiation of ESCs in the physoxia microenvironment.

Our qRT- PCR results showed no significant increases in ectoderm or endoderm markers expression in monolayer differentiated cells. At the same time, there was an increased mesoderm markers expression with slower onset of differentiation in physoxia. However, EBs can express three germ layer markers, including ectodermal (Nestin), mesodermal (KDR, Brachyury-T) and endodermal (α-fetoprotein) markers (Ferreira et al., 2007; Zhou et al., 2010; Garreta et al., 2014). Similar to previous studies, significant increases in expression of ectoderm, endoderm, and mesoderm markers were observed during spontaneous differentiation of EBs. Overall, 3D aggregates also displayed slower onset of differentiation in physoxia. Furthermore, the expression of differentiation markers Nestin, KDR, TBXT and AFP gradually

increased over the time course of EBs differentiation which correlates to a gradual decrease in pluripotency in three oxygen environments.

Many research has indicated the positive impact of reduced oxygen in cell growth and metabolic activity in stem cells and cancer (Forristal et al., 2010; Rajala et al., 2011). Low oxygen condition is associated with higher proliferation, colony initiating cells, stemness, survival, reduced chromosomal abnormalities, change of metabolic activity, and maintenance of the undifferentiated state in many types of stem cells (Ivanovic et al., 2000; Dunwoodie, 2009; Radan et al., 2014). Stem cells are best maintained in the range of 2–5% physiological normoxia, and low oxygen concentration enhances the proliferation, viability and self-renewal of cells (Ezashi T et al., 2005; Ma et al., 2009; Ghourichaee et al., 2017; Dogan et al., 2021). Our data demonstrated that physiological oxygen conditions elevated the proliferation and metabolic activity of ESCs when compared to air oxygen. Also, a shorter doubling time was noted in reduced oxygen culture compared to 21% AO in differentiated cells. Besides, cancer cells demonstrated different responses to reduced oxygen tension considering variability, proliferation, and metabolic activity. The difference in proliferative responses between cancer cells to reduced oxygen environment might be due to cell type and metabolic requirements (Abdollahi et al., 2011). Physoxia is a crucial component of the stem cell microenvironment and is involved in the regulation of stem cell behaviour. Next, we assessed the effect of oxygen on differentiation and telomerase activity.

Germ cells, stem cells, cancer, and specific immune cells possess high telomerase activity associated with proliferation and long telomeres, but TERT promoter activity and gene expression rapidly decrease after differentiation (Yui et al., 1998; Radan et al., 2014; Cheng et al., 2017). In addition, TERT knockout in hESCs exhibited reduced proliferation, increased the numbers of cells in the G1 phase, induced differentiation and inability to generate stable ESCs sublines (Yang et al., 2008; Sexton et al., 2014). Further, reduced oxygen conditions induce nuclear localization of TERT without significant changes in telomerase activity levels, and it was associated with increased cell survival and maintenance in stem cells (Ma et al., 2009; Radan et al., 2014). Consistent with the above, our TRAP assay and TERT protein data confirmed a gradual downregulation in telomerase activity during differentiation in ESCs and EBs. Telomerase enzyme activity was significantly higher in both ESCs cultured in physiological oxygen niches when compared to AO. Furthermore, EBs have about 40 population doublings *in vitro* due to senescence and telomeric shortening. After many population doublings and absence of telomerase lead cells to senescence and eventually

telomere attribution (Shamblott, 2001). Contrary to these results, a less decreased telomerase activity and TERT gene expression were noted in EBs than in undifferentiated cells. We emphasised that spontaneous differentiated ESCs derived EBs maintained more telomerase activity and TERT gene expression even after 20 days of culture following long telomeres compared to monolayer differentiated cells. In addition, telomerase activity was significantly higher in ESCs and EBs cultured in physiological oxygen niches when compared to 21% AO, which was correlated with slower onset of differentiation. Similar to these results, we observed a significant decrease in TERT expression during differentiation and a significantly higher gene expression was noted in reduced oxygen cultured cells. Telomere shortening was also consistent with telomerase activity and TERT expression. On the other hand, the mechanisms behind TERT reactivation in cancer cells and silencing of TERT in differentiation or embryonic development remain open to discussion. Several studies reported the effect of reduced oxygen conditions on telomerase and TERT gene. Reduced oxygen tension promotes the TERT promoter activity and enhances endogenous TERT expression in choriocarcinoma cell lines (Nishi et al., 2004). They suggested a correlation between telomerase activation and resistance to apoptotic cell death under reduced oxygen tension. We also performed telomerase assay, TERT expression and telomere length analysis for cancer cells. IMR-90, SH-SY5Y and Jurkat showed higher telomerase activity in reduced oxygen conditions, plus IMR-90 showed higher TERT expression and telomere length in 2% WKS. Consistent with the above, reduced oxygen increases TERT gene expression and telomerase activity in solid tumours (Seimiya et al., 1999; Yatabe et al., 2004). HIF1A induces telomerase activity via TERT transcription in cervical and choriocarcinoma cells and increases telomere length at low oxygen levels (Yatabe et al., 2004; Kyo et al., 2008; Wang et al., 2018). Therefore, low oxygen tension might be a selective advantage for tumour cell survival. Next, we performed a telomerase activity assay and qPCR for TERT expression in nanaomycin A treated cancer cells. There was an increase in TERT expression and telomerase activity after nanaomycin A treatment in cancer cells, while decitabine treated cells showed inconsistent results.

The importance of DNA methylation in stem cell differentiation, cell fate, and maintenance of characteristics and cellular programming has been shown in many studies (Gopalakrishnan et al., 2008; Altun et al., 2010; Pelosi et al., 2011). Especially, DNA methylation on gene promoters, enhancers or first exon can regulate specific genes that have important roles in stem cell differentiation and cellular programming (Wu and Sun, 2006; Brenet et al., 2011; Moore et al., 2013). DNA methylation at gene control elements, such as promoters and enhancers, is often associated with transcriptional repression (Di Croce L et al., 2002; Miller and Grant,

2013). TERT promoter methylation is associated with gene expression and telomerase regulation in cancer and stem cell biology. Therefore, we also investigated the impact of physoxia on DNA methylation of TERT promoter regions in human PSCs, EBs and cancers cells. TERT reactivation in cancer is commonly associated with genetic alterations in TERT promoter and epigenetic modifications through TERT promoter methylation (Castelo-Branco et al., 2013; Barthel et al., 2017; Leão et al., 2019). We noted a significant increase in methylation level during the differentiation of both ESCs and EBs. TERT transcriptional down-regulation was associated with increased promoter methylation in ESCs. Noteworthy, proximal TERT promoter methylation was oxygen-sensitive, and there was a decrease in methylation percentage in both ESCs and EBs cultured in physiological conditions. Also, pluripotent cell samples and somatic cell methylation results demonstrated that a distinct methylation pattern distinguishes pluripotent stem cells from somatic cells, similar to literature (Huang et al., 2014a). Distal promoter regions (-2056 and -1566 nt) of TERT were highly methylated like our results, while researchers showed distinct methylation signatures in pluripotent stem cells versus somatic cells correlated to gene expression levels at -1415 to -638 nt region (Takasawa et al., 2018). We observed that the distal promoter (region I, -1456, -1495 from TSS) has a high methylation level in both ESCs and EBs with no significant difference during differentiation compared to the proximal promoter. Altogether, we also observed that methylation alteration of the TERT promoter is strongly linked to telomerase activity and TERT regulation in stem cells (Seynnaeve et al., 2017). Interestingly, UTSS hypermethylation of the TERT gene is associated with tumour progression and poor prognosis in pediatric brain tumours (Castelo-Branco et al., 2013).

Different studies showed that low oxygen tension induces reduced global DNA methylation in cancer cell lines (Shahrzad et al., 2007; Skowronski et al., 2010). Kuck and colleagues showed that nanaomycin A (5 μmol/L) revealed selective inhibition of DNMT3B, which induced genomic demethylation using biochemical *in vitro* methylation assays. It showed antiproliferative effects in human cancer cells. (Kuck et al., 2010). To further investigate TERT methylation data, we used nanaomycin A selective inhibitor to target DNMT3B and performed a cytotoxicity assay to determine non-toxic drug doses for differentiated, undifferentiated ESCs and in cancer cells. We observed a significant decrease in DNMT3B enzyme and gene expression after nanaomycin A treatment. In addition, DNMT3B was down-regulated in physoxia in pluripotent stem cells. Importantly, DNMT3B inhibition positively regulates TERT gene expression and telomerase activity in stem cells and cancer cells. Also, results from ESCs and nanaomycin A treated cancer cells suggested the possible

effect of DNMT3B on TERT promoter methylation. Therefore, we investigated the methylation signature of stem cells and cancer cells after nanaomycin A treatment in reduced oxygen tension using pyrosequencing. Nanaomycin A treated cells showed a decrease in methylation in all TERT proximal promoter regions except distal promoter region I while decitabine treated cells displayed no significant changes in all regions. There was a correlation between increased TERT expression and promoter methylation in nanaomycin A treated cells.

Further, we performed CHIP experiments to explore more previous data from DNMT3B inhibition, decreased methylation and increased TERT expression. CHIP data showed a significant decrease in DNMT3B antibody binding to TERT promoter regions after nanaomycin A treatment compared to untreated cells. DNMT3B inhibitor treatment reduced TERT promoter methylation, associated with increased gene and enzyme activity. Most importantly, the first time, we showed that DNMT3B binding to TERT promoter increases methylation in differentiated stem cells and cancer cells using CHIP qPCR. On the other hand, elevated TERT and DNMT3B expression were associated with shorter survival of hepatocellular carcinoma patients (Yu et al., 2018b). Yu and colleagues suggested that TERT promotes DNMT3B transcription because TERT inhibition resulted in a decrease in both DNMT3B gene and protein expressions.

Downregulation of TERT expression during myeloid cell differentiation is a good tool to investigate TERT promoter methylation in cancer cells. Undifferentiated HL-60 cells have high levels of telomerase activity. But telomerase and TERT protein are suppressed in HL-60 cells after differentiation (Kim et al., 1999; Xu et al., 1999; Liu et al., 2004). Therefore, telomerase activity, gene expression and promoter methylation were analysed in a differentiated HL-60 model. We observed a reduced telomerase activity after ATRA and a combination of nanaomycin A/ATRA treatment during 20 days of differentiation. However, only nanaomycin A treated undifferentiated HL-60 cells represent higher telomerase and TERT expression versus controls. We noted no correlation between methylation and TERT expression in nanaomycin A/ATRA treated cells. Only nanaomycin A treated cells showed less methylation at promoter regions. It might explain increased TERT expression and telomerase activity in these samples.

This thesis aimed to identify the role of epigenetic modifications, especially methylation on the TERT gene in different cell lines, including stem cells and cancer associated with the oxygen level. Understanding the identification of the epigenetic memory of cell origin is essential to stem cell biology and cancer research. DNA methylation profiles will be necessary for developing precise epigenetic engineering tools. Understanding the development of

functional cells with epigenetic memory has massive potential for brand new clinical applications (Jones and Baylin, 2007). Previous data showed that routine culture of cells in low oxygen conditions resulted in a significant decrease in 5mC and 5hmC, accompanied by transcriptional-translational down-regulation of DNMT3B in MSCs (Dogan et al., 2021). We noted that continuous physoxic culture (2% WKS) is more consistent than semi-continuous physoxic culture (2% PG). There are some variations during changing media, passaging, seeding, handling cells in a standard safety cabinet, opening and closing of incubator doors in 2% PG condition, therefore, we might observe some fluctuations in some of the experiments between 2% conditions. We experienced that air oxygen is almost never 'normoxic' in mammalian cell culture. Finally, telomerase, TERT, DNMT3B genes and DNA methylation are regulated in an oxygen-sensitive manner in ESCs and cancer cells.

6.2 Conclusions

This research aimed to investigate the association between TERT promoter methylation, TERT expression, and physiological oxygen conditions in different cell lines, including stem cells and cancer. In addition, to identify the effect of low oxygen on cellular functions, including proliferation, metabolic activity, stemness and differentiation. The results from ESCs showed enhanced proliferation, metabolic activity, stemness and slower differentiation in the physoxia microenvironment. Cancer cells showed different growth profiles in reduced oxygen tension considering variability, proliferation and metabolic activity. Monolayer differentiated cells expressed only mesoderm markers following decreased expression of pluripotency markers, but 3D aggregates EBs expressed all ectoderm, endoderm, and mesoderm markers during spontaneous differentiation. Overall, both monolayer and 3D differentiated cells displayed slower onset of differentiation in physoxia. Downregulated TERT gene and protein expressions were correlated to telomerase activity during differentiation in ESCs and EBs. Physoxia cultured ESCs showed higher telomerase enzyme activity when compared to 21% AO. EBs showed higher telomerase activity and TERT gene expression than monolayer differentiated cells. Moreover, telomerase activity and TERT gene expression were significantly higher in ESCs and EBs cultured in physiological oxygen niches when compared to 21% AO.

Pyrosequencing data showed a significant increase in methylation level during the differentiation of ESCs and EBs correlated to decreased telomerase expression. It is noteworthy that promoter methylation was oxygen-sensitive, and there was a decrease in methylation percentage in physiological conditions. Further experiments suggested that DNMT3B inhibition decreased methylation on the promoter and increased TERT expression, associated with increased enzyme activity in stem cells and cancer cell models. CHIP experiments confirmed a significant decrease in DNMT3B antibody binding to TERT promoter regions after nanaomycin A treatment compared to untreated cells. Our data, for the first time demonstrated that DNMT3B binding to TERT promoter increases methylation in differentiated stem cells and cancer cells using CHIP qPCR. Together these data suggest that DNMT3B inhibition positively regulates TERT gene expression and telomerase activity in stem cells and cancer cells. Furthermore, results from CHIP experiments showed the possible effect of DNMT3B on TERT promoter methylation.

6.3 Future Work

Our study has raised a number of considerations for understanding the effect of physoxia on epigenetics in cell and telomerase biology. It will be helpful to extend follow-up studies in these areas.

- It is important to highlight the limitations of culturing cells in traditional monolayer culture and 3D models. ESCs differentiation in monolayer culture showed a particular type of cell differentiation that displayed significantly downregulated telomerase activity. On the other hand, 3D aggregates of ESCs expressed three germ layer markers and higher telomerase activity than monolayer culture. Further investigation of telomerase activity, TERT gene expression and epigenetics on each germ layer can provide more details about telomerase regulation during early embryonic development.
- There are limitations of culturing 3D aggregates of EBs more uniform in size, shape, and homogeneity, but EBs are a great model to mimic embryonic development without ethical concern. Improving the EBs culture can increase the data quality and reproducibility of experiments. EBs are holding great promise for a model of early embryonic development, although control over cell aggregation during EB aggregation is still challenging. Especially, cell-cell interactions involved in EB formation are considered to influence the course of ESCs differentiation, and it controls cell number, quality and size of EBs. Despite these limitations, it is also essential to acknowledge the benefits surrounding 3D culture models.
- Additionally, analysing different cell lines can minimise the variations and improve the confidence to compare the effect of oxygen at different oxygen tensions.
- The role of other epigenetic factors, including histone modification and 5-hydroxymethylcytosine (5hmC) on telomerase regulation and cell differentiation in different oxygen tension, can contribute to our knowledge.

- Second-generation methylation array technology can permit the identification of DNA methylation changes in physoxia relative to air oxygen. The potential functional roles of low oxygen can be investigated with associations between methylation and gene expression.
- Individual DNMTs' role in TERT promoter can be investigated further with knockdown and overexpression experiments.
- More insight may be gained by exploring the role of the individual HIFs factors after short term and long term culture in three oxygen conditions.

References

Aalami, O. O., Fang, T. D., Song, H. M., and Nacamuli, R. P. (2003). Physiological Features of Aging Persons. *Arch. Surg.* 138, 1068. doi:10.1001/archsurg.138.10.1068.

Abdollahi, H., Harris, L. J., Zhang, P., McIlhenny, S., Srinivas, V., Tulenko, T., et al. (2011). The role of hypoxia in stem cell differentiation and therapeutics. *J. Surg. Res.* 165, 112–117. doi:10.1016/J.JSS.2009.09.057.

Abe, K., Niwa, H., Iwase, K., Takiguchi, M., Mori, M., Abé, S. I., et al. (1996). Endoderm-Specific Gene Expression in Embryonic Stem Cells Differentiated to Embryoid Bodies. *Exp. Cell Res.* 229, 27–34. doi:10.1006/EXCR.1996.0340.

Adewumi, O., Aflatoonian, B., Ahrlund-Richter, L., Amit, M., Andrews, P. W., Beighton, G., et al. (2007). Characterization of human embryonic stem cell lines by the International Stem Cell Initiative. *Nat. Biotechnol.* 25, 803–816. doi:10.1038/nbt1318.

Aflatoonian, B., Ruban, L., Shamsuddin, S., Baker, D., Andrews, P., and Moore, H. (2010). Generation of Sheffield (Shef) human embryonic stem cell lines using a microdrop culture system. *Vitr. Cell. Dev. Biol. - Anim.* 46, 236–241. doi:10.1007/s11626-010-9294-2.

Agrawal, R., Dale, T. P., Al-Zubaidi, M. A., Benny Malgulwar, P., Forsyth, N. R., and Kulshreshtha, R. (2016). Pluripotent and Multipotent Stem Cells Display Distinct Hypoxic miRNA Expression Profiles. *PLoS One* 11, e0164976. doi:10.1371/journal.pone.0164976.

Aisner, D. L., Wright, W. E., and Shay, J. W. (2002). Telomerase regulation: not just flipping the switch. *Curr. Opin. Genet. Dev.* 12, 80–85. doi:10.1016/S0959-437X(01)00268-4.

Al Tanoury, Z., Piskunov, A., and Rochette-Egly, C. (2013). Vitamin A and retinoid signaling: genomic and nongenomic effects: Thematic Review Series: Fat-Soluble Vitamins: Vitamin A. *J. Lipid Res.* 54, 1761. doi:10.1194/JLR.R030833.

Albanell, J., Han, W., Mellado, B., Gunawardane, R., Scher, H. I., Dmitrovsky, E., et al. (1996). Telomerase activity is repressed during differentiation of maturation-sensitive but not resistant human tumor cell lines. *Cancer Res.* 56, 1503–8. Available at:

http://www.ncbi.nlm.nih.gov/pubmed/8603393 [Accessed February 27, 2019].

Allsopp, R. C., Cheshier, S., and Weissman, I. L. (2001). Telomere shortening accompanies increased cell cycle activity during serial transplantation of hematopoietic stem cells. *J. Exp. Med.* 193, 917–24. Available at: http://www.ncbi.nlm.nih.gov/pubmed/11304552 [Accessed April 6, 2019].

Altun, G., Loring, J. F., and Laurent, L. C. (2010). DNA methylation in embryonic stem cells. *J. Cell. Biochem.* 109, 1–6. doi:10.1002/jcb.22374.

An, J., Rao, A., and Ko, M. (2017). TET family dioxygenases and DNA demethylation in stem cells and cancers. *Exp. Mol. Med. 2017 494* 49, e323–e323. doi:10.1038/emm.2017.5.

Arita, H., Narita, Y., Takami, H., Fukushima, S., Matsushita, Y., Yoshida, A., et al. (2013). TERT promoter mutations rather than methylation are the main mechanism for TERT upregulation in adult gliomas. *Acta Neuropathol.* 126, 939–941. doi:10.1007/s00401-013-1203-9.

Armstrong, C. A., and Tomita, K. (2017). Fundamental mechanisms of telomerase action in yeasts and mammals : understanding telomeres and telomerase in cancer cells. *Open Biol.* 7. doi:10.1098/rsob.160338.

Armstrong, L., Lako, M., Lincoln, J., Cairns, P. M., and Hole, N. (2000). mTert expression correlates with telomerase activity during the differentiation of murine embryonic stem cells. *Mech. Dev.* 97, 109–116. doi:10.1016/S0925-4773(00)00423-8.

Armstrong, L., Saretzki, G., Peters, H., Wappler, I., Evans, J., Hole, N., et al. (2005). Overexpression of Telomerase Confers Growth Advantage, Stress Resistance, and Enhanced Differentiation of ESCs Toward the Hematopoietic Lineage. *Stem Cells* 23, 516–529. doi:10.1634/stemcells.2004-0269.

Arora, R., Lee, Y., Wischnewski, H., Brun, C. M., Schwarz, T., and Azzalin, C. M. (2014). RNaseH1 regulates TERRA-telomeric DNA hybrids and telomere maintenance in ALT tumour cells. *Nat. Commun.* 5. doi:10.1038/ncomms6220.

Ast, T., and Mootha, V. K. (2019). Oxygen and mammalian cell culture: are we repeating the experiment of Dr. Ox? *Nat. Metab.* 1, 858–860. doi:10.1038/S42255-019-0105-0.

Atkinson, S. P., Hoare, S. F., Glasspool, R. M., and Keith, W. N. (2005). Lack of Telomerase Gene Expression in Alternative Lengthening of Telomere Cells Is Associated with Chromatin Remodeling of the hTR and hTERT Gene Promoters. *Cancer Res.* 65.

Atkuri, K. R., Herzenberg, L. A., Niemi, A.-K., Cowan, T., and Herzenberg, L. A. (2007). Importance of culturing primary lymphocytes at physiological oxygen levels. *Proc. Natl. Acad. Sci. U. S. A.* 104, 4547. doi:10.1073/PNAS.0611732104.

Autexier, C., and Lue, N. F. (2006). The Structure and Function of Telomerase Reverse Transcriptase. *Annu. Rev. Biochem.* 75, 493–517. doi:10.1146/annurev.biochem.75.103004.142412.

Avilion, A. A., Piatyszek, M. A., Gupta, J., Shay, J. W., Bacchetti, S., and Greider, C. W. (1996). Human telomerase RNA and telomerase activity in immortal cell lines and tumor tissues. *Cancer Res.* 56, 645–50. Available at: http://www.ncbi.nlm.nih.gov/pubmed/8564985 [Accessed October 24, 2019].

Azzalin, C. M., Reichenbach, P., Khoriauli, L., Giulotto, E., and Lingner, J. (2007). Telomeric repeat containing RNA and RNA surveillance factors at mammalian chromosome ends. *Science* 318, 798–801. doi:10.1126/science.1147182.

B, F., and BD, B. (1993). Oxygen tension in the oviduct and uterus of rhesus monkeys, hamsters and rabbits. *J. Reprod. Fertil.* 99, 673–679. doi:10.1530/JRF.0.0990673.

Bailey, S. M., Brenneman, M. A., and Goodwin, E. H. (2004). Frequent recombination in telomeric DNA may extend the proliferative life of telomerase-negative cells. *Nucleic Acids Res.* 32, 3743–51. doi:10.1093/nar/gkh691.

Bannister, A. J., and Kouzarides, T. (2011). Regulation of chromatin by histone modifications. *Cell Res.* 21, 381–95. doi:10.1038/cr.2011.22.

Bárdos, J. I., and Ashcroft, M. (2004). Hypoxia-inducible factor-1 and oncogenic signalling. *Bioessays* 26, 262–269. doi:10.1002/BIES.20002.

Barthel, F. P., Wei, W., Tang, M., Martinez-Ledesma, E., Hu, X., Amin, S. B., et al. (2017). Systematic analysis of telomere length and somatic alterations in 31 cancer types. *Nat. Genet.* 49, 349–357. doi:10.1038/ng.3781.

Basciano, L., Nemos, C., Foliguet, B., de Isla, N., de Carvalho, M., Tran, N., et al. (2011).

Long term culture of mesenchymal stem cells in hypoxia promotes a genetic program maintaining their undifferentiated and multipotent status. *BMC Cell Biol.* 12, 12. doi:10.1186/1471-2121-12-12.

Baylin, S., and Bestor, T. H. (2002). Altered methylation patterns in cancer cell genomes: cause or consequence? *Cancer Cell* 1, 299–305. doi:10.1016/S1535-6108(02)00061-2.

Beaulieu, N., Morin, S., Chute, I. C., Robert, M.-F., Nguyen, H., and MacLeod, A. R. (2002). An Essential Role for DNA Methyltransferase DNMT3B in Cancer Cell Survival. *J. Biol. Chem.* 277, 28176–28181. doi:10.1074/jbc.M204734200.

BECKER, A. J., McCULLOCH, E. A., and TILL, J. E. (1963). Cytological demonstration of the clonal nature of spleen colonies derived from transplanted mouse marrow cells. *Nature* 197, 452–4. Available at: http://www.ncbi.nlm.nih.gov/pubmed/13970094 [Accessed March 2, 2019].

Bedford, M. T., and Clarke, S. G. (2009). Protein Arginine Methylation in Mammals: Who, What, and Why. *Mol. Cell* 33, 1–13. doi:10.1016/j.molcel.2008.12.013.

Benetti, R., García-Cao, M., and Blasco, M. A. (2007a). Telomere length regulates the epigenetic status of mammalian telomeres and subtelomeres. *Nat. Genet.* 39, 243–250. doi:10.1038/ng1952.

Benetti, R., Gonzalo, S., Jaco, I., Schotta, G., Klatt, P., Jenuwein, T., et al. (2007b). Suv4-20h deficiency results in telomere elongation and derepression of telomere recombination. *J. Cell Biol.* 178, 925–936. doi:10.1083/jcb.200703081.

Bentivegna, A., Miloso, M., Riva, G., Foudah, D., Butta, V., Dalprà, L., et al. (2013). DNA methylation changes during in vitro propagation of human mesenchymal stem cells: Implications for their genomic stability? *Stem Cells Int.* doi:10.1155/2013/192425.

Berletch, J. B., Liu, C., Love, W. K., Andrews, L. G., Katiyar, S. K., and Tollefsbol, T. O. (2008). Epigenetic and genetic mechanisms contribute to telomerase inhibition by EGCG. *J. Cell. Biochem.* 103, 509–19. doi:10.1002/jcb.21417.

Bibikova, M., Chudin, E., Wu, B., Zhou, L., Garcia, E. W., Liu, Y., et al. (2006). Human embryonic stem cells have a unique epigenetic signature. *Genome Res.* 16, 1075–1083. doi:10.1101/gr.5319906.

Biedler, J. L., Roffler-Tarlov, S., Schachner, M., and Freedman, L. S. (1978). Multiple neurotransmitter synthesis by human neuroblastoma cell lines and clones. *Cancer Res.* 38, 3751–7. Available at: http://www.ncbi.nlm.nih.gov/pubmed/29704 [Accessed August 22, 2019].

Billiau, A., Edy, V. G., Heremans, H., Van Damme, J., Desmyter, J., Georgiades, J. A., et al. (1977). Human interferon: mass production in a newly established cell line, MG-63. *Antimicrob. Agents Chemother.* 12, 11–5. doi:10.1128/aac.12.1.11.

Bindu A, H., and B, S. (2011). Potency of Various Types of Stem Cells and their Transplantation. *J. Stem Cell Res. Ther.* 01. doi:10.4172/2157-7633.1000115.

Bird, A. (2007). Perceptions of epigenetics. *Nature* 447, 396–398. doi:10.1038/nature05913.

Blackburn, E. H., and Gall, J. G. (1978). A tandemly repeated sequence at the termini of the extrachromosomal ribosomal RNA genes in Tetrahymena. *J. Mol. Biol.* 120, 33–53. Available at: http://www.ncbi.nlm.nih.gov/pubmed/642006 [Accessed May 13, 2019].

Blasco, M. A. (2007). The epigenetic regulation of mammalian telomeres. *Nat. Rev. Genet.* 8, 299–309. doi:10.1038/nrg2047.

Boheler, K. R., Czyz, J., Tweedie, D., Yang, H. T., Anisimov, S. V., and Wobus, A. M. (2002). Differentiation of pluripotent embryonic stem cells into cardiomyocytes. *Circ. Res.* 91, 189–201. doi:10.1161/01.RES.0000027865.61704.32.

Borah, S., Xi, L., Zaug, A. J., Powell, N. M., Dancik, G. M., Cohen, S. B., et al. (2015). Cancer. TERT promoter mutations and telomerase reactivation in urothelial cancer. *Science* 347, 1006–10. doi:10.1126/science.1260200.

Bork, S., Pfister, S., Witt, H., Horn, P., Korn, B., Ho, A. D., et al. (2010). DNA methylation pattern changes upon long-term culture and aging of human mesenchymal stromal cells. *Aging Cell* 9, 54–63. doi:10.1111/j.1474-9726.2009.00535.x.

Box, A. H., and Demetrick, D. J. (2004). Cell cycle kinase inhibitor expression and hypoxia-induced cell cycle arrest in human cancer cell lines. *Carcinogenesis* 25, 2325–2335. doi:10.1093/CARCIN/BGH274.

Bratt-Leal, A. M., Carpenedo, R. L., and McDevitt, T. C. (2009). Engineering the embryoid body microenvironment to direct embryonic stem cell differentiation. *Biotechnol. Prog.*

25, 43–51. doi:10.1002/BTPR.139.

Breitman, T. R., Selonick, S. E., and Collins, S. J. (1980). Induction of differentiation of the human promyelocytic leukemia cell line (HL-60) by retinoic acid. *Proc. Natl. Acad. Sci.* 77, 2936–2940. doi:10.1073/PNAS.77.5.2936.

Brenet, F., Moh, M., Funk, P., Feierstein, E., Viale, A. J., Socci, N. D., et al. (2011). DNA Methylation of the First Exon Is Tightly Linked to Transcriptional Silencing. *PLoS One* 6, e14524. doi:10.1371/journal.pone.0014524.

Bryan, T. M., Englezou, A., Gupta, J., Bacchetti, S., and Reddel, R. R. (1995). Telomere elongation in immortal human cells without detectable telomerase activity. *EMBO J.* 14, 4240–8. Available at: http://www.ncbi.nlm.nih.gov/pubmed/7556065 [Accessed November 2, 2017].

Burr, S., Caldwell, A., Chong, M., Beretta, M., Metcalf, S., Hancock, M., et al. (2018). Oxygen gradients can determine epigenetic asymmetry and cellular differentiation via differential regulation of Tet activity in embryonic stem cells. *Nucleic Acids Res.* 46, 1210–1226. doi:10.1093/NAR/GKX1197.

Cacchione, S., Biroccio, A., and Rizzo, A. (2019). Emerging roles of telomeric chromatin alterations in cancer 06 Biological Sciences 0601 Biochemistry and Cell Biology 11 Medical and Health Sciences 1112 Oncology and Carcinogenesis. *J. Exp. Clin. Cancer Res.* 38. doi:10.1186/s13046-019-1030-5.

Cameron, C. M., Harding, F., Hu, W. S., and Kaufman, D. S. (2008). Activation of Hypoxic Response in Human Embryonic Stem Cell–Derived Embryoid Bodies: *https://doi.org/10.3181/0709-RM-263* 233, 1044–1057. doi:10.3181/0709-RM-263.

Camuzi, D., de Amorim, Í., Ribeiro Pinto, L., Oliveira Trivilin, L., Mencalha, A., and Soares Lima, S. (2019). Regulation Is in the Air: The Relationship between Hypoxia and Epigenetics in Cancer. *Cells* 8, 300. doi:10.3390/CELLS8040300.

Castelo-Branco, P., Choufani, S., Mack, S., Gallagher, D., Zhang, C., Lipman, T., et al. (2013). Methylation of the TERT promoter and risk stratification of childhood brain tumours: An integrative genomic and molecular study. *Lancet Oncol.* 14, 534–542. doi:10.1016/S1470-2045(13)70110-4.

Castelo-Branco, P., Leão, R., Lipman, T., Campbell, B., Lee, D., Price, A., et al. (2016). A

cancer specific hypermethylation signature of the TERT promoter predicts biochemical relapse in prostate cancer: A retrospective cohort study. *Oncotarget* 7, 57726–57736. doi:10.18632/oncotarget.10639.

Caulfield, T., and Medina-Franco, J. L. (2011). Molecular dynamics simulations of human DNA methyltransferase 3B with selective inhibitor nanaomycin A. *J. Struct. Biol.* 176, 185–191. doi:10.1016/J.JSB.2011.07.015.

Cavaleri, F., and Schöler, H. R. (2003). Nanog: A New Recruit to the Embryonic Stem Cell Orchestra. *Cell* 113, 551–552. doi:10.1016/S0092-8674(03)00394-5.

Cheng, D., Wang, S., Jia, W., Zhao, Y., Zhang, F., Kang, J., et al. (2017). Regulation of human and mouse telomerase genes by genomic contexts and transcription factors during embryonic stem cell differentiation. *Sci. Rep.* 7, 1–12. doi:10.1038/s41598-017-16764-w.

Cheng, D., Zhao, Y., Zhang, F., Zhang, J., Wang, S., and Zhu, J. (2019). Engineering a humanized telomerase reverse transcriptase gene in mouse embryonic stem cells. *Sci. Reports 2019 91* 9, 1–11. doi:10.1038/s41598-019-46160-5.

ChiP_mag_flowchart_web_big.jpg (901×782) Available at: https://www.activemotif.com/images/products/ChiP_mag_flowchart_web_big.jpg [Accessed February 13, 2022].

Choi, J. R., Pingguan-Murphy, B., Abas, W. A. B. W., Yong, K. W., Poon, C. T., Azmi, A. N., et al. (2015). In Situ Normoxia Enhances Survival and Proliferation Rate of Human Adipose Tissue-Derived Stromal Cells without Increasing the Risk of Tumourigenesis. *PLoS One* 10, e0115034. doi:10.1371/JOURNAL.PONE.0115034.

Chu, H. P., Cifuentes-Rojas, C., Kesner, B., Aeby, E., Lee, H. goo, Wei, C., et al. (2017). TERRA RNA Antagonizes ATRX and Protects Telomeres. *Cell* 170, 86-101.e16. doi:10.1016/j.cell.2017.06.017.

Cong, Y.-S., Wright, W. E., and Shay, J. W. (2002). Human Telomerase and Its Regulation. *Microbiol. Mol. Biol. Rev.* 66, 407–425. doi:10.1128/mmbr.66.3.407-425.2002.

Cong, Y. S., Wen, J., and Bacchetti, S. (1999). The human telomerase catalytic subunit hTERT: Organization of the gene and characterization of the promoter. *Hum. Mol. Genet.* 8, 137–142. doi:10.1093/hmg/8.1.137.

Coucouvanis, E., and Ft Martin, G. (1995). Signals for Death and Survival: A Two-Step Mechanism for Cavitation in the Vertebrate Embryo. *Cell* 83, 279–287.

Counter, C. M., Meyerson, M., Eaton, E. N., Ellisen, L. W., Caddle, S. D., Haber, D. A., et al. (1998). Telomerase activity is restored in human cells by ectopic expression of hTERT (hEST2), the catalytic subunit of telomerase. *Oncogene* 16, 1217–1222. doi:10.1038/sj.onc.1201882.

Crowe, D. L., Nguyen, D. C., Tsang, K. J., and Kyo, S. (2001). E2F-1 represses transcription of the human telomerase reverse transcriptase gene. *Nucleic Acids Res.* 29, 2789–94. doi:10.1093/nar/29.13.2789.

Cubiles, M. D., Barroso, S., Vaquero-Sedas, M. I., Enguix, A., Aguilera, A., and Vega-Palas, M. A. (2018). Epigenetic features of human telomeres. *Nucleic Acids Res.* 46, 2347–2355. doi:10.1093/nar/gky006.

Cusanelli, E., Romero, C. A. P., and Chartrand, P. (2013). Telomeric Noncoding RNA TERRA Is Induced by Telomere Shortening to Nucleate Telomerase Molecules at Short Telomeres. *Mol. Cell* 51, 780–791. doi:10.1016/j.molcel.2013.08.029.

D, K., N, S., F, L., and JL, M.-F. (2010). Novel and selective DNA methyltransferase inhibitors: Docking-based virtual screening and experimental evaluation. *Bioorg. Med. Chem.* 18, 822–829. doi:10.1016/J.BMC.2009.11.050.

Dang, D. T., Chen, F., Gardner, L. B., Cummins, J. M., Rago, C., Bunz, F., et al. (2006). Hypoxia-Inducible Factor-1α Promotes Nonhypoxia-Mediated Proliferation in Colon Cancer Cells and Xenografts. *Cancer Res.* 66, 1684–1693. doi:10.1158/0008-5472.CAN-05-2887.

Dang, S. M., Kyba, M., Perlingeiro, R., Daley, G. Q., and Zandstra, P. W. (2002). Efficiency of embryoid body formation and hematopoietic development from embryonic stem cells in different culture systems. *Biotechnol. Bioeng.* 78, 442–453. doi:10.1002/BIT.10220/FORMAT/PDF.

Das, P. M., Ramachandran, K., VanWert, J., and Singal, R. (2004). Chromatin immunoprecipitation assay. *Biotechniques* 37, 961–969. doi:10.2144/04376RV01/ASSET/IMAGES/LARGE/FIGURE2.JPEG.

Deans, C., and Maggert, K. A. (2015). What do you mean, “Epigenetic”? *Genetics* 199, 887–

896. doi:10.1534/genetics.114.173492.

Deng, Z., Norseen, J., Wiedmer, A., Riethman, H., and Lieberman, P. M. (2009). TERRA RNA Binding to TRF2 Facilitates Heterochromatin Formation and ORC Recruitment at Telomeres. *Mol. Cell* 35, 403–413. doi:10.1016/j.molcel.2009.06.025.

Desbaillets, I., Ziegler, U., Groscurth, P., and Gassmann, M. (2000). Embryoid Bodies: An In Vitro Model of Mouse Embryogenesis. *Exp. Physiol.* 85, 645–651. doi:10.1111/J.1469-445X.2000.02104.X.

Dessain, S. K., Yu, H., Reddel, R. R., Beijersbergen, R. L., and Weinberg, R. A. (2000). Methylation of the human telomerase gene CpG island. *Cancer Res.* 60, 537–41. doi:10.1158/0008-5472.can-05-1715.

Devereux, T. R., Horikawa, I., Anna, C. H., Annab, L. A., Afshari, C. A., and Barrett, J. C. (1999). DNA methylation analysis of the promoter region of the human telomerase reverse transcriptase (hTERT) gene. *Cancer Res.* 59, 6087–6090.

Dogan, F., Aljumaily, R. M. K., Kitchen, M., and Forsyth, N. R. (2021). DNMT3B Is an Oxygen-Sensitive De Novo Methylase in Human Mesenchymal Stem Cells. *Cells 2021, Vol. 10, Page 1032* 10, 1032. doi:10.3390/CELLS10051032.

Dogan, F., Aljumaily, R. M. K., Kitchen, M., and Forsyth, N. R. (2022). Physoxia influences global and gene-specific methylation in pluripotent stem cells. *bioRxiv*, 2022.03.21.484908. doi:10.1101/2022.03.21.484908.

Dogan, F., and Forsyth, N. R. (2021). Telomerase Regulation: A Role for Epigenetics. *Cancers 2021, Vol. 13, Page 1213* 13, 1213. doi:10.3390/CANCERS13061213.

Dongmei, H. E., and Yuan, Z. (2003). Effects of AI/-trans Retinoic Acid on hTERT Gene Expression and Telornerase Activity of HL-60 Cells. *Chinese-German J. Clin. Oncol.* 2, 169–171.

Dratwa, M., Wysoczańska, B., Łacina, P., Kubik, T., and Bogunia-Kubik, K. (2020). TERT—Regulation and Roles in Cancer Formation. *Front. Immunol.* 11, 2930. doi:10.3389/FIMMU.2020.589929/BIBTEX.

Dunwoodie, S. L. (2009). The Role of Hypoxia in Development of the Mammalian Embryo. *Dev. Cell* 17, 755–773. doi:10.1016/J.DEVCEL.2009.11.008.

E, L., TH, B., and R, J. (1992). Targeted mutation of the DNA methyltransferase gene results in embryonic lethality. *Cell* 69, 915–926. doi:10.1016/0092-8674(92)90611-F.

Eitsuka, T., Nakagawa, K., Kato, S., Ito, J., Otoki, Y., Takasu, S., et al. (2018). Modulation of Telomerase Activity in Cancer Cells by Dietary Compounds: A Review. *Int. J. Mol. Sci.* 19, 478. doi:10.3390/ijms19020478.

Episkopou, H., Draskovic, I., Van Beneden, A., Tilman, G., Mattiussi, M., Gobin, M., et al. (2014). Alternative Lengthening of Telomeres is characterized by reduced compaction of telomeric chromatin. *Nucleic Acids Res.* 42, 4391–4405. doi:10.1093/nar/gku114.

Ernst, J., Kheradpour, P., Mikkelsen, T. S., Shoresh, N., Ward, L. D., Epstein, C. B., et al. (2011). Systematic analysis of chromatin state dynamics in nine human cell types. *Nature* 473, 43. doi:10.1038/NATURE09906.

Evseenko, D., Zhu, Y., Schenke-Layland, K., Kuo, J., Latour, B., Ge, S., et al. (2010). Mapping the first stages of mesoderm commitment during differentiation of human embryonic stem cells. *Proc. Natl. Acad. Sci. U. S. A.* 107, 13742. doi:10.1073/PNAS.1002077107.

Falahi, F., van Kruchten, M., Martinet, N., Hospers, G. A. P., and Rots, M. G. (2014). Current and upcoming approaches to exploit the reversibility of epigenetic mutations in breast cancer. *Breast Cancer Res.* 16, 1–11. doi:10.1186/S13058-014-0412-Z/TABLES/2.

Faleiro, I., Apolónio, J. D., Price, A. J., De Mello, R. A., Roberto, V. P., Tabori, U., et al. (2017). The TERT hypermethylated oncologic region predicts recurrence and survival in pancreatic cancer. *Futur. Oncol.* 13, 2045–2051. doi:10.2217/fon-2017-0167.

Farnung, B. O., Brun, C. M., Arora, R., Lorenzi, L. E., and Azzalin, C. M. (2012). Telomerase Efficiently Elongates Highly Transcribing Telomeres in Human Cancer Cells. *PLoS One* 7, e35714. doi:10.1371/journal.pone.0035714.

Feil, R., and Fraga, M. F. (2012). Epigenetics and the environment: emerging patterns and implications. *Nat. Rev. Genet.* 13, 97–109. doi:10.1038/nrg3142.

Ferreira, L. S., Gerecht, S., Fuller, J., Shieh, H. F., Vunjak-Novakovic, G., and Langer, R. (2007). Bioactive hydrogel scaffolds for controllable vascular differentiation of human embryonic stem cells. *Biomaterials* 28, 2706–2717. doi:10.1016/J.BIOMATERIALS.2007.01.021.

Ferron, S., Mira, H., Franco, S., Cano-Jaimez, M., Bellmunt, E., Ramírez, C., et al. (2004). Telomere shortening and chromosomal instability abrogates proliferation of adult but not embryonic neural stem cells. *Development* 131, 4059–4070. doi:10.1242/dev.01215.

Finley, K. R., Tennessen, J., and Shawlot, W. (2003). The mouse Secreted frizzled-related protein 5 gene is expressed in the anterior visceral endoderm and foregut endoderm during early post-implantation development. *Gene Expr. Patterns* 3, 681–684. doi:10.1016/S1567-133X(03)00091-7.

Fischbach, G. D., and Fischbach, R. L. (2004). Stem cells: science, policy, and ethics. *J. Clin. Invest.* 114, 1364–1370. doi:10.1172/JCI23549.

Flores, I., Cayuela, M. L., and Blasco, M. A. (2005). Effects of Telomerase and Telomere Length on Epidermal Stem Cell Behavior. *Science (80-.).* 309, 1253–1256. doi:10.1126/science.1115025.

Forristal, C. E., Wright, K. L., Hanley, N. A., Oreffo, R. O. C., and Houghton, F. D. (2010). Hypoxia inducible factors regulate pluripotency and proliferation in human embryonic stem cells cultured at reduced oxygen tensions. *Reproduction* 139, 85–97. doi:10.1530/REP-09-0300.

Forsyth, N. R., Musio, A., Vezzoni, P., Simpson, A. H. R. W., Noble, B. S., and McWhir, J. (2006). Physiologic oxygen enhances human embryonic stem cell clonal recovery and reduces chromosomal abnormalities. *Cloning Stem Cells* 8, 16–23. doi:10.1089/clo.2006.8.16.

Forsyth, N. R., Wright, W. E., and Shay, J. W. (2002). Telomerase and differentiation in multicellular organisms: Turn it off, turn it on, and turn it off again. *Differentiation* 69, 188–197. doi:10.1046/J.1432-0436.2002.690412.X.

Fouse, S. D., Shen, Y., Pellegrini, M., Cole, S., Meissner, A., Van Neste, L., et al. (2008). Promoter CpG Methylation Contributes to ES Cell Gene Regulation in Parallel with Oct4/Nanog, PcG Complex, and Histone H3 K4/K27 Trimethylation. *Cell Stem Cell* 2, 160–169. doi:10.1016/j.stem.2007.12.011.

García-Cao, M., O'Sullivan, R., Peters, A. H. F. M. F. M., Jenuwein, T., and Blasco, M. A. (2004). Epigenetic regulation of telomere length in mammalian cells by the Suv39h1 and Suv39h2 histone methyltransferases. *Nat. Genet.* 36, 94–99. doi:10.1038/ng1278.

Garreta, E., Melo, E., Navajas, D., and Farré, R. (2014). Low oxygen tension enhances the generation of lung progenitor cells from mouse embryonic and induced pluripotent stem cells. *Physiol. Rep.* 2, 12075. doi:10.14814/PHY2.12075.

George, S. L., Parmar, V., Lorenzi, F., Marshall, L. V., Jamin, Y., Poon, E., et al. (2020). Novel therapeutic strategies targeting telomere maintenance mechanisms in high-risk neuroblastoma. *J. Exp. Clin. Cancer Res.* 39, 1–10. doi:10.1186/S13046-020-01582-2/TABLES/1.

Ghourichaee, S. S., Powell, E. M., and Leach, J. B. (2017). Enhancement of human neural stem cell self-renewal in 3D hypoxic culture. *Biotechnol. Bioeng.* 114, 1096–1106. doi:10.1002/BIT.26224.

Giard, D. J., Aaronson, S. A., Todaro, G. J., Arnstein, P., Kersey, J. H., Dosik, H., et al. (1973). In Vitro Cultivation of Human Tumors: Establishment of Cell Lines Derived From a Series of Solid Tumors2. *JNCI J. Natl. Cancer Inst.* 51, 1417–1423. doi:10.1093/jnci/51.5.1417.

Gifford, C. A., Ziller, M. J., Gu, H., Trapnell, C., Donaghey, J., Tsankov, A., et al. (2013). Transcriptional and Epigenetic Dynamics during Specification of Human Embryonic Stem Cells. *Cell* 153, 1149–1163. doi:10.1016/J.CELL.2013.04.037.

Gomez, D. L. M., Armando, R. G., Cerrudo, C. S., Ghiringhelli, P. D., and Gomez, D. E. (2016). Telomerase as a Cancer Target. Development of New Molecules. *Curr. Top. Med. Chem.* 16, 2432. doi:10.2174/1568026616666160212122425.

Gopalakrishnan, S., Van Emburgh, B. O., and Robertson, K. D. (2008). DNA methylation in development and human disease. *Mutat. Res. - Fundam. Mol. Mech. Mutagen.* 647, 30–38. doi:10.1016/j.mrfmmm.2008.08.006.

Gordan, J. D., Bertout, J. A., Hu, C. J., Diehl, J. A., and Simon, M. C. (2007). HIF-2α promotes hypoxic cell proliferation by enhancing c-Myc transcriptional activity. *Cancer Cell* 11, 335. doi:10.1016/J.CCR.2007.02.006.

Gordon, C. A., Hartono, S. R., and Chédin, F. (2013). Inactive DNMT3B splice variants modulate de novo DNA methylation. *PLoS One* 8. doi:10.1371/JOURNAL.PONE.0069486.

Gossage, L., and Eisen, T. (2010). Alterations in VHL as potential biomarkers in renal-cell

carcinoma. *Nat. Rev. Clin. Oncol.* 7, 277–288. doi:10.1038/NRCLINONC.2010.42.

Greider, C. W., and Blackburn, E. H. (1985). Identification of a specific telomere terminal transferase activity in Tetrahymena extracts. *Cell* 43, 405–13. Available at: http://www.ncbi.nlm.nih.gov/pubmed/3907856 [Accessed May 13, 2019].

Grobelny, J. V., Godwin, A. K., and Broccoli, D. (2000). ALT-associated PML bodies are present in viable cells and are enriched in cells in the G2/M phase of the cell cycle. *J. Cell Sci.* 113, 4577–4585.

Guan, J.-Z., Guan, W.-P., Maeda, T., and Makino, N. (2012a). Alteration of Telomere Length and Subtelomeric Methylation in Human Endothelial Cell Under Different Levels of Hypoxia. *Arch. Med. Res.* 43, 15–20. doi:10.1016/j.arcmed.2012.02.001.

Guan, J.-Z., Guan, W.-P., Maeda, T., and Makino, N. (2012b). Different levels of hypoxia regulate telomere length and telomerase activity. *Aging Clin. Exp. Res.* 24, 213–7. Available at: http://www.ncbi.nlm.nih.gov/pubmed/23114548 [Accessed December 30, 2018].

Guccione, E., Martinato, F., Finocchiaro, G., Luzi, L., Tizzoni, L., Dall' Olio, V., et al. (2006). Myc-binding-site recognition in the human genome is determined by chromatin context. *Nat. Cell Biol.* 8, 764–770. doi:10.1038/ncb1434.

Guilleret, I., and Benhattar, J. (2004). Unusual distribution of DNA methylation within the hTERT CpG island in tissues and cell lines. *Biochem. Biophys. Res. Commun.* 325, 1037–1043. doi:10.1016/J.BBRC.2004.10.137.

Guilleret, I., Yan, P., Grange, F., Braunschweig, R., Bosman, F. T., and Benhattar, J. (2002). Hypermethylation of the human telomerase catalytic subunit (hTERT) gene correlates with telomerase activity. *Int. J. Cancer* 101, 335–341. doi:10.1002/ijc.10593.

Hackett, J. A., and Greider, C. W. (2002). Balancing instability: dual roles for telomerase and telomere dysfunction in tumorigenesis. *Oncogene* 21, 619–626. doi:10.1038/sj.onc.1205061.

Harley, C. B., Futcher, A. B., and Greider, C. W. (1990). Telomeres shorten during ageing of human fibroblasts. *Nat. 1990 3456274* 345, 458–460. doi:10.1038/345458a0.

Hata, K., Okano, M., Lei, H., and Li, E. (2002). Dnmt3L cooperates with the Dnmt3 family of

de novo DNA methyltransferases to establish maternal imprints in mice. *Development* 129, 1983–1993. doi:10.1242/DEV.129.8.1983.

Hayflick, L. (1965). The limited in vitro lifetime of human diploid cell strains. *Exp. Cell Res.* 37, 614–636. doi:10.1016/0014-4827(65)90211-9.

Henson, J. D., Neumann, A. A., Yeager, T. R., and Reddel, R. R. (2002). Alternative lengthening of telomeres in mammalian cells. *Oncogene* 21, 598–610. doi:10.1038/sj.onc.1205058.

Hermann, A., Goyal, R., and Jeltsch, A. (2004). The Dnmt1 DNA-(cytosine-C5)-methyltransferase methylates DNA processively with high preference for hemimethylated target sites. *J. Biol. Chem.* 279, 48350–48359. doi:10.1074/jbc.M403427200.

Hescheler, J., Fleischmann, B. K., Lentini, S., Maltsev, V. A., Rohwedel, J., Wobus, A. M., et al. (1997). Embryonic stem cells: A model to study structural and functional properties in cardiomyogenesis. *Cardiovasc. Res.* 36, 149–162. doi:10.1016/S0008-6363(97)00193-4/2/36-2-149-FIG5.GIF.

Hicksteinsgli, D. D., Back$#, A. L., and Collins, S. J. (1989). Regulation of Expression of the CD1lb and CD18 Subunits of the Neutrophil Adherence Receptor during Human Myeloid Differentiation*. *J. Biol. Chem.* 264, 21812–21817. doi:10.1016/S0021-9258(20)88256-8.

Hiyama, E., and Hiyama, K. (2007). Telomere and telomerase in stem cells. *Br. J. Cancer* 96, 1020–4. doi:10.1038/sj.bjc.6603671.

Hodges, E., Molaro, A., Dos Santos, C. O., Thekkat, P., Song, Q., Uren, P. J., et al. (2011). Directional DNA Methylation Changes and Complex Intermediate States Accompany Lineage Specificity in the Adult Hematopoietic Compartment. *Mol. Cell* 44, 17–28. doi:10.1016/J.MOLCEL.2011.08.026.

Horn, S., Figl, A., Rachakonda, P. S., Fischer, C., Sucker, A., Gast, A., et al. (2013). TERT Promoter Mutations in Familial and Sporadic Melanoma. *Science (80-.).* 339, 959–961. doi:10.1126/science.1230062.

Hornsby, P. J. (2007). Telomerase and the aging process. *Exp. Gerontol.* 42, 575–81. doi:10.1016/j.exger.2007.03.007.

Huang, K., Shen, Y., Xue, Z., Bibikova, M., April, C., Liu, Z., et al. (2014a). A Panel of CpG Methylation Sites Distinguishes Human Embryonic Stem Cells and Induced Pluripotent Stem Cells. *Stem Cell Reports* 2, 36–43. doi:10.1016/j.stemcr.2013.11.003.

Huang, Y., Liang, P., Liu, D., Huang, J., and Songyang, Z. (2014b). Telomere regulation in pluripotent stem cells. *Protein Cell 2014 53* 5, 194–202. doi:10.1007/S13238-014-0028-1.

Hubbi, M. E., Kshitiz, Gilkes, D. M., Rey, S., Wong, C. C., Luo, W., et al. (2013). A Nontranscriptional Role for HIF-1α as a Direct Inhibitor of DNA Replication. *Sci. Signal.* 6, ra10. doi:10.1126/SCISIGNAL.2003417.

Human Fertilisation and Embryology Act (1990) | The Embryo Project Encyclopedia Available at: https://embryo.asu.edu/pages/human-fertilisation-and-embryology-act-1990 [Accessed December 4, 2021].

I, C., D, C., M, R., J, N., S, L., S, T., et al. (2003). Functional expression cloning of Nanog, a pluripotency sustaining factor in embryonic stem cells. *Cell* 113, 643–655. doi:10.1016/S0092-8674(03)00392-1.

Issa, J. P. F., Gharibyan, V., Cortes, J., Jelinek, J., Morris, G., Verstovsek, S., et al. (2005). Phase II study of low-dose decitabine in patients with chronic myelogenous leukemia resistant to imatinib mesylate. *J. Clin. Oncol.* 23, 3948–3956. doi:10.1200/JCO.2005.11.981.

Ito, H., Kyo, S., Kanaya, T., Takakura, M., Koshida, K., Namiki, M., et al. (1998). Detection of Human Telomerase Reverse Transcriptase Messenger RNA in Voided Urine Samples as a Useful Diagnostic Tool for Bladder Cancer. *Clin. Cancer Res.* 4, 2807–2810. Available at: http://clincancerres.aacrjournals.org/content/clincanres/4/11/2807.full.pdf [Accessed October 12, 2017].

Itskovitz-Eldor, J., Schuldiner, M., Karsenti, D., Eden, A., Yanuka, O., Amit, M., et al. (2000a). Differentiation of Human Embryonic Stem Cells into Embryoid Bodies Comprising the Three Embryonic Germ Layers. *Mol. Med.* 6, 88–95. doi:10.1007/BF03401776.

Itskovitz-Eldor, J., Schuldiner, M., Karsenti, D., Eden, A., Yanuka, O., Amit, M., et al. (2000b). Differentiation of human embryonic stem cells into embryoid bodies

compromising the three embryonic germ layers. *Mol. Med.* 6, 88. doi:10.1007/bf03401776.

Ivanovic, Z. (2009). Hypoxia or in situ normoxia: The stem cell paradigm. *J. Cell. Physiol.* 219, 271–275. doi:10.1002/JCP.21690.

Ivanovic, Z., Sbarba, P. Dello, Trimoreau, F., Faucher, J. L., and Praloran, V. (2000). Primitive human HPCs are better maintained and expanded in vitro at 1 perent oxygen than at 20 percent. *Transfusion* 40, 1482–1488. doi:10.1046/j.1537-2995.2000.40121482.x.

JA, T., J, I.-E., SS, S., MA, W., JJ, S., VS, M., et al. (1998). Embryonic stem cell lines derived from human blastocysts. *Science* 282, 1145–1147. doi:10.1126/SCIENCE.282.5391.1145.

Jackson, M., Krassowska, A., Gilbert, N., Chevassut, T., Forrester, L., Ansell, J., et al. (2004). Severe Global DNA Hypomethylation Blocks Differentiation and Induces Histone Hyperacetylation in Embryonic Stem Cells. *Mol. Cell. Biol.* 24, 8862–8871. doi:10.1128/mcb.24.20.8862-8871.2004.

Jackson, M., Taylor, A. H., Jones, E. A., and Forrester, L. M. (2010). The culture of mouse embryonic stem cells and formation of embryoid bodies. *Methods Mol. Biol.* 633, 1–18. doi:10.1007/978-1-59745-019-5_1.

Jagannathan, L., Cuddapah, S., and Costa, M. (2016). Oxidative stress under ambient and physiological oxygen tension in tissue culture. *Curr. Pharmacol. reports* 2, 64–72. doi:10.1007/s40495-016-0050-5.

Januszkiewicz, D., Wysoki, J., Lewandowski, K., Pernak, M., Nowicka, K., Rembowska, J., et al. (2003). Lack of correlation between telomere length and telomerase activity and expression in leukemic cells. *Int. J. Mol. Med.* 12, 935–8. Available at: http://www.ncbi.nlm.nih.gov/pubmed/14612969 [Accessed February 10, 2019].

Jia, W., Wang, S., Horner, J. W., Wang, N., Wang, H., Gunther, E. J., et al. (2011). A BAC transgenic reporter recapitulates in vivo regulation of human telomerase reverse transcriptase in development and tumorigenesis. *FASEB J.* 25, 979–989. doi:10.1096/FJ.10-173989.

Johnson, A. B., Denko, N., and Barton, M. C. (2008). Hypoxia induces a novel signature of

chromatin modifications and global repression of transcription. *Mutat. Res. Mol. Mech. Mutagen.* 640, 174–179. doi:10.1016/j.mrfmmm.2008.01.001.

Jones, P. A., and Baylin, S. B. (2007). The epigenomics of cancer. *Cell* 128, 683–92. doi:10.1016/j.cell.2007.01.029.

Jones, P. A., and Laird, P. W. (1999). Cancer-epigenetics comes of age. *Nat. Genet.* 21, 163–167. doi:10.1038/5947.

Jones, P. A., and Liang, G. (2009). Rethinking how DNA Methylation Patterns are Maintained. *Nat. Rev. Genet.* 10, 805. doi:10.1038/NRG2651.

K, M., Y, T., H, I., K, S., M, M., K, T., et al. (2003). The homeoprotein Nanog is required for maintenance of pluripotency in mouse epiblast and ES cells. *Cell* 113, 631–642. doi:10.1016/S0092-8674(03)00393-3.

Kallio, P. J., Okamoto, K., O'Brien, S., Carrero, P., Makino, Y., Tanaka, H., et al. (1998). Signal transduction in hypoxic cells: inducible nuclear translocation and recruitment of the CBP/p300 coactivator by the hypoxia-inducible factor-1alpha. *EMBO J.* 17, 6573–86. doi:10.1093/emboj/17.22.6573.

Kanaya, T., Kyo, S., Hamada, K., Takakura, M., Kitagawa, Y., Harada, H., et al. (2000). Adenoviral expression of p53 represses telomerase activity through down-regulation of human telomerase reverse transcriptase transcription. *Clin. Cancer Res.* 6, 1239–1247.

Kato, K., Kawaguchi, A., and Nagata, K. (2021). Template activating factor-I epigenetically regulates the TERT transcription in human cancer cells. *Sci. Reports 2021 111* 11, 1–15. doi:10.1038/s41598-021-97009-9.

Kemp, C., Willems, E., Abdo, S., Lambiv, L., and Leyns, L. (2005). Expression of all Wnt genes and their secreted antagonists during mouse blastocyst and postimplantation development. *Dev. Dyn.* 233, 1064–1075. doi:10.1002/dvdy.20408.

Khan, Y. S., and Ackerman, K. M. (2021). Embryology, Week 1. *StatPearls*. Available at: https://www.ncbi.nlm.nih.gov/books/NBK554562/ [Accessed November 15, 2021].

Khanduja, J. S., Calvo, I. A., Joh, R. I., Hill, I. T., and Motamedi, M. (2016). Nuclear Noncoding RNAs and Genome Stability. *Mol. Cell* 63, 7–20. doi:10.1016/j.molcel.2016.06.011.

Khattar, E., and Tergaonkar, V. (2017). Transcriptional regulation of telomerase reverse transcriptase (TERT) by MYC. *Front. Cell Dev. Biol.* 5, 1. doi:10.3389/FCELL.2017.00001/BIBTEX.

Khaw, A. K., Silasudjana, M., Banerjee, B., Suzuki, M., Baskar, R., and Hande, M. P. (2007). Inhibition of telomerase activity and human telomerase reverse transcriptase gene expression by histone deacetylase inhibitor in human brain cancer cells. *Mutat. Res. Mol. Mech. Mutagen.* 625, 134–144. doi:10.1016/j.mrfmmm.2007.06.005.

Khoo, M. L. M., McQuade, L. R., Smith, M. S. R., Lees, J. G., Sidhu, K. S., and Tuch, B. E. (2005). Growth and Differentiation of Embryoid Bodies Derived from Human Embryonic Stem Cells: Effect of Glucose and Basic Fibroblast Growth Factor. *Biol. Reprod.* 73, 1147–1156. doi:10.1095/BIOLREPROD.104.036673.

Kietzmann, T., Petry, A., Shvetsova, A., Gerhold, J. M., and Görlach, A. (2017). The epigenetic landscape related to reactive oxygen species formation in the cardiovascular system. *Br. J. Pharmacol.* 174, 1533. doi:10.1111/BPH.13792.

Kikuno, N., Shiina, H., Urakami, S., Kawamoto, K., Hirata, H., Tanaka, Y., et al. (2008). Retracted: Genistein mediated histone acetylation and demethylation activates tumor suppressor genes in prostate cancer cells. *Int. J. Cancer* 123, 552–560. doi:10.1002/ijc.23590.

KIM, I.-H., KIM, S.-J., CHEONG, H.-J., PARK, S.-K., LEE, G.-T., WON, J.-H., et al. (1999). Telomerase Activity in HL-60 Cells After Treatment with Differentiating Agents. *Korean J. Hematol.*, 107–117. Available at: http://dx.doi.org/ [Accessed January 30, 2022].

Kim, N. W., Piatyszek, M. A., Prowse, K. R., Harley, C. B., West, M. D., Ho, P. L., et al. (1994). Specific association of human telomerase activity with immortal cells and cancer. *Science* 266, 2011–5. Available at: http://www.ncbi.nlm.nih.gov/pubmed/7605428 [Accessed April 2, 2019].

Kim, S.-Y., Lee, S., Hong, S.-W., Min, B.-H., Lee, K.-U., Bendayan, M., et al. (2010). Nestin Action During Insulin-secreting Cell Differentiation. *J. Histochem. Cytochem.* 58, 567. doi:10.1369/JHC.2010.955682.

Kim, W., and Shay, J. W. (2018). Long-range telomere regulation of gene expression:

Telomere looping and telomere position effect over long distances (TPE-OLD). *Differentiation* 99, 1–9. doi:10.1016/j.diff.2017.11.005.

Kinoshita, T., Nagamatsu, G., ¶1, §, Saito, S., Takubo, K., Horimoto, K., et al. (2014). Telomerase Reverse Transcriptase Has an Extratelomeric Function in Somatic Cell Reprogramming * □ S. *J. Biol. Chem.* 289, 15776–15787. doi:10.1074/jbc.M113.536037.

Klapper, W., Parwaresch, R., and Krupp, G. (2001). Telomere biology in human aging and aging syndromes. *Mech. Ageing Dev.* 122, 695–712. doi:10.1016/S0047-6374(01)00223-8.

Klimanskaya, I., Kimbrel, E. A., and Lanza, R. (2020). Embryonic stem cells. *Princ. Tissue Eng.*, 421–434. doi:10.1016/B978-0-12-818422-6.00024-1.

Kondo, S., Tanaka, Y., Kondo, Y., Hitomi, M., Barnett, G. H., Ishizaka, Y., et al. (1998). Antisense telomerase treatment: Induction of two distinct pathways, apoptosis and differentiation. *FASEB J.* 12, 801–811. doi:10.1096/fasebj.12.10.801.

Konstantinov, I. E. (2000). In search of Alexander A. Maximow: the man behind the unitarian theory of hematopoiesis. *Perspect. Biol. Med.* 43, 269–76. Available at: http://www.ncbi.nlm.nih.gov/pubmed/10804590 [Accessed March 2, 2019].

Kourmouli, N., Jeppesen, P., Mahadevhaiah, S., Burgoyne, P., Wu, R., Gilbert, D. M., et al. (2004). Heterochromatin and tri-methylated lysine 20 of histone H4 in animals. *J. Cell Sci.* 117, 2491–2501. doi:10.1242/jcs.01238.

Kremenskoy, M., Kremenska, Y., Ohgane, J., Hattori, N., Tanaka, S., Hashizume, K., et al. (2003). Genome-wide analysis of DNA methylation status of CpG islands in embryoid bodies, teratomas, and fetuses. *Biochem. Biophys. Res. Commun.* 311, 884–890. doi:10.1016/j.bbrc.2003.10.078.

Kuck, D., Caulfield, T., Lyko, F., and Medina-Franco, J. L. (2010). Nanaomycin A Selectively Inhibits DNMT3B and Reactivates Silenced Tumor Suppressor Genes in Human Cancer Cells. doi:10.1158/1535-7163.MCT-10-0609.

Kulić, A., Plavetić, N. D., Gamulin, S., Jakić-Razumović, J., Vrbanec, D., and Sirotković-Skerlev, M. (2016). Telomerase activity in breast cancer patients: association with poor prognosis and more aggressive phenotype. *Med. Oncol.* 33, 23. doi:10.1007/s12032-016-

0736-x.

Kumar, R., Sharma, A., Pattnaik, A. K., and Varadwaj, P. K. (2010). Stem cells: An overview with respect to cardiovascular and renal disease. *J. Nat. Sci. Biol. Med.* 1, 43–52. doi:10.4103/0976-9668.71674.

Kurosawa, H., Kimura, M., Noda, T., and Amano, Y. (2006). Effect of oxygen on in vitro differentiation of mouse embryonic stem cells. *J. Biosci. Bioeng.* 101, 26–30. doi:10.1263/jbb.101.26.

Kwon, S. Y., Chun, S. Y., Ha, Y. S., Kim, D. H., Kim, J., Song, P. H., et al. (2017). Hypoxia Enhances Cell Properties of Human Mesenchymal Stem Cells. *Tissue Eng. Regen. Med.* 14, 595–604. doi:10.1007/s13770-017-0068-8.

Kyo, S., Takakura, M., Fujiwara, T., and Inoue, M. (2008). Understanding and exploiting *hTERT* promoter regulation for diagnosis and treatment of human cancers. *Cancer Sci.* 99, 1528–1538. doi:10.1111/j.1349-7006.2008.00878.x.

L, D. C., VA, R., M, C., F, F., M, F., M, F., et al. (2002). Methyltransferase recruitment and DNA hypermethylation of target promoters by an oncogenic transcription factor. *Science* 295, 1079–1082. doi:10.1126/SCIENCE.1065173.

Lai, S. R., Phipps, S., Liu, L., Andrews, L., and Tollefsbol, T. (2005). Epigenetic Control of Telomerase and Modes of Telomere Maintenance in Aging and Abnormal Systems. *Front. Biosci.* 5, i779-1796. doi:10.1525/jer.2010.5.4.toc.

Lalonde, M., and Chartrand, P. (2020). TERRA, a Multifaceted Regulator of Telomerase Activity at Telomeres. *J. Mol. Biol.* doi:10.1016/j.jmb.2020.02.004.

Lane, S. W., Williams, D. A., and Watt, F. M. (2014). Modulating the stem cell niche for tissue regeneration. *Nat. Biotechnol.* 32, 795–803. doi:10.1038/NBT.2978.

Leão, R., Lee, D., Figueiredo, A., Hermanns, T., Wild, P., Komosa, M., et al. (2019). Combined genetic and epigenetic alterations of the TERT promoter affect clinical and biological behavior of bladder cancer. *Int. J. cancer* 144, 1676–1684. doi:10.1002/IJC.31935.

Lee, D. D., Leão, R., Komosa, M., Gallo, M., Zhang, C. H., Lipman, T., et al. (2019). DNA hypermethylation within TERT promoter upregulates TERT expression in cancer. *J.*

Clin. Invest. 129, 223–229. doi:10.1172/JCI121303.

Lewis, K. A., and Tollefsbol, T. O. (2016). Regulation of the telomerase reverse transcriptase subunit through epigenetic mechanisms. *Front. Genet.* 7, 1–12. doi:10.3389/fgene.2016.00083.

Li, C.-T., Hsiao, Y.-M., Wu, T.-C., Lin, Y., Yeh, K.-T., and Ko, J.-L. (2011). Vorinostat, SAHA, represses telomerase activity via epigenetic regulation of telomerase reverse transcriptase in non-small cell lung cancer cells. *J. Cell. Biochem.* 112, 3044–3053. doi:10.1002/jcb.23229.

Li, E. (2002). Chromatin modification and epigenetic reprogramming in mammalian development. *Nat. Rev. Genet.* 3, 662–673. doi:10.1038/nrg887.

Li, E., and Zhang, Y. (2014). DNA Methylation in Mammals. *Cold Spring Harb. Perspect. Biol.* 6, 19133–19134. doi:10.1101/CSHPERSPECT.A019133.

Li, J.-Y., Pu, M.-T., Hirasawa, R., Li, B.-Z., Huang, Y.-N., Zeng, R., et al. (2007). Synergistic function of DNA methyltransferases Dnmt3a and Dnmt3b in the methylation of Oct4 and Nanog. *Mol. Cell. Biol.* 27, 8748–59. doi:10.1128/MCB.01380-07.

Li, Y., Liu, L., Andrews, L. G., and Tollefsbol, T. O. (2009). Genistein depletes telomerase activity through cross-talk between genetic and epigenetic mechanisms. *Int. J. Cancer* 125, 286–296. doi:10.1002/ijc.24398.

Li, Y., and Tollefsbol, T. O. (2011). DNA methylation detection: bisulfite genomic sequencing analysis. *Methods Mol. Biol.* 791, 11–21. doi:10.1007/978-1-61779-316-5_2.

Liao, J., Karnik, R., Gu, H., Ziller, M. J., Clement, K., Tsankov, A. M., et al. (2015). Targeted disruption of DNMT1, DNMT3A and DNMT3B in human embryonic stem cells. *Nat. Genet.* 47, 469–478. doi:10.1038/ng.3258.

Lingner, J., Cooper, J. P., and Cech, T. R. (1995). Telomerase and DNA end replication: no longer a lagging strand problem? *Science* 269, 1533–4. Available at: http://www.ncbi.nlm.nih.gov/pubmed/7545310 [Accessed March 1, 2019].

Liu, C., Fang, X., Ge, Z., Jalink, M., Kyo, S., Bjorkholm, M., et al. (2007a). The Telomerase Reverse Transcriptase (hTERT) Gene Is a Direct Target of the Histone Methyltransferase SMYD3. *Cancer Res.* 67, 2626–2631. doi:10.1158/0008-5472.CAN-06-4126.

Liu, L., Bailey, S. M., Okuka, M., Muñoz, P., Li, C., Zhou, L., et al. (2007b). Telomere lengthening early in development. *Nat. Cell Biol.* 9, 1436–1441. doi:10.1038/ncb1664.

Liu, Q., Liu, L., Zhao, Y., Zhang, J., Wang, D., Chen, J., et al. (2011). Hypoxia Induces Genomic DNA Demethylation through the Activation of HIF-1α and Transcriptional Upregulation of MAT2A in Hepatoma Cells. *Mol. Cancer Ther.* 10, 1113–1123. doi:10.1158/1535-7163.MCT-10-1010.

Liu, T., Yuan, X., and Xu, D. (2016). Cancer-Specific Telomerase Reverse Transcriptase (TERT) Promoter Mutations: Biological and Clinical Implications. *Genes (Basel).* 7. doi:10.3390/genes7070038.

Liu, W. J., Zhang, Y. W., Zhang, Z. X., and Ding, J. (2004). Alternative splicing of human telomerase reverse transcriptase may not be involved in telomerase regulation during all-trans-retinoic acid-induced HL-60 cell differentiation. *J. Pharmacol. Sci.* 96, 106–114. doi:10.1254/JPHS.FP0030600.

Loh, Y. H., Ng, J. H., and Ng, H. H. (2008). Molecular framework underlying pluripotency. *Cell Cycle* 7, 885–891. doi:10.4161/cc.7.7.5636.

Love, W., Berletch, J., Andrews, L., and Tollefsbol, T. (2008). Epigenetic regulation of telomerase in retinoid-induced differentiation of human leukemia cells. *Int. J. Oncol.* 32, 625–631. doi:10.3892/ijo.32.3.625.

Lovejoy, C. A., Li, W., Reisenweber, S., Thongthip, S., Bruno, J., de Lange, T., et al. (2012). Loss of ATRX, Genome Instability, and an Altered DNA Damage Response Are Hallmarks of the Alternative Lengthening of Telomeres Pathway. *PLoS Genet.* 8, e1002772. doi:10.1371/journal.pgen.1002772.

Luo, Y., Wang, S. xiang, Zhou, Z. quan, Wang, Z., Zhang, Y. gao, Zhang, Y., et al. (2014). Apoptotic effect of genistein on human colon cancer cells via inhibiting the nuclear factor-kappa B (NF-κB) pathway. *Tumour Biol.* 35, 11483–11488. doi:10.1007/S13277-014-2487-7.

M, A., MK, C., MS, I., CP, C., CP, H., MA, W., et al. (2000). Clonally derived human embryonic stem cell lines maintain pluripotency and proliferative potential for prolonged periods of culture. *Dev. Biol.* 227, 271–278. doi:10.1006/DBIO.2000.9912.

M, S., M, L., T, S., and A, M. (2004). Derivation, growth and applications of human

embryonic stem cells. *Reproduction* 128, 259–267. doi:10.1530/REP.1.00243.

Ma, T., Grayson, W. L., Fröhlich, M., and Vunjak-Novakovic, G. (2009). Hypoxia and stem cell-based engineering of mesenchymal tissues. *Biotechnol. Prog.* 25, 32–42. doi:10.1002/btpr.128.

Madonna, R., Willerson, J. T., and Geng, Y.-J. (2008). Myocardin a enhances telomerase activities in adipose tissue mesenchymal cells and embryonic stem cells undergoing cardiovascular myogenic differentiation. *Stem Cells* 26, 202–211. doi:10.1634/STEMCELLS.2007-0490.

Majid, S., Kikuno, N., Nelles, J., Noonan, E., Tanaka, Y., Kawamoto, K., et al. (2008). Genistein Induces the p21WAF1/CIP1 and p16INK4a Tumor Suppressor Genes in Prostate Cancer Cells by Epigenetic Mechanisms Involving Active Chromatin Modification. doi:10.1158/0008-5472.CAN-07-2290.

Manda-Handzlik, A., Bystrzycka, W., Wachowska, M., Sieczkowska, S., Stelmaszczyk-Emmel, A., Demkow, U., et al. (2018). The influence of agents differentiating HL-60 cells toward granulocyte-like cells on their ability to release neutrophil extracellular traps. *Immunol. Cell Biol.* 96, 413–425. doi:10.1111/IMCB.12015.

Mansergh, F. C., Wride, M. A., Hunter, S. M., and Evans, M. J. (2009). Gene expression profiles during early differentiation of mouse embryonic stem cells. *BMC Dev. Biol.* 9, 5. doi:10.1186/1471-213X-9-5.

Mariani, C. J., Vasanthakumar, A., Madzo, J., Yesilkanal, A., Bhagat, T., Yu, Y., et al. (2014). TET1-mediated hydroxymethylation facilitates hypoxic gene induction in neuroblastoma. *Cell Rep.* 7, 1343–1352. doi:10.1016/j.celrep.2014.04.040.

Martin, S. J., Bradley, J. G., and Cotter, T. G. (1990). HL-60 cells induced to differentiate towards neutrophils subsequently die via apoptosis. *Clin. Exp. Immunol.* 79, 448–453. doi:10.1111/J.1365-2249.1990.TB08110.X.

Marzinke, M. A., and Dufour, D. R. (2020). Laboratory diagnosis of liver disease. *Contemp. Pract. Clin. Chem.*, 545–559. doi:10.1016/B978-0-12-815499-1.00031-4.

Mas-Bargues, C., Sanz-Ros, J., Román-Domínguez, A., Inglés, M., Gimeno-Mallench, L., Alami, M. El, et al. (2019). Relevance of Oxygen Concentration in Stem Cell Culture for Regenerative Medicine. *Int. J. Mol. Sci.* 20. doi:10.3390/IJMS20051195.

Mattick, J. S., and Makunin, I. V. (2006). Non-coding RNA. *Hum. Mol. Genet.* 15, R17–R29. doi:10.1093/hmg/ddl046.

Miller, J. L., and Grant, P. A. (2013). The Role of DNA Methylation and Histone Modifications in Transcriptional Regulation in Humans. *Subcell. Biochem.* 61, 289. doi:10.1007/978-94-007-4525-4_13.

Minasi, S., Baldi, C., Pietsch, T., Donofrio, V., Pollo, B., Antonelli, M., et al. (2019). Telomere elongation via alternative lengthening of telomeres (ALT) and telomerase activation in primary metastatic medulloblastoma of childhood. *J. Neurooncol.* 142, 435–444. doi:10.1007/s11060-019-03127-w.

Mizukoshi, E., and Kaneko, S. (2019). Telomerase-Targeted Cancer Immunotherapy. *Int. J. Mol. Sci.* 20. doi:10.3390/IJMS20081823.

Montero, J. J., López-Silanes, I., Megías, D., Fraga, M., Castells-García, Á., and Blasco, M. A. (2018). TERRA recruitment of polycomb to telomeres is essential for histone trymethylation marks at telomeric heterochromatin. *Nat. Commun.* 9, 1–14. doi:10.1038/s41467-018-03916-3.

Moore, L. D., Le, T., and Fan, G. (2013). DNA methylation and its basic function. *Neuropsychopharmacology* 38, 23–38. doi:10.1038/npp.2012.112.

Moravec, M., Wischnewski, H., Bah, A., Hu, Y., Liu, N., Lafranchi, L., et al. (2016). TERRA promotes telomerase-mediated telomere elongation in *Schizosaccharomyces pombe*. *EMBO Rep.* 17, 999–1012. doi:10.15252/embr.201541708.

Moyzis, R. K., Buckingham, J. M., Cram, L. S., Dani, M., Deaven, L. L., Jones, M. D., et al. (1988). A highly conserved repetitive DNA sequence, (TTAGGG)n, present at the telomeres of human chromosomes. *Proc. Natl. Acad. Sci. U. S. A.* 85, 6622–6. doi:10.1073/PNAS.85.18.6622.

Murray, P., and Edgar, D. (2000). Regulation of Programmed Cell Death by Basement Membranes in Embryonic Development. *J. Cell Biol.* 150. Available at: http://www.jcb.org [Accessed November 29, 2021].

Muz, B., Puente, P. de la, Azab, F., and Azab, A. K. (2015). The role of hypoxia in cancer progression, angiogenesis, metastasis, and resistance to therapy. *Hypoxia* 3, 83. doi:10.2147/HP.S93413.

N, F., I, D., A, M.-H., BB, K., and D, S. (1981). Immunohistochemical localization of the early embryonic antigen (SSEA-1) in postimplantation mouse embryos and fetal and adult tissues. *Dev. Biol.* 83, 391–398. doi:10.1016/0012-1606(81)90487-5.

Nakamura, T. M., Morin, G. B., Chapman, K. B., Weinrich, S. L., Andrews, W. H., Lingner, J., et al. (1997). Telomerase catalytic subunit homologs from fission yeast and human. *Science* 277, 955–9. Available at: http://www.ncbi.nlm.nih.gov/pubmed/9252327 [Accessed July 26, 2017].

Napier, C. E., Veas, L. A., Kan, C. Y., Taylor, L. M., Yuan, J., Wen, V. W., et al. (2010). Mild hyperoxia limits hTR levels, telomerase activity, and telomere length maintenance in hTERT-transduced bone marrow endothelial cells. *Biochim. Biophys. Acta - Mol. Cell Res.* 1803, 1142–1153. doi:10.1016/J.BBAMCR.2010.06.010.

Närvä, E., Pursiheimo, J. P., Laiho, A., Rahkonen, N., Emani, M. R., Viitala, M., et al. (2013). Continuous hypoxic culturing of human embryonic stem cells enhances SSEA-3 and MYC levels. *PLoS One* 8, e78847. doi:10.1371/journal.pone.0078847.

Nebbioso, A., Tambaro, F. P., Dell'Aversana, C., and Altucci, L. (2018). Cancer epigenetics: Moving forward. *PLOS Genet.* 14, e1007362. doi:10.1371/JOURNAL.PGEN.1007362.

Nelson, D. M., Jaber-Hijazi, F., Cole, J. J., Robertson, N. A., Pawlikowski, J. S., Norris, K. T., et al. (2016). Mapping H4K20me3 onto the chromatin landscape of senescent cells indicates a function in control of cell senescence and tumor suppression through preservation of genetic and epigenetic stability. *Genome Biol.* 17. doi:10.1186/s13059-016-1017-x.

Ng, E. S., Davis, R. P., Azzola, L., Stanley, E. G., and Elefanty, A. G. (2005). Forced aggregation of defined numbers of human embryonic stem cells into embryoid bodies fosters robust, reproducible hematopoietic differentiation. *Blood* 106, 1601–1603. doi:10.1182/BLOOD-2005-03-0987.

Ng, S. S., Yue, W. W., Oppermann, U., and Klose, R. J. (2009). Dynamic protein methylation in chromatin biology. *Cell. Mol. Life Sci.* 66, 407–422. doi:10.1007/s00018-008-8303-z.

Nichols, W., Murphy, D., Cristofalo, V., Toji, L., Greene, A., and Dwight, S. (1977). Characterization of a new human diploid cell strain, IMR-90. *Science (80-.).* 196, 60–63. doi:10.1126/science.841339.

Nishi, H., Nakada, T., Kyo, S., Inoue, M., Shay, J. W., and Isaka, K. (2004). Hypoxia-inducible factor 1 mediates upregulation of telomerase (hTERT). *Mol. Cell. Biol.* 24, 6076–83. doi:10.1128/MCB.24.13.6076-6083.2004.

Nishida, N., Nagasaka, T., Nishimura, T., Ikai, I., Boland, C. R., and Goel, A. (2008). Aberrant methylation of multiple tumor suppressor genes in aging liver, chronic hepatitis, and hepatocellular carcinoma. *Hepatology* 47, 908–918. doi:10.1002/HEP.22110.

Noisa, P., Ramasamy, T. S., Lamont, F. R., Yu, J. S. L., Sheldon, M. J., Russell, A., et al. (2012). Identification and Characterisation of the Early Differentiating Cells in Neural Differentiation of Human Embryonic Stem Cells. *PLoS One* 7, e37129. doi:10.1371/JOURNAL.PONE.0037129.

Norvil, A. B., Petell, C. J., Alabdi, L., Wu, L., Rossie, S., and Gowher, H. (2018). Dnmt3b Methylates DNA by a Noncooperative Mechanism, and Its Activity Is Unaffected by Manipulations at the Predicted Dimer Interface. *Biochemistry* 57, 4312. doi:10.1021/ACS.BIOCHEM.6B00964.

Novakovic, B., Napier, C. E., Vryer, R., Dimitriadis, E., Manuelpillai, U., Sharkey, A., et al. (2016). DNA methylation mediated up-regulation of TERRA non-coding RNA is coincident with elongated telomeres in the human placenta. *Mol. Hum. Reprod.* 22, 791–799. doi:10.1093/MOLEHR/GAW053.

Okano, M., Bell, D. W., Haber, D. A., and Li, E. (1999). DNA methyltransferases Dnmt3a and Dnmt3b are essential for de novo methylation and mammalian development. *Cell* 99, 247–257. doi:10.1016/S0092-8674(00)81656-6.

Okano, M., Xie, S., and Li, E. (1998). Cloning and characterization of a family of novel mammalian DNA (cytosine-5) methyltransferases. *Nat. Genet. 1998 193* 19, 219–220. doi:10.1038/890.

Okazaki, K., and Maltepe, E. (2006). Oxygen, epigenetics and stem cell fate. *Regen. Med.* 1, 71–83. doi:10.2217/17460751.1.1.71.

Ostenfeld, T., Caldwell, M. A., Prowse, K. R., Linskens, M. H., Jauniaux, E., and Svendsen, C. N. (2000). Human neural precursor cells express low levels of telomerase in vitro and show diminishing cell proliferation with extensive axonal outgrowth following

transplantation. *Exp. Neurol.* 164, 215–226. doi:10.1006/exnr.2000.7427.

Ostler, K. R., Davis, E. M., Payne, S. L., Gosalia, B. B., Expósito-Céspedes, J., Beau, M. M. Le, et al. (2007). Cancer cells express aberrant DNMT3B transcripts encoding truncated proteins. *Oncogene* 26, 5553–5563. doi:10.1038/sj.onc.1210351.

PASQUALINI, J. R., KINCL✠, F. A., and SUMIDA, C. (1991). The Binding of Hormones in Maternal and Fetal Biological Fluids. *Horm. Fetus*, 1–50. doi:10.1016/B978-0-08-035720-1.50005-0.

Pekkanen-Mattila, M., Pelto-Huikko, M., Kujala, V., Suuronen, R., Skottman, H., Aalto-Setälä, K., et al. (2010). Spatial and temporal expression pattern of germ layer markers during human embryonic stem cell differentiation in embryoid bodies. *Histochem. Cell Biol.* 133, 595–606. doi:10.1007/S00418-010-0689-7.

Pelosi, E., Forabosco, A., and Schlessinger, D. (2011). Germ cell formation from embryonic stem cells and the use of somatic cell nuclei in oocytes. *Ann. N. Y. Acad. Sci.* 1221, 18–26. doi:10.1111/j.1749-6632.2011.05982.x.

Perez-Perri, J. I., Acevedo, J. M., and Wappner, P. (2011). Epigenetics: new questions on the response to hypoxia. *Int. J. Mol. Sci.* 12, 4705–21. doi:10.3390/ijms12074705.

Pettinato, G., Wen, X., and Zhang, N. (2014). Formation of well-defined embryoid bodies from dissociated human induced pluripotent stem cells using microfabricated cell-repellent microwell arrays. *Sci. Rep.* 4, 1–11. doi:10.1038/srep07402.

Phipps, S. M. O., Love, W. K., Mott, T. E., Andrews, L. G., and Tollefsbol, T. O. (2009). Differential expression of epigenetic modulators during human embryonic stem cell differentiation. *Mol. Biotechnol.* 41, 201–207. doi:10.1007/s12033-008-9118-8.

Poh, Y.-C., Chen, J., Hong, Y., Yi, H., Zhang, S., Chen, J., et al. (2014). Generation of organized germ layers from a single mouse embryonic stem cell. *Nat. Commun. 2014 51* 5, 1–12. doi:10.1038/ncomms5000.

Poole, C. J., Zheng, W., Lodh, A., Yevtodiyenko, A., Liefwalker, D., Li, H., et al. (2017). DNMT3B overexpression contributes to aberrant DNA methylation and MYC-driven tumor maintenance in T-ALL and Burkitt's lymphoma. *Oncotarget* 8, 76898. doi:10.18632/ONCOTARGET.20176.

Poon, E., Harris, A. L., and Ashcroft, M. (2009). Targeting the hypoxia-inducible factor (HIF) pathway in cancer. doi:10.1017/S1462399409001173.

Prado-Lopez, S., Conesa, A., ArmiÃ±Ã¡n, A., MartÃ-nez-Losa, M., Escobedo-Lucea, C., Gandia, C., et al. (2009). Hypoxia Promotes Efficient Differentiation of Human Embryonic Stem Cells to Functional Endothelium. *Stem Cells* 28, N/A-N/A. doi:10.1002/stem.295.

Prado-Lopez, S., Conesa, A., Armiñán, A., Martínez-Losa, M., Escobedo-Lucea, C., Gandia, C., et al. (2010). Hypoxia promotes efficient differentiation of human embryonic stem cells to functional endothelium. *Stem Cells* 28, 407–418. doi:10.1002/stem.295.

Qin, J., Guo, X., Zhang, J., Cui, G., Gui, Y., and Cai, Z. (2008). Growth and differentiation of embryoid bodies derived from nouse embryonic stem cells. *Cell Res. 2008 181* 18, S135–S135. doi:10.1038/cr.2008.225.

Qing, H., Aono, J., Findeisen, H. M., Jones, K. L., Heywood, E. B., and Bruemmer, D. (2016). Differential Regulation of Telomerase Reverse Transcriptase Promoter Activation and Protein Degradation by Histone Deacetylase Inhibition. *J. Cell. Physiol.* 231, 1276–1282. doi:10.1002/jcp.25226.

RA, G., RC, A., L, C., GB, M., and RA, D. (1998). Expression of mouse telomerase reverse transcriptase during development, differentiation and proliferation. *Oncogene* 16, 1723–1730. doi:10.1038/SJ.ONC.1201933.

Radan, L., Hughes, C. S., Teichroeb, J. H., Vieira Zamora, F. M., Jewer, M., Postovit, L. M., et al. (2014). Microenvironmental regulation of telomerase isoforms in human embryonic stem cells. *Stem Cells Dev.* 23, 2046–2066. doi:10.1089/scd.2013.0373.

Rajala, K., Vaajasaari, H., Suuronen, R., Hovatta, O., and Skottman, H. (2011). Effects of the physiochemical culture environment on the stemness and pluripotency of human embryonic stem cells. *Stem Cell Stud.* 1, 3. doi:10.4081/scs.2011.e3.

Rasmussen, K. D., and Helin, K. (2016). Role of TET enzymes in DNA methylation, development, and cancer. *Genes Dev.* 30, 733. doi:10.1101/GAD.276568.115.

Rathjen, J., and Rathjen, P. (2013). Embryonic Stem Cells. *Brenner's Encycl. Genet. Second Ed.*, 479–481. doi:10.1016/B978-0-12-374984-0.00490-3.

Redon, S., Reichenbach, P., and Lingner, J. (2010). The non-coding RNA TERRA is a natural ligand and direct inhibitor of human telomerase. *Nucleic Acids Res.* 38, 5797–5806. doi:10.1093/nar/gkq296.

Reik, W. (2007). Stability and flexibility of epigenetic gene regulation in mammalian development. *Nature* 447, 425–432. doi:10.1038/nature05918.

Renaud, S., Loukinov, D., Abdullaev, Z., Guilleret, I., Bosman, F. T., Lobanenkov, V., et al. (2007). Dual role of DNA methylation inside and outside of CTCF-binding regions in the transcriptional regulation of the telomerase hTERT gene. *Nucleic Acids Res.* 35, 1245–56. doi:10.1093/nar/gkl1125.

Renaud, S., Loukinov, D., Bosman, F. T., Lobanenkov, V., and Benhattar, J. (2005). CTCF binds the proximal exonic region of hTERT and inhibits its transcription. *Nucleic Acids Res.* 33, 6850–60. doi:10.1093/nar/gki989.

Rice, J. C., Briggs, S. D., Ueberheide, B., Barber, C. M., Shabanowitz, J., Hunt, D. F., et al. (2003). Histone Methyltransferases Direct Different Degrees of Methylation to Define Distinct Chromatin Domains. *Mol. Cell* 12, 1591–1598. doi:10.1016/S1097-2765(03)00479-9.

Rios, C., D'Ippolito, G., Curtis, K. M., Delcroix, G. J. R., Gomez, L. A., El Hokayem, J., et al. (2016). Low Oxygen Modulates Multiple Signaling Pathways, Increasing Self-Renewal, While Decreasing Differentiation, Senescence, and Apoptosis in Stromal MIAMI Cells. *Stem Cells Dev.* 25, 848. doi:10.1089/SCD.2015.0362.

Rivera-Pérez, J. A., and Magnuson, T. (2005). Primitive streak formation in mice is preceded by localized activation of Brachyury and Wnt3. *Dev. Biol.* 288, 363–371. doi:10.1016/J.YDBIO.2005.09.012.

Robertson, K. D., Keyomarsi, K., Gonzales, F. A., Velicescu, M., and Jones, P. A. (2000). Differential mRNA expression of the human DNA methyltransferases (DNMTs) 1, 3a and 3b during the G(0)/G(1) to S phase transition in normal and tumor cells. *Nucleic Acids Res.* 28, 2108–2113. doi:10.1093/NAR/28.10.2108.

Romito, A., and Cobellis, G. (2016). Pluripotent Stem Cells: Current Understanding and Future Directions. *Stem Cells Int.* 2016. doi:10.1155/2016/9451492.

Sadasivam, A., Dunn, N. R., and Rust, W. L. (2007). Three-Dimensional Extracellular Matrix

Stimulates Gastrulation-like Events in Human Embryoid Bodies. *https://home.liebertpub.com/scd* 15, 889–904. doi:10.1089/SCD.2006.15.889.

Sadikovic, B., Al-Romaih, K., Squire, J., and Zielenska, M. (2008). Cause and Consequences of Genetic and Epigenetic Alterations in Human Cancer. *Curr. Genomics* 9, 394. doi:10.2174/138920208785699580.

Saha, A., Wittmeyer, J., and Cairns, B. R. (2006). Chromatin remodelling: The industrial revolution of DNA around histones. *Nat. Rev. Mol. Cell Biol.* 7, 437–447. doi:10.1038/NRM1945.

Saha, D., Singh, A., Hussain, T., Srivastava, V., Sengupta, S., Kar, A., et al. (2017). Epigenetic suppression of human telomerase (hTERT) is mediated by the metastasis suppressor NME2 in a G-quadruplex– dependent fashion. *J. Biol. Chem.* 292, 15205–15215. doi:10.1074/jbc.M117.792077.

Salani, S., Donadoni, C., Rizzo, F., Bresolin, N., Comi, G. P., and Corti, S. (2012). Generation of skeletal muscle cells from embryonic and induced pluripotent stem cells as an in vitro model and for therapy of muscular dystrophies. *J. Cell. Mol. Med.* 16, 1353. doi:10.1111/J.1582-4934.2011.01498.X.

Sathananthan, A. H., and Trounson, A. (2005). Human embryonic stem cells and their spontaneous differentiation. *Ital. J. Anat. Embryol.* 110, 151–7. Available at: http://www.ncbi.nlm.nih.gov/pubmed/16101033 [Accessed April 20, 2019].

Schneider, U., Schwenk, H.-U., and Bornkamm, G. (1977). Characterization of EBV-genome negative “null” and “T” cell lines derived from children with acute lymphoblastic leukemia and leukemic transformed non-Hodgkin lymphoma. *Int. J. Cancer* 19, 621–626. doi:10.1002/ijc.2910190505.

Schoeftner, S., and Blasco, M. A. (2008). Developmentally regulated transcription of mammalian telomeres by DNA-dependent RNA polymerase II. *Nat. Cell Biol.* 10, 228–36. doi:10.1038/ncb1685.

Schroeder, M., Niebruegge, S., Werner, A., Willbold, E., Burg, M., Ruediger, M., et al. (2005). Differentiation and lineage selection of mouse embryonic stem cells in a stirred bench scale bioreactor with automated process control. *Biotechnol. Bioeng.* 92, 920–933. doi:10.1002/BIT.20668.

Seimiya, H., Tanji, M., Oh-Hara, T., Tomida, A., Naasani, I., and Tsuruo, T. (1999). Hypoxia Up-Regulates Telomerase Activity via Mitogen-Activated Protein Kinase Signaling in Human Solid Tumor Cells. *Biochem. Biophys. Res. Commun.* 260, 365–370. doi:10.1006/BBRC.1999.0910.

Sell, S. (2008). Alpha-Fetoprotein, Stem Cells and Cancer: How Study of the Production of Alpha-Fetoprotein during Chemical Hepatocarcinogenesis Led to Reaffirmation of the Stem Cell Theory of Cancer. *Tumor Biol.* 29, 161–180. doi:10.1159/000143402.

Semenza, G. L. (2011). Oxygen Sensing, Homeostasis, and Disease. *N. Engl. J. Med.* 365, 537–547. doi:10.1056/NEJMra1011165.

Seto, E., and Yoshida, M. (2014). Erasers of histone acetylation: the histone deacetylase enzymes. *Cold Spring Harb. Perspect. Biol.* 6, a018713. doi:10.1101/cshperspect.a018713.

Sexton, A. N., Regalado, S. G., Lai, C. S., Cost, G. J., O'Neil, C. M., Urnov, F. D., et al. (2014). Genetic and molecular identification of three human TPP1 functions in telomerase action: Recruitment, activation, and homeostasis set point regulation. *Genes Dev.* 28, 1885–1899. doi:10.1101/gad.246819.114.

Seynnaeve, B., Lee, S., Borah, S., Park, Y., Pappo, A., Kirkwood, J. M., et al. (2017). Genetic and Epigenetic Alterations of TERT Are Associated with Inferior Outcome in Adolescent and Young Adult Patients with Melanoma. *Sci. Rep.* 7, 45704. doi:10.1038/srep45704.

Shaheen, F., Grammatopoulos, D. K., Müller, J., Zammit, V. A., and Lehnert, H. (2014). Extra-nuclear telomerase reverse transcriptase (TERT) regulates glucose transport in skeletal muscle cells. *Biochim. Biophys. Acta - Mol. Basis Dis.* 1842, 1762–1769. doi:10.1016/j.bbadis.2014.06.018.

Shahrzad, S., Bertrand, K., Minhas, K., and Coomber, B. L. (2007). Induction of DNA hypomethylation by tumor hypoxia. *Epigenetics* 2, 119–125. doi:10.4161/epi.2.2.4613.

Shamblott, M. J. (2001). Human embryonic germ cell derivatives express a broad range of developmentally distinct markers and proliferate extensively in vitro. *Proc. Natl. Acad. Sci.* 98, 113–118. doi:10.1073/PNAS.021537998.

Shao, Y., Taniguchi, K., Townshend, R. F., Miki, T., Gumucio, D. L., and Fu, J. (2017). A

pluripotent stem cell-based model for post-implantation human amniotic sac development. *Nat. Commun. 2017 81* 8, 1–15. doi:10.1038/s41467-017-00236-w.

Sharma, H. W., SOKOLOSKIt, J. A., Perez, J. R., Yves Maltese, J., SARTORELLIt, A. C., STEINt, C. A., et al. (1995). Differentiation of immortal cells inhibits telomerase activity (cancer/telomeres/ribonucleoprotein). Available at: https://www.pnas.org/content/pnas/92/26/12343.full.pdf [Accessed August 7, 2019].

Sharma, S., Kelly, T. K., and Jones, P. A. (2010). Epigenetics in cancer. *Carcinogenesis* 31, 27–36. doi:10.1093/carcin/bgp220.

Shay, J. W. (2016). Role of Telomeres and Telomerase in Aging and Cancer. *Cancer Discov.* 6, 584–593. doi:10.1158/2159-8290.CD-16-0062.

Shay, J. W., and Wright, W. E. (2011). Role of telomeres and telomerase in cancer. *Semin. Cancer Biol.* 21, 349–53. doi:10.1016/j.semcancer.2011.10.001.

Shevde, N. (2012). Stem Cells: Flexible friends. *Nat. 2012 4837387* 483, S22–S26. doi:10.1038/483s22a.

Shimada, H., Hashimoto, Y., Nakada, A., Shigeno, K., and Nakamura, T. (2012). Accelerated generation of human induced pluripotent stem cells with retroviral transduction and chemical inhibitors under physiological hypoxia. *Biochem. Biophys. Res. Commun.* 417, 659–664. doi:10.1016/J.BBRC.2011.11.111.

Simó-Riudalbas, L., Melo, S. A., and Esteller, M. (2011). DNMT3B gene amplification predicts resistance to DNA demethylating drugs. *Genes. Chromosomes Cancer* 50, 527–534. doi:10.1002/GCC.20877.

Simunovic, M., and Brivanlou, A. H. (2017). Embryoids, organoids and gastruloids: New approaches to understanding embryogenesis. *Dev.* 144, 976–985. doi:10.1242/dev.143529.

Skowronski, K., Dubey, S., Rodenhiser, D. I., and Coomber, B. (2010). Ischemia dysregulates DNA methyltransferases and *p16INK4a* methylation in human colorectal cancer cells. *Epigenetics* 5, 547–556. doi:10.4161/epi.5.6.12400.

Solter, D., and Knowles, B. B. (1978). Monoclonal antibody defining a stage-specific mouse embryonic antigen (SSEA-1)

(cytotoxicity/immunofluorescence/radioimmunoassay/preimplantation mouse embryo/teratocarcinoma stem cells). *Dev. Biol.* 75, 5565–5569.

Stephenson, R. O., Yamanaka, Y., and Rossant, J. (2010). Disorganized epithelial polarity and excess trophectoderm cell fate in preimplantation embryos lacking E-cadherin. *Development* 137, 3383–3391. doi:10.1242/DEV.050195.

Stewart, M. L., Tamayo, P., Wilson, A. J., Wang, S., Chang, Y. M., Kim, J. W., et al. (2015). KRAS Genomic Status Predicts the Sensitivity of Ovarian Cancer Cells to Decitabine. *Cancer Res.* 75, 2897–2906. doi:10.1158/0008-5472.CAN-14-2860.

Stögbauer, L., Thomas, C., Wagner, A., Warneke, N., Bunk, E. C., Grauer, O., et al. (2020). Efficacy of decitabine in malignant meningioma cells: relation to promoter demethylation of distinct tumor suppressor and oncogenes and independence from TERT. *J. Neurosurg.* 135, 845–854. doi:10.3171/2020.7.JNS193097.

Strahl, B. D., and Allis, C. D. (2000). The language of covalent histone modifications. *Nature* 403, 41–45. doi:10.1038/47412.

Suelves, M., Carrió, E., Núñez-Álvarez, Y., and Peinado, M. A. (2016). DNA methylation dynamics in cellular commitment and differentiation. *Brief. Funct. Genomics* 15, 443–453. doi:10.1093/bfgp/elw017.

Sui, X., Kong, N., Wang, Z., and Pan, H. (2013). Epigenetic regulation of the human telomerase reverse transciptase gene: A potential therapeutic target for the treatment of leukemia (Review). *Oncol. Lett.* 6, 317–322. doi:10.3892/ol.2013.1367.

T, E., P, D., and RM, R. (2005). Low O2 tensions and the prevention of differentiation of hES cells. *Proc. Natl. Acad. Sci. U. S. A.* 102, 4783–4788. doi:10.1073/PNAS.0501283102.

Takakura, M., Kyo, S., Kanaya, T., Hirano, H., Takeda, J., Yutsudo, M., et al. (1999). Cloning of human telomerase catalytic subunit (hTERT) gene promoter and identification of proximal core promoter sequences essential for transcriptional activation in immortalized and cancer cells. *Cancer Res.* 59, 551–7. Available at: http://www.ncbi.nlm.nih.gov/pubmed/9973199 [Accessed December 18, 2018].

Takakura, M., Kyo, S., Sowa, Y., Wang, Z., Yatabe, N., Maida, Y., et al. (2001). Telomerase activation by histone deacetylase inhibitor in normal cells. *Nucleic Acids Res.* 29, 3006–11. doi:10.1093/nar/29.14.3006.

Takasawa, K., Arai, Y., Yamazaki-Inoue, M., Toyoda, M., Akutsu, H., Umezawa, A., et al. (2018). DNA hypermethylation enhanced telomerase reverse transcriptase expression in human-induced pluripotent stem cells. *Hum. Cell* 31, 78–86. doi:10.1007/s13577-017-0190-x.

Takubo, K., Izumiyama-Shimomura, N., Honma, N., Sawabe, M., Arai, T., Kato, M., et al. (2002). Telomere lengths are characteristic in each human individual. *Exp. Gerontol.* 37, 523–31. doi:10.1016/s0531-5565(01)00218-2.

Tanaka, T., Kato, H., Kojima, I., Ohse, T., Son, D., Tawakami, T., et al. (2006). Hypoxia and Expression of Hypoxia-Inducible Factor in the Aging Kidney. *Journals Gerontol. Ser. A Biol. Sci. Med. Sci.* 61, 795–805. doi:10.1093/gerona/61.8.795.

Tang, M., Bolderson, E., O'Byrne, K. J., and Richard, D. J. (2021). Tumor Hypoxia Drives Genomic Instability. *Front. Cell Dev. Biol.* 9, 430. doi:10.3389/FCELL.2021.626229/BIBTEX.

TE, L., ME, L., JM, J., WT, B., ER, M., JL, F., et al. (2006). Derivation of human embryonic stem cells in defined conditions. *Nat. Biotechnol.* 24, 185–187. doi:10.1038/NBT1177.

Teichroeb, J. H., Kim, J., and Betts, D. H. (2016). The role of telomeres and telomerase reverse transcriptase isoforms in pluripotency induction and maintenance. *RNA Biol.* 13, 707–719. doi:10.1080/15476286.2015.1134413.

ten Berge, D., Koole, W., Fuerer, C., Fish, M., Eroglu, E., and Nusse, R. (2008). Wnt Signaling Mediates Self-Organization and Axis Formation in Embryoid Bodies. *Cell Stem Cell* 3, 508–518. doi:10.1016/j.stem.2008.09.013.

Thomson, J. A., Itskovitz-Eldor, J., Shapiro, S. S., Waknitz, M. A., Swiergiel, J. J., Marshall, V. S., et al. (1998). Embryonic stem cell lines derived from human blastocysts. *Science* 282, 1145–7. Available at: http://www.ncbi.nlm.nih.gov/pubmed/9804556 [Accessed February 19, 2019].

Ting, A. H., Jair, K., Schuebel, K. E., and Baylin, S. B. (2006). Differential Requirement for DNA Methyltransferase 1 in Maintaining Human Cancer Cell Gene Promoter Hypermethylation. *Cancer Res.* 66.

Torisawa, Y. S., Chueh, B. H., Huh, D., Ramamurthy, P., Roth, T. M., Barald, K. F., et al. (2007). Efficient formation of uniform-sized embryoid bodies using a compartmentalized

microchannel device. *Lab Chip* 7, 770–776. doi:10.1039/B618439A.

TRAPEZE® RT Telomerase Detection Kit | S7710 Available at: http://www.merckmillipore.com/GB/en/product/TRAPEZE-RT-Telomerase-Detection-Kit,MM_NF-S7710#documentation [Accessed July 28, 2019].

Turek-Plewa, J., and Jagodziński, P. P. (2005). THE ROLE OF MAMMALIAN DNA METHYLTRANSFERASES IN THE REGULATION OF GENE EXPRESSION. Available at: http://www.cmbl.org.pl [Accessed December 12, 2020].

Tzukerman, M., Shachaf, C., Ravel, Y., Braunstein, I., Cohen-Barak, O., Yalon-Hacohen, M., et al. (2000). Identification of a novel transcription factor binding element involved in the regulation by differentiation of the human telomerase (hTERT) promoter. *Mol. Biol. Cell* 11, 4381–4391. doi:10.1091/mbc.11.12.4381.

V, V., B, L., P, S., A, L., N, A., and M, S. (2011). Human stem cell research and regenerative medicine--present and future. *Br. Med. Bull.* 99, 155–168. doi:10.1093/BMB/LDR027.

van den Berg-Bakker, C. A. M., Hagemeijer, A., Franken-Postma, E. M., Smit, V. T. H. B. M., Kuppen, P. J. K., Claasen, H. H. V. R., et al. (1993). Establishment and characterization of 7 ovarian carcinoma cell lines and one granulosa tumor cell line: Growth features and cytogenetics. *Int. J. Cancer* 53, 613–620. doi:10.1002/ijc.2910530415.

van den Brink, S. C., Baillie-Johnson, P., Balayo, T., Hadjantonakis, A.-K., Nowotschin, S., Turner, D. A., et al. (2014). Symmetry breaking, germ layer specification and axial organisation in aggregates of mouse embryonic stem cells. *Development* 141, 4231–42. doi:10.1242/dev.113001.

Van Winkle, A. P., Gates, I. D., and Kallos, M. S. (2012). Mass transfer limitations in embryoid bodies during human embryonic stem cell differentiation. *Cells. Tissues. Organs* 196, 34–47. doi:10.1159/000330691.

Vaquero-Sedas, M. I., and Vega-Palas, M. A. (2019). Assessing the Epigenetic Status of Human Telomeres. *Cells* 8, 1050. doi:10.3390/cells8091050.

Vaziri, H., Dragowska, W., Allsopp, R. C., Thomas, T. E., Harley, C. B., and Lansdorp, P. M. (1994). Evidence for a mitotic clock in human hematopoietic stem cells: loss of telomeric DNA with age. *Proc. Natl. Acad. Sci. U. S. A.* 91, 9857–60. Available at:

http://www.ncbi.nlm.nih.gov/pubmed/7937905 [Accessed April 6, 2019].

Volkmer, E., Kallukalam, B. C., Maertz, J., Otto, S., Drosse, I., Polzer, H., et al. (2010). Hypoxic preconditioning of human mesenchymal stem cells overcomes hypoxia-induced inhibition of osteogenic differentiation. *Tissue Eng. Part A* 16, 153–64. doi:10.1089/ten.TEA.2009.0021.

Vonderheide, R. H. (2008). Prospects and challenges of building a cancer vaccine targeting telomerase. *Biochimie* 90, 173. doi:10.1016/J.BIOCHI.2007.07.005.

Waddington, C. H. (2012). The Epigenotype. *Int. J. Epidemiol.* 41, 10–13. doi:10.1093/ije/dyr184.

Wajed, S. A., Laird, P. W., and DeMeester, T. R. (2001). DNA Methylation: An Alternative Pathway to Cancer. *Ann. Surg.* 234, 10. doi:10.1097/00000658-200107000-00003.

Walker, J. M. METHODS I N MOLECULAR BIOLOGY TM Series Editor. Available at: www.springer.com/series/7651 [Accessed November 30, 2021].

Wang, F., Thirumangalathu, S., and Loeken, M. R. (2006). Establishment of new mouse embryonic stem cell lines is improved by physiological glucose and oxygen. *Cloning Stem Cells* 8, 108–116. doi:10.1089/CLO.2006.8.108.

Wang, Y., Zhao, Z., Zhu, Z., Li, P., Li, X., Xue, X., et al. (2018). Telomere elongation protects heart and lung tissue cells from fatal damage in rats exposed to severe hypoxia. *J. Physiol. Anthropol.* 37, 5. doi:10.1186/s40101-018-0165-y.

Watanabe, D., Suetake, I., Tada, T., and Tajima, S. (2002). Stage- and cell-specific expression of Dnmt3a and Dnmt3b during embryogenesis. *Mech. Dev.* 118, 187–190. doi:10.1016/S0925-4773(02)00242-3.

Watanabe, K., Ueno, M., Kamiya, D., Nishiyama, A., Matsumura, M., Wataya, T., et al. (2007). A ROCK inhibitor permits survival of dissociated human embryonic stem cells. *Nat. Biotechnol.* 25, 681–686. doi:10.1038/NBT1310.

Watson, C. J., Collier, P., Tea, I., Neary, R., Watson, J. A., Robinson, C., et al. (2014). Hypoxia-induced epigenetic modifications are associated with cardiac tissue fibrosis and the development of a myofibroblast-like phenotype. *Hum. Mol. Genet.* 23, 2176–2188. doi:10.1093/hmg/ddt614.

Watson, J. A., Watson, C. J., Mccann, A., and Baugh, J. (2010). Epigenetics: The epicenter of the hypoxic response. doi:10.4161/epi.5.4.11684.

Watson, J. A., Watson, C. J., McCrohan, A.-M., Woodfine, K., Tosetto, M., McDaid, J., et al. (2009). Generation of an epigenetic signature by chronic hypoxia in prostate cells. *Hum. Mol. Genet.* 18, 3594–3604. doi:10.1093/hmg/ddp307.

Watt, F. M., and Hogan, B. L. (2000). Out of Eden: stem cells and their niches. *Science* 287, 1427–30. doi:10.1126/SCIENCE.287.5457.1427.

Weng, N., Granger, L., and Hodes, R. J. (1997). Telomere lengthening and telomerase activation during human B cell differentiation. Available at: www.pnas.org. [Accessed August 7, 2019].

Wick, M., Zubov, D., and Hagen, G. (1999). Genomic organization and promoter characterization of the gene encoding the human telomerase reverse transcriptase (hTERT). *Gene* 232, 97–106. doi:10.1016/S0378-1119(99)00108-0.

Widowati, W., Rihibiha, D. D., Khiong, K., Widodo, M. A., Sumitro, S. B., and Bachtiar, I. (2017). "Hypoxia in Mesenchymal Stem Cell," in *Hypoxia and Human Diseases* (InTech). doi:10.5772/65510.

Wobus, A. M. (2001). Potential of embryonic stem cells. *Mol. Aspects Med.* 22, 149–164. doi:10.1016/S0098-2997(01)00006-1.

Wong, J. M. Y., Kusdra, L., and Collins, K. (2002). Subnuclear shuttling of human telomerase induced by transformation and DNA damage. *Nat. Cell Biol.* 4, 731–736. doi:10.1038/NCB846.

Wright, W. E., and Shay, J. W. (2000). Telomere dynamics in cancer progression and prevention: fundamental differences in human and mouse telomere biology. *Nat. Med.* 6, 849–851. doi:10.1038/78592.

Wu, H., and Sun, Y. E. (2006). Epigenetic Regulation of Stem Cell Differentiation. *Pediatr. Res. 2006 594* 59, 21–25. doi:10.1203/01.pdr.0000203565.76028.2a.

Wu, Y., Li, G., He, D., Yang, F., He, G., He, L., et al. (2016). Telomerase reverse transcriptase methylation predicts lymph node metastasis and prognosis in patients with gastric cancer. *Onco. Targets. Ther.* 9, 279–86. doi:10.2147/OTT.S97899.

Xhemalce, B., Dawson, M. A., and Bannister, A. J. (2011). “Histone Modifications,” in *Encyclopedia of Molecular Cell Biology and Molecular Medicine* (Weinheim, Germany: Wiley-VCH Verlag GmbH & Co. KGaA). doi:10.1002/3527600906.mcb.201100004.

Xiong, Z. M., LaDana, C., Wu, D., and Cao, K. (2013). An inhibitory role of progerin in the gene induction network of adipocyte differentiation from iPS cells. *Aging (Albany. NY).* 5, 288–303. doi:10.18632/AGING.100550.

Xu, D., Gruber, A., Björkholm, M., Peterson, C., and Pisa, P. (1999). Suppression of telomerase reverse transcriptase (hTERT) expression in differentiated HL-60 cells: regulatory mechanisms. *Br. J. Cancer 1999 808* 80, 1156–1161. doi:10.1038/sj.bjc.6690480.

Xu, Y., Wu, F., Tan, L., Kong, L., Xiong, L., Deng, J., et al. (2011). Genome-wide Regulation of 5hmC, 5mC, and Gene Expression by Tet1 Hydroxylase in Mouse Embryonic Stem Cells. *Mol. Cell* 42, 451–464. doi:10.1016/j.molcel.2011.04.005.

Y, H., A, H., R, A. H., M, D.-K., M, C., G, F., et al. (2020). Hyperbaric oxygen therapy increases telomere length and decreases immunosenescence in isolated blood cells: a prospective trial. *Aging (Albany. NY).* 12, 22445–22456. doi:10.18632/AGING.202188.

Yamanaka, Y., Ralston, A., Stephenson, R. O., and Rossant, J. (2006). Cell and molecular regulation of the mouse blastocyst. *Dev. Dyn.* 235, 2301–2314. doi:10.1002/DVDY.20844.

Yamashita, J., Itoh, H., Hirashima, M., Ogawa, M., Nishikawa, S., Yurugi, T., et al. (2000). Flk1-positive cells derived from embryonic stem cells serve as vascular progenitors. *Nat. 2000 4086808* 408, 92–96. doi:10.1038/35040568.

Yan, F., Shen, N., Pang, J., Molina, J. R., Yang, P., and Liu, S. (2015). The DNA Methyltransferase DNMT1 and Tyrosine-Protein Kinase KIT Cooperatively Promote Resistance to 5-Aza-2′-deoxycytidine (Decitabine) and Midostaurin (PKC412) in Lung Cancer Cells. *J. Biol. Chem.* 290, 18480. doi:10.1074/JBC.M114.633693.

Yang, C., Przyborski, S., Cooke, M. J., Zhang, X., Stewart, R., Anyfantis, G., et al. (2008). A Key Role for Telomerase Reverse Transcriptase Unit in Modulating Human Embryonic Stem Cell Proliferation, Cell Cycle Dynamics, and In Vitro Differentiation. *Stem Cells* 26, 850–863. doi:10.1634/stemcells.2007-0677.

Yatabe, N., Kyo, S., Maida, Y., Nishi, H., Nakamura, M., Kanaya, T., et al. (2004). HIF-1-mediated activation of telomerase in cervical cancer cells. *Oncogene* 23, 3708–3715. doi:10.1038/sj.onc.1207460.

Yoo, C. B., and Jones, P. A. (2006). Epigenetic therapy of cancer: past, present and future. *Nat. Rev. Drug Discov. 2006 51* 5, 37–50. doi:10.1038/nrd1930.

Yoshida, Y., Takahashi, K., Okita, K., Ichisaka, T., and Yamanaka, S. (2009). Hypoxia enhances the generation of induced pluripotent stem cells. *Cell Stem Cell* 5, 237–241. doi:10.1016/J.STEM.2009.08.001.

Yu, J., Qin, B., Moyer, A. M., Nowsheen, S., Liu, T., Qin, S., et al. (2018a). DNA methyltransferase expression in triple-negative breast cancer predicts sensitivity to decitabine. *J. Clin. Invest.* 128, 2376–2388. doi:10.1172/JCI97924.

Yu, J., Yuan, X., Sjöholm, L., Liu, T., Kong, F., Ekström, T. J., et al. (2018b). Telomerase reverse transcriptase regulates DNMT3B expression/aberrant DNA methylation phenotype and AKT activation in hepatocellular carcinoma. *Cancer Lett.* 434, 33–41. doi:10.1016/j.canlet.2018.07.013.

Yuan, X., Larsson, C., and Xu, D. (2019). Mechanisms underlying the activation of TERT transcription and telomerase activity in human cancer: old actors and new players. *Oncogene 2019 3834* 38, 6172–6183. doi:10.1038/s41388-019-0872-9.

Yuan, X., and Xu, D. Molecular Sciences Telomerase Reverse Transcriptase (TERT) in Action: Cross-Talking with Epigenetics. doi:10.3390/ijms20133338.

Yui, J., Chiu, C.-P., and Lansdorp, P. M. (1998). Telomerase Activity in Candidate Stem Cells From Fetal Liver and Adult Bone Marrow. *Blood* 91, 3255–3262. doi:10.1182/BLOOD.V91.9.3255.

Zhao, W., Ji, X., Zhang, F., Li, L., Ma, L., Zhao, W., et al. (2012). Embryonic Stem Cell Markers. *Molecules* 17, 6196–6236. doi:10.3390/molecules17066196.

Zheng, Y., Shao, Y., and Fu, J. (2020). A microfluidics-based stem cell model of early post-implantation human development. *Nat. Protoc. 2020 161* 16, 309–326. doi:10.1038/s41596-020-00417-w.

Zheng, Y., Xue, X., Shao, Y., Wang, S., Esfahani, S. N., Li, Z., et al. (2019). Controlled

modelling of human epiblast and amnion development using stem cells. *Nat. 2019 5737774* 573, 421–425. doi:10.1038/s41586-019-1535-2.

Zhi, X., Xiong, J., Wang, M., Zhang, H., Huang, G., Zhao, J., et al. (2018). Physiological Hypoxia Enhances Stemness Preservation, Proliferation, and Bidifferentiation of Induced Hepatic Stem Cells. *Oxid. Med. Cell. Longev.* 2018, 1–10. doi:10.1155/2018/7618704.

Zhou, J., Zhang, Y., Lin, Q., Liu, Z., Wang, H., Duan, C., et al. (2010). Embryoid bodies formation and differentiation from mouse embryonic stem cells in collagen/Matrigel scaffolds. *J. Genet. Genomics* 37, 451–460. doi:10.1016/S1673-8527(09)60064-3.

Zhu, H., and Bunn, H. F. (2001). How Do Cells Sense Oxygen? *Science* 292, 449. doi:10.1126/SCIENCE.1060849.

Zhu, J., Zhao, Y., and Wang, S. (2010). Chromatin and epigenetic regulation of the telomerase reverse transcriptase gene. *Protein Cell* 1, 22–32. doi:10.1007/S13238-010-0014-1.

Zhu, K., Qu, D., Sakamoto, T., Fukasawa, I., Hayashi, M., and Inaba, N. (2007). Telomerase expression and cell proliferation in ovarian cancer cells induced by histone deacetylase inhibitors. *Arch. Gynecol. Obstet.* 277, 15–19. doi:10.1007/s00404-007-0423-4.

Ziello, J. E., Jovin, I. S., and Huang, Y. (2007). Hypoxia-Inducible Factor (HIF)-1 regulatory pathway and its potential for therapeutic intervention in malignancy and ischemia. *Yale J. Biol. Med.* 80, 51–60. Available at: http://www.ncbi.nlm.nih.gov/pubmed/18160990 [Accessed April 9, 2019].

Ziller, M. J., Gu, H., Müller, F., Donaghey, J., Tsai, L. T. Y., Kohlbacher, O., et al. (2013). Charting a dynamic DNA methylation landscape of the human genome. *Nat. 2013 5007463* 500, 477–481. doi:10.1038/nature12433.

Zinn, R. L., Pruitt, K., Eguchi, S., Baylin, S. B., and Herman, J. G. (2007). hTERT is expressed in cancer cell lines despite promoter DNA methylation by preservation of unmethylated DNA and active chromatin around the transcription start site. *Cancer Res.* 67, 194–201. doi:10.1158/0008-5472.CAN-06-3396.